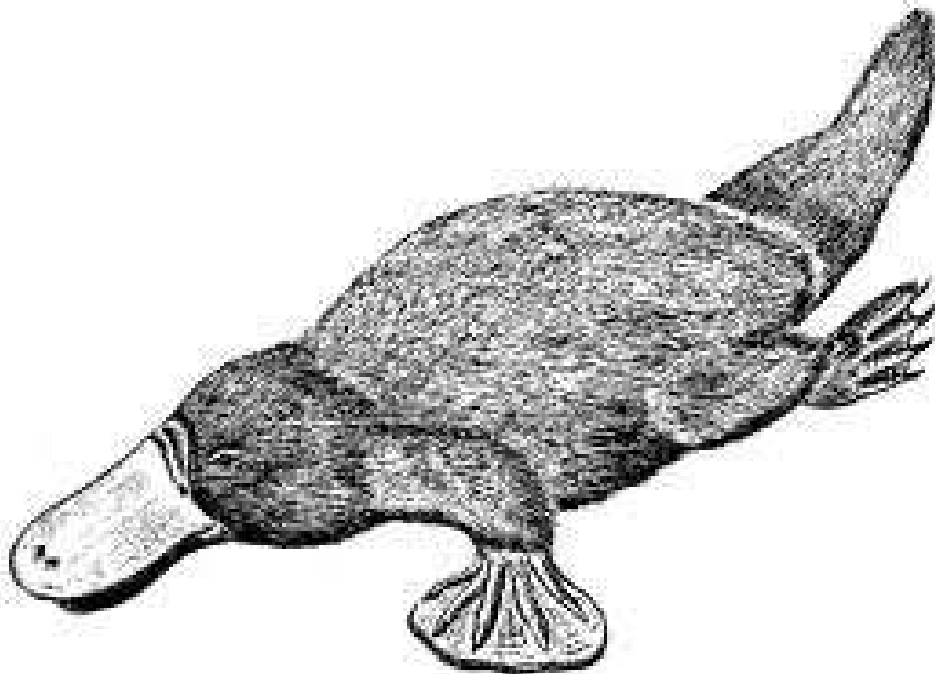


# TALYS-1.9

New  
Edition  
December 21, 2017

*A nuclear reaction program*



*User Manual*

**Arjan Koning  
Stephane Hilaire  
Stephane Goriely**

© User Manual  
2017 A.J. Koning, All rights reserved  
On cover page: a platypus.

First edition: December 21, 2017

# Contents

<b>Contents</b>	<b>i</b>
<b>Preface</b>	<b>ix</b>
<b>1 Introduction</b>	<b>1</b>
1.1 From TALYS-1.0 to TALYS-1.2 . . . . .	4
1.2 From TALYS-1.2 to TALYS-1.4 . . . . .	5
1.3 From TALYS-1.4 to TALYS-1.6 . . . . .	7
1.4 From TALYS-1.6 to TALYS-1.8 . . . . .	8
1.5 From TALYS-1.8 to TALYS-1.9 . . . . .	9
1.6 How to use this manual . . . . .	9
<b>2 Installation and getting started</b>	<b>11</b>
2.1 The TALYS package . . . . .	11
2.2 Installation . . . . .	12
2.3 Verification . . . . .	13
2.4 Getting started . . . . .	13
<b>3 Nuclear reactions: General approach</b>	<b>15</b>
3.1 Reaction mechanisms . . . . .	19
3.1.1 Low energies . . . . .	19
3.1.2 High energies . . . . .	21
3.2 Cross section definitions . . . . .	22
3.2.1 Total cross sections . . . . .	23

3.2.2	Exclusive cross sections . . . . .	23
3.2.3	Binary cross sections . . . . .	27
3.2.4	Total particle production cross sections . . . . .	28
3.2.5	Residual production cross sections . . . . .	29
3.3	Spectra and angular distributions . . . . .	29
3.3.1	Discrete angular distributions . . . . .	30
3.3.2	Exclusive spectra . . . . .	30
3.3.3	Binary spectra . . . . .	32
3.3.4	Total particle production spectra . . . . .	32
3.3.5	Double-differential cross sections . . . . .	33
3.4	Fission cross sections . . . . .	33
3.5	Recoils . . . . .	35
3.5.1	Qualitative analysis . . . . .	35
3.5.2	General method . . . . .	35
3.5.3	Quantitative analysis . . . . .	36
3.5.4	The recoil treatment in TALYS . . . . .	37
3.5.5	Method of average velocity . . . . .	39
3.5.6	Approximative recoil correction for binary ejectile spectra . . . . .	39
<b>4</b>	<b>Nuclear models</b>	<b>41</b>
4.1	Optical model . . . . .	41
4.1.1	Spherical OMP: Neutrons and protons . . . . .	43
4.1.2	Spherical dispersive OMP: Neutrons . . . . .	49
4.1.3	Spherical OMP: Complex particles . . . . .	50
4.1.4	Semi-microscopic optical model (JLM) . . . . .	52
4.1.5	Systematics for non-elastic cross sections . . . . .	54
4.2	Direct reactions . . . . .	54
4.2.1	Deformed nuclei: Coupled-channels . . . . .	54
4.2.2	Distorted Wave Born Approximation . . . . .	57
4.2.3	Odd nuclei: Weak coupling . . . . .	57
4.2.4	Giant resonances . . . . .	58
4.3	Gamma-ray transmission coefficients . . . . .	59
4.3.1	Gamma-ray strength functions . . . . .	60

4.3.2	Renormalization of gamma-ray strength functions . . . . .	61
4.3.3	Photoabsorption cross section . . . . .	62
4.4	Pre-equilibrium reactions . . . . .	63
4.4.1	Exciton model . . . . .	63
4.4.2	Photon exciton model . . . . .	76
4.4.3	Pre-equilibrium spin distribution . . . . .	77
4.4.4	Continuum stripping, pick-up, break-up and knock-out reactions . . . . .	78
4.4.5	Angular distribution systematics . . . . .	81
4.5	Compound reactions . . . . .	83
4.5.1	Binary compound cross section and angular distribution . . . . .	83
4.5.2	Width fluctuation correction factor . . . . .	86
4.6	Multiple emission . . . . .	92
4.6.1	Multiple Hauser-Feshbach decay . . . . .	92
4.6.2	Multiple pre-equilibrium emission . . . . .	93
4.7	Level densities . . . . .	96
4.7.1	Effective level density . . . . .	97
4.7.2	Collective effects in the level density . . . . .	110
4.7.3	Microscopic level densities . . . . .	112
4.8	Fission . . . . .	113
4.8.1	Level densities for fission barriers . . . . .	113
4.8.2	Fission transmission coefficients . . . . .	114
4.8.3	Transmission coefficient for multi-humped barriers . . . . .	115
4.8.4	Class II/III states . . . . .	116
4.8.5	Fission barrier parameters . . . . .	117
4.8.6	WKB approximation . . . . .	118
4.8.7	Fission fragment properties . . . . .	118
4.9	Thermal reactions . . . . .	125
4.9.1	Capture channel . . . . .	125
4.9.2	Other non-threshold reactions . . . . .	125
4.10	Direct capture . . . . .	127
4.11	Populated initial nucleus . . . . .	127
4.12	Astrophysical reaction rates . . . . .	127

4.13	Medical isotope production . . . . .	129
4.13.1	Production and depletion of isotopes . . . . .	129
4.13.2	Initial condition and stopping power . . . . .	132
4.13.3	Nuclear reaction and decay rates . . . . .	133
4.13.4	Activities . . . . .	134
<b>5</b>	<b>Nuclear structure and model parameters</b>	<b>135</b>
5.1	General setup of the database . . . . .	135
5.2	Nuclear masses and deformations . . . . .	135
5.3	Isotopic abundances . . . . .	136
5.4	Discrete level file . . . . .	137
5.5	Deformation parameters . . . . .	138
5.6	Level density parameters . . . . .	140
5.7	Resonance parameters . . . . .	142
5.8	Gamma-ray parameters . . . . .	142
5.9	Thermal cross sections . . . . .	143
5.10	Optical model parameters . . . . .	144
5.11	Fission parameters . . . . .	145
5.12	Integral validation library . . . . .	149
5.13	Decay data library . . . . .	149
5.14	Best TALYS input parameters . . . . .	149
<b>6</b>	<b>Input description</b>	<b>151</b>
6.1	Basic input rules . . . . .	152
6.2	Keywords . . . . .	153
6.2.1	Four main keywords . . . . .	154
6.2.2	Basic physical and numerical parameters . . . . .	158
6.2.3	Optical model . . . . .	178
6.2.4	Direct reactions . . . . .	200
6.2.5	Compound nucleus . . . . .	203
6.2.6	Gamma emission . . . . .	207
6.2.7	Pre-equilibrium . . . . .	216
6.2.8	Level densities . . . . .	224

6.2.9	Fission . . . . .	239
6.2.10	Medical isotope production . . . . .	247
6.2.11	Output . . . . .	250
6.2.12	Energy-dependent parameter adjustment . . . . .	266
6.2.13	Input parameter table . . . . .	268
<b>7</b>	<b>Verification and validation, sample cases and output</b>	<b>279</b>
7.1	Robustness test with DRIP . . . . .	279
7.2	Robustness test with MONKEY . . . . .	279
7.3	Validation with sample cases . . . . .	280
7.3.1	Sample 1: All results for 14 MeV $n + {}^{93}\text{Nb}$ . . . . .	282
7.3.2	Sample 2: Excitation functions: ${}^{208}\text{Pb}(n,n')$ , $(n,2n)$ , $(n,p)$ etc. . . . .	313
7.3.3	Sample 3: Comparison of compound nucleus WFC models: 10 keV $n + {}^{93}\text{Nb}$ . . . . .	319
7.3.4	Sample 4: Recoils: 20 MeV $n + {}^{28}\text{Si}$ . . . . .	322
7.3.5	Sample 5: Fission cross sections: $n + {}^{232}\text{Th}$ . . . . .	324
7.3.6	Sample 6: Continuum spectra at 63 MeV for $\text{Bi}(n, \text{xp}) \dots \text{Bi}(n, \text{x}\alpha)$ . . . . .	328
7.3.7	Sample 7: Pre-equilibrium angular dist. and multiple pre-equilibrium emission . . . . .	332
7.3.8	Sample 8: Residual production cross sections: $p + {}^{\text{nat}}\text{Fe}$ up to 100 MeV . . . . .	336
7.3.9	Sample 9: Spherical optical model and DWBA: $n + {}^{208}\text{Pb}$ . . . . .	338
7.3.10	Sample 10: Coupled-channels rotational model: $n + {}^{28}\text{Si}$ . . . . .	340
7.3.11	Sample 11: Coupled-channels vibrational model: $n + {}^{74}\text{Ge}$ . . . . .	342
7.3.12	Sample 12: Inelastic spectra at 20 MeV: Direct + Preeq + GR + Compound . . . . .	343
7.3.13	Sample 13: Gamma-ray intensities: ${}^{208}\text{Pb}(n, n\gamma)$ and ${}^{208}\text{Pb}(n, 2n\gamma)$ . . . . .	344
7.3.14	Sample 14: Fission yields for ${}^{238}\text{U}$ . . . . .	346
7.3.15	Sample 15: Photonuclear reactions: $g + {}^{90}\text{Zr}$ . . . . .	349
7.3.16	Sample 16: Different optical models : $n + {}^{120}\text{Sn}$ . . . . .	350
7.3.17	Sample 17: Different level density models : $n + {}^{99}\text{Tc}$ . . . . .	352
7.3.18	Sample 18: Astrophysical reaction rates : $n + {}^{187}\text{Os}$ . . . . .	356
7.3.19	Sample 19: Unresolved resonance range parameters: $n + {}^{136}\text{Ba}$ . . . . .	359
7.3.20	Sample 20: Maxwellian averaged cross section at 30 keV: $n + {}^{138}\text{Ba}$ . . . . .	360
7.3.21	Sample 21: Medical isotope production with $p + {}^{100}\text{Mo}$ . . . . .	361
7.3.22	Sample 22: Calculations up to 500 MeV for $p + {}^{209}\text{Bi}$ . . . . .	362
7.3.23	Sample 23: Neutron multiplicities and fission yields for $n + {}^{242}\text{Pu}$ . . . . .	364

7.3.24	Sample 24: Local parameter adjustment for $n + {}^{93}\text{Nb}$ . . . . .	365
7.3.25	Sample 25: Direct neutron capture for $n + {}^{89}\text{Y}$ . . . . .	369
7.3.26	Sample 26: Different alpha-particle optical model potentials: $\alpha + {}^{165}\text{Ho}$ . . .	370
7.3.27	Sample 27: Low energy resonance data for $n + {}^{107}\text{Ag}$ . . . . .	372
<b>8</b>	<b>Computational structure of TALYS</b> . . . . .	<b>377</b>
8.1	General structure of the source code . . . . .	377
8.1.1	machine . . . . .	377
8.1.2	constants . . . . .	378
8.1.3	talysinput . . . . .	378
8.1.4	talysinitial . . . . .	378
8.1.5	talysreaction . . . . .	378
8.1.6	natural . . . . .	378
8.1.7	ecis06t . . . . .	378
8.2	Input: talysinput . . . . .	379
8.2.1	readinput . . . . .	379
8.2.2	input1 . . . . .	379
8.2.3	input2, input3, input4, input5, input6 . . . . .	380
8.2.4	checkkeyword . . . . .	380
8.2.5	checkvalue . . . . .	380
8.3	Initialisation: talysinitial . . . . .	380
8.3.1	particles . . . . .	381
8.3.2	nuclides . . . . .	381
8.3.3	thermalxs . . . . .	390
8.3.4	grid . . . . .	391
8.3.5	mainout . . . . .	392
8.3.6	timer . . . . .	393
8.4	Nuclear models: talysreaction . . . . .	393
8.4.1	basicxs . . . . .	394
8.4.2	preeqinit . . . . .	398
8.4.3	excitoninit . . . . .	399
8.4.4	compoundinit . . . . .	399
8.4.5	astroinit . . . . .	399

8.4.6	reacinitial . . . . .	399
8.4.7	incident . . . . .	399
8.4.8	exgrid . . . . .	401
8.4.9	recoilinit . . . . .	401
8.4.10	direct . . . . .	401
8.4.11	preeq . . . . .	402
8.4.12	population . . . . .	410
8.4.13	compnorm . . . . .	411
8.4.14	comptarget . . . . .	411
8.4.15	binary . . . . .	415
8.4.16	angdis . . . . .	417
8.4.17	multiple . . . . .	417
8.4.18	channels . . . . .	421
8.4.19	totalxs . . . . .	421
8.4.20	spectra . . . . .	421
8.4.21	massdis . . . . .	421
8.4.22	residual . . . . .	424
8.4.23	totalrecoil . . . . .	424
8.4.24	normalization . . . . .	424
8.4.25	thermal . . . . .	424
8.4.26	output . . . . .	425
8.4.27	finalout . . . . .	426
8.4.28	astro . . . . .	427
8.4.29	endf . . . . .	427
8.5	Programming techniques . . . . .	428
8.6	Changing the array dimensions . . . . .	429
<b>9</b>	<b>Outlook and conclusions</b>	<b>433</b>
	<b>Bibliography</b>	<b>434</b>
<b>A</b>	<b>Log file of changes since the release of TALYS-1.0</b>	<b>495</b>
<b>B</b>	<b>Log file of changes since the release of TALYS-1.2</b>	<b>507</b>

<b>C</b>	<b>Log file of changes since the release of TALYS-1.4</b>	<b>515</b>
<b>D</b>	<b>Log file of changes since the release of TALYS-1.6</b>	<b>525</b>
<b>E</b>	<b>Log file of changes since the release of TALYS-1.6</b>	<b>531</b>
<b>F</b>	<b>Derivation of the isotope production equations</b>	<b>535</b>
<b>G</b>	<b>TERMS AND CONDITIONS FOR COPYING, DISTRIBUTION AND MODIFICATION</b>	<b>537</b>
	<b>Index</b>	<b>541</b>

# Preface

TALYS is a nuclear reaction program created at NRG Petten, the Netherlands and CEA Bruyères-le-Châtel, France. The idea to make TALYS was born in 1998, when we decided to implement our combined knowledge of nuclear reactions into one single software package. Our objective is to provide a complete and accurate simulation of nuclear reactions in the 1 keV-200 MeV energy range, through an optimal combination of reliable nuclear models, flexibility and user-friendliness. TALYS can be used for the analysis of basic scientific experiments or to generate nuclear data for applications.

Like most scientific projects, TALYS is always under development. Nevertheless, at certain moments in time, we freeze a well-defined version of TALYS and subject it to extensive verification and validation procedures. You are now reading the manual of version 1.9.

Many people have contributed to the present state of TALYS: In no particular order, and realizing that we probably forget someone, we thank Jacques Raynal for extending the ECIS-code according to our special wishes and for refusing to retire, Jean-Paul Delaroche and Olivier Bersillon for theoretical support, Emil Betak, Vivian Demetriou and Connie Kalbach for input on the pre-equilibrium models, Dimitri Rochman for helping to apply this code even more than initially thought possible, Eric Bauge for extending the optical model possibilities of TALYS, Pascal Romain, Emmeric Dupont and Michael Borchard for specific computational advice and code extensions, Steven van der Marck for careful reading of this manual, Roberto Capote and Mihaela Sin for input on fission models, Yi Xu for his direct capture model, Gilles Noguere for a better implementation of the unresolved resonance range model, Natalia Dzysiuk for parameter optimization, Vasily Simutkin and Michail Onegin to help implementing the GEF model for fission yields by Schmidt and Jurado, Arjan Plompen, Jura Kopecky and Robin Forrest for testing many of the results of TALYS, and Mark Chadwick, Phil Young and Mike Herman for helpful discussions and for providing us the motivation to compete with their software.

TALYS-1.9 falls in the category of GNU General Public License software. Please read the release conditions on the next page. Although we have invested a lot of effort in the validation of our code, we will not make the mistake to guarantee perfection. Therefore, in exchange for the free use of TALYS: If you find any errors, or in general have any comments, corrections, extensions, questions or advice, we would like to hear about it. You can reach us at [info@talys.eu](mailto:info@talys.eu), if you need us personally, but questions or information that is of possible interest to all TALYS users should be send to the mailing list [talys-1@nrg.eu](mailto:talys-1@nrg.eu). The webpage for TALYS is [www.talys.eu](http://www.talys.eu).

Arjan Koning

Stéphane Hilaire

Stephane Goriely



# TALYS release terms

TALYS-1.9 is copylefted free software: you can redistribute it and/or modify it under the terms of the GNU General Public License as published by the Free Software Foundation, see <http://www.gnu.org>.

This program is distributed in the hope that it will be useful, but WITHOUT ANY WARRANTY; without even the implied warranty of MERCHANTABILITY or FITNESS FOR A PARTICULAR PURPOSE. See the GNU General Public License in Appendix G for more details.

In addition to the GNU GPL *terms* we have a few *requests*:

- When TALYS is used for your reports, publications, etc., please make a proper reference to the code. At the moment this is:  
A.J. Koning, S. Hilaire and M.C. Duijvestijn, “TALYS-1.0”, *Proceedings of the International Conference on Nuclear Data for Science and Technology*, April 22-27, 2007, Nice, France, editors O.Bersillon, F.Gunsing, E.Bauge, R.Jacqmin, and S.Leray, EDP Sciences, 2008, p. 211-214.
- Please inform us about, or send, extensions you have built into TALYS. Of course, proper credit will be given to the authors of such extensions in future versions of the code.
- Please send us a copy/preprint of reports and publications in which TALYS is used. This will help us to maintain the TALYS-bibliography [133]-[748].

# Introduction

TALYS is a computer code system for the analysis and prediction of nuclear reactions. The basic objective behind its construction is the simulation of nuclear reactions that involve neutrons, photons, protons, deuterons, tritons,  $^3\text{He}$ - and alpha-particles, in the 1 keV - 200 MeV energy range and for target nuclides of mass 12 and heavier. To achieve this, we have implemented a suite of nuclear reaction models into a single code system. This enables us to evaluate nuclear reactions from the unresolved resonance range up to intermediate energies.

There are two main purposes of TALYS, which are strongly connected. First, it is a *nuclear physics* tool that can be used for the analysis of nuclear reaction experiments. The interplay between experiment and theory gives us insight in the fundamental interaction between particles and nuclei, and precise measurements enable us to constrain our models. In return, when the resulting nuclear models are believed to have sufficient predictive power, they can give an indication of the reliability of measurements. The many examples we present at the end of this manual confirm that this software project would be nowhere without the existing (and future) experimental database.

After the nuclear physics stage comes the second function of TALYS, namely as a *nuclear data* tool: Either in a default mode, when no measurements are available, or after fine-tuning the adjustable parameters of the various reaction models using available experimental data, TALYS can *generate* nuclear data for all open reaction channels, on a user-defined energy and angle grid, beyond the resonance region. The nuclear data libraries that are constructed with these calculated and experimental results provide essential information for existing and new nuclear technologies. Important applications that rely directly or indirectly on data generated by nuclear reaction simulation codes like TALYS are: conventional and innovative nuclear power reactors (GEN-IV), transmutation of radioactive waste, fusion reactors, accelerator applications, homeland security, medical isotope production, radiotherapy, single-event upsets in microprocessors, oil-well logging, geophysics and astrophysics.

Before this release, TALYS has already been extensively used for both basic and applied science. A large list of TALYS-related publications is given in Refs. [133]-[748]. We have ordered these references per topic, see the top of the bibliography, which should give a good indication of what the code can be used for.

The development of TALYS used to follow the “first completeness, then quality” principle. This

certainly should not suggest that we use toy models to arrive at some quick and dirty results since several reaction mechanisms coded in TALYS are based on theoretical models whose implementation is only possible with the current-day computer power. It rather means that, in our quest for completeness, we try to divide our effort equally among all nuclear reaction types. The precise description of *all* possible reaction channels in a single calculational scheme is such an enormous task that we have chosen, to put it bluntly, not to devote several years to the theoretical research and absolutely perfect implementation of one particular reaction channel which accounts for only a few millibarns of the total reaction cross section. Instead, we aim to enhance the quality of TALYS equally over the whole reaction range and always search for the largest shortcoming that remains after the last improvement. We now think that “completeness and quality” has been accomplished for several important parts of the program. The reward of this approach is that with TALYS we can cover the whole path from fundamental nuclear reaction models to the creation of complete data libraries for nuclear applications, with the obvious side note that the implemented nuclear models will always need to be upgraded using better physics. An additional long-term aim is full transparency of the implemented nuclear models, in other words, an *understandable* source program, and a modular coding structure.

The idea to construct a computer program that gives a simultaneous prediction of many nuclear reaction channels, rather than a very detailed description of only one or a few reaction channels, is not new. Well-known examples of all-in-one codes from the past decades are GNASH [2], ALICE [3], STAPRE [4], and EMPIRE [5]. They have been, and are still, extensively used, not only for academical purposes but also for the creation of the nuclear data libraries that exist around the world. GNASH and EMPIRE are still being maintained and extended by the original authors, whereas various local versions of ALICE and STAPRE exist around the world, all with different extensions and improvements. TALYS is new in the sense that it has recently been written completely from scratch (with the exception of one very essential module, the coupled-channels code ECIS), using a consistent set of programming procedures.

As specific features of the TALYS package we mention

- In general, an exact implementation of many of the latest nuclear models for direct, compound, pre-equilibrium and fission reactions.
- A continuous, smooth description of reaction mechanisms over a wide energy range (0.001- 200 MeV) and mass number range ( $12 < A < 339$ ).
- Completely integrated optical model and coupled-channels calculations by the ECIS-06 code [6].
- Incorporation of recent optical model parameterisations for many nuclei, both phenomenological (optionally including dispersion relations) and microscopical.
- Total and partial cross sections, energy spectra, angular distributions, double-differential spectra and recoils.
- Discrete and continuum photon production cross sections.
- Excitation functions for residual nuclide production, including isomeric cross sections.
- An exact modeling of exclusive channel cross sections, e.g.  $(n, 2np)$ , spectra, and recoils.

- Automatic reference to nuclear structure parameters as masses, discrete levels, resonances, level density parameters, deformation parameters, fission barrier and gamma-ray parameters, generally from the IAEA Reference Input Parameter Library [163].
- Various width fluctuation models for binary compound reactions and, at higher energies, multiple Hauser-Feshbach emission until all reaction channels are closed.
- Various phenomenological and microscopic level density models.
- Various fission models to predict cross sections and fission fragment and product yields, and neutron multiplicities.
- Models for pre-equilibrium reactions, and multiple pre-equilibrium reactions up to any order.
- Generation of parameters for the unresolved resonance range.
- Reconstruction of resonance range into pointwise cross sections using tabulated resonance parameters.
- Astrophysical reaction rates using Maxwellian averaging.
- Medical isotope production yields as a function of accelerator energy and beam current.
- Option to start with an excitation energy distribution instead of a projectile-target combination, helpful for coupling TALYS with intranuclear cascade codes or fission fragment studies.
- Use of systematics if an adequate theory for a particular reaction mechanism is not yet available or implemented, or simply as a predictive alternative for more physical nuclear models.
- Automatic generation of nuclear data in ENDF-6 format (not included in the free release).
- Automatic optimization to experimental data and generation of covariance data (not included in the free release).
- A transparent source program.
- Input/output communication that is easy to use and understand.
- An extensive user manual.
- A large collection of sample cases.

The central message is that we always provide a complete set of answers for a nuclear reaction, for all open channels and all associated cross sections, spectra and angular distributions. It depends on the current status of nuclear reaction theory, and our ability to implement that theory, whether these answers are generated by sophisticated physical methods or by a simpler empirical approach. With TALYS, a complete set of cross sections can already be obtained with minimal effort, through a four-line input file of the type:

```
projectile n
element     Fe
mass       56
energy    14.
```

which, if you are only interested in reasonably good answers for the most important quantities, will give you all you need. If you want to be more specific on nuclear models, their parameters and the level of output, you simply add some of the more than 340 keywords that can be specified in TALYS. We thus do not ask you to understand the precise meaning of all these keywords: you can make your input file as simple or as complex as you want. Let us immediately stress that we realize the danger of this approach. This ease of use may give the obviously false impression that one gets a *good* description of *all* the reaction channels, with minimum reaction specification, as if we would have solved virtually all nuclear reaction problems (in which case we would have been famous). Unfortunately, nuclear physics is not that simple. Clearly, many types of nuclear reactions are very difficult to model properly and can not be expected to be covered by simple default values. Moreover, other nuclear reaction codes may outperform TALYS on particular tasks because they were specifically designed for one or a few reaction channels. In this light, Section 7.3 is very important, as it contains many sample cases which should give the user an idea of what TALYS can do. We wish to mention that the above sketched method for handling input files was born out of frustration: We have encountered too many computer codes containing an implementation of beautiful physics, but with an unnecessary high threshold to use the code, since its input files are supposed to consist of a large collection of mixed, and correlated, integer and real values, for which values *must* be given, forcing the user to first read the entire manual, which often does not exist.

## 1.1 From TALYS-1.0 to TALYS-1.2

On December 21, 2007 the first official version of the code, TALYS-1.0, was released. Since then, the code has undergone changes that fall in the usual two categories: significant extensions and corrections that may affect a large part of the user community, and several small bug fixes. As appendix to this manual, we add the full log file of changes since the release of TALYS-1.0. Here we list the most important updates:

- Further unification of microscopic structure information from Hartree-Fock-Bogolyubov (HFB) calculations. Next to masses, HFB deformation parameters are now also provided. The latest HFB-based tabulated level densities for both the ground state and fission barriers were included in the structure database. Another new addition is a database of microscopic particle-hole densities for preequilibrium calculations.
- Introduction of more keywords for adjustment. Often, these are defined relative to the default values, and thus often have a default value of 1. This is convenient since one does not have to look up the current value of the parameter if it is to be changed by a certain amount. Instead, giving e.g. **adjust 41 93 1.04** means multiplying the built-in value for the level density parameter  $a$  by 1.04. Such keywords are now available for many parameters of the optical model, level density, etc., enabling easy sensitivity and covariance analyses with TALYS.
- An alternative fission model has been added, or more precisely, revived. Pascal Romain and colleagues of CEA Bruyeres-le-Chatel has been more successful to fit actinide data with older TALYS

options for fission (present in versions of the code before the first released beta version TALYS-0.64) using effective level densities, than with the newer options with explicit collective enhancement for the level densities[8, 9]. Therefore we decided to re-include that option again, through the **colldamp** keyword. Also his corrections for the class-II states were adopted. We generally use this option now for our actinide evaluations, until someone is able to do that with the newer fission models built in the code.

- Average resonance parameters for the unresolved resonance range are calculated.
- More flexibility has been added for cases where TALYS fails to fit experimental data. It is now possible to normalize TALYS directly to experimental or evaluated data for each reaction channel. This is not physical, but needed for several application projects.
- Perhaps the most important error was found by Arjan Plompen and Olivier Bersillon. In the discrete level database of TALYS-1.0, the internal conversion coefficients were wrongly applied to the gamma-ray branching ratios. A new discrete level database has been generated and internal conversion is now correctly taken into account. In some cases, this affects the production of discrete gamma lines and the cross section for isomer production.
- TALYS can be turned into a "pure" optical model program with the keyword **omponly y**. After the optical model calculation and output it then skips the calculation for all nonelastic reaction channels. In this mode, TALYS basically becomes a driver for ECIS.
- It is now possible to save and use your best input parameters for a particular isotope in the structure database (helpful for data evaluation). With the **best** keyword these parameter settings can automatically be invoked. We include part of our collection in the current version.
- Pygmy resonance parameters for gamma-ray strength functions can be included.

To accommodate all this, plus other options, the following new keywords were introduced: **aadjust**, see page 229, **rvadjustF**, see page 193, **avadjustF**, see page 193, **rvdadjustF**, see page 195, **avdadjustF**, see page 195, **rvsoadjustF**, see page 196, **avsoadjustF**, see page 196, **best**, see page 175, **colldamp**, see page 225, **coulomb**, see page 184, **epr**, see page 214, **fiso**, see page 213, **gamgamadjust**, see page 211, **gnadjust**, see page 239, **gpadjust**, see page 238, **gpr**, see page 215, **hbstate**, see page 243, **jlmmodel**, see page 180, **micro**, see page 113, **ompenenergyfile**, see page 260, **omponly**, see page 181, **phmodel**, see page 237, **radialmodel**, see page 181, **rescuefile**, see page 177, **s2adjust**, see page 235, **soswitch**, see page 185, **spr**, see page 215, **strengthM1**, see page 208, **urr**, see page 205, **xsalphatherm**, see page 174, **xscaptherm**, see page 174, **xsptherm**, see page 175.

## 1.2 From TALYS-1.2 to TALYS-1.4

On December 23, 2009 the second official version of the code, TALYS-1.2, was released. Since then, the code has undergone changes that fall in the usual two categories: significant extensions and corrections that may affect a large part of the user community, and several small bug fixes. As appendix to this

manual, we add the full log file of changes since the release of TALYS-1.2. Here we list the most important updates:

- A new phenomenological model for break-up reactions by Connie Kalbach was included. This model is documented in an unpublished report to the FENDL-3 meeting at the IAEA, december 2010, and resolves some of the cross section prediction problems that were observed in earlier versions of TALYS. The contribution can be scaled by a normalization factor (**Cbreak** keyword).
- The alpha double-folding potential by Demetriou et al[22] was added as an option.
- Several deuteron OMP's were added to provide a better prediction of deuteron reaction cross sections and transmission coefficients.
- As part of the output of the binary reaction information, the compound nucleus formation cross section as a function of spin and parity is now also printed.
- TALYS is now able to produce unresolved resonance range (URR) parameters with a higher quality than that of TALYS-1.2, thanks to modelling and programming help by Gilles Noguere, CEA-Cadarache, and testing by Paul Koehler, ORNL.
- We increased the flexibility of using level densities. Up to TALYS-1.2, it was possible to choose between 5 level density models, which were then used for *all* nuclides in the calculation. It is now possible to choose one of these 5 level density models *per nuclide*, e.g. the Constant Temperature model for the target nucleus and the Backshifted Fermi Gas model for the compound nucleus. The **ldmodel** and **colenhance** keywords have been extended with (optional) Z,A identifiers.
- We have added the possibility to print the direct, pre-equilibrium and compound components of each cross section in the output files, in order to check which reaction mechanism is responsible for different parts of the excitation function. This can be enabled with the new **components** keyword.
- It is now possible to calculate the Maxwellian averaged cross section (MACS) at a user-defined energy. By using the **astroE** keyword, one can for example compare TALYS with experimental 30 keV averaged capture cross sections.
- We have included the possibility to calculate the so-called effective cross section for integral activation measurements, by folding the excitation functions by an experimental flux. In *talys/structure/flux*, we have stored more than 40 spectra which have been used in past activation benchmarks.

For TALYS-1.4 the following new keywords were introduced: **Cbreak**, see page 222, **deuteronomp**, see page 199, **rwadjustF**, see page 194, **awadjustF**, see page 194, **rwdadjustF**, see page 195, **awdadjustF**, see page 195, **rwsoadjustF**, see page 196, **awsoadjustF**, see page 197, **integral**, see page 259, **urnnjoy**, see page 205, **components**, see page 264, **astroE**, see page 172, **astroT**, see page 173, while the possibilities of **alphaomp**, see page 199, **ldmodel**, see page 224, **colenhance**, see page 225, were extended.

It is worthwhile to mention here that the structure database has almost not changed since the release of version 1.2. The only exceptions are the *structure/mass/hfb* directory, which contains the

latest Hartree-Fock-Bogolyubov + Skyrme-based theoretical masses, and the *structure/flux* directory, which contains a collection of experimental neutron spectra for the calculation of effective integral cross sections.

### 1.3 From TALYS-1.4 to TALYS-1.6

On December 28, 2011 the third official version of the code, TALYS-1.4, was released. Since then, the code has undergone changes that fall in the usual two categories: significant extensions and corrections that may affect a large part of the user community, and several small bug fixes. As appendix to this manual, we add the full log file of changes since the release of TALYS-1.4. Here we list the most important updates:

- The activity of all residual products can be given in the output. This means that TALYS can now directly be used for medical isotope production with accelerators through the use of the **production keyword**. For this the decay data library is added to the TALYS structure database. Excitation functions are thus automatically transferred into isotope production rates in MBq or Ci, as a function of time. Various extra keywords for this are included for flexibility.
- Part of the GEF code for fission yields, by Schmidt and Jurado, has been translated into FORTRAN and into a TALYS subroutine by Vasily Simutkin and Michail Onegin. This now allows the calculation of fission yields and fission neutron multiplicities as a function of Z, N, A and the number of emitted neutrons, while the calculation of fission neutron spectra will be done in a future version of TALYS. GEF is designed to produce this information starting from an excited state of a fissile system. Hence, the TALYS-GEF combination can now give estimates for these fission quantities in the case of multi-chance fission.
- Non-equidistant binning for the excitation energy grid was introduced. The excitation energies can now be tracked on a logarithmic grid, and has now become the default. It allows to use less excitation energy bins while not losing precision. The old situation of TALYS-1.4 and before can be invoked with the new **equidistant** keyword, but from now on the default will be **equidistant n**. Especially for cross sections above 100 MeV the improvement is significant in terms of smoothness and more reliable absolute values.
- Thanks to the previous improvement, TALYS can now technically be used up to 1 GeV. For this, the Koning-Delaroche OMP was extended as well.
- A radiative capture model for the direct capture cross section was added.
- An extra option for the pre-equilibrium spin distribution was included, see the **preeqspin** keyword.
- The **energy** keyword has been made more flexible, avoiding long files with energy values to be constructed by the user.
- About 70 keywords can now have energy-dependent values. After the keyword and its value are given in the input, an energy range can be specified over which the corresponding model parameter

is altered. Hence, it is for example possible to have a (usual) constant value for the optical model radius  $r_V$ , but to increase its value between e.g. 6 and 10 MeV, through a simple addition on the input line.

For TALYS-1.6 the following new keywords were introduced: **equidistant**, see page 161, **disctable**, see page 163, **Tladjust**, see page 197, **branch**, see page 164, **racap**, see page 213, **sfexp**, see page 214, **sfth**, see page 214, **ldmodelracap**, see page 213, **Vinf**, see page 192, **Ejoin**, see page 192, **w3adjust**, see page 188, **w4adjust**, see page 188, **incadjust**, see page 182, **Liso**, see page 164, **fisfeed**, see page 251, **production**, see page 247, **Ebeam**, see page 247, **Eback**, see page 247, **Tcool**, see page 250, **Tirrad**, see page 249, **rho**, see page 248, **Ibeam**, see page 248, **Area**, see page 248, **radiounit**, see page 248, **yieldunit**, see page 249, **cpang**, see page 185, **egradjust**, see page 210, **ggradjust**, see page 210, **sgradjust**, see page 210, **epradjust**, see page 215, **gpradjust**, see page 216, **spradjust**, see page 215, **E0adjust**, see page 232, **Exmatchadjust**, see page 232, **Tadjust**, see page 232, **fisbaradjust**, see page 242, **fishwadjust**, see page 242, **fymodel**, see page 245, **outfy**, see page 246, **gefran**, see page 246, while the possibilities of **preeqspin**, see page 218, **ldmodel**, see page 224, were extended.

## 1.4 From TALYS-1.6 to TALYS-1.8

On December 23, 2013 the fourth official version of the code, TALYS-1.6, was released. Since then, the code has undergone changes that fall in the usual two categories: significant extensions and corrections that may affect a large part of the user community, and several small bug fixes. As appendix to this manual, we add the full log file of changes since the release of TALYS-1.6. Here we list the most important updates:

- Low energy resonance cross sections were added to the output. For this, the resonance keyword was introduced. If **resonance y**, TALYS will read in resonance parameters, from various possible sources, and call the RECENT code of Red Cullen's PREPRO package[23]. Low energy pointwise resonance cross sections are added to channels like total, elastic, fission and capture. Choices for adoption of resonance parameters from various libraries can be made with the **reslib** keyword, which can be equal to default, endfb7.1, jeff3.1, jendl4.0. In addition, use can be made of Cullen's SIGMA1 code, for resonance broadening, and GROUPIE, for groupwise cross sections.
- The stand-alone Fortran version of the GEF code was added as a subroutine to enable, in principle, the evaporation of fission fragments by TALYS. For this, TALYS "loops over itself", i.e. it is restarted internally for every excited fission fragment. The results are not yet good however. The option for this is **fymodel 3**. In principle, quantities like the neutron spectrum for evaporated fission fragments, nubar etc. are available now.
- The range of elements that is allowed in the input is extended up to  $Z=124$ , with nuclear symbols Rg(111), Cn(112), Nh(113), Fl(114), Mc(115), Lv(116), Ts(117), Og(118), B9(119), C0-4(120-124).
- More models (**strength 6, 7, 8** for gamma-ray strength functions) are added.

- More models (**alphaomp 6, 7, 8** for the alpha optical model potential are added. *alphaomp 6*, i.e. of Avrigeanu et al [25] is now the default alpha OMP potential.

For TALYS-1.8 the following new keywords were introduced: **pshiftadjust**, see page 233, **resonance**, see page 206, **Tres**, see page 207, **group**, see page 206, **reslib**, see page 206, **bestend**, see page 176, **E1file**, see page 212, **Estop**, see page 168, **popMeV**, see page 168, **bestbranch**, see page 176, **breakup-model**, see page 223, **outbinspectra**, see page 256, **ffspin**, see page 246, **skipCN**, see page 207, while the possibilities of **strength**, see page 208, **element**, see page 154, **alphaomp**, see page 199, **fymodel**, see page 245, were extended.

## 1.5 From TALYS-1.8 to TALYS-1.9

On December 28, 2015 the fifth official version of the code, TALYS-1.8, was released. Since then, the code has undergone changes that fall in the usual two categories: significant extensions and corrections that may affect a large part of the user community, and several small bug fixes. As appendix to this manual, we add the full log file of changes since the release of TALYS-1.8. Here we list the most important updates:

- More flexibility for gamma-ray strength functions, such as the possibility to read in M1 strength function tables.
- Extension of astrophysical reaction rate calculations to excited states.
- Addition of fission yield isomeric ratio's to the output.

For TALYS-1.9 the following new keywords were introduced: **M1file**, see page 212, **massdir**, see page 166, **upbendc**, see page 216, **upbende**, see page 216, **astroex**, see page 173, **nonthermlev**, see page 173, while the possibilities of **etable**, see page 212, **fable**, see page 212, were extended.

## 1.6 How to use this manual

Although we would be honored if you would read this manual from the beginning to the end, we can imagine that not all parts are necessary, relevant or suitable to you. For example if you are just an interested physicist who does not own a computer, you may skip

Chapter 2: Installation guide.

while everybody else probably needs Chapter 2 to use TALYS. A complete description of all nuclear models and other basic information present in TALYS, as well as the description of the types of cross sections, spectra, angular distributions etc. that can be produced with the code can be found in the next three chapters:

Chapter 3: A general discussion of nuclear reactions and the types of observables that can be obtained.

Chapter 4: An outline of the theory behind the various nuclear models that are implemented in TALYS.

Chapter 5: A description of the various nuclear structure parameters that are used.

If you are an experienced nuclear physicist and want to compute your own specific cases directly after a successful installation, then instead of reading Chapters 3-5 you may go directly to

Chapter 6: Input description.

The next chapter we consider to be quite important, since it contains ready to use starting points (sample cases) for your own work. At the same time, it gives an impression of what TALYS can be used for. That and associated matters can be found in

Chapter 7: Output description, sample cases and verification and validation.

People planning to enter the source code for extensions, changes or debugging, may be interested in

Chapter 8: The detailed computational structure of TALYS.

Finally, this manual ends with

Chapter 9: Conclusions and ideas for future work.

# Installation and getting started

## 2.1 The TALYS package

In what follows we assume TALYS will be installed on a Unix/Linux operating system. In total, you will need about 6 Gb of free disk space to install TALYS. (This rather large amount of memory is almost completely due to microscopic level density, radial density, gamma and fission tables in the nuclear structure database. Since these are, at the moment, not the default models for TALYS you could omit these if total hard disk storage poses a problem.) If you obtain the entire TALYS package from [www.talys.eu](http://www.talys.eu), you should do

- **tar zxvf talys.tar**

and the total TALYS package will be automatically stored in the *talys/* directory. It contains the following directories and files:

- *README* outlines the contents of the package.
- *talys.setup* is a script that takes care of the installation.
- *source/* contains the source code of TALYS: 324 Fortran subroutines, and the files *talys.cmb*, *mom.cmb*, *gef.cmb*, *gefsubdcl2.cmb*, which contains all variable declarations and common blocks, and a few *.h* files for the PREPRO subroutines. The package includes the file *ecis06t.f*. This is basically Jacques Raynal's code ECIS-06, which we have transformed into a subroutine and have slightly modified to enable communication with the rest of TALYS.
- *structure/* contains the nuclear structure database in various subdirectories. See Chapter 5 for more information.
- *doc/* contains the documentation: this manual in postscript and pdf format and the description of ECIS-06.

- *samples/* contains the input and output files of the sample cases.

The code has so far been tested by us on various Unix/Linux systems, so we can not guarantee that it works on all operating systems, although we know that some users have easily installed TALYS under Windows. The only machine dependencies we can think of are the directory separators '/' we use in pathnames that are hardwired in the code. If there is any dependence on the operating system, the associated statements can be altered in the subroutine *machine.f*. Also, the output of the execution time in *timer.f* may be machine dependent. The rest of the code should work on any computer.

TALYS has been tested for the following compilers and operating systems:

- gfortran Fortran compiler on various Linux systems
- Intel ifort Fortran compiler on various Linux systems
- Portland pgf95 Fortran compiler on various Linux systems
- Fujitsu/Lahey Fortran90/95 compiler on various Linux systems
- g95 Fortran compiler on various Linux systems

## 2.2 Installation

The installation of TALYS is straightforward. For a Unix/Linux system, the installation is expected to be handled by the *talys.setup* script, as follows

- edit *talys.setup* and set the first two variables: the name of your compiler and the place where you want to store the TALYS executable.
- **talys.setup**

If this does not work for some reason, we here provide the necessary steps to do the installation manually. For a Unix/Linux system, the following steps should be taken:

- **chmod -R u+rwX talys** to ensure that all directories and files have read and write permission and the directories have execute permission. (This may no longer be needed, since these permissions are usually only disabled when reading from a CD or DVD).
- **cd talys/source**
- Ensure that TALYS can read the nuclear structure database. This is done in subroutine *machine.f*. If *talys.setup* has not already replaced the path name in *machine.f*, do it yourself. We think this is the only Unix/Linux machine dependence of TALYS. Apart from a few trivial warning messages for *ecis06t.f*, we expect no complaints from the compiler.
- **f95 -c \*.f**

- **f95 \*.o -o talys**
- **mv talys ~/bin** (assuming you have a *~/bin* directory which contains all executables that can be called from any working directory)

After you or *talys.setup* have completed this, type

- **rehash**, to update your table with commands.

The above commands represent the standard compilation options. Consult the manual of your compiler to get an enhanced performance with optimization flags enabled. The only restriction for compilation is that *ecis06t.f* should *not* be compiled in double precision.

## 2.3 Verification

If TALYS is installed, testing the sample cases is the logical next step. The *samples/* directory contains the script *verify* that runs all the test cases. Each sample case has its own subdirectory, which contains a subdirectory *org/*, where we stored the input files and **our** calculated results, obtained with the Fujitsu/Lahey v8.0 compiler on Linux Red Hat Enterprise 6. It also contains a subdirectory *new*, where we have stored the input files only and where the *verify* script will produce **your** output files. A full description of the keywords used in the input files is given in Chapter 6. Section 7.3 describes all sample cases in full detail. Note that under Linux/Unix, in each subdirectory a file with differences with our original output is created.

Should you encounter error messages upon running TALYS, like *'killed'* or *'segmentation fault'*, then probably the memory of your processor is not large enough (i.e. smaller than 256 Mb). Edit *talys.cmb* and reduce the value of **memorypar**.

## 2.4 Getting started

If you have created your own working directory with an input file named e.g. *input*, then a TALYS calculation can easily be started with:

```
talys < input > output
```

where the names *input* and *output* are not obligatory: you can use any name for these files.



## Nuclear reactions: General approach

An outline of the general theory and modeling of nuclear reactions can be given in many ways. A common classification is in terms of time scales: short reaction times are associated with direct reactions and long reaction times with compound nucleus processes. At intermediate time scales, pre-equilibrium processes occur. An alternative, more or less equivalent, classification can be given with the number of intranuclear collisions, which is one or two for direct reactions, a few for pre-equilibrium reactions and many for compound reactions, respectively. As a consequence, the coupling between the incident and outgoing channels decreases with the number of collisions and the statistical nature of the nuclear reaction theories increases with the number of collisions. Figs. 3.1 and 3.2 explain the role of the different reaction mechanisms during an arbitrary nucleon-induced reaction in a schematic manner. They will all be discussed in this manual.

This distinction between nuclear reaction mechanisms can be obtained in a more formal way by means of a proper division of the nuclear wave functions into open and closed configurations, as detailed for example by Feshbach's many contributions to the field. This is the subject of several textbooks and will not be repeated here. When appropriate, we will return to the most important theoretical aspects of the nuclear models in TALYS in Chapter 4.

When discussing nuclear reactions in the context of a computer code, as in this manual, a different starting point is more appropriate. We think it is best illustrated by Fig. 3.3. A particle incident on a target nucleus will induce several *binary* reactions which are described by the various competing reaction mechanisms that were mentioned above. The end products of the binary reaction are the emitted particle and the corresponding recoiling residual nucleus. In general this is, however, not the end of the process. A total nuclear reaction may involve a whole sequence of residual nuclei, especially at higher energies, resulting from multiple particle emission. All these residual nuclides have their own separation energies, optical model parameters, level densities, fission barriers, gamma strength functions, etc., that must properly be taken into account along the reaction chain. The implementation of this entire reaction chain forms the backbone of TALYS. The program has been written in a way that enables a clear and easy inclusion of all possible nuclear model ingredients for any number of nuclides in the reaction chain. Of course, in this whole chain the target and primary compound nucleus have a special status, since they

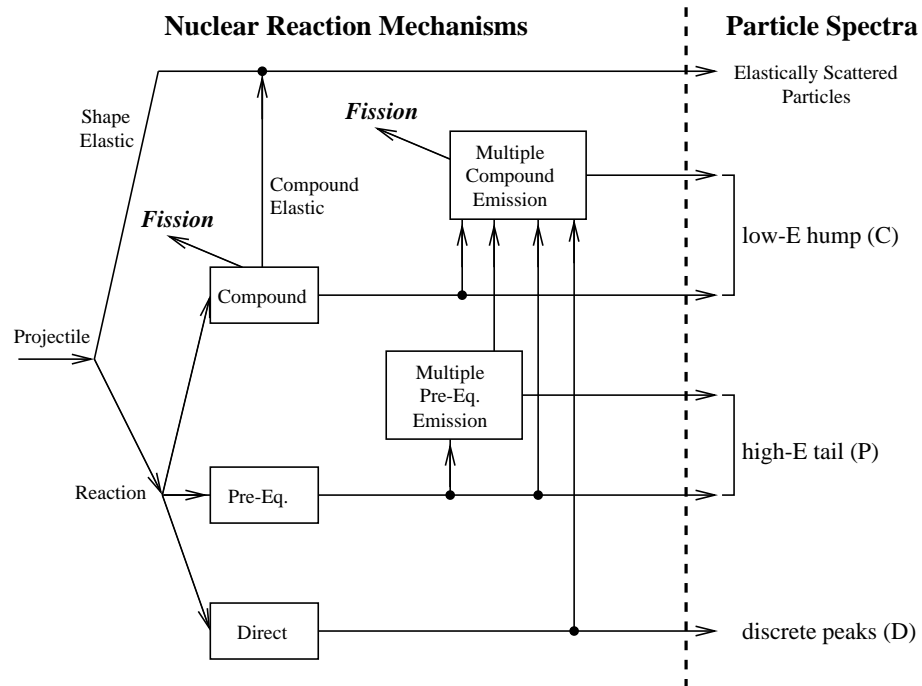


Figure 3.1: The role of direct, pre-equilibrium and compound processes in the description of a nuclear reaction and the outgoing particle spectra. The C, P and D labels correspond to those in Fig. 3.2

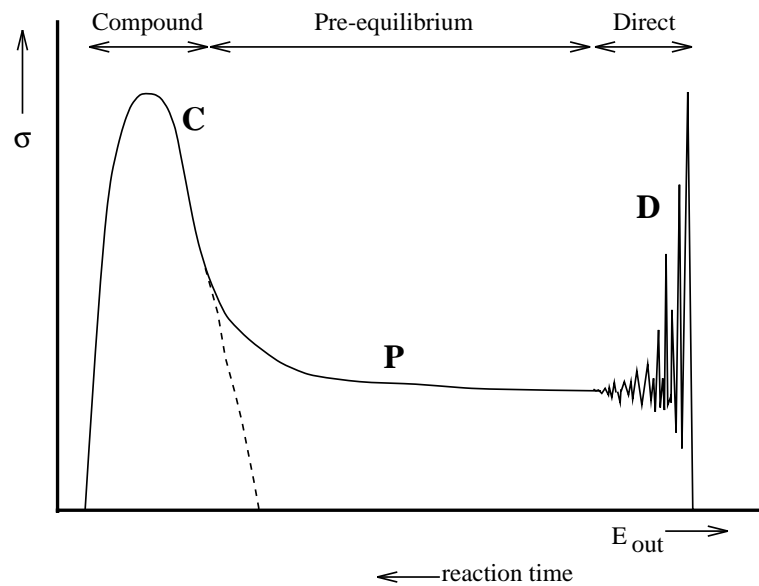


Figure 3.2: Schematic drawing of an outgoing particle spectrum. The energy regions to which direct (D), pre-equilibrium (P) and compound (C) mechanisms contribute are indicated. The dashed curve distinguishes the compound contribution from the rest in the transitional energy region.

are subject to *all* reaction mechanisms, i.e. direct, pre-equilibrium, compound and fission and, at low incident energies, with fluctuation corrections in compound nucleus decay. Also, at incident energies below a few MeV, only binary reactions take place and the target and compound nucleus are often the only two nuclei involved in the whole reaction. Historically, it is for the binary reactions that most of the theoretical methods have been developed and refined, mainly because their validity, and their relation with nuclear structure, could best be tested with exclusive measurements. In general, however, Fig. 3.3 should serve as the illustration of a total nuclear reaction at any incident energy. The projectile, in this case a neutron, and the target  $(Z_C, N_C - 1)$  form a compound nucleus  $(Z_C, N_C)$  with a total energy

$$(3.1) \quad E^{tot} = E_{CM} + S_n(Z_C, N_C) + E_x^0,$$

where  $E_{CM}$  is the incident energy in the CM frame,  $S_n$  is the neutron separation energy of the compound nucleus, and  $E_x^0$  the excitation energy of the target (which is usually zero, i.e. representing the ground state). The compound nucleus is described by a range of possible spin ( $J$ ) and parity ( $\Pi$ ) combinations, which for simplicity are left out of Fig. 3.3. From this state, transitions to all open channels may occur by means of direct, pre-equilibrium and compound processes. The residual nuclei formed by these binary reactions may be populated in the discrete level part and in the continuum part of the available excitation energy range. In Fig. 3.3, we have only drawn three binary channels, namely the  $(Z_C, N_C - 1)$ ,  $(Z_C - 1, N_C)$  and  $(Z_C - 1, N_C - 1)$  nuclei that result from binary neutron, proton and deuteron emission, respectively. Each nucleus is characterized by a separation energy per possible ejectile. If the populated residual nucleus has a maximal excitation energy  $E_x^{max}(Z, N)$  that is still above the separation energies for one or more different particles for that nucleus, further emission of these particles may occur and nuclei with lower  $Z$  and  $N$  will be populated. At the end of the nuclear reaction (left bottom part of Fig. 3.3), all the reaction population is below the lowest particle separation energy, and the residual nucleus  $(Z_C - z, N_C - n)$  can only decay to its ground or isomeric states by means of gamma decay. In a computer program, the continuum must be discretized in excitation energy ( $E_x$ ) bins. We can take these bins equidistant or non-equidistant (the default), although we already want to stress the important fact here that the *emission* energy grid for the outgoing particles is non-equidistant in TALYS. After the aforementioned binary reaction, every continuum excitation energy bin will be further depleted by means of particle emission, gamma decay or fission. Computationally, this process starts at the initial compound nucleus and its highest energy bin, i.e. the bin just below  $E_x^{max}(Z_C, N_C) = E^{tot}$ , and subsequently in order of decreasing energy bin/level, decreasing  $N$  and decreasing  $Z$ . Inside each continuum bin, there is an additional loop over all possible  $J$  and  $\Pi$ , whereas for each discrete level,  $J$  and  $\Pi$  have unique values. Hence, a bin/level is characterized by the set  $\{Z, N, E_x, J, \Pi\}$  and by means of gamma or particle emission, it can decay into all accessible  $\{Z', N', E_{x'}, J', \Pi'\}$  bins/levels. In this way, the whole reaction chain is followed until all bins and levels are depleted and thus all channels are closed. In the process, all particle production cross sections and residual production cross sections are accumulated to their final values.

We will now zoom in on the various parts of Fig. 3.3 to describe the various stages of the reaction, depending on the incident energy, and we will mention the nuclear reaction mechanisms that apply.

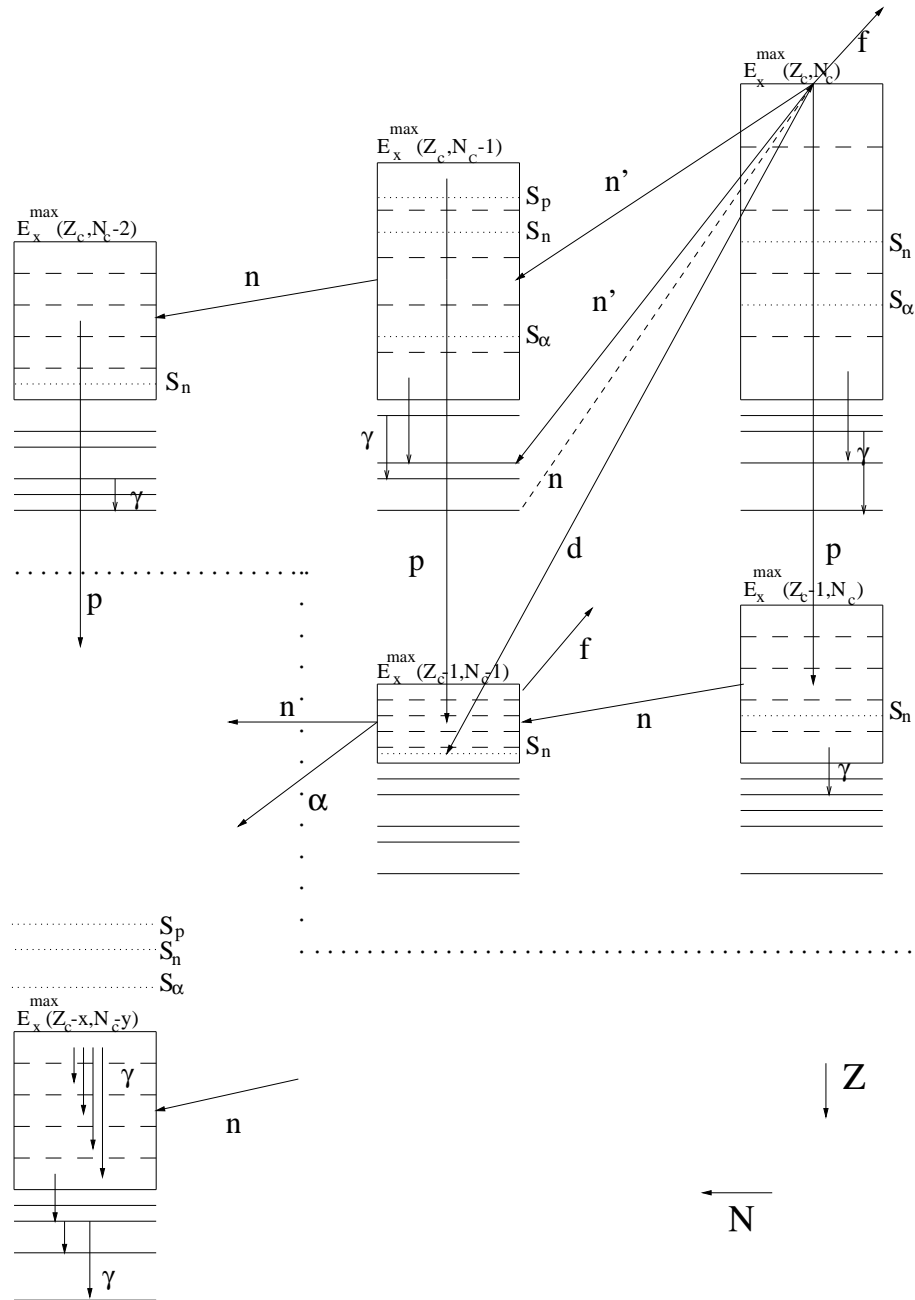


Figure 3.3: Neutron-induced reaction. The dashed arrow represents the incident channel, while the continuous arrows represent the decay possibilities.  $E_x^{\max}$  denotes the maximal possible excitation energy of each nucleus and  $S_k$  is the particle separation energy for particle  $k$ . For each nucleus a few discrete levels are drawn, together with a few continuum energy bins. Spin and parity degrees of freedom are left out of this figure for simplicity. Fission is indicated by an  $f$ .

## 3.1 Reaction mechanisms

In the projectile energy range between 1 keV and several hundreds of MeV, the importance of a particular nuclear reaction mechanism appears and disappears upon varying the incident energy. We will now describe the particle decay scheme that typically applies in the various energy regions. Because of the Coulomb barrier for charged particles, it will be clear that the discussion for low energy reactions usually concerns incident neutrons. In general, however, what follows can be generalized to incident charged particles. The energy ranges mentioned in each paragraph heading are just meant as helpful indications, which apply for a typical medium mass nucleus.

### 3.1.1 Low energies

#### Elastic scattering and capture ( $E < 0.2$ MeV)

If the energy of an incident neutron is below the excitation energy of the first inelastic level, and if there are no  $(n, p)$ , etc. reactions that are energetically possible, then the only reaction possibilities are elastic scattering, neutron capture and, for fissile nuclides, fission. At these low energies, only the  $(Z_C, N_C - 1)$  and  $(Z_C, N_C)$  nuclides of Fig. 3.3 are involved, see Fig. 3.4. First, the shape (or direct) elastic scattering cross section can directly be determined from the optical model, which will be discussed in Section 4.1. The compound nucleus, which is populated by a reaction population equal to the reaction cross section, is formed at one single energy  $E^{tot} = E_x^{max}(Z_C, N_C)$  and a range of  $J, \Pi$ -values. This compound nucleus either decays by means of compound elastic scattering back to the initial state of the target nucleus, or by means of neutron capture, after which gamma decay follows to the continuum and to discrete states of the compound nucleus. The competition between the compound elastic and capture channels is described by the compound nucleus theory, which we will discuss in Section 4.5. To be precise, the elastic and capture processes comprise the first *binary* reaction. To complete the description of the total reaction, the excited  $(Z_C, N_C)$  nucleus, which is populated over its whole excitation energy range by the primary gamma emission, must complete its decay. The highest continuum bin is depleted first, for all  $J$  and  $\Pi$ . The subsequent gamma decay increases the population of the lower bins, before the latter are depleted themselves. Also, continuum bins that are above the neutron separation energy  $S_n$  of the compound nucleus contribute to the feeding of the  $(n, \gamma n)$  channel. This results in a weak continuous neutron spectrum, even though the elastic channel is the only true binary neutron channel that is open. The continuum bins and the discrete levels of the compound nucleus are depleted one by one, in decreasing order, until the ground or an isomeric state of the compound nucleus is reached by subsequent gamma decay. If a nuclide is fissile, fission may compete as well, both from the initial compound state  $E_x^{max}(Z_C, N_C)$  and from the continuum bins of the compound nucleus, the latter resulting in a  $(n, \gamma f)$  cross section. Both contributions add up to the so called first-chance fission cross section.

#### Inelastic scattering to discrete states ( $0.2 < E < 4$ MeV)

At somewhat higher incident energies, the first inelastic channels open up, see Fig. 3.5. Reactions to these discrete levels have a compound and a direct component. The former is again described by the com-

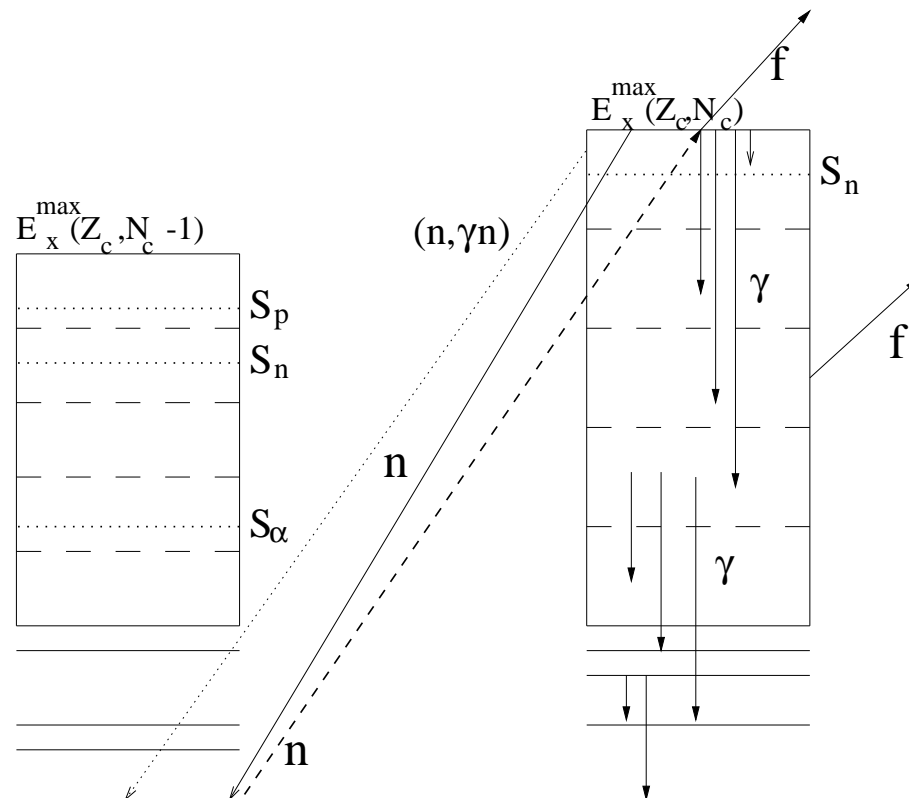


Figure 3.4: Neutron-induced reaction at low energy. The dashed arrow represents the incident channel, while the continuous arrows represents the elastic channel. The only possibilities are elastic scattering and capture of the neutron in the compound nucleus, with subsequent decay to the ground state or an isomeric state of the compound nucleus. A small part of the population may decay to the target nucleus by means of the  $(n, \gamma n)$  channel (dotted arrow). For fissile nuclei, fission may be another open channel.

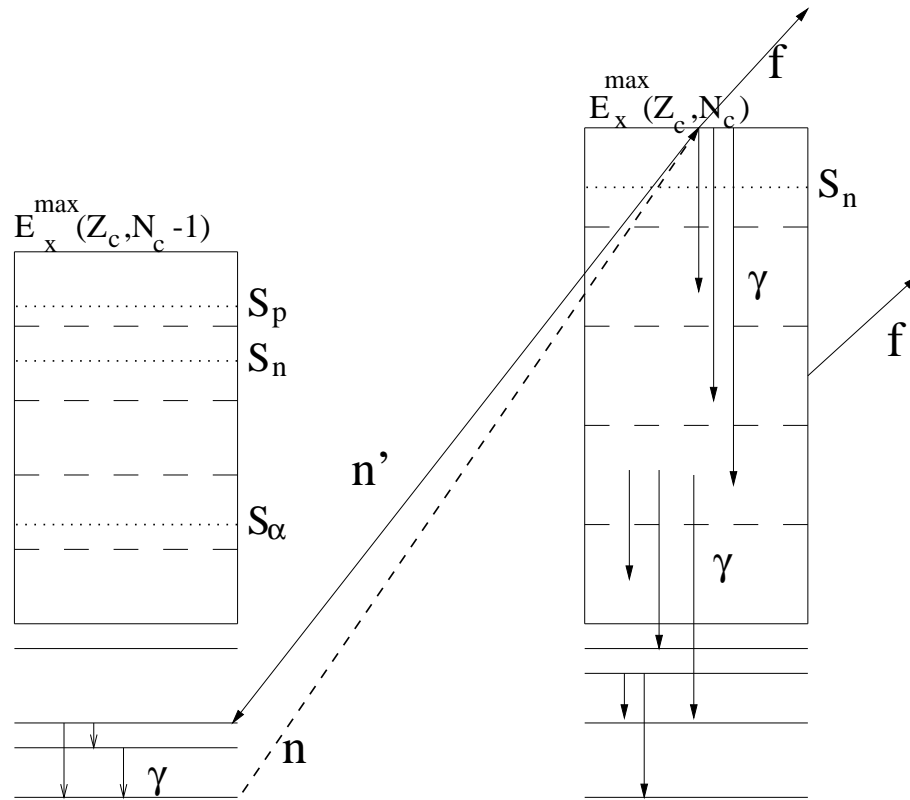


Figure 3.5: Neutron-induced reaction at somewhat higher energy. The dashed arrow represents the incident channel, while the continuous arrows represent the decay possibilities. In addition to the possibilities sketched in the previous figure, there is now inelastic scattering followed by gamma decay in the target nucleus.

pound nucleus theory, while the latter is described by the Distorted Wave Born Approximation (DWBA) for spherical nuclei and by coupled-channels equations for deformed nuclei, see Section 4.2. When the incident energy crosses an inelastic threshold, the compound inelastic contribution rises rapidly and predominates, whereas the direct component increases more gradually. Obviously, the elastic scattering, capture and fission processes described in the previous subsection also apply here. In addition, there is now gamma decay to an isomeric state or the ground state in the target nucleus after inelastic scattering. When there are several, say 10, inelastic levels open to decay, the compound contribution to each individual level is still significant. However, the effect of the width fluctuation correction on the compound cross section is already small in this case, as will be outlined in Section 4.5.

### 3.1.2 High energies

#### Pre-equilibrium reactions ( $E > 4$ MeV)

At higher incident energies, inelastic cross sections to both the discrete states and the continuum are possible, see Fig. 3.3. Like reactions to discrete states, reactions to the continuum also have a compound

and a direct-like component. The latter are usually described by pre-equilibrium reactions which, by definition, include direct reactions to the continuum. They will be discussed in Section 4.4. Also non-elastic channels to other nuclides, through charge-exchange, e.g.  $(n,p)$ , and transfer reactions, e.g.  $(n,\alpha)$ , generally open up at these energies, and decay to these nuclides can take place by the same direct, pre-equilibrium and compound mechanisms. Again, the channels described in the previous subsections also apply here. In addition, gamma decay to ground and isomeric states of all residual nuclides occurs. When many channels open up, particle decay to individual states (e.g. compound elastic scattering) rapidly becomes negligible. For the excitation of a discrete state, the direct component now becomes predominant, since that involves no statistical competition with the other channels. At about 15 MeV, the *total* compound cross section, i.e. summed over all final discrete states and the excited continuum, is however still larger than the summed direct and pre-equilibrium contributions.

### Multiple compound emission ( $E > 8$ MeV)

At incident energies above about the neutron separation energy, the residual nuclides formed after the first binary reaction contain enough excitation energy to enable further decay by compound nucleus particle emission or fission. This gives rise to multiple reaction channels such as  $(n,2n)$ ,  $(n,np)$ , etc. For higher energies, this picture can be generalized to many residual nuclei, and thus more complex reaction channels, as explained in the introduction of this Chapter, see also Fig. 3.3. If fission is possible, this may occur for all residual nuclides, which is known as multiple chance fission. All excited nuclides will eventually decay to their isomeric and ground states.

### Multiple pre-equilibrium emission ( $E > 40$ MeV)

At still higher incident energies, above several tens of MeV, the residual nuclides formed after binary emission may contain so much excitation energy that the presence of further *fast* particles inside the nucleus becomes possible. These can be imagined as strongly excited particle-hole pairs resulting from the first binary interaction with the projectile. The residual system is then clearly non-equilibrated and the excited particle that is high in the continuum may, in addition to the first emitted particle, also be emitted on a short time scale. This so-called multiple pre-equilibrium emission forms an alternative theoretical picture of the intra-nuclear cascade process, whereby now not the exact location and momentum of the particles is followed, but instead the total energy of the system and the number of particle-hole excitations (exciton number). In TALYS, this process can be generalized to any number of multiple pre-equilibrium stages in the reaction by keeping track of all successive particle-hole excitations, see Section 4.6.2. For these incident energies, the binary compound cross section becomes small: the non-elastic cross section is almost completely exhausted by primary pre-equilibrium emission. Again, Fig. 3.3 applies.

## 3.2 Cross section definitions

In TALYS, cross sections for reactions to all open channels are calculated. Although the types of most of these partial cross sections are generally well known, it is appropriate to define them for completeness.

This section concerns basically the book-keeping of the various cross sections, including all the sum rules they obey. The particular nuclear models that are needed to obtain them are described in Chapter 4. Thus, we do not yet give the definition of cross sections in terms of more fundamental quantities. Unless otherwise stated, we use incident neutrons as example in what follows and we consider only photons ( $\gamma$ ), neutrons (n), protons (p), deuterons (d), tritons (t), helium-3 particles (h) and alpha particles ( $\alpha$ ) as competing particles. Also, to avoid an overburdening of the notation and the explanation, we will postpone the competition of fission to the last section of this Chapter.

### 3.2.1 Total cross sections

The most basic nuclear reaction calculation is that with the optical model, which will be explained in more detail in Section 4.1. Here, it is sufficient to summarize the relations that can be found in many nuclear reaction textbooks, namely that the optical model yields the *reaction cross section*  $\sigma_{reac}$  and, in the case of neutrons, the *total cross section*  $\sigma_{tot}$  and the *shape-elastic cross section*  $\sigma_{shape-el}$ . They are related by

$$(3.2) \quad \sigma_{tot} = \sigma_{shape-el} + \sigma_{reac}.$$

If the elastic channel is, besides shape elastic scattering, also fed by compound nucleus decay, the latter component is a part of the reaction cross section and is called the *compound elastic cross section*  $\sigma_{comp-el}$ . With this, we can define the *total elastic cross section*  $\sigma_{el}$ ,

$$(3.3) \quad \sigma_{el} = \sigma_{shape-el} + \sigma_{comp-el},$$

and the *non-elastic cross section*  $\sigma_{non-el}$ ,

$$(3.4) \quad \sigma_{non-el} = \sigma_{reac} - \sigma_{comp-el},$$

so that we can combine these equations to give

$$(3.5) \quad \sigma_{tot} = \sigma_{el} + \sigma_{non-el}.$$

The last equation contains the quantities that can actually be measured in an experiment. We also note that the competition between the many compound nucleus decay channels ensures that  $\sigma_{comp-el}$  rapidly diminishes for incident neutron energies above a few MeV, in which case  $\sigma_{non-el}$  becomes practically equal to  $\sigma_{reac}$ .

A further subdivision of the outcome of a nuclear reaction concerns the breakdown of  $\sigma_{non-el}$ : this cross section contains all the partial cross sections. For this we introduce the exclusive cross sections, from which all other cross sections of interest can be derived.

### 3.2.2 Exclusive cross sections

In this manual, we call a cross section *exclusive* when the outgoing channel is precisely specified by the type and number of outgoing particles (+ any number of photons). Well-known examples are the

inelastic or  $(n, n')$  cross section and the  $(n, 2n)$  cross section, which corresponds with two, *and only* two, neutrons (+ accompanying photons) in the outgoing channel. We denote the *exclusive cross section* as  $\sigma^{ex}(i_n, i_p, i_d, i_t, i_h, i_\alpha)$ , where  $i_n$  stands for the number of outgoing neutrons, etc. In this notation, where the incident particle is assumed implicit, e.g. the  $(n, 2np)$  cross section is given by  $\sigma^{ex}(2, 1, 0, 0, 0, 0)$ , for which we will also use the shorthand notation  $\sigma_{n,2np}$ . For a non-fissile nucleus, the sum over all exclusive cross sections is equal to the non-elastic cross section

$$(3.6) \quad \sigma_{non-el} = \sum_{i_n=0}^{\infty} \sum_{i_p=0}^{\infty} \sum_{i_d=0}^{\infty} \sum_{i_t=0}^{\infty} \sum_{i_h=0}^{\infty} \sum_{i_\alpha=0}^{\infty} \sigma^{ex}(i_n, i_p, i_d, i_t, i_h, i_\alpha),$$

provided we impose that  $\sigma^{ex}(1, 0, 0, 0, 0, 0)$  is the exclusive *inelastic* cross section  $\sigma_{n,n'}$ , i.e. it does not include shape- or compound elastic scattering.

The precise calculation of exclusive cross sections and spectra is a complicated book-keeping problem which, to our knowledge, has not been properly documented. We will describe the exact formalism here. In what follows we use quantities with a prime for daughter nuclides and quantities without a prime for mother nuclides in a decay chain. Consider an excitation energy bin or discrete level  $E_x$  in a nucleus  $(Z, N)$ . Let  $P(Z, N, E_x)$  represent the population of this bin/level before it decays. Let  $s_k(Z, N, E_x, E_{x'})$  be the part of the population that decays from the  $(Z, N, E_x)$  bin/level to the residual  $(Z', N', E_{x'})$  bin/level, whereby  $(Z, N)$  and  $(Z', N')$  are connected through the particle type  $k$ , with the index  $k$  running from  $\gamma$ -rays up to  $\alpha$ -particles. With these definitions, we can link the various residual nuclides while keeping track of all intermediate particle emissions. A special case for the population is the initial compound nucleus  $(Z_C, N_C)$ , which contains all the initial reaction population at its total excitation energy  $E_x^{max}$  (projectile energy + binding energy), i.e.

$$(3.7) \quad P(Z_C, N_C, E_x^{max}) = \sigma_{non-el},$$

while all other population bins/levels are zero. For the initial compound nucleus,  $s_k(Z_C, N_C, E_x^{max}, E_{x'})$  represents the binary feeding to the excitation energy bins of the first set of residual nuclides. This term generally consists of direct, pre-equilibrium and compound components.

The population of any bin in the decay chain is equal to the sum of the decay parts for all particles that can reach this bin from the associated mother bins, i.e.

$$(3.8) \quad P(Z', N', E_{x'}(i')) = \sum_{k=\gamma, n, p, d, t, h, \alpha} \sum_i s_k(Z, N, E_x(i), E_{x'}(i')),$$

where the sum over  $i$  runs over discrete level and continuum energy bins in the energy range from  $E_{x'}(i') + S_k$  to  $E_x^{max}(Z, N)$ , where  $S_k$  is the separation energy of particle  $k$  so that the sum only includes decay that is energetically allowed, and  $E_x^{max}(Z, N)$  is the maximum possible excitation energy of the  $(Z, N)$  nucleus. Note again that the particle type  $k$  determines  $(Z, N)$ .

To obtain the exclusive cross sections, we need to start with the initial compound nucleus and work our way down to the last nucleus that can be reached. First, consider a daughter nucleus  $(Z', N')$  somewhere in the reaction chain. We identify all exclusive channels  $(i_n, i_p, i_d, i_t, i_h, i_\alpha)$  that lead to this residual  $(Z', N')$  nucleus, i.e. all channels that satisfy

$$(3.9) \quad \begin{aligned} i_n + i_d + 2i_t + i_h + 2i_\alpha &= N_C - N' \\ i_p + i_d + i_t + 2i_h + 2i_\alpha &= Z_C - Z'. \end{aligned}$$

For each of these channels, the *inclusive* cross section per excitation energy bin  $S$  is equal to the sum of the feeding from all possible mother bins, i.e.

$$(3.10) \quad S(i_n, i_p, i_d, i_t, i_h, i_\alpha, E_{x'}(i')) = \sum_{k=\gamma, n, p, d, t, h, \alpha} \sum_i \frac{s_k(Z, N, E_x(i), E_{x'}(i'))}{P(Z, N, E_x(i))} \\ \times S(i_n - \delta_{nk}, i_p - \delta_{pk}, i_d - \delta_{dk}, i_t - \delta_{tk}, i_h - \delta_{hk}, i_\alpha - \delta_{\alpha k}, E_x(i)),$$

where we introduce Kronecker delta's, with characters as subscript, as

$$(3.11) \quad \delta_{nk} = 1 \text{ if } k = n \text{ (neutron)} \\ = 0, \text{ otherwise}$$

and similarly for the other particles. Note that  $S$  is still inclusive in the sense that it is not yet depleted for further decay. The summation runs over the excitation energies of the mother bin from which decay into the  $E_{x'}(i')$  bin of the residual nucleus is energetically allowed. Feeding by gamma decay from bins above the  $(Z', N', E_{x'}(i'))$  bin is taken into account by the  $k = \gamma$  term, in which case all of the Kronecker delta's are zero.

With Eq. (3.7) as initial condition, the recursive procedure is completely defined. For a fixed nucleus, Eq. (3.10) is calculated for all excitation energy bins, in decreasing order, until the remaining population is in an isomeric or the ground state of the nucleus. When there is no further decay possible, the exclusive cross section per ground state/isomer, numbered by  $i$ , can be identified,

$$(3.12) \quad \sigma_i^{ex}(i_n, i_p, i_d, i_t, i_h, i_\alpha) = S(i_n, i_p, i_d, i_t, i_h, i_\alpha, E_i).$$

The total exclusive cross section for a particular channel is then calculated as

$$(3.13) \quad \sigma^{ex}(i_n, i_p, i_d, i_t, i_h, i_\alpha) = \sum_{i=0, \text{isomers}} \sigma_i^{ex}(i_n, i_p, i_d, i_t, i_h, i_\alpha).$$

The procedure outlined above automatically sorts and stores all exclusive cross sections, irrespective of the order of particle emission within the reaction chain. For example, the  $(n, np)$  and  $(n, pn)$  channels are automatically added. The above formalism holds *exactly* for an arbitrary number of emitted particles.

We stress that keeping track of the excitation energy  $E_x$  throughout this formalism is essential to get the exact exclusive cross sections for two reasons:

- (i) the exact determination of the branching ratios for exclusive isomeric ratios. The isomeric ratios for different exclusive reactions that lead to the same residual product, e.g.  $(n, np)$  and  $(n, d)$ , both leading to  $(Z_C - 1, N_C - 1)$ , are generally different from each other and thus also from the isomeric ratios of the total residual product. Hence, it would be an approximation to apply isomeric branching ratios for residual products, obtained after the full reaction calculation, a posteriori on the exclusive channels. This is avoided with our method,
- (ii) the exclusive spectra, which we will explain in Section 3.3.2.

Suppose one would only be interested in the total exclusive cross sections of Eq. (3.13), i.e. neither in the exclusive isomeric ratios, nor in the exclusive spectra. Only in that case, a simpler method would be sufficient. Since only the total reaction population that decays from nucleus to nucleus needs to be tracked, the total exclusive cross section for a certain channel is easily determined by subtracting the total ongoing flux from the total feeding flux to this channel. This is described in e.g. Section II.E.f of the GNASH manual[2]. We note that the exact treatment of TALYS does not require a large amount of computing time, certainly not when compared with more time-expensive parts of the full calculation.

When TALYS computes the binary reaction models and the multiple pre-equilibrium and Hauser-Feshbach models, it stores both  $P(Z, N, E_x)$  (through the **popexcl** array) and  $s_k(Z, N, E_x, E_{x'})$  (through the **feedexcl** array) for all residual nuclei and particles. This temporary storage enables us to first complete the full reaction calculation, including all its physical aspects, until all channels are closed. Then, we turn to the exclusive cross section and spectra problem afterwards in a separate subroutine: *channels.f*. It is thus considered as an isolated book-keeping problem.

The total number of different exclusive channels rapidly increases with the number of reaction stages. It can be shown that for  $m$  outgoing particles (i.e. reaction stages) which can be of  $k$  different types, the maximum number of exclusive cross sections is  $\binom{m+k-1}{m}$ . In general, we include neutrons up to alpha-particles as competing particles, i.e.  $k = 6$ , giving  $\binom{m+5}{m}$  possible exclusive channels, or 6, 21, 56 and 126, respectively, for the first 4 stages. This clarifies why exclusive channels are usually only of interest for only a few outgoing particles (the ENDF format for evaluated data libraries includes reactions up to 4 particles). At higher energies, and thus more outgoing particles, exclusive cross sections lose their relevance and the cross sections per channel are usually accumulated in the total particle production cross sections and residual production cross sections. Certainly at higher energies, this apparent loss of information is no longer an issue, since the observable quantities to which nuclear models can be tested are of a cumulative nature anyway, when many particles are involved.

In TALYS, the cumulated particle production cross sections and residual production cross sections are always *completely* tracked down until all residual nuclides have decayed to an isomer or the ground state, regardless of the incident energy, whereas exclusive cross sections are only tracked up to a user-defined depth. To elucidate this important point we discuss the low and the high energy case. For low energies, say up to 20 MeV, keeping track of the exclusive cross section is important from both the fundamental and the applied point of view. It can be imagined that in a  $(n, np)$  measurement both the emitted neutron and proton have been measured in the detector. Hence the cross section is *not* the same as that of an activation measurement of the final residual nucleus, since the latter would also include a contribution from the  $(n, d)$  channel. Another example is the  $(n, 2n)$  channel, distinguished from the  $(n, n')$  or the general  $(n, xn)$  cross section, which is of importance in some integral reactor benchmarks. If, on the other hand, we encounter in the literature a cross section of the type  $^{120}\text{Sn}(p, 7p18n)^{96}\text{Ru}$ , we can be sure that the residual product  $^{96}\text{Ru}$  was measured and not the indicated number of neutrons and protons in a detector. The  $(p, 7p18n)$  symbol merely represents the number of neutron and proton units, while other light ions are generally included in the emission channel. Hence, for high energies the outcome of a nuclear reaction is usually tracked in parallel by two sets of quantities: the  $(proj, xn), \dots (proj, x\alpha)$  particle production cross sections and spectra, and the residual production cross sections. These will be exactly defined in the next sections.

### 3.2.3 Binary cross sections

Some of the exclusive channels need, and get, more attention than others. The exclusive binary cross sections, for reactions that are characterized by one, and only one, particle out, are special in the sense that they comprise both discrete and continuous energy transitions. Inelastic scattering can occur through both direct collective and compound transitions to the first few excited levels and through pre-equilibrium and compound reactions to the continuum. Let us assume that for a target nucleus the basic structure properties (spin, parity, deformation parameters) of the first  $N$  levels are known. Then, the *inelastic cross section*,  $\sigma_{n,n'}$  is the sum of a *total discrete inelastic cross section*  $\sigma_{n,n'}^{disc}$  and a *continuum inelastic cross section*  $\sigma_{n,n'}^{cont}$

$$(3.14) \quad \sigma_{n,n'} = \sigma_{n,n'}^{disc} + \sigma_{n,n'}^{cont},$$

where  $\sigma_{n,n'}^{disc}$  is the sum over the inelastic cross sections for all the individual discrete states

$$(3.15) \quad \sigma_{n,n'}^{disc} = \sum_{i=1}^N \sigma_{n,n'}^i.$$

A further breakdown of each term is possible by means of reaction mechanisms. The inelastic cross section for each individual state  $i$  has a direct and a compound contribution:

$$(3.16) \quad \sigma_{n,n'}^i = \sigma_{n,n'}^{i,direct} + \sigma_{n,n'}^{i,comp},$$

where the direct component comes from DWBA or coupled-channels calculations. Similarly, for the inelastic scattering to the continuum we can consider a pre-equilibrium and a compound contribution

$$(3.17) \quad \sigma_{n,n'}^{cont} = \sigma_{n,n'}^{PE} + \sigma_{n,n'}^{cont,comp}.$$

The set of definitions (3.14-3.17) can be given in a completely analogous way for the other binary channels  $\sigma_{n,p}$ , i.e.  $\sigma^{ex}(0, 1, 0, 0, 0, 0)$ ,  $\sigma_{n,d}$ ,  $\sigma_{n,t}$ ,  $\sigma_{n,h}$  and  $\sigma_{n,\alpha}$ . For the depletion of the reaction population that goes into the pre-equilibrium channels, which will be discussed in Section 4.4, it is helpful to define here the *total discrete direct cross section*,

$$(3.18) \quad \sigma^{disc,direct} = \sum_i \sum_{k=n',p,d,t,h,\alpha} \sigma_{n,k}^{i,direct}.$$

Finally, we also consider an alternative division for the non-elastic cross section. It is equal to the sum of the *inclusive* binary cross sections

$$(3.19) \quad \sigma_{non-el} = \sum_{k=\gamma,n',p,d,t,h,\alpha} \sigma_{n,k}^{inc,bin},$$

where again at the present stage of the outline we do not consider fission and ejectiles heavier than  $\alpha$ -particles. This is what we actually use in the inclusive nuclear reaction calculations. With the direct, pre-equilibrium and compound models, several residual nuclides can be formed after the binary reaction, with a total population per nucleus that is equal to the terms of Eq. (3.19). The residual nuclides then decay further until all channels are closed. Note that  $\sigma^{inc,bin}$  is not a “true” cross section in the sense of a quantity for a final combination of a product and light particle(s).

### 3.2.4 Total particle production cross sections

Especially for incident energies higher than about 10 MeV, it is appropriate to define the composite or *total neutron production cross section*,  $\sigma_{n,xn}$ . It can be expressed in terms of the exclusive cross sections as follows

$$(3.20) \quad \sigma_{n,xn} = \sum_{i_n=0}^{\infty} \sum_{i_p=0}^{\infty} \sum_{i_d=0}^{\infty} \sum_{i_t=0}^{\infty} \sum_{i_h=0}^{\infty} \sum_{i_\alpha=0}^{\infty} i_n \sigma^{ex}(i_n, i_p, i_d, i_t, i_h, i_\alpha),$$

i.e. in the more common notation,

$$(3.21) \quad \sigma_{n,xn} = \sigma_{n,n'} + 2\sigma_{n,2n} + \sigma_{n,np} + 2\sigma_{n,2np} + \dots$$

Again,  $\sigma_{n,xn}$  is not a true cross section since the incident and outgoing channels are not exactly defined by its individual reaction components. (Contrary to our definition, in some publications  $\sigma_{n,xn}$  is used to indicate activation measurements of a whole string of isotopes (e.g.  $^{202-208}\text{Pb}$ ) in which case  $x$  is a number that varies case by case. In our work, this is called an exclusive cross section). The *neutron multiplicity*, or *yield*,  $Y_n$  is defined as

$$(3.22) \quad Y_n = \frac{\sigma_{n,xn}}{\sigma_{non-el}}.$$

Similarly, the *total proton production cross section*,  $\sigma_{n,xp}$  is defined as

$$(3.23) \quad \sigma_{n,xp} = \sum_{i_n=0}^{\infty} \sum_{i_p=0}^{\infty} \sum_{i_d=0}^{\infty} \sum_{i_t=0}^{\infty} \sum_{i_h=0}^{\infty} \sum_{i_\alpha=0}^{\infty} i_p \sigma^{ex}(i_n, i_p, i_d, i_t, i_h, i_\alpha),$$

and the proton multiplicity, or yield,  $Y_p$  is defined as

$$(3.24) \quad Y_p = \frac{\sigma_{n,xp}}{\sigma_{non-el}},$$

and similarly for the other particles. We note that we do not, in practice, use Eq. (3.20) to calculate the composite particle production cross section. Instead, we first calculate the inclusive binary cross section of Eq. (3.19) and then, during the depletion of each residual nucleus by further decay we directly add the reaction flux, equal to the  $s_k(Z, N, E_x, E_{x'})$  term of Eq. (3.8), to  $\sigma_{n,xn}$ ,  $\sigma_{n,xp}$ , etc. This procedure has already been sketched in the multiple decay scheme at the beginning of this Chapter. In the output of TALYS, we include Eq. (3.20) only as a numerical check. For a few outgoing particles Eq. (3.20) should exactly hold. For higher energies and thus more outgoing particles (typically more than 4, see the **maxchannel** keyword on page 169) the exclusive cross sections are no longer tracked by TALYS and Eq. (3.20) can no longer be expected to hold numerically. Remember, however, that we always calculate the total particle production cross sections, irrespective of the number of outgoing particles, since we continue the multiple emission calculation until all residual nuclides are in their isomeric or ground states.

### 3.2.5 Residual production cross sections

We can define another important type of derived cross section using the exclusive cross section, namely the residual production cross section  $\sigma_{prod}$ . All exclusive cross sections with the same number of neutron and proton units in the outgoing channel sum up to the same residual nucleus production cross section for the final nucleus  $(Z, N)$ , i.e.

$$(3.25) \quad \sigma_{prod}(Z, N) = \sum_{i_n=0}^{\infty} \sum_{i_p=0}^{\infty} \sum_{i_d=0}^{\infty} \sum_{i_t=0}^{\infty} \sum_{i_h=0}^{\infty} \sum_{i_\alpha=0}^{\infty} \sigma^{ex}(i_n, i_p, i_d, i_t, i_h, i_\alpha) \delta_N \delta_Z,$$

where the Kronecker delta's are defined by

$$(3.26) \quad \begin{aligned} \delta_N &= 1 \text{ if } i_n + i_d + 2i_t + i_h + 2i_\alpha = N_C - N \\ &= 0 \text{ otherwise} \\ \delta_Z &= 1 \text{ if } i_p + i_d + i_t + 2i_h + 2i_\alpha = Z_C - Z \\ &= 0 \text{ otherwise,} \end{aligned}$$

where the first compound nucleus that is formed from the projectile and target nucleus is denoted by  $(Z_C, N_C)$ . As an example, consider the  $n + {}^{56}\text{Fe} \rightarrow {}^{54}\text{Mn} + x$  reaction. The exclusive cross sections that add up to the  ${}^{54}\text{Mn}$  production cross section are  $\sigma_{n,2np}$ ,  $\sigma_{n,nd}$ , and  $\sigma_{n,t}$ , or  $\sigma^{ex}(2, 1, 0, 0, 0, 0)$ ,  $\sigma^{ex}(1, 0, 1, 0, 0, 0)$ , and  $\sigma^{ex}(0, 0, 0, 1, 0, 0)$ , respectively.

Since all exclusive cross sections contribute to the residual production cross section for one nuclide  $(Z, N)$  only, Eq. (3.6) automatically implies

$$(3.27) \quad \sigma_{non-el} = \sum_Z \sum_N \sigma_{prod}(Z, N).$$

Similar to Eq. (3.13), Eq. (3.25) is separated per isomer

$$(3.28) \quad \sigma_{prod,i}(Z, N) = \sum_{i_n=0}^{\infty} \sum_{i_p=0}^{\infty} \sum_{i_d=0}^{\infty} \sum_{i_t=0}^{\infty} \sum_{i_h=0}^{\infty} \sum_{i_\alpha=0}^{\infty} \sigma_i^{ex}(i_n, i_p, i_d, i_t, i_h, i_\alpha) \delta_N \delta_Z,$$

and the equivalent of Eq. (3.13) is

$$(3.29) \quad \sigma_{prod}(Z, N) = \sum_{i=0, \text{isomers}} \sigma_{prod,i}(Z, N).$$

Also here, we do not calculate  $\sigma_{prod}$  and  $\sigma_{prod,i}$  using Eqs. (3.25) and (3.28), although optionally TALYS includes it as a numerical check in the output for residual nuclides close to the target. Analogous to the total particle production, we determine the residual production cross section, for both the isomers and the ground state, after the complete decay of each nucleus by means of an inclusive calculation.

## 3.3 Spectra and angular distributions

In addition to cross sections, TALYS also predicts energy spectra, angular distributions and energy-angle distributions.

### 3.3.1 Discrete angular distributions

The elastic angular distribution  $\frac{d\sigma^{el}}{d\Omega}$  has a direct and a compound component:

$$(3.30) \quad \frac{d\sigma^{el}}{d\Omega} = \frac{d\sigma^{shape-el}}{d\Omega} + \frac{d\sigma^{comp-el}}{d\Omega},$$

where the shape-elastic part comes directly from the optical model while the compound part comes from compound nucleus theory, namely Eq. (4.180). An analogous relation holds for inelastic scattering to a single discrete state  $i$

$$(3.31) \quad \frac{d\sigma_{n,n'}^i}{d\Omega} = \frac{d\sigma_{n,n'}^{i,direct}}{d\Omega} + \frac{d\sigma_{n,n'}^{i,compound}}{d\Omega},$$

where the direct component comes from DWBA or coupled-channels calculations. For charge exchange, we can write

$$(3.32) \quad \frac{d\sigma_{n,p}^i}{d\Omega} = \frac{d\sigma_{n,p}^{i,direct}}{d\Omega} + \frac{d\sigma_{n,p}^{i,compound}}{d\Omega}$$

and analogous expressions can be written for the other binary reactions  $(n, d)$ , etc.

Of course, the integration over solid angle of every angular distribution defined here must be equal to the corresponding cross section, e.g.

$$(3.33) \quad \sigma_{n,n'}^{i,direct} = \int d\Omega \frac{d\sigma_{n,n'}^{i,direct}}{d\Omega}.$$

In the output of TALYS, we use a representation in terms of outgoing angle and one in terms of Legendre coefficients, i.e. Eq. (3.30) can also be written as

$$(3.34) \quad \frac{d\sigma^{el}}{d\Omega} = \sum_L (C_L^{shape-el} + C_L^{comp-el}) P_L(\cos \Theta),$$

where  $P_L$  are Legendre polynomials. For inelastic scattering we have

$$(3.35) \quad \frac{d\sigma_{n,n'}^i}{d\Omega} = \sum_L (C_L^{i,direct} + C_L^{i,comp}) P_L(\cos \Theta),$$

and similarly for the other binary channels. The Legendre expansion is required for the storage of the results in ENDF data libraries.

### 3.3.2 Exclusive spectra

An exclusive spectrum is not only specified by the exact number of emitted particles, but also by their outgoing energies.

In TALYS, exclusive spectra are calculated in the same loops that take care of the exclusive cross sections. The inclusive continuum spectra are obtained by taking the derivative of the inclusive cross sections per excitation energy of Eq. (3.10) with respect to the outgoing particle energy  $E_{k'}$ ,

$$(3.36) \quad E_{k'} = E_x - E_{x'}(i') - S_{k'},$$

where  $S_{k'}$  is the separation energy for outgoing particle  $k'$ . Note that since the inclusive cross section per excitation energy  $S$  depends on  $E_{k'}$  via  $s_k$ , the product rule of differentiation applies to Eq. (3.10). Therefore, the inclusive spectrum per excitation energy for an outgoing particle  $k'$  of a given  $(i_n, i_p, i_d, i_t, i_h, i_\alpha)$  channel is

$$(3.37) \quad \begin{aligned} \frac{dS}{dE_{k'}}(i_n, i_p, i_d, i_t, i_h, i_\alpha, E_{x'}(i')) &= \sum_{k=\gamma, n, p, d, t, h, \alpha} \sum_i \\ & \left[ \frac{s_k(Z, N, E_x(i), E_{x'}(i'))}{P(Z, N, E_x(i))} \frac{dS}{dE_{k'}}(i_n - \delta_{nk}, i_p - \delta_{pk}, i_d - \delta_{dk}, i_t - \delta_{tk}, i_h - \delta_{hk}, i_\alpha - \delta_{\alpha k}, E_x(i)) \right. \\ & \left. + \delta_{kk'} \frac{ds_k(Z, N, E_x(i), E_{x'}(i'))}{dE_{k'}} \frac{S(i_n - \delta_{nk}, i_p - \delta_{pk}, i_d - \delta_{dk}, i_t - \delta_{tk}, i_h - \delta_{hk}, i_\alpha - \delta_{\alpha k}, E_x(i))}{P(Z, N, E_x(i))} \right], \end{aligned}$$

where, as initial condition, the derivatives of  $s_k(Z_C, N_C, E_x^{max}, E_{x'}(i'))$  are the binary emission spectra. The first term on the right-hand side corresponds to the spectrum of the feeding channel and the second term denotes the contribution of the last emitted particle. The calculation of Eq. (3.37) can be done simultaneously with the exclusive cross section calculation, i.e. we follow exactly the same recursive procedure. The final exclusive spectrum for outgoing particle  $k'$  is given by

$$(3.38) \quad \frac{d\sigma^{ex}}{dE_{k'}}(i_n, i_p, i_d, i_t, i_h, i_\alpha) = \sum_{i=0, isomers} \frac{dS}{dE_{k'}}(i_n, i_p, i_d, i_t, i_h, i_\alpha, E_i),$$

The terms on the right hand side are the exclusive spectra per ground state or isomer. The latter naturally result from our method, even though only the total exclusive spectra of the left hand side are of interest.

We stress that for a given  $(i_n, i_p, i_d, i_t, i_h, i_\alpha)$  channel, Eq. (3.37) is calculated for *every* outgoing particle  $k'$  (i.e. n, p, d, t, h and  $\alpha$ ). Hence, e.g. the  $(n, 2np\alpha)$  channel is characterized by only one exclusive cross section,  $\sigma_{n, 2np\alpha}$ , but by three spectra, one for outgoing neutrons, protons and alpha's, respectively, whereby all three spectra are constructed from components from the first up to the fourth particle emission (i.e. the  $\alpha$  can have been emitted in each of the four stages). In practice, this means that all spectra have a first order pre-equilibrium component (and for higher energies also higher order pre-equilibrium components), and a compound component from multiple emission. Upon integration over outgoing energy, the exclusive cross sections may be obtained,

$$(3.39) \quad \sigma^{ex}(i_n, i_p, i_d, i_t, i_h, i_\alpha) = \frac{1}{i_n + i_p + i_d + i_t + i_h + i_\alpha} \sum_{k'=n, p, d, t, h, \alpha} \int dE_{k'} \frac{d\sigma^{ex}}{dE_{k'}}(i_n, i_p, i_d, i_t, i_h, i_\alpha).$$

### 3.3.3 Binary spectra

Similar to the cross sections, the exclusive spectra determine various other specific spectra of interest. The exclusive *inelastic spectrum* is a special case of Eq. (3.38)

$$(3.40) \quad \frac{d\sigma_{n,n'}}{dE_{n'}} = \frac{d\sigma^{ex}}{dE_{n'}}(1, 0, 0, 0, 0, 0).$$

Since Eq. (3.37) represents an energy spectrum, it includes by definition only continuum transitions, i.e. it does not include the binary reactions to discrete states. Hence, upon integration, Eq. (3.40) only gives the continuum inelastic cross section of Eq. (3.14):

$$(3.41) \quad \sigma_{n,n'}^{cont} = \int dE_{n'} \frac{d\sigma_{n,n'}}{dE_{n'}}.$$

Similar relations hold for the binary  $(n, p)$ ,  $(n, d)$ ,  $(n, t)$ ,  $(n, h)$  and  $(n, \alpha)$  spectra. The contributions to the binary spectra generally come from pre-equilibrium and continuum compound spectra.

### 3.3.4 Total particle production spectra

Similar to the total particle production cross sections, the *composite* or *total neutron spectrum* can be expressed in terms of exclusive spectra as follows

$$(3.42) \quad \frac{d\sigma_{n,xn}}{dE_{n'}} = \sum_{i_n=0}^{\infty} \sum_{i_p=0}^{\infty} \sum_{i_d=0}^{\infty} \sum_{i_t=0}^{\infty} \sum_{i_h=0}^{\infty} \sum_{i_\alpha=0}^{\infty} \frac{d\sigma^{ex}}{dE_{n'}}(i_n, i_p, i_d, i_t, i_h, i_\alpha),$$

i.e. in the other notation,

$$(3.43) \quad \frac{d\sigma_{n,xn}}{dE_{n'}} = \frac{d\sigma_{n,n'}}{dE_{n'}} + \frac{d\sigma_{n,2n}}{dE_{n'}} + \frac{d\sigma_{n,np}}{dE_{n'}} + \frac{d\sigma_{n,2np}}{dE_{n'}} + \dots$$

Similar relations hold for the  $(n, xp)$ , etc. spectra. Note that, in contrast with Eq. (3.20), the multiplicity is already implicit in the exclusive spectra.

Again, in practice we do not use Eq. (3.42) to calculate the composite spectra but instead add the  $ds_k(Z, N, E_x, E_{x'})/dE_k'$  term that appears in Eq. (3.37) to the composite spectra while depleting all nuclides in an inclusive calculation. We do use Eq. (3.42) as a numerical check in the case of a few outgoing particles. Finally, integration of the total neutron spectrum and addition of the binary discrete cross section gives the total particle production cross section

$$(3.44) \quad \sigma_{n,xn} = \int dE_{n'} \frac{d\sigma_{n,xn}}{dE_{n'}} + \sigma_{n,n'}^{disc},$$

and similarly for the other particles.

### 3.3.5 Double-differential cross sections

The generalization of the exclusive spectra to angular dependent cross sections is done by means of the exclusive double-differential cross sections

$$(3.45) \quad \frac{d^2\sigma^{ex}}{dE_{k'}d\Omega}(i_n, i_p, i_d, i_t, i_h, i_\alpha),$$

which are obtained by either physical models or systematics. Integration over angles yields the exclusive spectrum

$$(3.46) \quad \frac{d\sigma^{ex}}{dE_{k'}}(i_n, i_p, i_d, i_t, i_h, i_\alpha) = \int d\Omega \frac{d^2\sigma^{ex}}{dE_{k'}d\Omega}(i_n, i_p, i_d, i_t, i_h, i_\alpha).$$

The other relations are analogous to those of the spectra, e.g. the inelastic double-differential cross section for the continuum is

$$(3.47) \quad \frac{d^2\sigma_{n,n'}}{dE_{n'}d\Omega} = \frac{d^2\sigma^{ex}}{dE_{n'}d\Omega}(1, 0, 0, 0, 0, 0),$$

and the total neutron double-differential cross section can be expressed as

$$(3.48) \quad \frac{d^2\sigma_{n,xn}}{dE_{n'}d\Omega} = \sum_{i_n=0}^{\infty} \sum_{i_p=0}^{\infty} \sum_{i_d=0}^{\infty} \sum_{i_t=0}^{\infty} \sum_{i_h=0}^{\infty} \sum_{i_\alpha=0}^{\infty} \frac{d^2\sigma^{ex}}{dE_{n'}d\Omega}(i_n, i_p, i_d, i_t, i_h, i_\alpha).$$

For the *exclusive* calculation, the angular information is only tracked for the first particle emission. The reason is that for incident energies up to about 20 to 30 MeV, only the first emitted particle deviates from an isotropic angular distribution. Multiple compound emission to the continuum is essentially isotropic. The isotropic contribution to the exclusive double-differential spectrum is then simply determined by the part of the corresponding cross section that comes from Hauser-Feshbach decay. At higher incident energies, where the approximation of only one forward-peaked particle becomes incorrect, the interest in exclusive spectra, or for that matter, the computational check of Eq. (3.48), is no longer there. The presence of multiple pre-equilibrium emission at energies above several tens of MeV requires that we include angular information for every emitted particle in the *total* double-differential cross section, i.e. the left-hand side of Eq. (3.48). Again, this is all tracked correctly in the full inclusive calculation.

## 3.4 Fission cross sections

For clarity, we have kept the fission channel out of the discussion so far. The generalization to a picture in which fission is possible is however not too difficult. For fissile nuclides, the first expression that needs generalization is that of the non-elastic cross section expressed as a sum of exclusive cross sections, Eq. (3.6). It should read

$$(3.49) \quad \sigma_{non-el} = \sum_{i_n=0}^{\infty} \sum_{i_p=0}^{\infty} \sum_{i_d=0}^{\infty} \sum_{i_t=0}^{\infty} \sum_{i_h=0}^{\infty} \sum_{i_\alpha=0}^{\infty} \sigma^{ex}(i_n, i_p, i_d, i_t, i_h, i_\alpha) + \sigma_f,$$

where the *total fission* cross section  $\sigma_f$  is the sum over exclusive fission cross sections

$$(3.50) \quad \sigma_f = \sum_{i_n=0}^{\infty} \sum_{i_p=0}^{\infty} \sum_{i_d=0}^{\infty} \sum_{i_t=0}^{\infty} \sum_{i_h=0}^{\infty} \sum_{i_\alpha=0}^{\infty} \sigma_f^{ex}(i_n, i_p, i_d, i_t, i_h, i_\alpha),$$

where  $\sigma_f^{ex}(i_n, i_p, i_d, i_t, i_h, i_\alpha)$  represents the cross section for fissioning *after* the emission of  $i_n$  neutrons,  $i_p$  protons, etc. Well-known special cases are  $\sigma_{n,f} = \sigma_f^{ex}(0, 0, 0, 0, 0, 0)$ ,  $\sigma_{n,nf} = \sigma_f^{ex}(1, 0, 0, 0, 0, 0)$  and  $\sigma_{n,2nf} = \sigma_f^{ex}(2, 0, 0, 0, 0, 0)$ , which are also known as first-chance, second-chance and third-chance fission cross section, respectively. Eq. (3.50) is more general in the sense that it also includes cases where particles other than neutrons can be emitted before the residual nucleus fissions, e.g.  $(n, npf)$ , which may occur at higher incident energies.

The generalization of the non-elastic cross section of Eq. (3.19) is

$$(3.51) \quad \sigma_{non-el} = \sum_{k=\gamma, n', p, d, t, h, \alpha} \sigma_{n,k}^{inc, bin} + \sigma_f^{bin},$$

where  $\sigma_f^{bin}$  represents fission from the initial compound state (i.e. excluding  $(n, \gamma f)$  processes).

Analogous to Eq. (3.25), we can define a cross section for each fissioning residual product

$$(3.52) \quad \sigma_{prod}^{fis}(Z, N) = \sum_{i_n=0}^{\infty} \sum_{i_p=0}^{\infty} \sum_{i_d=0}^{\infty} \sum_{i_t=0}^{\infty} \sum_{i_h=0}^{\infty} \sum_{i_\alpha=0}^{\infty} \sigma_f^{ex}(i_n, i_p, i_d, i_t, i_h, i_\alpha) \delta_N \delta_Z.$$

At higher energies, the meaning of  $\sigma_{prod}^{fis}(Z, N)$  is more relevant than the exclusive fission cross sections. Consequently, for the total fission cross section we have

$$(3.53) \quad \sigma_f = \sum_Z \sum_N \sigma_{prod}^{fis}(Z, N).$$

What remains to be explained is how  $\sigma_f^{ex}$  is computed. First, we need to add to Eq. (3.8) a term we denote by  $s_f(Z, N, E_x(i))$ , which is the part of the population that fissions from the  $(Z, N, E_x(i))$  bin. Hence, for fissile nuclides we have

$$(3.54) \quad P(Z, N, E_x(i)) = s_f(Z, N, E_x(i)) + \sum_{k=\gamma, n, p, d, t, h, \alpha} \sum_i s_k(Z, N, E_x(i), E_{x'}(i')).$$

where in this case the sum over  $i$  runs over discrete levels and continuum bins from 0 to  $E_x(i) - S_k$ . The exclusive fission cross section  $\sigma_f^{ex}$  is

$$(3.55) \quad \sigma_f^{ex}(i_n, i_p, i_d, i_t, i_h, i_\alpha) = \sum_i \frac{s_f(Z, N, E_x(i))}{P(Z, N, E_x(i))} S(i_n, i_p, i_d, i_t, i_h, i_\alpha, E_x(i)).$$

where  $i$  runs from 0 to  $E_x^{max}(Z, N)$ . The rest of the calculation of the exclusive particle cross section proceeds exactly as before. Eq. (3.10) is now automatically depleted from the fission cross section (3.55), in the sense that the  $s_k$  terms alone, summed over  $\gamma$  and particles only, no longer add up to the population  $P$ .

Finally, the exclusive fission cross sections are also accompanied by spectra. For example, the first two neutrons emitted in the  $(n, 2nf)$  channel (third-chance fission) are described by an outgoing neutron spectrum. The exclusive spectrum of outgoing particle  $k'$  in a fission channel is

$$(3.56) \quad \frac{d\sigma_f^{ex}}{dE_{k'}}(i_n, i_p, i_d, i_t, i_h, i_\alpha) = \sum_i \frac{s_f(Z, N, E_x(i))}{P(Z, N, E_x(i))} \frac{dS}{dE_{k'}}(i_n, i_p, i_d, i_t, i_h, i_\alpha),$$

while the exclusive particle spectra are again described by Eq. (3.37). For double-differential spectra, the usual generalization holds. We also repeat here that the total (observable) fission cross section is always calculated by letting reaction population go into the fission channel from each  $(Z, N, E_x, J, \Pi)$  channel until all nuclides have ended up in their ground or isomeric state, irrespective of the user request for an exclusive channel calculation.

## 3.5 Recoils

### 3.5.1 Qualitative analysis

In a nuclear reaction code, the calculations are usually performed in the center of mass (CM) frame, while the experimental data are obtained in the Laboratory (LAB) frame. It is therefore necessary to perform a transformation either by (i) expressing the experimental data in the CM frame or by (ii) expressing the CM model results in the LAB frame. Of course, the cross sections are the same in both frames, but the spectra are certainly different. The best example is given by the elastic peak in an emission spectrum which is a Dirac delta peak in the CM frame and rather looks like a Gaussian when measured experimentally. The reason for this, apart from the fact that the projectile beam is not perfectly mono-energetic, is that the composite system has a velocity in the LAB frame before decay occurs. Consequently if one considers the emission of an ejectile with a well defined energy in the CM frame, the ejectile energy in the LAB frame will not be unique because of all the CM emission angles. More precisely, a maximum ejectile energy will be obtained when the emission occurs at  $0^\circ$ , and a minimum will be obtained at  $180^\circ$ , together with all the intermediate situations. Dealing with this situation is simple if only one nucleus decays, but if two particles are sequentially emitted, the first emission probabilities create a velocity distribution of the residual nuclei in the LAB frame. One must first loop over these velocities before one can compute the secondary emission.

### 3.5.2 General method

As mentioned in section 3.2.2, in TALYS each nucleus that can decay is described by an array  $P(Z, N, E_x)$  which gives the population in a bin/level with excitation energy  $E_x$  of the nucleus  $(Z, N)$ . A special case is the initial compound nucleus which contains all the initial reaction population at its total excitation energy  $E_x^{max}$ . For the kinematics of the binary reactions, it is necessary to keep track of the velocities and moving directions of these nuclei in the LAB frame, so that we can reconstruct the LAB spectra from the decays in the CM frame. We therefore have to add in principle three dimensions to the  $P$  array. The first one to keep track of the recoil energy, and the two other ones for the emission angles. However, such book-keeping would become very time consuming, especially for high energies.

Hence, we only take into account the recoil energies and the usual  $\Theta$  angle and define another array  $P_{rec}(Z, N, E_x, E_r, \Theta_r)$  which indicates the fraction of the total population  $P(Z, N, E_x)$  moving with the kinetic energy  $E_r$  in the direction  $\Theta_r$  with respect to the beam direction in the LAB frame. Obviously,

$$(3.57) \quad P(Z, N, E_x) = \sum_{E_r \text{ bins}} \sum_{\Theta_r \text{ bins}} P_{rec}(Z, N, E_x, E_r, \Theta_r).$$

Again, the initial compound nucleus  $(Z_C, N_C)$  is a special one. Its kinetic energy  $E_r^0$  in the LAB frame is unique and is given by

$$(3.58) \quad E_r^0 = \sqrt{(E_p^2 + 2M_p E_p + M_C^2)} - M_C,$$

where  $E_p$  is the projectile kinetic energy in the LAB,  $M_p$  the projectile mass and  $M_C$  the compound nucleus mass, and it moves in the beam direction (i.e.  $0^\circ$ ). Before any emission is calculated, the initial reaction population is stored in the array element  $P_{rec}(Z_c, N_c, E_x^{max}, E_r^0, 0)$ . As explained before, the population of the residual nuclei bins are calculated by looping over all possible ejectiles, emission energies and angles in the CM frame. Therefore, each time we decay from a mother bin to a residual bin, we know exactly what fraction of the total bin population is emitted in a given CM (energy,angle) bin. We then simply couple the CM emission energies and angles with the CM kinetic energy and moving direction in the LAB frame to determine simultaneously the ejectile double-differential spectrum in the LAB and the residual nucleus population in the corresponding LAB (energy,angle) bin. This may seem simple from a qualitative point of view, it is however not trivial to implement numerically and can be time consuming.

### 3.5.3 Quantitative analysis

From now on, for simplicity, we assume that the kinematics of the binary reactions can be considered as a classical process, i.e. we exclude  $\gamma$  decay and relativistic kinematics in the recoil calculation. We here consider the emission of a given ejectile from a given energy bin  $i$  of the decaying nucleus  $(Z, N)$  which moves with a given velocity  $v_{cm}$  (or kinetic energy  $E_{cm}$ ) in the direction  $\Theta_{cm}$  with respect to the beam direction. The total population that is going to decay is  $P(Z, N, E_i)$  and the fraction of this population moving with the velocity  $v_{cm}$  in the direction  $\Theta_{cm}$  is given by  $P_{rec}(Z, N, E_i, E_{cm}, \Theta_{cm})$ . We can determine the total emitted flux for a given emission energy and a given emission angle in the CM frame. In practice, we rather decay from a initial bin to a residual bin in a given angular bin in the CM frame. If recoil effects are neglected we directly derive from such a decay an energy bin  $[E_{low}^{CM}, E_{up}^{CM}]$  and an angular bin  $[\Theta_{low}^{CM}, \Theta_{up}^{CM}]$  in which the total flux  $\Phi_{ej}^{CM}$  is emitted. Accounting for recoil effects requires an intermediate step to share the available energy  $\Delta E$  (difference between the energy bins of the initial nucleus and final nucleus) among the ejectile with mass  $m_{ej}$  and the residual nucleus with mass  $M_R$ .

To do this, we use the classical relation

$$(3.59) \quad \vec{v}_{ej}^{LAB} = \vec{v}_{cm} + \vec{v}_{ej}^{CM},$$

which connects the LAB velocity  $\vec{v}_{ej}^{LAB}$  of the ejectile with its velocity  $\vec{v}_{ej}^{CM}$  in the CM frame and the CM frame velocity  $\vec{v}_{cm}$ . We need to connect  $\vec{v}_{ej}^{CM}$  with  $\Delta E$ .

This can be done upon writing

$$(3.60) \quad \Delta E = \frac{1}{2}m_{ej}(\vec{v}_{ej}^{CM})^2 + \frac{1}{2}M_R(\vec{v}_R^{CM})^2,$$

where  $\vec{v}_R^{CM}$  is the residual nucleus velocity in the CM frame, and using the relation

$$(3.61) \quad m_{ej}\vec{v}_{ej}^{CM} + m_R\vec{v}_R^{CM} = \vec{0}.$$

Combining (3.60) and (3.61) yields

$$(3.62) \quad v_{ej}^{CM} = \sqrt{2\frac{M_R}{m_{ej}(m_{ej} + M_R)}\Delta E},$$

which reduces to the classical relation

$$(3.63) \quad v_{ej}^{CM} = \sqrt{\frac{2\Delta E}{m_{ej}}},$$

if recoil effects are neglected (i.e. in the limit  $M_R \rightarrow +\infty$ ).

Once this connection is established, Eq. (3.59) is used to determine the velocity and angle of both the emitted light particle and the residual nucleus by simple projections on the LAB axis.

Hence, given a decay situation in the CM frame, we can reconstruct both the energy and angle of emission in the LAB frame. We now have to determine the link between the double-differential decay characteristics in both frames. The solution is well known (see Ref. [7] for instance) and consists of using a Jacobian which accounts for the modification of an elementary solid angle  $d\Omega$  in the CM frame when going into the LAB frame. However, in TALYS we have to employ another method because we do not generally calculate decays for well defined energies and angles but rather for a given energy bin and angular bin. Moreover, since we do not account for the azimuthal angle, we may also encounter some problems when calculating recoil for secondary emission. Indeed, only the first binary process has the azimuthal symmetry with respect to the beam direction.

### 3.5.4 The recoil treatment in TALYS

The way the double-differential spectra are calculated by TALYS in the LAB frame from those obtained in the CM frame is illustrated in Fig. 3.6. As stressed in Chapter 3, the emission energy grid for the outgoing particles is non-equidistant. Moreover, one has to keep in mind that the total flux  $\Phi(i, j)$  in an energy-angular bin  $(i, j)$  is connected with the double differential cross section  $xs(i, j)$  by

$$(3.64) \quad \Phi(i, j) = xs(i, j)\Delta E(i)\Delta\cos\Theta(j).$$

Consequently, it is appropriate to locate the grid points using an energy-cosine grid. As an example, in Fig. 3.6, we consider the decay in the CM bin defined by the energy interval  $[2, 3]$  and the cosine interval

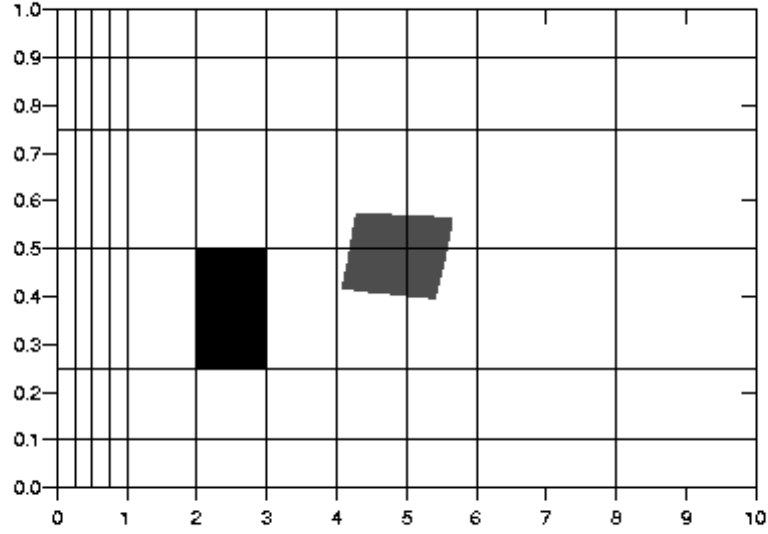


Figure 3.6: CM and LAB double-differential spectra in TALYS.

[0.25, 0.5] (black region). We assume that the decay occurs from a composite system moving with a kinetic energy of 1 MeV in the direction  $45^\circ$  with respect to the initial beam direction. The mass of the ejectile is assumed to be  $m_e = 1$  arb.unit, and that of the composite system 20 arb.unit. In that case, the region reached by the ejectile is a slightly deformed trapezoid (gray region) which covers several bins. Therefore, if the emitted flux is located in a single bin in the CM, it must be distributed over several bins when going to the LAB frame. This is the key problem to be solved in TALYS. To solve this problem, we need to make assumptions to be able (i) to calculate the area covered in the LAB frame (gray region) and (ii) the way this global area is distributed over the bins it partially covers. The assumption made in TALYS consists of neglecting the deformation of the boundaries of the grey area and assuming this area to be a trapezoid. In other words, we make the assumption that a triangle in the CM frame is transformed into a triangle when going in the LAB. This is helpful since the area of a triangle is given by a simple analytic expression as function of the coordinates of the summits of the triangle. Therefore, we divide the starting CM bins into two triangles to determine the two triangles obtained in the LAB frame. With such a method, the whole problem can be solved and the decay calculated in the CM frame can be transformed to the LAB frame without any further approximations.

However, in practice, coupling the angular direction (in the LAB) of the nucleus that decays with the ejectile emission angle in the CM frame, while neglecting the azimuthal angle, gives double differential ejectile spectra in the LAB which are generally not correct. In fact, we believe that it is better not to account for the angular distribution of the decaying nucleus unless both  $\Theta$  and  $\phi$  are explicitly treated. Fortunately, the final angular distribution of the recoiling nucleus is seldom of interest.

### 3.5.5 Method of average velocity

As mentioned above, we do not loop over the angular distribution of the decaying nucleus. This is equivalent to replacing the array  $P_{rec}(Z, N, E_i, E_r, \Theta_r)$  by  $P_{rec}(Z, N, E_i, E_r)$ . Then, we only have to keep track of the velocities of the nucleus that is going to decay, i.e. we have to loop over the  $E_r$  bins to reconstruct both the ejectile and residual nuclei spectra. Another approximation that we have implemented as an option (**recoilaverage y**) consists of using an average velocity before this reconstruction, a method first applied by Chadwick et al. [10, 11]. This approach avoids the loop over the  $E_r$  bins altogether and reduces the calculation time. However, for high energies, this might be too crude an approximation.

### 3.5.6 Approximative recoil correction for binary ejectile spectra

Maybe you are not interested in a full recoil calculation, but merely want to correct the outgoing particle spectra for the recoil of the nucleus. In that case you may use the following method which is implemented in TALYS for just that purpose and which is outlined below.

The assumptions are made that (i) only binary emission takes place, and that (ii) emission only occurs under  $0^\circ$ . Hence, this approximation is basically expected to be valid for angle-integrated spectra only. The CM to LAB conversion of the ejectile spectra takes under these conditions the following simple form:

$$(3.65) \quad E_{ej}^{lab} = \frac{M_R}{M_C} \Delta E + \frac{m_{ej} M_p}{M_C^2} E_p + 2 \sqrt{\frac{m_{ej} M_R M_p}{M_C^3} E_p \Delta E},$$

in which  $E_{ej}^{lab}$  is the LAB ejectile energy. This correction is applied to the *full* ejectile spectrum including the multiple emission contributions. Hence, the approximation is rather crude. It saves, however, a lot of computer time. Since the high-energy tail originates completely from binary emission, this tail is correctly converted to the LAB system. Furthermore, the correction is small at low energies where the largest contributions from multiple emission reside.



# Nuclear models

Fig. 4.1 gives an overview of the nuclear models that are included in TALYS. They can generally be categorized into optical, direct, pre-equilibrium, compound and fission models, all driven by a comprehensive database of nuclear structure and model parameters. We will first describe the optical model and the various models for direct reactions that are used. Next, we give an outline of the various pre-equilibrium models that are included. Then, we describe compound nucleus models for both binary and multiple emission, and level densities, which are important ingredients of pre-equilibrium and compound models. Finally, we give an outline of the fission models.

## 4.1 Optical model

The central assumption underlying the optical model is that the complicated interaction between an incident particle and a nucleus can be represented by a complex mean-field potential, which divides the reaction flux into a part covering shape elastic scattering and a part describing all competing non-elastic channels. Solving the Schrödinger equation numerically with this complex potential yields a wealth of valuable information. First, it returns a prediction for the basic observables, namely the elastic angular distribution and polarisation, the reaction and total cross section and, for low energies, the  $s, p$ -wave strength functions and the potential scattering radius  $R'$ . The essential value of a good optical model is that it can reliably predict these quantities for energies and nuclides for which no measurements exist. Also, the quality of the not directly observable quantities that are provided by the optical model has an equally important impact on the evaluation of the various reaction channels. Well-known examples are transmission coefficients, for compound nucleus and multi-step compound decay, and the distorted wave functions that are used for direct inelastic reactions and for transitions to the continuum that describe statistical multi-step direct reactions. Also, the reaction cross sections that are calculated with the optical model are crucial for the semi-classical pre-equilibrium models.

All optical model calculations are performed by ECIS-06 [6], which is used as a subroutine in TALYS.

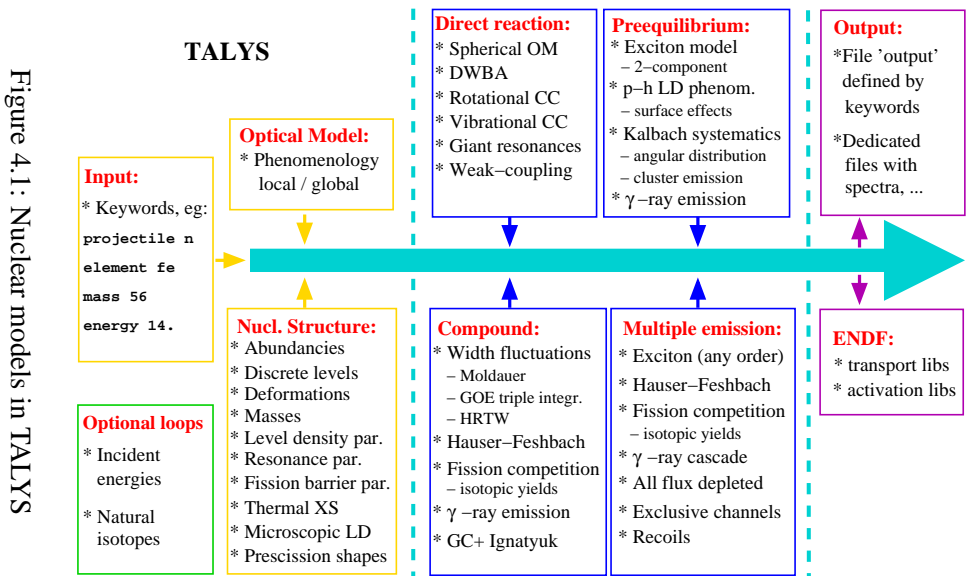


Figure 4.1: Nuclear models in TALYS

### 4.1.1 Spherical OMP: Neutrons and protons

The default optical model potentials (OMP) used in TALYS are the local and global parameterisations of Koning and Delaroche [182].

The phenomenological OMP for nucleon-nucleus scattering,  $\mathcal{U}$ , is defined as:

$$(4.1) \quad \begin{aligned} \mathcal{U}(r, E) = & -\mathcal{V}_V(r, E) - i\mathcal{W}_V(r, E) - i\mathcal{W}_D(r, E) \\ & + \mathcal{V}_{SO}(r, E) \cdot \mathbf{l} \cdot \boldsymbol{\sigma} + i\mathcal{W}_{SO}(r, E) \cdot \mathbf{l} \cdot \boldsymbol{\sigma} + \mathcal{V}_C(r), \end{aligned}$$

where  $\mathcal{V}_{V,SO}$  and  $\mathcal{W}_{V,D,SO}$  are the real and imaginary components of the volume-central ( $V$ ), surface-central ( $D$ ) and spin-orbit ( $SO$ ) potentials, respectively.  $E$  is the LAB energy of the incident particle in MeV. All components are separated in energy-dependent well depths,  $V_V, W_V, W_D, V_{SO}$ , and  $W_{SO}$ , and energy-independent radial parts  $f$ , namely

$$(4.2) \quad \begin{aligned} \mathcal{V}_V(r, E) &= V_V(E) f(r, R_V, a_V), \\ \mathcal{W}_V(r, E) &= W_V(E) f(r, R_V, a_V), \\ \mathcal{W}_D(r, E) &= -4a_D W_D(E) \frac{d}{dr} f(r, R_D, a_D), \\ \mathcal{V}_{SO}(r, E) &= V_{SO}(E) \left( \frac{\hbar}{m_\pi c} \right)^2 \frac{1}{r} \frac{d}{dr} f(r, R_{SO}, a_{SO}), \\ \mathcal{W}_{SO}(r, E) &= W_{SO}(E) \left( \frac{\hbar}{m_\pi c} \right)^2 \frac{1}{r} \frac{d}{dr} f(r, R_{SO}, a_{SO}). \end{aligned}$$

The form factor  $f(r, R_i, a_i)$  is a Woods-Saxon shape

$$(4.3) \quad f(r, R_i, a_i) = (1 + \exp[(r - R_i)/a_i])^{-1},$$

where the geometry parameters are the radius  $R_i = r_i A^{1/3}$ , with  $A$  being the atomic mass number, and the diffuseness parameters  $a_i$ . For charged projectiles, the Coulomb term  $\mathcal{V}_C$ , as usual, is given by that of a uniformly charged sphere

$$(4.4) \quad \begin{aligned} \mathcal{V}_C(r) &= \frac{Zze^2}{2R_C} \left( 3 - \frac{r^2}{R_C^2} \right), \quad \text{for } r \leq R_C \\ &= \frac{Zze^2}{r}, \quad \text{for } r \geq R_C, \end{aligned}$$

with  $Z(z)$  the charge of the target (projectile), and  $R_C = r_C A^{1/3}$  the Coulomb radius.

The functional forms for the potential depths depend on  $(E - E_f)$ , where  $E_f$ , the Fermi energy in MeV, is defined as the energy halfway between the last occupied and the first unoccupied shell of the nucleus. For incident neutrons,

$$(4.5) \quad E_f^n = -\frac{1}{2}[S_n(Z, N) + S_n(Z, N + 1)],$$

with  $S_n$  the neutron separation energy for a nucleus with proton number  $Z$  and neutron number  $N$ , while for incident protons

$$(4.6) \quad E_f^p = -\frac{1}{2}[S_p(Z, N) + S_p(Z + 1, N)],$$

with  $S_p$  the proton separation energy. We use the mass table of the nuclear structure database to obtain the values of the separation energies.

Our OMP parameterisation for either incident neutrons or protons is

$$\begin{aligned}
 V_V(E) &= v_1[1 - v_2(E - E_f) + v_3(E - E_f)^2 - v_4(E - E_f)^3] \\
 W_V(E) &= w_1 \frac{(E - E_f)^2}{(E - E_f)^2 + (w_2)^2} \\
 r_V &= \text{constant} \\
 a_V &= \text{constant} \\
 W_D(E) &= d_1 \frac{(E - E_f)^2}{(E - E_f)^2 + (d_3)^2} \exp[-d_2(E - E_f)] \\
 r_D &= \text{constant} \\
 a_D &= \text{constant} \\
 V_{SO}(E) &= v_{so1} \exp[-v_{so2}(E - E_f)] \\
 W_{SO}(E) &= w_{so1} \frac{(E - E_f)^2}{(E - E_f)^2 + (w_{so2})^2} \\
 r_{SO} &= \text{constant} \\
 a_{SO} &= \text{constant} \\
 (4.7) \quad r_C &= \text{constant,}
 \end{aligned}$$

where  $E_f = E_f^n$  for incident neutrons and  $E_f = E_f^p$  for incident protons. Here  $E$  is the incident energy in the LAB system. This representation is valid for incident energies from 1 keV up to 200 MeV. Note that  $V_V$  and  $W_V$  share the same geometry parameters  $r_V$  and  $a_V$ , and likewise for the spin-orbit terms.

In general, all parameters appearing in Eq. (4.7) differ from nucleus to nucleus. When enough experimental scattering data of a certain nucleus is available, a so called local OMP can be constructed. TALYS retrieves all the parameters  $v_1, v_2$ , etc. of these local OMPs automatically from the nuclear structure and model parameter database, see the next Chapter, which contains the same information as the various tables of Ref. [182]. If a local OMP parameterisation is not available in the database, the built-in global optical models are automatically used, which can be applied for any  $Z, A$  combination. A flag exists (the **localomp** keyword) to overrule the local OMP by the global OMP. The global neutron

OMP, validated for  $0.001 \leq E \leq 200$  MeV and  $24 \leq A \leq 209$ , is given by

$$\begin{aligned}
V_V(E) &= v_1^n [1 - v_2^n (E - E_f^n) + v_3^n (E - E_f^n)^2 - v_4^n (E - E_f^n)^3] \\
W_V(E) &= w_1^n \frac{(E - E_f^n)^2}{(E - E_f^n)^2 + (w_2^n)^2} \\
r_V &= 1.3039 - 0.4054A^{-1/3} \\
a_V &= 0.6778 - 1.487 \cdot 10^{-4} A \\
W_D(E) &= d_1^n \frac{(E - E_f^n)^2}{(E - E_f^n)^2 + (d_3^n)^2} \exp[-d_2^n (E - E_f^n)] \\
r_D &= 1.3424 - 0.01585A^{1/3} \\
a_D &= 0.5446 - 1.656 \cdot 10^{-4} A \\
V_{SO}(E) &= v_{so1}^n \exp[-v_{so2}^n (E - E_f^n)] \\
W_{SO}(E) &= w_{so1}^n \frac{(E - E_f^n)^2}{(E - E_f^n)^2 + (w_{so2}^n)^2} \\
r_{SO} &= 1.1854 - 0.647A^{-1/3} \\
a_{SO} &= 0.59,
\end{aligned} \tag{4.8}$$

where the units are in fm and MeV and the parameters for the potential depths and  $E_f^n$  are given in Table 4.1.

The global proton OMP is given by

$$\begin{aligned}
V_V(E) &= v_1^p [1 - v_2^p (E - E_f^p) + v_3^p (E - E_f^p)^2 - v_4^p (E - E_f^p)^3] \\
&\quad + \bar{V}_C \cdot v_1^p \left[ v_2^p - 2v_3^p (E - E_f^p) + 3v_4^p (E - E_f^p)^2 \right] \\
W_V(E) &= w_1^p \frac{(E - E_f^p)^2}{(E - E_f^p)^2 + (w_2^p)^2} \\
r_V &= 1.3039 - 0.4054A^{-1/3} \\
a_V &= 0.6778 - 1.487 \cdot 10^{-4} A \\
W_D(E) &= d_1^p \frac{(E - E_f^p)^2}{(E - E_f^p)^2 + (d_3^p)^2} \exp[-d_2^p (E - E_f^p)] \\
r_D &= 1.3424 - 0.01585A^{1/3} \\
a_D &= 0.5187 + 5.205 \cdot 10^{-4} A \\
V_{SO}(E) &= v_{so1}^p \exp[-v_{so2}^p (E - E_f^p)] \\
W_{SO}(E) &= w_{so1}^p \frac{(E - E_f^p)^2}{(E - E_f^p)^2 + (w_{so2}^p)^2} \\
r_{SO} &= 1.1854 - 0.647A^{-1/3} \\
a_{SO} &= 0.59 \\
r_C &= 1.198 + 0.697A^{-2/3} + 12.994A^{-5/3},
\end{aligned} \tag{4.9}$$

$v_1^n$	$= 59.30 - 21.0(N - Z)/A - 0.024A$	MeV
$v_2^n$	$= 0.007228 - 1.48.10^{-6}A$	MeV <sup>-1</sup>
$v_3^n$	$= 1.994.10^{-5} - 2.0.10^{-8}A$	MeV <sup>-2</sup>
$v_4^n$	$= 7.10^{-9}$	MeV <sup>-3</sup>
$w_1^n$	$= 12.195 + 0.0167A$	MeV
$w_2^n$	$= 73.55 + 0.0795A$	MeV
$d_1^n$	$= 16.0 - 16.0(N - Z)/A$	MeV
$d_2^n$	$= 0.0180 + 0.003802/(1 + \exp[(A - 156.)/8.])$	MeV <sup>-1</sup>
$d_3^n$	$= 11.5$	MeV
$v_{so1}^n$	$= 5.922 + 0.0030A$	MeV
$v_{so2}^n$	$= 0.0040$	MeV <sup>-1</sup>
$w_{so1}^n$	$= -3.1$	MeV
$w_{so2}^n$	$= 160.$	MeV
$E_f^n$	$= -11.2814 + 0.02646A$	MeV

Table 4.1: Potential depth parameters and Fermi energy for the neutron global OMP of Eq. (4.8).

where the parameters for the potential depths,  $\bar{V}_C$  and  $E_f^p$  are given in Table 4.2. The functional form of the proton global OMP differs from the neutron global OMP only by the Coulomb correction term in  $V_V(E)$ .

The spherical optical model described above provides the transmission coefficients, DWBA cross sections, total and elastic cross sections, etc., mentioned in the beginning of this section. For deformed nuclides, strongly coupled collective levels need to be included. This will be explained in Section 4.2 on direct reactions.

All optical model parameters mentioned in this Section can be adjusted, not only by means of a local parameter file (see the **optmodfileN** keyword), but also via adjustable parameters through the **v1adjust**, **v2adjust** etc. keywords, with which the standard values can be multiplied. Even energy-dependent adjustment of the geometry is possible as a last resort to fit data, using the **rvadjustF**, etc. keywords.

### Extension to 1 GeV

To be able to predict the total, elastic and non-elastic cross sections up to 1 GeV, the OMP described above has been extended [12]. It is emphasized here that this was just done to test at which energy the validity of TALYS in predicting other (residual) cross section will fail. We are well aware of the fact that the usual Schrödinger picture of the OMP is valid up to about 180 MeV, and should then be taken over by a Dirac approach. Nevertheless, a functional form was be constructed which leaves all KD03 parameter values below a joining energy  $E_J$ , at or around 200 MeV, unaltered while smoothly extending the energy dependence above  $E_J$ . This was only applied to the real,  $V_V$ , and imaginary,  $W_V$ , volume parts of the

$v_1^p$	$= 59.30 + 21.0(N - Z)/A - 0.024A$	MeV
$v_2^p$	$= 0.007067 + 4.23 \cdot 10^{-6} A$	MeV <sup>-1</sup>
$v_3^p$	$= 1.729 \cdot 10^{-5} + 1.136 \cdot 10^{-8} A$	MeV <sup>-2</sup>
$v_4^p$	$= v_4^n$	MeV <sup>-3</sup>
$w_1^p$	$= 14.667 + 0.009629A$	MeV
$w_2^p$	$= w_2^n$	MeV
$d_1^p$	$= 16.0 + 16.0(N - Z)/A$	MeV
$d_2^p$	$= d_2^n$	MeV <sup>-1</sup>
$d_3^p$	$= d_3^n$	MeV
$v_{so1}^p$	$= v_{so1}^n$	MeV
$v_{so2}^p$	$= v_{so2}^n$	MeV <sup>-1</sup>
$w_{so1}^p$	$= w_{so1}^n$	MeV
$w_{so2}^p$	$= w_{so2}^n$	MeV
$E_f^p$	$= -8.4075 + 0.01378A$	MeV
$\bar{V}_C$	$= 1.73 \cdot Z \cdot A^{-1/3} / r_C$	MeV

Table 4.2: Potential depth parameters and Fermi energy for the proton global OMP of Eq. (4.9). The parameter values for neutrons are given in Table 4.1.  $\bar{V}_C$  appears in the Coulomb correction term  $\Delta V_C(E)$ , of the real central potential.

potential. For that, the KD03 OMP for neutrons below  $E_J$  reads [182],

$$\begin{aligned}
 V_V(E) &= v_1^n [1 - v_2^n (E - E_f^n) + v_3^n (E - E_f^n)^2 - \\
 &\quad v_4^n (E - E_f^n)^3] \\
 W_V(E) &= w_1^n \frac{(E - E_f^n)^2}{(E - E_f^n)^2 + (w_2^n)^2},
 \end{aligned}$$

(4.10)

where  $E_f^n$  is the Fermi energy. For  $V_V$ , we assume that the exponential decrease should continue beyond  $E_J$ . After all, the KD03 form of Eq. (4.10) for  $V_V$  is just a Taylor expansion of the exponential function, in which we gave ourselves the freedom to alter the individual coefficients  $v_1$ , etc. Also, following studies like [13, 14], we assume that it converges to a negative value  $V_\infty$ . Hence, the form chosen for  $E > E_J$  is

$$(4.11) \quad V_V(E) = V_\infty + b \cdot \exp(-c(E - E_f^n)).$$

We determine the new parameters  $b$  and  $c$  by calculating the value at  $E = E_f^n$ , giving

$$(4.12) \quad b = V_V(E_f^n) - V_\infty.$$

Hence,

$$(4.13) \quad V_V(E) = V_\infty + (V_V(E_f^n) - V_\infty) \exp(-c(E - E_f^n)).$$

Next,  $c$  can be determined by requiring that the high-energy potential is equal to that of the low energy expression Eq. (4.10) at the joining energy:

$$(4.14) \quad V_V(E_J) = V_\infty + (V_V(E_f^n) - V_\infty) \exp(-c(E_J - E_f^n)),$$

giving

$$(4.15) \quad c = -\frac{1}{(E_J - E_f^n)} \log\left(\frac{V_V(E_J) - V_\infty}{V_V(E_f^n) - V_\infty}\right).$$

For  $W_V$  it is expected that at high energies new absorption channels, such as pion production, emerge and that  $W_V$  will show another smooth increase as function of energy. Hence, the form of  $W_V$  for  $E > E_J$  is

$$(4.16) \quad W_V(E) = w_3^n \frac{(E - E_f^n)^4}{(E - E_f^n)^4 + (w_4^n)^4} + d,$$

where we find that a power of 4, instead of the usual 2, gives a better description of experimental data. Also here, a parameter  $d$  was added to ensure a value exactly equal to KD03 at  $E_J$ , i.e. at  $E = E_J$  we have

$$(4.17) \quad d = W_V(E_J) - w_3^n \frac{(E_J - E_f^n)^4}{(E_J - E_f^n)^4 + (w_4^n)^4}$$

In sum, we have the following simple extension of the KD03 OMP for  $E > E_J$ :

$$(4.18) \quad \begin{aligned} V_V(E) &= V_\infty + (V_V(E_f^n) - V_\infty) \\ &\quad * \exp\left(\frac{E - E_f^n}{E_J - E_f^n} * \log\left(\frac{V_V(E_J) - V_\infty}{V_V(E_f^n) - V_\infty}\right)\right) \\ W_V(E) &= W_V(E_J) - w_3^n \frac{(E_J - E_f^n)^4}{(E_J - E_f^n)^4 + (w_4^n)^4} \\ &\quad + w_3^n \frac{(E - E_f^n)^4}{(E - E_f^n)^4 + (w_4^n)^4} \end{aligned}$$

which joins smoothly with the KD03 expression of Eq. (4.10) for  $E < E_J$ . The following, preliminary, values were obtained from a fit to neutron total and proton non-elastic cross sections up to 1 GeV:

$$(4.19) \quad \begin{aligned} E_J &= 200. \\ V_\infty &= -30. \\ w_3^n &= 25. - 0.0417A \\ w_4^n &= 250. \end{aligned}$$

All parameters can be adjusted with keywords. In Eq. (4.18),  $V_V(E_f)$ ,  $V_V(E_J)$  and  $W_V(E_J)$  are obtained from Eq. (4.10). The above extension, and parameters, also hold for incident protons.

### 4.1.2 Spherical dispersive OMP: Neutrons

The theory of the nuclear optical model can be reformulated in terms of dispersion relations that connect the real and imaginary parts of the optical potential, and we have added an option in TALYS to take them into account. These dispersion relations are a natural result of the causality principle that a scattered wave cannot be emitted before the arrival of the incident wave. The dispersion component stems directly from the absorptive part of the potential,

$$(4.20) \quad \Delta\mathcal{V}(r, E) = \frac{\mathcal{P}}{\pi} \int_{-\infty}^{\infty} \frac{\mathcal{W}(r, E')}{E' - E} dE',$$

where  $\mathcal{P}$  denotes the principal value. The total real central potential can be written as the sum of a Hartree-Fock term  $\mathcal{V}_{HF}(r, E)$  and the total dispersion potential  $\Delta\mathcal{V}(r, E)$

$$(4.21) \quad \mathcal{V}(r, E) = \mathcal{V}_{HF}(r, E) + \Delta\mathcal{V}(r, E).$$

Since  $\mathcal{W}(r, E)$  has a volume and a surface component, the dispersive addition is,

$$(4.22) \quad \begin{aligned} \Delta\mathcal{V}(r, E) &= \Delta\mathcal{V}_V(r, E) + \Delta\mathcal{V}_D(r, E) \\ &= \Delta V_V(E) f(r, R_V, a_V) - 4a_D \Delta V_D(E) \frac{d}{dr} f(r, R_D, a_D) \end{aligned}$$

where the volume dispersion term is given by

$$(4.23) \quad \Delta V_V(E) = \frac{\mathcal{P}}{\pi} \int_{-\infty}^{\infty} \frac{W_V(E')}{E' - E} dE',$$

and the surface dispersion term is given by

$$(4.24) \quad \Delta V_D(E) = \frac{\mathcal{P}}{\pi} \int_{-\infty}^{\infty} \frac{W_D(E')}{E' - E} dE'.$$

Hence, the real volume well depth of Eq. (4.2) becomes

$$(4.25) \quad V_V(E) = V_{HF}(E) + \Delta V_V(E),$$

and the real surface well depth is

$$(4.26) \quad V_D(E) = \Delta V_D(E).$$

In general, Eqs. (4.23)-(4.24) cannot be solved analytically. However, under certain plausible conditions, analytical solutions exist. Under the assumption that the imaginary potential is symmetric with respect to the Fermi energy  $E_F$ ,

$$(4.27) \quad W(E_F - E) = W(E_F + E),$$

where  $W$  denotes either the volume or surface term, we can rewrite the dispersion relation as,

$$(4.28) \quad \Delta V(E) = \frac{2}{\pi} (E - E_F) \mathcal{P} \int_{E_F}^{\infty} \frac{W(E')}{(E' - E_F)^2 - (E - E_F)^2} dE',$$

from which it easily follows that  $\Delta V(E)$  is skew-symmetric around  $E_F$ ,

$$(4.29) \quad \Delta V(E + E_F) = -\Delta V(E - E_F),$$

and hence  $\Delta V(E_F) = 0$ . This can then be used to rewrite Eq. (4.20) as

$$(4.30) \quad \begin{aligned} \Delta V(E) &= \Delta V(E) - \Delta V(E_F) \\ &= \frac{\mathcal{P}}{\pi} \int_{-\infty}^{\infty} W(E') \left( \frac{1}{E' - E} - \frac{1}{E' - E_F} \right) dE' \\ &= \frac{E - E_F}{\pi} \int_{-\infty}^{\infty} \frac{W(E')}{(E' - E)(E' - E_F)} dE'. \end{aligned}$$

For the Hartree-Fock term we adopt the usual form for  $V_V(E)$  given in Eq. (4.7). The dispersion integrals for the functions for absorption can be calculated analytically and are included as options in ECIS-06. This makes the use of a dispersive optical model parameterization completely equivalent to that of a non-dispersive OMP: the dispersive contributions are calculated automatically once the OMP parameters are given. Upon comparison with a nondispersive parameterization, we find that  $v_1$  is rather different (as expected) and that  $r_V, a_V, v_2, v_3, w_1$  and  $w_2$  are slightly different. We have included dispersive spherical neutron OMP parameterization for about 70 nuclides (unpublished). They can be used with the keyword **dispersion y**.

### 4.1.3 Spherical OMP: Complex particles

For deuterons, tritons, Helium-3 and alpha particles, we use a simplification of the folding approach of Watanabe [15], see Ref. [16]. We take the nucleon OMPs described in the previous section, either local or global, as the basis for these complex particle potentials.

#### Deuterons

For deuterons, the real central potential depth at incident energy  $E$  is

$$(4.31) \quad V_V^{deuteron}(E) = V_V^{neutron}(E/2) + V_V^{proton}(E/2),$$

and similarly for  $W_V$  and  $W_D$ . For the spin-orbit potential depth we have

$$(4.32) \quad V_{SO}^{deuteron}(E) = (V_{SO}^{neutron}(E) + V_{SO}^{proton}(E))/2,$$

and similarly for  $W_{SO}$ . For the radius and diffuseness parameter of the real central potential we have

$$(4.33) \quad \begin{aligned} r_V^{deuteron} &= (r_V^{neutron} + r_V^{proton})/2, \\ a_V^{deuteron} &= (a_V^{neutron} + a_V^{proton})/2, \end{aligned}$$

and similarly for the geometry parameters of the other potentials.

Note that several of these formulae are somewhat more general than necessary, since the nucleon potentials mostly have geometry parameters, and also potential depths such as  $V_{SO}$ , which are equal for

neutrons and protons ( $a_D$  is an exception). The general formulae above have been implemented to also account for other potentials, if necessary.

We are well aware of the fact that others have constructed specific potentials for deuterons that may outperform the Watanabe-type potential described here. Therefore, we have also added the deuteron potentials of Daehnick et al. [17], Bojowald et al.[18], Han et al.[19], and Haixia An et al.[20] as options.

### Tritons

For tritons, the real central potential depth at incident energy  $E$  is

$$(4.34) \quad V_V^{triton}(E) = 2V_V^{neutron}(E/3) + V_V^{proton}(E/3),$$

and similarly for  $W_V$  and  $W_D$ . For the spin-orbit potential depth we have

$$(4.35) \quad V_{SO}^{triton}(E) = (V_{SO}^{neutron}(E) + V_{SO}^{proton}(E))/6,$$

and similarly for  $W_{SO}$ . For the radius and diffuseness parameter of the real central potential we have

$$(4.36) \quad \begin{aligned} r_V^{triton} &= (2r_V^{neutron} + r_V^{proton})/3, \\ a_V^{triton} &= (2a_V^{neutron} + a_V^{proton})/3, \end{aligned}$$

and similarly for the geometry parameters of the other potentials.

### Helium-3

For Helium-3, the real central potential depth at incident energy  $E$  is

$$(4.37) \quad V_V^{Helium-3}(E) = V_V^{neutron}(E/3) + 2V_V^{proton}(E/3),$$

and similarly for  $W_V$  and  $W_D$ . For the spin-orbit potential depth we have

$$(4.38) \quad V_{SO}^{Helium-3}(E) = (V_{SO}^{neutron}(E) + V_{SO}^{proton}(E))/6,$$

and similarly for  $W_{SO}$ . For the radius and diffuseness parameter of the real central potential we have

$$(4.39) \quad \begin{aligned} r_V^{Helium-3} &= (r_V^{neutron} + 2r_V^{proton})/3, \\ a_V^{Helium-3} &= (a_V^{neutron} + 2a_V^{proton})/3, \end{aligned}$$

and similarly for the geometry parameters of the other potentials.

### Alpha particles

For alpha's, the real central potential depth at incident energy  $E$  is

$$(4.40) \quad V_V^{alphas}(E) = 2V_V^{neutron}(E/4) + 2V_V^{proton}(E/4),$$

and similarly for  $W_V$  and  $W_D$ . For the spin-orbit potential depth we have

$$(4.41) \quad V_{SO}^{alphas}(E) = W_{SO}^{alphas}(E) = 0.$$

For the radius and diffuseness parameter of the real central potential we have

$$(4.42) \quad \begin{aligned} r_V^{alphas} &= (r_V^{neutron} + r_V^{proton})/2, \\ a_V^{alphas} &= (a_V^{neutron} + a_V^{proton})/2, \end{aligned}$$

and similarly for the geometry parameters of the other potentials.

As extra options the alpha potentials by McFadden and Satchler [21] and Demetriou et al [22] are available.

All optical model parameters for complex particles can be altered via adjustable parameters through the **v1adjust**, **rvadjust** etc. keywords, with which the standard values can be multiplied. Also local energy-dependent adjustment of the geometry is possible as a last resort to fit data, using the **rvadjustF**, etc. keywords.

#### 4.1.4 Semi-microscopic optical model (JLM)

Besides the phenomenological OMP, it is also possible to perform TALYS calculations with the semi-microscopic nucleon-nucleus spherical optical model potential as described in [28]. We have implemented Eric Bauge's MOM code [163] as a subroutine to perform so called Jeukenne-Lejeune-Mahaux (JLM) OMP calculations. The optical model potential of [28] and its extension to deformed and unstable nuclei has been widely tested [28, 29, 30, 31, 32] and produces predictions from  $A=30$  to 240 and for energies ranging from 10 keV up to 200 MeV. MOM stands for "Modèle Optique Microscopique" in French, or "Microscopic Optical Model" in English. In this version of TALYS, only spherical JLM OMP's are included.

The MOM module reads the radial matter densities from the nuclear structure database and performs the folding of the Nuclear Matter (NM) optical model potential described in [28] with the densities to obtain a local OMP. This is then put in the ECIS-06 routine to compute observables by solving the Schrödinger equation for the interaction of the projectile with the aforementioned OMP. The OMP's are calculated by folding the target radial matter density with an OMP in nuclear matter based on the Brückner-Hartree-Fock work of Jeukenne, Lejeune and Mahaux [33, 34, 35, 36]. This NM OMP was then phenomenologically altered in [28, 37] in order to improve the agreement of predicted finite nuclei observables with a large set of experimental data. These improvements consist in unifying the low and high energy parameterizations of the NM interaction in [37], and in studying the energy variations of the potential depth normalization factors in [28]. These factors now include non-negligible normalizations of isovector components [28] that are needed in order to account simultaneously for (p,p) and (n,n) elastic scattering as well as (p,n)<sub>IAS</sub> quasi-elastic scattering. The final NM potential for a given nuclear matter density  $\rho = \rho_n - \rho_p$  and asymmetry  $\alpha = (\rho_n + \rho_p)/\rho$  reads

$$(4.43) \quad U_{NM}(E)_{\rho,\alpha} = \lambda_V(E) \left[ V_0(\tilde{E}) \pm \lambda_{V1}(E)\alpha V_1(\tilde{E}) \right] + i\lambda_W(E) \left[ W_0(\tilde{E}) \pm \lambda_{W1}(E)\alpha W_1(\tilde{E}) \right],$$

with  $E$  the incident nucleon energy,  $\tilde{E} = E - V_c$  (where  $V_c$  is the Coulomb field),  $V_0$ ,  $V_1$ ,  $W_0$ , and  $W_1$  the real isoscalar, real isovector, imaginary isoscalar, and imaginary isovector NM OMP components respectively, and  $\lambda_V$ ,  $\lambda_{V1}$ ,  $\lambda_W$ , and  $\lambda_{W1}$  the real (isoscalar+isovector), real isovector, imaginary, and imaginary isovector normalization factors respectively. The values of  $\lambda_V$ ,  $\lambda_{V1}$ ,  $\lambda_W$ , and  $\lambda_{W1}$  given in [28] read

$$(4.44) \quad \lambda_V(E) = 0.951 + 0.0008 \ln(1000E) + 0.00018 [\ln(1000E)]^2$$

$$(4.45) \quad \lambda_W(E) = \left[ 1.24 - \left[ 1 + e^{\left(\frac{E-4.5}{2.9}\right)} \right]^{-1} \right] \left[ 1 + 0.06 e^{-\left(\frac{E-14}{3.7}\right)^2} \right] \times \left[ 1 - 0.09 e^{-\left(\frac{E-80}{78}\right)^2} \right] \left[ 1 + \left( \frac{E-80}{400} \right) \Theta(E-80) \right]$$

$$(4.46) \quad \lambda_{V1}(E) = 1.5 - 0.65 \left[ 1 + e^{\frac{E-1.3}{3}} \right]^{-1}$$

$$(4.47) \quad \lambda_{W1}(E) = \left[ 1.1 + 0.44 \left[ 1 + \left( e^{\frac{E-40}{50.9}} \right)^4 \right]^{-1} \right] \times \left[ 1 - 0.065 e^{-\left(\frac{E-40}{13}\right)^2} \right] \left[ 1 - 0.083 e^{-\left(\frac{E-200}{80}\right)^2} \right].$$

with the energy  $E$  expressed in MeV. As stated in [28], in the 20 to 50 MeV range, the uncertainties related to  $\lambda_V$ ,  $\lambda_{V1}$ ,  $\lambda_W$ , and  $\lambda_{W1}$  are estimated to be 1.5%, 10%, 10%, and 10%, respectively. Outside this energy range, uncertainties are estimated to be 1.5 times larger.

In order to apply the NM OMP to finite nuclei an approximation had to be performed. This is the Local Density Approximation (LDA) where the local value of the finite nucleus OMP is taken to be the NM OMP value for the local finite nucleus density:  $U_{FN}(r) = U_{NM}(\rho(r))$ . Since this LDA produces potentials with too small rms radii, the improved LDA, which broadens the OMP with a Gaussian form factor (4.48), is introduced. In [37, 28] different prescriptions for the improved Local Density approximation are compared and LDA range parameters are optimized.

$$(4.48) \quad U_{FN}(r, E) = (t\sqrt{\pi})^{-3} \int \frac{U_{NM}(\rho(r'), E)}{\rho(r')} \exp(-|\vec{r} - \vec{r}'|^2/t_r^2) \rho(r') d\vec{r}',$$

with  $t$  the range of the Gaussian form factor. The  $t_r = 1.25$  fm and  $t_i = 1.35$  fm values were found [28] to be global optimal values for the real and imaginary ranges, respectively.

Finally, since no spin-orbit (SO) potential exists between a nucleon and NM, the Scheerbaum [38] prescription was selected in [37], coupled with the phenomenological complex potential depths  $\lambda_{v_{so}}$ , and  $\lambda_{w_{so}}$ . The SO potential reads

$$(4.49) \quad U_{n(p)}^{so}(r) = (\lambda_{v_{so}}(E) + i\lambda_{w_{so}}(E)) \frac{1}{r} \frac{d}{dr} \left( \frac{2}{3}\rho_p(n) + \frac{1}{3}\rho_n(p) \right),$$

with

$$(4.50) \quad \lambda_{v_{so}} = 130 \exp(-0.013 E) + 40$$

and

$$(4.51) \quad \lambda_{w_{so}} = -0.2 (E - 20).$$

All JLM OMP parameters can be altered via adjustable parameters through the **lvadjust**, **lwadjust** etc. keywords, with which the standard values can be multiplied.

### 4.1.5 Systematics for non-elastic cross sections

Since the reaction cross sections for complex particles as predicted by the OMP have not been tested and rely on a relatively simple folding model, we added a possibility to estimate the non-elastic cross sections from empirical expressions. The adopted *tripathi.f* subroutine that provides this does not coincide with the published expression as given by Tripathi et al. [39], but checking our results with the published figures of Ref. [39] made us decide to adopt this empirical model as an option. We sometimes use it for deuterons up to alpha-particles. A high-quality OMP for complex particles would make this option redundant.

## 4.2 Direct reactions

Various models for direct reactions are included in the program: DWBA for (near-)spherical nuclides, coupled-channels for deformed nuclides, the weak-coupling model for odd nuclei, and also a giant resonance contribution in the continuum. In all cases, TALYS drives the ECIS-06 code to perform the calculations. The results are presented as discrete state cross sections and angular distributions, or as contributions to the continuum.

### 4.2.1 Deformed nuclei: Coupled-channels

The formalism outlined in the previous section works, theoretically, for nuclides which are spherical and, in practice, for nuclides which are not too strongly deformed. In general, however, the more general

coupled-channels method should be invoked to describe simultaneously the elastic scattering channel and the low-lying states which are, due to their collective nature, strongly excited in inelastic scattering. These collective excitations can be described as the result of static or dynamic deformations, which cause the homogeneous neutron-proton fluid to rotate or vibrate. The associated deformation parameters can be predicted from a (semi-)microscopic model or can be derived from an analysis of the experimental angular distributions.

The coupled-channels formalism for scattering and reaction studies is well known and will not be described in this manual. For a detailed presentation, we refer to Ref. [40]. We will only state the main aspects here to put the formalism into practice. Refs. [41] and [42] have been used as guidance. In general various different channels, usually the ground state and several inelastic states, are included in a coupling scheme while the associated coupled equations are solved. In ECIS-06, this is done in a so called sequential iterative approach [6]. Besides Ref. [6], Ref. [43] is also recommended for more insight in the use of the ECIS code.

Various collective models for deformed nuclei exist. Note that the spherical optical model of Eq. (4.2) is described in terms of the nuclear radius  $R_i = r_i A^{1/3}$ . For deformed nuclei, this expression is generalized to include collective motions. Various models have been implemented in ECIS-06, which enables us to cover many nuclides of interest. We will describe the ones that can be invoked by TALYS. The collective models are automatically applied upon reading the deformation parameter database, see Section 5.5.

### Symmetric rotational model

In the symmetric rotational model, the radii of the different terms of the OMP are expressed as

$$(4.52) \quad R_i = r_i A^{1/3} \left[ 1 + \sum_{\lambda=2,4,\dots} \beta_\lambda Y_\lambda^0(\Omega) \right],$$

where the  $\beta_\lambda$ 's are permanent, static deformation parameters, and the  $Y$  functions are spherical harmonics. The quadrupole deformation  $\beta_2$  plays a leading role in the interaction process. Higher order deformations  $\beta_\lambda$  (with  $\lambda = 4, 6, \dots$ ) are systematically smaller in magnitude than  $\beta_2$ . The inclusion of  $\beta_4$  and  $\beta_6$  deformations in coupled-channels calculations produces changes in the predicted observables, but in general, only  $\beta_2$  and  $\beta_4$  are important in describing inelastic scattering to the first few levels in a rotational band. For even-even nuclides like  $^{184}\text{W}$  and  $^{232}\text{Th}$ , the symmetric rotational model provides a good description of the lowest  $0^+, 2^+, 4^+$  (and often  $6^+, 8^+$ , etc.) rotational band. The nuclear model and parameter database of TALYS specifies whether a rotational model can be used for a particular nucleus, together with the included levels and deformation parameters. Either a deformation parameter  $\beta_\lambda$  or a deformation length  $\delta_\lambda = \beta_\lambda r_i A^{1/3}$  may be given. The latter one is generally recommended since it has more physical meaning than  $\beta_\lambda$  and should not depend on incident energy (while  $r_i$  may, in some optical models, depend on energy). We take  $\delta_\lambda$  equal for the three OMP components  $V_V, W_V$  and  $W_D$  and take the spin-orbit potential undeformed. The same holds for the vibrational and other collective models.

By default, TALYS uses the global optical model by Soukhovitskii et al. [44] for actinides. For

rotational non-fissile nuclides, if no specific potential is specified through one of the various input methods, we take our local or global spherical potential and subtract 15% from the imaginary surface potential parameter  $d_1$ , if rotational or vibrational levels are included in the coupling scheme.

### Harmonic vibrational model

A vibrational nucleus possesses a spherically symmetric ground state. Its excited states undergo shape oscillations about the spherical equilibrium model. In the harmonic vibrational model, the radii of the different terms of the OMP are expressed as

$$(4.53) \quad R_i = r_i A^{1/3} \left[ 1 + \sum_{\lambda\mu} \alpha_{\lambda\mu} Y_{\lambda}^{\mu}(\Omega) \right],$$

where the  $\alpha_{\lambda\mu}$  operators can be related to the coupling strengths  $\beta_{\lambda}$ , describing the vibration amplitude with multipolarity  $\lambda$ . Expanding the OMP to first or second order with this radius gives the OMP expressions for the excitation of one-phonon (first order vibrational model) and two-phonon (second order vibrational model) states [6]. For vibrational nuclei, the minimum number of states to couple is two. For even-even nuclei, we generally use the  $(0^+, 2^+)$  coupling, where the  $2^+$  level is a one-quadrupole phonon excitation. The level scheme of a vibrational nucleus (e.g.  $^{110}\text{Pd}$ ) often consists of a one-phonon state ( $2^+$ ) followed by a  $(0^+, 2^+, 4^+)$  triplet of two-phonon states. When this occurs, all levels are included in the coupling scheme with the associated deformation length  $\delta_2$  (or deformation parameter  $\beta_2$ ). If the  $3^-$  and  $5^-$  states are strongly collective excitations, that is when  $\beta_3$  and  $\beta_5$  are larger than 0.1, these levels may also be included in the coupling scheme. An example is  $^{120}\text{Sn}$  [45], where the low lying  $(0^+, 2^+, 3^-, 4^+, 5^-)$  states can all be included as one-phonon states in a single coupling scheme.

Again, if no specific potential is specified through one of the various input methods, we take our local or global spherical potential and subtract 15% from the imaginary surface potential parameter  $d_1$ .

### Vibration-rotational model

For certain nuclides, the level scheme consists not only of one or more rotational bands, but also of one or more vibrational bands that can be included in the coupling scheme. An example is  $^{238}\text{U}$ , where many vibrational bands can be coupled. In Chapter 5 on nuclear model parameters, it is explained how such calculations are automatically performed by TALYS. Depending on the number of levels included, the calculations can be time-consuming.

### Asymmetric rotational model

In the asymmetric rotational model, in addition to the spheroidal equilibrium deformation, the nucleus can oscillate such that ellipsoidal shapes are produced. In this model the nucleus has rotational bands built on the statically deformed ground state and on the  $\gamma$ -vibrational state. The radius is now angular

dependent,

$$(4.54) \quad R_i(\Theta) = r_i A^{1/3} \left[ 1 + \beta_2 \cos \gamma Y_2^0(\Omega) + \sqrt{\frac{1}{2}} \beta_2 \sin \gamma (Y_2^2(\Omega) + Y_2^{-2}(\Omega)) + \beta_4 Y_4^0(\Omega) \right],$$

where we restrict ourselves to a few terms. The deformation parameters  $\beta_2$ ,  $\beta_4$  and  $\gamma$  need to be specified.  $^{24}\text{Mg}$  is an example of a nucleus that can be analyzed with the asymmetric rotational model. Mixing between bands is not yet automated as an option in TALYS.

### 4.2.2 Distorted Wave Born Approximation

The Distorted Wave Born Approximation (DWBA) is only valid for small deformations. Until the advent of the more general coupled-channels formalism, it was the commonly used method to describe inelastic scattering, for both weakly and strongly coupled levels. Nowadays, we see DWBA as a first order vibrational model for small deformation, with only a single iteration to be performed for the coupled-channels solution. (See, however Satchler [46] for the exact difference between this so called distorted wave method and DWBA). The interaction between the projectile and the target nucleus is modeled by the derivative of the OMP for elastic scattering times a strength parameter. The latter, the deformation parameter  $\beta_\lambda$ , is then often used to vary the overall magnitude of the cross section (which is proportional to  $\beta_\lambda^2$ ).

In TALYS, we use DWBA

- (a) if a deformed OMP is not available. This applies for the spherical OMPs mentioned in the previous Section, which are all based on elastic scattering observables only. Hence, if we have not constructed a coupled-channels potential, TALYS will automatically use (tabulated or systematic) deformation parameters for DWBA calculations.
- (b) if a deformed OMP is used for the first excited states only. For the levels that do not belong to that basic coupling scheme, e.g. for the many states at somewhat higher excitation energy, we use DWBA with (very) small deformation parameters.

### 4.2.3 Odd nuclei: Weak coupling

Direct inelastic scattering off odd- $A$  nuclei can be described by the weak-coupling model [47], which assumes that a valence particle or hole interacts only weakly with a collective core excitation. Hence the model implies that the nucleon inelastic scattering by the odd- $A$  nucleus is very similar to that by the even core alone, i.e. the angular distributions have a similar shape. Let  $L$  be the spin of the even core state, and  $J_0$  and  $J$  the spin of the ground and excited state, respectively, of the odd- $A$  nucleus, resulting from the angular momentum coupling. Then, the spins  $J$  of the multiplet states in the odd- $A$  nucleus range from  $|L - J_0|$  to  $(L + J_0)$ . If the strength of the inelastic scattering is characterized by the square of the deformation parameters  $\beta_{L,J}^2$ , then the sum of all  $\beta_{L,J}^2$  or  $\sigma(E)$  for the transitions in the odd- $A$  nucleus should be equal to the value  $\beta_L^2$  or  $\sigma(E)$  for the single transition in the even core nucleus:

$$(4.55) \quad \sum_J \beta_{L,J}^2 = \beta_L^2, \quad \sum_J \sigma_{J_0 \rightarrow J} = \sigma_{0 \rightarrow L},$$

where the symbol  $0 \rightarrow L$  indicates a transition between the ground state to the excited state with spin  $L$  in the even core nucleus. The deformation parameters  $\beta_{L,J}^2$  are now given by

$$(4.56) \quad \beta_{L,J}^2 = \frac{2J+1}{(2J_0+1)(2L+1)} \beta_L^2.$$

In practice, the DWBA cross sections are calculated for the real mass of the target nucleus and at the exact excitation energies of the odd-A states, but for the even-core spin  $L$  and with deformation parameters  $\beta_{L,J}$ .

We stress that our weak-coupling model is not full-proof. First of all, there are always two choices for the even-even core. The default used in TALYS (by means of the keyword **core -1**) is to use the even-even core obtained by subtracting a nucleon, but the other choice (**core 1**), to obtain the even-even core by adding a nucleon, may sometimes be more appropriate. The next uncertainty is the choice of levels in the odd-A core. We select the levels that are closest to the excitation energy of the even-spin state of the even-even core. Again, this may not always be the most appropriate choice. A future option is to designate these levels manually.

#### 4.2.4 Giant resonances

The high-energy part of the continuum spectra are generally described by pre-equilibrium models. These models are essentially of a single-particle nature. Upon inspection of continuum spectra, some structure in the high-energy tail is observed that can not be accounted for by the smooth background of the single-particle pre-equilibrium model. For example, many 14 MeV inelastic neutron spectra show a little hump at excitation energies around 6-10 MeV. This structure is due to collective excitations of the nucleus that are known as giant resonances [48, 49]. We use a macroscopic, phenomenological model to describe giant resonances in the inelastic channel. For each multipolarity, an energy weighted sum rule (EWSR)  $S_\ell$  applies,

$$(4.57) \quad S_\ell = \sum_i E_{\ell,i} \beta_{\ell,i}^2 = 57.5 A^{-5/3} l(l+1) \text{ MeV},$$

where  $E_{\ell,i}$  is the excitation energy of the  $i$ -th state with multipolarity  $\ell$ . The summation includes all the low-lying collective states, for each  $\ell$ , that have already been included in the coupled-channels or DWBA formalism. The EWSR thus determines the remaining collective strength that is spread over the continuum. Our treatment is phenomenological in the sense that we perform a DWBA calculation with ECIS-06 for each giant resonance state and spread the cross section over the continuum with a Gaussian distribution. The central excitation energy for these states and the spreading width is different for each multipolarity and has been empirically determined. For the giant monopole resonance (GMR) EWSR we have

$$(4.58) \quad S_0 = 23 A^{-5/3} \text{ MeV},$$

with excitation energy and width

$$(4.59) \quad E_{0,GMR} = 18.7 - 0.025A \text{ MeV}, \quad \Gamma_{GMR} = 3 \text{ MeV}.$$

The EWSR for the giant quadrupole resonance (GQR) is

$$(4.60) \quad S_2 = 575A^{-5/3}\text{MeV},$$

with

$$(4.61) \quad E_{0,GQR} = 65A^{-1/3}\text{MeV}, \quad \Gamma_{GQR} = 85A^{-2/3}\text{MeV}.$$

The EWSR for the giant octupole resonance is

$$(4.62) \quad S_3 = 1208A^{-5/3}\text{MeV},$$

which has a low-energy (LEOR) and a high-energy (HEOR) component. Following Kalbach [49], we assume

$$(4.63) \quad S_{3,LEOR} = 0.3S_3, \quad S_{3,HEOR} = 0.7S_3,$$

with excitation energy and width

$$(4.64) \quad E_{0,LEOR} = 31A^{-1/3}\text{MeV}, \quad \Gamma_{LEOR} = 5\text{MeV},$$

and

$$(4.65) \quad E_{0,HEOR} = 115A^{-1/3}\text{MeV}, \quad \Gamma_{HEOR} = 9.3 - A/48\text{MeV},$$

respectively. We also take as width for the actual Gaussian distribution  $\Gamma_{Gauss} = 0.42\Gamma_\ell$ .

The contribution from giant resonances is automatically included in the total inelastic cross section. The effect is most noticeable in the single- and double-differential energy spectra.

### 4.3 Gamma-ray transmission coefficients

Gamma-ray transmission coefficients are important for the description of the gamma emission channel in nuclear reactions. This is an almost universal channel since gamma rays, in general, may accompany emission of any other emitted particle. Like the particle transmission coefficients that emerge from the optical model, gamma-ray transmission coefficients enter the Hauser-Feshbach model for the calculation of the competition of photons with other particles.

The gamma-ray transmission coefficient for multipolarity  $\ell$  of type  $X$  (where  $X = M$  or  $E$ ) is given by

$$(4.66) \quad T_{X\ell}(E_\gamma) = 2\pi f_{X\ell}(E_\gamma)E_\gamma^{2\ell+1},$$

where  $E_\gamma$  denotes the gamma energy and  $f_{X\ell}(E_\gamma)$  is the energy-dependent gamma-ray strength function.

### 4.3.1 Gamma-ray strength functions

We have included 4 models for the gamma-ray strength function. The first is the so-called Brink-Axel option [50], in which a standard Lorentzian form describes the giant dipole resonance shape, i.e.

$$(4.67) \quad f_{X\ell}(E_\gamma) = K_{X\ell} \frac{\sigma_{X\ell} E_\gamma \Gamma_{X\ell}^2}{(E_\gamma^2 - E_{X\ell}^2)^2 + E_\gamma^2 \Gamma_{X\ell}^2},$$

where  $\sigma_{X\ell}$ ,  $E_{X\ell}$  and  $\Gamma_{X\ell}$  are the strength, energy and width of the giant resonance, respectively, and

$$(4.68) \quad K_{X\ell} = \frac{1}{(2\ell + 1)\pi^2 \hbar^2 c^2}.$$

At present, we use the Brink-Axel option for all transition types other than  $E1$ . For  $E1$  radiation, the default option used in TALYS is the generalized Lorentzian form of Kopecky and Uhl [51],

$$(4.69) \quad f_{E1}(E_\gamma, T) = K_{E1} \left[ \frac{E_\gamma \tilde{\Gamma}_{E1}(E_\gamma)}{(E_\gamma^2 - E_{E1}^2)^2 + E_\gamma^2 \tilde{\Gamma}_{E1}(E_\gamma)^2} + \frac{0.7 \Gamma_{E1} 4\pi^2 T^2}{E_{E1}^3} \right] \sigma_{E1} \Gamma_{E1},$$

where the energy-dependent damping width  $\tilde{\Gamma}(E_\gamma)$  is given by

$$(4.70) \quad \tilde{\Gamma}_{E1}(E_\gamma) = \Gamma_{E1} \frac{E_\gamma^2 + 4\pi^2 T^2}{E_{E1}^2},$$

and  $T$  is the nuclear temperature given by [52]

$$(4.71) \quad T = \sqrt{\frac{E_n + S_n - \Delta - E_\gamma}{a(S_n)}},$$

where  $S_n$  is the neutron separation energy,  $E_n$  the incident neutron energy,  $\Delta$  the pairing correction (see the Section on level densities) and  $a$  the level density parameter at  $S_n$ .

For  $E1$ -transitions, GDR parameters for various individual nuclides exist. These are stored in the nuclear structure database of TALYS, see Chapter 5. Certain nuclides have a split GDR, i.e. a second set of Lorentzian parameters. For these cases, the incoherent sum of two strength functions is taken. For all transitions other than  $E1$ , systematic formulae compiled by Kopecky [163], for the resonance parameters are used. For  $E1$  transitions for which no tabulated data exist, we use

$$(4.72) \quad \sigma_{E1} = 1.2 \times 120NZ / (A\pi\Gamma_{E1}) \text{ mb}, \quad E_{E1} = 31.2A^{-1/3} + 20.6A^{-1/6} \text{ MeV}, \quad \Gamma_{E1} = 0.026E_{E1}^{1.91} \text{ MeV}.$$

For  $E2$  transitions we use

$$(4.73) \quad \sigma_{E2} = 0.00014Z^2 E_{E2} / (A^{1/3}\Gamma_{E2}) \text{ mb}, \quad E_{E2} = 63.A^{-1/3} \text{ MeV}, \quad \Gamma_{E2} = 6.11 - 0.012A \text{ MeV}.$$

For multipole radiation higher than  $E2$ , we use

$$(4.74) \quad \sigma_{E\ell} = 8.10^{-4} \sigma_{E(\ell-1)}, \quad E_{E\ell} = E_{E(\ell-1)}, \quad \Gamma_{E\ell} = \Gamma_{E(\ell-1)},$$

For  $M1$  transitions we use

$$(4.75) \quad f_{M1} = 1.58e - 9A^{0.47} \text{ at } 7 \text{ MeV}, \quad E_{M1} = 41.A^{-1/3} \text{ MeV}, \quad \Gamma_{M1} = 4 \text{ MeV},$$

where Eq. (4.67) thus needs to be applied at 7 MeV to obtain the  $\sigma_{M1}$  value. For multipole radiation higher than  $M1$ , we use

$$(4.76) \quad \sigma_{M\ell} = 8.10^{-4} \sigma_{M(\ell-1)}, \quad E_{M\ell} = E_{M(\ell-1)} \quad \Gamma_{M\ell} = \Gamma_{M(\ell-1)},$$

For all cases, the systematics can be overruled with user-defined input parameters.

In addition to the GDR contribution above, we can include Pygmy resonances by adding another contribution of the form (4.67) to the strength function. The Pygmy resonance parameters do not have a default but can be given through the **epr**, etc. keywords, see page 214.

There are also two microscopic options for  $E1$  radiation. Stephane Goriely calculated gamma-ray strength functions according to the Hartree-Fock BCS model (**strength 3**) and the Hartree-Fock-Bogolyubov model (**strength 4**), see also Ref. [163]. Since these microscopical strength functions, which we will call  $f_{\text{HFM}}$ , have not been adjusted to experimental data, we add adjustment flexibility through a scaling function, i.e.

$$(4.77) \quad f_{E1}(E_\gamma) = f^{\text{nor}} f_{\text{HFM}}(E_\gamma + E_{\text{shift}})$$

where by default  $f^{\text{nor}} = 1$  and  $E_{\text{shift}} = 0$  (i.e. unaltered values from the tables). The energy shift  $E_{\text{shift}}$  simply implies obtaining the level density from the table at a different energy. Adjusting  $f^{\text{nor}}$  and  $E_{\text{shift}}$  together gives enough adjustment flexibility.

### 4.3.2 Renormalization of gamma-ray strength functions

At sufficiently low incident neutron energies, the average radiative capture width  $\Gamma_\gamma$  is due entirely to the  $s$ -wave interaction, and it is  $\Gamma_\gamma$  at the neutron separation energy  $S_n$  that is often used to normalize gamma-ray transmission coefficients [53]. The  $\Gamma_\gamma$  values are, when available, read from our nuclear structure database. For nuclides for which no experimental value is available, we use an interpolation table by Kopecky [54] for  $40 < A < 250$ , the simple form

$$(4.78) \quad \Gamma_\gamma = 1593/A^2 \text{ eV},$$

for  $A > 250$ , while we apply no gamma normalization for  $A < 40$ .

The  $s$ -wave radiation width may be obtained by integrating the gamma-ray transmission coefficients over the density of final states that may be reached in the first step of the gamma-ray cascade. The normalization is then carried out as follows

$$(4.79) \quad \frac{2\pi\Gamma_\gamma}{D_0} = G_{\text{norm}} \sum_J \sum_\Pi \sum_{X\ell} \sum_{\ell'=|J-\ell|}^{J+\ell} \sum_{\Pi'} \int_0^{S_n} dE_\gamma T_{X\ell}(E_\gamma) \rho(S_n - E_\gamma, I', \Pi') f(X, \Pi', \ell),$$

where  $D_0$  is the average resonance spacing and  $\rho$  is the level density. The  $J, \Pi$  sum is over the compound nucleus states with spin  $J$  and parity  $\Pi$  that can be formed with  $s$ -wave incident particles, and  $I', \Pi'$

denote the spin and parity of the final states. The multipole selection rules are  $f(E, \Pi', \ell) = 1$  if  $\Pi = \Pi'(-1)^\ell$ ,  $f(M, \Pi', \ell) = 1$  if  $\Pi = \Pi'(-1)^{\ell+1}$ , and 0 otherwise. It is understood that the integral over  $dE_\gamma$  includes a summation over discrete states.  $G_{norm}$  is the normalization factor that ensures the equality (4.79). In practice, the transmission coefficients (4.66) are thus multiplied by  $G_{norm}$  before they enter the nuclear reaction calculation.  $G_{norm}$  can be specified by the user. The default is the value returned by Eq. (4.79). If  $G_{norm} = 1$  is specified, no normalization is carried out and strength functions purely determined from giant resonance parameters are taken. Other values can be entered for  $G_{norm}$ , e.g. for fitting of the neutron capture cross section. Normalisation per multipolarity can be performed by adjusting the  $\sigma_{X\ell}$  values in the input, see Chapter 6.

### 4.3.3 Photoabsorption cross section

TALYS requires photo-absorption cross sections for photo-nuclear reactions and for pre-equilibrium gamma-ray emission. Following Chadwick et al. [55], the photo-absorption cross section is given by

$$(4.80) \quad \sigma_{abs}(E_\gamma) = \sigma_{GDR}(E_\gamma) + \sigma_{QD}(E_\gamma).$$

The GDR component is related to the strength functions outlined above. It is given by

$$(4.81) \quad \sigma_{GDR}(E_\gamma) = \sum_i \sigma_{E1} \frac{(E_\gamma \Gamma_{E1,i})^2}{(E_\gamma^2 - E_{E1,i}^2)^2 + E_\gamma^2 \Gamma_{E1,i}^2},$$

where the parameters were specified in the previous subsection. The sum over  $i$  is over the number of parts into which the GDR is split.

The quasi-deuteron component  $\sigma_{QD}$  is given by

$$(4.82) \quad \sigma_{QD}(E_\gamma) = L \frac{NZ}{A} \sigma_d(E_\gamma) f(E_\gamma).$$

Here,  $\sigma_d(E_\gamma)$  is the experimental deuteron photo-disintegration cross section, parameterized as

$$(4.83) \quad \sigma_d(E_\gamma) = 61.2 \frac{(E_\gamma - 2.224)^{3/2}}{E_\gamma^3},$$

for  $E_\gamma > 2.224$  MeV and zero otherwise. The so-called Levinger parameter is  $L = 6.5$  and the Pauli-blocking function is approximated by the polynomial expression

$$(4.84) \quad f(E_\gamma) = 8.3714 \cdot 10^{-2} - 9.8343 \cdot 10^{-3} E_\gamma + 4.1222 \cdot 10^{-4} E_\gamma^2 - 3.4762 \cdot 10^{-6} E_\gamma^3 + 9.3537 \cdot 10^{-9} E_\gamma^4$$

for  $20 < E_\gamma < 140$  MeV,

$$(4.85) \quad f(E_\gamma) = \exp(-73.3/E_\gamma)$$

for  $E_\gamma < 20$  MeV, and

$$(4.86) \quad f(E_\gamma) = \exp(-24.2348/E_\gamma)$$

for  $E_\gamma > 140$  MeV.

## 4.4 Pre-equilibrium reactions

It is now well-known that the separation of nuclear reaction mechanisms into direct and compound is too simplistic. As Fig. 3.2 shows, the cross section as predicted by the pure compound process is too small with respect to measured continuum spectra, and the direct processes described in the previous section only excite the discrete levels at the highest outgoing energies. Furthermore, the measured angular distributions in the region between direct and compound are anisotropic, indicating the existence of a memory-preserving, direct-like reaction process. Apparently, as an intermediate between the two extremes, there exists a reaction type that embodies both direct- and compound-like features. These reactions are referred to as *pre-equilibrium*, *precompound* or, when discussed in a quantum-mechanical context, *multi-step processes*. Pre-equilibrium emission takes place after the first stage of the reaction but long before statistical equilibrium of the compound nucleus is attained. It is imagined that the incident particle step-by-step creates more complex states in the compound system and gradually loses its memory of the initial energy and direction. Pre-equilibrium processes cover a sizable part of the reaction cross section for incident energies between 10 and (at least) 200 MeV. Pre-equilibrium reactions have been modeled both classically and quantum-mechanically and both are included in TALYS.

### 4.4.1 Exciton model

In the exciton model (see Refs. [181, 56, 57] for extensive reviews), the nuclear state is characterized at any moment during the reaction by the total energy  $E^{tot}$  and the total number of particles above and holes below the Fermi surface. Particles ( $p$ ) and holes ( $h$ ) are indiscriminately referred to as excitons. Furthermore, it is assumed that all possible ways of sharing the excitation energy between different particle-hole configurations with the same exciton number  $n = p + h$  have equal a-priori probability. To keep track of the evolution of the scattering process, one merely traces the temporal development of the exciton number, which changes in time as a result of intranuclear two-body collisions. The basic starting point of the exciton model is a time-dependent master equation, which describes the probability of transitions to more and less complex particle-hole states as well as transitions to the continuum (emission). Upon integration over time, the energy-averaged emission spectrum is obtained. These assumptions makes the exciton model amenable for practical calculations. The price to be paid, however, is the introduction of a free parameter, namely the average matrix element of the residual two-body interaction, occurring in the transition rates between two exciton states. When this matrix element is properly parameterized, a very powerful model is obtained.

Qualitatively, the equilibration process of the excited nucleus is imagined to proceed as follows, see Fig. 4.2. After entering the target nucleus, the incident particle collides with one of the nucleons of the Fermi sea, with depth  $E_F$ . The formed state with  $n = 3$  (2p1h), in the case of a nucleon-induced reaction, is the first that is subject to particle emission, confirming the picture of the exciton model as a compound-like model rather than a direct-like model. Subsequent interactions result in changes in the number of excitons, characterized by  $\Delta n = +2$  (a new particle-hole pair) or  $\Delta n = -2$  (annihilation of a particle-hole pair) or  $\Delta n = 0$  (creation of a different configuration with the same exciton number). In the first stage of the process, corresponding to low exciton numbers, the  $\Delta n = +2$  transitions are predominant. Apart from transitions to more complex or less complex exciton states, at any stage there is a

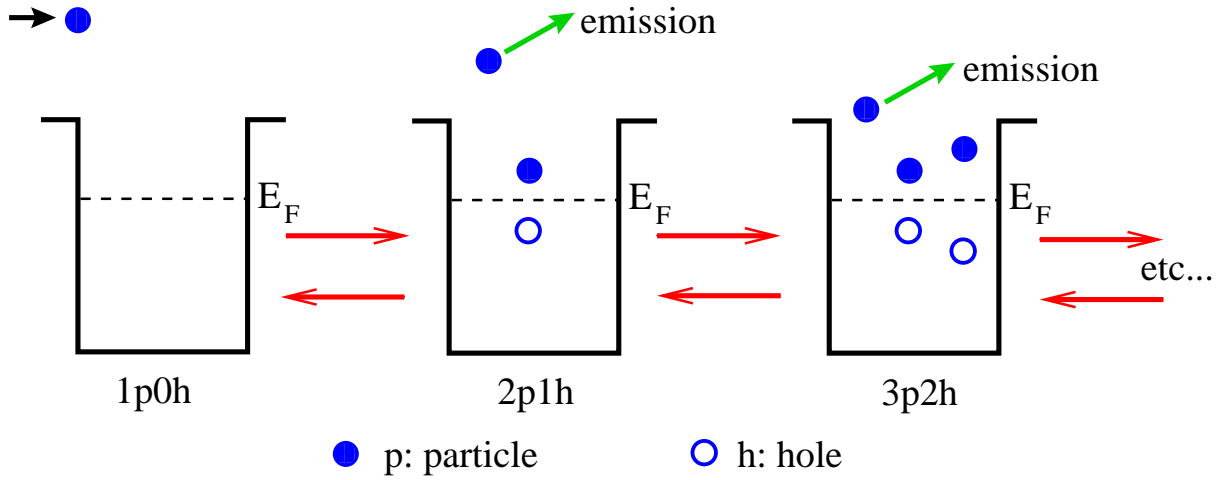


Figure 4.2: Reaction flow in exciton model

non-zero probability that a particle is emitted. Should this happen at an early stage, it is intuitively clear that the emitted particle retains some “memory” of the incident energy and direction: the hypothesis of a fully equilibrated compound nucleus is not valid. This phase is called the pre-equilibrium phase, and it is responsible for the experimentally observed high-energy tails and forward-peaked angular distributions. If emission does not occur at an early stage, the system eventually reaches a (quasi-) equilibrium. The equilibrium situation, corresponding to high exciton numbers, is established after a large number of interactions, i.e. after a long lapse of time, and the system has “forgotten” about the initial state. Accordingly, this stage may be called the compound or evaporation stage. Hence, in principle the exciton model enables to compute the emission cross sections in a unified way, without introducing adjustments between equilibrium and pre-equilibrium contributions. However, in practical cases it turns out that it is simpler and even more accurate to distinguish between a pre-equilibrium and an equilibrium phase and to perform the latter with the usual Hauser-Feshbach formalism. This is the approach followed in TALYS.

Two versions of the exciton model are implemented in TALYS: The default is the two-component model in which the neutron or proton types of particles and holes are followed throughout the reaction. We describe this model first, and then discuss the simpler, and more generally known, one-component model which is also implemented as an option. The following Section contains basically the most important equations of the recent exciton model study of [181].

### Two-component exciton model

In the following reaction equations, we use a notation in which  $p_\pi$  ( $p_\nu$ ) is the proton (neutron) particle number and  $h_\pi$  ( $h_\nu$ ) the proton (neutron) hole number. From this, we define the proton exciton number  $n_\pi = p_\pi + h_\pi$  and the neutron exciton number  $n_\nu = p_\nu + h_\nu$ . From this, we can construct the charge-independent particle number  $p = p_\pi + p_\nu$ , the hole number  $h = h_\pi + h_\nu$  and the exciton number  $n = n_\pi + n_\nu$ .

The temporal development of the system can be described by a master equation, describing the gain and loss terms for a particular class of exciton states, see [181]. Integrating the master equation over time up to the equilibration time  $\tau_{eq}$  yields the mean lifetime of the exciton state  $\tau$  that can be used to calculate the differential cross section [58]. The primary pre-equilibrium differential cross section for the emission of a particle  $k$  with emission energy  $E_k$  can then be expressed in terms of  $\tau$ , the composite-nucleus formation cross section  $\sigma^{CF}$ , and an emission rate  $W_k$ ,

$$(4.87) \quad \frac{d\sigma_k^{PE}}{dE_k} = \sigma^{CF} \sum_{p_\pi=p_\pi^0}^{p_\pi^{\max}} \sum_{p_\nu=p_\nu^0}^{p_\nu^{\max}} W_k(p_\pi, h_\pi, p_\nu, h_\nu, E_k) \tau(p_\pi, h_\pi, p_\nu, h_\nu) \times P(p_\pi, h_\pi, p_\nu, h_\nu),$$

where the factor  $P$  represents the part of the pre-equilibrium population that has survived emission from the previous states and now passes through the  $(p_\pi, h_\pi, p_\nu, h_\nu)$  configurations, averaged over time. Expressions for all quantities appearing in this expression will be detailed in the rest of this Section. The initial proton and neutron particle numbers are  $p_\pi^0 = Z_p$ , and  $p_\nu^0 = N_p$ , respectively with  $Z_p$  ( $N_p$ ) the proton (neutron) number of the projectile. For any exciton state in the reaction process,  $h_\pi = p_\pi - p_\pi^0$  and  $h_\nu = p_\nu - p_\nu^0$ , so that for primary pre-equilibrium emission the initial hole numbers are  $h_\pi^0 = h_\nu^0 = 0$ . For e.g. a neutron-induced reaction, the initial exciton number is given by  $n^0 = n_\nu^0 = 1$  ( $0p_\pi 0h_\pi 1p_\nu 0h_\nu$ ), but only pre-equilibrium gamma emission can occur from this state (nucleon emission from this state is essentially elastic scattering and this is already covered by the optical model). Particle emission only occurs from  $n = 3$  ( $2p1h$ ) and higher exciton states. We use a hardwired value of  $p_\pi^{\max} = p_\nu^{\max} = 6$  as the upper limit of the summation, see [181]. We use the never-come-back approximation, i.e. throughout the cascade one neglects the interactions that decrease the exciton number, although the adopted solution of Eq. (4.87) does include transitions that convert a proton particle-hole pair into a neutron pair and vice versa. The maximum values  $p_\pi^{\max}$  and  $p_\nu^{\max}$  thus entail an automatic separation of the pre-equilibrium population and the compound nucleus population. The latter is then handled by the more adequate Hauser-Feshbach mechanism. We now discuss the various ingredients of Eq. (4.87).

**A. Reaction cross sections** The basic feeding term for pre-equilibrium emission is the compound formation cross section  $\sigma^{CF}$ , which is given by

$$(4.88) \quad \sigma^{CF} = \sigma_{\text{reac}} - \sigma_{\text{direct}},$$

where the reaction cross section  $\sigma_{\text{reac}}$  is directly obtained from the optical model and  $\sigma_{\text{direct}}$  is the sum of the cross sections for direct reactions to discrete states  $\sigma^{disc, direct}$  as defined in Eq. (3.18), and for giant resonances, see Section 4.2.4.

**B. Emission rates and particle-hole state densities** The emission rate  $W_k$  has been derived by Cline and Blann [59] from the principle of microreversibility, and can easily be generalized to a two-component version [60]. The emission rate for an ejectile  $k$  with relative mass  $\mu_k$  and spin  $s_k$  is

$$(4.89) \quad W_k(p_\pi, h_\pi, p_\nu, h_\nu, E_k) = \frac{2s_k + 1}{\pi^2 \hbar^3} \mu_k E_k \sigma_{k, \text{inv}}(E_k) \times \frac{\omega(p_\pi - Z_k, h_\pi, p_\nu - N_k, h_\nu, E^{\text{tot}} - E_k)}{\omega(p_\pi, h_\pi, p_\nu, h_\nu, E^{\text{tot}})},$$

where  $\sigma_{k,\text{inv}}(E_k)$  is the inverse reaction cross section, again calculated with the optical model,  $Z_k$  ( $N_k$ ) is the charge (neutron) number of the ejectile and  $E^{\text{tot}}$  is the total energy of the composite system.

For the particle-hole state density  $\omega(p_\pi, h_\pi, p_\nu, h_\nu, E_x)$  we use the expression of Běťák and Dobeš [60, 61]. Their formula is based on the assumption of equidistant level spacing and is corrected for the effect of the Pauli exclusion principle and for the finite depth of the potential well. The two-component particle-hole state density is

$$(4.90) \quad \omega(p_\pi, h_\pi, p_\nu, h_\nu, E_x) = \frac{g_\pi^{n_\pi} g_\nu^{n_\nu}}{p_\pi! h_\pi! p_\nu! h_\nu! (n-1)!} (U - A(p_\pi, h_\pi, p_\nu, h_\nu))^{n-1} \times f(p, h, U, V),$$

where  $g_\pi$  and  $g_\nu$  are the single-particle state densities,  $A$  the Pauli correction,  $f$  the finite well function, and  $U = E_x - P_{p,h}$  with  $P_{p,h}$  Fu's pairing correction [62],

$$(4.91) \quad P_{p,h} = \Delta - \Delta \left[ 0.996 - 1.76 \left( \frac{n}{n_{\text{crit}}} \right)^{1.6} / \left( \frac{E_x}{\Delta} \right)^{0.68} \right]^2$$

$$\text{if } E_x/\Delta \geq 0.716 + 2.44 \left( \frac{n}{n_{\text{crit}}} \right)^{2.17},$$

$$= \Delta \text{ otherwise,}$$

with

$$(4.92) \quad n_{\text{crit}} = 2gT_{\text{crit}} \ln 2,$$

where  $T_{\text{crit}} = 2\sqrt{\Delta/1/4g/3.5}$  and  $g = g_\pi + g_\nu$ . The pairing energy  $\Delta$  for total level densities is given by

$$(4.93) \quad \Delta = \chi \frac{12}{\sqrt{A}},$$

where here  $A$  is the mass number and  $\chi = 0, 1$  or  $2$  for odd-odd, odd or even-even nuclei. The Pauli correction term is given by

$$(4.94) \quad A(p_\pi, h_\pi, p_\nu, h_\nu) = \frac{[\max(p_\pi, h_\pi)]^2}{g_\pi} + \frac{[\max(p_\nu, h_\nu)]^2}{g_\nu} - \frac{p_\pi^2 + h_\pi^2 + p_\pi + h_\pi}{4g_\pi} - \frac{p_\nu^2 + h_\nu^2 + p_\nu + h_\nu}{4g_\nu}.$$

For the single-particle state densities we take

$$(4.95) \quad g_\pi = Z/15, \quad g_\nu = N/15,$$

which is, through the relationship  $g = a\pi^2/6$ , in line with the values for our total level density parameter  $a$ , see Eq. (4.242), and also provides a globally better description of spectra than the generally adopted  $g = A/13$ .

The finite well function  $f(p, h, E_x, V)$  accounts for the fact that a hole cannot have an energy below that of the bottom of the potential well depth  $V$ . It is given by

$$(4.96) \quad f(p, h, E_x, V) = 1 + \sum_{i=1}^h (-1)^i \binom{h}{i} \left[ \frac{E_x - iV}{E_x} \right]^{n-1} \Theta(E_x - iV),$$

where  $\Theta$  is the unit step function. Note that  $f$  is different from 1 only for excitation energies greater than  $V$ . In the original version of Běťák and Dobeš,  $V$  is given by the depth  $E_f$  of the Fermi well. This was generalized by Kalbach [63, 49] to obtain an effective method to include surface effects in the first stage of the interaction, leading to a harder pre-equilibrium spectrum. For the first stage the maximum depth of the hole should be significantly reduced, since in the surface region the potential is shallower than in the interior. This automatically leaves more energy to be adopted by the excited particle, yielding more emission at the highest outgoing energies. We use the following functional form for  $V$  in terms of the projectile energy  $E_p$  and the mass  $A$ ,

$$(4.97) \quad \begin{aligned} V &= 22 + 16 \frac{E_p^4}{E_p^4 + (450/A^{1/3})^4} \text{ MeV for } h = 1 \text{ and incident protons,} \\ V &= 12 + 26 \frac{E_p^4}{E_p^4 + (245/A^{1/3})^4} \text{ MeV for } h = 1 \text{ and incident neutrons,} \\ V &= E_f = 38 \text{ MeV for } h > 1. \end{aligned}$$

See Ref. [181] for a further justification of this parameterisation.

**C. Lifetimes** The lifetime  $\tau$  of exciton state  $(p_\pi, h_\pi, p_\nu, h_\nu)$  in Eq. (4.87) is defined as the inverse sum of the total emission rate and the various internal transition rates,

$$(4.98) \quad \tau(p_\pi, h_\pi, p_\nu, h_\nu) = [\lambda_\pi^+(p_\pi, h_\pi, p_\nu, h_\nu) + \lambda_\nu^+(p_\pi, h_\pi, p_\nu, h_\nu) + \lambda_{\pi\nu}^0(p_\pi, h_\pi, p_\nu, h_\nu) + \lambda_{\nu\pi}^0(p_\pi, h_\pi, p_\nu, h_\nu) + W(p_\pi, h_\pi, p_\nu, h_\nu)]^{-1},$$

where  $\lambda_\pi^+$  ( $\lambda_\nu^+$ ) is the internal transition rate for proton (neutron) particle-hole pair creation,  $\lambda_{\pi\nu}^0$  ( $\lambda_{\nu\pi}^0$ ) is the rate for the conversion of a proton (neutron) particle-hole pair into a neutron (proton) particle-hole pair, and  $\lambda_\pi^-$  ( $\lambda_\nu^-$ ) is the rate for particle-hole annihilation. These transition rates will be discussed in Sec. 4.4.1. The total emission rate  $W$  is the integral of Eq. (4.89) over all outgoing energies, summed over all outgoing particles,

$$(4.99) \quad W(p_\pi, h_\pi, p_\nu, h_\nu) = \sum_{k=\gamma, n, p, d, t, h, \alpha} \int dE_k W_k(p_\pi, h_\pi, p_\nu, h_\nu, E_k).$$

The final ingredient of the exciton model equation, Eq. (4.87), is the part of the pre-equilibrium population  $P$  that has survived emission from all previous steps and has arrived at the exciton state  $(p_\pi, h_\pi, p_\nu, h_\nu)$ . The expression for  $P$  is somewhat more complicated than that of the depletion factor that appears in the one-component exciton model [57]. For two components, contributions from both particle creation *and* charge exchange reactions need to be taken into account, whereas transitions that do not change the exciton number cancel out in the one-component model.

For the  $(p_\pi, h_\pi, p_\nu, h_\nu)$  state,  $P$  is given by a recursive relation:

$$\begin{aligned}
P(p_\pi, h_\pi, p_\nu, h_\nu) &= P(p_\pi - 1, h_\pi - 1, p_\nu, h_\nu)\Gamma_\pi^+(p_\pi - 1, h_\pi - 1, p_\nu, h_\nu) & (A) \\
&+ P(p_\pi, h_\pi, p_\nu - 1, h_\nu - 1)\Gamma_\nu^+(p_\pi, h_\pi, p_\nu - 1, h_\nu - 1) & (B) \\
&+ [P(p_\pi - 2, h_\pi - 2, p_\nu + 1, h_\nu + 1)\Gamma_\pi^+(p_\pi - 2, h_\pi - 2, p_\nu + 1, h_\nu + 1) \\
&+ P(p_\pi - 1, h_\pi - 1, p_\nu, h_\nu)\Gamma_\nu^+(p_\pi - 1, h_\pi - 1, p_\nu, h_\nu)] \\
&\times \Gamma_{\nu\pi}^0(p_\pi - 1, h_\pi - 1, p_\nu + 1, h_\nu + 1) & (C + D) \\
&+ [P(p_\pi, h_\pi, p_\nu - 1, h_\nu - 1)\Gamma_\pi^+(p_\pi, h_\pi, p_\nu - 1, h_\nu - 1) \\
&+ P(p_\pi + 1, h_\pi + 1, p_\nu - 2, h_\nu - 2)\Gamma_\nu^+(p_\pi + 1, h_\pi + 1, p_\nu - 2, h_\nu - 2)] \\
&\times \Gamma_{\pi\nu}^0(p_\pi + 1, h_\pi + 1, p_\nu - 1, h_\nu - 1) & (E + F).
\end{aligned}
\tag{4.100}$$

This relation contains 6 distinct feeding terms: (A) creation of a proton particle-hole pair from the  $(p_\pi - 1, h_\pi - 1, p_\nu, h_\nu)$  state, (C) creation of a proton particle-hole pair from the  $(p_\pi - 2, h_\pi - 2, p_\nu + 1, h_\nu + 1)$  state followed by the conversion of a neutron particle-hole pair into a proton particle-hole pair, and (D) creation of a neutron particle-hole pair from the  $(p_\pi - 1, h_\pi - 1, p_\nu, h_\nu)$  state followed by its conversion into a proton particle-hole pair. The three remaining terms (B), (E), and (F) are obtained by changing protons into neutrons and vice versa. The probabilities of creating new proton or neutron particle-hole pairs and for converting a proton (neutron) pair into a neutron (proton) pair are calculated as follows:

$$\begin{aligned}
\Gamma_\pi^+(p_\pi, h_\pi, p_\nu, h_\nu) &= \lambda_\pi^+(p_\pi, h_\pi, p_\nu, h_\nu)\tau(p_\pi, h_\pi, p_\nu, h_\nu), \\
\Gamma_\nu^+(p_\pi, h_\pi, p_\nu, h_\nu) &= \lambda_\nu^+(p_\pi, h_\pi, p_\nu, h_\nu)\tau(p_\pi, h_\pi, p_\nu, h_\nu), \\
\Gamma_\pi^{\prime+}(p_\pi, h_\pi, p_\nu, h_\nu) &= \lambda_\pi^+(p_\pi, h_\pi, p_\nu, h_\nu)\tau'(p_\pi, h_\pi, p_\nu, h_\nu), \\
\Gamma_\nu^{\prime+}(p_\pi, h_\pi, p_\nu, h_\nu) &= \lambda_\nu^+(p_\pi, h_\pi, p_\nu, h_\nu)\tau'(p_\pi, h_\pi, p_\nu, h_\nu), \\
\Gamma_{\pi\nu}^0(p_\pi, h_\pi, p_\nu, h_\nu) &= \lambda_{\pi\nu}^0(p_\pi, h_\pi, p_\nu, h_\nu)\tau(p_\pi, h_\pi, p_\nu, h_\nu), \\
\Gamma_{\nu\pi}^0(p_\pi, h_\pi, p_\nu, h_\nu) &= \lambda_{\nu\pi}^0(p_\pi, h_\pi, p_\nu, h_\nu)\tau(p_\pi, h_\pi, p_\nu, h_\nu), \\
\tau'(p_\pi, h_\pi, p_\nu, h_\nu) &= [\lambda_\pi^+(p_\pi, h_\pi, p_\nu, h_\nu) + \lambda_\nu^+(p_\pi, h_\pi, p_\nu, h_\nu) \\
&+ W(p_\pi, h_\pi, p_\nu, h_\nu)]^{-1}.
\end{aligned}
\tag{4.101}$$

The use of  $\tau'$  in the probability  $\Gamma_\pi^{\prime+}$  ( $\Gamma_\nu^{\prime+}$ ), to create a new proton (neutron) particle-hole pair preceding an exchange interaction, originates from the approximation that only one exchange interaction is allowed in each pair-creation step. The appropriate lifetime in this case consists merely of pair creation and emission rates [58].

The initial condition for the recursive equations is

$$P(p_\pi^0, h_\pi^0, p_\nu^0, h_\nu^0) = 1,
\tag{4.102}$$

after which  $P$  can be solved for any configuration.

To calculate the pre-equilibrium spectrum, the only quantities left to determine are the internal transition rates  $\lambda_\pi^+$ ,  $\lambda_\nu^+$ ,  $\lambda_{\pi\nu}^0$  and  $\lambda_{\nu\pi}^0$ .

**D. Internal transition rates** The transition rate  $\lambda_{\pi}^{\pm}$  for the creation of a proton particle-hole pair is given by four terms, accounting for  $p_{\pi}$ ,  $h_{\pi}$ ,  $p_{\nu}$  and  $h_{\nu}$  scattering that leads to a new  $(p_{\pi}, h_{\pi})$  pair,

$$\begin{aligned}
\lambda_{\pi}^{+}(p_{\pi}, h_{\pi}, p_{\nu}, h_{\nu}) &= \frac{1}{\omega(p_{\pi}, h_{\pi}, p_{\nu}, h_{\nu}, E^{\text{tot}})} \\
& \left[ \int_{L_1^{p\pi}}^{L_2^{p\pi}} \lambda_{\pi\pi}^{1p}(u) \omega(p_{\pi} - 1, h_{\pi}, p_{\nu}, h_{\nu}, E^{\text{tot}} - u) \omega(1, 0, 0, 0, u) du \right. \\
& + \int_{L_1^{h\pi}}^{L_2^{h\pi}} \lambda_{\pi\pi}^{1h}(u) \omega(p_{\pi}, h_{\pi} - 1, p_{\nu}, h_{\nu}, E^{\text{tot}} - u) \omega(0, 1, 0, 0, u) du \\
& + \int_{L_1^{p\nu}}^{L_2^{p\nu}} \lambda_{\nu\pi}^{1p}(u) \omega(p_{\pi}, h_{\pi}, p_{\nu} - 1, h_{\nu}, E^{\text{tot}} - u) \omega(0, 0, 1, 0, u) du \\
& \left. + \int_{L_1^{h\nu}}^{L_2^{h\nu}} \lambda_{\nu\pi}^{1h}(u) \omega(p_{\pi}, h_{\pi}, p_{\nu}, h_{\nu} - 1, E^{\text{tot}} - u) \omega(0, 0, 0, 1, u) du \right],
\end{aligned}
\tag{4.103}$$

where the first and third term represent particle scattering and the second and fourth term hole scattering. The integration limits correct for the Pauli exclusion principle,

$$\begin{aligned}
L_1^{p\pi} &= A(p_{\pi} + 1, h_{\pi} + 1, p_{\nu}, h_{\nu}) - A(p_{\pi} - 1, h_{\pi}, p_{\nu}, h_{\nu}), \\
L_2^{p\pi} &= E^{\text{tot}} - A(p_{\pi} - 1, h_{\pi}, p_{\nu}, h_{\nu}), \\
L_1^{h\pi} &= A(p_{\pi} + 1, h_{\pi} + 1, p_{\nu}, h_{\nu}) - A(p_{\pi}, h_{\pi} - 1, p_{\nu}, h_{\nu}), \\
L_2^{h\pi} &= E^{\text{tot}} - A(p_{\pi}, h_{\pi} - 1, p_{\nu}, h_{\nu}), \\
L_1^{p\nu} &= A(p_{\pi}, h_{\pi}, p_{\nu} + 1, h_{\nu} + 1) - A(p_{\pi}, h_{\pi}, p_{\nu} - 1, h_{\nu}), \\
L_2^{p\nu} &= E^{\text{tot}} - A(p_{\pi}, h_{\pi}, p_{\nu} - 1, h_{\nu}), \\
L_1^{h\nu} &= A(p_{\pi} + 1, h_{\pi} + 1, p_{\nu}, h_{\nu}) - A(p_{\pi}, h_{\pi}, p_{\nu}, h_{\nu} - 1), \\
L_2^{h\nu} &= E^{\text{tot}} - A(p_{\pi}, h_{\pi}, p_{\nu}, h_{\nu} - 1),
\end{aligned}
\tag{4.104}$$

which demands that (a) the minimal energy available to the scattering particle or hole creating a new particle-hole pair equals the Pauli energy of the final state minus the Pauli energy of the inactive particles and holes not involved in the scattering process, and (b) the maximal energy available equals the total excitation energy minus the latter Pauli energy.

The term  $\lambda_{\pi\pi}^{1p}(u)$  is the collision probability per unit time for a proton-proton interaction leading to an additional proton particle-hole pair. In general, the corresponding term for a hole is obtained by relating it to the particle collision probability through the accessible state density of the interacting particles and holes,

$$\lambda_{\pi\pi}^{1h}(u) = \lambda_{\pi\pi}^{1p}(u) \frac{\omega(1, 2, 0, 0, u)}{\omega(2, 1, 0, 0, u)}.
\tag{4.105}$$

Similarly,  $\lambda_{\nu\pi}^{1p}(u)$  is the collision probability per unit time for a neutron-proton interaction leading to an additional proton particle-hole pair, and for the corresponding hole term we have

$$\lambda_{\nu\pi}^{1h}(u) = \lambda_{\nu\pi}^{1p}(u) \frac{\omega(1, 1, 0, 1, u)}{\omega(1, 1, 1, 0, u)}.
\tag{4.106}$$

The transition rate for conversion of a proton particle-hole pair into a neutron pair is

$$(4.107) \quad \lambda_{\pi\nu}^0(p_\pi, h_\pi, p_\nu, h_\nu) = \frac{1}{\omega(p_\pi, h_\pi, p_\nu, h_\nu, E^{\text{tot}})} \int_{L_1^{p\pi}}^{L_2^{p\pi}} \lambda_{\pi\nu}^{1p1h}(u) \omega(p_\pi - 1, h_\pi - 1, p_\nu, h_\nu, E^{\text{tot}} - u) \omega(1, 1, 0, 0, u) du,$$

with integration limits

$$(4.108) \quad \begin{aligned} L_1^{p\pi} &= A(p_\pi, h_\pi, p_\nu, h_\nu) - A(p_\pi - 1, h_\pi - 1, p_\nu, h_\nu) \\ L_2^{p\pi} &= E^{\text{tot}} - A(p_\pi - 1, h_\pi - 1, p_\nu, h_\nu). \end{aligned}$$

The term  $\lambda_{\pi\nu}^{1p1h}$  is the associated collision probability. Interchanging  $\pi$  and  $\nu$  in Eqs. (4.103-4.108) gives the expressions for  $\lambda_\nu^+$ ,  $\lambda_{\nu\nu}^{1h}$ ,  $\lambda_{\pi\nu}^{1h}$  and  $\lambda_{\nu\pi}^0$ .

We distinguish between two options for the collision probabilities:

#### D1. Effective squared matrix element

Expressing the transition rate in terms of an effective squared matrix element has been used in many exciton model analyses. Also in TALYS, it is one of the options for our calculations and comparisons with data. The collision probabilities of Eqs. (4.103) and (4.107) are determined with the aid of Fermi's golden rule of time-dependent perturbation theory, which for a two-component model gives

$$(4.109) \quad \begin{aligned} \lambda_{\pi\pi}^{1p}(u) &= \frac{2\pi}{\hbar} M_{\pi\pi}^2 \omega(2, 1, 0, 0, u), \\ \lambda_{\pi\pi}^{1h}(u) &= \frac{2\pi}{\hbar} M_{\pi\pi}^2 \omega(1, 2, 0, 0, u), \\ \lambda_{\nu\pi}^{1p}(u) &= \frac{2\pi}{\hbar} M_{\nu\pi}^2 \omega(1, 1, 1, 0, u), \\ \lambda_{\nu\pi}^{1h}(u) &= \frac{2\pi}{\hbar} M_{\nu\pi}^2 \omega(1, 1, 0, 1, u), \\ \lambda_{\pi\nu}^{1p1h}(u) &= \frac{2\pi}{\hbar} M_{\pi\nu}^2 \omega(0, 0, 1, 1, u), \end{aligned}$$

where the relations (4.105)-(4.106) have been applied. Interchanging  $\pi$  and  $\nu$  gives the expressions for  $\lambda_{\nu\nu}^{1p}$ ,  $\lambda_{\nu\nu}^{1h}$ ,  $\lambda_{\pi\nu}^{1p}$ ,  $\lambda_{\pi\nu}^{1h}$ , and  $\lambda_{\nu\pi}^{1p1h}$ . Here, the  $M_{\pi\pi}^2$ , etc. are average squared matrix elements of the residual interaction, which are assumed to depend on the total energy  $E^{\text{tot}}$  of the whole composite nucleus only. Such a matrix element thus represents a truly *effective* residual interaction, whereby all individual residual interactions taking place inside the nucleus can be cast into an average form for the squared matrix element to which one assigns a global  $E^{\text{tot}}$ -dependence a posteriori.

The average residual interaction inside the nucleus is not necessarily the same for like and unlike nucleons. The two-component matrix elements are given, in terms of an average  $M^2$ , by

$$(4.110) \quad \begin{aligned} M_{\pi\pi}^2 &= R_{\pi\pi} M^2, \\ M_{\nu\nu}^2 &= R_{\nu\nu} M^2, \\ M_{\pi\nu}^2 &= R_{\pi\nu} M^2, \\ M_{\nu\pi}^2 &= R_{\nu\pi} M^2. \end{aligned}$$

In TALYS, we take

$$(4.111) \quad R_{\nu\nu} = 1.5, R_{\nu\pi} = R_{\pi\pi} = R_{\pi\nu} = 1.,$$

which is in line with the, more parameter-free, optical model based exciton model that we describe later. Note that this deviates somewhat from the parameters adopted in Ref. [181]. The current parameterization gives slightly better performance for cross section excitation functions. In TALYS, the above parameters are adjustable (**Rpinu**, etc. keywords) with Eq. (4.111) as default. The following semi-empirical expression for the squared matrix element has been shown to work for incident energies between 7 and 200 MeV [181]:

$$(4.112) \quad M^2 = \frac{C_1 A_p}{A^3} \left[ 7.48 C_2 + \frac{4.62 \times 10^5}{\left( \frac{E^{tot}}{n \cdot A_p} + 10.7 C_3 \right)^3} \right].$$

Eq. (4.112) is a generalization of older parameterisations such as given in Refs. [58, 49], which apply in smaller (lower) energy ranges. Here  $C_1, C_2$  and  $C_3$  are adjustable constants (see the **M2constant**, **M2limit** and **M2shift** keywords) that are all equal to 1 by default, and  $A_p$  is the mass number of the projectile, which allows generalization for complex-particle reactions. Again, Eq. (4.112) is slightly different (10%) from the expression given in Ref. [181] to allow for better fits of excitation functions.

Finally, for matrix element based transition rates and equidistant particle-hole level densities, the integrals in the transition rates can be approximated analytically [58], giving

$$(4.113) \quad \begin{aligned} \lambda_{\pi+}(p_\pi, h_\pi, p_\nu, h_\nu) &= \frac{2\pi}{\hbar} \frac{g_\pi^2}{2n(n+1)} \frac{[E^{tot} - A(p_\pi + 1, h_\pi + 1, p_\nu, h_\nu)]^{n+1}}{[E^{tot} - A(p_\pi, h_\pi, p_\nu, h_\nu)]^{n-1}} \\ &\times (n_\pi g_\pi M_{\pi\pi}^2 + 2n_\nu g_\nu M_{\nu\nu}^2) f(p+1, h+1, E^{tot}, V) \\ \lambda_{\nu+}(p_\pi, h_\pi, p_\nu, h_\nu) &= \frac{2\pi}{\hbar} \frac{g_\nu^2}{2n(n+1)} \frac{[E^{tot} - A(p_\pi, h_\pi, p_\nu + 1, h_\nu + 1)]^{n+1}}{[E^{tot} - A(p_\pi, h_\pi, p_\nu, h_\nu)]^{n-1}} \\ &\times (n_\nu g_\nu M_{\nu\nu}^2 + 2n_\pi g_\pi M_{\pi\pi}^2) f(p+1, h+1, E^{tot}, V) \\ \lambda_{\pi\nu}(p_\pi, h_\pi, p_\nu, h_\nu) &= \frac{2\pi}{\hbar} M_{\pi\nu}^2 \frac{p_\pi h_\pi}{n} g_\nu^2 f(p, h, E^{tot}, V) \left[ \frac{E^{tot} - B_{\pi\nu}(p_\pi, h_\pi, p_\nu, h_\nu)}{E^{tot} - A(p_\pi, h_\pi, p_\nu, h_\nu)} \right]^{n-1} \\ &\times (2[E^{tot} - B_{\pi\nu}(p_\pi, h_\pi, p_\nu, h_\nu)] \\ &+ n|A(p_\pi, h_\pi, p_\nu, h_\nu) - A(p_\pi - 1, h_\pi - 1, p_\nu + 1, h_\nu + 1)|) \\ \lambda_{\nu\pi}(p_\pi, h_\pi, p_\nu, h_\nu) &= \frac{2\pi}{\hbar} M_{\nu\pi}^2 \frac{p_\nu h_\nu}{n} g_\pi^2 f(p, h, E^{tot}, V) \left[ \frac{E^{tot} - B_{\nu\pi}(p_\pi, h_\pi, p_\nu, h_\nu)}{E^{tot} - A(p_\pi, h_\pi, p_\nu, h_\nu)} \right]^{n-1} \\ &\times (2[E^{tot} - B_{\nu\pi}(p_\pi, h_\pi, p_\nu, h_\nu)] \\ &+ n|A(p_\pi, h_\pi, p_\nu, h_\nu) - A(p_\pi + 1, h_\pi + 1, p_\nu - 1, h_\nu - 1)|), \end{aligned}$$

with

$$(4.114) \quad \begin{aligned} B_{\pi\nu}(p_\pi, h_\pi, p_\nu, h_\nu) &= \max[A(p_\pi, h_\pi, p_\nu, h_\nu), A(p_\pi - 1, h_\pi - 1, p_\nu + 1, h_\nu + 1)] \\ B_{\nu\pi}(p_\pi, h_\pi, p_\nu, h_\nu) &= \max[A(p_\pi, h_\pi, p_\nu, h_\nu), A(p_\pi + 1, h_\pi + 1, p_\nu - 1, h_\nu - 1)]. \end{aligned}$$

which is also included as an option. The default is however to use the numerical solutions for the internal transition rates. This analytical solution requires a value for  $M^2$  that is 20% larger than that of

Eq. (4.112), which apparently is the energy-averaged effect of introducing such approximations.

### D2. Collision rates based on the optical model

Instead of modeling the intranuclear transition rate by an average squared matrix element, one may also relate the transition rate to the average imaginary optical model potential depth [181]. The collision probabilities, when properly averaged over all particle-hole configurations as in Eq. (4.103), in principle would yield a parameter free expression for the transition rate.

The average well depth  $W_i$  can be obtained by averaging the total imaginary part of the potential  $\mathcal{W}$  over the whole volume of the nucleus

$$(4.115) \quad W_i(E) = \frac{\int \mathcal{W}_i(r, E) \rho(r) dr}{\int \rho(r) dr},$$

where  $\rho$  represents the density of nuclear matter for which we take the form factor  $f(r, R, a)$  of the volume part of the optical model potential, given by the usual Woods-Saxon shape of Eq. (4.3). The total imaginary potential is given by

$$(4.116) \quad \mathcal{W}_i(r, E) = \mathcal{W}_{V,i}(E) f(r, R_{V,i}, a_{V,i}) - 4a_{D,i} \mathcal{W}_{D,i}(E) \frac{d}{dr} f(r, R_{D,i}, a_{D,i}).$$

Next, we define an *effective* imaginary optical potential [181] related to nucleon-nucleon collisions in nuclear matter:

$$(4.117) \quad W_i^{\text{eff}}(E) = C^{\text{omp}} W_i(E).$$

We use as best overall parameter

$$(4.118) \quad C^{\text{omp}} = 0.55.$$

This parameter can be adjusted with the **M2constant** keyword, which serves as a multiplier for the value given in Eq. (4.118). The collision probabilities are now related as follows to the *effective* imaginary optical potential:

$$(4.119) \quad \begin{aligned} \lambda_{\pi\pi}^{1p}(u) &= \frac{1}{4} \frac{2W_p^{\text{eff}}(u - S(p))}{\hbar} \\ \lambda_{\pi\pi}^{1h}(u) &= \frac{1}{4} \frac{2W_p^{\text{eff}}(u - S(p))}{\hbar} \frac{\omega(1, 2, 0, 0, u)}{\omega(2, 1, 0, 0, u)} \\ \lambda_{\nu\pi}^{1p}(u) &= \frac{3}{4} \frac{2W_n^{\text{eff}}(u - S(n))}{\hbar} \\ \lambda_{\nu\pi}^{1h}(u) &= \frac{3}{4} \frac{2W_n^{\text{eff}}(u - S(n))}{\hbar} \frac{\omega(1, 1, 0, 1, u)}{\omega(1, 1, 1, 0, u)} \\ \lambda_{\nu\pi}^{1p1h}(u) &= \frac{1}{2} \frac{2W_n^{\text{eff}}(u - S(n))}{\hbar}, \end{aligned}$$

and similarly for the components of  $\lambda_{\nu}^{+}$  and  $\lambda_{\nu\pi}^0$ . The transition rates for the exciton model are then obtained by inserting these terms in Eqs. (4.103) and (4.107). Apart from Eq. (4.118), a parameter-free model is obtained.

### One-component exciton model

The one-component exciton model has been made redundant by the more flexible and physically more justified two-component model. Nevertheless, it is included as an option since it connects to many older pre-equilibrium studies and thus may be helpful as comparison. In the one-component exciton model, the pre-equilibrium spectrum for the emission of a particle  $k$  at an energy  $E_k$  is given by

$$(4.120) \quad \frac{d\sigma_k^{\text{PE}}}{dE_k} = \sigma^{\text{CF}} \sum_{p=p_0}^{p_{\text{max}}} W_k(p, h, E_k) \tau(p, h),$$

where  $p_{\text{max}} = 6$  and  $\sigma^{\text{CF}}$  are defined as below Eq. (4.87). For the initial particle number  $p_0$  we have  $p_0 = A_p$  with  $A_p$  the mass number of the projectile. In general, the hole number  $h = p - p_0$  in Eq. (4.120), so that the initial hole number is always zero, i.e.  $h_0 = 0$  for primary pre-equilibrium emission.

The emission rate  $W_k$  is

$$(4.121) \quad W_k(p, h, E_k) = \frac{2s_k + 1}{\pi^2 \hbar^3} \mu_k E_k \sigma_{k, \text{inv}}(E_k) \frac{\omega(p - A_k, h, E_{\text{tot}} - E_k)}{\omega(p, h, E_{\text{tot}})} Q_k(p),$$

with all quantities explained below Eq. (4.89), and  $A_k$  is the mass number of the ejectile and  $Q_k(p)$  is a factor accounting for the distinguishability of neutrons and protons [64]

$$(4.122) \quad Q_k(p) = \frac{(p - A_k)!}{p!} \left[ \sum_{p_\pi = Z_k}^{p - N_k} \left(\frac{Z}{A}\right)^{n_\pi - Z_k} \left(\frac{A}{N}\right)^{n_\nu - N_k} \frac{1}{h_\pi! h_\nu!} \frac{1}{(p_\pi - Z_k)! (p_\nu - N_k)!} \right] \\ / \left[ \sum_{p_\pi = Z_k}^{p - N_k} \left(\frac{Z}{A}\right)^{n_\pi} \left(\frac{N}{A}\right)^{n_\nu} \frac{1}{p_\pi! p_\nu! h_\pi! h_\nu!} \right].$$

For gamma's we set  $Q_\gamma(p) = 1$ .

Finally,  $\omega(p, h, E_x)$  is the particle-hole state density for which we use the one-component expression by Běťák and Dobeš [61], again corrected for the effect of the Pauli exclusion principle and for the finite depth of the potential well. The one-component particle-hole state density has a simpler form than that of Eq. (4.90),

$$(4.123) \quad \omega(p, h, E_x) = \frac{g^n}{p! h! (n-1)!} [E_x - A(p, h)]^{n-1} f(p, h, E_x, V),$$

where  $g = A/15$  is the single-particle state density and

$$(4.124) \quad A(p, h) = \frac{[\text{max}(p, h)]^2}{g} - \frac{p^2 + h^2 + p + h}{4g},$$

is the Pauli correction factor. The finite well function  $f$  is given by Eq. (4.96).

To obtain the lifetimes  $\tau(p, h)$  that appear in Eq. (4.120), we first define the total emission rate  $W(p, h)$  as the integral of Eq. (4.121) over all outgoing energies, summed over all outgoing particles:

$$(4.125) \quad W(p, h) = \sum_{k=\gamma, n, p, d, t, h, \alpha} \int dE_k W_k(p, h, E_k).$$

As mentioned already, we have implemented the never-come-back solution of the master equation. This is based on the assumption that at the beginning of the cascade one neglects the interactions that decrease the exciton number. Then, for the one-component model the expression for the lifetime is (see e.g. Ref. [57])

$$(4.126) \quad \tau(p, h) = \frac{1}{\lambda^+(p, h) + W(p, h)} D_{p, h},$$

where  $D_{p, h}$  is a depletion factor that accounts for the removal of reaction flux, through emission, by the previous stages

$$(4.127) \quad D_{p, h} = \prod_{p'=p_0}^{p-1} \frac{\lambda^+(p', h')}{\lambda^+(p', h') + W(p', h')},$$

with again  $h' = p' - p_0$ . The initial case of Eq. (4.126) is

$$(4.128) \quad \tau(p_0, h_0) = \frac{1}{\lambda^+(p_0, h_0) + W(p_0, h_0)}.$$

To calculate the pre-equilibrium spectrum, the only quantity left to determine is the internal transition rate  $\lambda^+(p, h)$  from state  $(p, h)$  to state  $(p + 1, h + 1)$ . The general definition of  $\lambda^+(p, h)$  is

$$(4.129) \quad \begin{aligned} \lambda^+(p, h) = & \frac{1}{\omega(p, h, E^{\text{tot}})} \left[ \int_{L_1^p}^{L_2^p} du \lambda^{1p}(u) \omega(p-1, h, E^{\text{tot}} - u) \omega(1, 0, u) \right. \\ & \left. + \int_{L_1^h}^{L_2^h} du \lambda^{1h}(u) \omega(p, h-1, E^{\text{tot}} - u) \omega(0, 1, u) \right]. \end{aligned}$$

where the two terms account for particle and hole scattering, respectively, and the integration limits

$$(4.130) \quad \begin{aligned} L_1^p &= A(p+1, h+1) - A(p-1, h) \\ L_2^p &= E^{\text{tot}} - A(p-1, h) \\ L_1^h &= A(p+1, h+1) - A(p, h-1) \\ L_2^h &= E^{\text{tot}} - A(p, h-1), \end{aligned}$$

correct for the Pauli exclusion principle.

We again distinguish between two options:

### 1. Effective squared matrix element

The collision probabilities are determined with the aid of Fermi's golden rule of time-dependent perturbation theory, which for the one-component model are

$$(4.131) \quad \begin{aligned} \lambda^{1p}(u) &= \frac{2\pi}{\hbar} M^2 \omega(2, 1, u) \\ \lambda^{1h}(u) &= \frac{2\pi}{\hbar} M^2 \omega(1, 2, u), \end{aligned}$$

with  $M^2$  the average squared matrix element of the residual interaction. In the one-component model, “forbidden” transitions are taken into account, so that a squared matrix element smaller than that of Eq. (4.112) of the two-component model is needed to compensate for these transitions. We find that for the one-component model we need to multiply  $M^2$  of Eq. (4.112) by 0.5 to obtain a global comparison with data that is closest to our two-component result, i.e.

$$(4.132) \quad M^2 = \frac{0.5C_1A_p}{A^3} \left[ 7.48C_2 + \frac{4.62 \times 10^5}{\left(\frac{E^{\text{tot}}}{n.A_p} + 10.7C_3\right)^3} \right].$$

For completeness, we note that the transition rate can be well approximated by an analytical form as discussed in Refs. [65, 61, 63]. The result is

$$(4.133) \quad \lambda^+(p, h) = \frac{2\pi}{\hbar} M^2 \frac{g^3}{2(n+1)} \frac{[E^{\text{tot}} - A(p+1, h+1)]^{n+1}}{[E^{\text{tot}} - A(p, h)]^{n-1}} f(p+1, h+1, E^{\text{tot}}, V).$$

However, the overall description of experimental data obtained with the one-component model is however worse than that of the two-component model, so we rarely use it.

## 2. Collision rates based on the optical model

Also in the one-component model the transition rates can be related to the effective nucleon-nucleon interaction  $\bar{\sigma}$  and thereby to the imaginary optical potential,

$$(4.134) \quad \begin{aligned} \lambda^{1p}(u) &= \frac{1}{2} \frac{2W^{\text{eff}}(u-S)}{\hbar} \\ \lambda^{1h}(u) &= \frac{1}{2} \frac{2W^{\text{eff}}(u-S)}{\hbar} \frac{\omega(1, 2, u)}{\omega(2, 1, u)}, \end{aligned}$$

with  $S$  the separation energy of the particle. Since the one-component model makes no distinction between neutron and proton particle-hole pairs,  $W_V^{\text{eff}}$  is evaluated as follows,

$$(4.135) \quad W_i^{\text{eff}}(E) = 0.5C^{\text{omp}} W_i(E),$$

analogous to the multiplication with a factor 0.5 for  $M^2$ .

**Energy width representation** The formalism given above, i.e. Eqs. (4.120), (4.121) and (4.126), forms a representation in which the time appears, i.e. the dimensions of  $W(p, h)$  and  $\tau(p, h)$  are  $[s]^{-1}$  and  $[s]$  respectively. An alternative expression for the exciton model that is often used is in terms of energy widths. Since this may be more recognisable to some users we also give it here. The partial escape width  $\Gamma_k^\dagger(p, h, E_k)$  is related to the emission rate by

$$(4.136) \quad \Gamma_k^\dagger(p, h, E_k) = \hbar W_k(p, h, E_k).$$

Integrated over energy we have

$$(4.137) \quad \Gamma_k^\uparrow(p, h) = \hbar W_k(p, h),$$

and the total escape width is

$$(4.138) \quad \Gamma^\uparrow(p, h) = \sum_{k=\gamma, n, p, d, t, h, \alpha} \Gamma_k^\uparrow(p, h) = \hbar W(p, h).$$

The damping width  $\Gamma^\downarrow$  is related to the internal transition rate by

$$(4.139) \quad \Gamma^\downarrow(p, h) = \hbar \lambda^+(p, h).$$

Defining the total width by

$$(4.140) \quad \Gamma^{\text{tot}}(p, h) = \Gamma^\downarrow(p, h) + \Gamma^\uparrow(p, h),$$

we can rewrite the exciton model cross section (4.120) as

$$(4.141) \quad \frac{d\sigma_k^{\text{PE}}}{dE_k} = \sigma^{\text{CF}} \sum_{p=p_0}^{p_{\text{max}}} \frac{\Gamma_k^\uparrow(p, h, E_k)}{\Gamma^{\text{tot}}(p, h)} \left( \prod_{p'=p_0}^{p-1} \frac{\Gamma^\downarrow(p', h')}{\Gamma^{\text{tot}}(p', h')} \right).$$

In the output file of TALYS, the results for the various quantities in both the time and the energy width representation are given.

In sum, the default model used by TALYS is the two-component exciton model with collision probabilities based on the effective squared matrix element of Eq. (4.112).

#### 4.4.2 Photon exciton model

For pre-equilibrium photon emission, we have implemented the model of Akkermans and Gruppelaar [66]. This model gives a simple but powerful simulation of the direct-semidirect capture process within the framework of the exciton model. Analogous to the particle emission rates, the continuum  $\gamma$ -ray emission rates may be derived from the principle of detailed balance or microscopic reversibility, assuming that only  $E1$ -transitions contribute. This yields

$$(4.142) \quad W_\gamma(p, h, E_\gamma) = \frac{E_\gamma^2}{\pi^2 \hbar^3 c^2} \frac{\sigma_{\gamma, \text{abs}}(E_\gamma)}{\omega(p, h, E^{\text{tot}})} \left( \frac{g^2 E_\gamma \omega(p-1, h-1, E_x - E_\gamma)}{g(n-2) + g^2 E_\gamma} + \frac{gn\omega(p, h, E_x - E_\gamma)}{gn + g^2 E_\gamma} \right)$$

where  $\sigma_{\gamma, \text{abs}}(E_\gamma)$  is the photon absorption cross section of Eq. (4.80). The initial particle-hole configuration in Eq. (4.120) is  $n_0 = 1$  ( $1p0h$ ) for photon emission. For “direct”  $\gamma$ -ray emission in nucleon-induced reactions only the second term between brackets ( $n = 1$ ) contributes. The “semi-direct”  $\gamma$ -ray emission ( $n = 3$ ) consists of both terms.

The emission rate (4.142) is included in Eqs. (4.120) and (4.125) so that the pre-equilibrium photon cross section automatically emerges.

For the two-component model, we use

$$(4.143) \quad W_\gamma(p_\pi, h_\pi, p_\nu, h_\nu, E_\gamma) = \frac{E_\gamma^2}{\pi^2 \hbar^3 c^2} \frac{\sigma_{\gamma,abs}(E_\gamma)}{\omega(p_\pi, h_\pi, p_\nu, h_\nu, E^{tot})} \\ \times \left( \frac{g^2 E_\gamma^{\frac{1}{2}} [\omega(p_\pi - 1, h_\pi - 1, p_\nu, h_\nu, E_x - E_\gamma) + \omega(p_\pi, h_\pi, p_\nu - 1, h_\nu - 1, E_x - E_\gamma)]}{g(n - 2) + g^2 E_\gamma} \right) \\ + \frac{gn\omega(p_\pi, h_\pi, p_\nu, h_\nu, E_x - E_\gamma)}{gn + g^2 E_\gamma}.$$

#### 4.4.3 Pre-equilibrium spin distribution

Since the exciton model described above does not provide a spin distribution for the residual states after pre-equilibrium emission, a model needs to be adopted that provides the spin population in the continuum in binary reactions. TALYS provides two options for this. The default is to adopt the compound nucleus spin distribution (described in Section 4.5) also for the excited states resulting from pre-equilibrium emission. Another option that has been quite often used in the past is to assign a spin distribution to the particle-hole state density. For that, we adopt the usual decomposition of the state density into a  $J$ -dependent part and an energy-dependent part,

$$(4.144) \quad \rho(p, h, J, E_x) = (2J + 1)R_n(J)\omega(p, h, E_x).$$

The function  $R_n(J)$  represents the spin distribution of the states in the continuum. It is given by

$$(4.145) \quad R_n(J) = \frac{2J + 1}{\pi^{1/2} n^{3/2} \sigma^3} \exp \left[ -\frac{(J + \frac{1}{2})^2}{n\sigma^2} \right],$$

and satisfies, for any exciton number  $n$ ,

$$(4.146) \quad \sum_J (2J + 1)R_n(J) = 1.$$

The used expression for the spin cut-off parameter  $\sigma$  is [67],

$$(4.147) \quad \sigma^2 = 0.24nA^{\frac{2}{3}},$$

where  $A$  is the mass number of the nucleus. Similarly, for the two-component particle-hole level density we have

$$(4.148) \quad \rho(p_\pi, h_\pi, p_\nu, h_\nu, J, E_x) = (2J + 1)R_n(J)\omega(p_\pi, h_\pi, p_\nu, h_\nu, E_x).$$

In practice, with this option (**preeqspin y**) the residual states formed by pre-equilibrium reactions would be multiplied by  $R_n$  a posteriori. There are various arguments to prefer the compound nucleus spin distribution, so we use that default.

#### 4.4.4 Continuum stripping, pick-up, break-up and knock-out reactions

For pre-equilibrium reactions involving deuterons, tritons, Helium-3 and alpha particles, a contribution from the exciton model is automatically calculated with the formalism of the previous subsections. It is however well-known that for nuclear reactions involving projectiles and ejectiles with different particle numbers, mechanisms like stripping, pick-up, break-up and knock-out play an important role and these direct-like reactions are not covered by the exciton model. Therefore, Kalbach [68] developed a phenomenological contribution for these mechanisms, which we have included in TALYS. In total, the pre-equilibrium cross section for these reactions is given by the sum of an exciton model (EM), nucleon transfer (NT), and knock-out (KO) contribution:

$$(4.149) \quad \frac{d\sigma_k^{\text{PE}}}{dE_k} = \frac{d\sigma_k^{\text{EM}}}{dE_k} + \frac{d\sigma_k^{\text{NT}}}{dE_k} + \frac{d\sigma_k^{\text{KO}}}{dE_k}$$

where the contribution from the exciton model was outlined in the previous subsection.

#### Transfer reactions

The general differential cross section formula for a nucleon transfer reaction of the type  $A(a, b)B$  is

$$(4.150) \quad \frac{d\sigma_{a,b}^{\text{NT}}}{dE_b} = \frac{2s_b + 1}{2s_a + 1} \frac{A_b}{A_a} \frac{E_b \sigma_{b,inv}(E_b)}{A_a} K \left( \frac{A_a}{E_a + V_a} \right)^{2n} \left( \frac{C}{A_B} \right)^n \\ \times N_a \left( \frac{2Z_A}{A_A} \right)^{2(Z_a+2)h_\pi+2p_\nu} \omega_{\text{NT}}(p_\pi, h_\pi, p_\nu, h_\nu, U)$$

where

$$(4.151) \quad C_a = 5500 \text{ for incident neutrons,} \\ = 3800 \text{ for incident charged particles,}$$

$$(4.152) \quad N_a = \frac{1}{80E_a} \text{ for pickup,} \\ = \frac{1}{580\sqrt{E_a}} \text{ for stripping,} \\ = \frac{1}{1160\sqrt{E_a}} \text{ for exchange.}$$

$K$  is an enhancement factor taking into account the fact that d, t and 3-He are loosely bound:

$$(4.153) \quad K = 12 \text{ for } (N, \alpha), \\ = 12 - 11 \frac{E_a - 20}{E_a} \text{ for } (\alpha, N) \text{ and } E_a > 20, \\ = 1 \text{ otherwise,}$$

where  $N$  stands for either neutron or proton. The well depth  $V_a$  is set at

$$(4.154) \quad V_a = 12.5A_a \text{ MeV,}$$

and represents the average potential drop seen by the projectile between infinity and the Fermi level. The possible degrees of freedom for the reaction are all included in the residual state density  $\omega_{NT}(p_\pi, h_\pi, p_\nu, h_\nu, U)$ . Since we do not use this model to describe exchange reactions in inelastic scattering, there is no need to sum the various terms of Eq. (4.150) over  $p_\pi$ , as in Ref. [68]. The exciton numbers are automatically determined by the transfer reaction, i.e.  $n = |A_a - A_b|$ ,  $n_\pi = h_\pi = |Z_a - Z_b|$ ,  $n_\nu = h_\nu = |N_a - N_b|$ ,  $p_\pi = p_\nu = 0$ . The accessible state density that is directly determined by the reaction is  $\omega(p_\pi, h_\pi, p_\nu, h_\nu, U)$ , given by Eq. (4.90). The total residual state density however also takes into account more complex configurations that can be excited by the transfer reaction. It is given by

$$(4.155) \quad \omega_{NT}(p_\pi, h_\pi, p_\nu, h_\nu, U) = \sum_{i=0}^3 \sum_{j=0}^{3-i} (X_{NT})^{i+j} \omega(p_\pi + i, h_\pi + i, p_\nu + j, h_\nu + j, U) \\ + \sum_{i=0}^{p_\pi} \sum_{j=0}^{h_\pi} \sum_{k=0}^{p_\nu} \sum_{l=0}^{h_\nu} \omega(p_\pi - i, h_\pi - j, p_\nu - k, h_\nu - l, U) \Theta(i + j + k + l - \frac{1}{2})$$

The first term allows that up to three particle-hole pairs can be excited in a transfer reaction. The factor  $X_{NT}$  represents the probability for exciting such a pair and is given by

$$(4.156) \quad X_{NT} = \frac{7\sqrt{E_a/A_a}}{V_1 A_A^2} (p_\nu^2 + p_\pi^2 + h_\nu^2 + 1.5h_\pi^2)$$

For neutrons and protons we adopt for  $V_1$  the value given by Eq.(4.97), for deuterons and tritons we take  $V_1=17$  MeV, and for Helium-3 and alpha particles we take  $V_1=25$  MeV. The finite well depth correction for Eq. (4.155) are made using a well depth of

$$(4.157) \quad V = V_1 \left( \frac{2Z}{A} \right) \text{ if } n_\pi = 0 \\ = V_1 \text{ otherwise.}$$

The second term of Eq. (4.155) allows for transfer of nucleons at the Fermi level. Here, the Heaviside function is merely used to avoid double counting of  $\omega(p_\pi, h_\pi, p_\nu, h_\nu, U)$ .

### Knockout reactions

For (*nucleon*,  $\alpha$ ) reactions a knockout contribution is added. The general differential cross section formula for a knockout reaction of the type  $A(a, b)B$  is

$$(4.158) \quad \frac{d\sigma_{a,b}^{KO}}{dE_b} = \frac{\sigma_{a,inv}(E_a)}{14} (2s_b + 1) A_b E_b \sigma_{b,inv}(E_b) \\ \times \frac{P_b g_a g_b [U - A_{KO}(p_a, h_b)]}{\sum_{c=a,b} (2s_c + 1) A_c \langle \sigma_c \rangle (E_{max} + 2B_{coul,c})(E_{max} - B_{coul,c})^2 g_a g_b^2 / 6g_c}$$

where  $P_b$  is the probability of exciting a  $b$ -type particle-hole pair,  $E_{max}$  is the maximum emission energy, and  $B_{coul,c}$  is the Coulomb barrier for a particle  $c$ . The average inverse cross section  $\langle \sigma_c \rangle$  is given by

$$(4.159) \quad \langle \sigma_c \rangle = \int_{B_{coul,c}}^{E_{max}} dE \sigma_c(E)$$

For the knockout model, the single-particle state density parameters for the cluster degrees of freedom  $g$  represent the number of cluster states per unit energy. The relevant values are given by

$$(4.160) \quad g_n = N/13, \quad g_p = Z/13, \quad g_\alpha = A/208 \text{ MeV}.$$

The Pauli correction factor  $A_{KO}$  is given by

$$(4.161) \quad A_{KO}(p_a, h_b) = \frac{1}{2g_a^2} - \frac{1}{2g_b^2}$$

The probabilities for exciting the various particle-hole pairs are

$$(4.162) \quad \begin{aligned} P_n &= \frac{N_A - \phi Z_A}{A_A - 2\phi Z_A + \phi Z_A/2} \\ P_p &= \frac{Z_A - \phi Z_A}{A_A - 2\phi Z_A + \phi Z_A/2} \\ P_\alpha &= \frac{\phi Z_A/2}{A_A - 2\phi Z_A + \phi Z_A/2} \end{aligned}$$

The factors  $\phi$  are a kind of pre-formation parameters [68]. The following values are adopted

$$(4.163) \quad \begin{aligned} N_A \leq 116 & : \phi = 0.08 \\ 116 \leq N_A < 126 & : \phi = 0.02 + 0.06(126 - N_A)/10 \\ 126 \leq N_A < 129 & : \phi = 0.02 + 0.06(N_A - 126)/3 \\ 129 \leq N_A & : \phi = 0.08 \end{aligned}$$

### Break-up reactions

For reactions induced by complex particles, break-up may play an important role. This holds especially for weakly bound projectiles like deuterons. Break-up is here defined as having a projectile fragment emerge from the reaction in a relatively narrow peak centered close to the beam velocity and strongly directed toward forward angles. For deuterons only, a simple model by Kalbach has been included [69]. This leads to an extra contribution in the (d,n) and (d,p) channels.

The centroid energy of the breakup peak, in MeV, is given by

$$(4.164) \quad \epsilon_0 = \frac{A_b}{A_a} \left( \epsilon_a - B_{a,b} - \frac{Z_a Z_A}{9.5} \right) + \frac{Z_b Z_B}{9.5},$$

where  $\epsilon_a$  represents the channel energy (the energy of both the emitted particle and the recoiling nucleus in the center of mass), and  $B_{a,b}$  is the binding energy in the projectile for the indicated breakup channel (2.224 MeV for deuterons). The peak is assumed to be described by a Gaussian line shape with a width parameter of

$$(4.165) \quad \Gamma = 1.15 + 0.12E_a - \frac{A_A}{140},$$

where  $E_a$  is the laboratory energy of the incident deuteron, and the width parameter is given in MeV. The break-up cross section is assumed to be

$$(4.166) \quad \sigma_{BU} = K_{d,b} \frac{(A_A^{1/3} + 0.8)^2}{1 + \exp(\frac{13-E_a}{6})},$$

where the normalization factors are

$$(4.167) \quad \begin{aligned} K_{d,n} &= 18, \\ K_{d,p} &= 21. \end{aligned}$$

Finally, the differential break-up cross section is given by

$$(4.168) \quad \frac{d\sigma_{a,b}^{BU}}{dE_b} = \sigma_{BU} \frac{1}{\Gamma\sqrt{2\pi}} \exp\left(-\frac{(\epsilon_0 - E_b)^2}{\Gamma^2}\right).$$

In the output, we have stored the break-up contribution in the column “knockout” (which is normally only used for nucleon-induced reactions with alpha particles as ejectiles).

The stripping, pick-up, break-up and knock-out contributions can be adjusted with the **Cstrip** and **Cknock** keywords.

#### 4.4.5 Angular distribution systematics

A sound pre-equilibrium theory should, besides the angle-integrated spectra, also describe the smooth forward peaked angular distributions in the continuum. A physics method to do so will be included in a future version of TALYS (multi-step direct reactions). Semi-classical models, such as the exciton model, have always had some problems to describe angular distributions (essentially because it is based on a compound-like concept instead of a direct one [70]). A powerful phenomenological method is given by Kalbach [71]. It is based on experimental information only and the insight that in general, a pre-equilibrium process consists of a forward peaked part (multi-step direct) and an isotropic part (multi-step compound), and that the angular distributions are fairly structureless and all look alike. The Kalbach formula for the double-differential cross section for a projectile  $a$  and an ejectile  $b$  is

$$(4.169) \quad \frac{d^2\sigma_{a,xb}}{dE_b d\Omega} = \frac{1}{4\pi} \left[ \frac{d\sigma^{PE}}{dE_b} + \frac{d\sigma^{comp}}{dE_b} \right] \frac{a}{\sinh(a)} [\cosh(a \cos \Theta) + f_{MSD}(E_b) \sinh(a \cos \Theta)]$$

where  $\frac{d\sigma^{PE}}{dE_b}$  and  $\frac{d\sigma^{comp}}{dE_b}$  are the angle-integrated pre-equilibrium and compound spectra, respectively, and  $f_{MSD}$  is the so-called multi-step direct or pre-equilibrium ratio:

$$(4.170) \quad f_{MSD}(E_b) = \frac{d\sigma^{PE}}{dE_b} / \left[ \frac{d\sigma^{PE}}{dE_b} + \frac{d\sigma^{comp}}{dE_b} \right]$$

which thus increases from practically 0 at very low emission energy to 1 at the highest emission energies. Hence, once the angle-integrated spectra are known, the parameter  $a$  determines the angular distribution.

Kalbach parameterized it as

$$\begin{aligned}
a(e'_a, e'_b) &= 0.04 \frac{E_1 e'_b}{e'_a} + 1.8 \times 10^{-6} \left( \frac{E_1 e'_b}{e'_a} \right)^3 + 6.7 \times 10^{-7} M_a m_b \left( \frac{E_3 e'_b}{e'_a} \right)^4, \\
E_1 &= \min(e'_a, 130 \text{MeV}) \\
E_3 &= \min(e'_a, 41 \text{MeV}) \\
e'_b &= E_b + S_b \\
e'_a &= E_a + S_a. \\
M_a &= 1 \text{ for neutrons, protons, deuterons, tritons and Helium} - 3 \\
&= 0 \text{ for alpha's} \\
m_b &= 1 \text{ for protons, deuterons, tritons and Helium} - 3 \\
&= \frac{1}{2} \text{ for neutrons} \\
&= 2 \text{ for alpha's} \\
S_b &= 15.68(A_C - A_B) - 28.07 \left[ \frac{(N_C - Z_C)^2}{A_C} - \frac{(N_B - Z_B)^2}{A_B} \right] \\
&\quad - 18.56(A_C^{2/3} - A_B^{2/3}) + 33.22 \left[ \frac{(N_C - Z_C)^2}{A_C^{4/3}} - \frac{(N_B - Z_B)^2}{A_B^{4/3}} \right] \\
&\quad - 0.717 \left[ \frac{Z_C^2}{A_C^{1/3}} - \frac{Z_B^2}{A_B^{1/3}} \right] + 1.211 \left[ \frac{Z_C^2}{A_C} - \frac{Z_B^2}{A_B} \right] - I_b \\
I_d &= 2.225 \\
I_t &= 8.482 \\
I_h &= 7.718 \\
(4.171) \quad I_\alpha &= 28.296,
\end{aligned}$$

Here,  $E_a$  and  $E_b$  are the incident and the outgoing energy, respectively. The number  $M_a$  represents the incident particle, while  $m_b$  represents the outgoing particle, C is a label for the compound nucleus, B for the final nucleus and the Myers and Swiatecki mass formula [72] for spherical nuclides should be used here to determine the separation energy  $S$ . Finally  $I_b$  is the energy required to break the emitted particle up into its constituents.

Since we calculate the pre-equilibrium and compound cross sections explicitly (and actually only use  $f_{MSD}$  for ENDF-6 data libraries), Eq. (4.169) can be reduced to a formula for the double-differential pre-equilibrium cross section

$$(4.172) \quad \frac{d^2 \sigma_{a,xb}^{\text{PE}}}{dE_b d\Omega} = \frac{1}{4\pi} \frac{d\sigma^{\text{PE}}}{dE_b} \frac{a}{\sinh(a)} \exp(a \cos \Theta),$$

to which the isotropic compound angular distribution can be added. In sum, given the angle-integrated spectrum  $\frac{d\sigma^{\text{PE}}}{dE_b}$  by some physics model, the double-differential cross section is returned quite simply and reasonably accurate by Eq. (4.172).

## 4.5 Compound reactions

The term compound nucleus reaction is commonly used for two different mechanisms: (i) the process of the capture of the projectile in the target nucleus to form a compound nucleus, which subsequently emits a particle or gamma, (ii) the multiple emission process of highly excited residual nuclei formed after the binary reaction. The latter, which is known as multiple compound emission, will be explained in Section 4.6. We first treat the binary compound nucleus reaction that plays a role at low incident energy. It differs from the multiple compound emission at two important points: (a) the presence of width fluctuation corrections and (b) non-isotropic, though still symmetric, angular distributions.

### 4.5.1 Binary compound cross section and angular distribution

In the compound nucleus picture, the projectile and the target nucleus form a compound nucleus with a total energy  $E^{tot}$  and a range of values for the total spin  $J$  and parity  $\Pi$ . The following energy, angular momentum and parity conservation laws need to be obeyed,

$$(4.173) \quad \begin{aligned} E_a + S_a &= E_{a'} + E_x + S_{a'} = E^{tot} \\ s + I + l &= s' + I' + l' = J \\ \pi_0 \Pi_0 (-1)^l &= \pi_f \Pi_f (-1)^{l'} = \Pi. \end{aligned}$$

The compound nucleus formula for the binary cross section is given by

$$(4.174) \quad \begin{aligned} \sigma_{\alpha\alpha'}^{comp} &= D^{comp} \frac{\pi}{k^2} \sum_{J=\text{mod}(I+s,1)}^{l_{max}+I+s} \sum_{\Pi=-1}^1 \frac{2J+1}{(2I+1)(2s+1)} \sum_{j=|J-I|}^{J+I} \sum_{l=|j-s|}^{j+s} \sum_{j'=|J-I'|}^{J+I'} \sum_{l'=|j'-s'|}^{j'+s'} \\ &\times \delta_{\pi}(\alpha) \delta_{\pi}(\alpha') \frac{T_{\alpha l j}^J(E_a) \langle T_{\alpha' l' j'}^J(E_{a'}) \rangle}{\sum_{\alpha'', l'', j''} \delta_{\pi}(\alpha'') \langle T_{\alpha'' l'' j''}^J(E_{a'')} \rangle} W_{\alpha l j \alpha' l' j'}^J, \end{aligned}$$

In the above equations, the symbols have the following meaning:

$E_a$  = projectile energy

$s$  = spin of the projectile

$\pi_0$  = parity of the projectile

$l$  = orbital angular momentum of the projectile

$j$  = total angular momentum of the projectile

$\delta_{\pi}(\alpha) = 1$ , if  $(-1)^l \pi_0 \Pi_0 = \Pi$  and 0 otherwise

$\alpha$  = channel designation of the initial system of projectile and target nucleus:

$\alpha = \{a, s, E_a, E_x^0, I, \Pi_0\}$ , where  $a$  is the projectile type and  $E_x^0$  the excitation energy of the target nucleus (usually zero)

$l_{max}$  = maximum l-value for projectile

$S_a$  = separation energy

$E_{a'}$  = ejectile energy

$s'$  = spin of the ejectile

$\pi_f$  = parity of the ejectile

$l'$  = orbital angular momentum of the ejectile

$j'$  = total angular momentum of the ejectile

$\delta_\pi(\alpha') = 1$ , if  $(-1)^{l'} \pi_f \Pi_f = \Pi$  and 0 otherwise

$\alpha'$  = channel designation of the final system of ejectile and residual nucleus:

$\alpha' = \{a', s', E_{a'}, E_x, I', \Pi_f\}$ , where  $a'$  is the ejectile type,  $E_x$  the excitation energy of the residual nucleus

$I$  = spin of the target nucleus

$\Pi_0$  = parity of the target

$I'$  = spin of the residual nucleus

$\Pi_f$  = parity of the residual nucleus

$\Pi$  = parity of the compound system

$J$  = total angular momentum of the compound system

$D^{comp}$  = depletion factor to account for direct and pre-equilibrium effects

$k$  = wave number of relative motion

$T$  = transmission coefficient

$W$  = width fluctuation correction (WFC) factor, see the next Section.

In order to let Eq. (4.174) represent the general case, we have denoted the outgoing transmission coefficient by  $\langle T_{\alpha'l'j'}^J \rangle$ . For this, two cases can be distinguished. If the excitation energy  $E_x$ , that is implicit in the definition of channel  $\alpha'$ , corresponds to a discrete state of the final nucleus, then we simply have

$$(4.175) \quad \langle T_{\alpha'l'j'}^J(E_{a'}) \rangle = T_{\alpha'l'j'}^J(E_{a'})$$

and  $E_{a'}$  is exactly determined by Eq. (4.173). For  $\alpha'$  channels in which  $E_x$  is in the continuum, we have an effective transmission coefficient for an excitation energy bin with width  $\Delta E_x$ ,

$$(4.176) \quad \langle T_{\alpha'l'j'}^J(E_{a'}) \rangle = \int_{E_x - \frac{1}{2}\Delta E_x}^{E_x + \frac{1}{2}\Delta E_x} dE_{x'} \rho(E_{x'}, J, \Pi) T_{\alpha'l'j'}^J(E_{a'})$$

where  $\rho$  is the level density, which will be discussed in Section 4.7, and  $T$  is evaluated at an emission energy  $E_{a'}$  that corresponds to the middle of the excitation energy bin, i.e.  $E_{a'} = E^{tot} - E_x - S_{a'}$ . Hence, both transitions to discrete states and transitions to the whole accessible continuum are covered by the sum over  $\alpha'$  in Eq. (4.174). The normalization factor  $D^{comp}$  is

$$(4.177) \quad D^{comp} = [\sigma_{react} - \sigma^{disc,direct} - \sigma^{PE}] / \sigma_{react}$$

This indicates that in TALYS we assume that direct and compound contributions can be added incoherently. This formula for  $D^{comp}$  is only applied for weakly coupled channels that deplete the flux, such as contributions from DWBA or pre-equilibrium. In the case of coupled-channels calculations for the discrete collective states, the transmission coefficients of Eq. (4.174) are automatically reduced by ECIS-06 to account for direct effects and TALYS only subtracts the direct cross section for the weakly coupled levels (DWBA), i.e. if

$$(4.178) \quad \sigma^{disc,direct} = \sigma^{disc,cc} + \sigma^{disc,DWBA}$$

then

$$(4.179) \quad D^{comp} = [\sigma_{react} - \sigma^{disc,DWBA} - \sigma^{PE}] / \sigma_{react}$$

TALYS also computes the compound nucleus formula for the angular distribution. It is given by

$$(4.180) \quad \frac{d\sigma_{\alpha\alpha'}^{comp}(\theta)}{d\Omega} = \sum_L C_L^{comp} P_L(\cos \Theta),$$

where  $P_L$  are Legendre polynomials. The Legendre coefficients  $C_L^{comp}$  are given by

$$(4.181) \quad C_L^{comp} = D^{comp} \frac{\pi}{k^2} \sum_{J,\Pi} \frac{2J+1}{(2I+1)(2s+1)} \sum_{j=|J-I|}^{J+I} \sum_{l=|j-s|}^{j+s} \sum_{j'=|J-I'|}^{J+I'} \sum_{l'=|j'-s'}^{j'+s'} \\ \times \delta_{\pi}(\alpha) \delta_{\pi}(\alpha') \frac{T_{\alpha l j}^J(E_a) \langle T_{\alpha' l' j'}^J(E_{a'}) \rangle}{\sum_{\alpha'', l'', j''} \delta_{\pi}(\alpha'') \langle T_{\alpha'' l'' j''}^J(E_{a''}) \rangle} W_{\alpha l j \alpha' l' j'}^J A_{l l' j j'; L}^J,$$

where the Blatt-Biedenharn factor  $A$  is given by

$$(4.182) \quad A_{l l' j j'; L}^J = \frac{(-1)^{l'-s'-I+s}}{4\pi} (2J+1)(2j+1)(2l+1)(2j'+1)(2l'+1) \\ (l l 0 0 | L 0) \mathcal{W}(J j J j; I L) \mathcal{W}(j j l l; L s) (l' l' 0 0 | L 0) \mathcal{W}(J j' J j'; I' L) \mathcal{W}(j' j' l' l'; L s'),$$

where  $( \quad | \quad )$  are Clebsch-Gordan coefficients and  $\mathcal{W}$  are Racah coefficients.

Formulae (4.174) and (4.180-4.182) show that the width fluctuation correction factors and the angular distribution factors depend on all the angular momentum quantum numbers involved, and thus have to be re-evaluated each time inside all the summations. We generally need these formulae for relatively low incident energy, where the WFC has a significant impact and where the compound nucleus cross section to each individual discrete state is large enough to make its angular distribution of interest.

For projectile energies above several MeV (we generally take the neutron separation energy for safety), the width fluctuations have disappeared, meaning that  $W_{\alpha l j \alpha' l' j'}^J = 1$  for all channels. Then for the angle-integrated compound cross section, instead of performing the full calculation, Eq. (4.174) can be decoupled into two parts that represent the incoming and outgoing reaction flux, respectively. It simplifies to

$$(4.183) \quad \sigma_{\alpha\alpha'}^{comp} = \sum_{J=mod(I+s,1)}^{l_{max}+I+s} \sum_{\Pi=-1}^1 \sigma_{J\Pi}^{CF}(E^{tot}) \frac{\Gamma_{\alpha'}(E^{tot}, J, \Pi \longrightarrow E_x, I', \Pi_f)}{\Gamma^{tot}(E^{tot}, J, \Pi)}$$

where  $\sigma_{J\Pi}^{CF}$  is the compound formation cross section per spin and parity:

$$(4.184) \quad \sigma_{J\Pi}^{CF}(E^{tot}) = D^{comp} \frac{\pi}{k^2} \frac{2J+1}{(2I+1)(2s+1)} \sum_{j=|J-I|}^{J+I} \sum_{l=|j-s|}^{j+s} T_{\alpha l j}^J(E_a) \delta_{\pi}(\alpha)$$

which itself obeys

$$(4.185) \quad \sum_{J=mod(I+s,1)}^{l_{max}+I+s} \sum_{\Pi=-1}^1 \sigma_{J\Pi}^{CF}(E^{tot}) = D^{comp} \sigma_{reac}$$

The partial decay widths are

$$(4.186) \quad \Gamma_{\alpha'}(E^{tot}, J, \Pi \longrightarrow E_x, I', \Pi_f) = \frac{1}{2\pi\rho(E^{tot}, J, \Pi)} \sum_{j=|J-I'|}^{J+I'} \sum_{l'=|j'-s'|}^{j'+s'} \delta_{\pi}(\alpha') \langle T_{\alpha' l' j'}^J(E_{a'}) \rangle$$

and the total decay width is

$$(4.187) \quad \Gamma^{tot}(E^{tot}, J, \Pi) = \sum_{\alpha''} \Gamma_{\alpha''}(E^{tot}, J, \Pi \longrightarrow E_x, I'', \Pi_f)$$

where we sum over all possible states in the residual nuclides through the sum over  $\alpha''$ . Note that the term with the compound nucleus level density,  $2\pi\rho$ , is present in both Eq. (4.186) and Eq. (4.187) and therefore does not need to be calculated in practice for Eq. (4.183). A formula similar to Eq. (4.183) is used for multiple emission, see Section 4.6.

In sum, we use Eqs. (4.174) and (4.181) if either width fluctuations (**widthfluc y**, p. 203) or compound angular distributions (**outangle y**, p. 257) are to be calculated and Eq. (4.183) if they are both not of interest.

A final note to make here is that the formulae of this whole Section can also be applied for excited (isomeric) target states.

## 4.5.2 Width fluctuation correction factor

The WFC factor  $W$  accounts for the correlations that exist between the incident and outgoing waves. From a qualitative point of view, these correlations enhance the elastic channel and accordingly decrease

the other open channels. Above a few MeV of projectile energy, when many competing channels are open, the WFC factor can be neglected and the simple Hauser-Feshbach model is adequate to describe the compound nucleus decay. To explain the WFC factors, we now switch to a more compact notation in which we leave out  $J$  and define  $a = \{\alpha, l, j\}$  and  $b = \{\alpha', l', j'\}$ . With such a notation the compound nucleus cross section can be written in the compact form

$$(4.188) \quad \sigma_{ab} = \frac{\pi}{k_a^2} \frac{T_a T_b}{\sum_c T_c} W_{ab}$$

for each combination of  $a$  and  $b$ . In general, the WFC factor may be calculated using three different expressions, which have all been implemented in TALYS: The Hofmann-Richert-Tepel-Weidenmüller (HRTW) model [73, 74, 75], the Moldauer model [76, 77], and the model using the Gaussian Orthogonal Ensemble (GOE) of Hamiltonian matrices [78]. A comparison between the three models is given in Ref. [183].

For each expression, flux conservation implies that

$$(4.189) \quad T_a = \sum_b \frac{T_a T_b}{\sum_c T_c} W_{ab}$$

This equation can be used to check the numerical accuracy of the WFC calculation (see the **flagcheck** keyword in Chapter 6).

### The HRTW method

The simplest approach is the HRTW method. It is based on the assumption that the main effect of the correlation between incident and outgoing waves is in the elastic channel. In that case, it is convenient to express the compound nucleus cross section (4.188) as

$$(4.190) \quad \sigma_{ab} = \frac{\pi}{k^2} \frac{V_a V_b}{\sum_c V_c} [1 + \delta_{ab}(W_a - 1)],$$

where the  $V_i$ 's are effective transmission coefficients that take into account the correlations.

This expression means that only the elastic channel enhancement is described since for  $a = b$ , Eq. (4.190) becomes

$$(4.191) \quad \sigma_{aa} = \frac{\pi}{k_a^2} \frac{V_a^2}{\sum_c V_c} W_a$$

while for  $a \neq b$ ,

$$(4.192) \quad \sigma_{ab} = \frac{\pi}{k_a^2} \frac{V_a V_b}{\sum_c V_c}$$

An expression for the  $V_i$  values can be determined from the flux conservation condition

$$(4.193) \quad \sum_b \sigma_{ab} = \frac{\pi}{k_a^2} T_a,$$

which yields using Eq. (4.190)

$$(4.194) \quad T_a = V_a + (W_a - 1) \frac{V_a^2}{\sum_c V_c},$$

or

$$(4.195) \quad V_a = \frac{T_a}{1 + \frac{(W_a - 1)V_a}{\sum_c V_c}}.$$

The only required information is thus the expression for  $W_a$ , which can be derived from an analysis using random matrix calculations. In TALYS, the expression of Ref. [75] is used. It reads

$$(4.196) \quad W_a = 1 + \frac{2}{1 + T_a^F} + 87 \left( \frac{T_a - \bar{T}}{\sum_c T_c} \right)^2 \left( \frac{T_a}{\sum_c T_c} \right)^5,$$

with  $\bar{T} = \frac{\sum_c T_c^2}{\sum_c T_c}$  and the exponent  $F = \frac{4 \frac{\bar{T}}{\sum_c T_c} \left( 1 + \frac{T_a}{\sum_c T_c} \right)}{1 + \frac{3\bar{T}}{\sum_c T_c}}$ .

The result for  $V_a$  is obtained after iterating Eq. (4.195) several times, starting from the initial value

$$(4.197) \quad V_a(i = 0) = \frac{T_a}{1 + (W_a - 1) \frac{T_a}{\sum_c T_c}}$$

and calculating  $V_a(i + 1)$  using

$$(4.198) \quad V_a(i + 1) = \frac{T_a}{1 + (W_a - 1) \frac{V_a(i)}{\sum_c V_c(i)}}$$

until  $V_a(i + 1) \approx V_a(i)$ . In a calculation, a few tens of iterations are generally required to reach a stable result.

For each  $J$  and  $\Pi$ , expressions (4.195)-(4.198) only need to be evaluated once. This is done in *hrtwprepare.f*, before all the loops over  $l$ ,  $j$ ,  $l'$  and  $j'$ , etc. quantum numbers are performed. For the calculation of  $W_{\alpha l j \alpha' l' j'}^J$  in Eq. (4.174), which takes place inside all loops, the correct  $V_a$  and  $V_b$  are then addressed. The WFC factor can then be derived from Eqs. (4.188) and (4.190),

$$(4.199) \quad W_{ab} = \frac{V_a V_b}{\sum_c V_c} [1 + \delta_{ab} (W_a - 1)] \frac{\sum_c T_c}{T_a T_b}$$

which is calculated in *hrtw.f*.

**Moldauer expression**

This is the default option for the WFC in TALYS. Moldauer's expression for  $W_{ab}$  is based on the assumption that a  $\chi^2$  law with  $\nu$  degrees of freedom applies for the partial widths  $\Gamma$ , which can be calculated from a Porter-Thomas distribution. These are associated with transmission coefficients as

$$(4.200) \quad T = \frac{2\pi \langle \Gamma \rangle}{D}$$

provided  $\langle \Gamma \rangle \ll D$ , where  $D$  is the mean level spacing. The WFC factor  $W_{ab}$  reads

$$(4.201) \quad W_{ab} = \left(1 + \frac{2\delta_{ab}}{\nu_a}\right) \int_0^{+\infty} \prod_c \left(1 + \frac{2T_c x}{\nu_c \sum_i T_i}\right)^{-(\delta_{ac} + \delta_{bc} + \nu_c/2)} dx$$

Moldauer has parameterised  $\nu$  using Monte Carlo calculations, giving

$$(4.202) \quad \nu_a = 1.78 + (T_a^{1.212} - 0.78) \exp\left(-0.228 \sum_c T_c\right)$$

In TALYS, the integral in Eq. (4.201) is evaluated numerically. For this, the Gauss-Laguerre method has been chosen and we find that 40 integration points are enough to reach convergence, the criterion being the flux conservation of Eq. (4.189). As for the HRTW model, the calculation can be split into parts dependent and independent of the channel quantum numbers. First, in *molprepare.f*, for each  $J$  and  $\Pi$ , we calculate Eq. (4.202) for all channels and the product  $\prod_c \left(1 + \frac{2T_c x}{\nu_c \sum_i T_i}\right)^{-\nu_c/2}$  that appears in Eq. (4.201). Inside all the loops, we single out the correct  $a$  and  $b$  channel and calculate Eq. (4.201) in *moldauer.f*.

Eq. (4.201) involves a product over all possible open channels. When the number of channels is large, the product calculation drastically increases the time of computation, forcing us to consider another method. Many open channels are considered for capture reactions and reactions to the continuum.

**A. Capture reactions** If the projectile is captured by the target nucleus, the compound nucleus is formed with an excitation energy at least equal to the projectile separation energy in the compound system. Since the  $\gamma$  transmission coefficient calculation involves all the possible states to which a photon can be emitted from the initial compound nucleus state, the number of radiative open channels is almost infinite, but each has a very small transmission coefficient. Following Ref. [79], the product over the radiative channels in Eq. (4.201) can be transformed as

$$(4.203) \quad \prod_{c \in \gamma} \left(1 + \frac{2T_c x}{\nu_c \sum_i T_i}\right)^{-\nu_c/2} \approx \lim_{\nu_\gamma \rightarrow +\infty} \left(1 + \frac{2T_\gamma x}{\nu_\gamma \sum_i T_i}\right)^{-\bar{\nu}_\gamma/2} = \exp\left(-\frac{T_\gamma^{eff} x}{\sum_i T_i}\right)$$

where  $T_\gamma^{eff}$  is given by the procedure sketched in Section 4.3. The derivation is based on the hypothesis that all the individual  $T_\gamma$  are almost identical to 0. Therefore, to calculate  $W_{ab}$  when  $b$  denotes the gamma channel, we set  $T_b = 0$  in Eqs. (4.201) and use Eqs. (4.203) to calculate the product for  $\gamma$  channels.

**B. Continuum reactions** For high excitation energies, it is impossible to describe all the open channels individually. It is then necessary to introduce energy bins to discretize the continuum of levels and define continuum (or effective) transmission coefficients as

$$(4.204) \quad T_{eff}(U) = \int_{E_{min}}^{E_{max}} \rho(\varepsilon)T(\varepsilon)d\varepsilon,$$

where  $U$  is generally taken as the middle of the interval  $[E_{min}, E_{max}]$  and  $\rho$  is the density of levels under consideration. This effective transmission coefficient corresponds to an effective number of channels  $N_{eff}(U)$ , given by

$$(4.205) \quad N_{eff}(U) = \int_{E_{min}}^{E_{max}} \rho(\varepsilon)d\varepsilon.$$

Calculating the product term in Eq. (4.201) is tedious, unless one assumes that the energy variation of  $T(\varepsilon)$  is smooth enough to warrant that each of the  $N_{eff}(U)$  channels has the same average transmission coefficient

$$(4.206) \quad T_{mean}(U) = \frac{T_{eff}(U)}{N_{eff}(U)}.$$

Then, the product over the channels  $c$  belonging to such a continuum bin in the Moldauer integral Eq. (4.201) can be replaced by a single term, i.e.

$$(4.207) \quad \prod_c \left( 1 + \frac{2T_c}{\nu_c \sum_i T_i} x \right)^{-\nu_c/2} \approx \left( 1 + \frac{2T_{mean}(U)}{\nu_{mean} \sum_i T_i} x \right)^{-N_{eff}(U)\nu_{mean}/2},$$

where

$$(4.208) \quad \nu_{mean} = 1.78 + (T_{mean}^{1.212} - 0.78) \exp \left( -0.228 \sum_c T_c \right)$$

**C. Fission reactions** The fission reaction is treated as one global channel, regardless of the nature of the fission fragments that result from fission. We will see later on in Section 4.8, how the global fission transmission coefficient is calculated. It is however important to state here that the fission transmission coefficient is generally greater than 1 since it results from a summation over several fission paths and can therefore be defined as

$$(4.209) \quad T_{fis}(U) = \int_{E_{min}}^{E_{max}} \rho_{fis}(\varepsilon)T_f(\varepsilon)d\varepsilon.$$

Of course, one has  $0 \leq T_f(\varepsilon) \leq 1$ , but one can not assume that  $T_f$  is constant over the whole integration energy range as in the case of continuum reactions. To bypass this problem, instead of using a

global fission transmission coefficient, we have grouped the various components of Eq. (4.209) according to their values. Instead of dealing with a global fission transmission coefficient, we use  $N$  different global transmission coefficients (where  $N$  is an adjustable parameter) such that

$$(4.210) \quad T_{fis}(U) = \sum_{i=0}^N T_{fis}(i, U)$$

where

$$(4.211) \quad T_{fis}(i, U) = \int_{E_{min}}^{E_{max}} \rho_{fis}(\varepsilon) T_f(\varepsilon) \delta_{i,N} d\varepsilon$$

and  $\delta_{i,N} = 1$  is  $i/N \leq T_f(\varepsilon) \leq (i+1)/N$  and 0 otherwise.

In this case one can define, as for continuum reactions, an effective number of channels  $N_{fis}(i, U)$ , and use  $N$  average fission transmission coefficients defined by

$$(4.212) \quad T_{fismean}(i) = \frac{T_{fis}(i, U)}{N_{fis}(i, U)}.$$

If  $N$  is large enough, these  $N$  average coefficients can be used for the width fluctuation calculation without making a too crude approximation.

### The GOE triple integral

The two previously described methods to obtain  $W_{ab}$  are readily obtained since both are relatively simple to implement. However, in each case, a semi-empirical parameterisation is used. The GOE formulation avoids such a parameterisation, in which sense it is the more general expression. In the GOE approach,  $W_{ab}$  reads

$$(4.213) \quad W_{ab} = \frac{\sum_c T_c}{8} \int_0^{+\infty} d\lambda_1 \int_0^{+\infty} d\lambda_2 \int_0^1 d\lambda f(\lambda_1, \lambda_2, \lambda) \prod_c (\lambda_1, \lambda_2, \lambda) g_{ab}(\lambda_1, \lambda_2, \lambda)$$

with

$$(4.214) \quad f(\lambda_1, \lambda_2, \lambda) = \frac{\lambda(1-\lambda)|\lambda_1 - \lambda_2|}{\sqrt{\lambda_1 \lambda_2 (1+\lambda_1)(1+\lambda_2)} (\lambda + \lambda_1)^2 (\lambda + \lambda_2)^2},$$

$$(4.215) \quad \prod_c (\lambda_1, \lambda_2, \lambda) = \prod_c \frac{1 - \lambda T_c}{\sqrt{(1 + \lambda_1 T_c)(1 + \lambda_2 T_c)}},$$

and

$$(4.216) \quad g_{ab}(\lambda_1, \lambda_2, \lambda) = \delta_{ab}(1 - T_a) \left( \frac{\lambda_1}{1 + \lambda_1 T_a} + \frac{\lambda_2}{1 + \lambda_2 T_a} + \frac{2\lambda}{1 - \lambda T_a} \right)^2 + (1 + \delta_{ab}) \\ \times \left[ \frac{\lambda_1(1 + \lambda_1)}{(1 + \lambda_1 T_a)(1 + \lambda_1 T_b)} + \frac{\lambda_2(1 + \lambda_2)}{(1 + \lambda_2 T_a)(1 + \lambda_2 T_b)} + \frac{2\lambda(1 - \lambda)}{(1 - \lambda T_a)(1 - \lambda T_b)} \right]$$

The numerical method employed to compute this complicated triple integral is explained in Ref. [183].

Also here, a particular situation exists for the capture channel, where we set

$$(4.217) \quad \prod_{c \in \gamma} \frac{1 - \lambda T_c}{\sqrt{(1 + \lambda_1 T_c)(1 + \lambda_2 T_c)}} \approx \exp \left[ - (2\lambda + \lambda_1 + \lambda_2) T_\gamma^{eff} / 2 \right]$$

and for the continuum, for which we set

$$(4.218) \quad \prod_c (\lambda_1, \lambda_2, \lambda) = \prod_{c \in \text{continuum}} \frac{(1 - \lambda \bar{T}_c)^{N_c}}{\sqrt{(1 + \lambda_1 \bar{T}_c)^{N_c} (1 + \lambda_2 \bar{T}_c)^{N_c}}}.$$

Again, for each  $J$  and  $\Pi$ , the multiplications that do not depend on  $a$  or  $b$  are first prepared in *goeprepare.f*, while the actual WFC calculation takes place in *goef.f*.

## 4.6 Multiple emission

At incident energies above approximately the neutron separation energy, the residual nuclides formed after the first binary reaction are populated with enough excitation energy to enable further decay by particle emission or fission. This is called multiple emission. We distinguish between two mechanisms: multiple compound (Hauser-Feshbach) decay and multiple pre-equilibrium decay.

### 4.6.1 Multiple Hauser-Feshbach decay

This is the conventional way, and for incident energies up to several tens of MeV a sufficient way, to treat multiple emission. It is assumed that pre-equilibrium processes can only take place in the binary reaction and that secondary and further particles are emitted by compound emission.

After the binary reaction, the residual nucleus may be left in an excited discrete state  $i'$  or an excited state within a bin  $i'$  which is characterized by excitation energy  $E_{x'}(i')$ , spin  $I'$  and parity  $\Pi'$ . The population of this state or set of states is given by a probability distribution for Hauser-Feshbach decay  $P^{\text{HF}}$  that is completely determined by the binary reaction mechanism. For a binary neutron-induced reaction to a discrete state  $i'$ , i.e. when  $E_{x'}(i')$ ,  $I'$  and  $\Pi'$  have unique values, the residual population is given by

$$(4.219) \quad P^{\text{HF}}(Z', N', E_{x'}(i'), I', \Pi') = \sigma_{n,k'}^{i'}(E^{\text{tot}}, I, \Pi \rightarrow E_{x'}(i'), I', \Pi'),$$

where the non-elastic reaction cross section for a discrete state  $\sigma_{n,k'}^{i'}$  was defined in Section 3.2.3 and where the ejectile  $k'$  connects the initial compound nucleus  $(Z_C, N_C)$  and the residual nucleus  $(Z', N')$ .

For binary reactions to the continuum, the residual population of states characterised by  $(I', \Pi')$  per  $E_{x'}(i')$  bin is given by the sum of a pre-equilibrium and a compound contribution

$$(4.220) \quad P^{\text{HF}}(Z', N', E_{x'}(i'), I', \Pi') = \int dE_{k'} \frac{d\sigma^{\text{comp,cont}}(E^{\text{tot}}, I, \Pi \rightarrow E_{x'}(i'), I', \Pi')}{dE_{k'}} + \mathcal{P}^{\text{pre}}(Z', N', p_{\pi}^{\text{max}} + 1, h_{\pi}^{\text{max}} + 1, p_{\nu}^{\text{max}} + 1, h_{\nu}^{\text{max}} + 1, E_{x'}(i')),$$

where the integration range over  $dE_{k'}$  corresponds exactly with the bin width of  $E_{x'}(i')$  and  $\mathcal{P}^{\text{pre}}$  denotes the population entering the compound stage after primary preequilibrium emission. The expression for  $\mathcal{P}^{\text{pre}}$  will be given in Eq. (4.224) of the next section. Once the first generation of residual nuclides/states has been filled, the picture can be generalized to tertiary and higher order multiple emission.

In general, the population  $P^{\text{HF}}$  before decay of a level  $i'$  or a set of states  $(I', \Pi', E_{x'}(i'))$  in bin  $i'$  of a nucleus  $(Z', N')$  in the reaction chain is proportional to the feeding, through the ejectiles  $k'$ , from all possible mother bins  $i$  with an energy  $E_x(i)$  in the  $(Z, N)$  nuclides, i.e.

$$(4.221) \quad \begin{aligned} P^{\text{HF}}(Z', N', E_{x'}(i'), I', \Pi') &= \sum_{I, \Pi} \sum_{k'} \sum_i [P^{\text{HF}}(Z, N, E_x(i), I, \Pi) \\ &+ \mathcal{P}^{\text{pre}}(Z, N, p_{\pi}^{\text{max}} + 1, h_{\pi}^{\text{max}} + 1, p_{\nu}^{\text{max}} + 1, h_{\nu}^{\text{max}} + 1, E_x(i))] \\ &\times \frac{\Gamma_{k'}(E_x(i), I, \Pi \rightarrow E_{x'}(i'), I', \Pi')}{\Gamma^{\text{tot}}(E_x(i), I, \Pi)}. \end{aligned}$$

The appearance of the indices  $p_{\pi}^{\text{max}}$  indicates that only the reaction population that has not been emitted via the (multiple) pre-equilibrium mechanism propagates to the multiple compound stage. Similar to Eq. (4.186) the decay widths are given by (4.222)

$$\Gamma_{k'}(E_x(i), I, \Pi \rightarrow E_{x'}(i'), I', \Pi') = \frac{1}{2\pi\rho(E_x(i), I, \Pi)} \sum_{j'=|J-I'|}^{J+I'} \sum_{l'=|j'-s'|}^{j'+s'} \delta_{\pi}(\alpha') \langle T_{\alpha'l'j'}^J(E'_{\alpha'}) \rangle.$$

Again, the term  $2\pi\rho$  (compound nucleus level density) of the decay width (4.222) falls out of the multiple emission equation (4.221) and therefore does not need to be calculated in practice. The total decay width is

$$(4.223) \quad \Gamma^{\text{tot}}(E_x(i), I, \Pi) = \sum_{k''} \sum_{I''=\text{mod}(J+s,1)}^{J+I_{\text{max}}} \sum_{\Pi''=-1}^1 \sum_{i''} \Gamma_{k''}(E_x(i), I, \Pi \rightarrow E_{x''}(i''), I'', \Pi'').$$

In sum, the only differences between binary and multiple compound emission are that width fluctuations and angular distributions do not enter the model and that the initial compound nucleus energy  $E^{\text{tot}}$  is replaced by an excitation energy bin  $E_x$  of the mother nucleus. The calculational procedure, in terms of sequences of decaying bins, was already explained in Chapter 3.

#### 4.6.2 Multiple pre-equilibrium emission

At high excitation energies, resulting from high incident energies, the composite nucleus is far from equilibrated and it is obvious that the excited nucleus should be described by more degrees of freedom

than just  $E_x$ ,  $J$  and  $\Pi$ . In general, we need to keep track of the particle-hole configurations that are excited throughout the reaction chain and thereby calculate multiple pre-equilibrium emission up to any order. This is accomplished by treating multiple pre-equilibrium emission within the exciton model. This is the default option for multiple pre-equilibrium calculations in TALYS (selected with the keyword **mpreeqmode 1**). TALYS contains, furthermore, an alternative more approximative model for multiple pre-equilibrium emission (**mpreeqmode 2**), called the *s-wave transmission coefficient method*. Both approaches are discussed below.

### Multiple pre-equilibrium emission within the exciton model

We introduce the pre-equilibrium population  $\mathcal{P}^{\text{pre}}(Z, N, p_\pi, h_\pi, p_\nu, h_\nu, E_x(i))$  which holds the amount of the reaction population present in a unique  $(Z, N)$  nucleus,  $(p_\pi, h_\pi, p_\nu, h_\nu)$  exciton state and excitation energy bin  $E_x(i)$ . A special case is the pre-equilibrium population for a particular exciton state after binary emission, which can be written as

$$\begin{aligned}
 & \mathcal{P}^{\text{pre}}(Z', N', p_\pi - Z_{k'}, h_\pi, p_\nu - N_{k'}, h_\nu, E_{x'}(i')) = \\
 & = \sigma^{\text{CF}}(Z_C, N_C, E^{\text{tot}}) W_{k'}(Z_C, N_C, E^{\text{tot}}, p_\pi, h_\pi, p_\nu, h_\nu, E_{k'}) \\
 (4.224) \quad & \times \tau(Z_C, N_C, E^{\text{tot}}, p_\pi, h_\pi, p_\nu, h_\nu) P(Z_C, N_C, E^{\text{tot}}, p_\pi, h_\pi, p_\nu, h_\nu),
 \end{aligned}$$

where  $Z_C$  ( $N_C$ ) again is the compound nucleus charge (neutron) number and  $Z_{k'}$  ( $N_{k'}$ ) corresponds to the ejectile charge (neutron) number. The residual excitation energy  $E_x(i')$  is linked to the total energy  $E^{\text{tot}}$ , the ejectile energy  $E_{k'}$ , and its separation energy  $S(k')$  by  $E_x(i') = E^{\text{tot}} - E_{k'} - S(k')$ . This  $\mathcal{P}^{\text{pre}}$  represents the feeding term for secondary pre-equilibrium emission. Note that for several particle-hole configurations this population is equal to zero.

In general, the pre-equilibrium population can be expressed in terms of the mother nucleus, excitation energy bins, and particle-hole configurations from which it is fed. The residual population is given by a generalization of Eq. (4.87), in which  $\sigma^{\text{CF}}(Z_C, N_C, E^{\text{tot}})$  is replaced by the population of the particle-hole states left after the previous emission stage  $\mathcal{P}^{\text{pre}}(Z, N, p_\pi^0, h_\pi^0, p_\nu^0, h_\nu^0, E_x(i))$ . Since several combinations of emission and internal transitions may lead to the same configuration, a summation is applied over the ejectiles treated in multiple pre-equilibrium (neutrons and protons), over the  $(p_\pi^0, h_\pi^0, p_\nu^0, h_\nu^0)$  configurations with which the next step is started and over the mother excitation energy bins:

$$\begin{aligned}
 \mathcal{P}^{\text{pre}}(Z', N', p'_\pi, h'_\pi, p'_\nu, h'_\nu, E_{x'}(i')) & = \sum_{k'=n,p} \sum_{p_\pi^0=1}^{p_\pi^{\text{max}}} \sum_{h_\pi^0=1}^{h_\pi^{\text{max}}} \sum_{p_\nu^0=1}^{p_\nu^{\text{max}}} \sum_{h_\nu^0=1}^{h_\nu^{\text{max}}} \\
 & \sum_i \mathcal{P}^{\text{pre}}(Z, N, p_\pi^0, h_\pi^0, p_\nu^0, h_\nu^0, E_x(i)) \\
 & W_k(Z, N, p_\pi, h_\pi, p_\nu, h_\nu, E_x(i), E_{k'}) \tau(Z, N, p_\pi, h_\pi, p_\nu, h_\nu, E_x(i)) \\
 (4.225) \quad & \times P(Z, N, p_\pi, h_\pi, p_\nu, h_\nu, E_x(i)),
 \end{aligned}$$

where the mother and daughter quantities are related by

$$\begin{aligned}
 Z &= Z' + Z_{k'}, \\
 N &= N' + N_{k'}, \\
 p_\pi &= p'_\pi + Z_{k'}, \\
 h_\pi &= h'_\pi, \\
 p_\nu &= p'_\nu + N_{k'}, \\
 h_\nu &= h'_\nu, \\
 E_x &= E_{x'}(i') + E_{k'} + S_{k'}.
 \end{aligned}
 \tag{4.226}$$

In the computation, we thus need to keep track of every possible  $(Z', N', p'_\pi, h'_\pi, p'_\nu, h'_\nu, E_{x'}(i'))$  configuration, which is uniquely linked to a mother exciton state  $(Z, N, p_\pi, h_\pi, p_\nu, h_\nu, E_x(i))$  through the ejectile characterized by  $(Z_{k'}, N_{k'}, E_{k'})$ . The term  $P(Z, N, p_\pi, h_\pi, p_\nu, h_\nu, E_x(i))$  represents the part of the pre-equilibrium cross section that starts in  $(Z, N, p_\pi^0, h_\pi^0, p_\nu^0, h_\nu^0, E_x(i))$  and survives emission up to a new particle-hole state  $(Z, N, p_\pi, h_\pi, p_\nu, h_\nu, E_x(i))$ . Again (see Eq. (4.102)),

$$P(Z, N, p_\pi^0, h_\pi^0, p_\nu^0, h_\nu^0, E_x(i)) = 1,
 \tag{4.227}$$

and the calculation for each newly encountered  $(Z, N, p_\pi, h_\pi, p_\nu, h_\nu, E_x(i))$  configuration proceeds according to Eq. (4.100).

The part of  $\mathcal{P}^{\text{pre}}$  that does not feed a new multiple pre-equilibrium population automatically goes to the multiple Hauser-Feshbach chain of Eq. (4.221).

The final expression for the multiple pre-equilibrium spectrum is very similar to Eq.( 4.87)

$$\begin{aligned}
 \frac{d\sigma_k^{\text{MPE}}}{dE_{k'}} &= \sum_{p_\pi^0=1}^{p_\pi^{\text{max}}} \sum_{h_\pi^0=1}^{h_\pi^{\text{max}}} \sum_{p_\nu^0=1}^{p_\nu^{\text{max}}} \sum_{h_\nu^0=1}^{h_\nu^{\text{max}}} \\
 &\sum_i \mathcal{P}^{\text{pre}}(Z, N, p_\pi^0, h_\pi^0, p_\nu^0, h_\nu^0, E_x(i)) \\
 &\sum_{p_\pi=p_\pi^0}^{p_\pi^{\text{max}}} \sum_{h_\pi=h_\pi^0}^{h_\pi^{\text{max}}} \sum_{p_\nu=p_\nu^0}^{p_\nu^{\text{max}}} \sum_{h_\nu=h_\nu^0}^{h_\nu^{\text{max}}} W_k(Z, N, p_\pi, h_\pi, p_\nu, h_\nu, E_x(i), E_{k'}) \\
 &\times \tau(Z, N, p_\pi, h_\pi, p_\nu, h_\nu, E_x(i)) P(Z, N, p_\pi, h_\pi, p_\nu, h_\nu, E_x(i))
 \end{aligned}
 \tag{4.228}$$

### Multiple pre-equilibrium emission with the s-wave transmission coefficient method

Apart from the exciton model, TALYS offers another, slightly faster, method to determine multiple pre-equilibrium emission [80, 81]. Within this approach the multiple pre-equilibrium spectrum is given by

the following expression:

$$\begin{aligned}
 \frac{d\sigma_k^{\text{MPE}}}{dE_{k'}} &= \sum_{p_\pi^0=1}^{p_\pi^{\text{max}}} \sum_{h_\pi^0=1}^{h_\pi^{\text{max}}} \sum_{p_\nu^0=1}^{p_\nu^{\text{max}}} \sum_{h_\nu^0=1}^{h_\nu^{\text{max}}} \\
 &\sum_i \mathcal{P}^{\text{pre}}(Z, N, p_\pi^0, h_\pi^0, p_\nu^0, h_\nu^0, E_x(i)) \\
 &\frac{1}{p_\pi^0 + p_\nu^0} \frac{\omega(Z_{k'}, h_\pi^0, N_{k'}, h_\nu^0, E_{k'} + S_{k'}) \omega(p_\pi^0 - Z_{k'}, h_\pi^0, p_\nu^0 - N_{k'}, h_\nu^0, E_x(i) - E_{k'} - S_{k'})}{\omega(p_\pi^0, h_\pi^0, p_\nu^0, h_\nu^0, E_x(i))} \\
 (4.229) \quad &\times T_s(E_{k'})
 \end{aligned}$$

In this approach each residual particle-hole configuration created in the primary pre-equilibrium decay may have one or more excited particles in the continuum. Each of these excited particles can either be emitted or captured. The emission probability is assumed to be well represented by the s-wave transmission coefficient  $T_s(E_{k'})$ .

## 4.7 Level densities

In statistical models for predicting cross sections, nuclear level densities are used at excitation energies where discrete level information is not available or incomplete. We use several models for the level density in TALYS, which range from phenomenological analytical expressions to tabulated level densities derived from microscopic models. The complete details can be found in Ref. [168].

To set the notation, we first give some general definitions. The *level density*  $\rho(E_x, J, \Pi)$  corresponds to the number of nuclear levels per MeV around an excitation energy  $E_x$ , for a certain spin  $J$  and parity  $\Pi$ . The *total level density*  $\rho^{\text{tot}}(E_x)$  corresponds to the total number of levels per MeV around  $E_x$ , and is obtained by summing the level density over spin and parity:

$$(4.230) \quad \rho^{\text{tot}}(E_x) = \sum_J \sum_\Pi \rho(E_x, J, \Pi).$$

The nuclear levels are degenerate in  $M$ , the magnetic quantum number, which gives rise to the *total state density*  $\omega^{\text{tot}}(E_x)$  which includes the  $2J + 1$  states for each level, i.e.

$$(4.231) \quad \omega^{\text{tot}}(E_x) = \sum_J \sum_\Pi (2J + 1) \rho(E_x, J, \Pi).$$

When level densities are given by analytical expressions they are usually factorized as follows

$$(4.232) \quad \rho(E_x, J, \Pi) = P(E_x, J, \Pi) R(E_x, J) \rho^{\text{tot}}(E_x),$$

where  $P(E_x, J, \Pi)$  is the parity distribution and  $R(E_x, J)$  the spin distribution. In all but two level density models in TALYS (**ldmodel 5,6**), the parity equipartition is assumed, i.e.

$$(4.233) \quad P(E_x, J, \Pi) = \frac{1}{2},$$

However, in our programming, we have accounted for the possibility to adopt non-equal parities, such as e.g. in the case of microscopic level density tables.

### 4.7.1 Effective level density

We first describe the simplest expressions that are included in TALYS for level densities. We here use the term "effective" to denote that the nuclear collective effects are not explicitly considered, but instead are effectively included in the level density expression.

#### The Fermi Gas Model

Arguably the best known analytical level density expression is that of the Fermi Gas model (FGM). It is based on the assumption that the single particle states which construct the excited levels of the nucleus are equally spaced, and that collective levels are absent. For a two-fermion system, i.e. distinguishing between excited neutrons and protons, the total Fermi gas state density reads

$$(4.234) \quad \omega_F^{\text{tot}}(E_x) = \frac{\sqrt{\pi} \exp \left[ 2\sqrt{aU} \right]}{12 a^{1/4} U^{5/4}},$$

with  $U$  defined by

$$(4.235) \quad U = E_x - \Delta,$$

where the energy shift  $\Delta$  is an empirical parameter which is equal to, or for some models closely related to, the pairing energy which is included to simulate the known odd-even effects in nuclei. The underlying idea is that  $\Delta$  accounts for the fact that pairs of nucleons must be separated before each component can be excited individually. In practice,  $\Delta$  plays an important role as adjustable parameter to reproduce observables, and its definition can be different for the various models we discuss here. Eq. (4.234) indicates that throughout this manual we will use both the *true* excitation energy  $E_x$ , as basic running variable and for expressions related to discrete levels, and the *effective* excitation energy  $U$ , mostly for expressions related to the continuum.

Eq. (4.234) also contains the level density parameter  $a$ , which theoretically is given by  $a = \frac{\pi^2}{6}(g_\pi + g_\nu)$ , with  $g_\pi$  ( $g_\nu$ ) denoting the spacing of the proton (neutron) single particle states near the Fermi energy. In practice  $a$  is determined, through Eq. (4.234), from experimental information of the specific nucleus under consideration or from global systematics. In contemporary analytical models, it is energy-dependent. This will be discussed in more detail below.

Under the assumption that the projections of the total angular momentum are randomly coupled, it can be derived [82] that the Fermi gas level density is

$$(4.236) \quad \rho_F(E_x, J, \Pi) = \frac{1}{2} \frac{2J+1}{2\sqrt{2\pi}\sigma^3} \exp \left[ -\frac{(J + \frac{1}{2})^2}{2\sigma^2} \right] \frac{\sqrt{\pi} \exp \left[ 2\sqrt{aU} \right]}{12 a^{1/4} U^{5/4}},$$

where the first factor  $\frac{1}{2}$  represents the aforementioned equiparity distribution and  $\sigma^2$  is the spin cut-off parameter, which represents the width of the angular momentum distribution. It depends on excitation energy and will also be discussed in more detail below. Eq. (4.236) is a special case of the factorization

of Eq. (4.232), with the Fermi gas spin distribution given by,

$$(4.237) \quad R_F(E_x, J) = \frac{2J+1}{2\sigma^2} \exp \left[ -\frac{(J + \frac{1}{2})^2}{2\sigma^2} \right].$$

Summing  $\rho_F(E_x, J, \Pi)$  over all spins and parities yields for the total Fermi gas level density

$$(4.238) \quad \rho_F^{\text{tot}}(E_x) = \frac{1}{\sqrt{2\pi}\sigma} \frac{\sqrt{\pi} \exp \left[ 2\sqrt{aU} \right]}{12 a^{1/4} U^{5/4}},$$

which is, through Eq. (4.234), related to the total Fermi gas state density as

$$(4.239) \quad \rho_F^{\text{tot}}(E_x) = \frac{\omega_F^{\text{tot}}(E_x)}{\sqrt{2\pi}\sigma}.$$

These equations show that  $\rho_F^{\text{tot}}$  and  $\rho_F$  are determined by three parameters,  $a$ ,  $\sigma$  and  $\Delta$ . The first two of these have specific energy dependencies that will now be discussed separately, while we postpone the discussion of  $\Delta$  to the Section on the various specific level density models.

In the Fermi gas model, the level density parameter  $a$  can be derived from  $D_0$ , the average s-wave level spacing at the neutron separation energy  $S_n$ , which is usually obtained from the available experimental set of s-wave resonances. The following equation can be used:

$$(4.240) \quad \frac{1}{D_0} = \sum_{J=|I-\frac{1}{2}|}^{J=I+\frac{1}{2}} \rho_F(S_n, J, \Pi)$$

where  $I$  is the spin of the target nucleus. From this equation, the level density parameter  $a$  can be extracted by an iterative search procedure.

In the TALYS-output, all quantities of interest are printed, if requested.

### The level density parameter $a$

The formulae described above may suggest a nuclide-specific constant value for the level density parameter  $a$ , and the first level density analyses spanning an entire range of nuclides [83, 84, 85] indeed treated  $a$  as a parameter independent of energy. Later, Ignatyuk et al. [86] recognized the correlation between the parameter  $a$  and the shell correction term of the liquid-drop component of the mass formula. They argued that a more realistic level density is obtained by assuming that the Fermi gas formulae outlined above are still valid, but that energy-dependent shell effects should be effectively included through an energy dependent expression for  $a$ . This expression takes into account the presence of shell effects at low energy and their disappearance at high energy in a phenomenological manner. It reads,

$$(4.241) \quad a = a(E_x) = \tilde{a} \left( 1 + \delta W \frac{1 - \exp[-\gamma U]}{U} \right).$$

Here,  $\tilde{a}$  is the asymptotic level density value one would obtain in the absence of any shell effects, i.e.  $\tilde{a} = a(E_x \rightarrow \infty)$  in general, but also  $\tilde{a} = a(E_x)$  for all  $E_x$  if  $\delta W = 0$ . The damping parameter  $\gamma$

Model	$\alpha$	$\beta$	$\gamma_1$	$\delta_{\text{global}}$
BFM effective	0.0722396	0.195267	0.410289	0.173015
BFM collective	0.0381563	0.105378	0.546474	0.743229
CTM effective	0.0692559	0.282769	0.433090	0.
CTM collective	0.0207305	0.229537	0.473625	0.
GSM effective	0.110575	0.0313662	0.648723	1.13208
GSM collective	0.0357750	0.135307	0.699663	-0.149106

Table 4.3: Global level density parameters for the phenomenological models

determines how rapidly  $a(E_x)$  approaches  $\tilde{a}$ . Finally,  $\delta W$  is the shell correction energy. The absolute magnitude of  $\delta W$  determines how different  $a(E_x)$  is from  $\tilde{a}$  at low energies, while the sign of  $\delta W$  determines whether  $a(E_x)$  decreases or increases as a function of  $E_x$ .

The asymptotic value  $\tilde{a}$  is given by the smooth form

$$(4.242) \quad \tilde{a} = \alpha A + \beta A^{2/3},$$

where  $A$  is the mass number, while the following systematical formula for the damping parameter is used,

$$(4.243) \quad \gamma = \frac{\gamma_1}{A^{1/3}} + \gamma_2.$$

In Eqs. (4.242)-(4.243),  $\alpha$ ,  $\beta$  and  $\gamma_{1,2}$  are global parameters that have been determined to give the best average level density description over a whole range of nuclides. They are given in Table 4.3, where also the average pairing correction  $\delta_{\text{global}}$  is given. Also,  $\gamma_2 = 0$  by default. The  $\alpha$  and  $\beta$  parameters can be changed with the **alphald** and **betald** keywords, see page 227. The parameters  $\gamma_1$  and  $\gamma_2$  can be adjusted with the **gammashell1** and **gammashell2** keywords, see page 228, and  $\delta_{\text{global}}$  with the **Pshiftconstant** keyword, see page 233.

We define  $\delta W$ , expressed in MeV, as the difference between the experimental mass of the nucleus  $M_{\text{exp}}$  and its mass according to the spherical liquid-drop model mass  $M_{\text{LDM}}$  (both expressed in MeV),

$$(4.244) \quad \delta W = M_{\text{exp}} - M_{\text{LDM}}.$$

For the real mass we take the value from the experimental mass compilation [87]. Following Mengoni

and Nakajima [88], for  $M_{\text{LDM}}$  we take the formula by Myers and Swiatecki [72]:

$$\begin{aligned}
 M_{\text{LDM}} &= M_n N + M_H Z + E_{\text{vol}} + E_{\text{sur}} + E_{\text{coul}} + \delta \\
 M_n &= 8.07144 \text{ MeV} \\
 M_H &= 7.28899 \text{ MeV} \\
 E_{\text{vol}} &= -c_1 A \\
 E_{\text{sur}} &= c_2 A^{2/3} \\
 E_{\text{coul}} &= c_3 \frac{Z^2}{A^{1/3}} - c_4 \frac{Z^2}{A} \\
 c_i &= a_i \left[ 1 - \kappa \left( \frac{N - Z}{A} \right)^2 \right], \quad i = 1, 2 \\
 a_1 &= 15.677 \text{ MeV} \\
 a_2 &= 18.56 \text{ MeV} \\
 \kappa &= 1.79 \\
 c_3 &= 0.717 \text{ MeV} \\
 c_4 &= 1.21129 \text{ MeV} \\
 \delta &= -\frac{11}{\sqrt{A}} \text{ even - even} \\
 &= 0 \text{ odd} \\
 &= \frac{11}{\sqrt{A}} \text{ odd - odd.}
 \end{aligned}
 \tag{4.245}$$

Eq. (4.241) should in principle be applied at all excitation energies, unless a different level density prescription is used at low energies, as e.g. for the CTM. Therefore, a helpful extra note for practical calculations is that for small excitation energies, i.e.  $E_x \leq \Delta$ , the limiting value of Eq. (4.241) is given by its first order Taylor expansion

$$\lim_{E_x - \Delta \rightarrow 0} a(E_x) = \tilde{a} [1 + \gamma \delta W].
 \tag{4.246}$$

From now on, wherever the level density parameter  $a$  appears in the formalism, we implicitly assume the form (4.241) for  $a(E_x)$ .

It is important to define the order in which the various parameters of Eq. (4.241) are calculated in TALYS, because they can be given as an adjustable parameter in the input file, they can be known from experiment or they can be determined from systematics.

If the level density parameter at the neutron separation energy  $a(S_n)$  is *not* known from an experimental  $D_0$  value, we use the above systematical formulae for the global level density parameters. In this case, all parameters in Eq. (4.241) are defined and  $a(E_x)$  can be completely computed at any excitation energy. However, for several nuclei  $a(S_n)$  can be derived from an experimental  $D_0$  value through Eq. (4.240), and one may want to use this information. In TALYS, this occurs when an input value for  $a(S_n)$  is given and when **asys n** is set, meaning that instead of using the systematical formulae (4.242)-(4.244) the resonance parameter database is used to determine level density parameters. If we want to use this “experimental”  $a(S_n)$  we are immediately facing a constraint: Eq. (4.241) gives the following

condition that must be obeyed

$$(4.247) \quad a(S_n) = \tilde{a} \left[ 1 + \delta W \frac{1 - \exp(-\gamma(S_n - \Delta))}{S_n - \Delta} \right]$$

This means also that  $a(S_n)$ ,  $\tilde{a}$ ,  $\delta W$  and  $\gamma$  cannot *all* be given simultaneously in the input, since it would lead to inconsistency. In the case of an experimental  $a(S_n)$ , at least another parameter must be re-adjusted. The asymptotic level density parameter  $\tilde{a}$  is the first choice. This is not as strange as it seems at first sight. Even though the values for  $\delta W$  depend strongly on the particular theoretical mass model and are merely adopted to reproduce the global trend of shell effects for various regions of the nuclide chart, we do not alter them when going from a global to a local model. Likewise, we feel that it is dangerous to adjust  $\gamma_1$  merely on the basis of discrete level information and the mean resonance spacing at the neutron separation energy, since its presence in the exponent of Eq. (4.241) may lead to level density values that deviate strongly from the global average at high energy.

Hence, if  $a(S_n)$  is given, and also  $\gamma$  and  $\delta W$  are given in the input or from tables then the asymptotic level density parameter  $\tilde{a}$  is automatically obtained from

$$(4.248) \quad \tilde{a} = a(S_n) / \left[ 1 + \delta W \frac{1 - \exp(-\gamma(S_n - \Delta))}{S_n - \Delta} \right]$$

Other choices can however be forced with the input file. If  $a(S_n)$ ,  $\tilde{a}$  and  $\delta W$  are given while  $\gamma$  is not given in the input,  $\gamma$  is eliminated as a free parameter and is obtained by inverting Eq. (4.247),

$$(4.249) \quad \gamma = -\frac{1}{S_n - \Delta} \ln \left[ 1 - \frac{S_n - \Delta}{\delta W} \left( \frac{\tilde{a}}{a(S_n)} - 1 \right) \right]$$

If  $\delta W$  is the only parameter not given in the input, it is automatically determined by inverting Eq. (4.247),

$$(4.250) \quad \delta W = \frac{(S_n - \Delta) \left( \frac{a(S_n)}{\tilde{a}} - 1 \right)}{1 - \exp(-\gamma(S_n - \Delta))}$$

All this flexibility is not completely without danger. Since both  $\delta W$  and  $a(S_n)$  are independently derived from experimental values, it may occur that Eq. (4.249) poses problems. In particular,  $\delta W$  may have a sign opposite to  $[a(S_n) - \tilde{a}]$ . In other words, if the argument of the natural logarithm is not between 0 and 1, our escape route is to return to Eq. (4.243) for  $\gamma$  and to readjust  $\delta W$  through Eq. (4.250).

The recipe outlined above represents a full-proof method to deal with all the parameters of Eq. (4.241), i.e. it always gives a reasonable answer since we are able to invert the Ignatyuk formula in all possible ways. We emphasize that in general, consistent calculations are obtained with Eqs. (4.244), (4.242), (4.243), and when available, a specific  $a(S_n)$  value from the tables. The full range of possibilities of parameter specification for the Ignatyuk formula is summarized in Table 4.4. The reason to include all these parameter possibilities is simple: fitting experiments. Moreover, these variations are not as unphysical as they may seem: Regardless of whether they are derived from experimental data or from microscopic nuclear structure models, the parameters  $a(S_n)$ ,  $\tilde{a}$ ,  $\delta W$  and  $\gamma$  always have an uncertainty. Hence, as long as the deviation from their default values is kept within bounds, they can be helpful fitting parameters.

Table 4.4: Specification of parameter handling for Ignatyuk formula

Input	Calculation
- (Default)	$\gamma$ : Eq. (4.243), $\tilde{a}$ : Eq. (4.242) or Eq. (4.248), $\delta W$ : Eq. (4.244), $a(S_n)$ : Eq. (4.247)
$a(S_n), \gamma, \tilde{a}, \delta W$	TALYS-Error: Conflict
$a(S_n)$ (table), $\gamma, \tilde{a}, \delta W$	$a(S_n)$ : Eq. (4.247) (Input overruled)
$\gamma, \tilde{a}, \delta W$	$a(S_n)$ : Eq. (4.247)
$\gamma, \tilde{a}$	$\delta W$ : Eq. (4.244), $a(S_n)$ : Eq. (4.247)
$\gamma, \delta W$	$\tilde{a}$ : Eq. (4.242), $a(S_n)$ : Eq. (4.247)
$\tilde{a}, \delta W$	$\gamma$ : Eq. (4.243), $a(S_n)$ : Eq. (4.247)
$\gamma$	$\tilde{a}$ : Eq. (4.242), $\delta W$ : Eq. (4.244), $a(S_n)$ : Eq. (4.247)
$\tilde{a}$	$\gamma$ : Eq. (4.243), $\delta W$ : Eq. (4.244), $a(S_n)$ : Eq. (4.247)
$\delta W$	$\gamma$ : Eq. (4.243), $\tilde{a}$ : Eq. (4.242), $a(S_n)$ : Eq. (4.247)
$a(S_n)$	$\gamma$ : Eq. (4.249) or (4.243), $\tilde{a}$ : Eq. (4.248), $\delta W$ : Eq. (4.244) or (4.250)
$a(S_n), \tilde{a}, \delta W$	$\gamma$ : Eq. (4.249)
$a(S_n), \delta W$	$\tilde{a}$ : Eq. (4.248) $\gamma$ : Eq. (4.249)
$a(S_n), \tilde{a}$	$\delta W$ : Eq. (4.244), $\gamma$ : Eq. (4.249) or $\gamma$ : Eq. (4.243), $\delta W$ : Eq. (4.250)
$a(S_n), \gamma$	$\delta W$ : Eq. (4.244), $\tilde{a}$ : Eq. (4.248)
$a(S_n), \gamma, \delta W$	$\tilde{a}$ : Eq. (4.248)
$a(S_n), \gamma, \tilde{a}$	$\delta W$ : Eq. (4.250)

### The spin cut-off parameter

The spin cut-off parameter  $\sigma^2$  represents the width of the angular momentum distribution of the level density. The general expression for the continuum is based on the observation that a nucleus possesses collective rotational energy that can not be used to excite the individual nucleons. In this picture, one can relate  $\sigma^2$  to the (undeformed) moment of inertia of the nucleus  $I_0$  and the thermodynamic temperature  $t$ ,

$$(4.251) \quad t = \sqrt{\frac{U}{a}}.$$

Indeed, an often used expression is  $\sigma^2 = \sigma_{\parallel}^2 = I_0 t$ , where the symbol  $\sigma_{\parallel}^2$  designates the parallel spin cut-off parameter, obtained from the projection of the angular momentum of the single-particle states on the symmetry axis. However, it has been observed from microscopic level density studies that the quantity  $\sigma^2/t$  is not constant [89, 90], but instead shows marked shell effects, similar to the level density parameter  $a$ . To take that effect into account we follow Refs. [89, 91] and adopt the following expression,

$$(4.252) \quad \sigma^2 = \sigma_{\parallel}^2 = \sigma_F^2(E_x) = I_0 \frac{a}{\tilde{a}} t,$$

with  $\tilde{a}$  from Eq. (4.242) and

$$(4.253) \quad I_0 = \frac{\frac{2}{5} m_0 R^2 A}{(\hbar c)^2},$$

where  $R = 1.2A^{1/3}$  is the radius, and  $m_0$  the neutron mass in amu. This gives

$$(4.254) \quad \sigma_F^2(E_x) = 0.01389 \frac{A^{5/3}}{\tilde{a}} \sqrt{aU}.$$

On average, the  $\sqrt{aU}/\tilde{a}$  has the same energy- and mass-dependent behaviour as the temperature  $\sqrt{U/a}$ . The differences occur in the regions with large shell effects. Eq. (4.254) can be altered by means of the **spincut** keyword, see page 235.

Analogous to the level density parameter, we have to account for low excitation energies for which Eq. (4.254) is not defined ( $E_x \leq \Delta$ ) or less appropriate. This leads us to an alternative method to determine the spin cut-off parameter, namely from the spins of the low-lying discrete levels. Suppose we want to determine this discrete spin cut-off parameter  $\sigma_d^2$  in the energy range where the total level density agrees well with the discrete level sequence, i.e. from a lower discrete level  $N_L$  with energy  $E_L$  to an upper level  $N_U$  with energy  $E_U$ . It can be derived that

$$(4.255) \quad \sigma_d^2 = \frac{1}{3 \sum_{i=N_L}^{N_U} (2J_i + 1)} \sum_{i=N_L}^{N_U} J_i(J_i + 1)(2J_i + 1).$$

where  $J_i$  is the spin of discrete level  $i$ . Reading these spins from the discrete level file readily gives the value for  $\sigma_d^2$ . In TALYS,  $\sigma_d^2$  can be used on a nucleus-by-nucleus basis, when discrete levels are known. For cases where either Eqs. (4.254) or (4.255) are not applicable, e.g. because there are no discrete levels and  $U = E_x - P$  is negative, we take the systematical formula

$$(4.256) \quad \sigma^2 = (0.83A^{0.26})^2$$

which gives a reasonable estimate for energies in the order of 1-2 MeV.

The final functional form for  $\sigma^2(E_x)$  is a combination of Eqs. (4.254) and (4.255). Defining  $E_d = \frac{1}{2}(E_L + E_U)$  as the energy in the middle of the  $N_L - N_U$  region, we assume  $\sigma_d^2$  is constant up to this energy and can then be linearly interpolated to the expression given by Eq. (4.254). We choose the matching point to be the neutron separation energy  $S_n$  of the nucleus under consideration, i.e.

$$(4.257) \quad \begin{aligned} \sigma^2(E_x) &= \sigma_d^2 && \text{for } 0 \leq E_x \leq E_d \\ &= \sigma_d^2 + \frac{E_x - E_d}{S_n - E_d} (\sigma_F^2(E_x) - \sigma_d^2) && \text{for } E_d \leq E_x \leq S_n \\ &= \sigma_F^2(E_x) && \text{for } E_x \geq S_n. \end{aligned}$$

Analogous to the level density parameter  $a$ , from now on we implicitly assume the energy dependence for  $\sigma^2(E_x)$  whenever  $\sigma^2$  appears in the formalism.

### Constant Temperature Model

In the Constant Temperature Model (CTM), as introduced by Gilbert and Cameron [83], the excitation energy range is divided into a low energy part from 0 MeV up to a matching energy  $E_M$ , where the

so-called constant temperature law applies and a high energy part above  $E_M$ , where the Fermi gas model applies. Hence, for the total level density we have

$$(4.258) \quad \begin{aligned} \rho^{\text{tot}}(E_x) &= \rho_T^{\text{tot}}(E_x), \quad \text{if } E_x \leq E_M, \\ &= \rho_F^{\text{tot}}(E_x), \quad \text{if } E_x \geq E_M, \end{aligned}$$

and similarly for the level density

$$(4.259) \quad \begin{aligned} \rho(E_x, J, \Pi) &= \frac{1}{2} R_F(E_x, J) \rho_T^{\text{tot}}(E_x), \quad \text{if } E_x \leq E_M, \\ &= \rho_F(E_x, J, \Pi), \quad \text{if } E_x \geq E_M. \end{aligned}$$

Note that the spin distribution of Eq. (4.237) is also used in the constant temperature region, including the low-energy behaviour for the spin cut-off parameter as expressed by Eq. (4.257).

For the Fermi gas expression, we use the effective excitation energy  $U = E_x - \Delta^{\text{CTM}}$ , where the energy shift is given by

$$(4.260) \quad \Delta^{\text{CTM}} = \chi \frac{12}{\sqrt{A}},$$

with

$$(4.261) \quad \begin{aligned} \chi &= 0, \quad \text{for odd - odd,} \\ &= 1, \quad \text{for odd - even,} \\ &= 2, \quad \text{for even - even.} \end{aligned}$$

Note that by default no adjustable pairing shift parameter is used in the CTM. In TALYS, the number 12 in the numerator of Eq. (4.260) can be altered using the **pairconstant** keyword, see page 229. This also applies to the other level density models.

For low excitation energy, the CTM is based on the experimental evidence that the cumulated histogram  $N(E_x)$  of the first discrete levels can be well reproduced by an exponential law of the type

$$(4.262) \quad N(E_x) = \exp\left(\frac{E_x - E_0}{T}\right),$$

which is called the constant temperature law. The nuclear temperature  $T$  and  $E_0$  are parameters that serve to adjust the formula to the experimental discrete levels. Accordingly, the constant temperature part of the total level density reads

$$(4.263) \quad \rho_T^{\text{tot}}(E_x) = \frac{dN(E_x)}{dE_x} = \frac{1}{T} \exp\left(\frac{E_x - E_0}{T}\right).$$

For higher energies, the Fermi gas model is more suitable and the total level density is given by Eq. (4.238). The expressions for  $\rho_T^{\text{tot}}$  and  $\rho_F^{\text{tot}}$  have to be matched at a matching energy  $E_M$  where they, and their derivatives, are identical. First, continuity requires that

$$(4.264) \quad \rho_T^{\text{tot}}(E_M) = \rho_F^{\text{tot}}(E_M).$$

Inserting Eq. (4.263) in this equation directly leads to the condition

$$(4.265) \quad E_0 = E_M - T \ln [T \rho_F^{\text{tot}}(E_M)].$$

Second, continuity of the derivatives requires that

$$(4.266) \quad \frac{d\rho_T^{\text{tot}}}{dE_x}(E_M) = \frac{d\rho_F^{\text{tot}}}{dE_x}(E_M).$$

Inserting Eq. (4.263) in this equation directly leads to the condition

$$(4.267) \quad \frac{\rho_T^{\text{tot}}(E_M)}{T} = \frac{d\rho_F^{\text{tot}}}{dE_x}(E_M),$$

or

$$(4.268) \quad \frac{1}{T} = \frac{d \ln \rho_F^{\text{tot}}}{dE_x}(E_M).$$

In principle, for all Fermi gas type expressions, including the energy dependent expressions for  $a$ ,  $\sigma^2$ ,  $K_{\text{rot}}$  etc., Eq. (4.268) could be elaborated analytically, but in practice we use a numerical approach to allow any level density model to be used in the matching problem. For this, we determine the inverse temperature of Eq. (4.268) numerically by calculating  $\rho_F^{\text{tot}}$  on a sufficiently dense energy grid.

The matching problem gives us two conditions, given by Eqs. (4.265) and (4.268), with three unknowns:  $T$ ,  $E_0$  and  $E_M$ . Hence, we need another constraint. This is obtained by demanding that in the discrete level region the constant temperature law reproduces the experimental discrete levels, i.e.  $\rho_T^{\text{tot}}$  needs to obey

$$(4.269) \quad N_U = N_L + \int_{E_L}^{E_U} dE_x \rho^{\text{tot}}(E_x),$$

or, after inserting Eq. (4.263),

$$(4.270) \quad N_U = N_L + \left( \exp\left[\frac{E_U}{T}\right] - \exp\left[\frac{E_L}{T}\right] \right) \exp\left[\frac{-E_0}{T}\right].$$

The combination of Eqs. (4.265), (4.268) and (4.270) determines  $T$ ,  $E_0$  and  $E_M$ . Inserting Eq. (4.265) in Eq. (4.270) yields:

$$(4.271) \quad T \rho_F^{\text{tot}}(E_M) \exp\left[\frac{-E_M}{T}\right] \left( \exp\left[\frac{E_U}{T}\right] - \exp\left[\frac{E_L}{T}\right] \right) + N_L - N_U = 0,$$

from which  $E_M$  can be solved by an iterative procedure with the simultaneous use of the tabulated values given by Eq. (4.268). The levels  $N_L$  and  $N_U$  are chosen such that  $\rho_T(E_x)$  gives the best description of the observed discrete states and are stored in the nuclear structure database. For nuclides for which no, or not enough, discrete levels are given we rely on empirical formula for the temperature. For the effective model,

$$(4.272) \quad T = -0.22 + \frac{9.4}{\sqrt{A(1 + \gamma \delta W)}}$$

and for the collective model

$$(4.273) \quad T = -0.25 + \frac{10.2}{\sqrt{A(1 + \gamma\delta W)}}$$

where  $\gamma$  is taken from Eq. (4.243) and Table 4.3. Next, we directly obtain  $E_M$  from Eq. (4.268) and  $E_0$  from Eq. (4.265). Again, Eqs. (4.272) and (4.273) were obtained by fitting all individual values of the nuclides for which sufficient discrete level information exists. In a few cases, the global expression for  $T$  leads to a value for  $E_M$  which is clearly off scale. In that case, we resort to empirical expressions for the matching energy. For the effective model

$$(4.274) \quad E_M = 2.33 + 253/A + \Delta^{CTM},$$

and for the collective model

$$(4.275) \quad E_M = 2.67 + 253/A + \Delta^{CTM},$$

after which we obtain  $T$  from Eq. (4.268).

### The Back-shifted Fermi gas Model

In the Back-shifted Fermi gas Model (BFM) [84], the pairing energy is treated as an adjustable parameter and the Fermi gas expression is used all the way down to 0 MeV. Hence for the total level density we have

$$(4.276) \quad \rho_F^{\text{tot}}(E_x) = \frac{1}{\sqrt{2\pi}\sigma} \frac{\sqrt{\pi} \exp[2\sqrt{aU}]}{12 a^{1/4} U^{5/4}},$$

and for the level density,

$$(4.277) \quad \rho_F(E_x, J, \Pi) = \frac{1}{2} \frac{2J+1}{2\sqrt{2\pi}\sigma^3} \exp\left[-\frac{(J+\frac{1}{2})^2}{2\sigma^2}\right] \frac{\sqrt{\pi} \exp[2\sqrt{aU}]}{12 a^{1/4} U^{5/4}},$$

respectively. These expressions, as well as the energy-dependent expressions for  $a$  and  $\sigma^2$ , contain the effective excitation energy  $U = E_x - \Delta^{\text{BFM}}$ , where the energy shift is given by

$$(4.278) \quad \Delta^{\text{BFM}} = \chi \frac{12}{\sqrt{A}} + \delta,$$

with

$$(4.279) \quad \begin{aligned} \chi &= -1, \text{ for odd - odd,} \\ &= 0, \text{ for odd - even,} \\ &= 1, \text{ for even - even,} \end{aligned}$$

and  $\delta$  an adjustable parameter to fit experimental data per nucleus.

A problem of the original BFM, which may have hampered its use as the default level density option in nuclear model analyses, is the divergence of Eqs. (4.276)-(4.277) when  $U$  goes to zero. A solution to this problem has been provided by Grossjean and Feldmeier [93], has been put into a practical form by Demetriou and Goriely [97], and is adopted in TALYS. The expression for the total BFM level density is

$$(4.280) \quad \rho_{\text{BFM}}^{\text{tot}}(E_x) = \left[ \frac{1}{\rho_F^{\text{tot}}(E_x)} + \frac{1}{\rho_0(t)} \right]^{-1},$$

where  $\rho_0$  is given by

$$(4.281) \quad \rho_0(t) = \frac{\exp(1) (a_n + a_p)^2}{24\sigma \sqrt{a_n a_p}} \exp(4a_n a_p t^2),$$

where  $a_n = a_p = a/2$  and  $t$  is given by Eq. (4.251).

With the usual spin distribution, the level density reads

$$(4.282) \quad \rho_{\text{BFM}}(E_x, J, \Pi) = \frac{1}{2} \frac{2J+1}{2\sigma^2} \exp \left[ -\frac{(J + \frac{1}{2})^2}{2\sigma^2} \right] \rho_{\text{BFM}}^{\text{tot}}(E_x).$$

In sum, there are two adjustable parameters for the BFM,  $a$  and  $\delta$ .

### The Generalized Superfluid Model

The Generalized Superfluid Model (GSM) takes superconductive pairing correlations into account according to the Bardeen-Cooper-Schrieffer theory. The phenomenological version of the model [101, 102] is characterized by a phase transition from a superfluid behaviour at low energy, where pairing correlations strongly influence the level density, to a high energy region which is described by the FGM. The GSM thus resembles the CTM to the extent that it distinguishes between a low energy and a high energy region, although for the GSM this distinction follows naturally from the theory and does not depend on specific discrete levels that determine a matching energy. Instead, the model automatically provides a constant temperature-like behaviour at low energies. For the level density expressions, it is useful to recall the general formula for the total level density,

$$(4.283) \quad \rho^{\text{tot}}(E_x) = \frac{1}{\sqrt{2\pi\sigma}} \frac{e^S}{\sqrt{D}},$$

where  $S$  is the entropy and  $D$  is the determinant related to the saddle-point approximation. For the GSM this expression has two forms: one below and one above the so called critical energy  $U_c$ .

For energies below  $U_c$ , the level density is described in terms of thermodynamical functions defined at  $U_c$ , which is given by

$$(4.284) \quad U_c = a_c T_c^2 + E_{\text{cond}}.$$

Here, the critical temperature  $T_c$  is

$$(4.285) \quad T_c = 0.567\Delta_0,$$

where the pairing correlation function is given by

$$(4.286) \quad \Delta_0 = \frac{12}{\sqrt{A}}.$$

This correlation function also determines the condensation energy  $E_{\text{cond}}$ , which characterizes the decrease of the superfluid phase relative to the Fermi gas phase. It is given by the expression

$$(4.287) \quad E_{\text{cond}} = \frac{3}{2\pi^2} a_c \Delta_0^2,$$

where the critical level density parameter  $a_c$  is given by the iterative equation

$$(4.288) \quad a_c = \tilde{a} \left[ 1 + \delta W \frac{1 - \exp(-\gamma a_c T_c^2)}{a_c T_c^2} \right],$$

which is easily obtained once  $\tilde{a}$ ,  $\delta W$  and  $\gamma$  are known. Eq. (4.288) indicates that shell effects are again appropriately taken into account. For the determination of the level density we also invoke the expression for the critical entropy  $S_c$ ,

$$(4.289) \quad S_c = 2 a_c T_c,$$

the critical determinant  $D_c$ ,

$$(4.290) \quad D_c = \frac{144}{\pi} a_c^3 T_c^5,$$

and the critical spin cut-off parameter  $\sigma_c^2$ ,

$$(4.291) \quad \sigma_c^2 = 0.01389 A^{5/3} \frac{a_c}{\tilde{a}} T_c.$$

Now that everything is specified at  $U_c$ , we can use the superfluid Equation Of State (EOS) to define the level density below  $U_c$ . For this, we define an effective excitation energy

$$(4.292) \quad U' = E_x + \chi \Delta_0 + \delta,$$

where

$$(4.293) \quad \begin{aligned} \chi &= 2, \text{ for odd - odd,} \\ &= 1, \text{ for odd - even,} \\ &= 0, \text{ for even - even,} \end{aligned}$$

and  $\delta$  is an adjustable shift parameter to obtain the best description of experimental data per nucleus. Note that the convention for  $\chi$  is again different from that of the BFM or CTM. Defining

$$(4.294) \quad \varphi^2 = 1 - \frac{U'}{U_c},$$

then for  $U' \leq U_c$  the quantities  $\varphi$  and  $T$  obey the superfluid EOS [101],

$$(4.295) \quad \varphi = \tanh \left( \frac{T_c}{T} \varphi \right),$$

which is equivalent to

$$(4.296) \quad T = 2T_c \varphi \left[ \ln \frac{1+\varphi}{1-\varphi} \right]^{-1}.$$

The other required functions for  $U' \leq U_c$  are the entropy  $S$ ,

$$(4.297) \quad S = S_c \frac{T_c}{T} (1 - \varphi^2) = S_c \frac{T_c}{T} \frac{U'}{U_c},$$

the determinant  $D$ ,

$$(4.298) \quad D = D_c (1 - \varphi^2) (1 + \varphi^2)^2 = D_c \frac{U'}{U_c} \left( 2 - \frac{U'}{U_c} \right)^2,$$

and the spin cut-off parameter

$$(4.299) \quad \sigma^2 = \sigma_c^2 (1 - \varphi^2) = \sigma_c^2 \frac{U'}{U_c}.$$

In sum, the level density can now be specified for the entire energy range. For  $U' \leq U_c$ , the total level density is given by

$$(4.300) \quad \rho_{\text{GSM}}^{\text{tot}}(E_x) = \frac{1}{\sqrt{2\pi\sigma}} \frac{e^S}{\sqrt{D}},$$

using Eqs. (4.297)-(4.299). Similarly, the level density is

$$(4.301) \quad \rho_{\text{GSM}}(E_x, J, \Pi) = \frac{1}{2} R_F(E_x, J) \rho_{\text{GSM}}^{\text{tot}}(E_x).$$

For  $U' \geq U_c$  the FGM applies, though with an energy shift that is different from the pairing correction of the CTM and BFM. The total level density is

$$(4.302) \quad \rho_{\text{GSM}}^{\text{tot}}(E_x) = \frac{1}{\sqrt{2\pi\sigma}} \frac{\sqrt{\pi} \exp[2\sqrt{aU}]}{12 a^{1/4} U^{5/4}},$$

where the effective excitation energy is defined by  $U = E_x - \Delta^{\text{GSM}}$ , with

$$(4.303) \quad \Delta^{\text{GSM}} = E_{\text{cond}} - \chi \Delta_0 - \delta.$$

The spin cut-off parameter in the high-energy region reads

$$(4.304) \quad \sigma^2 = I_0 \frac{a}{\bar{a}} \sqrt{\frac{U}{a}},$$

and  $I_0$  is given by Eq. (4.253). The level density is given by

$$(4.305) \quad \rho_{\text{GSM}}(E_x, J, \Pi) = \frac{1}{2} R_F(E_x, J) \rho_{\text{GSM}}^{\text{tot}}(E_x).$$

At the matching energy, i.e., for  $E'_x = U_c - \chi \Delta_0 - \delta$ , it is easy to verify that Eqs. (4.300) and (4.302) match so that the total level density is perfectly continuous. In sum, there are two adjustable parameters for the GSM,  $a$  and  $\delta$ .

### 4.7.2 Collective effects in the level density

All the previously described models do not explicitly account for collective effects. However, it is well known that generally the first excited levels of nuclei result from coherent excitations of the fermions it contains. The Fermi gas model is not appropriate to describe such levels. Nevertheless, the models presented so far can still be applied successfully in most cases since they incorporate collectivity in the level density in an effective way through a proper choice of the energy-dependent level density parameter values.

In some calculations, especially if the disappearance of collective effects with excitation energy plays a role (e.g. in the case of fission), one would like to model the collective effects in more detail. It can be shown that the collective effects may be accounted for explicitly by introducing collective enhancement factors on top of an intrinsic level density  $\rho_{F,\text{int}}(E_x, J, \Pi)$ . Then the deformed Fermi gas level density  $\rho_{F,\text{def}}(E_x, J, \Pi)$  reads

$$(4.306) \quad \rho_{F,\text{def}}(E_x, J, \Pi) = K_{\text{rot}}(E_x)K_{\text{vib}}(E_x)\rho_{F,\text{int}}(E_x, J, \Pi),$$

while the total level densities  $\rho_{F,\text{def}}^{\text{tot}}$  and  $\rho_{F,\text{int}}^{\text{tot}}$  are related in the same way.  $K_{\text{rot}}$  and  $K_{\text{vib}}$  are called the rotational and vibrational enhancement factors, respectively. If  $K_{\text{rot}}$  and  $K_{\text{vib}}$  are explicitly accounted for,  $\rho_{F,\text{int}}(E_x, J, \Pi)$  should now describe purely single-particle excitations, and can be determined again by using the Fermi gas formula. Obviously, the level density parameter  $a$  of  $\rho_{F,\text{int}}$  will be different from that of the effective level density described before.

The vibrational enhancement of the level density is approximated [163] by

$$(4.307) \quad K_{\text{vib}} = \exp[\delta S - (\delta U/t)],$$

where  $\delta S$  and  $\delta U$  are changes in the entropy and excitation energy, respectively, resulting from the vibrational modes and  $T$  is the nuclear temperature given by Eq. (4.251). These changes are described by the Bose gas relationships, i.e

$$(4.308) \quad \begin{aligned} \delta S &= \sum_i (2\lambda_i + 1) \left[ (1 + n_i) \ln(1 + n_i) - n_i \ln n_i \right], \\ \delta U &= \sum_i (2\lambda_i + 1) \omega_i n_i, \end{aligned}$$

where  $\omega_i$  are the energies,  $\lambda_i$  the multipolarities, and  $n_i$  the occupation numbers for vibrational excitations at a given temperature. The disappearance of collective enhancement of the level density at high temperatures can be taken into account by defining the occupation numbers in terms of the equation

$$(4.309) \quad n_i = \frac{\exp(-\gamma_i/2\omega_i)}{\exp(\omega_i/T) - 1},$$

where  $\gamma_i$  are the spreading widths of the vibrational excitations. This spreading of collective excitations in nuclei should be similar to the zero-sound damping in a Fermi liquid, and the corresponding width can be written as

$$(4.310) \quad \gamma_i = C(\omega_i^2 + 4\pi^2 T^2).$$

The value of  $C = 0.0075 A^{1/3}$  was obtained from the systematics of the neutron resonance densities of medium-weight nuclei [94]. We use a modified systematics [163] which includes shell effects to estimate the phonon energies (in MeV), namely

$$(4.311) \quad \omega_2 = 65A^{-5/6}/(1 + 0.05\delta W),$$

for the quadrupole vibrations and

$$(4.312) \quad \omega_3 = 100A^{-5/6}/(1 + 0.05\delta W),$$

for the octupole excitations.

An alternative, liquid drop model, estimation of the vibrational collective enhancement factor is given by [92]

$$(4.313) \quad K_{\text{vib}}(E_x) = \exp\left(0.0555A^{\frac{2}{3}}t^{\frac{4}{3}}\right).$$

The **kvibmodel** keyword can be used to choose between these models.

A more important contribution to the collective enhancement of the level density originates from rotational excitations. Its effect is not only much stronger ( $K_{\text{rot}} \sim 10 - 100$  whereas  $K_{\text{vib}} \sim 3$ ), but the form for the rotational enhancement depends on the nuclear shape as well. This makes it crucial, among others, for the description of fission cross sections.

The expression for the rotational enhancement factor depends on the deformation [163, 95]. Basically,  $K_{\text{rot}}$  is equal to the perpendicular spin cut-off parameter  $\sigma_{\perp}^2$ ,

$$(4.314) \quad \sigma_{\perp}^2 = I_{\perp}t,$$

with the rigid-body moment of inertia perpendicular to the symmetry axis given by

$$(4.315) \quad I_{\perp} = I_0 \left(1 + \frac{\beta_2}{3}\right) = 0.01389A^{5/3} \left(1 + \frac{\beta_2}{3}\right),$$

where  $\beta_2$  is the ground-state quadrupole deformation, which we take from the nuclear structure database. Hence,

$$(4.316) \quad \sigma_{\perp}^2 = 0.01389A^{5/3} \left(1 + \frac{\beta_2}{3}\right) \sqrt{\frac{U}{a}}.$$

For high excitation energies, it is known that the rotational behavior vanishes. To take this into account, it is customary to introduce a phenomenological damping function  $f(E_x)$  which is equal to 1 in the purely deformed case and 0 in the spherical case. The expression for the level density is then

$$(4.317) \quad \begin{aligned} \rho(E_x, J, \Pi) &= [1 - f(E_x)]K_{\text{vib}}(E_x)\rho_{F,\text{int}}(E_x, J, \Pi) + f(E_x)\rho_{F,\text{def}}(E_x, J, \Pi) \\ &= K_{\text{rot}}(E_x)K_{\text{vib}}(E_x)\rho_{F,\text{int}}(E_x, J, \Pi) \end{aligned}$$

where

$$(4.318) \quad K_{\text{rot}}(E_x) = \max([\sigma_{\perp}^2 - 1]f(E_x) + 1, 1).$$

The function  $f(E_x)$  is taken as a combination of Fermi functions,

$$(4.319) \quad f(E_x) = \frac{1}{1 + \exp\left(\frac{E_x - E_{col}^{g.s.}}{d_{col}^{g.s.}}\right)},$$

which yields the desired property of  $K_{rot}$  going to 1 for high excitation energy. Little is known about the parameters that govern this damping, although attempts have been made (see e.g. [96]). We arbitrarily take  $E_{col}^{g.s.} = 30$  MeV,  $d_{col}^{g.s.} = 5$  MeV.

Finally, these collective enhancement expressions can be applied to the various phenomenological level density models. The CTM formalism can be extended with explicit collective enhancement, i.e. the total level density reads

$$(4.320) \quad \begin{aligned} \rho^{tot}(E_x) &= \rho_T^{tot}(E_x), \quad \text{if } E_x \leq E_M, \\ &= K_{rot}(E_x)K_{vib}(E_x)\rho_{F,int}^{tot}(E_x), \quad \text{if } E_x \geq E_M, \end{aligned}$$

and similarly for the level density  $\rho(E_x, J, \Pi)$ . Note that the collective enhancement is not applied to the constant temperature region, since collectivity is assumed to be already implicitly included in the discrete levels. The matching problem is completely analogous to that described before, although the resulting parameters  $E_M$ ,  $E_0$  and  $T$  will of course be different.

The BFM can also be extended with explicit collective enhancement, i.e.

$$(4.321) \quad \rho_{BFM}^{tot}(E_x) = K_{rot}(E_x)K_{vib}(E_x) \left[ \frac{1}{\rho_{F,int}^{tot}(E_x)} + \frac{1}{\rho_0(t)} \right]^{-1},$$

and similarly for the level density  $\rho(E_x, J, \Pi)$ . Finally, the GSM can be extended as follows

$$(4.322) \quad \rho_{GSM}^{tot}(E_x) = K_{rot}(E_x)K_{vib}(E_x)\rho_{GSM,int}^{tot}(E_x).$$

(In fact, the term ‘‘general’’ in the GSM was originally meant for the collective enhancement).

### 4.7.3 Microscopic level densities

Besides the phenomenological models that are used in TALYS, there is also an option to employ more microscopic approaches. For the RIPL database, S. Goriely has calculated level densities from drip line to drip line on the basis of Hartree-Fock calculations [98] for excitation energies up to 150 MeV and for spin values up to  $I = 30$ . If **ldmodel 4**, see page 224, these tables with microscopic level densities can be read. Moreover, new energy-, spin- and parity-dependent nuclear level densities based on the microscopic combinatorial model have been proposed by Hilaire and Goriely [169]. The combinatorial model includes a detailed microscopic calculation of the intrinsic state density and collective enhancement. The only phenomenological aspect of the model is a simple damping function for the transition from spherical to deformed, see also Eq. (4.317). The calculations make coherent use of nuclear structure properties determined within the deformed Skyrme-Hartree-Fock-Bogolyubov framework. Level densities for more than 8500 nuclei are made available in tabular format, for excitation energies up to 200 MeV and for spin values up to  $J = 49$ . These level densities are used with **ldmodel 5**.

The most recent option, invoked with **ldmodel 6**, is based on temperature-dependent Hartree-Fock-Bogolyubov calculations using the Gogny force [138].

Since these microscopical level densities, which we will call  $\rho_{\text{HFMB}}$ , have not been adjusted to experimental data, we add adjustment flexibility through a scaling function, i.e.

$$(4.323) \quad \rho(E_x, J, \pi) = \exp(c\sqrt{E_x - \delta})\rho_{\text{HFMB}}(E_x - \delta, J, \pi)$$

where by default  $c = 0$  and  $\delta = 0$  (i.e. unaltered values from the tables). The “pairing shift”  $\delta$  simply implies obtaining the level density from the table at a different energy. The constant  $c$  plays a role similar to that of the level density parameter  $a$  of phenomenological models. Adjusting  $c$  and  $\delta$  together gives adjustment flexibility at both low and higher energies.

For both microscopic level density models, tables for level densities on top of the fission barriers are automatically invoked for **ldmodel 4, 5** or **6**, when available in the structure database. For nuclides outside the tabulated microscopic database, the default Fermi gas model is used.

## 4.8 Fission

The probability that a nucleus fissions can be estimated by TALYS on both phenomenological and microscopic grounds. Cross sections for (multi-chance) fission can be calculated. For this, various nuclear quantities are required.

### 4.8.1 Level densities for fission barriers

The level density formulae given in Section 4.7 for the ground state of the nucleus can all be applied for the fission barriers. In general, only the ingredients for a few level density expressions change as compared to the non-fissile case. In TALYS, two methods for fission level densities are programmed. The level densities are used in the calculation of fission transmission coefficients.

#### Explicit treatment of collective effects

Eq. (4.318) for the rotational enhancement also holds for inner barriers with neutron number  $N \leq 144$ , which are all assumed to be axially symmetric (specified by the keyword **axtype 1**). Inner barriers with  $N > 144$ , e.g. the Am-isotopes, are taken to be axially asymmetric (**axtype 3**), and in that case the rotational enhancement is

$$(4.324) \quad K_{rot}(E_x) = K_{rot}^{asym}(E_x, \beta_2) = \max([\sqrt{\frac{\pi}{2}}\sigma_{\perp}^2(1 - \frac{2\beta_2}{3})\sigma_{\parallel} - 1]f(E_x) + 1, 1).$$

For outer barriers, we apply an extra factor of 2 to  $K_{rot}$ , due to the mass asymmetry. For all fission barriers, the default parameters for the damping function Eq. (4.319) are  $U_f^{bar} = 45$  MeV,  $C_f^{bar} = 5$  MeV.

The shell correction is also different: For the inner barrier,  $\delta W = 1.5$  MeV for an axially symmetric barrier, and 2.5 MeV otherwise. For the other barriers, we take 0.6 MeV in general.

### Effective treatment of collective effects

Despite being of a more “effective” nature than the approach described above, this method (invoked with **colldamp y**) has been more successful in the description of fission cross sections, see e.g. [459]. An essential aspect is that the damping of collective effects are taken into account in a phenomenological way through the level density parameter  $a$ . The asymptotic level density parameter  $\tilde{a}$ , see Eq. (4.242) is damped from its effective limit  $A/8$  to its intrinsic limit  $A/13$  as follows

$$(4.325) \quad \tilde{a}^{\text{eff}} = \frac{A}{13}f(E_x) + \tilde{a}(1 - f(E_x))$$

where

$$(4.326) \quad f(E_x) = \frac{1}{1 + \exp\left(-\frac{E_x - E_{col}^{g.s.}}{a_{col}^{g.s.}}\right)},$$

with the same values as mentioned below Eq. (4.319). Next, the resulting  $a(E_x)$  is used in all equations. After this, an extra rotational enhancement needs only to be taken into account for tri-axial barriers (**axtype 2**). Instead of Eq. (4.318), this is taken as

$$(4.327) \quad K_{rot}(E_x) = \left(\frac{U}{a_{\text{eff}}}\right)^{1/4}(1 - f(E_x)) + f(E_x),$$

where  $a_{\text{eff}} = 8a/13$  and

$$(4.328) \quad f(E_x) = \frac{1}{1 + \exp\left(-\frac{1}{2}(E_x - 18)\right)},$$

For barriers other than tri-axial,  $K_{rot} = 1$ . There is no vibrational enhancement in this model. For the shell correction, for all barriers  $\delta W = \frac{2}{3}|\delta W^{g.s.}|$ . Finally, the spin cut-off parameter (4.257) is multiplied by  $\left(1 + \frac{\beta_2}{3}\right)$  as done in Eq. (4.315) for the perpendicular spin cut-off parameter.

## 4.8.2 Fission transmission coefficients

For fission, the default model implemented in TALYS is based on the transition state hypothesis of Bohr and the Hill-Wheeler expression. This yields transmission coefficients that enter the Hauser-Feshbach model to compete with the particle and photon transmission coefficients.

### Transmission coefficient for one fission barrier

The Hill-Wheeler expression gives the probability of tunneling through a barrier with height  $B_f$  and width  $\hbar\omega_f$  for a compound nucleus with excitation energy  $E_x$ . It reads

$$(4.329) \quad T_f(E_x) = \frac{1}{1 + \exp\left[-2\pi\frac{(E_x - B_f)}{\hbar\omega_f}\right]}$$

For a transition state with excitation energy  $\varepsilon_i$  above the top of the same barrier, one has

$$(4.330) \quad T_f(E_x, \varepsilon_i) = \frac{1}{1 + \exp \left[ -2\pi \frac{(E_x - B_f - \varepsilon_i)}{\hbar\omega_f} \right]}$$

which means that the barrier is simply shifted up by  $\varepsilon_i$ .

For a compound nucleus with excitation energy  $E_x$ , spin  $J$ , and parity  $\Pi$ , the total fission transmission coefficient is the sum of the individual transmissions coefficients for each barrier through which the nucleus may tunnel, and thus reads in terms of the previously introduced  $T_f(E_x, \varepsilon_i)$

$$(4.331) \quad T_f^{J,\Pi}(E_x) = \sum_i T_f(E_x, \varepsilon_i) f(i, J, \Pi) + \int_{E_{th}}^{E_x} \rho(\varepsilon, J, \Pi) T_f(E_x, \varepsilon) d\varepsilon$$

The summation runs over all discrete transition states on top of the barrier and  $E_{th}$  marks the beginning of the continuum. In this equation,  $f(i, J, \Pi) = 1$  if the spin and parity of the transition state equal that of the compound nucleus and 0 otherwise. Moreover,  $\rho(\varepsilon, J, \Pi)$  is the level density of fission channels with spin  $J$  and parity  $\Pi$  for an excitation energy  $\varepsilon$ . The main difference with the usually employed expressions is that the upper limit in the integration is finite. This expression also enables to define the number of fission channels by replacing  $T_f(E_x, \varepsilon_i)$  by 1 in Eq. (4.331). This is needed for width fluctuation calculations where the fission transmission coefficient is treated as a continuum transmission coefficient.

### 4.8.3 Transmission coefficient for multi-humped barriers

For double humped barriers, the generally employed expression is based on an effective transmission coefficient  $T_{eff}$  defined by

$$(4.332) \quad T_{eff} = \frac{T_A T_B}{T_A + T_B}$$

where  $T_A$  and  $T_B$  are the transmission coefficients for barrier  $A$  and  $B$  respectively, calculated with Eq. (4.331).

If a triple humped barrier needs to be considered, the expression for  $T_{eff}$  reads

$$(4.333) \quad T_{eff} = \frac{T_{AB} T_C}{T_{AB} + T_C}$$

where  $T_{AB}$  is given by Eq. (4.332). Consequently, the expression used in TALYS reads

$$(4.334) \quad T_{eff} = \frac{T_A T_B T_C}{T_A T_B + T_A T_C + T_B T_C}$$

For any number of barrier, the effective number of fission channels is calculated as in the case for one barrier [183].

#### 4.8.4 Class II/III states

Class II (resp. III) states may be introduced when double (resp. triple) humped barriers are considered. In the particular situation where the excitation energy  $E_{CN}$  of the compound nucleus is lower than the barrier heights, fission transmission coefficients display resonant structures which are due to the presence of nuclear excited levels (Class II) in the second, or in the third (Class III) well of the potential energy surface. When such resonant structures occur, the expression for the effective fission transmission coefficient has to be modified (generally enhanced).

The way this resonant effect is determined depends on the number of barriers that are considered.

##### Double humped fission barrier

In the case where two barriers occur, the effective fission transmission coefficient  $T_{eff}$  can be written as

$$(4.335) \quad T_{eff} = \frac{T_A T_B}{T_A + T_B} \times F_{AB}(E_{CN})$$

where  $F_{AB}(E_{CN})$  is a factor whose value depends on the energy difference between the excitation energy of the nucleus and that of the a class II state located in the well between barrier  $A$  and  $B$ . It has been shown [100] that the maximum value of  $F_{AB}(E)$  reaches  $\frac{4}{T_A + T_B}$  and gradually decreases over an energy interval defined as the width  $\Gamma_{II}$  of the class II state with excitation energy  $E_{II}$ . This is accounted for using the empirical quadratic expression

$$(4.336) \quad F_{AB}(E) = \frac{4}{T_A + T_B} + \left( \frac{E - E_{II}}{0.5\Gamma_{II}} \right)^2 \times \left( 1 - \frac{4}{T_A + T_B} \right)$$

if  $E_{II} - 0.5\Gamma_{II} \leq E \leq E_{II} + 0.5\Gamma_{II}$  and  $F_{AB} = 1$  otherwise.

Theoretically, this expression is valid for the tunneling through a single double humped barrier whereas in realistic situations, both  $T_A$  and  $T_B$  are obtained from a summation over several transition states. One may thus have large  $T_A$  and  $T_B$  values so that Eq. 4.336 may give  $F_{AB}(E) \leq 1$ . Such a situation can only occur for high enough excitation energies for which the individual Hill-Wheeler contributions in Eq. (4.331) are large enough. However, in TALYS, we only consider class II states with excitation energies lower than the height of the first barrier. Consequently, the resonant effect can only occur if the compound nucleus energy  $E_{CN}$  is (i) lower than the top of the first barrier and (ii) close to a resonant class II state ( $E_{II} - 0.5\Gamma_{II} \leq E_{CN} \leq E_{II} + 0.5\Gamma_{II}$ ). With such requirements, the individual Hill-Wheeler terms are clearly small, and  $T_A + T_B \ll 1$ .

##### Triple humped fission barrier

If three barriers  $A$ ,  $B$  and  $C$  are considered, the situation is more complicated. In this case, three situations can occur depending on the positions of the class II and class III states. Indeed the enhancement

can be due either to a class II state or to a class III state, but on top of that, a double resonant effect can also occur if both a class II and a class III state have an excitation energy close to the compound nucleus energy. For any situation, the enhancement is first calculated for the first and the second barrier giving the transmission coefficient

$$(4.337) \quad T_{eff}^{AB} = T_{AB} \times F_{AB}$$

with  $F_{AB}$  given by Eq. (4.336) as in the previous case.

Next, the eventual coupling with a class III state with energy  $E_{III}$  of width  $\Gamma_{III}$  is accounted for by generalizing Eq. (4.335) writing

$$(4.338) \quad T_{eff}^{ABC} = \frac{T_{eff}^{AB} T_C}{T_{eff}^{AB} + T_C} \times F_{ABC}(E_{CN})$$

where  $F_{ABC}(E_{CN})$  is given by generalizing Eq. (4.336) writing

$$(4.339) \quad F_{ABC}(E) = \frac{4}{T_{eff}^{AB} + T_C} + \left( \frac{E - E_{III}}{0.5\Gamma_{III}} \right)^2 \times \left( 1 - \frac{4}{T_{eff}^{AB} + T_C} \right)$$

if  $E_{III} - 0.5\Gamma_{III} \leq E \leq E_{III} + 0.5\Gamma_{III}$  and  $F_{ABC} = 1$  otherwise.

#### 4.8.5 Fission barrier parameters

In TALYS several options are included for the choice of the fission barrier parameters:

1. Experimental parameters [163]: collection of a large set of actinide fission barrier heights and curvatures for both the inner and outer barrier based on a fit to experimental data, compiled by V. Maslov. Moreover, this compilation contains head band transition states.
2. Mamdough parameters [106]: set of double-humped fission barrier heights for numerous isotopes derived from Extended Thomas-Fermi plus Strutinsky Integral calculations.
3. Rotating-Finite-Range Model (RFRM) by Sierk [103]: single-humped fission barrier heights are determined within a rotating liquid drop model, extended with finite-range effects in the nuclear surface energy and finite surface-diffuseness effects in the Coulomb energy.
4. Rotating-Liquid-Drop Model (RLDM) by Cohen *et al* [104].

In the current version of TALYS, the dependence on angular momentum of the fission barriers is discarded. If LDM barriers are employed in the calculation, they are corrected for the difference between the ground-state and fission barrier shell correction energy:

$$(4.340) \quad B_f^{LDM}(T) = B_f^{LDM}(0) - (\delta W_{groundstate} - \delta W_{barrier}) * g(T)$$

This correction gradually disappears with temperature due to the washing out of the shell effects [107]:

$$(4.341) \quad g(T) = \begin{cases} 1 & \text{for } T < 1.65\text{MeV}, \\ g(T) = 5.809 \exp(-1.066 T) & \text{for } T \geq 1.65\text{MeV}. \end{cases}$$

Shell corrections on top of the fission barrier are generally unknown. They obviously play an important role for the level density as well. Default values are adopted: for subactinides  $\delta W_{\text{barrier}} = 0$  MeV, for actinides  $\delta W_{\text{barrier,inner}} = 2.5$  MeV and  $\delta W_{\text{barrier,outer}} = 0.6$  MeV [163].

#### 4.8.6 WKB approximation

As an alternative to the Hill-Wheeler approach, it is also possible to use the WKB approximation to calculate fission transmission coefficients. We use an implementation by Mihaela Sin and Roberto Capote and refer to Ref. [105] for the full details of this method. It can be invoked with the keyword **fismodel 5**.

#### 4.8.7 Fission fragment properties

Since TALYS-1.6, two models for fission fragments are available, the temperature dependent Brosa model, and the GEF model.

##### GEF model

A fission model has been developed model by Schmidt-Jurado [115] It is based on the statistical population of states in the fission valleys at the moment of dynamical freeze-out, which is specific to each collective degree of freedom. Three fission channels are considered. The separability principle governs the interplay of macroscopic and microscopic effects. The newly discovered energy-sorting mechanism determines the division of intrinsic excitation energy between the fragments at scission and the creation of a strong even-odd effect at large mass asymmetry. This model gives a new insight into several dynamical times. Most parameters are fixed from independent sources, only about 20 parameters have specifically been adjusted. Since the parameters of the model are closely related to physical properties of the systems, valuable conclusions on the fission process can be deduced. The good reproduction of measured data and the high predictive power of the code make it useful for applications in nuclear technology and complement the use of purely empirical models.

##### Temperature-dependent Brosa model

The description of fission fragment and product yields follows the procedure outlined in Ref. [109]. The Hauser-Feshbach formalism gives a fission cross section per excitation energy bin for each fissioning system. The fission fragment masses and charges are, subsequently, determined per given excitation energy bin  $E_x$ , in a fissioning system FS, characterised by  $(Z_{FS}, A_{FS}, E_x)$ , for which the fission cross section exceeds some minimum value. The total fragment mass distribution is given by a sum over all

contributing bins weighted with the corresponding fission cross sections:

$$(4.342) \quad \sigma(A_{FF}) = \sum_{Z_{FS}, A_{FS}, E_x} \sigma_f(Z_{FS}, A_{FS}, E_x) Y(A_{FF}; Z_{FS}, A_{FS}, E_x),$$

where  $Y(A_{FF}; Z_{FS}, A_{FS}, E_x)$  is the relative yield of a fission fragment with mass  $A_{FF}$  originating from a fissioning system. Combining this expression with the result of a fission fragment charge distribution calculation yields the final production cross section of a fission fragment with mass  $A_{FF}$  and charge  $Z_{FF}$ :

$$(4.343) \quad \sigma_{prod}(Z_{FF}, A_{FF}) = \sum_{Z_{FS}, A_{FS}, E_x} \sigma_f(Z_{FS}, A_{FS}, E_x) Y(A_{FF}; Z_{FS}, A_{FS}, E_x) \times Y(Z_{FF}; A_{FF}, Z_{FS}, A_{FS}, E_x)$$

$Y(Z_{FF}; A_{FF}, Z_{FS}, A_{FS}, E_x)$  is the relative yield of a fission fragment with charge  $Z_{FF}$  given its mass  $A_{FF}$  and the fissioning system characterised by  $(Z_{FS}, A_{FS}, E_x)$ .

In general, an excitation energy distribution is connected to these fission *fragment* production cross sections. In theory, this could be used to deduce the fission *product* yields through a full evaporation calculation of the fission fragments. This is not yet possible in TALYS. Instead a rather crude approximation, outlined later in this section, is adopted to estimate the number of post-scission neutrons emitted from each fragment. This procedure leads to relative yields for the fission product masses  $Y(A_{FP}; Z_{FS}, A_{FS}, E_x)$  and charges  $Y(Z_{FP}; A_{FP}, Z_{FS}, A_{FS}, E_x)$  and, hence, to expressions similar to Eq. (4.342) and Eq. (4.343) for the final fission products.

### Fission fragment mass distribution

The fission fragment mass distribution is determined with a revised version of the multi-modal random neck-rupture model (MM-RNRM). The original model has been developed by Brosa to calculate properties of fission fragments at zero temperature [108]. However, fission calculations within TALYS require fragment mass distributions up to higher temperatures.

In the recent version of the model [109] the temperature is added to the calculation of the potential energy landscape of the nucleus. A search for the fission channels in deformation space yields the superlong (SL), standard I (ST I), and standard II (ST II) fission barriers and pre-scission shapes as a function of temperature. In this manner, the incorporated melting of shell effects naturally gives rise to the vanishing of the asymmetric fission modes ST I and ST II with increasing excitation energies. The obtained temperature-dependent fission barrier and pre-scission shape parameters serve as input for the fragment mass distribution computations in TALYS.

Each mass distribution is a sum over contributions of the three dominant fission modes FM:

$$(4.344) \quad Y(A_{FF}; Z_{FS}, A_{FS}, E_x) = \sum_{FM=SL, STI, STII} W_{FM}(Z_{FS}, A_{FS}, E_x) Y_{FM}(A_{FF}; Z_{FS}, A_{FS}, E_x),$$

where  $W_{FM}(Z_{FS}, A_{FS}, E_x)$  denotes the weight of a fission mode, and  $Y_{FM}(A_{FF}; Z_{FS}, A_{FS}, E_x)$  is the corresponding mass distribution.  $Y(A_{FF}; Z_{FS}, A_{FS}, E_x)$  can then be substituted in Eq. (4.342) to

determine the full fission fragment mass distribution for the reaction under consideration. An analogous expression can be written down for  $Y(A_{FP}; Z_{FS}, A_{FS}, E_x)$ .

Each mass distribution calculation is started by determining the relative contributions of the different fission modes. These are evaluated with the Hill-Wheeler penetrability through inverted parabolic barriers using temperature-dependent barrier parameters and, consequently (the reader is referred to [109] for a detailed explanation), ground-state level densities:

$$(4.345) \quad T_{f,FM}(Z_{FS}, A_{FS}, E_x) = \int_0^\infty d\epsilon \rho_{gs}(Z_{FS}, A_{FS}, \epsilon) \frac{1}{1 + \exp \left[ \frac{2\pi(B_{f,FM}(Z_{FS}, A_{FS}, T(\epsilon)) + \epsilon - E_x)}{\hbar\omega_{f,FM}(Z_{FS}, A_{FS}, T(\epsilon))} \right]}.$$

All actinides encounter a double-humped barrier on their way to fission. The effective transmission coefficient can be expressed in terms of the transmission coefficient through the first and second barrier denoted by  $T_f^A$  and  $T_f^B$  respectively by Eq. (4.332). Since, however, the theoretical inner barrier is much lower than the outer barrier, the relative contribution  $W_{FM}(Z_{FS}, A_{FS}, E_x)$  of the three fission modes may simply be determined by an equation of the following form:

$$(4.346) \quad W_{SL}(Z_{FS}, A_{FS}, E_x) = \frac{T_{f,SL}^B}{T_{f,SL}^B + T_{f,STI}^B + T_{f,STII}^B}.$$

Equivalent formulas hold for  $W_{STI}(Z_{FS}, A_{FS}, E_x)$  and  $W_{STII}(Z_{FS}, A_{FS}, E_x)$ .

For subactinides it is not possible to calculate the competition between symmetric and asymmetric fission modes, since the computed fission channels exhibit rather broad and strangely shaped outer barriers, which makes a parabola fit to these barriers impossible. Hence, the Hill-Wheeler approach cannot be applied. Fortunately, the SL barriers are much lower than the ST barriers. Therefore, in all these calculations the asymmetric fission modes are simply discarded and the dominant symmetric SL mode is solely taken into account for subactinides.

The RNRM is employed to calculate the mass distribution per fission mode. An extensive description of the RNRM may be found in [108]. Here it is merely attempted to communicate its main ideas. In this model, the fission process is regarded as a series of instabilities. After the passage over the barriers, a neck starts to form. If this neck becomes flat its rupture may happen anywhere, which means that the point of future constriction can shift over the neck. This motion of the dent is called the shift instability. In the instant that the Rayleigh instability starts to deepen the dent, the position of the asymmetry is frozen and rupture is taking place. The RNRM translates the effect of both mechanisms into measurable quantities.

In order for the shift instability to do its work, a perfectly flat neck is required. Hence, the so-called flat-neck parameterisation is introduced: (see Fig. 4.3):

$$(4.347) \quad \rho(\zeta) = \begin{cases} (r_1^2 - \zeta^2)^{1/2} & -r_1 \leq \zeta \leq \zeta_1 \\ r + a^2 c \left( \cosh \left( \frac{\zeta - z + l - r_1}{a} \right) - 1 \right) & \zeta_1 \leq \zeta \leq \zeta_2 \\ (r_2^2 - (2l - r_1 - r_2 - \zeta)^2)^{1/2} & \zeta_2 \leq \zeta \leq 2l - r_1. \end{cases}$$

The radius of the nucleus is given by  $\rho$  as a function of a parameter  $\zeta$  in terms of several parameters: the semilength  $l$ , the neck radius  $r$ , the position  $z$  of the dent, the curvature  $c$ , the extension of the neck  $a$ , the

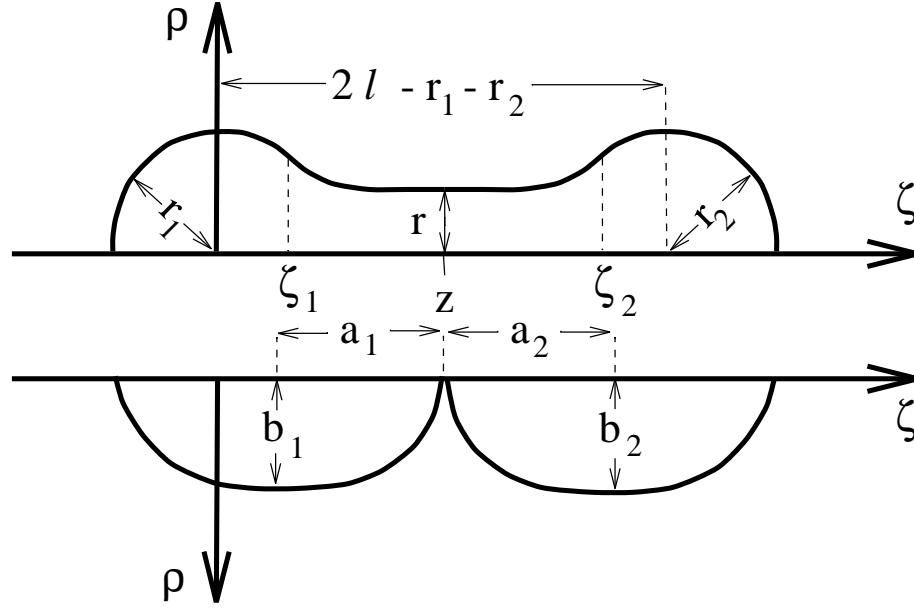


Figure 4.3: The upper part illustrates the flat-neck representation. The lower part contains the embedded spheroids parameterisation.

radii of the spherical heads  $r_1$  and  $r_2$ , and the transitional points  $\zeta_1$  and  $\zeta_2$ . By requiring continuity and differentiability of the shape, volume conservation and a minimal value of  $c$  for a really flat neck, only  $(l, r, z)$  remain as independent parameters. Subsequently, the neck radius is eliminated by the Rayleigh criterion, which relates the total length  $2l$  of the precission shape to the neck radius  $r$  by  $2l = 11r$ . The value of  $z$  can be transformed into the heavy fragment mass  $A_h$  by:

$$(4.348) \quad A_h = \frac{3A}{4r_{cn}^3} \int_{-l}^z \rho^2(\zeta) d\zeta,$$

where  $r_{cn}$  is the compound nucleus radius. The actual values of  $A_h$  and  $l$  originate from the channel searches and are called the precission shape parameters. They have been stored in the structure database and are input to the RNRM calculations.

One last ingredient is missing for the computation of the mass distribution, namely the surface tension:

$$(4.349) \quad \gamma_0 = 0.9517 \left( 1 - 1.7828 \left( \frac{N - Z}{A} \right)^2 \right) \text{ MeV fm}^{-2}.$$

This is taken from the LDM by Myers and Swiatecki [72].

Fluctuations amplified by the shift instability alter the shape slightly and enable the rupture of the nucleus to take place at another point than the most probable point  $z$ . In order to determine the fission-fragment mass distribution, the probability of cutting the neck at an arbitrary position  $z_r$  has to be calculated. This probability is given by the change in potential energy from  $z_r$  to  $z$ :  $E(z_r) - E(z)$ . This is replaced by the energy to cut the nucleus at the two positions:  $E_{cut}(z_r) - E_{cut}(z)$ , with  $E_{cut}(z_r) =$

$2\pi\gamma_0\rho^2(z_r)$ . The rupture probability is now proportional to the Boltzmann factor:

$$(4.350) \quad y(A_{FF}) \propto \exp\left(\frac{-2\pi\gamma_0(\rho^2(z_r) - \rho^2(z))}{T}\right).$$

The fragment mass number  $A_{FF}$  can be computed according to the analogue of Eq. (4.348):

$$(4.351) \quad A_{FF}(z_r) = \frac{3A}{4r_{cn}^3} \int_{-l}^{z_r} \rho^2(\zeta) d\zeta.$$

The theoretical yield is finally determined with the following relation in which  $Y(A_{FF})$  stands for the normalized fission fragment mass yield:

$$(4.352) \quad Y_{FM}(A_{FF}; Z_{FS}, A_{FS}, E_x) = y(A_{FF}) + y(A - A_{FF}).$$

In Eq. (4.350) the temperature of the scissioning nucleus must be provided. All calculations of the PES and the crossing of the fission barriers have been isothermal. However, for the RNRM the loss and gain of excitation energy in crossing the barrier is taken into account into a new excitation energy and temperature at scission:

$$(4.353) \quad E_x^{scission} = E_x^{groundstate} + F_{def,scission}.$$

The new excitation energy has two components: the original excitation energy in the ground state  $E_x^{groundstate}$  and the deformation energy at scission  $F_{def,scission}$ .  $F_{def,scission}$  is positive for actinides and becomes negative in the subactinide region. The new excitation energy is related to a new temperature  $T_{scission}$ . However, a new prescission temperature corresponds to a different prescission shape with a somewhat different value for  $F_{def,scission}$ . Therefore, the temperature  $T_{scission}$  has to be determined in a self-consistent manner together with the final prescission shape. If a prescission shape has a high temperature or a very long neck, the mass distribution will be broad. Low temperatures and short necks result in a narrow mass distribution.

### Post-scission neutron multiplicities

The mass distribution calculated above belongs to the primary fission fragments. Most fragments, however, are highly excited directly after their creation. They take their share of total excitation energy available at scission (4.353). Moreover, they are strongly deformed, which manifests itself in an extra amount of excitation energy set free when this deformation relaxes towards the ground-state deformation of the fragments by the strong surface tension. The superfluous excitation energy is released during the process of post-scission neutron and gamma emission. The neutron emission is responsible for a shift of the pre-neutron emission mass distribution to somewhat smaller masses.

The total excitation energy in a newly created fragment with mass  $A_{FF}$  results from:

$$(4.354) \quad E_x^{fragment}(A_{FF}) = E_{def,fragment}(A_{FF}) + \frac{A_{FF}}{A} E_x^{scission}.$$

$E_{def,fragment}(A_{FF})$  denotes the deformation energy of the fragment, and the second term contains the portion of the thermal energy at scission of the whole fissioning system picked up by the fragment. The assumption is that the fragment receives a share proportional to its mass.

For the calculation of  $E_{def,fragment}(A_{FF})$  another shape parameterisation is employed: the embedded spheroids (see Fig. 4.3). The newborn fragments are modeled as two contacting spheroids with major axes  $a_1$  and  $a_2$ , which are linked to  $2l$  and  $z_r$  by:

$$(4.355) \quad a_1 = \frac{1}{2}(r_1 + z_r), \quad a_2 = l - \frac{1}{2}(r_1 + z_r).$$

The minor axes  $b_1$  and  $b_2$  follow from volume conservation:

$$(4.356) \quad b_1^2 = \frac{3}{4a_1} \int_{-r_1}^{z_r} \rho^2 d\zeta, \quad b_2^2 = \frac{3}{4a_2} \int_{z_r}^{2l-r_1} \rho^2 d\zeta.$$

The energy difference of the spheroidally deformed and the spherical fragment  $E_{def,fragment}(A_{FF})$  is given by:

$$(4.357) \quad \begin{aligned} E_{def,fragment}(A_{FF}, \epsilon) = & E_{surf}^{sph}(A_{FF}) \left( \frac{\arcsin(\epsilon) + \epsilon(1 - \epsilon^2)^{1/2}}{2\epsilon(1 - \epsilon^2)^{1/6}} - 1 \right) + \\ & E_{Coul}^{sph}(A_{FF}) \left( \frac{(1 - \epsilon^2)^{1/3}}{2\epsilon} \ln \left( \frac{1 + \epsilon}{1 - \epsilon} \right) - 1 \right). \end{aligned}$$

The eccentricity is defined as:

$$(4.358) \quad \epsilon_i = \left( 1 - \left( \frac{b_i}{a_i} \right)^2 \right)^{1/2},$$

and  $E_{surf}^{sph}(A_{FF})$  and  $E_{Coul}^{sph}(A_{FF})$  represent the LDM surface and the Coulomb energy of a spherical nucleus obtained from Ref. [110].

The neutron multiplicity  $\nu_{FM}(A_{FF})$  for a fragment with mass  $A_{FF}$  is now derived by finding the root of the following relation:

$$(4.359) \quad E_x^{fragment}(A_{FF}) = \sum_{n=1}^{\nu_{FM}(A_{FF})} (S_n + \eta_n) + E_\gamma.$$

The separation energy  $S_n$  is calculated from the mass formula [110]. The average kinetic energy of the neutrons is taken to be  $\frac{3}{2}$  times the fragment temperature, and the energy carried off by  $\gamma$ -rays  $E_\gamma$  is approximately half the separation energy of the first non-evaporated neutron.

The final fission product mass yield per fission mode is given by:

$$(4.360) \quad Y_{FM}(A_{FP}; Z_{FS}, A_{FS}, E_x) = Y_{FM}(A_{FF} - \nu_{FM}(A_{FF})) + Y_{FM}(A - A_{FF} - \nu_{FM}(A - A_{FF})).$$

### Fission fragment charge distribution

Unfortunately, the MM-RNRM only yields information on the mass yields of the fission fragments. Predictions of charge distributions are performed in TALYS within a scission-point-model-like approach (Wilkins *et al.* [111]). Corresponding to each fission fragment mass  $A_{FF}$  a charge distribution is computed using the fact that the probability of producing a fragment with a charge  $Z_{FF}$  is given by the total potential energy of the two fragment system inside a Boltzmann factor:

$$(4.361) \quad Y_{FM}(Z_{FF}; A_{FF}, Z_{FS}, A_{FS}, E_x) = \frac{\exp\left(\frac{-E(Z_{FF}, A_{FF}, Z, A)}{T}\right)}{\sum_{Z_{FF_i}} \exp\left(\frac{-E(Z_{FF_i}, A_{FF}, Z, A)}{T}\right)}$$

In the original scission-point model this potential energy is integrated over all deformation space. Within the MM-RNRM, however, fission channel calculations already define the deformation at the scission point. Furthermore, a strong coupling between the collective and single particle degrees of freedom is assumed near the scission point. This means that the nucleus is characterised by a single temperature  $T$ .

The potential energy for the creation of one fragment with  $(Z_{FF}, A_{FF})$  and a second fragment with  $(Z - Z_{FF}, A - A_{FF})$  consists of a sum over the binding energy of the deformed fragments by the droplet model without shell corrections and their mutual Coulomb repulsion energy as well as the nuclear proximity repulsion energy:

$$(4.362) \quad E(Z_{FF}, A_{FF}, Z, A) = B(Z_{FF}, A_{FF}) + B(Z - Z_{FF}, A - A_{FF}) + E_{Coul} + V_{prox}.$$

The single constituents of this formula are defined by the following relations:

$$(4.363) \quad B(Z_{FF}, A_{FF}) = -a_1 \left[ 1 - \kappa \left( \frac{A_{FF} - 2Z_{FF}}{A_{FF}} \right)^2 \right] A_{FF} \\ + a_2 \left[ 1 - \kappa \left( \frac{A_{FF} - 2Z_{FF}}{A_{FF}} \right)^2 \right] A_{FF}^{\frac{2}{3}} f(shape)$$

$$(4.364) \quad + \frac{3e^2}{5r_0} \frac{Z_{FF}^2}{A_{FF}^{\frac{1}{3}}} g(shape) - \frac{\pi^2 e^2}{2r_0} \left( \frac{d}{r_0} \right)^2 \frac{Z_{FF}^2}{A_{FF}}$$

$$(4.365) \quad E_{Coul} = e^2 Z_{FF} (Z - Z_{FF}) S_{form} / (a_1 + a_2)$$

$$(4.366) \quad V_{prox} = -1.7817 \frac{4\pi\gamma_0 b_1^2 b_2^2}{a_1 b_2^2 + a_2 b_1^2}$$

The parameters in the binding energy formula are taken from Ref. [110]. The function  $f(shape)$  is the form factor for the Coulomb term whereas  $g(shape)$  denotes the form factor for the surface energy.  $S_{form}$  is the form factor for the Coulomb interaction energy between two spheroids.

The fission product charge distribution is obtained from the calculated fission fragment charge distribution by shifting the corresponding fragment masses  $A_{FF}$  to the fission product masses  $A_{FP}$  with the aid of the post-scission neutron multiplicity  $\nu_{FM}(A_{FF})$ :

$$(4.367) \quad Y_{FM}(Z_{FP}; A_{FP}, Z_{FS}, A_{FS}, E_x) = Y_{FM}(Z_{FF}; A_{FF} - \nu_{FM}(A_{FF}), Z_{FS}, A_{FS}, E_x).$$

Since proton evaporation of the fission fragments is neglected, the charge distribution connected with  $A_{FF}$  becomes simply linked to the fission product mass  $A_{FP}$ .

## 4.9 Thermal reactions

The Introduction states that TALYS is meant for the analysis of data in the 1 keV - 200 MeV energy region. The lower energy of 1 keV should not be taken too literally. More accurate is: above the resolved resonance range. The start of the unresolved resonance range differs from nucleus to nucleus and is related to the average resonance spacing  $D_0$  or, equivalently, the level density at the binding energy. Generally, the starting energy region is higher for light nuclides than for heavy nuclides. Only beyond this energy, the optical and statistical models are expected to yield reasonable results, at least for the non-fluctuating cross sections. The lower energies are the domain of R-matrix theory, which describes the resonances. Nevertheless, it would be useful to have a first-order estimate of the non-threshold reactions, not only for the obvious neutron capture channel, but also for the exothermal  $(n, p)$ ,  $(n, \alpha)$  and fission channels. The fact that a nuclear model calculation in TALYS is only performed down to about 1 keV should not prevent us to give at least an estimate of the  $1/v$ -like behaviour of the excitation function down to  $10^{-5}$  eV (the lower energy limit in ENDF-6 files). In collaboration with J. Kopecky, we constructed a method that provides this.

### 4.9.1 Capture channel

First, we decide on the lower energy of validity of a TALYS nuclear model calculation  $E_L$ . Somewhat arbitrarily, we set as default  $E_L = D_0$  when we wish to construct evaluated data libraries, where  $D_0$  is taken from the nuclear model database or, if not present, derived from the level density.  $E_L$  can also be entered as an input keyword (**Elow**). Next, we determine the neutron capture cross section at the thermal energy  $E_{th} = 2.53 \cdot 10^{-8}$  MeV, either from the experimental database, see Chapter 5, or, if not present, from the systematical relation [112]

$$(4.368) \quad \sigma_{n,\gamma}(E_{th}) = 1.5 \times 10^{-3} a(S_n - \Delta)^{3.5} \text{ mb}$$

with  $a$  the level density parameter at the separation energy  $S_n$  and  $\Delta$  the pairing energy. We assign a  $1/v$ , i.e.  $1/\sqrt{E}$ , dependence to the cross section from  $10^{-5}$  eV to an upper limit  $E_{1/v}$  which we set, again arbitrarily, at  $E_{1/v} = 0.2E_L$ . The  $1/v$  line obviously crosses  $\sigma_{n,\gamma}(E_{th})$  at  $E_{th}$ . The points at  $E_{1/v}$  and  $E_L$  are connected by a straight line. The resulting capture cross section then looks like Fig. 4.4. In reality, the region between  $E_{1/v}$  and  $E_L$  is filled with resolved resonances, the only feature we did not try to simulate.

### 4.9.2 Other non-threshold reactions

For other reactions with positive Q-values, such as  $(n, p)$  and  $(n, \alpha)$ , only a few experimental values at thermal energy are available and a systematical formula as for  $(n, \gamma)$  is hard to construct. If we do have a value for these reactions at thermal energy, the same method as for capture is followed. If not, we assume that the ratio between the gamma decay width and e.g. the proton decay width is constant for incident energies up to  $E_L$ . Hence, we determine  $R_p = \sigma_{n,p}/\sigma_{n,\gamma}$  at  $E_L$ , and since we know the thermal  $(n, \gamma)$  value we can produce the (n,p) excitation function down to  $10^{-5}$  eV by multiplying the capture cross section by  $R_p$ . A similar procedure is applied to all other non-threshold reactions.

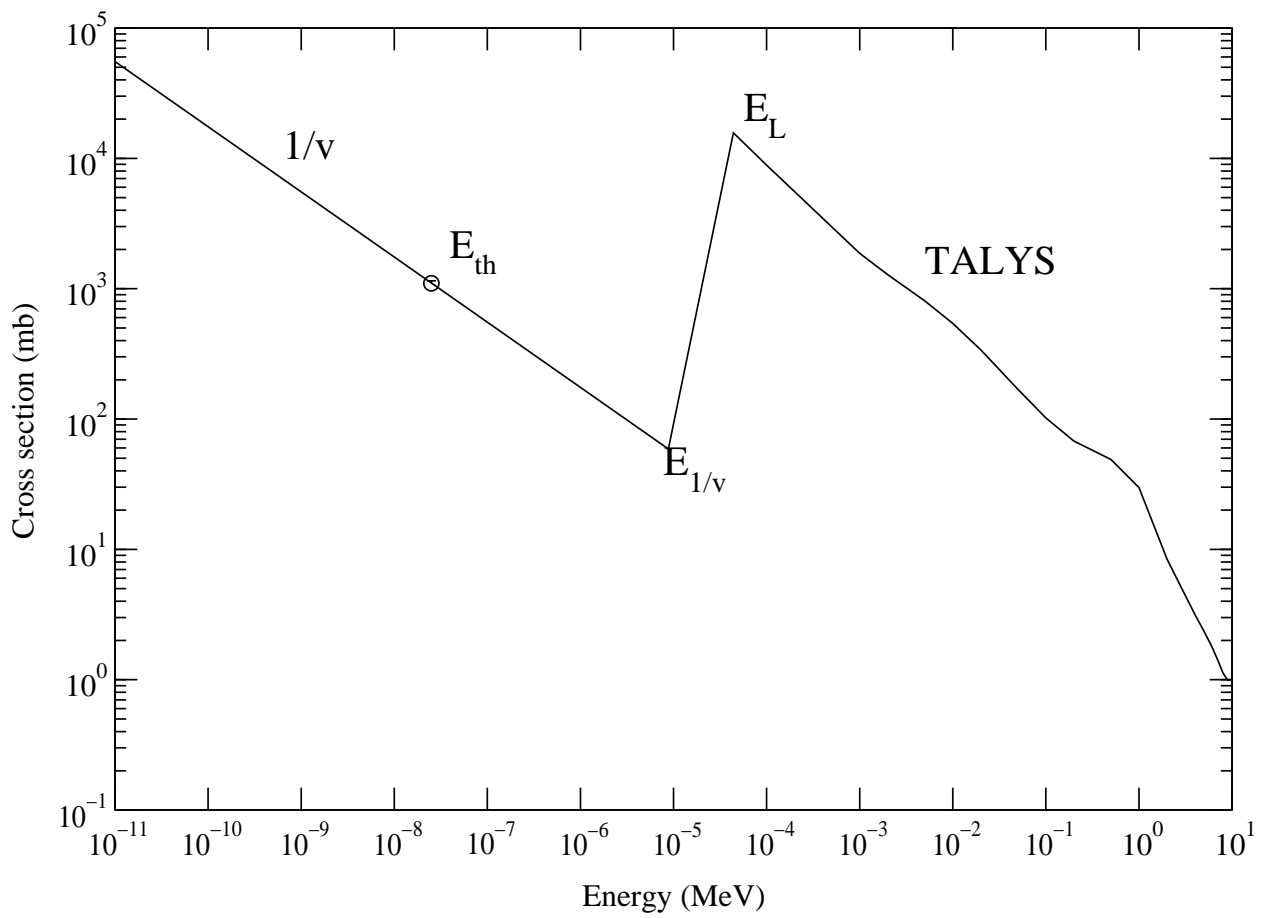


Figure 4.4: Capture cross section at low energies. The origin of the various energy regions are indicated.

## 4.10 Direct capture

For light nuclides and (very) neutron-rich nuclides, the direct capture process may have a significant contribution. Therefore, a direct capture model was implemented, to be activated with the **racap** keyword, see page 213. More details may become available in future versions of this manual. For the moment we refer to Ref. [139].

## 4.11 Populated initial nucleus

Usually, a TALYS calculation will concern a projectile with a certain incident energy and a target, either in its ground or an excited state. For various reasons, we have introduced the possibility to start the decay from an initial population, i.e. an excited nucleus with a population distributed over excitation energy. An example of an interesting application is the neutron spectrum from fission fragments. One could calculate the fragment distribution from fission, e.g. as described in Section 4.8.7 or from empirical methods, and assume a population per excitation energy and spin, of the excited light and heavy fission fragment (models for such distributions exist, see e.g. Ref. [113]). This distribution can then be the starting point for a TALYS calculation. The initial population enters the Hauser-Feshbach scheme and the compound nucleus calculation proceeds as usual. The emitted neutrons can be recorded as well as the path from fission fragment to fission product. All relevant nuclear structure quantities are available since we simulate the process by a photon-induced reaction, the only difference being that we do not excite a single compound nucleus energy but directly fill the continuum bins and discrete levels according to our specified starting population. TALYS can be used in this mode by simply specifying **projectile 0**, see page 154, and providing an energy file as input, see page 155. The initial population can be provided at two levels of detail. A full excitation energy-spin-parity population can be given, which is then interpolated on the internal excitation energy scheme of TALYS. Alternatively, only the total population per excitation energy can be given, after which the spin-parity-dependent population is determined by multiplying it with the spin distribution of Eq. (4.237). For the fission neutron spectrum example mentioned above, one could loop over all fission fragments (by writing a clever script), sum the results, and obtain the fission neutron spectrum. There are more applications for this feature, such as coupling a high-energy intranuclear cascade code with TALYS, the latter taking care of the low energy evaporation part including all its quantum-mechanical conservation rules.

## 4.12 Astrophysical reaction rates

A complete calculation of astrophysical reaction rates is possible with TALYS. In stellar interiors, nuclides not only exist in their ground states but also in different thermally excited states and a thermodynamic equilibrium holds locally to a very good approximation. Therefore, most of nuclear astrophysics calculations have made use of nuclear reaction rates evaluated within the statistical model [114]. The assumption of a thermodynamic equilibrium combined with the compound nucleus cross sections for the various excited states then allows to produce Maxwellian-averaged reaction rates, which is important input for stellar evolution models. Calculation of stellar reaction rates is obviously not new, but TALYS

provides some features which automatically makes the extension to reaction rate calculations very worthwhile. In contrast with existing dedicated astrophysical reaction rate codes, the present Chapter shows that we provide the inclusion of pre-equilibrium reaction mechanism, the detailed competition between all open channels, the inclusion of multi-particle emission (neglected in most astrophysics codes), the inclusion of detailed width fluctuation corrections, the inclusion of parity-dependent level densities, the inclusion of coupled channel description for deformed nuclei, and the coherent inclusion of fission channel. Different prescriptions are also used when normalizing nuclear models on available experimental data, such as level densities on s-wave spacings or E1 resonance strength on photoabsorption data.

The energies of both the targets and projectiles, as well as their relative energies  $E$ , obey Maxwell-Boltzmann distributions corresponding to the temperature  $T$  at that location (or a black-body Planck spectrum for photons). The astrophysical rate is obtained by integrating the cross section given by Eq. (4.174) over a Maxwell-Boltzmann distribution of energies  $E$  at the given temperature  $T$ . In addition, in hot astrophysical plasmas, a target nucleus exists in its ground as well as excited states. In a thermodynamic equilibrium situation, the relative populations of the various levels of nucleus with spins  $I^\mu$  and excitation energies  $E_x^\mu$  obey a Maxwell-Boltzmann distribution. Hence, in the formulae to follow, it is understood that the definition of the incident  $\alpha$  channel, see below Eq. (4.174), now includes an explicit superscript  $\mu$  to distinguish between the excited states. The effective stellar rate of  $\alpha \rightarrow \alpha'$  in the entrance channel at temperature  $T$  taking due account of the contributions of the various target excited states is finally expressed as

$$(4.369) \quad N_A \langle \sigma v \rangle_{\alpha\alpha'}^*(T) = \left( \frac{8}{\pi m} \right)^{1/2} \frac{N_A}{(kT)^{3/2} G(T)} \int_0^\infty \sum_\mu \frac{(2I^\mu + 1)}{(2I^0 + 1)} \times \sigma_{\alpha\alpha'}^\mu(E) E \exp\left(-\frac{E + E_x^\mu}{kT}\right) dE,$$

where  $k$  is the Boltzmann constant,  $m$  the reduced mass of the  $\alpha$  channel,  $N_A$  the Avogadro number, and

$$(4.370) \quad G(T) = \sum_\mu (2I^\mu + 1) / (2I^0 + 1) \exp(-E_x^\mu / kT)$$

the  $T$ -dependent normalized partition function. Reverse reactions can also be estimated making use of the reciprocity theorem [114]. In particular, the stellar photodissociation rates are classically derived from the radiative capture rates by

$$(4.371) \quad \lambda_{(\gamma,\alpha)}^*(T) = \frac{(2I + 1)(2j + 1)}{(2I' + 1)} \frac{G_I(T)}{G_{I'}(T)} \left( \frac{AA_a}{A'} \right)^{3/2} \left( \frac{kT}{2\pi\hbar^2 N_A} \right)^{3/2} \times N_A \langle \sigma v \rangle_{(\alpha,\gamma)}^* e^{-Q_{\alpha\gamma}/kT},$$

where  $Q_{\alpha\gamma}$  is the Q-value of the  $I^0(\alpha, \gamma)I'^0$  capture channel. Note that, in stellar conditions, the reaction rates for targets in thermal equilibrium are usually believed to obey reciprocity since the forward and reverse channels are symmetrical, in contrast to the situation which would be encountered for targets in their ground states only [114]. In TALYS, the total stellar photodissociation rate is determined from

$$(4.372) \quad \lambda_{(\gamma,j)}^*(T) = \frac{\sum_\mu (2J^\mu + 1) \lambda_{(\gamma,\alpha)}^\mu(T) \exp(-E_x^\mu / kT)}{\sum_\mu (2J^\mu + 1) \exp(-E_x^\mu / kT)},$$

where the photodissociation rate  $\lambda_{(\gamma,\alpha)}^\mu$  of state  $\mu$  with excitation energy  $E_x^\mu$  is given by

$$(4.373) \quad \lambda_{(\gamma,\alpha)}^\mu(T) = \int_0^\infty c n_\gamma(E, T) \sigma_{(\gamma,\alpha)}^\mu(E) dE,$$

where  $c$  is the speed of light,  $\sigma_{(\gamma,j)}^\mu(E)$  the photodisintegration cross section at energy  $E$ , and  $n_\gamma$  the stellar  $\gamma$ -ray distribution well described by the back-body Planck spectrum at the given temperature  $T$ .

In TALYS, if **astro y**, an appropriate incident energy grid for astrophysical calculations is made which overrules any incident energy given by the user.

## 4.13 Medical isotope production

This section describes the formalism to calculate the production yield of a radioactive nucleus by a nuclear reaction. Starting from the general formalism we will introduce realistic approximations and derive simpler equations that hold in basically all cases of interest. In TALYS we have implemented only analytical solutions to the production and depletion equations. This may be generalized in future versions.

### 4.13.1 Production and depletion of isotopes

The most general situation is that of the irradiation of a piece of material, consisting of many different isotopes, which were either present at the start of the irradiation, have been formed, or will be formed during the irradiation, by either the primary flux of particles, by secondary particles, or by radioactive decay. If we have a total of  $K$  different isotopes (theoretically  $K$  may stand for the the entire nuclide chart) and the number of each isotope  $k$  is  $N_k$ , then the temporal development of such a system is described by  $K$  differential equations:

$$(4.374) \quad \begin{aligned} \frac{dN_1(t)}{dt} &= \sum_{k=1, k \neq 1}^K \Lambda_{k \rightarrow 1} N_k(t) - \Lambda_1 N_1(t) \\ &\dots \\ \frac{dN_i(t)}{dt} &= \sum_{k=1, k \neq i}^K \Lambda_{k \rightarrow i} N_k(t) - \Lambda_i N_i(t) \\ &\dots \\ \frac{dN_K(t)}{dt} &= \sum_{k=1, k \neq K}^K \Lambda_{k \rightarrow K} N_k(t) - \Lambda_K N_K(t) \end{aligned}$$

In each equation, the first term is a feeding term. In the most general case, various parent nuclides may contribute to the formation of isotope  $i$ , hence the summation over parent nuclides  $k$ , with  $\Lambda_{k \rightarrow i}$  the partial formation rate for any possible parent isotope  $k$  to isotope  $i$ . Each partial formation rate can be expressed as

$$(4.375) \quad \Lambda_{k \rightarrow i} = \lambda_{k \rightarrow i} + R_{k \rightarrow i}$$

with  $\lambda_{k \rightarrow i}$  the (partial) radioactive decay rate and  $R_{k \rightarrow i}$  the (partial) nuclear reaction rate for any possible parent isotope  $k$  to isotope  $i$ . The second terms of Eq. (4.374) are loss terms due to radioactive decay and nuclear reactions from isotope  $i$  to any other isotope. Here the total depletion rate (we interchange “depletion” with “formation” whenever appropriate) for isotope  $i$  is

$$(4.376) \quad \Lambda_i = \lambda_i + R_i$$

where the total decay rate for isotope  $i$  is

$$\lambda_i = \sum_{k=1, k \neq i}^K \lambda_{i \rightarrow k}$$

and the total nuclear reaction rate for isotope  $i$  is

$$(4.377) \quad R_i = \sum_{k=1, k \neq i}^K R_{i \rightarrow k}$$

The entire loop over  $k$  may run over isotopes in their ground or isomeric states. Theoretically, the sum over reaction rates could include secondary particles (neutrons, photons, alpha particles etc.) formed after the first interaction of the incident beam with the material, over the entire outgoing energy spectrum. Since the number of isotopes  $i$ ,  $N_i(t)$  may appear simultaneously in many equations, due to its possible formation, or depletion, by many different nuclear reactions, it is clear that such a coupled system can only be solved by complicated mathematical and computational techniques. In fact, the most exact simulation would involve a Monte Carlo 3D transport calculation in which all primary and secondary particles are taken into account, including complete cross section libraries for all possible particles, coupled with an activation code that keeps track of the nuclide inventory. If we neglect such thick target transport issues, a system of equations like (4.374) is often solved by methods developed by Bateman [116] for radioactive decay and later generalized for source terms by Rubinson [117].

Fortunately, the situation is often not as complex as sketched above, since very reasonable approximations can be introduced into Eq. (4.374), certainly for charged-particle induced reactions. First, let us start with the common case of the irradiation of a target which contains only one natural element at the start of the irradiation. This set of equations can be then be separated into a linear combination of contributions by each target *isotope*. Hence, we solve Eq. (4.374) one by one for each target isotope and add these contributions at the end to get the answer for the target material. Then, for such a mono-isotopic target  $T$  we have at the start of the irradiation

$$(4.378) \quad \begin{aligned} t = 0 : N_T &= N_T(0) \\ N_i &= 0 \\ &\dots \\ N_K &= 0 \end{aligned}$$

Since in practice our target isotope is not radioactive, the loss terms reduce to  $\Lambda_T = R_T$  in Eq. (4.374) for  $N_T$ . Next, if a substantial part of the target is converted into other isotopes, beam

particles may interact with atoms other than the original target atoms. However, this is only a concern for irradiation times of the order of months or longer. For most practical applications, like medical isotope production, we can often assume that the burn-up of the target is small and that the target composition does not change much during the irradiation (this will be confirmed by some of our sample cases). Hence, in addition we will assume there are no nuclear reaction or radioactive decay feeding terms for the *target* isotope  $T$ .

This means that the target isotope is described by the following simple equation

$$(4.379) \quad \frac{dN_T(t)}{dt} = -R_T N_T(t)$$

which basically assumes that the only thing that happens to the target material is burn-up through nuclear reactions.

For the isotopes that are produced during the irradiation we can make similar reasonable assumptions. We assume there is no loss of a *produced* isotope of interest through nuclear reactions with beam particles, i.e. we assume nuclides are not hit twice (again, this assumption becomes less accurate at very long irradiation times). This is equivalent to stating that the isotopes of interest are only produced from nuclear reactions on the target isotopes or from decay of other products formed during the irradiation. Also, consistent with the assumption for the target isotope that nuclides are not hit twice, we have  $\Lambda_i = \lambda_i$  for the depletion term, and assume that no other nuclear reactions lead to the isotope of interest. Thus for the produced isotopes  $i$  we obtain

$$(4.380) \quad \frac{dN_i(t)}{dt} = \sum_{k=1, k \neq i}^K \lambda_{k \rightarrow i} N_k(t) + R_{T \rightarrow i} N_T(t) - \lambda_i N_i(t)$$

Nuclides often have only one or a few radioactive decay modes. Usually, only beta decay to the ground state or an isomer needs to be considered, although in some cases alpha decay may occur as well. If we neglect alpha decay, the summation in the first term above reduces to only one term. Thus, Eq. (4.380) reduces to

$$(4.381) \quad \frac{dN_i(t)}{dt} = \lambda_{p \rightarrow i} N_p(t) + R_{T \rightarrow i} N_T(t) - \lambda_i N_i(t)$$

where we now use the subscript  $p$  for the parent isotope which decays to isotope  $i$ . The parent isotope itself is described by the equation,

$$(4.382) \quad \frac{dN_p(t)}{dt} = R_{T \rightarrow p} N_T(t) - \lambda_p N_p(t)$$

where for simplicity we have left out a possible feeding term  $\lambda_{g \rightarrow p} N_g(t)$  from its own parent (i.e. the grandparent of isotope  $i$ ). It neglects radioactive decay to channels produced by multiple proton emission, e.g.  $^{120}\text{Te}(p,2p)^{119}\text{Sb}$  and the contribution from its feeding channel  $^{120}\text{Te}(p,2n)^{119}\text{I} + 2\beta^+$ . Although the (p,2p) channel is generally smaller and therefore often not relevant for most practical medical isotope production routes, it would be safer that at higher energies feeding from radioactive decay is taken into account. For that a more general solution of Eq. (4.374) would have to be implemented, similar to solutions for neutron-induced problems where processes like e.g. multiple fission yield decay need to be

taken into account. For most charged-particle induced reactions of interest, the current approximation is justified.

If we now use the boundary conditions  $N_T(t = 0) = N_T(0)$  and  $N_p(t = 0) = N_i(t = 0) = 0$ , the solutions to these equations are given by:

$$\begin{aligned} N_T(t) &= N_T(0) e^{-R_T t}, \\ N_p(t) &= N_T(0) \frac{R_{T \rightarrow p}}{\lambda_p - R_T} [e^{-R_T t} - e^{-\lambda_p t}], \\ N_i(t) &= N_T(0) \frac{R_{T \rightarrow i}}{\lambda_i - R_T} [e^{-R_T t} - e^{-\lambda_i t}] + N_T(0) \frac{R_{T \rightarrow p} \lambda_{p \rightarrow i}}{\lambda_p - R_T} \left[ \frac{e^{-R_T t} - e^{-\lambda_i t}}{\lambda_i - R_T} - \frac{e^{-\lambda_p t} - e^{-\lambda_i t}}{\lambda_i - \lambda_p} \right]. \end{aligned} \quad (4.383)$$

This is derived in the Appendix.

By setting the derivative of  $N_i(t)$  to zero, the irradiation time for which a maximal yield is obtained can be easily derived:

$$(4.384) \quad t_{max} = \frac{\ln(\lambda_i/R_T)}{\lambda_i - R_T}$$

The production of  $i$  is restrained by its  $\beta$ -decay on the one hand and by the decreasing number of available target atoms on the other hand. Hence, this observable  $t_{max}$  depends on the decay constant  $\lambda_i$  and the total production rate  $R_T$ .

Now that the analytical formulae for production are set with Eq. (4.383), the remaining ingredients needed to evaluate Eqs.(4.383) and (4.384) are:  $N_1(0), \dots, N_I(0)$ ,  $R$ , and  $\lambda$ , and this will be done in the next two sections.

### 4.13.2 Initial condition and stopping power

The number of target atoms at  $t=0$ ,  $N_i(0)$ , for  $1 \leq i \leq I$  equals:

$$(4.385) \quad N_i(0) = \frac{N_A}{A} B_i \rho V_{tar},$$

where  $N_A = 6.022 \cdot 10^{23}$  is Avogadro's number,  $A$  is the mass number,  $B_i$  is the abundance of isotope  $i$  with  $\sum_i^I B_i = 1$ ,  $\rho$  the mass density in  $[\text{g}/\text{cm}^3]$ , and  $V_{tar}$  the active target volume in  $[\text{cm}^3]$ .  $V_{tar}$  is given by the product of the beam surface  $S_{beam}$  in  $[\text{cm}^2]$  and the effective target thickness in  $[\text{cm}]$ , which can be expressed in terms of the stopping power  $\frac{dE}{dx}$ ,

$$(4.386) \quad V_{tar} = S_{beam} \int_{E_{back}}^{E_{beam}} \left( \frac{dE}{dx} \right)^{-1} dE,$$

where  $E_{beam}$  denotes the incident beam energy and  $E_{back}$  is the average projectile energy available at the backside of the target. If the projectiles travels through the target, the average projectile beam energy will decrease. The amount of energy loss inside the target is determined by the target thickness and the stopping power. The integration limits  $E_{beam}$  and  $E_{back}$  are fixed by the requested projectile

energy range inside the target, which is determined by the cross section as function of projectile energy (excitation function). This formula neglects the spreading of the beam inside the target.

The stopping power describes the average energy loss of projectiles in the target by atomic collisions as a function of their energy in [MeV/cm]. We use the Bethe-Bloch formula [118]:

$$(4.387) \quad \frac{dE}{dx} = 0.1535 \rho \frac{Z}{A} \frac{z_p^2}{\beta^2} \left[ \ln \left( \frac{2m_e \gamma^2 v^2 W_{max}}{I^2} \right) - 2\beta^2 \right], \text{ MeV/cm}$$

with  $Z$  the target charge number, and  $z_p$  the projectile charge number, while  $\beta$  represents a beam particle traveling at a relative velocity

$$(4.388) \quad \beta = \frac{v}{c} = \sqrt{\frac{E_{beam}(E_{beam} + 2m_0c^2)}{(E_{beam} + m_0c^2)^2}},$$

with rest mass  $m_0$ . Further,  $m_e$  is the electron mass, and  $\gamma = \frac{1}{\sqrt{1-\beta^2}}$ . The maximum energy transfer in a single collision,  $W_{max}$  is given by

$$(4.389) \quad W_{max} = 2m_e c^2 (\beta\gamma)^2,$$

if the incident particle is much heavier than the electron mass. For the mean excitation potential  $I$  a semi-empirical formula is adopted:

$$(4.390) \quad \frac{I}{Z} = 9.76 + 58.8Z^{-1.19} \text{ eV}.$$

This expression is claimed to be tested only if  $Z \geq 13$ , but we use it for all values.

### 4.13.3 Nuclear reaction and decay rates

When the full beam hits the target (i.e., assuming that the beam diameter is smaller than the target dimensions), the production rate in [atoms/s] of isotope  $i$  through the nuclear reaction on the target isotope  $T$  is given by the following expression

$$(4.391) \quad R_{T \rightarrow i} = \frac{I_{beam}}{z_p q_e} \frac{1}{V_{tar}} \int_{E_{back}}^{E_{beam}} \left( \frac{dE}{dx} \right)^{-1} \sigma_i^{rp}(E) dE$$

where  $I_{beam}$  is the beam current in [A] and  $q_e$  is the electron charge. The factor  $I_{beam}/(z_p q_e)$  corresponds to the number of projectiles impinging on the target per [s]. The residual production cross section of  $i$  in [mb] is denoted by  $\sigma_i^{rp}(E)$ .

Analogously, the production rate in [ $s^{-1}$ ] of all reaction channels, from the target, is given by:

$$(4.392) \quad R_T = \frac{I_{beam}}{z_p q_e} \frac{1}{V_{tar}} \int_{E_{back}}^{E_{beam}} \left( \frac{dE}{dx} \right)^{-1} (\sigma_{non}(E) - \sigma_{in}(E)) dE$$

where  $\sigma_{non}(E)$  is the non-elastic cross section and  $\sigma_{in}(E)$  is the inelastic cross section of  $i$  in [mb], which is nothing else than the residual production cross section  $\sigma_i^{rp}(E)$ . The difference  $\sigma_{non}(E) -$

$\sigma_{in}(E)$  provides the probability to create an isotope different from the original target atom in the nuclear reaction.

The decay rate of  $i$  is given by the simple relation

$$(4.393) \quad \lambda_i = \frac{\ln 2}{T_i^{1/2}},$$

where  $T_i^{1/2}$  is the half-life of isotope  $i$  in [s]. The  $\lambda_i$  in the loss term usually feeds only one or two different channels, namely by beta decay to the ground state or isomer of the daughter isotope  $d$ ,

$$(4.394) \quad \lambda_i = \lambda_{i \rightarrow d} = \lambda_{i \rightarrow d}^{g.s.} + \lambda_{i \rightarrow d}^{iso}.$$

With this, all ingredients of Eq. (4.383) are defined and we may calculate the nuclide inventory  $N_i(t)$  at any time during or after the irradiation process.

#### 4.13.4 Activities

With  $N_i(t)$  known, the final expression for the activity of the produced isotope  $i$ ,  $A_i$ , as a function of the irradiation time  $t$  can now be given by

$$(4.395) \quad A_i(t) = \lambda_i N_i(t).$$

For small irradiation times the expression for  $N_i(t)$ , Eq. (4.383), behaves as:

$$(4.396) \quad N_i(t) = N_T(0) R_{T \rightarrow i} t,$$

and hence the activity of  $i$  as

$$(4.397) \quad A_i(t) = \lambda_i N_T(0) R_{T \rightarrow i} t,$$

Under these circumstances, the yield scales linearly with the irradiation time  $t$  and the production rate  $R_{T \rightarrow i}$ . Only then, the production yield expressed in [MBq/mAh] is a meaningful quantity, which can be used to determine the yield, given a certain irradiation time and beam current.

# Nuclear structure and model parameters

## 5.1 General setup of the database

We have aimed to unify the nuclear structure and model parameter database of TALYS as much as possible. In the *talys/structure/* directory you can find the *masses/*, *abundance/*, *levels/*, *fission/*, *resonances/*, *deformation/*, *optical/*, *thermal/*, *gamma/*, *density/*, *decay/* *integral/* and *best/* subdirectories. Most subdirectories contain about 100 files, where each individual file points to a nuclear element. One file contains the info for all the isotopes of one element. For example, the file *talys/structure/levels/Fe.lev* contains the discrete levels of all Fe ( $Z=26$ ) isotopes. As you will see below, the chemical symbol is always present in the file itself, allowing an easy search. Every directory has this same substructure and also the formats in which the data are stored have been kept uniform as much as possible.

The nuclear structure database has been created from a collection of “raw” data files, which for a large part come from the Reference Input Parameter Library RIPL [163], that we used as a basis for TALYS.

## 5.2 Nuclear masses and deformations

The nuclear masses are stored in the *talys/structure/masses/* directory. In TALYS, we use three different sources. In order of priority:

- Experimental masses: The Audi Wapstra table (2003) [87]
- Theoretical masses: Goriely’s mass table using either the Skyrme force [119] or the Gogny force, or the Möller mass table [120].
- The Duflo-Zuker mass formula [121], included as a subroutine in TALYS.

All these masses have been processed into our database. There, we have stored both the real mass  $M$  in atomic mass units ( $amu = 931.49386$  MeV) and the mass excess  $\Delta M = (M - A) * amu$  in MeV for

both the experimental mass (if available) and the theoretical mass. The mass excesses are stored for a more precise calculation of separation energies. There are 4 subdirectories, *audi/* for Audi-Wapstra, *hfb/* for Hartree-Fock-Bogolyubov with Skyrme force, *hfbdlm/* for Hartree-Fock-Bogolyubov with Gogny force, and *moller/* for Moller.

For reaction Q-values one needs the masses of two nuclides. If for only one of them the experimental mass is known, we take the two *theoretical* mass excesses to calculate the Q-value, for consistency. This only occurs for nuclides far from the line of stability. If a nuclide is even outside the tables given in the database, we use the formula of Duflo-Zuker, which is included as a subroutine in TALYS.

As an example, below are the masses of some of the Fe-isotopes as given in file *masses/audi/Fe.mass*. We have stored  $Z$ ,  $A$ , mass (*amu*), mass excess (MeV), nuclear symbol with the format (2i4,2f12.6,42x,i4,a2).

26	45	45.014578	13.579000					45Fe
26	46	46.000810	0.755000					46Fe
26	47	46.992890	-6.623000					47Fe
26	48	47.980504	-18.160000					48Fe
26	49	48.973610	-24.582000					49Fe
26	50	49.962988	-34.475541					50Fe

For the 3 directories with theoretical masses, also the ground state deformation parameters  $\beta_2$  and  $\beta_4$  are given. The parameters in the *hfb/* directory are used by default for deformed nuclides. Moreover, the ground state spin and parity (for *hfb/* and *hfbdlm/*, not for *moller/*) are given. As an example, below are the masses of some of the Fe-isotopes as given in file *masses/hfb/Fe.mass*. We have stored  $Z$ ,  $A$ , mass (*amu*), mass excess (MeV),  $\beta_2$ ,  $\beta_4$ , nuclear symbol with the format (2i4,2f12.6,2f8.4,20x,f4.1,i2,i4,a2).

26	42	42.055503	51.701000	0.3200	0.0400	0.0	1	42Fe
26	43	43.041632	38.780000	0.2700	0.0300	0.5	1	43Fe
26	44	44.026225	24.428000	-0.2100	0.0400	0.0	1	44Fe
26	45	45.014192	13.220000	-0.1800	0.0300	1.5	1	45Fe
26	46	45.999931	-0.064000	-0.1100	0.0200	0.0	1	46Fe
26	47	46.992187	-7.278000	-0.0900	0.0200	3.5	-1	47Fe
26	48	47.979358	-19.228000	0.1800	0.0700	0.0	1	48Fe

### 5.3 Isotopic abundances

We have included the possibility to evaluate nuclear reactions for natural elements. If **mass 0**, see page 155, a calculation is performed for each isotope, after which the results are averaged with the isotopic abundance as weight. The isotopic abundances are stored in the *talys/structure/abundance/* directory and they are taken from RIPL (which are equal to those of the Nuclear Wallet Cards from Brookhaven National Laboratory). As an example, below are the isotopic abundances for Fe from the file *abundance/Fe.abun*. For each isotope, we have stored  $Z$ ,  $A$ , its abundance, its uncertainty (not used in TALYS), nuclear symbol with the format (2i4,f11.6,f10.6,45x,i4,a2).

26	54	5.845000	0.035000					54Fe
----	----	----------	----------	--	--	--	--	------



					3	0.021580	7.670E-01		
					0	0.978420	1.200E-03		
5	0.810320	2.5	-1	2			1.000E-12		5/2-
					2	0.000000	1.273E-01		
					1	1.000000	1.310E-03		
6	0.949800	6.5	1	1			4.360E-12		13/2+
					0	1.000000	8.120E-04		
7	0.970000	1.5	-1	2				J	1/2-, 3/2-
					4	0.500000	0.000E+00	B	
					2	0.500000	0.000E+00	B	
8	0.978910	5.5	1	1			2.580E-13		11/2+
					0	1.000000	7.690E-04		
9	1.082680	4.5	1	3			2.800E-12		9/2+
					8	0.073863	2.044E-01		
					3	0.687527	9.110E-03		
					0	0.238610	6.080E-04		
10	1.127090	1.5	1	1				J	3/2, 5/2, 7/2
					4	1.000000	1.050E-02		

For nuclides very far away from the line of stability, the discrete level database has been completed with the ground state information from the mass database, so that it spans the same range of nuclides. For these nuclides, the string 'HFB' has been added as a comment to denote that the information comes from structure calculations.

There is a directory *levels/spectrn* with spectroscopical factors for the direct capture process.

## 5.5 Deformation parameters

Deformation parameters, lengths and coupling schemes for coupled channels calculations are put in directory *talys/structure/deformation/*. They are strongly linked to the discrete level file. For each isotope, we first write  $Z$ ,  $A$ , number of levels, type of collectivity, the type of parameter, nuclear symbol with the format (3i4,3x,a1,3x,a1,54x,i4,a2). The type of parameter can be D (deformation length  $\delta_L$ ) or B (deformation parameter  $\beta_L$ ). The type of collectivity can be S (spherical), V (vibrational), R (rotational) and A (asymmetric rotational). Next, we read for each level the number of the level corresponding to that of the discrete level database, the type of collectivity per level, the number of the vibrational band, multipolarity, magnetic quantum number, phonon number of the level, deformation parameter(s) with the format (i4,3x,a1,4i4,4f9.4). The type of collectivity per level can be either D (DWBA), V (vibrational) or R (rotational). In the case of levels that belong to a rotational band, only the level number and an 'R' are given. For the first level of the rotational band, the deformation parameter  $\beta_2$  (and, if present,  $\beta_4$  and  $\beta_6$ ) can be given. If these  $\beta$  parameters are not given they are retrieved from the *talys/structure/mass/* directory. In certain cases, the deformation parameters have been adjusted to fit data. In those cases, they are added to the coupling schemes. Also, for the first level of a vibrational band the deformation parameter is given. The vibration-rotational model is thus invoked if within the rotational model also states belonging to a vibrational band can be specified. The level of complexity of rotational or vibrational-rotational

calculations can be specified with the **maxrot** (see page 201) and **maxband** (see page 201) keywords. For weakly coupled levels that can be treated with DWBA, the level number, a 'D' and the deformation parameter is given.

As an example, below are the deformation parameters for some even Ca isotopes, taken from *Ca.def*. This file ensures that for a reaction on  $^{40}\text{Ca}$ , a coupled-channels calculation with a vibrational model will automatically be invoked. Levels 2 ( $3^-$  at 3.737 MeV, with  $\delta_3 = 1.34$ ), 3 ( $2^+$  at 3.904 MeV, with  $\delta_2 = 0.36$ ), 4 ( $5^-$  at 4.491 MeV, with  $\delta_5 = 0.93$ ), will all be coupled individually as one-phonon states. There is an option to enforce a spherical OMP calculation through **spherical y** in the input, see page 201. In that case all levels will be treated with DWBA. The table below reveals that for the other Ca-isotopes the direct calculation will always be done with DWBA, but with deformation parameters  $\beta_L$  instead of deformation lengths  $\delta_L$ .

20	40	4	V	D					40Ca
0	V	0							
2	V	1	3		1	1.34000			
3	V	2	2		1	0.36000			
4	V	3	5		1	0.93000			
20	42	3	S	B					42Ca
0	V	0							
1	D					0.24700			
9	D					0.30264			
20	44	3	S	B					44Ca
0	V	0							
1	D					0.25300			
8	D					0.24012			
20	46	3	S	B					46Ca
0	V	0							
1	D					0.15300			
6	D					0.20408			
20	48	3	S	B					48Ca
0	V	0							
1	D					0.10600			
4	D					0.23003			

As a second example, below is the info for  $^{238}\text{U}$  from the *U.def* file. The basis for the coupling scheme is a rotational model with deformation lengths  $\delta_2 = 1.546$  and  $\delta_4 = 0.445$ , in which levels 1, 2, 3, 4, 7 and 22 can be coupled. In practice, we would include at least levels 1 and 2 (and if the results are important enough also levels 3 and 4) as rotational levels. There are 5 vibrational bands which can be included. By default we include no vibrational bands in a rotational model, but if e.g. **maxband 1** in the input, the levels 5, 6, 8 and 13 would be included with deformation length  $\delta_3 = 0.9$ .

92	238	23	R	D					238U
0	R	0			1.54606	0.44508			
1	R	0							
2	R	0							

3	R	0						
4	R	0						
5	V	1	3	0	0.90000			
6	V	1						
7	R	0						
8	V	1						
9	V	2	4	0	0.20000			
10	V	3	3	1	0.10000			
11	V	3						
12	V	2						
13	V	1						
14	V	4	2	0	0.10000			
15	V	3						
16	V	4						
17	V	2						
21	V	5	2	2	0.10000			
22	R	0						
23	V	5						
25	V	4						
31	V	5						

Finally, we note that in principle all level numbers in the *deformation/* database need to be re-checked if a new discrete level database (see the previous Section) is installed. It is however unlikely that new low-lying levels will be discovered for nuclides for which the coupling scheme is given.

## 5.6 Level density parameters

The level density parameters are stored in the *talys/structure/density/* directory. First, there are 4 sub-directories, *ground/*, *fission/*, *ph/*, *phjp* for ground state, fission barrier, particle-hole level densities, and spin-parity dependent particle-hole level densities, respectively. In *ground/ctm/*, *ground/bfm/*, and *ground/gsm/*, phenomenological level density parameters are stored. When the level density parameter **a** is given, it is derived from a fit to the  $D_0$  resonance spacing of the RIPL database. As an example, below are the parameters for the Zr-isotopes from *ground/bfm/Zr.ld*. For each isotope, we have stored  $Z$ ,  $A$ , and then for both the effective and explicit collective model  $N_L$ ,  $N_U$ , level density parameter  $a$  in  $\text{MeV}^{-1}$ , and pairing correction in MeV, nuclear symbol. The format is (2i4,2(2i4,2f12.5)4x,i4,a2).

40	86	8	17	0.00000	0.51730	8	17	0.00000	1.04574	86Zr
40	87	8	26	0.00000	0.15936	8	26	0.00000	0.65313	87Zr
40	88	5	17	0.00000	-0.04425	5	17	0.00000	0.46704	88Zr
40	89	2	15	0.00000	0.39230	2	15	0.00000	0.96543	89Zr
40	90	8	16	0.00000	0.99793	8	16	0.00000	1.80236	90Zr
40	91	3	17	9.57730	0.40553	3	17	5.13903	1.15428	91Zr
40	92	3	16	9.94736	-0.03571	3	16	5.00387	0.39829	92Zr
40	93	8	18	11.07918	0.50929	8	18	5.92169	1.07202	93Zr
40	94	4	16	12.51538	0.28941	4	16	6.66540	0.60420	94Zr

40	95	3	18	11.98832	0.83535	3	18	5.97084	1.28803	95Zr
40	96	3	16	0.00000	0.64799	3	16	0.00000	1.06393	96Zr
40	98	8	16	0.00000	0.32758	8	16	0.00000	0.67594	98Zr
40	99	2	21	0.00000	-0.01325	2	21	0.00000	0.26100	99Zr
40	100	8	17	0.00000	-0.25519	8	17	0.00000	0.00789	100Zr
40	101	8	15	0.00000	-0.13926	8	15	0.00000	0.17608	101Zr
40	102	8	17	0.00000	-0.37952	8	17	0.00000	-0.12167	102Zr

The other two subdirectories *ground/hilaire/* and *ground/goriely/*, contain the tabulated microscopic level densities of Hilaire [169] and Goriely [98], respectively, also present in RIPL. For each isotope, there are first 4 comment lines, indicating the nucleus under consideration. Next, the excitation energy, temperature, number of cumulative levels, total level density, total state density and level density per spin are read in the format (f7.2,7.3,e10.2,31e9.2). Below is an example for the first energies of  $^{42}\text{Fe}$  from *ground/goriely/Fe.tab*

```
*****
* Z= 26 A= 42: Total and Spin-dependent Level Density [MeV-1] for Fe 42 *
*****
U[MeV]  T[MeV]  NCUMUL  RHOBS  RHOTOT  J=0  J=1  J=2
  0.25  0.224  1.09E+00  7.33E-01  2.07E+00  2.44E-01  3.39E-01  1.26E-01
  0.50  0.302  1.33E+00  1.17E+00  4.14E+00  2.74E-01  4.83E-01  2.88E-01
  0.75  0.365  1.71E+00  1.86E+00  7.60E+00  3.45E-01  6.76E-01  4.95E-01
  1.00  0.419  2.29E+00  2.82E+00  1.31E+01  4.33E-01  9.05E-01  7.55E-01
```

Level densities for fission barriers are tabulated in *fission/hilaire/* and *fission/goriely/*. There is an *inner/* and *outer/* subdirectory, for the inner and outer barrier, respectively. Here is an example for the first few energy/spin points of  $^{230}\text{U}$  from *fission/goriely/inner/Th.ld*. The format is the same as for the ground state, see above.

```
*****
* Z= 92 A=230: Total and Spin-dependent Level Density [MeV-1] at the inner
  saddle point c= 1.24 h= 0.00 a= 0.00 B= 3.80 MeV *
*****
U[MeV]  T[MeV]  NCUMUL  RHOBS  RHOTOT  J=0  J=1  J=2
  0.25  0.162  1.11E+00  8.86E-01  5.92E+00  6.44E-02  1.64E-01  1.98E-01
  0.50  0.190  1.51E+00  2.32E+00  1.81E+01  1.19E-01  3.20E-01  4.31E-01
  0.75  0.209  2.56E+00  6.10E+00  5.25E+01  2.54E-01  7.01E-01  9.85E-01
```

In *density/ph/* microscopic particle-hole state densities are stored for 72 two-component ph combinations and 14 one-component ph combinations. The same energy grid and format as for total level densities is used. The particle-hole combinations are denoted as  $p_{\pi}h_{\pi}p_{\nu}h_{\nu}$ .

Here is an example for the first few energy/ph points of  $^{42}\text{Fe}$  from *density/ph/Fe.ph*.

```
*****
```

```

* Z= 26 A= 42 Particle-hole density [MeV-1] *
* Proton Fermi energy = -49.556 MeV *
* Neutron Fermi energy = -31.217 MeV *
*****
U[MeV]  0010    1000    0011    0020    0110    1001    1010
0.25 0.00E+00 0.00E+00 0.00E+00 0.00E+00 0.00E+00 0.00E+00 0.00E+00
0.50 0.00E+00 2.00E+00 0.00E+00 0.00E+00 0.00E+00 4.00E+00 0.00E+00
0.75 0.00E+00 2.00E+00 0.00E+00 0.00E+00 0.00E+00 4.00E+00 0.00E+00
1.00 0.00E+00 2.00E+00 0.00E+00 0.00E+00 0.00E+00 8.00E+00 0.00E+00
1.25 0.00E+00 2.00E+00 0.00E+00 0.00E+00 0.00E+00 8.00E+00 0.00E+00
1.50 0.00E+00 0.00E+00 0.00E+00 0.00E+00 0.00E+00 4.00E+00 0.00E+00

```

Finally, in *density/phjp/* microscopic particle-hole state densities, dependent on spin and parity, are tabulated for direct capture calculations.

## 5.7 Resonance parameters

Neutron resonance parameters are provided in the *talys/structure/resonances/* directory and stem from the the RIPL-2 database. As an example, below are the parameters for the Fe-isotopes from *resonances/Fe.res*. For each isotope, we have stored  $Z$ ,  $A$ , the experimental s-wave resonance spacing  $D_0$  in keV, its uncertainty, the experimental s-wave strength function  $S_0$  ( $\times 10^{-4}$ ), its uncertainty, the experimental total radiative width in eV and its uncertainty, nuclear symbol. The format is (2i4,2e9.2,2f5.2,2f9.5,20x,i4,a2).

26	55	1.80E+01	2.40E+00	6.90	1.80	1.80000	0.50000		55Fe
26	57	2.54E+01	2.20E+00	2.30	0.60	0.92000	0.41000		57Fe
26	58	6.50E+00	1.00E+00	4.70	1.10	1.90000	0.60000		58Fe
26	59	2.54E+01	4.90E+00	4.40	1.30	3.00000	0.90000		59Fe

## 5.8 Gamma-ray parameters

The Giant Dipole Resonance (GDR) parameters, stored in the *talys/structure/gamma/gdr/* directory, originate from the Beijing GDR compilation, as present in the RIPL database. As an example, below are the GDR parameters for the U-isotopes from *U.gdr*. For each isotope, we have stored  $Z$ ,  $A$ , energy  $E_0$  in MeV, strength  $\sigma_0$  in mb, width of the GDR  $\Gamma_0$  in MeV and, if present, another energy, strength and width for the second peak, nuclear symbol. The format is (2i4,6f8.2,18x,i4,a2).

92	233	11.08	221.00	1.94	13.86	433.00	5.47		233U
92	234	11.13	371.00	2.26	13.94	401.00	4.46		234U
92	235	10.90	328.00	2.30	13.96	459.00	4.75		235U
92	236	10.92	271.00	2.55	13.78	415.00	4.88		236U
92	238	10.77	311.00	2.37	13.80	459.00	5.13		238U

The second subdirectory *gamma/hbfc/*, contains the tabulated microscopic gamma ray strength functions of Goriely [737], calculated according to Hartree-Fock BCS theory. For each isotope, there is first a line indicating the nucleus under consideration, read in the format (2(4x,i3)). Next, one line with units is given after which comes a table of excitation energies and strength functions, in the format (f9.3,e12.3). Below is an example for the first energies of  $^{110}\text{Ba}$  from *gamma/hbfc/Ba.psf*

```
Z= 56 A= 121 Ba
U[MeV]  fE1[mb/MeV]
0.100   5.581E-05
0.200   2.233E-04
0.300   5.028E-04
0.400   8.947E-04
0.500   1.400E-03
0.600   2.018E-03
0.700   2.752E-03
0.800   3.601E-03
```

The third subdirectory *gamma/hbf/*, contains the tabulated microscopic gamma ray strength functions of Goriely [737], calculated according to Hartree-Fock QRPA theory. For each isotope, there is first a line indicating the nucleus under consideration, read in the format (2(4x,i3)). Next, one line with units is given after which comes a table of excitation energies and strength functions, in the format (f9.3,e12.3). Below is an example for the first energies of  $^{110}\text{Ba}$  from *gamma/hbf/Ba.psf*

```
Z= 56 A= 110
U[MeV]  fE1[mb/MeV]
0.100   8.463E-03
0.200   9.116E-03
0.300   9.822E-03
0.400   1.058E-02
0.500   1.139E-02
0.600   1.226E-02
0.700   1.318E-02
0.800   1.416E-02
```

## 5.9 Thermal cross sections

In *talys/structure/thermal/*, the thermal cross sections for  $(n, \gamma)$ ,  $(n, p)$ ,  $(n, \alpha)$  and  $(n, f)$  cross sections are stored. The values come from Mughabghab [99] and Kopecky, who has compiled this database for use in the EAF library. In TALYS, we use this to determine cross sections for non-threshold reactions at low energies. For each isotope, we read  $Z$ ,  $A$ , target state (ground state or isomer), final state (ground state or isomer), the thermal  $(n, \gamma)$  cross section, its error, the thermal  $(n, p)$  cross section, its error, the thermal  $(n, \alpha)$  cross section, its error, the thermal  $(n, f)$  cross section, its error, nuclear symbol. The format is (4i4,8e9.2,7x,i4,a2). As an example, below are the values for the Fe-isotopes from *Fe.ther*.

26	54	0	0	2.25E+03	1.80E+02		1.00E-02	...	54Fe
26	55	0	0	1.30E+04	2.00E+03		1.70E+05	...	55Fe
26	56	0	0	2.59E+03	1.40E+02			...	56Fe
26	57	0	0	2.48E+03	3.00E+02			...	57Fe
26	58	0	0	1.32E+03	3.00E+01			...	58Fe
26	59	0	0	1.30E+04	3.00E+03		1.00E+04	...	59Fe

## 5.10 Optical model parameters

The optical model parameters are stored in the *talys/structure/optical/* directory. All the parameters are based on one and the same functional form, see Section 4.1. There are two subdirectories: *neutron/* and *proton/*. For each isotope, optical potential parameters can be given. Per isotope, we have stored  $Z$ ,  $A$ , number of different optical potentials (2), character to determine coupled-channels potential, nuclear symbol with the format (3i4,3x,a1,58x,i4,a2). On the next line we read the OMP index (1: non-dispersive, 2: dispersive). Fermi energy and reduced Coulomb radius with the format (i4,f7.2,f8.3). On the next 3 lines we read the optical model parameters as defined in Section 4.1 with the following format

```
(2f8.3,f6.1,f10.4,f9.6,f6.1,f7.1) rv,av,v1,v2,v3,w1,w2
(2f8.3,f6.1,f10.4,f7.2) rvd,avd,d1,d2,d3
(2f8.3,f6.1,f10.4,f7.2,f6.1) rvso,avso,vso1,vso2,wsol,wsol2
```

For neutrons, a dispersive potential may also be available. (These potentials have not (yet) been unpublished). In that case, another block of data is given per isotope, but now with an OMP index equal to 2, to denote the parameters for a dispersive potential. As an example, here are the parameters for the Fe-isotopes from *neutron/n-Fe.omp*.

26	54	2							54Fe
1	-11.34	0.000							
1.186	0.663	58.2	0.0071	0.000019	13.2	78.0			
1.278	0.536	15.4	0.0223	10.90					
1.000	0.580	6.1	0.0040	-3.1	160.0				
2	-11.34	0.000							
1.215	0.670	54.2	0.0077	0.000022	9.5	88.0			
1.278	0.536	15.4	0.0223	10.90					
1.000	0.580	6.1	0.0040	-3.1	160.0				
26	56	2							56Fe
1	-9.42	0.000							
1.186	0.663	56.8	0.0071	0.000019	13.0	80.0			
1.282	0.532	15.3	0.0211	10.90					
1.000	0.580	6.1	0.0040	-3.1	160.0				
2	-9.42	0.000							
1.212	0.670	53.2	0.0079	0.000023	10.0	88.0			
1.282	0.532	15.3	0.0211	10.90					
1.000	0.580	6.1	0.0040	-3.1	160.0				

For the calculation of the JLM OMP, both Stephane Goriely and Stephane Hilaire have provided radial matter densities from dripline to dripline. They are stored in *talys/structure/optical/jlm/*. As an example, below are the data of some of the Fe-isotopes as given in file *talys/structure/optical/jlm/goriely/Fe.rad*. First we give  $Z$ ,  $A$ , number of radii (lines), incremental step between radii, all in fm, with the format (2i4,i5,f7.3). Next we give the radius, and the radial densities for different deformations, first for protons and then for neutrons, with the format (f8.3,10(e12.5)),

```
26 56 200 0.100
0.100 8.04162E-02 0.00000E+00 0.00000E+00 0.00000E+00 0.00000E+00 9.06018E-02
0.200 8.02269E-02 0.00000E+00 0.00000E+00 0.00000E+00 0.00000E+00 9.05443E-02
0.300 7.98895E-02 0.00000E+00 0.00000E+00 0.00000E+00 0.00000E+00 9.04407E-02
0.400 7.94588E-02 0.00000E+00 0.00000E+00 0.00000E+00 0.00000E+00 9.03063E-02
0.500 7.89124E-02 0.00000E+00 0.00000E+00 0.00000E+00 0.00000E+00 9.01315E-02
```

Note that only the spherical components in this database are non-zero. In the files of Hilaire, see *talys/structure/optical/jlm/hilaire/*, there are also deformed components, but they will only become relevant when deformed JLM calculations are included in TALYS.

## 5.11 Fission parameters

The fission parameters are stored in the *talys/structure/fission/* directory. There are various subdirectories: *barrier/*, *states/*, *gef*, *brosa/*, *mamdouh/*, and *hfbpath/*.

First, the experimental fission parameter set can be found in directory *barrier/*. The directory *states/* includes headband transition states for even-even, even-odd, odd-odd, and odd-even nuclides. The parameters are the result of an extensive fit to many experimental fission cross sections, compiled by V. Maslov for the RIPL library. As an example we show the available parameters for the uranium isotopes which are present in the file *barrier/U.bar*. We have stored  $Z$ ,  $A$ , a parameter specifying the symmetry of the inner barrier, height of the inner barrier, curvature of the inner barrier, a parameter specifying the symmetry of the outer barrier, height of the outer barrier, curvature of the outer barrier, the pairing correlation function at the barrier (which is not used in the calculation) and the nuclear symbol with the format (2i4,a5,2f8.3,a5,2f8.3,f9.4,15x,i4,a2).

92	231	S	4.40	0.70	MA	5.50	0.50	0.869	231U
92	232	S	4.90	0.90	MA	5.40	0.60	0.848	232U
92	233	S	4.35	0.80	MA	5.55	0.50	0.946	233U
92	234	S	4.80	0.90	MA	5.50	0.60	0.889	234U
92	235	S	5.25	0.70	MA	6.00	0.50	0.803	235U
92	236	S	5.00	0.90	MA	5.67	0.60	0.833	236U
92	237	GA	6.40	0.70	MA	6.15	0.50	0.809	237U
92	238	GA	6.30	1.00	MA	5.50	0.60	0.818	238U
92	239	GA	6.45	0.70	MA	6.00	0.50	0.816	239U

In *states*, we have stored files with default head band and class II-states for even-even, even-odd, odd-odd, and odd-even nuclides. An example of a file containing the head band transition states is given

below for *states/hbstates.ee*. This file is used for even-even nuclides. We loop over the two barriers. On the first line one finds the barrier number, the number of head band states and the energy at which the continuum starts with the format(2i4,f8.3). Next we loop over the transition states, in which we read the level number, level energy in MeV, spin and parity with the format (i4,f11.6,f6.1,i5).

```

1  8  0.800
1  0.000000  0.0  1
2  0.500000  2.0  1
3  0.400000  0.0 -1
4  0.400000  1.0 -1
5  0.500000  2.0  1
6  0.400000  2.0 -1
7  0.800000  0.0  1
8  0.800000  0.0  1
2  4  0.500
1  0.000000  0.0  1
2  0.500000  2.0  1
3  0.200000  0.0 -1
4  0.500000  1.0 -1

```

We also include the possibility to incorporate the effect of class II states in the calculation. For this purpose we take four parameter sets with class II states for even-even, even-odd, odd-odd, and odd-even nuclides. As an example we show the file *states/class2states.ee*. This file contains the well number, and the number of class II states. Subsequent lines contain the level number, the level energy in MeV, spin and parity with the format (i4,f8.3,f9.1,i5).

```

1  10
1  2.700      0.0  1
2  3.400      0.0 -1
3  4.100      1.0 -1
4  4.800      2.0 -1
5  5.000      1.0  1
6  5.200      0.0  1
7  5.400      0.0 -1
8  5.500      1.0 -1
9  5.600      2.0 -1
10 5.700      1.0  1

```

The directory *brosa/* contains three subdirectories: *barrier/*, *groundstate/*, and *prescission/*. In *brosa/barrier/* temperature-dependent fission barrier parameters per fission mode can be found. They are the results of calculations performed within the Brosa model. The extension in the filename reveals the fission mode: *sl* for superlong, *st* for standard I, and *st2* for standard II. As an example, below are the superlong parameters for several U isotopes taken from *brosa/barrier/U.sl*. Each line gives Z, A, temperature T in MeV,  $B_F$  in MeV,  $\hbar\omega$  in MeV, and the barrier position in terms of the distance between the fragment centers d in fm. The format is (2i4,4f15.5).

```

92 240      0.00000      11.40470      3.92020      10.37450

```

92 240	0.30000	11.23440	4.18630	10.34980
92 240	0.60000	11.64780	4.25390	10.44170
92 240	0.90000	9.58680	2.58900	10.35970
92 240	1.20000	7.88030	2.36520	10.53400
92 240	1.60000	5.69890	1.58010	10.43420
92 240	2.00000	4.17750	1.07010	10.28590
92 240	2.50000	2.76320	0.47300	9.69080
92 240	3.00000	1.84230	0.25520	8.57080
92 238	0.00000	10.88450	4.67530	10.27930
92 238	0.30000	10.97680	4.87110	10.27090
92 238	0.60000	10.59680	4.44100	10.29590
92 238	0.90000	9.31080	3.69600	10.37940
92 238	1.20000	7.55620	2.32260	10.40990
92 238	1.60000	5.46180	1.51320	10.33670
92 238	2.00000	3.98050	0.82730	10.15860
92 238	2.50000	2.74050	0.43440	9.43930
92 238	3.00000	1.87030	0.34600	8.62610

The ground state energies as a function of temperature are stored in *brosa/barrier/groundstate/*. Each line has the same format: Z, A, T in MeV, and  $E_{groundstate}$  in MeV (2i4,2f15.5). An example is included for U isotopes, see *brosa/groundstate/U.fis*.

92 240	0.00000	-1811.82104
92 240	0.30000	-1813.38599
92 240	0.60000	-1818.06006
92 240	0.90000	-1825.59497
92 240	1.20000	-1836.26599
92 240	1.60000	-1855.76294
92 240	2.00000	-1881.23901
92 240	2.50000	-1921.08105
92 240	3.00000	-1969.60205
92 238	0.00000	-1800.57996
92 238	0.30000	-1802.16504
92 238	0.60000	-1806.85205
92 238	0.90000	-1814.34302
92 238	1.20000	-1825.23596
92 238	1.60000	-1844.68799
92 238	2.00000	-1870.17004
92 238	2.50000	-1910.02905
92 238	3.00000	-1958.52405

The third directory, *brosa/barrier/precission/*, contains parameters that fix the precission shape of the nucleus in each fission mode. They mark the end of the fission path found in the same fission channel calculations that resulted in the Brosa barrier parameters. Again each line has the same format: Z, A, T in MeV,  $A_h$  the heavy fragment mass in amu,  $l$  the nucleus half length in fm, and  $E_{precission}$  in MeV (2i4,4f15.5). An example is included for precission shape parameters in the superlong mode of U isotopes, see *brosa/precission/U.sl*,

92 240	0.00000	120.45900	21.29700	-1840.84900
92 240	0.30000	120.83730	21.48670	-1826.35022
92 240	0.60000	120.83670	20.74300	-1831.38477
92 240	0.90000	120.30430	20.21950	-1840.12256
92 240	1.20000	120.65520	20.13060	-1854.43555
92 240	1.60000	120.83060	19.56120	-1874.16174
92 240	2.00000	120.74340	19.33610	-1902.75671
92 240	2.50000	120.62800	18.38600	-1945.59497
92 240	3.00000	120.78300	18.45000	-1998.50598
92 238	0.00000	120.00730	21.40630	-1815.46497
92 238	0.30000	119.64770	21.36200	-1816.33203
92 238	0.60000	119.50730	20.50950	-1821.51123
92 238	0.90000	119.27930	20.50120	-1830.13428
92 238	1.20000	119.47550	19.91770	-1842.70630
92 238	1.60000	123.00390	19.23990	-1864.13489
92 238	2.00000	120.49580	19.24370	-1892.63281
92 238	2.50000	119.62200	18.37100	-1935.14502
92 238	3.00000	119.37600	18.38000	-1988.42395

In directory *gef*, masses and shell correction energies for the GEF model are stored.

The Mamdouh fission parameter set can be found in directory *mamdouh/*. This parameter set has been derived from Extended Thomas-Fermi plus Strutinsky Integral calculations and comprise double-humped fission barrier heights and curvatures for numerous isotopes. As an example we show the available parameters for the various U isotopes which are present in the file *mamdouh/U.bar*. We have stored Z, A, height of the inner barrier, height of the outer barrier in MeV and the nuclear symbol with the format (i3,i4,2(24x,f8.2),5x,i3,a2).

92 230	1.24	0.00	0.00	3.80	1.77	-0.02	0.35	3.90	230U
92 231	1.24	0.01	0.00	4.10	1.83	0.05	0.50	4.30	231U
92 232	1.25	0.02	0.00	4.20	1.83	0.05	0.53	4.20	232U
92 233	1.28	0.05	0.00	4.70	1.84	0.06	0.53	4.40	233U
92 234	1.28	0.03	0.00	4.80	1.83	0.06	0.53	4.40	234U
92 235	1.28	0.04	0.00	5.40	1.63	0.01	0.53	4.10	235U
92 236	1.29	0.04	0.00	5.20	1.64	0.01	0.53	4.00	236U
92 237	1.28	0.04	0.00	5.70	1.63	0.01	0.53	4.30	237U
92 238	1.29	0.03	0.00	5.70	1.91	0.07	0.47	4.90	238U
92 239	1.29	0.03	0.00	6.10	1.81	-0.07	0.35	5.50	239U
92 240	1.29	0.03	0.00	6.00	1.90	-0.04	0.53	6.30	240U
92 241	1.30	0.04	0.00	6.30	1.91	-0.03	0.55	5.70	241U
92 242	1.30	0.04	0.00	5.90	1.90	-0.04	0.53	6.00	242U

If we use the WKB approximation to calculate fission transmission coefficients, **fismodel 5**, we need potential energy curves. They can be found in the directory *hfbpath/*. As an example, we show the data for  $^{235}\text{U}$  as present in the file *hfbpath/U.fis*. We have stored Z, A, number of fission width values, total energy (not used) with the format (3i4,f12.3). Next, we give the values for the fission width and height with the format (f10.3,20x,f10.3),

92	235	100	-1781.682	
	0.269	0.000	0.152	0.000
	0.298	0.000	0.180	0.332
	0.326	0.000	0.189	1.047
	0.355	0.000	0.171	1.987
	0.383	0.000	0.216	2.846
	0.412	0.000	0.199	3.921
	0.440	0.000	0.194	4.695
	0.470	0.000	0.158	5.002
	0.501	0.000	0.136	5.391
	0.531	0.000	0.156	5.390
	0.563	0.000	0.173	5.186

## 5.12 Integral validation library

Since all excitation functions are available in TALYS after a run with many incident energies, it is relatively easy to calculate production or reaction rates for various applications. This is for example done for astrophysics and medical isotope production. Another possibility is to calculate the so called effective cross section for integral activation measurements, by folding the excitation functions by an experimental flux. In *talys/structure/flux*, we have stored more than 40 spectra, coming from the EASY package [432, 529], which have been used in past activation benchmarks. Also the effective cross sections are stored, allowing direct comparison with experimental data.

## 5.13 Decay data library

For medical isotope production, the decay paths to the produced isotopes need to be known. Therefore, in *talys/structure/decay* we have stored the JEFF-3.1.1 Radioactive Decay Data File in the usual element by element files.

## 5.14 Best TALYS input parameters

We have created the possibility to store the “best” set of model input parameters per nuclide. This is a helpful feature to ensure reproducibility of earlier obtained results, i.e. a nuclear reaction analysis with TALYS is stored in the best possible way (rather than scattered over input files in several working directories). Theoretically, a complete collection of best TALYS input parameter files would enable a high-quality description of nuclear reactions on all nuclides simultaneously (when used e.g. in a script to produce a complete nuclear data library), especially if the work is divided among more than a few persons. One would thus be able to get the best possible results with a seemingly default input file. The only requirement is that the keyword **best y** is set in the input file. All adjusted optical model, level density etc. parameters are stored in the *talys/structure/best* directory. As subdirectories, full isotope names should be used in the format (a1,i3.3) or (a2,i3.3), depending on the element symbol. Furthermore, the first character of the Symbol should be in upper case. In other words, valid examples of subdirectories

are *Yb174/*, *F019/*, *Be009/*, and *U235*. For the sets of best parameters in these subdirectories, we use filenames *zZZZaAAAS.best* where *ZZZ* and *AAA* are the *Z* and *A* of the nuclide in i3.3 format, and *S* is the particle symbol (g, n, p, d, t, h, or a). This strict naming procedure is required for software that uses TALYS for nuclear data evaluation purposes. As an example, we show the best parameters for neutrons incident on  $^{80}\text{Se}$  as present in the file *talys/structure/best/Se080/n-Se080.best*,

```
gamgamadjust 34 81 0.35
rvadjust a 1.05
avadjust a 1.05
gnadjust 34 81 0.92
gpadjust 34 81 0.92
Cstrip a 1.40
Cknock a 1.40
```

If we use **best y**, the above set of keywords will automatically be added to the TALYS input file. This directory is also the best place to store other TALYS input files such as files with tabular optical model parameters. They need to be copied to the working directory when the **best y** option is used. It is also possible to create alternative “best” database under *talys/structure* with a different collection of best input files. These can then be invoked with the **bestpath** keyword, see page 6.2.2.

## Input description

For the communication between TALYS and its users, we have constructed an input/output method which shields beginners from all the possible options for nuclear model parameters that can be specified in TALYS, while enabling at the same time maximal flexibility for experienced users.

An input file of TALYS consists of keywords and their associated values. Before we list all the input possibilities, let us illustrate the use of the input by the following example. It represents a minimum input file for TALYS:

```
projectile n
element    al
mass      27
energy    14.
```

This input file represents the simplest question that can be asked to TALYS: if a  $^{27}\text{Al}$  nucleus is hit by 14 MeV neutrons, what happens? Behind this simple input file, however, there are more than a few hundred default values for the various nuclear models, parameters, output flags, etc., that you may or may not be interested in. When you use a minimal input file like the one above, you leave it to the authors of TALYS to choose all the parameters and models for you, as well as the level of detail of the output file. If you want to use specific nuclear models other than the default, adjust parameters or want to have more specific information in the output file(s), more keywords are required. Obviously, more keywords means more flexibility and, in the case of adequate use, better results, though often at the expense of increasing the level of phenomenology. In this Chapter, we will first give the basic rules that must be obeyed when constructing an input file for TALYS. Next, we give an outline of all the keywords, which have been categorised in several groups. Finally, we summarize all keywords in one table.

## 6.1 Basic input rules

Theoretically, it would be possible to make the use of TALYS completely idiot-proof, i.e. to prevent the user from any input mistakes that possibly can be made and to continue a calculation with “assumed” values. Although we have invested a relatively large effort in the user-friendliness of TALYS, we have not taken such safety measures to the extreme limit and ask at least some minimal responsibility from the user. Once you have accepted that, only very little effort is required to work with the code. Successful execution of TALYS can be expected if you remember the following simple rules and possibilities of the input file:

1. One input line contains one keyword. Usually it is accompanied by only one value, as in the simple example given above, but some keywords for model parameters need to be accompanied by indices (usually  $Z$  and  $A$ ) on the same line.
2. A keyword and its value(s) *must* be separated by at least 1 blank character.
3. The keywords can be given in arbitrary order. If, by mistake, you use the same keyword more than once, the value of the last one will be adopted. This does not hold for keywords which are labeled with different  $Z$  and  $A$  indices, see the beginning of Section 6.2.
4. All characters can be given in either lowercase or uppercase.
5. A keyword *must* be accompanied by a value. (There is one exception, the **rotational** keyword). To use default values, the keywords should simply be left out of the input file.
6. An input line starting with a  $\#$  in column 1 is neglected. This is helpful for including comments in the input file or to temporarily deactivate keywords.
7. A minimal input file always consists of 4 lines and contains the keywords **projectile**, **element**, **mass** and **energy**. These 4 keywords *must* be given in any input file.
8. An input line may not exceed 80 characters.

As an example of rules 2, 3, 4 and 6, it can be seen that the following input file is completely equivalent to the one given in the beginning of this Chapter:

```
# Equivalent input file
energy          14.
projectile n
mass 27
Element AL
#outbasic y
```

In the following erroneous input file, only the first 2 lines are correct, while rules 2 and 5 are violated in the other lines.

```

projectile n
element al
mass27
energy

```

In cases like this, the execution will be stopped and TALYS will give an appropriate error message for the first encountered problem. We like to believe that we have covered all such cases and that it is impossible to let TALYS crash (at least with our compilers, see also Chapter 7), but you are of course invited to prove and let us know about the contrary (Sorry, no cash rewards). Typing errors in the input file will be spotted by TALYS, e.g. if you write **projectile n**, it will tell you the keyword is not in our list.

## 6.2 Keywords

The four-line input file given above was an example of a minimum input file for TALYS. In general, you probably want to be more specific, as in the following example:

```

projectile    n
element      nb
mass         93
energy       1.
Ltarget      1
relativistic n
widthmode    2
outinverse   y
a 41 93 13.115
a 41 94 13.421

```

which will simulate the reaction of a 1 MeV neutron incident on  $^{93}\text{Nb}$ , with the target in its first excited state (**Ltarget 1**, a 16-year isomer), using non-relativistic kinematics, the HRTW-model for width fluctuation corrections (**widthmode 2**) in the compound nucleus calculation, with the particle transmission coefficients and inverse reaction cross sections written on the output file (**outinverse y**) and with user-defined level density parameters **a** for  $^{93}\text{Nb}$  and  $^{94}\text{Nb}$ .

In this Section, we will explain all the possible keywords. We have classified them according to their meaning and importance. For each keyword, we give an explanation, a few examples, the default value, and the theoretically allowed numerical range. As the input file above shows, there is usually one value per keyword. Often, however, in cases where several residual nuclides are involved, nuclear model parameters differ from nuclide to nuclide. Then, the particular nuclide under consideration must also be given in the input line. In general, for these model parameters, we read keyword,  $Z$ ,  $A$ , a physical value and sometimes a possible further index (e.g. the fission barrier, index for the giant resonance, etc.), all separated by blanks. As the example above shows for the level density parameter  $a$ , the same keyword can appear more than once in an input file, to cover several different nuclides. Again, remember that all such keywords, if you don't specify them, have a default value from either the nuclear structure and model parameter database or from systematics. The usual reason to change them is to fit experimental

data, to use new information that is not yet in the TALYS database, or simply because the user may not agree with our default values. A final important point to note is that some keywords induce defaults for other keywords. This may seem confusing, but in practice this is not so. As an example, for a  $^{56}\text{Fe}$  target the **fission** keyword is automatically disabled whereas for  $^{232}\text{Th}$  it is by default enabled. Hence, the default value of the **fission** keyword is mass dependent. In the input description that follows, you will find a few similar cases. Anyway, you can always find all adopted default values for all parameters at the top of the *output* file, see which values have been set by the user or by default, and overrule them in a new input file.

### 6.2.1 Four main keywords

As explained above there are 4 basic keywords that form the highest level of input. They determine the fundamental parameters for any nuclear reaction induced by a light particle.

#### projectile

Eight different symbols can be given as **projectile**, namely **n, p, d, t, h, a, g** representing neutron, proton, deuteron, triton,  $^3\text{He}$ , alpha and gamma, respectively, and **0**, which is used if instead of a nuclear reaction (projectile + target) we start with an initial population of an excited nucleus.

*Examples:*

**projectile n**

**projectile d**

*Range:* **projectile** must be equal to **n, p, d, t, h, a, g** or **0**.

*Default:* None.

#### element

Either the nuclear symbol or the charge number  $Z$  of the target nucleus can be given. Possible values for **element** range from Li (3) to C4 (124). To accommodate target nuclides with  $Z > 110$  the element names are defined as follows: Rg(111), Cn(112), Nh(113), Fl(114), Mc(115), Lv(116), Ts(117), Og(118), B9(119), C0-4(120-124). Obviously the symbols for  $Z$  above 118 will be changed when official names are assigned to them.

*Examples:*

**element pu**

**element 41**

**element V**

**element B9**

*Range:*  $3 \leq \text{element} \leq 124$  or  $\text{Li} \leq \text{element} \leq \text{C4}$ .

*Default:* None.

### mass

The target mass number  $A$ . The case of a natural element can be specified by **mass 0**. Then, a TALYS calculation for each naturally occurring isotope will be performed (see also the **abundance** keyword, p. 173), after which the results will be properly weighted and summed.

*Examples:*

**mass 239**

**mass 0**

*Range:* **mass 0** or  $5 < \text{mass} \leq 339$ . The extra condition is that the target nucleus, i.e. the combination of **mass** and **element** must be present in the mass database, which corresponds to all nuclei between the proton and neutron drip lines.

*Default:* None.

### energy

The incident energy in MeV. The user has four possibilities: (1) A single incident energy is specified in the input as a real number, (2) A filename is specified, where the corresponding file contains a series of incident energies, with one incident energy per line. Any name can be given to this file, provided it starts with a character, and it is present in your working directory. Option (2) is helpful for the calculation of excitation functions or for the creation of nuclear data libraries. Option (2) is mandatory if **projectile 0**, i.e., if instead of a nuclear reaction we start with a population of an excited nucleus (see the **Special cases** below). Since TALYS-1.6, there are an additional 2 options which allows to use a whole range of incident energies without having to make a file for this: (3) A filename that is predefined by TALYS. This contains a hardwired energy grids with for example for neutrons a finer energy grid at low energies and a progressively wider grid at high energies. These have the form  $pE-E.grid$  where  $p$  is the name of the projectile, and the two  $E$ 's are the start and end energy in integer form respectively. The *.grid* specifies that this concerns a predefined energy grid. An often used example is *n0-200.grid* which is the neutron energy grid of the TENDL library. More energies are used in the eV and keV range while at high energies automatically a course grid is used. With the file *n0-20.grid* exactly the same incident energy grid is used, but only up to the final energy of 20 MeV. Finally, option (4) is to give after the *energy* keyword 3 numbers: the starting energy, the end energy and the energy step. Next, an equidistant grid is made based on these 3 numbers.

*Examples:*

**energy 140.**

**energy 0.002**

**energy range**

**energy n0-30.grid**

**energy p10-100.grid**

**energy 0.5 20. 0.5** (Incident energies: 0.5, 1, 1.5, ...20 MeV)

*Range:*  $10^{-11}$  MeV  $\leq$  **energy** < 1000 MeV or a *filename*, whereby the corresponding file contains at least 1 and a maximum of **numenin** incident energies, where **numenin** is an array dimension specified in *talys.cmb*. Currently **numenin=500**.

*Default:* None.

### Using the four main keywords

To summarize the use of the four basic keywords, consider the following input file

```
projectile n
element    pd
mass      110
energy range
```

The file *range* looks e.g. as follows

```
0.1
0.2
0.5
1.
1.5
2.
5.
8.
10.
15.
20.
```

In the source code, the number of incident energies, here 11, is known as **numinc**. For the four-line input given above, TALYS will simulate all open reaction channels for  $n + {}^{110}\text{Pd}$  for all incident energies given in the file *range*, using defaults for all models and parameters. The most important cross sections will automatically be written to the output file, see Chapter 7.

### Special cases

There are two examples for which the **energy** keyword does not represent the incident energy of the projectile.

**1. Populated initial nucleus** If **projectile 0**, the user *must* give a filename for the **energy** keyword. This time however, the file does not consist of incident energies but of the excitation energy grid of the initial population, see Section 4.11. On the first line of the file we read the number of energies (lines), number of spins, and number of parities. The excitation energies that are read represent the middle values of the bins, and are followed by either (a) if the number of spins is zero, the total population in that bin, or (b) if the number of spins is not zero, the population per excitation energy bin and spin, using one column per spin. The values given in the second column represent either a histogram, if **popMeV n** (the default) or spectrum (**popMeV y**). If **popMeV y**, these spectral values are multiplied by the energy bin width and we obtain the population, which has a dimension of millibarns. If the population for only 1 parity is given, the population is equally distributed over both parities. Hence, if we let TALYS determine the spin-parity distribution (case (a)), an example of such a file is

```

      8      0      1
0.25 0.1342
0.75 0.2176
1.25 0.3344
1.75 0.6522
2.25 0.6464
2.75 0.2897
3.25 0.1154
3.75 0.0653

```

and if we give the full spin-dependent population (case (b)), with equal parity distribution, we could e.g. have

```

      8      3      1
0.25 0.0334 0.0542 0.0112
0.75 0.0698 0.1043 0.0441
1.25 0.1131 0.2303 0.0971
1.75 0.1578 0.3333 0.1143
2.25 0.1499 0.3290 0.1212
2.75 0.1003 0.2678 0.0845
3.25 0.0844 0.1313 0.0661
3.75 0.0211 0.0889 0.0021

```

If in addition the population should be parity-dependent, one would have e.g.

```

      8      3      2
0.25 0.0134 0.0542 0.0112
0.75 0.0298 0.1043 0.0441
1.25 0.0531 0.2303 0.0971
1.75 0.0578 0.3333 0.1143
2.25 0.0599 0.3290 0.1212
2.75 0.0603 0.2678 0.0845
3.25 0.0444 0.1313 0.0661
3.75 0.0111 0.0889 0.0021

```

```

0.25 0.0234 0.0142 0.0008
0.75 0.0498 0.0943 0.0141
1.25 0.0666 0.1103 0.0471
1.75 0.0678 0.1333 0.0343
2.25 0.0299 0.1290 0.0512
2.75 0.0403 0.1678 0.0245
3.25 0.0344 0.1013 0.0361
3.75 0.0100 0.0489 0.0011

```

Note that in this case the energy restarts in the middle; first the energy grid for 3 spin values and parity -1 is given, then for parity +1.

**2. Astrophysical reaction rates** If **astro y**, see page 172 for astrophysical reaction rate calculations, the incident energy as given in the input is overruled by a hardwired incident energy grid that is appropriate for the calculation of reaction rates. However, to avoid unnecessary programming complications, the **energy** keyword *must* still be given in the input, and it can have any value. Hence if **astro y** one could e.g. give **energy 1**. in the input file. The adopted incident energies that overrule this value will be given in the output.

#### Four main keywords: summary

The first four keywords are clearly the most important: they do *not* have a default value while they determine default values for some of the other keywords which, in other words, may be projectile-, energy-, element- or mass-dependent. All the keywords that follow now in this manual have default values and can hypothetically be left out of the input file if you are only interested in a minimal reaction specification. If you want to add keywords, you can enter them one by one in the format that will be described below. Another way is to go to the top of the output file that is generated by the simple input file given above. You will find all the keywords with their values as adopted in the calculation, either user-specified or as defaults. All nuclear model parameters per nucleus are printed in the file *parameters.dat*, provided **partable y** was set in the input. You can copy this part and paste it into the input file, after which the values can be changed.

## 6.2.2 Basic physical and numerical parameters

The keywords described in this subsection are rather general and do not belong to particular nuclear models. They determine the completeness and precision of the calculations and most of them can have a significant impact on the calculation time.

### ejectiles

The outgoing particles that are considered in competing reaction channels. By default, all competing channels are included even if one is interested in only one type of outgoing particle. This is neces-

sary since there is always competition with other particles, in e.g. Hauser-Feshbach and pre-equilibrium models, that determines the outcome for the particle under study. Furthermore, reaction Q-values automatically keep channels closed at low incident energies. However, for diagnostic or time-economical purposes, or cases where e.g. one is only interested in high-energy  $(p, p')$  and  $(p, n)$  multi-step direct reactions, one may save computing time and output by skipping certain ejectiles as competing particles. For neutron-induced reactions on actinides up to 20 MeV, setting **ejectiles g n** is a rather good approximation that saves time. Also comparisons with computer codes that do not include the whole range of particles will be facilitated by this keyword.

*Examples:*

**ejectiles n**

**ejectiles g n p a**

*Range:* **ejectiles** can be any combination of **g, n, p, d, t, h** and **a**.

*Default:* Include all possible outgoing particles, i.e. **ejectiles g n p d t h a**

### Ltarget

The excited state of the target as given in the discrete level database. This keyword allows to compute cross sections for isomeric targets.

*Examples:*

**Ltarget 2**

*Range:*  $0 \leq \mathbf{Ltarget} \leq \mathbf{numlev}$ , where **numlev** is specified in the file *talys.cmb*. Currently, **numlev=30**

*Default:* **Ltarget 0**, i.e. the target is in its ground state.

### maxZ

The maximal number of protons away from the initial compound nucleus that is considered in a chain of residual nuclides. For example, if **maxZ 3**, then for a  $n + {}^{56}\text{Fe}$  ( $Z=26$ ) reaction, the V-isotopes ( $Z=23$ ) are the last to be considered for further particle evaporation in the multiple emission chain. **maxZ** is normally only changed for diagnostic purposes. For example, if you are only interested in the  $(n, n')$ ,  $(n, 2n), \dots, (n, xn)$  residual production cross sections, or the associated discrete gamma ray intensities, **maxZ 0** is appropriate. (Note that in this case, the competition of emission of protons up to alpha particles is *still* taken into account for all the nuclides along the  $(n, xn)$  chain, only the decay of the residual nuclides associated with this charged-particle emission are not tracked further).

*Examples:*

**maxZ 6**

*Range:*  $0 \leq \mathbf{maxZ} \leq \mathbf{numZ}-2$ , where  $\mathbf{numZ}=2+2*\mathbf{memorypar}$  is specified in the file *talys.cmb*, where  $\mathbf{memorypar}=5$  for a computer with at least 256 Mb of memory.

*Default:* Continue until all possible reaction channels are closed or until the maximal possible value for  $\mathbf{maxZ}$  is reached (which rarely occurs). By default  $\mathbf{maxZ}=\mathbf{numZ}-2$  where the parameter  $\mathbf{numZ}$  is specified in the file *talys.cmb*. This parameter should be large enough to ensure complete evaporation of all daughter nuclei.

### maxN

The maximal number of neutrons away from the initial compound nucleus that is considered in a chain of nuclides. For example, if  $\mathbf{maxN} 3$ , then for a  $n + {}^{56}\text{Fe}$  ( $N=31$ ) reaction, residual nuclei with  $N=28$  ( $=31-3$ ) are the last to be considered for further particle evaporation in the multiple emission chain.  $\mathbf{maxN}$  is normally only changed for diagnostic or economical purposes.

*Examples:*

**maxN 6**

*Range:*  $0 \leq \mathbf{maxN} \leq \mathbf{numN}-2$ , where  $\mathbf{numN}=4+4*\mathbf{memorypar}$  is specified in the file *talys.cmb*, where  $\mathbf{memorypar}=5$  for a computer with at least 256 Mb of memory.

*Default:* Continue until all possible reaction channels are closed or until the maximal possible value for  $\mathbf{maxN}$  is reached (which rarely occurs). By default  $\mathbf{maxN}=\mathbf{numN}-2$  where the parameter  $\mathbf{numN}$  is specified in the file *talys.cmb*. This parameter should be large enough to ensure complete evaporation of all daughter nuclei.

### bins

The number of excitation energy bins in which the continuum of the initial compound nucleus is divided for further decay. The excitation energy region between the last discrete level and the total excitation energy for the initial compound nucleus is divided into **bins** energy bins. The resulting bin width then also determines that for the neighboring residual nuclei, in the sense that for any residual nucleus we ensure that the bins fit exactly between the last discrete level and the maximal possible excitation energy. For residual nuclides far away from the target, a smaller number of bins is automatically adopted. If **bins 0** a simple formula is invoked to take into account the fact that more bins are needed when the incident energy increases. Instead of a constant number of bins, it is then incident energy ( $E$ ) dependent. More specifically, **nbins 0** means

$$(6.1) \quad \text{Nbins} = 30 + 50 \frac{E^2}{(E^2 + 60^2)}$$

It is obvious that **bins** has a large impact on the computation time.

*Examples:*

**bins 25**

*Range:*  $\text{bins} = 0$  or  $2 \leq \text{bins} \leq \text{numbins}$ , where **numbins** is specified in the file *talys.cmb*. Currently, **numbins=100**

*Default:* **bins 40**

### equidistant

Flag for adopting an equidistant or non-equidistant (logarithmic) excitation energy grid for the continuum of each residual nucleus. The latter option makes the calculation more efficient since it uses more precision when it is needed.

*Examples:*

**equidistant y**

**equidistant n**

*Range:* **y** or **n**

*Default:* **equidistant n**

### segment

The number of segments to divide the standard emission energy grid. The basic emission energy grid we use for spectra and transmission coefficient calculations is:

```
0.001, 0.002, 0.005    MeV
0.01, 0.02, 0.05     MeV
0.1- 2 MeV : dE= 0.1 MeV
2 - 4 MeV : dE= 0.2 MeV
4 - 20 MeV : dE= 0.5 MeV
20 - 40 MeV : dE= 1.0 MeV
40 - 200 MeV : dE= 2.0 MeV
200 - 300 MeV : dE= 5.0 MeV
above 300 MeV : dE=10.0 MeV
```

This grid is divided into a finer grid by subdividing each interval by **segment**.

*Examples:*

**segment 3**

*Range:*  $1 \leq \text{segment} \leq 4$ . Extra conditions:  $1 \leq \text{segment} \leq 3$  if the maximum incident energy is larger than 20 MeV,  $1 \leq \text{segment} \leq 2$  if the maximum incident energy is larger than 40 MeV, **segment=1** if the maximum incident energy is larger than 100 MeV. (These rules are imposed due to memory limitations).

*Default:* **segment 1**

**maxlevelstar**

The number of included discrete levels for the *target* nucleus that is considered in Hauser-Feshbach decay and the gamma-ray cascade. For nuclides that do not have **maxlevelstar** available in the discrete level file, we take the last known level as the last discrete level in our calculation.

*Examples:*

**maxlevelstar 0**

**maxlevelstar 12**

*Range:*  $0 \leq \text{maxlevelstar} \leq \text{numlev}$ , where **numlev** is specified in the file *talys.cmb*. Currently, **numlev=30**

*Default:* **maxlevelstar 20**

**maxlevelsres**

The number of included discrete levels for all *residual* nuclides that is considered in Hauser-Feshbach decay and the gamma-ray cascade. For nuclides that do not have **maxlevelsres** available in the discrete level file, we take the last known level as the last discrete level in our calculation. This keyword is overruled by **maxlevelsbin** and **maxlevelstar** for specified nuclides.

*Examples:*

**maxlevelsres 0**

**maxlevelsres 12**

*Range:*  $0 \leq \text{maxlevelsres} \leq \text{numlev}$ , where **numlev** is specified in the file *talys.cmb*. Currently, **numlev=30**

*Default:* **maxlevelsres 10**

**maxlevelsbin**

The number of included discrete levels for the nuclides resulting from *binary* emission that is considered in Hauser-Feshbach decay and the gamma-ray cascade. For nuclides that do not have **maxlevelsbin** available in the discrete level file, we take the last known level as the last discrete level in our calculation. On the input line we read **maxlevelsbin**, the symbol of the ejectile and the number of levels of the associated residual nucleus.

*Examples:*

**maxlevelsbin a 8**

**maxlevelsbin p 12**

*Range:*  $0 \leq \text{maxlevelsbin} \leq \text{numlev}$ , where **numlev** is specified in the file *talys.cmb*. Currently, **numlev=30**

*Default:* **maxlevelsbin g 10, maxlevelsbin n 10, maxlevelsbin p 10, maxlevelsbin d 5, maxlevelsbin t 5, maxlevelsbin h 5, maxlevelsbin a 10**. The value for the inelastic channel will however always be overruled by the **maxlevelstar** keyword, for the target nucleus, or the value for its default.

### Nlevels

The number of included discrete levels for a *specific residual* nucleus that is considered in Hauser-Feshbach decay and the gamma-ray cascade. For nuclides that do not have **Nlevels** available in the discrete level file, we take the last known level as the last discrete level in our calculation. On the input line we read **Nlevels**, *Z*, *A*, and the number of levels.

*Examples:*

**Nlevels 41 93 8**

*Range:*  $0 \leq \text{Nlevels} \leq \text{numlev}$ , where **numlev** is specified in the file *talys.cmb*. Currently, **numlev=30**

*Default:* **Nlevels** has the value specified by the defaults of **maxlevelstar**, **maxlevelsbin**, and **maxlevelsres**.

### disctable

Keyword to change the used discrete level database. The standard discrete level database from RIPL can be updated with theoretical levels calculated from the microscopic level densities from **ldmodel 5**, for nuclides with no or few experimental levels. Note that **disctable 3** gives the option to do nuclear reaction calculations using purely theoretically estimated levels.

*Examples:*

**disctable 1:** RIPL database with experimental levels + theoretical levels added until the 100th level

**disctable 2:** RIPL database with experimental levels (the only option until TALYS-1.4)

**disctable 3:** Theoretical levels for all nuclides

*Range:*  $0 \leq \text{disctable} \leq 3$

*Default:* **disctable 1**

### levelfile

File with discrete levels. The format of the file is exactly the same as that of the nuclear structure database *talys/structure/levels/*. In practice, the user can copy a file from this database, e.g. *Fe.lev*, to the working directory and change it. In this way, changes in the “official” database are avoided. Note that even if

only changes for one isotope are required, the entire file needs to be copied if for the other isotopes the originally tabulated values are to be used. On the input line, we read **levelfile**,  $Z$ , filename.

*Examples:*

**levelfile 26 Fe.loc**

*Range:* **levelfile** can be equal to any filename, provided it starts with a character.

*Default:* If **levelfile** is not given in the input file, the discrete levels are taken from the *talys/structure/levels* database per nucleus.

### Liso

Level number of isomer. This user assigned value can overrule the one determined from the discrete level file.

*Examples:*

**Liso 2**

*Range:*  $0 \leq \mathbf{Liso} \leq \mathbf{numlev}$ , where **numlev** is specified in the file *talys.cmb*. *Default:* **Liso** not given.

### branch

Branching ratio for discrete level to overrule that given by the discrete level file. With this keyword one can change for example the "guessed" branching ratios put in the discrete level file, or even overrule the original values from RIPL. On the input line we read **branch**,  $Z$ ,  $A$ , mother level, the number of branching levels nbr, and next the daughter level and branching ratio for each level up to nbr.

*Examples:*

**branch 38 85 7 2 2 0.7 0 0.3:** 70% decay of 7th level of  $^{85}\text{Sr}$  to level 2, and 30% to the ground state

**branch 38 87 17 1 1 1.:** 100% decay of 17th level of  $^{87}\text{Sr}$  to level 1.

*Range:*  $0 \leq \mathbf{number\ of\ levels}, \mathbf{mother\ level}, \mathbf{daughter\ level} \leq \mathbf{numlev}$ , where **numlev** is specified in the file *talys.cmb*.

*Default:* **branch** is not given.

### massmodel

Model for nuclear masses. There are 4 theoretical mass models and an analytic formula, see Section 5.2. They are only used when no experimental mass is available or when **expmass n**.

*Examples:*

**massmodel 0:** Duflo-Zucker formula

**massmodel 1:** Möller table

**massmodel 2:** Goriely HFB-Skyrme table

**massmodel 3:** HFB-Gogny DIM table

*Range:*  $0 \leq \text{massmodel} \leq 3$

*Default:* **massmodel 2**

### expmass

Flag for using the experimental nuclear mass when available. Use **expmass n** to overrule the experimental mass by the theoretical nuclear mass (i.e. the Audi-Wapstra values will not be used). This will then be done for all nuclides encountered in the calculation.

*Examples:*

**expmass y**

**expmass n**

*Range:* **y** or **n**

*Default:* **expmass y**

### massnucleus

The mass of the nucleus in amu. Use **massnucleus** to overrule the value given in the mass table. On the input line, we read **massnucleus**,  $Z$ ,  $A$ , value.

*Examples:*

**massnucleus 41 93 92.12345**

**massnucleus 94 239 239.10101**

*Range:*  $A - 1 \leq \text{massnucleus} \leq A + 1$ , where  $A$  is the mass number.

*Default:* **massnucleus 0.**, i.e. the nuclear mass is read from the mass table.

### massexcess

The mass excess of the nucleus in MeV. Use **massexcess** to overrule the value given in the mass table. On the input line, we read **massexcess**,  $Z$ ,  $A$ , value.

*Examples:*

**massexcess 41 93 -45.678**

**massexcess 94 239 39.98765**

*Range:*  $-500. \leq \text{massexcess} \leq 500.$ ,

*Default:* **massexcess 0.**, i.e. the mass excess is read from the mass table.

### massdir

User made directory with nuclear masses. With this keyword, extra flexibility for nuclear masses is added. The directory should be placed under talys/structure/masses, and the individual files should have the same structure as the other mass tables. On the input line, we read **massdir**, directory name.

*Examples:*

**massdir hfb69**

*Range:* **massdir** can be equal to any appropriate directory name. The maximum length of the directory name is 72 characters.

*Default:* **massdir** is not used, i.e. the masses are read from an existing mass table.

### isomer

The definition of an isomer in seconds. In the discrete level database, the lifetimes of most of the levels are given. With **isomer**, it can be specified whether a level is treated as an isomer or not. Use **isomer 0.** to treat all levels, with any lifetime, as isomer and use **isomer 1.e38**, or any other number larger than the longest living isomer present in the problem, to include no isomers at all.

*Examples:*

**isomer 86400.** (86400 sec.=one day)

*Range:*  $0. \leq \text{isomer} \leq 1.e38$

*Default:* **isomer 1.** (second)

### Elow

Lowest incident energy in MeV for which TALYS performs a full nuclear model calculation. Below this energy, cross sections result from inter- and extrapolation using the calculated values at **Elow** and tabulated values and systematics at thermal energy, see Section 4.9. This keyword should only be used in the case of several incident energies.

*Examples:*

**Elow 0.001**

*Range:*  $1.e - 6 \leq \text{Elow} \leq 1.$

*Default:* **Elow**= $D_0$  for datafiles (**endf y**), **1.e-6** otherwise.

**transpower**

A limit for considering transmission coefficients in the calculation. Transmission coefficients  $T_{lj}$  smaller than  $T_{0\frac{1}{2}} \times 10^{-\text{transpower}} / (2l + 1)$  are not used in Hauser-Feshbach calculations, in order to reduce the computation time.

*Examples:*

**transpower 12**

*Range:*  $2 \leq \text{transpower} \leq 20$

*Default:* **transpower 5**

**transeps**

A limit for considering transmission coefficients in the calculation. Transmission coefficients smaller than **transeps** are not used in Hauser-Feshbach calculations, irrespective of the value of **transpower**, in order to reduce the computation time.

*Examples:*

**transeps 1.e-12**

*Range:*  $0. \leq \text{transeps} \leq 1.$

*Default:* **transeps 1.e-8**

**xseps**

The limit for considering cross sections in the calculation, in mb. Reaction cross sections smaller than **xseps** are not used in the calculations, in order to reduce the computation time.

*Examples:*

**xseps 1.e-10**

*Range:*  $0. \leq \text{xseps} \leq 1000.$

*Default:* **xseps 1.e-7**

**popeps**

The limit for considering population cross sections in the multiple emission calculation, in mb. Nuclides which, before their decay, are populated with a total cross section less than **popeps** are skipped, in order to reduce the computation time. From **popeps**, also the criteria for continuation of the decay per excitation energy bin (variable **popepsA**) and per  $(E_x, J, \Pi)$  bin (variable **popepsB**) in Hauser-Feshbach calculations are automatically derived.

*Examples:*

**popeps 1.e-6**

*Range:*  $0. \leq \text{popeps} \leq 1000.$

*Default:* **popeps 1.e-3**

**popMeV**

Flag to use initial population per MeV instead of per histogram, in the case of an excited energy distribution to be used with **projectile 0**. This keyword is given for backward compatibility. It is now seen that it is more natural to input the absolute value of the initial population per continuum bin or level, as histograms.

*Examples:*

**popMeV y**

**popMeV n**

*Range:* **y** or **n**

*Default:* **popMeV n**

**Estop**

Incident energy above which TALYS stops. This keyword is needed to speed up some uncertainty applications involving random TALYS calculations. No matter which incident energies are given in the input file, TALYS will stop when the incident energy exceeds **Estop**.

*Examples:*

**Estop 50.**

*Range:*  $1.e - 5 \leq \text{Estop} \leq 1000.$

*Default:* **Estop 1000.**

**angles**

Number of emission angles for reactions to discrete states.

*Examples:*

**angles 18**

*Range:*  $1 \leq \text{angles} \leq \text{numang}$ , where **numang** is specified in the file *talys.cmb*. Currently, **numang=90**

*Default:* **angles 90**

**anglescont**

Number of emission angles for reactions to the continuum.

*Examples:*

**anglescont 18**

*Range:*  $1 \leq \mathbf{anglescont} \leq \mathbf{numangcont}$ , where **numangcont** is specified in the file *talys.cmb*. Currently, **numangcont=36**

*Default:* **anglescont 36**

**channels**

Flag for the calculation and output of all exclusive reaction channel cross sections, e.g.  $(n, p)$ ,  $(n, 2n)$ ,  $(n, 2npa)$ , etc. The **channels** keyword can be used in combination with the keywords **outspectra** and **outangle** (see next Section) to give the exclusive spectra and angular distributions.

*Examples:*

**channels y**

**channels n**

*Range:* **y** or **n**

*Default:* **channels n**

**maxchannel**

Maximal number of outgoing particles in exclusive channel description, e.g. if **maxchannel 3**, then reactions up to 3 outgoing particles, e.g.  $(n, 2np)$ , will be given in the output. **maxchannel** is only active if **channels y**. We emphasize that, irrespective of the value of **maxchannel** and **channels**, all reaction chains are, by default, followed until all possible reaction channels are closed to determine cumulative particle production cross sections and residual production cross sections.

*Examples:*

**maxchannel 2**

*Range:*  $0 \leq \mathbf{maxchannel} \leq 8$ ,

*Default:* **maxchannel 4**

**relativistic**

Flag for relativistic kinematics.

*Examples:*

**relativistic y**

**relativistic n**

*Range:* y or n

*Default:* relativistic y

### **reaction**

Flag to disable nuclear reaction calculation. This may be helpful if one is e.g. only interested in a level density calculation. A TALYS run will then last only a few hundreds of a second. (This keyword was used for the large scale level density analysis of [168]).

*Examples:*

**reaction y**

**reaction n**

*Range:* y or n

*Default:* reaction y

### **recoil**

Flag for the calculation of the recoils of the residual nuclides and the associated corrections to the light-particle spectra, see Section 3.5.

*Examples:*

**recoil y**

**recoil n**

*Range:* y or n

*Default:* recoil n

### **labddx**

Flag for the calculation of double-differential cross sections in the LAB system. This is only active if **recoil y**. If **labddx n**, only the recoils of the nuclides are computed.

*Examples:*

**labddx y**

**labddx n**

*Range:* y or n

*Default:* labddx n

**anglesrec**

Number of emission angles for recoiling nuclides. This is only active if **recoil y**.

*Examples:*

**anglesrec 4**

*Range:*  $1 \leq \text{anglesrec} \leq \text{numangrec}$ , where **numangrec** is specified in the file *talys.cmb*. Currently, **numangrec=9**

*Default:* **anglesrec 9** if **labddx y**, **anglesrec 1** if **labddx n**

**maxenrec**

Number of emission energies for recoiling nuclides. This is only active if **recoil y**.

*Examples:*

**maxenrec 4**

*Range:*  $1 \leq \text{maxenrec} \leq \text{numenrec}$ , where **numenrec** is specified in the file *talys.cmb*. Currently, **numenrec=5\*memorypar**, where we suggest **memorypar=5** for a computer with at least 256 Mb of memory.

*Default:* **maxenrec 10**

**recoilaverage**

Flag to consider only one average kinetic energy of the recoiling nucleus per excitation energy bin (instead of a full kinetic energy distribution). This approximation significantly decreases the calculation time. This is only active if **recoil y**.

*Examples:*

**recoilaverage y**

**recoilaverage n**

*Range:* **y** or **n**

*Default:* **recoilaverage n**

**channelenergy**

Flag to use the channel energy instead of the center-of-mass energy for the emission spectrum.

*Examples:*

**channelenergy y**

**channelenergy n***Range:* y or n*Default:* channelenergy n**astro**

Flag for the calculation of thermonuclear reaction rates for astrophysics, see Section 4.12.

*Examples:***astro y****astro n***Range:* y or n*Default:* astro n**astrogs**Flag for treating the target in the ground state only, for astrophysical reaction calculations. In the default case, **astrogs n**, an average between excited target states will be made. This keyword is only active if **astro y**.*Examples:***astrogs y****astrogs n***Range:* y or n*Default:* astrogs n**astroE**Energy, in MeV, for thermonuclear reactions around which Maxwellian averaging should take place. This is only active if **astro y**. Actually, specifying this value will automatically activate **astro y** and **astrogs y**. Hence, if you require the Maxwellian averaged 30 keV capture cross section, all you need to give is the input line below. **astroE** may not be specified simultaneously with **astroT9**. The **energy** keyword must still be given in the TALYS input file, but becomes irrelevant since it concerns an average over a large number of incident energies.*Examples:***astroE 0.03***Range:*  $0.00001 \leq \text{astroE} \leq 1.$ *Default:* astroE 0.

**astroT**

Temperature, in units of  $10^9$  K, for thermonuclear reactions and Maxwellian averaging. This is only active if **astro y**. Actually, specifying this value will automatically activate **astro y**. **astroT** may not be specified simultaneously with **astroE**. The **energy** keyword must still be given in the TALYS input file, but becomes irrelevant since it concerns an average over a large number of incident energies.

*Examples:*

**astroT 0.53**

*Range:*  $0.0001 \leq \text{astroT} \leq 10.$

*Default:* **astroT 0.**

**astroex**

Flag for calculation of astrophysics reaction rate to final long-lived excited states. This extends the calculation of the rate for the ground state only. This keyword is only active if **astro y**.

*Examples:*

**astroex y**

**astroex n**

*Range:* **y** or **n**

*Default:* **astroex n**

**nonthermlev**

Non-thermalized level in the calculation of astrophysics rate.

*Examples:*

**nonthermlev 2**

*Range:*  $0 \leq \text{nonthermlev} \leq \text{numlev}$ , where **numlev** is specified in the file *talys.cmb*.

*Default:* **nonthermlev** is not used.

**abundance**

File with tabulated abundances. The **abundance** keyword is only active for the case of a natural target, i.e. if **mass 0**. By default, the isotopic abundances are read from the structure database, see Chapter 5. It can however be imagined that one wants to include only the most abundant isotopes of an element, to save some computing time. Also, **abundance** may be used to analyze experimental data for targets of a certain isotopic enrichment. On the input line, we read **abundance** and the filename. From each line of

the file, TALYS reads  $Z$ ,  $A$  and the isotopic abundance with the format (2i4,f11.6). An example of an abundance file, e.g. *abnew*, different from that of the database, is

```
82 206 24.100000
82 207 22.100000
82 208 52.400000
```

where we have left out the “unimportant”  $^{204}\text{Pb}$  (1.4%). TALYS automatically normalizes the abundances to a sum of 1, leading in the above case to 24.44 % of  $^{206}\text{Pb}$ , 22.41 % of  $^{207}\text{Pb}$  and 53.14 % of  $^{208}\text{Pb}$  in the actual calculation.

*Examples:*

### **abundance abnew**

*Range:* **abundance** can be equal to any filename, provided it is present in the working directory.

*Default:* If **abundance** is not given in the input file, abundances are taken from *talys/structure/abundance* and calculations for all isotopes are performed.

### **xscaptherm**

The thermal capture cross section in millibarn. By default, these are read from the nuclear structure database or taken from systematics. The **xscaptherm** keyword gives the possibility to overwrite this by using the input file.

*Examples:*

### **xscaptherm 320.2**

*Range:*  $10^{-20} \leq \text{xscaptherm} \leq 10^{10}$

*Default:* **xscaptherm** is read from the nuclear structure database or taken from systematics.

### **xsalphatherm**

The thermal ( $n, \alpha$ ) cross section in millibarn. By default, these are read from the nuclear structure database or taken from systematics. The **xsalphatherm** keyword gives the possibility to overwrite this by using the input file.

*Examples:*

### **xsalphatherm 0.2**

*Range:*  $10^{-20} \leq \text{xsalphatherm} \leq 10^{10}$

*Default:* **xsalphatherm** is read from the nuclear structure database or taken from systematics.

### **xsptherm**

The thermal (n,p) cross section in millibarn. By default, these are read from the nuclear structure database or taken from systematics. The **xsptherm** keyword gives the possibility to overwrite this by using the input file.

*Examples:*

**xsptherm 0.2**

*Range:*  $10^{-20} \leq \text{xsptherm} \leq 10^{10}$

*Default:* **xsptherm** is read from the nuclear structure database or taken from systematics.

### **partable**

Flag to write the all the model parameters used in a calculation on a separate file, *parameters.dat*. This can be a very powerful option when one wishes to vary any nuclear model parameter in the input. The file *parameters.dat* has the exact input format, so it can be easily copied and pasted into any input file. This is helpful for a quick look-up of all the parameters used in a calculation. We have used this ourselves for automatic (random) TALYS-input generators for e.g. covariance data.

*Examples:*

**partable y**

**partable n**

*Range:* **y** or **n**

*Default:* **partable n**

### **best**

Flag to use the set of adjusted nuclear model parameters that produces the optimal fit for measurements of all reaction channels of the nuclide under consideration. TALYS will look in the *talys/structure/best* directory for such a set, see Section 5.14. With the addition of the single line **best y** to the input file, TALYS will automatically use all detailed adjusted parameter fits that are stored in *talys/structure/best*.

*Examples:*

**best y**

**best n**

*Range:* **y** or **n**

*Default:* **best n**

### **bestend**

Flag to put the best set of parameters at end of input file, instead of at the beginning. With **bestend n**, the parameters can be overruled later in the input file, while this is no longer possible with **bestend y**. Obviously, this keyword is only relevant if **best y**.

*Examples:*

**bestend y**

**bestend n**

*Range:* **y** or **n**

*Default:* **bestend n**

### **bestbranch**

Flag to use the set of adjusted branching ratios for discrete levels.

*Examples:*

**bestbranch y**

**bestbranch n**

*Range:* **y** or **n**

*Default:* **bestbranch y**

### **bestpath**

Keyword to enable to use your own collection of “best” TALYS input parameters. This directory should be created under *talys/structure/* after which the current keyword can be used with that directory name. In practice, the user can copy a file from the standard *talys/structure/best/* database to his/her own database and change it. In this way, changes in the “official” database are avoided. See Section 5.14 for the format of the files in this database.

*Examples:*

**bestpath mybest**

For this keyword to work, information needs to be present in the *talys/structure/mybest/* with a format equal to that of the original *talys/structure/best/* directory, see Section 5.14. *Range:* **bestpath** can be equal to any filename, provided it starts with a character. Furthermore, the library must exist in the *talys/structure/* directory. This keyword is only active if **best y**.

*Default:* **bestpath** is equal to *talys/structure/best/*.

**rescuefile**

File with incident energy dependent normalization factors. If TALYS is not able to produce the “ultimate fit”, it is possible to invoke a “rescuefile” as a last resort. By giving a table of incident energies and normalization factors, the result of TALYS can be made exactly equal to that of experimental data, an evaluate data set, or any other data set. The contents of the file consist of a simple x-y table with x the incident energy and y the normalization factor. A rescuefile can be used for the reactions (n,n'), (n, $\gamma$ ), (n,f), (n,p), (n,d), (n,t), (n,h), (n,'alpha'), (n,2n) and (n,total). To invoke this, the ENDF-6 format for MT numbers representing a reaction channel is used, see the sample cases below. Moreover, a global multiplication factor can be applied. On the input line, we read **rescuefile**, reaction identifier (MT number), global multiplication factor (optional).

*Examples:*

**rescuefile 0 rescue.001 1.01** (n,total)

**rescuefile 4 rescue.004** (n,n')

**rescuefile 16 rescue.016** (n,2n)

**rescuefile 18 rescue.018 0.995** (n,f)

**rescuefile 102 rescue.102** (n, $\gamma$ )

**rescuefile 103 rescue.103 1.02** (n,p)

**rescuefile 104 rescue.104** (n,d)

**rescuefile 105 rescue.105** (n,t)

**rescuefile 106 rescue.106** (n,h)

**rescuefile 107 rescue.107** (n, $\alpha$ )

*Range:* **rescuefile** can be equal to any filename, provided it starts with a character.

*Default:* no default.

**nulldev**

Path for the null device. The null device is a “black hole” for output that is produced, but not of interest to the user. Some ECIS output files fall in this category. To ensure compatibility with Unix, Linux, Windows and other systems a null device string is used, of which the default setting is given in machine.f. With this keyword, extra flexibility is added. If the null device is properly set in machine.f, this keyword is not needed. On the input line, we read **nulldev**, filename.

*Examples:*

**nulldev /dev/null**

**nulldev nul**

*Range:* **nulldev** can be equal to any appropriate filename, provided it starts with a character.

*Default:* The default is set in subroutine *machine.f*.

**strucpath**

Path for the directory with nuclear structure information. With this keyword, extra flexibility is added. Nuclear structure databases other than the default can be invoked with this keyword. If the path name is properly set in *machine.f*, this keyword is not needed for standard use. On the input line, we read **strucpath**, filename.

*Examples:*

**strucpath /home/raynal/mon-structure/**

*Range:* **strucpath** can be equal to any appropriate directory. The maximum length of the path is 60 characters.

*Default:* The default is set in subroutine *machine.f*.

**6.2.3 Optical model****optmod**

File with tabulated phenomenological optical model parameters as a function of energy, see Section 4.1. This can be helpful if one wishes to use an optical model parameterisation which is not hardwired in TALYS. One could write a driver to automatically generate a table with parameters. On the input line, we read **optmod**,  $Z$ ,  $A$ , filename, and (optionally) particle type. TALYS first reads the number of lines to be read with format (8x,i4). Next, from each line of the file, TALYS reads  $E$ ,  $v$ ,  $rv$ ,  $av$ ,  $w$ ,  $rw$ ,  $aw$ ,  $vd$ ,  $rvd$ ,  $avd$ ,  $wd$ ,  $rwd$ ,  $awd$ ,  $vso$ ,  $rvso$ ,  $avso$ ,  $wso$ ,  $rwso$ ,  $awso$ , and  $rc$ .

*Examples:*

**optmod 40 90 ompzr90 d**

**optmod 94 239 omppu239**

*Range:* **optmod** can be equal to any filename, provided it starts with a character. The particle type must be equal to either **n**, **p**, **d**, **t**, **h** or **a**. A table of up to 500 incident energies (this is set by **numomp** in *talys.cmb*) and associated parameters can be specified.

*Default:* If the particle type is not given, as in the second example above, neutrons are assumed. If **optmod** is not given in the input file, the optical model parameters are taken from the *talys/structure/optical* database per nucleus or, if not present there, from the global optical model.

**optmodfileN**

File with the neutron optical model parameters of Eq. (4.7). The format of the file is exactly the same as that of the nuclear structure database *talys/structure/optical/*. In practice, the user can copy a file from this database, e.g. *Fe.omp*, to the working directory and change it. In this way, changes in the “official” database are avoided. Note that even if only changes for one isotope are required, the file for the whole element needs to be copied if for the other isotopes the originally tabulated values are to be used. On the input line, we read **optmodfileN**, *Z*, filename.

*Examples:*

**optmodfileN 26 Fe.loc**

*Range:* **optmodfileN** can be equal to any filename, provided it starts with a character.

*Default:* If **optmodfileN** is not given in the input file, the optical model parameters are taken from the *talys/structure/optical* database per nucleus or, if not present there, from the global optical model.

**optmodfileP**

File with the proton optical model parameters of Eq. (4.7). The format of the file is exactly the same as that of the nuclear structure database *talys/structure/optical/*. In practice, the user can copy a file from this database, e.g. *n-Fe.omp*, to the working directory and change it. In this way, changes in the “official” database are avoided. Note that even if only changes for one isotope are required, the file for the whole element needs to be copied if for the other isotopes the originally tabulated values are to be used. On the input line, we read **optmodfileP**, *Z*, filename.

*Examples:*

**optmodfileP 26 Fe.loc**

*Range:* **optmodfileP** can be equal to any filename, provided it starts with a character.

*Default:* If **optmodfileP** is not given in the input file, the optical model parameters are taken from the *talys/structure/optical* database per nucleus or, if not present there, from the global optical model.

**localomp**

Flag to overrule the local, nucleus-specific optical model by the global optical model of Eqs. (4.8) or (4.9). This may be helpful to study global mass-dependent trends.

*Examples:*

**localomp n**

*Range:* **y** or **n**

*Default:* **localomp y**, i.e. a nucleus-specific optical model, when available.

**dispersion**

Flag to invoke the dispersive optical model, see Section 4.1.2. These potentials are only available as tabulated neutron local potentials. If not available, TALYS will automatically resort to normal OMP's.

*Examples:*

**dispersion n**

*Range:* **y** or **n**

*Default:* **dispersion n**.

**jlmomp**

Flag to use the JLM microscopic optical model potential instead of the phenomenological optical model potential, see Section 4.1.4.

*Examples:*

**jlmomp n**

*Range:* **y** or **n**

*Default:* **jlmomp n**, i.e. to use the phenomenological OMP.

**jlmmode**

Keyword to enable different normalizations for the imaginary potential of the JLM optical model, as explained in Ref. [1] These different normalizations apply to the constant 0.44 in Eq. (4.47). This keyword is only active if 'jlmomp y'.

*Examples:*

**jlmmode 0:** standard JLM imaginary potential of Eq. (4.47)

**jlmmode 1:** 0.44 replaced by  $1.1 \exp(-0.4E^{1/2})$

**jlmmode 2:** 0.44 replaced by  $1.25 \exp(-0.2E^{1/2})$

**jlmmode 3:** as jlmmode 2 but with  $\lambda_W(E)$  twice as large, recommended for energies below 1 MeV.

*Range:*  $0 \leq \mathbf{jlmmode} \leq 3$

*Default:* **jlmmode 0**, i.e. the standard JLM OMP.

**radialmodel**

Model for radial matter densities in the JLM optical model. There are two options. This keyword is only active if 'jlmomp y'.

*Examples:*

**radialmodel 1:** HFB-Skyrme based matter densities

**radialmodel 2:** HFB-Gogny based matter densities

*Range:*  $1 \leq \text{radialmodel} \leq 2$

*Default:* **radialmodel 2.**

**omponly**

Flag to let TALYS perform *only* an optical model calculation. In this way, TALYS acts simply as a driver for ECIS. All non-elastic calculations for the various reaction channels are skipped. This is helpful for systematic, and quick, testing of optical model potentials.

*Examples:*

**omponly y**

*Range:* **y** or **n**

*Default:* **omponly n**

**sysreaction**

The types of particles for which the optical model reaction cross section is overruled by values obtained from systematics, see Section 4.1.5. The optical model transmission coefficients will be accordingly normalized.

*Examples:*

**sysreaction p**

**sysreaction d a**

*Range:* **sysreaction** can be any combination of **n**, **p**, **d**, **t**, **h** and **a**

*Default:* **sysreaction** is disabled for any particle.

*Warning:* setting e.g. **sysreaction p** will thus automatically disable the default setting. If this needs to be retained as well, set **sysreaction p d t h a**.

**statepot**

Flag for a different optical model parameterisation for each excited state in a DWBA or coupled-channels calculation. This may be appropriate if the emission energy of the ejectile, corresponding to a large excitation energy, differs considerably from the incident energy.

*Examples:*

**statepot y**

*Range:* **y** or **n**

*Default:* **statepot n**

**optmodall**

Flag for a new optical model calculation for each compound nucleus in the decay chain. In usual multiple Hauser-Feshbach decay, the transmission coefficients for the first compound nucleus are used for the whole decay chain. When a residual nucleus is far away from the initial compound nucleus, this approximation may become dubious. With **optmodall y**, new optical model calculations are performed for every compound nucleus that is depleted, for all types of emitted particles.

*Examples:*

**optmodall y**

*Range:* **y** or **n**

*Default:* **optmodall n**

**autorot**

Flag for automatic rotational coupled-channels calculations, see Section 4.2.1 for  $A > 150$ . The discrete level file is scanned and an attempt is made to automatically identify the lowest rotational band. Deformation parameters are also read in from the database so automated coupled-channels calculations can be performed. This option is possible for the rare earth and actinide region. Note that for all natural isotopes, the coupling scheme is already given in the *talys/structure/deformation* database.

*Examples:*

**autorot y**

*Range:* **y** or **n**

*Default:* **autorot n**

**incadjust**

Flag to use adjusted optical model parameters for the incident channel *and* exit channels. Disabling this flag allows to use a different OMP for the exit channels than for the incident channel, e.g. using **rvadjust**

**n 1.10** together with **incadjust n** means that the OMP for the incident channel is unaltered, while that for the outgoing channel has an adjust  $r_V$  parameter. This can be used to simulate e.g. temperature-dependent OMP effects.

*Examples:*

**incadjust n**

*Range:* y or n

*Default:* **incadjust y**

### **ecissave**

Flag for saving ECIS input and output files. This has two purposes: (a) if the next calculation will be performed with already existing reaction cross sections and transmission coefficients. This is helpful for time-consuming coupled-channels calculations, (b) to study the ECIS input and output files in detail. **ecissave** *must* be set to y, if in the next run **inccalc n** or **eciscalc n** will be used. If not, an appropriate error message will be given and TALYS stops.

*Examples:*

**ecissave y**

**ecissave n**

*Range:* y or n

*Default:* **ecissave n**

### **eciscalc**

Flag for the ECIS calculation of transmission coefficients and reaction cross sections for the inverse channels. If this calculation has already been performed in a previous run, and in that previous run **ecissave y** has been set, it may be helpful to put **eciscalc n**, which avoids a new calculation. This saves time, especially in the case of coupled-channels calculations. We stress that it is the responsibility of the user to ensure that the first run of a particular problem is done with **ecissave y**. You also have to make sure that the same energy grid for inverse channels is used.

*Examples:*

**eciscalc y**

**eciscalc n**

*Range:* y or n

*Default:* **eciscalc y**

**inccalc**

Flag for the ECIS calculation of transmission coefficients and reaction cross sections for the incident channel. If this calculation has already been performed in a previous run, and in that previous run **ecissave y** has been set, it may be helpful to put **inccalc n**, which avoids a new ECIS calculation. This saves time, especially in the case of coupled-channels calculations. We stress that it is the responsibility of the user to ensure that the first run of a particular problem is done with **eciscalc y**. If not, an appropriate error message will be given and TALYS stops. You also have to make sure that the same grid of incident energies is used.

*Examples:*

**inccalc y**

**inccalc n**

*Range:* **y** or **n**

*Default:* **inccalc y**

**endfecis**

Flag for the ECIS calculation of transmission coefficients and reaction cross sections for the ENDF-6 energy grid. If this calculation has already been performed in a previous run, it may be helpful to put **endfecis n**, which avoids a new calculation. This saves time, especially in the case of coupled-channels calculations. We stress that it is the responsibility of the user to ensure that the first run of a particular problem is done with **endfecis y** and **endfecis y**. If not, an appropriate error message will be given and TALYS stops.

*Examples:*

**endfecis y**

**endfecis n**

*Range:* **y** or **n**

*Default:* **endfecis y**

**coulomb**

Flag for Coulomb excitation calculation with ECIS, to be used for incident charged particles.

*Examples:*

**coulomb y**

*Range:* **y** or **n**

*Default:* **coulomb y**

**cpang**

Flag for compound angular distribution calculation for incident charged particles.

*Examples:*

**cpang y**

*Range:* y or n

*Default:* **cpang n**

**soswitch**

Energy switch to on-set deformed spin-orbit calculation and sequential iterations in ECIS. For coupled-channels calculations on rotational nuclei, such a switch needs to be made. On the input line, we read **soswitch**, value.

*Examples:*

**soswitch 1.2**

*Range:*  $0.1 \leq \text{soswitch} \leq 10$ .

*Default:* **soswitch 3**. MeV.

**v1adjust**

Multiplier to adjust the OMP parameter  $v_1$  of Eq. (4.7). This keyword can also be used for double-folding and complex particle potentials. On the input line, we read **v1adjust**, particle symbol, and value.

*Examples:*

**v1adjust a 1.12**

*Range:*  $0.1 \leq \text{v1adjust} \leq 10$ .

*Default:* **v1adjust particle 1**.

**v2adjust**

Multiplier to adjust the OMP parameter  $v_2$  of Eq. (4.7). This keyword can only be used for a potential of the Koning-Delaroche form. On the input line, we read **v2adjust**, particle symbol, and value.

*Examples:*

**v2adjust n 0.96**

*Range:*  $0.1 \leq \text{v2adjust} \leq 10$ . This keyword does not apply to deuterons up to alpha's.

*Default:* **v2adjust particle 1**.

**v3adjust**

Multiplier to adjust the OMP parameter  $v_3$  of Eq. (4.7). This keyword can only be used for a potential of the Koning-Delaroche form. On the input line, we read **v3adjust**, particle symbol, and value.

*Examples:*

**v3adjust p 1.10**

*Range:*  $0.1 \leq \mathbf{v3adjust} \leq 10$ . This keyword does not apply to deuterons up to alpha's.

*Default:* **v3adjust particle 1**.

**v4adjust**

Multiplier to adjust the OMP parameter  $v_4$  of Eq. (4.7). This keyword can only be used for a potential of the Koning-Delaroche form. On the input line, we read **v4adjust**, particle symbol, and value.

*Examples:*

**v4adjust n 0.98**

*Range:*  $0.1 \leq \mathbf{v4adjust} \leq 10$ . This keyword does not apply to deuterons up to alpha's.

*Default:* **v4adjust particle 1**.

**rvadjust**

Multiplier to adjust the OMP parameter  $r_v$  of Eq. (4.7). This keyword can also be used for complex particle potentials. On the input line, we read **rvadjust**, particle symbol, and value.

*Examples:*

**rvadjust t 1.04**

*Range:*  $0.1 \leq \mathbf{rvadjust} \leq 10$ .

*Default:* **rvadjust particle 1**.

**avadjust**

Multiplier to adjust the OMP parameter  $a_v$  of Eq. (4.7). This keyword can also be used for complex particle potentials. On the input line, we read **avadjust**, particle symbol, and value.

*Examples:*

**avadjust d 0.97**

*Range:*  $0.1 \leq \mathbf{avadjust} \leq 10$ .

*Default:* **avadjust particle 1**.

**rwadjust**

Multiplier to adjust the OMP parameter  $rw$  of Eq. (4.7). This keyword can also be used for complex particle potentials. On the input line, we read **rwadjust**, particle symbol, and value.

*Examples:*

**rwadjust t 1.04**

*Range:*  $0.1 \leq \text{rwadjust} \leq 10$ .

*Default:* **rwadjust particle 1**.

**awadjust**

Multiplier to adjust the OMP parameter  $aw$  of Eq. (4.7). This keyword can also be used for complex particle potentials. On the input line, we read **awadjust**, particle symbol, and value.

*Examples:*

**awadjust d 0.97**

*Range:*  $0.1 \leq \text{awadjust} \leq 10$ .

*Default:* **awadjust particle 1**.

**w1adjust**

Multiplier to adjust the OMP parameter  $w1$  of Eq. (4.7). This keyword can also be used for double-folding and complex particle potentials. On the input line, we read **w1adjust**, particle symbol, and value.

*Examples:*

**w1adjust p 1.10**

*Range:*  $0.1 \leq \text{w1adjust} \leq 10$ .

*Default:* **w1adjust particle 1**.

**w2adjust**

Multiplier to adjust the OMP parameter  $w2$  of Eq. (4.7). This keyword can only be used for a potential of the Koning-Delaroche form. On the input line, we read **w2adjust**, particle symbol, and value.

*Examples:*

**w2adjust n 0.80**

*Range:*  $0.1 \leq \text{w2adjust} \leq 10$ . This keyword does not apply to deuterons up to alpha's.

*Default:* **w2adjust particle 1**.

**w3adjust**

Multiplier to adjust the OMP parameter  $w_3$  of Eq. (4.18). This keyword can only be used for the high-energy extension of the Koning-Delaroche form. On the input line, we read **w3adjust**, particle symbol, and value.

*Examples:*

**w3adjust n 0.80**

*Range:*  $0.1 \leq \mathbf{w3adjust} \leq 10$ . This keyword does not apply to deuterons up to alpha's.

*Default:* **w3adjust particle 1**.

**w4adjust**

Multiplier to adjust the OMP parameter  $w_4$  of Eq. (4.18). This keyword can only be used for the high-energy extension of the Koning-Delaroche form. On the input line, we read **w4adjust**, particle symbol, and value.

*Examples:*

**w4adjust n 0.80**

*Range:*  $0.1 \leq \mathbf{w4adjust} \leq 10$ . This keyword does not apply to deuterons up to alpha's.

*Default:* **w4adjust particle 1**.

**rvdadjust**

Multiplier to adjust the OMP parameter  $r_{vd}$  of Eq. (4.7). This keyword can also be used for complex particle potentials. On the input line, we read **rvdadjust**, particle symbol, and value.

*Examples:*

**rvdadjust d 0.97**

*Range:*  $0.1 \leq \mathbf{rvdadjust} \leq 10$ .

*Default:* **rvdadjust particle 1**.

**avdadjust**

Multiplier to adjust the OMP parameter  $av_d$  of Eq. (4.7). This keyword can also be used for complex particle potentials. On the input line, we read **avdadjust**, particle symbol, and value.

*Examples:*

**avdadjust d 0.97**

*Range:*  $0.1 \leq \mathbf{avdadjust} \leq 10$ .

*Default:* **avdadjust particle 1**.

### rwdadjust

Multiplier to adjust the OMP parameter *rwd* of Eq. (4.7). This keyword can also be used for complex particle potentials. On the input line, we read **rwdadjust**, particle symbol, and value.

*Examples:*

**rwdadjust d 0.97**

*Range:*  $0.1 \leq \text{rwdadjust} \leq 10$ .

*Default:* **rwdadjust particle 1**.

### awdadjust

Multiplier to adjust the OMP parameter *awd* of Eq. (4.7). This keyword can also be used for complex particle potentials. On the input line, we read **awdadjust**, particle symbol, and value.

*Examples:*

**awdadjust d 0.97**

*Range:*  $0.1 \leq \text{awdadjust} \leq 10$ .

*Default:* **awdadjust particle 1**.

### d1adjust

Multiplier to adjust the OMP parameter *d1* of Eq. (4.7). This keyword can also be used for double-folding and complex particle potentials. On the input line, we read **d1adjust**, particle symbol, and value.

*Examples:*

**d1adjust d 0.97**

*Range:*  $0.1 \leq \text{d1adjust} \leq 10$ .

*Default:* **d1adjust particle 1**.

### d2adjust

Multiplier to adjust the OMP parameter *d2* of Eq. (4.7). This keyword can only be used for a potential of the Koning-Delaroche form. On the input line, we read **d2adjust**, particle symbol, and value.

*Examples:*

**d2adjust n 1.06**

*Range:*  $0.1 \leq \text{d2adjust} \leq 10$ . This keyword does not apply to deuterons up to alpha's.

*Default:* **d2adjust particle 1**.

**d3adjust**

Multiplier to adjust the OMP parameter  $d3$  of Eq. (4.7). This keyword can only be used for a potential of the Koning-Delaroche form. On the input line, we read **d3adjust**, particle symbol, and value.

*Examples:*

**d3adjust n 1.06**

*Range:*  $0.1 \leq \mathbf{d3adjust} \leq 10$ . This keyword does not apply to deuterons up to alpha's.

*Default:* **d3adjust particle 1**.

**vso1adjust**

Multiplier to adjust the OMP parameter  $vso1$  of Eq. (4.7). This keyword can also be used for complex particle potentials. On the input line, we read **vso1adjust**, particle symbol, and value.

*Examples:*

**vso1adjust d 1.15**

*Range:*  $0.1 \leq \mathbf{vso1adjust} \leq 10$ .

*Default:* **vso1adjust particle 1**.

**vso2adjust**

Multiplier to adjust the OMP parameter  $vso2$  of Eq. (4.7). This keyword can only be used for a potential of the Koning-Delaroche form. On the input line, we read **vso2adjust**, particle symbol, and value.

*Examples:*

**vso2adjust n 1.06**

*Range:*  $0.1 \leq \mathbf{vso2adjust} \leq 10$ . This keyword does not apply to deuterons up to alpha's.

*Default:* **vso2adjust particle 1**.

**wso1adjust**

Multiplier to adjust the OMP parameter  $wso1$  of Eq. (4.7). This keyword can also be used for complex particle potentials. On the input line, we read **wso1adjust**, particle symbol, and value.

*Examples:*

**wso1adjust d 1.15**

*Range:*  $0.1 \leq \mathbf{wso1adjust} \leq 10$ .

*Default:* **wso1adjust particle 1**.

**wso2adjust**

Multiplier to adjust the OMP parameter wso2 of Eq. (4.7). This keyword can only be used for a potential of the Koning-Delaroche form. On the input line, we read **wso2adjust**, particle symbol, and value.

*Examples:*

**wso2adjust n 1.06**

*Range:*  $0.1 \leq \mathbf{wso2adjust} \leq 10$ . This keyword does not apply to deuterons up to alpha's.

*Default:* **wso2adjust particle 1**.

**rvsoadjust**

Multiplier to adjust the OMP parameter rvso of Eq. (4.7). This keyword can also be used for complex particle potentials. On the input line, we read **rvsoadjust**, particle symbol, and value.

*Examples:*

**rvsoadjust d 1.15**

*Range:*  $0.1 \leq \mathbf{rvsoadjust} \leq 10$ .

*Default:* **rvsoadjust particle 1**.

**avsoadjust**

Multiplier to adjust the OMP parameter avso of Eq. (4.7). This keyword can also be used for complex particle potentials. On the input line, we read **avsoadjust**, particle symbol, and value.

*Examples:*

**avsoadjust d 1.15**

*Range:*  $0.1 \leq \mathbf{avsoadjust} \leq 10$ .

*Default:* **avsoadjust particle 1**.

**rwsadjust**

Multiplier to adjust the OMP parameter rwso of Eq. (4.7). This keyword can also be used for complex particle potentials. On the input line, we read **rwsadjust**, particle symbol, and value.

*Examples:*

**rwsadjust d 1.15**

*Range:*  $0.1 \leq \mathbf{rwsadjust} \leq 10$ .

*Default:* **rwsadjust particle 1**.

**awsoadjust**

Multiplier to adjust the OMP parameter  $awso$  of Eq. (4.7). This keyword can also be used for complex particle potentials. On the input line, we read **awsoadjust**, particle symbol, and value.

*Examples:*

**awsoadjust d 1.15**

*Range:*  $0.1 \leq \text{awsoadjust} \leq 10$ .

*Default:* **awsoadjust particle 1.**

**rcadjust**

Multiplier to adjust the OMP parameter  $rc$  of Eq. (4.7). On the input line, we read **rcadjust**, particle symbol, and value.

*Examples:*

**rcadjust d 1.15**

*Range:*  $0.1 \leq \text{rcadjust} \leq 10$ .

*Default:* **rcadjust particle 1.**

**Ejoin**

Joining energy  $E_J$ , in MeV, for the original form and high-energy extension of the KD03 OMP, see Eq. (4.18). On the input line, we read **Ejoin**, particle symbol, and value.

*Examples:*

**Ejoin n 250.**

*Range:*  $0. \leq \text{Ejoin} \leq 1000..$

*Default:* **Ejoin 200.**

**Vinf**

Limiting value  $V_\infty$  for the real volume potential of Eq. (4.18). This keyword can only be used for the high-energy extension of the Koning-Delaroche form. On the input line, we read **Vinf**, particle symbol, and value.

*Examples:*

**Vinf n -22.**

*Range:*  $-200. \leq \text{Vinf} \leq 0..$

*Default:* **Vinf -30.**

**rvadjustF**

Energy-dependent function to adjust the OMP parameter  $r_V$ . If physically adequate OMPs fail, such energy-dependent adjustment can be invoked as a last resort. As long as the deviation from the original model is not too large, unpleasant surprises in the various reaction channels are avoided. On the input line, we read **rvadjustF**, particle symbol, begin energy  $E_b$  and end energy  $E_e$  in MeV, maximal deviation  $D$  in % , and variance  $\sigma$  in MeV, of the function. If this keyword is specified,  $r_V$  will keep its original constant value for  $E < E_b$  and  $E > E_e$  while in between these two values it will be multiplied by the function

$$(6.2) \quad f(E) = 1 + D \exp(-(E - E_m)^2 / 2\sigma^2) + R$$

where  $E_m = (E_e + E_b)/2$  and the offset value

$$(6.3) \quad R = -D \exp(-(E_e - E_m)^2 / 2\sigma^2)$$

ensures continuity at  $E_b$  and  $E_e$ . Fig. 6.1 shows an example for  $r_V$  with an original value of 1.20, which is locally multiplied by the function  $f$  with parameters  $E_b=2$ ,  $E_e=10$ ,  $D = 5$ ,  $\sigma = 2$ . Up to 10 energy ranges, i.e. **rvadjustF** keywords, per particle can be used. We suggest however that the keyword **rvadjustF** is now replaced by the method explained in Section 6.2.12 for all parameters. We keep **rvadjustF** and related OMP keywords for backward compatibility reasons.

*Examples:*

**rvadjustF n 2. 10. 5. 2.**

*Range:* The particle symbol should be equal to n, p, d, t, h or a,  $0 \leq E_b \leq 250$ ,  $0 \leq E_e \leq 250$ ,  $E_b < E_e$ ,  $-100 \leq D \leq 100$ ,  $0 \leq \sigma \leq 100$ . If  $\sigma = 0$ , then the value  $\sigma = (E_e - E_b)/2$  will be adopted.

*Default:* **rvadjustF** is not applied.

**avadjustF**

Energy-dependent function to adjust the OMP parameter  $a_V$ . On the input line, we read **avadjustF**, particle symbol, begin energy  $E_b$  and end energy  $E_e$  in MeV, maximal deviation  $D$  in % , and variance  $\sigma$  in MeV, of the function. The same formalism as explained for the **rvadjustF** keyword applies.

*Examples:*

**avadjustF n 2. 10. 5. 2.**

*Range:* See **rvadjustF** keyword.

*Default:* **avadjustF** is not applied.

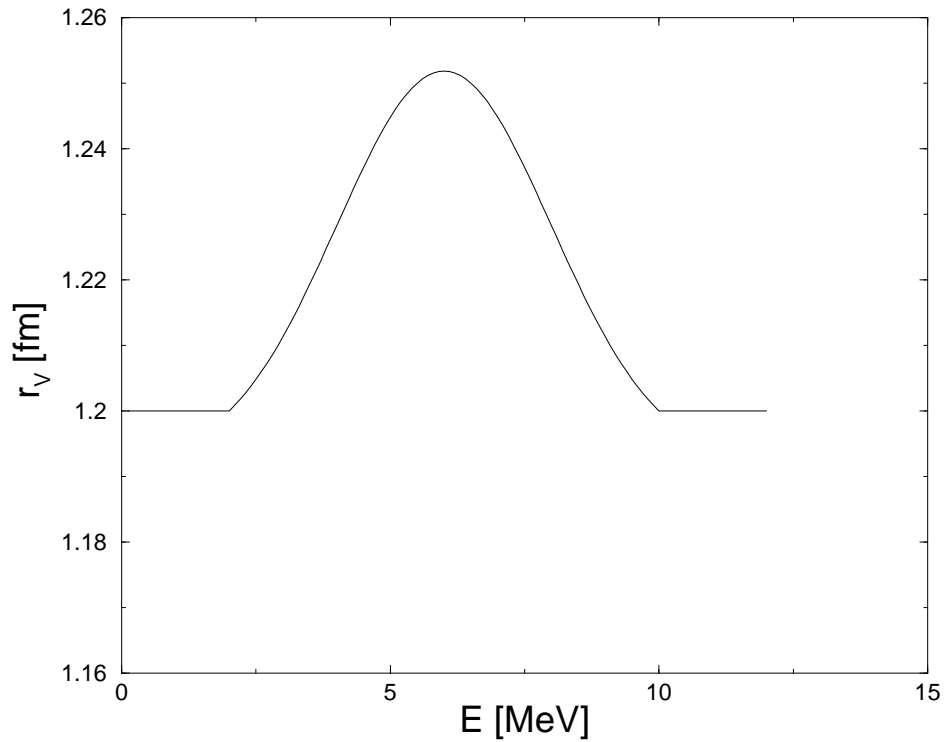


Figure 6.1: Energy-dependent radius  $r_V$  obtained with the **rvadjustF** keyword

### rvadjustF

Energy-dependent function to adjust the OMP parameter  $a_V$ . On the input line, we read **rvadjustF**, particle symbol, begin energy  $E_b$  and end energy  $E_e$  in MeV, maximal deviation D in % , and variance  $\sigma$  in MeV, of the function. The same formalism as explained for the **rvadjustF** keyword applies.

*Examples:*

**rvadjustF n 2. 10. 5. 2.**

*Range:* See **rvadjustF** keyword.

*Default:* **rvadjustF** is not applied.

### awadjustF

Energy-dependent function to adjust the OMP parameter  $a_V$ . On the input line, we read **awadjustF**, particle symbol, begin energy  $E_b$  and end energy  $E_e$  in MeV, maximal deviation D in % , and variance  $\sigma$  in MeV, of the function. The same formalism as explained for the **rvadjustF** keyword applies.

*Examples:*

**awadjustF n 2. 10. 5. 2.**

*Range:* See **rvadjustF** keyword.

*Default:* **awadjustF** is not applied.

### rvdadjustF

Energy-dependent function to adjust the OMP parameter rvd. On the input line, we read **rvdadjustF**, particle symbol, begin energy  $E_b$  and end energy  $E_e$  in MeV, maximal deviation D in % , and variance  $\sigma$  in MeV, of the function. The same formalism as explained for the **rvadjustF** keyword applies.

*Examples:*

**rvdadjustF n 2. 10. 5. 2.**

*Range:* See **rvadjustF** keyword.

*Default:* **rvdadjustF** is not applied.

### avdadjustF

Energy-dependent function to adjust the OMP parameter avd. On the input line, we read **avdadjustF**, particle symbol, begin energy  $E_b$  and end energy  $E_e$  in MeV, maximal deviation D in % , and variance  $\sigma$  in MeV, of the function. The same formalism as explained for the **rvadjustF** keyword applies.

*Examples:*

**avdadjustF n 2. 10. 5. 2.**

*Range:* See **rvadjustF** keyword.

*Default:* **avdadjustF** is not applied.

### rwdadjustF

Energy-dependent function to adjust the OMP parameter rwd. On the input line, we read **rwdadjustF**, particle symbol, begin energy  $E_b$  and end energy  $E_e$  in MeV, maximal deviation D in % , and variance  $\sigma$  in MeV, of the function. The same formalism as explained for the **rvadjustF** keyword applies.

*Examples:*

**rwdadjustF n 2. 10. 5. 2.**

*Range:* See **rvadjustF** keyword.

*Default:* **rwdadjustF** is not applied.

### awdadjustF

Energy-dependent function to adjust the OMP parameter awd. On the input line, we read **awdadjustF**, particle symbol, begin energy  $E_b$  and end energy  $E_e$  in MeV, maximal deviation D in % , and variance  $\sigma$

in MeV, of the function. The same formalism as explained for the **rvadjustF** keyword applies.

*Examples:*

**awdadjustF n 2. 10. 5. 2.**

*Range:* See **rvadjustF** keyword.

*Default:* **awdadjustF** is not applied.

### **rvsoadjustF**

Energy-dependent function to adjust the OMP parameter rvso. On the input line, we read **rvsoadjustF**, particle symbol, begin energy  $E_b$  and end energy  $E_e$  in MeV, maximal deviation D in % , and variance  $\sigma$  in MeV, of the function. The same formalism as explained for the **rvadjustF** keyword applies.

*Examples:*

**rvsoadjustF n 2. 10. 5. 2.**

*Range:* See **rvadjustF** keyword.

*Default:* **rvsoadjustF** is not applied.

### **avsoadjustF**

Energy-dependent function to adjust the OMP parameter avso. On the input line, we read **avsoadjustF**, particle symbol, begin energy  $E_b$  and end energy  $E_e$  in MeV, maximal deviation D in % , and variance  $\sigma$  in MeV, of the function. The same formalism as explained for the **rvadjustF** keyword applies.

*Examples:*

**avsoadjustF n 2. 10. 5. 2.**

*Range:* See **rvadjustF** keyword.

*Default:* **avsoadjustF** is not applied.

### **rwsadjustF**

Energy-dependent function to adjust the OMP parameter rwso. On the input line, we read **rwsadjustF**, particle symbol, begin energy  $E_b$  and end energy  $E_e$  in MeV, maximal deviation D in % , and variance  $\sigma$  in MeV, of the function. The same formalism as explained for the **rvadjustF** keyword applies.

*Examples:*

**rwsadjustF n 2. 10. 5. 2.**

*Range:* See **rvadjustF** keyword.

*Default:* **rwsadjustF** is not applied.

**awsoadjustF**

Energy-dependent function to adjust the OMP parameter `awso`. On the input line, we read **awsoadjustF**, particle symbol, begin energy  $E_b$  and end energy  $E_e$  in MeV, maximal deviation  $D$  in % , and variance  $\sigma$  in MeV, of the function. The same formalism as explained for the **rvadjustF** keyword applies.

*Examples:*

**awsoadjustF n 2. 10. 5. 2.**

*Range:* See **rvadjustF** keyword.

*Default:* **awsoadjustF** is not applied.

**Tladjust**

Multiplier to adjust the OMP transmission coefficient per  $l$ -value. On the input line, we read **Tladjust**, particle symbol, value and  $l$ -value.

*Examples:*

**Tladjust n 0.80 0**

*Range:*  $0.001 \leq \text{Tladjust} \leq 1000$ .

*Default:* **Tladjust** particle **1**.  $l$ -value

**radialfile**

File with radial matter densities. The format of the file is exactly the same as that of the nuclear structure database `talys/structure/optical/jlm/`. In practice, the user can copy a file from this database, e.g. `Fe.rad`, to the working directory and change it. In this way, changes in the “official” database are avoided. Note that even if only changes for one isotope are required, the entire file needs to be copied if for the other isotopes the originally tabulated values are to be used. On the input line, we read **radialfile**,  $Z$ , filename.

*Examples:*

**radialfile 26 Fe.loc**

*Range:* **radialfile** can be equal to any filename, provided it starts with a character.

*Default:* If **radialfile** is not given in the input, radial matter densities are taken from `talys/structure/optical/jlm`.

**lvadjust**

Normalization factor for the real central potential for JLM calculations, see Eq. (4.44). On the input line, we read **lvadjust** and value.

*Examples:*

**lvadjust 1.15***Range:*  $0.5 \leq \text{lvadjust} \leq 1.5$ *Default:* **lvadjust 1.****lwadjust**

Normalization factor for the imaginary central potential for JLM calculations, see Eq. (4.45). On the input line, we read **lwadjust** and value.

*Examples:***lwadjust 1.15***Range:*  $0.5 \leq \text{lwadjust} \leq 1.5$ *Default:* **lwadjust 1.****lv1adjust**

Normalization factor for the real isovector potential for JLM calculations, see Eq. (4.46). On the input line, we read **lv1adjust** and value.

*Examples:***lv1adjust 1.15***Range:*  $0.5 \leq \text{lv1adjust} \leq 1.5$ *Default:* **lv1adjust 1.****lw1adjust**

Normalization factor for the imaginary isovector potential for JLM calculations, see Eq. (4.47). On the input line, we read **lw1adjust** and value.

*Examples:***lw1adjust 1.15***Range:*  $0.5 \leq \text{lw1adjust} \leq 1.5$ *Default:* **lw1adjust 1.****lvsoadjust**

Normalization factor for the real spin-orbit potential for JLM calculations, see Eq. (4.50). On the input line, we read **lvsoadjust** and value.

*Examples:*

**lvsoadjust 1.15***Range:*  $0.5 \leq \text{lvsoadjust} \leq 1.5$ *Default:* **lvsoadjust 1.****lwsoadjust**

Normalization factor for the imaginary spin-orbit potential for JLM calculations, see Eq. (4.51). On the input line, we read **lwsoadjust** and value.

*Examples:***lwsoadjust 1.15***Range:*  $0.5 \leq \text{lwsoadjust} \leq 1.5$ *Default:* **lwsoadjust 1.****deuteronomp**

The default deuteron optical model coming from standard Watanabe folding does not always perform well. Therefore, we have included various other options:

*Examples:***deuteronomp 1:** Normal deuteron potential [15]**deuteronomp 2:** Deuteron potential of Daehnick et al. [17]**deuteronomp 3:** Deuteron potential of Bojowald et al.[18]**deuteronomp 4:** Deuteron potential of Han et al.[19]**deuteronomp 5:** Deuteron potential of Haixia An et al.[20]*Range:*  $1 \leq \text{deuteronomp} \leq 5$ *Default:* **deuteronomp 1****alphaomp**

Some of our users need a very old alpha optical model potential for their applications, namely that of McFadden and Satchler[21]. Therefore, we included an option for that. Also, there is an option to use the double folding potential of Demetriou, Grama and Goriely[22], which comes in three different versions. Since 2014, also the alpha OMPs of Avrigeanu et al. [27, 25] and Nolte [26] have been added.

*Examples:***alphaomp 1:** Normal alpha potential

**alphaomp 2:** Alpha potential of McFadden and Satchler

**alphaomp 3:** Alpha potential of Ref. [22], table 1.

**alphaomp 4:** Alpha potential of Ref. [22], table 2.

**alphaomp 5:** Alpha potential of Ref. [22], dispersive model.

**alphaomp 6:** Alpha potential of Avrigeanu et al. [25].

**alphaomp 7:** Alpha potential of Nolte et al. [26].

**alphaomp 8:** Alpha potential of Avrigeanu et al. [27].

*Range:*  $1 \leq \text{alphaomp} \leq 8$

*Default:* **alphaomp 6**

### **aradialcor**

Normalization factor for the shape of the double-folding alpha potential. This keyword is only relevant for **alphaomp**  $\geq 3$ . On the input line, we read **aradialcor** and value.

*Examples:*

**aradialcor 1.07**

*Range:*  $0.5 \leq \text{aradialcor} \leq 1.5$

*Default:* **aradialcor 1.**

### **adepthcor**

Normalization factor for the depth of the double-folding alpha potential. This keyword is only relevant for **alphaomp**  $\geq 3$ . On the input line, we read **adepthcor** and value.

*Examples:*

**adepthcor 1.07**

*Range:*  $0.5 \leq \text{adepthcor} \leq 1.5$

*Default:* **adepthcor 1.**

## **6.2.4 Direct reactions**

### **rotational**

Flag to enable or disable the rotational optical model for the various particles appearing in the calculation. This flag is to enable or disable coupled-channels calculations for the inverse channels provided a

coupling scheme is given in the deformation database. Using no rotational model at all can be set with another keyword: **spherical y**.

*Examples:*

**rotational n**

**rotational n p a**

*Range:* **rotational** can be any combination of **n, p, d, t, h** and **a**

*Default:* **rotational n p**. Warning: setting e.g. **rotational a** will thus automatically disable the default setting. If this needs to be retained as well, set **rotational n p a**

### spherical

Flag to enforce a spherical OMP calculation, regardless of the availability of a deformed OMP and a coupling scheme. Direct inelastic scattering will then be treated by DWBA.

*Examples:*

**spherical n**

*Range:* **y** or **n**

*Default:* **spherical n**

### maxrot

Number of excited levels to be included in a rotational band of a deformed nucleus for coupled-channels calculations. For example, use **maxrot 4** if the  $0^+ - 2^+ - 4^+ - 6^+ - 8^+$  states need to be included.

*Examples:*

**maxrot 4**

*Range:*  $0 \leq \text{maxrot} \leq 10$

*Default:* **maxrot 2**

### maxband

Maximum number of vibrational bands added to the rotational coupling scheme, regardless of the number of bands specified in the deformation database.

*Examples:*

**maxband 4**

*Range:*  $0 \leq \text{maxband} \leq 10$

*Default:* **maxband 0**

**deformfile**

File with deformation parameters and coupling schemes. The format of the file is exactly the same as that of the nuclear structure database *talys/structure/deformation/*. In practice, the user can copy a file from this database, e.g. *Fe.def*, to the working directory and change it. In this way, changes in the “official” database are avoided. Note that even if only changes for one isotope are required, the entire file needs to be copied if for the other isotopes the originally tabulated values are to be used. On the input line, we read **deformfile**, *Z*, filename.

*Examples:*

**deformfile 26 Fe.loc**

*Range:* **deformfile** can be equal to any filename, provided it starts with a character.

*Default:* If **deformfile** is not given in the input file, discrete levels are taken from *talys/structure/deformation*.

**giantresonance**

Flag for the calculation of giant resonance contributions to the continuum part of the spectrum. The GMR, GQR, LEOR and HEOR are included.

*Examples:*

**giantresonance y**

**giantresonance n**

*Range:* **y** or **n**

*Default:* **giantresonance y** for incident neutrons and protons, **giantresonance n** otherwise.

**core**

Integer to denote the even-even core for the weak-coupling model for direct scattering of odd-*A* nuclei. A value of -1 means the even-even core is determined by subtracting a nucleon from the target nucleus, while a value of +1 means a nucleon is added.

*Examples:*

**core 1**

*Range:* **-1** or **1**

*Default:* **core -1**

### 6.2.5 Compound nucleus

#### compound

Flag for compound nucleus calculation. This keyword can be used to disable compound nucleus evaporation if one is for example only interested in high-energy pre-equilibrium spectra.

*Examples:*

**compound y**

**compound n**

*Range:* **y** or **n**

*Default:* **compound y**

#### widthfluc

Enabling or disabling width fluctuation corrections (WFC) in compound nucleus calculations, see Section 4.5.2. For **widthfluc**, the user has 3 possibilities: **y**, **n** or a value for the energy above which WFC's are disabled. The latter option is helpful in the case of a calculation with several incident energies. Then, the user may want to set the width fluctuation off as soon as the incident energy is high enough, in order to save computing time. We have taken care of this by the default, **widthfluc=S**, where S is the projectile separation energy ( $\sim 8$  MeV), of the target nucleus. This default is rather safe, since in practice width fluctuation corrections are already negligible for incident energies above a few MeV, because the presence of many open channels reduces the correction to practically zero, i.e. the WFC factors to 1. Note that the disabling of width fluctuations for *any* incident energy can be accomplished by **widthfluc n**, which is equivalent to **widthfluc 0**. or any other energy lower than the (lowest) incident energy. Similarly, **widthfluc y**, equivalent to **widthfluc 20.**, will activate width fluctuations for any incident energy. To avoid numerical problems, width fluctuations are never calculated for incident energies beyond 20 MeV.

*Examples:*

**widthfluc y**

**widthfluc n**

**widthfluc 4.5**

*Range:* **y** or **n** or  $0. \leq \text{widthfluc} < 20.$

*Default:* **widthfluc** is equal to the projectile separation energy S, i.e. width fluctuation corrections are only used for incident energies below this value.

**widthmode**

Model for width fluctuation corrections in compound nucleus calculations, see Section 4.5.2.

*Examples:*

**widthmode 0:** no width fluctuation, i.e. pure Hauser-Feshbach model

**widthmode 1:** Moldauer model

**widthmode 2:** Hofmann-Richert-Tepel-Weidenmüller model

**widthmode 3:** GOE triple integral model

*Range:*  $0 \leq \text{widthmode} \leq 3$

*Default:* **widthmode 1**

**fullhf**

Flag for Hauser-Feshbach calculation using the full  $j,l$  coupling. This keyword can be used to enable/disable the loop over total angular momentum of the ejectile  $j'$  in Eq. (4.174). If **fullhf n**, the transmission coefficients are averaged over  $j$ , reducing the calculation time of the full Hauser-Feshbach model. In practice, the difference with the results from the full calculation is negligible.

*Examples:*

**fullhf y**

**fullhf n**

*Range:* **y** or **n**

*Default:* **fullhf n**

**eciscompound**

Flag for compound nucleus calculation by ECIS-06, done in parallel with TALYS. This keyword is used for checking purposes only and does not influence the TALYS results. An ECIS input file is created that contains the same discrete levels, level density parameters etc., as the TALYS calculation. The compound nucleus results given by ECIS can be compared with the results from TALYS, but are not used in TALYS. The results are written on a separate ECIS output file.

*Examples:*

**eciscompound y**

**eciscompound n**

*Range:* **y** or **n**

*Default:* **eciscompound n**

**urr**

Flag for the output of unresolved resonance parameters (URR). Since a full compound nucleus model and all its parameters are included in TALYS, it is only a small step to produce the URR parameters in the output. All calculated parameters, per incident energy, are stored in the file *urr.dat*. Energy-dependent tables can be found in the files *urrspacinglj.LL*, with LL the orbital angular momentum in (i2.2) format, for the l,j-dependent neutron spacing, *urrneustrengthl.100* for the l-dependent neutron spacing, *urrneuwidth.LL* for the neutron width, *urrgamwidth.LL* for the gamma width, *urrfiswidth.LL* for the fission width, and *urrcomwidth.LL* for the competitive width, These can be used for evaluated nuclear data files.

*Examples:*

**urr y**

**urr n**

*Range:* y or n

*Default:* **urr y**

**lurr**

Maximum orbital angular momentum taken into account for URR calculations. This keyword is only active if **urr y**.

*Examples:*

**lurr 1**

**lurr 4**

*Range:*  $0 \leq \text{lurr} \leq \text{numl}$ , where *numl* is specified in *talys.cmb* (currently *lurr*=60).

*Default:* **lurr 2**

**urrnjoy**

Flag for normalization of URR parameters with NJOY method. This keyword is only active if **urr y**. In addition to the files mentioned under the **urr** keyword, a few other files are produced: *urrtalys.tot*, the cross sections as calculated with the TALYS URR parameters, *urrnjoy.tot*, the cross sections as calculated with the NJOY URR method, and *urrratio.tot*, containing the ratio between the aforementioned two.

*Examples:*

**urrnjoy y**

**urrnjoy n**

*Range:* y or n

*Default:* **urrnjoy y**

**resonance**

Flag for the output of low energy resonance cross sections. If **resonance y**, TALYS will read in resonance parameters, from various possible sources, and call the RECENT code of Red Cullen's PREPRO package. Low energy pointwise resonance cross sections will be added to channels like total, elastic, fission and capture.

*Examples:*

**resonance y**

**resonance n**

*Range:* **y** or **n**

*Default:* **resonance n**

**group**

Flag for processing pointwise resonance cross sections into energy groups. This keyword is only relevant if **resonance y**.

*Examples:*

**group y**

**group n**

*Range:* **y** or **n**

*Default:* **group n**

**reslib**

Choice for the source of the resonance parameters. This keyword is only relevant if **resonance y**.

*Examples:*

**reslib default**

**reslib endfb7.1**

**reslib jendl4.0**

**reslib jeff3.2**

*Range:* One of the 4 choices listed above.

*Default:* **reslib default**

**Tres**

Temperature, in Kelvin, for the broadening of resonances. This keyword is only relevant if **resonance y**.

*Examples:*

**Tres 600.**

**Tres 0.**

*Range:* **0. < Tres < 1.e12**

*Default:* **Tres 293.16**

**skipCN**

Flag to skip the decay of a compound nucleus altogether. In this way, for example (n, $\gamma$ n) reactions can be skipped. Furthermore, the flag can be used for debugging purposes or other tests.

*Examples:*

**skipCN 40 91**

**skipCN 92 239**

*Range:* **skipCN Z A.**

*Default:* **skipCN** not used.

**6.2.6 Gamma emission****gammax**

Maximum number of  $l$ -values for gamma multipolarity, whereby  $l = 1$  stands for M1 and E1 transitions,  $l = 2$  for M2 and E2 transitions, etc.

*Examples:*

**gammax 1**

*Range:* **1  $\leq$  gammax  $\leq$  6**

*Default:* **gammax 2**

**gnorm**

Normalisation factor for gamma-ray transmission coefficient. This adjustable parameter can be used to scale e.g. the ( $n, \gamma$ ) cross section.

*Examples:*

**gnorm 1.6****gnorm -1.** (enforce automatic normalization)*Range:*  $0. \leq \mathbf{gnorm} \leq 100.$  or **gnorm -1.***Default:* **gnorm** is given by the normalization factor of Eq. (4.79) for **strength 1** or **2**.**strength**Model for  $E1$  gamma-ray strength function, see Section 4.3. There are 8 possibilities.*Examples:***strength 1** : Kopecky-Uhl generalized Lorentzian**strength 2** : Brink-Axel Lorentzian**strength 3** : Hartree-Fock BCS tables**strength 4** : Hartree-Fock-Bogolyubov tables**strength 5** : Goriely's hybrid model [126]**strength 6** : Goriely T-dependent HFB**strength 7** : T-dependent RMF**strength 8** : Gogny D1M HFB+QRPA*Range:* **1 - 8***Default:* **strength 1** for incident neutrons, **strength 2** for other incident particles.**strengthM1**Model for  $M1$  gamma-ray strength function. There are two possibilities.*Examples:***strengthM1 1** : Use Eq. (4.75)**strengthM1 2** : Normalize the  $M1$  gamma-ray strength function with that of  $E1$  as  $f_{E1}/(0.0588A^{0.878})$ .*Range:* **1 - 2***Default:* **strengthM1 2**

**electronconv**

Flag for the application of an electron-conversion coefficient on the gamma-ray branching ratios from the discrete level file.

*Examples:*

**electronconv y**

**electronconv n**

*Range:* y or n

*Default:* **electronconv y**

**egr**

Energy of the giant dipole resonance in MeV. On the input line, we read **egr**,  $Z$ ,  $A$ , value, type of radiation (the full symbol, i.e. M1, E1, E2, etc.), number of resonance (optional). If the number of the resonance is not given, it is assumed the keyword concerns the first Lorentzian.

*Examples:*

**egr 41 93 16.2 E1**

**egr 94 239 13.7 E1 2**

*Range:*  $1. \leq \text{egr} \leq 100$ . The optional number of the resonance must be either 1 or 2.

*Default:* **egr** is read from the *talys/structure/gamma/* directory. If the value for the first resonance is not present in the directory, it is calculated from systematics, see Section 4.3. If no parameter for the second resonance is given, this term is omitted altogether.

**sgr**

Strength of the giant dipole resonance in millibarns. On the input line, we read **sgr**,  $Z$ ,  $A$ , value, type of radiation (the full symbol, i.e. M1, E1, E2, etc.), number of resonance (optional). If the number of the resonance is not given, it is assumed the keyword concerns the first Lorentzian.

*Examples:*

**sgr 41 93 221. E1**

**sgr 94 239 384. E1 2**

*Range:*  $0. \leq \text{sgr} \leq 10000$ . The optional number of the resonance must be either 1 or 2.

*Default:* **sgr** is read from the *talys/structure/gamma/* directory. If the value for the first resonance is not present in the directory, it is calculated from systematics, see Section 4.3. If no parameter for the second resonance is given, this term is omitted altogether.

**ggr**

Width of the giant dipole resonance in MeV. On the input line, we read **ggr**,  $Z$ ,  $A$ , value, type of radiation (the full symbol, i.e. M1, E1, E2, etc.), number of resonance (optional). If the number of the resonance is not given, it is assumed the keyword concerns the first Lorentzian.

*Examples:*

**ggr 41 93 5.03 E1**

**ggr 94 239 4.25 E1 2**

*Range:*  $1. \leq \mathbf{ggr} \leq 100$ . The optional number of the resonance must be either 1 or 2.

*Default:* **ggr** is read from the *talys/structure/gamma/* directory. If the value for the first resonance is not present in the directory, it is calculated from systematics, see Section 4.3. If no parameter for the second resonance is given, this term is omitted altogether.

**egradjust**

Normalisation factor for the energy of the giant dipole resonance. This parameter can be used as a relative normalisation instead of the absolute value of **egr**.

*Examples:*

**egradjust 45 104 0.9**

*Range:*  $0.1 \leq \mathbf{egradjust} \leq 10$ .

*Default:* **egradjust Z A 1.**

**sgradjust**

Normalisation factor for the strength of the giant dipole resonance. This parameter can be used as a relative normalisation instead of the absolute value of **sgr**.

*Examples:*

**sgradjust 45 104 0.9**

*Range:*  $0.1 \leq \mathbf{sgradjust} \leq 10$ .

*Default:* **sgradjustZ A 1.**

**ggradjust**

Normalisation factor for the width of the giant dipole resonance. This parameter can be used as a relative normalisation instead of the absolute value of **ggr**.

*Examples:*

**ggradjust 45 104 0.9**

*Range:*  $0.1 \leq \text{ggradjust} \leq 10$ .

*Default:* **ggradjust**Z A 1..

### gamgam

The total radiative width,  $\Gamma_\gamma$  in eV. On the input line, we read **gamgam**, Z, A, value.

*Examples:*

**gamgam 26 55 1.8**

*Range:*  $0. \leq \text{gamgam} \leq 10$ .

*Default:* **gamgam** is read from the *talys/structure/resonances/* directory, or, if not present there, is taken from interpolation, see Section 4.3.

### gamgamadjust

Normalisation factor for the average radiative width  $\Gamma_\gamma$ . This parameter can be used to scale e.g. the  $(n, \gamma)$  cross section.

*Examples:*

**gamgamadjust 45 104 0.9**

*Range:*  $0.1 \leq \text{gamgamadjust} \leq 10$ .

*Default:* **gamgamadjust**Z A 1..

### D0

The s-wave resonance spacing  $D_0$  in keV. On the input line, we read **D0**, Z, A, value.

*Examples:*

**D0 26 55 13.**

*Range:*  $1.e - 6 \leq \text{D0} \leq 10000$ .

*Default:* **D0** is read from the *talys/structure/resonances/* directory.

### S0

The s-wave strength function  $S_0$  in units of  $10^{-4}$ . On the input line, we read **S0**, Z, A, value.

*Examples:*

**S0 26 55 6.90**

*Range:*  $0. \leq \mathbf{S0} \leq 10.$

*Default:* **S0** is read from the *talys/structure/resonances/* directory.

**etable**

Constant  $E_{\text{shift}}$  of the adjustment function (4.77) for tabulated gamma strength functions densities, per nucleus. On the input line, we read **etable**,  $Z$ ,  $A$ , value.

*Examples:*

**etable 29 65 -0.6**

*Range:*  $-10. \leq \mathbf{etable} \leq 10.$

*Default:* **etable** $Z A 0.$

**ftable**

Constant  $f^{nor}$  of the adjustment function (4.77) for tabulated gamma strength functions densities, per nucleus. On the input line, we read **ftable**,  $Z$ ,  $A$ , value.

*Examples:*

**ftable 29 65 1.2**

*Range:*  $0.1 \leq \mathbf{ftable} \leq 10.$

*Default:* **ftable** $Z A 1.$

**E1file**

File with tabulated E1 gamma-ray strength function. The format of the file is the same as that of the nuclear structure database *talys/structure/gamma/hfb/*. On the input line, we read **E1file**,  $Z$ ,  $A$ , filename.

*Examples:*

**E1file 26 56 gam.loc**

*Range:* **E1file** can be equal to any filename, provided it starts with a character.

*Default:* If **E1file** is not given in the input file, the default applies.

**M1file**

File with tabulated M1 gamma-ray strength function. The format of the file is the same as that of the nuclear structure database *talys/structure/gamma/hfb/*. On the input line, we read **M1file**,  $Z$ ,  $A$ , filename.

*Examples:*

**M1file 26 56 gam.loc**

*Range:* **M1file** can be equal to any filename, provided it starts with a character.

*Default:* If **M1file** is not given in the input file, the default applies.

**fiso**

Correction factor for isospin-forbidden transitions to self-conjugate nuclei [114]. Since isospin-dependent level densities are currently not implemented in TALYS, this is a way to handle transitions to  $Z = N$  or  $Z = N \pm 1$  nuclei. On the input line, we read **fiso**, projectile  $Z$ ,  $A$ , value.

*Examples:*

**fiso n 20 40 2.2**

*Range:*  $0.01 \leq \mathbf{fiso} \leq 100$ .

*Default:* If  $Z = N$ , **fiso 2**. for incident neutrons and protons, **fiso 5**. for incident alpha's. If  $Z = N \pm 1$ , **fiso 1.5** for incident neutrons, protons and alpha's. In all other cases **fiso 1**.

**racap**

Flag for the inclusion of the direct capture model, for addition to the gamma cross section.

*Examples:*

**racap y**

**racap n**

*Range:* **y** or **n**

*Default:* **racap n**

**ldmodelracap**

Level density model for direct capture model. There are 3 options.

*Examples:*

**ldmodelracap 1:** Spin-parity dependent ph-state densities

**ldmodelracap 2:** Total ph-state densities

**ldmodelracap 3:** Spin-parity dependent total level densities (**ldmodel 5**)

*Range:*  $1 \leq \mathbf{ldmodelracap} \leq 3$

*Default:* **ldmodelracap 1**

**sfexp**

Experimental spectroscopic factor for direct capture reactions. This keyword is only active if **racap y**. On the input line, we read **sfexp**,  $Z$ ,  $A$ , discrete level, value. The input for  $Z$ ,  $A$ , discrete level, is optional.

*Examples:*

**sfexp 20 40 2 0.1**

**sfexp 2 0.3**

**sfexp 20 40 0.1**

**sfexp 0.2**

*Range:*  $0. \leq \text{sfexp} \leq 10.$

*Default:* **sfexp** is taken from *talys/structure/levels/spectn*, and if not available there, **sfexp**  $Z A level$  **0.347**.

**sfth**

Theoretical spectroscopic factor for direct capture reactions, for levels in the continuum. This keyword is only active if **racap y**. On the input line, we read **sfth**,  $Z$ ,  $A$ , value. The input for  $Z$ ,  $A$ , is optional.

*Examples:*

**sfth 20 40 0.1**

**sfth 0.3**

*Range:*  $0. \leq \text{sfth} \leq 10.$

*Default:* **sfth**  $Z A$  **0.5**.

**epr**

Energy of the Pygmy resonance in MeV. On the input line, we read **epr**,  $Z$ ,  $A$ , value, type of radiation (the full symbol, i.e. M1, E1, E2, etc.), number of resonance (optional). If the number of the resonance is not given, it is assumed the keyword concerns the first Lorentzian.

*Examples:*

**epr 41 93 10.2 E1**

**epr 94 239 8.7 E1 2**

*Range:*  $1. \leq \text{epr} \leq 100.$  The optional number of the resonance must be either 1 or 2.

*Default:* no default.

**spr**

Strength of the Pygmy resonance in millibarns. On the input line, we read **spr**,  $Z$ ,  $A$ , value, type of radiation (the full symbol, i.e. M1, E1, E2, etc.), number of resonance (optional). If the number of the resonance is not given, it is assumed the keyword concerns the first Lorentzian.

*Examples:*

**spr 41 93 21.6 E1**

**spr 94 239 3.4 E1 2**

*Range:*  $0. \leq \mathbf{spr} \leq 10000$ . The optional number of the resonance must be either 1 or 2.

*Default:* no default.

**gpr**

Width of the Pygmy resonance in MeV. On the input line, we read **gpr**,  $Z$ ,  $A$ , value, type of radiation (the full symbol, i.e. M1, E1, E2, etc.), number of resonance (optional). If the number of the resonance is not given, it is assumed the keyword concerns the first Lorentzian.

*Examples:*

**gpr 41 93 5.03 E1**

**gpr 94 239 4.25 E1 2**

*Range:*  $0.1 \leq \mathbf{gpr} \leq 100$ . The optional number of the resonance must be either 1 or 2.

*Default:* no default.

**epradjust**

Normalisation factor for the energy of the Pygmy resonance. This parameter can be used as a relative normalisation instead of the absolute value of **epr**.

*Examples:*

**epradjust 45 104 0.9**

*Range:*  $0.1 \leq \mathbf{epradjust} \leq 10$ .

*Default:* **epradjust Z A 1.**

**spradjust**

Normalisation factor for the strength of the Pygmy resonance. This parameter can be used as a relative normalisation instead of the absolute value of **spr**.

*Examples:*

**spradjust 45 104 0.9**

*Range:*  $0.1 \leq \text{spradjust} \leq 10$ .

*Default:* **spradjust Z A 1.**

### **gpradjust**

Normalisation factor for the width of the Pygmy resonance. This parameter can be used as a relative normalisation instead of the absolute value of **gpr**.

*Examples:*

**gpradjust 45 104 0.9**

*Range:*  $0.1 \leq \text{gpradjust} \leq 10$ .

*Default:* **gpradjust Z A 1.**

### **upbendc**

Normalisation factor for the low-energy upbend of the gamma ray strength function.

*Examples:*

**upbendc 57 138 1.e-7 M1**

*Range:*  $0. \leq \text{upbendc} \leq 1.e-5$

*Default:* **upbendc Z A 0.**

### **upbende**

Energy-dependent factor for the low-energy upbend of the gamma ray strength function.

*Examples:*

**upbende 57 138 1.5 M1**

*Range:*  $0. \leq \text{upbende} \leq 10$ .

*Default:* **upbende Z A 0.**

## **6.2.7 Pre-equilibrium**

### **preequilibrium**

Enabling or disabling the pre-equilibrium reaction mechanism. For **preequilibrium**, the user has 3 possibilities: **y**, **n** or a value for the starting energy. The latter option is helpful in the case of a calculation

with several incident energies. Then, the user may want to set pre-equilibrium contributions on as soon as the incident energy is high enough. We have taken care of this by the default, **preequilibrium=Ex(Nm)**, where  $Ex(Nm)$  is the excitation energy of the last discrete level  $Nm$  of the target nucleus. This default is very safe, since in practice the pre-equilibrium contribution becomes only sizable for incident energies several MeV higher than  $Ex(Nm)$ . Note that the disabling of pre-equilibrium for *any* incident energy can be accomplished by **preequilibrium n**. Similarly, **preequilibrium y**, equivalent to **preequilibrium 0.**, will enable pre-equilibrium for any incident energy.

*Examples:*

**preequilibrium y**

**preequilibrium n**

**preequilibrium 4.5**

*Range:* **y** or **n** or  $0. \leq \text{preequilibrium} < 250$ .

*Default:* **preequilibrium** is equal to  $Ex(NL)$ , i.e. pre-equilibrium calculations are included for incident energies above the energy of the last discrete level of the target nucleus.

### preeqmode

Model for pre-equilibrium reactions. There are four possibilities, see Section 4.4.

*Examples:*

**preeqmode 1:** Exciton model: Analytical transition rates with energy-dependent matrix element.

**preeqmode 2:** Exciton model: Numerical transition rates with energy-dependent matrix element.

**preeqmode 3:** Exciton model: Numerical transition rates with optical model for collision probability.

**preeqmode 4:** Multi-step direct/compound model

*Range:*  $1 \leq \text{preeqmode} \leq 4$

*Default:* **preeqmode 2**

### multipreeq

Enabling or disabling multiple pre-equilibrium reaction mechanism. For **multipreeq**, the user has 3 possibilities: **y**, **n** or a value for the starting energy. The latter option is helpful in the case of a calculation with several incident energies. Then, the user may want to set multiple pre-equilibrium contributions on as soon as the incident energy is high enough. We have taken care of this by the default, **multipreeq 20.** This default is very safe, since in practice the multiple pre-equilibrium contribution becomes only sizable for incident energies a few tens of MeV higher than the default. Note that the disabling of multiple pre-equilibrium for *any* incident energy can be accomplished by **multipreeq n**. Similarly, **multipreeq y**,

equivalent to **multipreeq 0.**, will activate multiple pre-equilibrium for any incident energy.

*Examples:*

**multipreeq y**

**multipreeq n**

**multipreeq 40.**

*Range:* **y** or **n** or  $0. \leq \text{multipreeq} < 250.$

*Default:* **multipreeq 20.**, i.e. multiple pre-equilibrium calculations are included for incident energies above this value. TALYS always sets **multipreeq n** if **preequilibrium n**.

### m\_preeqmode

Model for multiple pre-equilibrium reactions. There are two possibilities, see Section 4.6.2 for an explanation.

*Examples:*

**m\_preeqmode 1:** Multiple exciton model

**m\_preeqmode 2:** Transmission coefficient method

*Range:*  $1 \leq \text{m_preeqmode} \leq 2$

*Default:* **m\_preeqmode 2**

### preeqspin

Flag to use the pre-equilibrium or compound nucleus spin distribution for the pre-equilibrium population of the residual nuclides. For backward-compatibility with earlier versions of TALYS, the following options are now possible:

*Examples:*

**preeqspin n** or **preeqspin 1:** the pre-equilibrium spin distribution is made equal to the relative spin-dependent population after compound nucleus emission

**preeqspin 2:** the spin distribution from total level densities is adopted

**preeqspin y** or **preeqspin 3:** the pre-equilibrium spin distribution is based on particle-hole state densities

*Range:* **y** or **n**, or  $1 \leq \text{preeqspin} \leq 3.$

*Default:* **preeqspin n**

**preeqsurface**

Flag to use surface corrections in the exciton model.

*Examples:*

**preeqsurface y**

**preeqsurface n**

*Range:* y or n

*Default:* **preeqsurface y**

**Esurf**

Effective well depth for surface effects in MeV in the exciton model, see Eq. (4.97).

*Examples:*

**Esurf 25.**

*Range:*  $0. \leq \mathbf{Esurf} \leq \mathbf{Efermi}$ , where **Efermi** = 38 MeV is the Fermi well depth.

*Default:* **Esurf** is given by Eq. (4.97).

**preeqcomplex**

Flag to use the Kalbach model for pickup, stripping and knockout reactions, in addition to the exciton model, in the pre-equilibrium region.

*Examples:*

**preeqcomplex y**

**preeqcomplex n**

*Range:* y or n

*Default:* **preeqcomplex y**

**twocomponent**

Flag to use the two-component (y) or one-component (n) exciton model.

*Examples:*

**twocomponent y**

**twocomponent n**

*Range:* y or n

*Default:* **twocomponent y**

**pairmodel**

Model for pairing correction for pre-equilibrium model.

*Examples:*

**pairmodel 1:** Fu's pairing energy correction, see Eq. (4.91).

**pairmodel 2:** Compound nucleus pairing correction

*Range:*  $1 \leq \text{pairmodel} \leq 2$

*Default:* **pairmodel 1**

**M2constant**

Overall constant for the matrix element, or the optical model strength, in the exciton model. The parameterisation of the matrix element is given by Eq. (4.132) for the one-component model, and by Eq. (4.112) for the two-component model. **M2constant** is also used to scale the MSD cross section (preeqmode 4).

*Examples:*

**M2constant 1.22**

*Range:*  $0. \leq \text{M2constant} \leq 100.$

*Default:* **M2constant 1.**

**M2limit**

Constant to scale the asymptotic value of the matrix element in the exciton model. The parameterisation of the matrix element is given by Eq. (4.132) for the one-component model, and by Eq. (4.112) for the two-component model.

*Examples:*

**M2limit 1.22**

*Range:*  $0. \leq \text{M2limit} \leq 100.$

*Default:* **M2limit 1.**

**M2shift**

Constant to scale the energy shift of the matrix element in the exciton model. The parameterisation of the matrix element is given by Eq. (4.132) for the one-component model, and by Eq. (4.112) for the two-component model.

*Examples:*

**M2shift 1.22**

*Range:*  $0. \leq \mathbf{M2shift} \leq 100.$

*Default:* **M2shift 1.**

**Rnnu**

Neutron-neutron ratio for the matrix element in the two-component exciton model, see Eq. (4.110).

*Examples:*

**Rnnu 1.6**

*Range:*  $0. \leq \mathbf{Rnnu} \leq 100.$

*Default:* **Rnnu 1.5**

**Rnupi**

Neutron-proton ratio for the matrix element in the two-component exciton model, see Eq. (4.110).

*Examples:*

**Rnupi 1.6**

*Range:*  $0. \leq \mathbf{Rnupi} \leq 100.$

*Default:* **Rnupi 1.**

**Rpipi**

Proton-proton ratio for the matrix element in the two-component exciton model, see Eq. (4.110).

*Examples:*

**Rpipi 1.6**

*Range:*  $0. < \mathbf{Rpipi} \leq 100.$

*Default:* **Rpipi 1.**

**Rpinu**

Proton-neutron ratio for the matrix element in the two-component exciton model, see Eq. (4.110).

*Examples:*

**Rpinu 1.6**

*Range:*  $0. \leq \mathbf{Rpinu} \leq 100.$

*Default:* **Rpinu 1.**

**Rgamma**

Adjustable parameter for pre-equilibrium gamma decay.

*Examples:*

**Rgamma 1.22**

*Range:*  $0. \leq \mathbf{Rgamma} \leq 100.$

*Default:* **Rgamma 2.**

**Cstrip**

Adjustable parameter for the stripping or pick-up process, to scale the complex-particle pre-equilibrium cross section per outgoing particle, see Section 4.4.4. On the input line, we read **Cstrip**, particle symbol, and value.

*Examples:*

**Cstrip d 1.3**

**Cstrip a 0.4**

*Range:*  $0. \leq \mathbf{Cstrip} \leq 10.$

*Default:* **Cstrip 1.**

**Cknock**

Adjustable parameter for the knock-out process, to scale the complex-particle pre-equilibrium cross section per outgoing particle, see Section 4.4.4. In practice, for nucleon-induced reactions this parameter affects only alpha-particles. This parameter is however also used as scaling factor for break-up reactions (such as (d,p) and (d,n)). On the input line, we read **Cknock**, particle symbol, and value.

*Examples:*

**Cknock a 0.4**

*Range:*  $0. \leq \mathbf{Cknock} \leq 10.$

*Default:* **Cknock 1.**

**Cbreak**

Adjustable parameter for the break-up process, to scale the complex-particle pre-equilibrium cross section per outgoing particle, see Section 4.4.4. On the input line, we read **Cbreak**, particle symbol, and value.

*Examples:*

**Cbreak d 1.3**

**Cbreak a 0.4**

*Range:*  $0. \leq \text{Cbreak} \leq 10.$

*Default:* **Cbreak 1.**

### **breakupmodel**

Model for break-up reactions.

*Examples:*

**breakupmodel 1:** Kalbach model

**breakupmodel 2:** Avrigeanu model

*Range:*  $1 \leq \text{breakupmodel} \leq 2$

*Default:* **breakupmodel 1**

### **ecisdwba**

Flag for DWBA calculations for multi-step direct calculations. If this calculation has already been performed in a previous run, it may be helpful to put **ecisdwba n**, which avoids a new calculation and thus saves time. We stress that it is the responsibility of the user to ensure that the first run of a particular problem is done with **ecisdwba y**. If not, an appropriate error message will be given and TALYS stops.

*Examples:*

**ecisdwba y**

**ecisdwba n**

*Range:* **y** or **n**

*Default:* **ecisdwba y**

### **onestep**

Flag for inclusion of *only* the one-step direct contribution in the continuum multi-step direct model. This is generally enough for incident energies up to about 14 MeV, and thus saves computing time.

*Examples:*

**onestep y**

**onestep n**

*Range:* **y** or **n**

*Default:* **onestep n**

**msdbins**

The number of emission energy points for the DWBA calculation for the multi-step direct model.

*Examples:*

**msdbins 8**

*Range:*  $2 \leq \text{msdbins} \leq \text{numenmsd}/2-1$ , where **numenmsd** is specified in the file *talys.cmb*. Currently, **numenmsd=18**

*Default:* **msdbins 6**

**Emsdmin**

The minimal emission energy in MeV for the multi-step direct calculation.

*Examples:*

**Emsdmin 8.**

*Range:*  $0. \leq \text{Emsdmin}$

*Default:* **Emsdmin** is equal to **eninc/5**. where **eninc** is the incident energy.

**6.2.8 Level densities****ldmodel**

Model for level densities. There are 3 phenomenological level density models and 3 options for microscopic level densities, see Section 4.7. Since TALYS-1.4, it is possible to choose a level density model per nuclide considered in the reaction.

*Examples:*

**ldmodel 1:** Constant temperature + Fermi gas model

**ldmodel 2:** Back-shifted Fermi gas model

**ldmodel 3:** Generalised superfluid model

**ldmodel 4:** Microscopic level densities (Skyrme force) from Goriely's tables

**ldmodel 5:** Microscopic level densities (Skyrme force) from Hilaire's combinatorial tables

**ldmodel 6:** Microscopic level densities (temperature dependent HFB, Gogny force) from Hilaire's combinatorial tables

**ldmodel 2 41 93:** Back-shifted Fermi gas model just for this particular nucleus

*Range:*  $1 \leq \text{ldmodel} \leq 6$

*Default:* **ldmodel 1**

**colenhance**

Flag to enable or disable explicit collective enhancement of the level density, using the  $K_{rot}$  and  $K_{vib}$  factors. This keyword can be used in combination with the **ldmodel** keyword. For fission, if **colenhance n**, collective effects for the ground state are included implicitly in the intrinsic level density, and collective effects on the barrier are determined relative to the ground state. Since TALYS-1.4, it is possible to enable or disable the collective enhancement per nuclide considered in the reaction.

*Examples:*

**colenhance y**

**colenhance y 41 93**

*Range:* **y** or **n**

*Default:* **colenhance y** if **fission y**, **colenhance n** otherwise.

**colldamp**

Flag for damping of collective effects in effective level density, i.e. in a formulation without explicit collective enhancement. In practice, this option is only used for fission model parameterization as employed in Bruyeres-le-Chatel actinide evaluations (Pascal Romain). Using it affects also the spin cutoff parameterization. For fission, collective effects for the ground state are included implicitly in the intrinsic level density, and collective effects on the barrier are determined relative to the ground state, see Section 4.8.1.

*Examples:*

**colldamp y**

*Range:* **y** or **n**

*Default:* **colldamp n**

**ctmglobal**

Flag to enforce global formulae for the Constant Temperature Model (CTM), see Section 4.7.1. By default, if enough discrete levels are available the CTM will always make use of them for the estimation of the level density at low energies. For an honest comparison with other level density models, and also to test the predictive power for nuclides for which no discrete levels are known, we have included the possibility to perform a level density calculation with a truly global CTM. In practice it means that the matching energy  $E_M$  is always determined from the empirical formula (4.274), while  $T$  and  $E_0$  are determined from  $E_M$  through Eqs.(4.268) and (4.265), respectively. This flag is only relevant if **ldmodel 1**.

*Examples:*

**ctmglobal y***Range:* y or n*Default:* ctmglobal n**spincutmodel**

Model for spin cut-off parameter for the ground state level densities, see Section 4.7.1. There are 2 expressions.

*Examples:*

$$\text{spincutmodel 1: } \sigma^2 = c \frac{a}{a} \sqrt{\frac{U}{a}}$$

$$\text{spincutmodel 2: } \sigma^2 = c \sqrt{\frac{U}{a}}$$

*Range:*  $1 \leq \text{spincutmodel} \leq 2$ *Default:* spincutmodel 1**asys**

Flag to use all level density parameters from systematics by default, i.e. to neglect the connection between  $a$  and  $D_0$ , even if an experimental value is available for the latter.

*Examples:***asys y***Range:* y or n*Default:* asys n**parity**

Flag to enable or disable non-equiparity level densities. At present, this option only serves to average tabulated parity-dependent level densities (**ldmodel 5, 6**) over the two parities (using **parity n**), for comparison purposes.

*Examples:***parity y***Range:* y or n*Default:* parity n for ldmodel 1-4, parity y for ldmodel 5, 6.

**a**

The level density parameter **a** at the neutron separation energy in  $\text{MeV}^{-1}$ . On the input line, we read **a**,  $Z$ ,  $A$ , value.

*Examples:*

**a 41 93 11.220**

**a 94 239 28.385**

*Range:*  $1. \leq \mathbf{a} \leq 100.$

*Default:* **a** is read from the *talys/structure/density/* directory or, if not present, is calculated from systematics, see Eq. (4.241).

**alimit**

The asymptotic level density parameter  $\tilde{a}$ , for a particular nucleus, in  $\text{MeV}^{-1}$ , see Eq. (4.241). On the input line, we read **alimit**,  $Z$ ,  $A$ , value.

*Examples:*

**alimit 41 93 10.8**

**alimit 94 239 28.010**

*Range:*  $1. \leq \mathbf{alimit} \leq 100.$

*Default:* **alimit** is determined from the systematics given by Eq. (4.242).

**alphald**

Constant for the global expression for the asymptotic level density parameter  $\tilde{a}$ , see Eq. (4.242).

*Examples:*

**alphald 0.054**

*Range:*  $0.01 \leq \mathbf{alphald} \leq 0.2$

*Default:* **alphald** is determined from the systematics given by Table 4.3, depending on the used level density model.

**betald**

Constant for the global expression for the asymptotic level density parameter  $\tilde{a}$ , see Eq. (4.242).

*Examples:*

**betald 0.15**

*Range:*  $-0.5 \leq \mathbf{betald} \leq 0.5$  with the extra condition that if  $\mathbf{betald} < 0$ , then  $\mathbf{abs(betald)} < \mathbf{alphald}$  (to avoid negative  $\mathbf{a}$  values).

*Default:* **betald** is determined from the systematics given by Table 4.3, depending on the used level density model.

**gammald**

The damping parameter for shell effects in the level density parameter, for a particular nucleus, in  $\text{MeV}^{-1}$ , see Eq. (4.241). On the input line, we read **gammald**,  $Z$ ,  $A$ , value.

*Examples:*

**gammald 41 93 0.051**

*Range:*  $0. \leq \mathbf{gammald} \leq 1$ .

*Default:* **gammald** is determined from either Eq. (4.243) or (4.249).

**gammashell1**

Constant for the global expression for the damping parameter for shell effects in the level density parameter  $\gamma$ , see Eq. (4.243).

*Examples:*

**gammashell1 0.5**

**gammashell1 0.**

*Range:*  $0. \leq \mathbf{gammashell1} \leq 1$ .

*Default:* **gammashell1** is determined from the systematics given by Table 4.3.

**gammashell2**

Constant for the global expression for the damping parameter for shell effects in the level density parameter  $\gamma$ , see Eq. (4.243).

*Examples:*

**gammashell2 0.054**

**gammashell1 0.**

*Range:*  $0. \leq \mathbf{gammashell2} \leq 0.2$

*Default:* **gammashell2=0.**

**aadjust**

Multiplier to adjust the level density parameter  $a$ . On the input line, we read **aadjust**, Z, A and value.

*Examples:*

**aadjust 41 93 1.04**

*Range:*  $0.5 \leq \text{aadjust} \leq 2$ .

*Default:* **aadjust Z A 1**.

**shellmodel**

Model for liquid drop expression for nuclear mass, to be used to calculate the shell correction. There are 2 expressions.

*Examples:*

**shellmodel 1:** Myers-Siatecki

**shellmodel 2:** Goriely

*Range:*  $1 \leq \text{shellmodel} \leq 2$

*Default:* **shellmodel 1**

**kvibmodel**

Model for the vibrational enhancement of the level density. There are 2 expressions.

*Examples:*

**kvibmodel 1:** Eq. (4.313)

**kvibmodel 2:** Eq. (4.307)

*Range:*  $1 \leq \text{kvibmodel} \leq 2$

*Default:* **kvibmodel 2**

**pairconstant**

Constant for the pairing energy expression in MeV, see Eq. (4.260).

*Examples:*

**pairconstant 11.3**

*Range:*  $0. \leq \text{pairconstant} \leq 30$ .

*Default:* **pairconstant=12**.

**pair**

The pairing correction in MeV. On the input line, we read **pair**,  $Z$ ,  $A$ , value.

*Examples:*

**pair 94 239 0.76**

*Range:*  $0. \leq \text{pair} \leq 10.$

*Default:* **pair** is determined from Eq. (4.278).

**deltaW**

Shell correction of the mass in MeV, see Eq. (4.241). On the input line, we read **deltaW**,  $Z$ ,  $A$ , value, the ground state or fission barrier to which it applies (optional). If the fission barrier is not given or is equal to 0, it concerns the ground state of the nucleus.

*Examples:*

**deltaW 41 93 0.110**

**deltaW 94 239 -0.262 1**

*Range:*  $-20. \leq \text{deltaW} \leq 20.$

*Default:* **deltaW** is determined from Eq. (4.244).

**Nlow**

Lower level to be used in the temperature matching problem of the Gilbert and Cameron formula. On the input line, we read **Nlow**,  $Z$ ,  $A$ , value, the ground state or fission barrier to which it applies (optional). If the fission barrier is not given or equal to 0, it concerns the ground state of the nucleus.

*Examples:*

**Nlow 41 93 4**

**Nlow 94 239 2 1**

*Range:*  $0 \leq \text{Nlow} \leq 200$

*Default:* **Nlow**  $Z A 2$

**Ntop**

Upper level to be used in the temperature matching problem of the Gilbert and Cameron formula. On the input line, we read **Ntop**,  $Z$ ,  $A$ , value, the ground state or fission barrier to which it applies (optional). If the fission barrier is not given or equal to 0, it concerns the ground state of the nucleus.

*Examples:*

**Ntop 41 93 14**

**Ntop 94 239 20 1**

*Range:*  $0 \leq \mathbf{Ntop} \leq 200$ , and  $\mathbf{Ntop} \geq \mathbf{Nlow}$ .

*Default:* **Ntop** is read from the *talys/structure/density/nmax* directory. If not present there, **Ntop** is equal to the last discrete level used for the Hauser-Feshbach calculation.

### **Exmatch**

The matching energy between the constant temperature and Fermi gas region in MeV, see Eq. (4.264). On the input line, we read **Exmatch**, *Z*, *A*, value, the ground state or fission barrier to which it applies (optional). If the fission barrier is not given or is equal to 0, it concerns the ground state of the nucleus.

*Examples:*

**Exmatch 41 93 4.213**

**Exmatch 94 239 5.556 2**

*Range:*  $0.1 \leq \mathbf{Exmatch} \leq 20$ .

*Default:* **Exmatch** is determined from Eq. (4.271).

### **T**

The temperature of the Gilbert-Cameron formula in MeV, see Eq. (4.268). On the input line, we read **T**, *Z*, *A*, value, the ground state or fission barrier to which it applies (optional). If the fission barrier is not given or is equal to 0, it concerns the ground state of the nucleus.

*Examples:*

**T 41 93 0.332**

**T 94 239 0.673 1**

*Range:*  $0.001 \leq \mathbf{T} \leq 10$ .

*Default:* **T** is determined from Eq. (4.268).

### **E0**

The "back-shift" energy of the four-component formula in MeV, see Eq. (4.265). On the input line, we read **E0**, *Z*, *A*, value, the ground state or fission barrier to which it applies (optional). If the fission barrier is not given or is equal to 0, it concerns the ground state of the nucleus.

*Examples:*

**E0 41 93 0.101**

**E0 94 239 -0.451 1**

*Range:*  $-10. \leq \mathbf{E0} \leq 10.$

*Default:* **E0** is determined from Eq. (4.265).

### Exmatchadjust

Normalisation factor for the matching energy of the four-component formula. This parameter can be used as a relative normalisation instead of the absolute value of **T**. On the input line, we read **Exmatchadjust**, *Z*, *A*, value, the ground state or fission barrier to which it applies (optional). If the fission barrier is not given or is equal to 0, it concerns the ground state

*Examples:*

**Exmatchadjust 41 93 0.9**

**Exmatchadjust 94 239 -1.13 1**

*Range:*  $0.1 \leq \mathbf{Exmatchadjust} \leq 10.$

*Default:* **Exmatchadjust** *Z A 1.*

### Tadjust

Normalisation factor for the temperature of the four-component formula. This parameter can be used as a relative normalisation instead of the absolute value of **T**. On the input line, we read **Tadjust**, *Z*, *A*, value, the ground state or fission barrier to which it applies (optional). If the fission barrier is not given or is equal to 0, it concerns the ground state

*Examples:*

**Tadjust 41 93 0.9**

**Tadjust 94 239 -1.13 1**

*Range:*  $0.1 \leq \mathbf{Tadjust} \leq 10.$

*Default:* **Tadjust** *Z A 1.*

### E0adjust

Normalisation factor for the "back-shift" energy of the four-component formula. This parameter can be used as a relative normalisation instead of the absolute value of **E0**. On the input line, we read **E0adjust**, *Z*, *A*, value, the ground state or fission barrier to which it applies (optional). If the fission barrier is not given or is equal to 0, it concerns the ground state

*Examples:*

**E0adjust 41 93 0.9**

**E0adjust 94 239 -1.13 1**

*Range:*  $0.1 \leq \mathbf{E0adjust} \leq 10$ .

*Default:* **E0adjust Z A 1.**

### **Pshift**

An extra pairing shift for adjustment of the Fermi Gas level density, in MeV. On the input line, we read **Pshift**,  $Z$ ,  $A$ , value.

*Examples:*

**Pshift 60 142 0.26**

*Range:*  $-10. \leq \mathbf{Pshift} \leq 10$ .

*Default:* **Pshift** is determined from Eqs. (4.260), (4.278), or (4.292), depending on the level density model.

### **Pshiftadjust**

Adjustable pairing shift for adjustment of the Fermi Gas level density, in MeV. The difference with **Pshift** is that the default is 0. On the input line, we read **Pshiftadjust**,  $Z$ ,  $A$ , value.

*Examples:*

**Pshiftadjust 60 142 -0.13**

*Range:*  $-10. \leq \mathbf{Pshift} \leq 10$ .

*Default:* **Pshift 0.**

### **Pshiftconstant**

Global constant for the adjustable pairing shift in MeV.

*Examples:*

**Pshiftconstant 1.03**

*Range:*  $-5. \leq \mathbf{Pshiftconstant} \leq 5$ .

*Default:* **Pshiftconstant=1.09** for **ldmodel 3** and **Pshiftconstant=0.** otherwise.

**Ufermi**

Constant  $U_f$  of the phenomenological function (4.319) for damping of collective effects, in MeV.

*Examples:*

**Ufermi 45.**

*Range:*  $0. \leq \text{Ufermi} \leq 1000.$

*Default:* **Ufermi 30.**

**cfermi**

Width  $C_f$  of the phenomenological Fermi distribution (4.319) for damping of collective effects, in MeV.

*Examples:*

**cfermi 16.**

*Range:*  $0. \leq \text{cfermi} \leq 1000.$

*Default:* **cfermi 10.**

**Ufermibf**

Constant  $U_f$  of the phenomenological function (4.319) for damping of collective effects on the fission barrier, in MeV.

*Examples:*

**Ufermibf 90.**

*Range:*  $0. \leq \text{Ufermibf} \leq 1000.$

*Default:* **Ufermibf 45.**

**cfermibf**

Width  $C_f$  of the phenomenological Fermi distribution (4.319) for damping of collective effects on the fission barrier, in MeV.

*Examples:*

**cfermibf 16.**

*Range:*  $0. \leq \text{cfermibf} \leq 1000.$

*Default:* **cfermibf 10.**

**Rspincut**

Global adjustable constant for spin cut-off parameter. Eq. (4.254) is multiplied by **Rspincut** for all nuclides in the calculation.

*Examples:*

**Rspincut 0.8**

*Range:*  $0. \leq \mathbf{Rspincut} \leq 10.$

*Default:* **Rspincut 1.**

**s2adjust**

Adjustable constant for spin cut-off parameter per nuclide. Eq. (4.254) is multiplied by **s2adjust**. On the input line, we read **s2adjust**, *Z*, *A*, value, fission barrier. If the number of the fission barrier is not given or is equal to 0, it concerns the ground state.

*Examples:*

**s2adjust 41 93 0.8**

**s2adjust 94 239 1.1 2**

*Range:*  $0.01 \leq \mathbf{s2adjust} \leq 10.$

*Default:* **s2adjust Z A 1.**

**beta2**

Deformation parameter for moment of inertia for the ground state or fission barrier, see Eq. (4.315). On the input line, we read **beta2**, *Z*, *A*, value, fission barrier. If the number of the fission barrier is not given or is equal to 0, it concerns the ground state.

*Examples:*

**beta2 90 232 0.3**

**beta2 94 239 1.1 2**

*Range:*  $0. \leq \mathbf{beta2} < 1.5$

*Default:* **beta2 Z A 0.** for the ground state, **beta2 Z A 0.6** for the first barrier, **beta2 0.8** for the second barrier, and **beta2 Z A 1.** for the third barrier, if present.

**Krotconstant**

Normalization constant for rotational enhancement for the ground state or fission barrier, to be multiplied with the r.h.s. of Eq. (4.316). On the input line, we read **Krotconstant**, *Z*, *A*, value, fission barrier. If

the number of the fission barrier is not given or is equal to 0, it concerns the ground state.

*Examples:*

**Krotconstant 90 232 0.4**

**Krotconstant 94 239 1.1 2**

*Range:*  $0.01 \leq \mathbf{Krotconstant} \leq 100$ .

*Default:* **Krotconstant Z A 1.**

### ctable

Constant  $c$  of the adjustment function (4.323) for tabulated level densities, per nucleus. On the input line, we read **ctable**,  $Z$ ,  $A$ , value, and (optionally) fission barrier.

*Examples:*

**ctable 29 65 2.8**

**ctable 92 234 0.1 1**

*Range:*  $-10. \leq \mathbf{ctable} \leq 10$ .

*Default:* **ctable Z A 0.**

### ptable

Constant  $\delta$  of the adjustment function (4.323) for tabulated level densities, per nucleus. On the input line, we read **ptable**,  $Z$ ,  $A$ , value, and (optionally) fission barrier.

*Examples:*

**ptable 29 65 -0.6**

**ptable 92 237 0.2 1**

*Range:*  $-10. \leq \mathbf{ptable} \leq 10$ .

*Default:* **ptable Z A 0.**

### cglobal

Constant  $c$  of the adjustment function (4.323) for tabulated level densities, applied for all nuclides at the same time. Individual cases can be overruled by the **ctable** keyword. On the input line, we read **cglobal**, value.

*Examples:*

**cglobal 1.5**

*Range:* **-10.  $\leq$  cglobal  $\leq$  10.**

*Default:* **cgloba 0.**

### **pglobal**

Constant  $\delta$  of the adjustment function (4.323) for tabulated level densities, applied for all nuclides at the same time. Individual cases can be overruled by the **ptable** keyword. On the input line, we read **pglobal**, value.

*Examples:*

**pglobal 0.5**

*Range:* **-10.**

*eq* **pglobal  $\leq$  10**

*Default:* **pgloba 0.**

### **phmodel**

Model for particle-hole state densities. There are two possibilities.

*Examples:*

**phmodel 1:** Phenomenological particle-hole state densities

**phmodel 2:** Microscopic particle-hole state densities

*Range:* **1  $\leq$  phmodel  $\leq$  2**

*Default:* **phmodel 1**

### **Kph**

Value for the constant of the single-particle level density parameter, i.e.  $g = A/K_{ph}$ , or  $g_{\pi} = Z/K_{ph}$  and  $g_{\nu} = N/K_{ph}$

*Examples:*

**Kph 12.5**

*Range:* **1.  $\leq$  Kph  $\leq$  100.**

*Default:* **Kph 15.**

### **g**

The single-particle level density parameter **g** in  $\text{MeV}^{-1}$ . On the input line, we read **g**, **Z**, **A**, value.

*Examples:*

**g 41 93 7.15**

**g 94 239 17.5**

*Range:*  $0.1 \leq g \leq 100$ .

*Default:*  $g = A/Kph$

### **gp**

The single-particle proton level density parameter  $g_\pi$  in  $\text{MeV}^{-1}$ . On the input line, we read **gp**,  $Z$ ,  $A$ , value.

*Examples:*

**gp 41 93 3.15**

**gp 94 239 7.2**

*Range:*  $0.1 \leq gp \leq 100$ .

*Default:*  $gp = Z/Kph$

### **gn**

The single-particle neutron level density parameter  $g_\nu$  in  $\text{MeV}^{-1}$ . On the input line, we read **gn**,  $Z$ ,  $A$ , value.

*Examples:*

**gn 41 93 4.1**

**gn 94 239 11.021**

*Range:*  $0.1 \leq gn \leq 100$ .

*Default:*  $gn = N/Kph$

### **gpadjust**

Multiplier to adjust the partial level density parameter  $g_\pi$ . On the input line, we read **gpadjust**,  $Z$ ,  $A$  and value.

*Examples:*

**gpadjust 41 93 1.04**

*Range:*  $0.5 \leq gpadjust \leq 2$ .

*Default:* **gpadjust**  $Z A 1$ .

**gnadjust**

Multiplier to adjust the partial level density parameter  $g_\nu$ . On the input line, we read **gnadjust**, Z, A and value.

*Examples:*

**gnadjust 41 93 1.04**

*Range:*  $0.5 \leq \text{gnadjust} \leq 2$ .

*Default:* **gnadjust Z A 1**.

**gshell**

Flag to include the damping of shell effects with excitation energy in single-particle level densities. The Ignatyuk parameterisation for total level densities is also applied to the single-particle level density parameters.

*Examples:*

**gshell y**

**gshell n**

*Range:* **y** or **n**

*Default:* **gshell n**

**6.2.9 Fission****fission**

Flag for enabling or disabling fission. By default **fission** is enabled if the target mass is above 209. Hence, for lower masses, it is necessary to set **fission y** manually at high incident energies (subactinide fission).

*Examples:*

**fission y**

**fission n**

*Range:* **y** or **n**. Fission is not allowed for  $A \leq 56$

*Default:* **fission y** for  $A > 209$ , **fission n** for  $A \leq 209$ . The default enabling or disabling of fission is thus mass dependent.

**fismodel**

Model for fission barriers. **fismodel** is only active if **fission y**. There are 5 possibilities:

*Examples:*

**fismodel 1:** “experimental” fission barriers

**fismodel 2:** theoretical fission barriers, Mamdouh table

**fismodel 3:** theoretical fission barriers, Sierk model

**fismodel 4:** theoretical fission barriers, rotating liquid drop

**fismodel 5:** WKB approximation for fission path model

*Range:*  $1 \leq \text{fismodel} \leq 5$

*Default:* **fismodel 1**

**fismodelalt**

”Back-up” model for fission barriers, for the case that the parameters of the tables used in **fismodel 1-2** are not available. There are two possibilities:

*Examples:*

**fismodelalt 3 :** theoretical fission barriers, Sierk model

**fismodelalt 4 :** theoretical fission barriers, rotating liquid drop model

*Range:*  $3 \leq \text{fismodelalt} \leq 4$

*Default:* **fismodelalt 4**

**axtype**

Type of axiality of the fission barrier. There are five options:

- 1: axial symmetry
- 2: left-right asymmetry
- 3: triaxial and left-right asymmetry
- 4: triaxial no left-right asymmetry
- 5: no symmetry

On the input line, we read **axtype**,  $Z$ ,  $A$ , value, fission barrier. If the number of the fission barrier is not given or is equal to 0, it concerns the first barrier.

*Examples:*

**axtype 90 232 3**

**axtype 94 239 1 2**

*Range:*  $1 \leq \text{axtype} \leq 5$

*Default:* **axtype 2** for the second barrier and  $N > 144$ , **axtype 3** for the first barrier and  $N > 144$ , **axtype 1** for the rest.

### **fisbar**

Fission barrier in MeV. On the input line, we read **fisbar**,  $Z$ ,  $A$ , value, fission barrier. This keyword overrules the value given in the nuclear structure database. If the number of the fission barrier is not given or is equal to 0, it concerns the first barrier.

*Examples:*

**fisbar 90 232 5.6**

**fisbar 94 239 6.1 2**

*Range:*  $0. \leq \text{fisbar} \leq 100.$

*Default:* **fisbar** is read from the *talys/structure/fission/* directory, or determined by systematics according to the choice of **fismodel**.

### **fishw**

Fission barrier width in MeV. On the input line, we read **fishw**,  $Z$ ,  $A$ , value, fission barrier. This keyword overrules the value given in the nuclear structure database. If the number of the fission barrier is not given or is equal to 0, it concerns the first barrier.

*Examples:*

**fishw 90 232 0.8**

**fishw 94 239 1.1 2**

*Range:*  $0.01 \leq \text{fishw} \leq 10.$

*Default:* **fishw** is read from the *talys/structure/fission/* directory or determined by systematics, according to the choice of **fismodel**.

**fisbaradjust**

Normalisation factor for the fission barrier. This parameter can be used as a relative normalisation instead of the absolute value of **fisbar**. On the input line, we read **fisbaradjust**,  $Z$ ,  $A$ , value, fission barrier. If the number of the fission barrier is not given or is equal to 0, it concerns the first barrier.

*Examples:*

**fisbaradjust 90 232 0.9**

**fisbaradjust 94 239 1.13 2**

*Range:*  $0.1 \leq \text{fisbaradjust} \leq 10$ .

*Default:* **fisbaradjust**  $Z A 1$ .

**fishwadjust**

Normalisation factor for the fission barrier width. This parameter can be used as a relative normalisation instead of the absolute value of **fishw**. On the input line, we read **fishwadjust**,  $Z$ ,  $A$ , value, fission barrier. If the number of the fission barrier is not given or is equal to 0, it concerns the first barrier.

*Examples:*

**fishwadjust 90 232 0.9**

**fishwadjust 94 239 1.13 2**

*Range:*  $0.1 \leq \text{fishwadjust} \leq 10$ .

*Default:* **fishwadjust**  $Z A 1$ .

**Rtransmom**

Normalization constant for moment of inertia for transition states, see Eq. (4.315). On the input line, we read **Rtransmom**,  $Z$ ,  $A$ , value, fission barrier. If the number of the fission barrier is not given or is equal to 0, it concerns the first barrier.

*Examples:*

**Rtransmom 90 232 1.15**

**Rtransmom 94 239 1.1 2**

*Range:*  $0.1 \leq \text{Rtransmom} \leq 10$ .

*Default:* **Rtransmom 0.6** for the first barrier, **Rtransmom 1.0** for the other barriers.

**hbstate**

Flag to use head band states in fission.

*Examples:*

**hbstate y**

**hbstate n**

*Range:* y or n.

*Default:* **hbstate y**.

**hbtransfile**

File with head band transition states. The format of the file is exactly the same as that of the nuclear structure database *talys/structure/fission/barrier/*. In practice, the user can copy a file from this database, e.g. *U.bar*, to the working directory and change it. In this way, changes in the “official” database are avoided. Note that one file in the working directory can only be used for one isotope. On the input line, we read **hbtransfile**, *Z*, *A*, filename.

*Examples:*

**hbtransfile 92 238 u238.hb**

*Range:* **hbtransfile** can be equal to any filename, provided it starts with a character.

*Default:* If **hbtransfile** is not given in the input file, the head band transition states are taken from the *talys/structure/fission/states* database.

**class2**

Flag for the enabling or disabling of class II/III states in fission. **class2** is only active if **fission y**.

*Examples:*

**class2 y**

**class2 n**

*Range:* y or n

*Default:* **class2 y**

**Rclass2mom**

Normalization constant for moment of inertia for class II/III states, see Eq. (4.315). On the input line, we read **Rclass2mom**, *Z*, *A*, value, fission barrier. If the number of the fission barrier is not given or is

equal to 0, it concerns the first barrier well.

*Examples:*

**Rclass2mom 90 232 1.15**

**Rclass2mom 94 239 1.1 2**

*Range:*  $0.1 \leq \mathbf{Rclass2mom} \leq 10$ .

*Default:* **Rclass2mom Z A 1**.

### **class2width**

Width of class II/III states. On the input line, we read **class2width**, *Z*, *A*, value, fission barrier. If the number of the fission barrier is not given or is equal to 0, it concerns the first barrier well.

*Examples:*

**class2width 90 232 0.35**

**class2width 94 239 0.15 2**

*Range:*  $0.01 \leq \mathbf{class2width} \leq 10$ .

*Default:* **class2width Z A 0.2**

### **class2file**

File with class II/III transition states. The format of the file is exactly the same as that of the nuclear structure database *talys/structure/fission/states/*. In practice, the user can copy a file from this database, e.g. *class2states.ee*, to the working directory and change it. In this way, changes in the “official” database are avoided. Note that one file in the working directory can only be used for one isotope. On the input line, we read **class2file**, *Z*, *A*, filename.

*Examples:*

**class2file 92 238 u238.c2**

*Range:* **class2file** can be equal to any filename, provided it starts with a character.

*Default:* If **class2file** is not given in the input file, the head band transition states are taken from the *talys/structure/fission/states* database.

### **betafiscor**

Factor to adjust the width of the WKB fission path. (only applies for **fismodel 5**). On the input line, we read **betafiscor**, *Z*, *A*, value.

*Examples:*

**betafiscor 92 239 1.2**

*Range:*  $0.1 \leq \text{betafiscor} \leq 10$ .

*Default:* **betafiscor Z A 1**.

### **vfiscor**

Factor to adjust the height of the WKB fission path. (only applies for **fismodel 5**). On the input line, we read **vfiscor**, Z, A, value.

*Examples:*

**vfiscor 92 239 0.9**

*Range:*  $0.1 \leq \text{vfiscor} \leq 10$ .

*Default:* **vfiscor Z A 1**.

### **Rfiseps**

Ratio for limit for fission cross section per nucleus. This parameter determines whether the mass distribution for a residual fissioning nucleus will be calculated. Cross sections smaller than **Rfiseps** times the fission cross section are not used in the calculations, in order to reduce the computation time.

*Examples:*

**Rfiseps 1.e-5**

*Range:*  $0. \leq \text{Rfiseps} \leq 1$ .

*Default:* **Rfiseps 1.e-3**

### **fymodel**

Model for the calculation of fission yields.

*Examples:*

**fymodel 1:** Brosa model (the only option until TALYS-1.4)

**fymodel 2:** GEF model from Schmidt-Jurado [115]

**fymodel 3:** GEF model from Schmidt-Jurado [115], but evaporation of fission fragments done by Hauser-Feshbach model of TALYS

*Range:*  $1 \leq \text{fymodel} \leq 3$

*Default:* **fymodel 1**

**outfy**

Detailed output of fission yields from each excited bin.

*Examples:*

**outfy y**

**outfy n**

*Range:* y or n

*Default:* **outfy n**

**ffspin**

Flag to enable a choice between spin dependent excitation functions for excited fission fragments as emerging from GEF, or assignment of spin distributions by TALYS. This only applied to **fymodel 3**.

*Examples:*

**ffspin y**

**ffspin n**

*Range:* y or n

*Default:* **ffspin n**

**gefran**

Number of random samples for GEF calculation.

*Examples:*

**gefran 18000**

*Range:*  $1000 \leq \text{gefran} \leq 1000000$

*Default:* **gefran 50000**

**massdis**

Flag for the calculation of the fission-fragment mass distribution.

*Examples:*

**massdis y**

**massdis n**

*Range:* y or n

*Default:* **massdis n**

**ffevaporation**

Flag to enable phenomenological correction for evaporated neutrons from fission fragments with the Brosa model.

*Examples:*

**ffevaporation y**

**ffevaporation n**

*Range:* y or n

*Default:* **ffevaporation n**

**6.2.10 Medical isotope production****production**

Flag to calculate medical isotope production.

*Examples:*

**production y**

**production n**

*Range:* y or n

*Default:* **production n**

**Ebeam**

The incident energy of the particle beam in MeV. This keyword is only active if **production y**.

*Examples:*

**Ebeam 140.**

**Ebeam 16.**

*Range:*  $10^{-11}$  MeV  $\leq$  **Ebeam** < **E<sub>max</sub>** MeV, where **E<sub>max</sub>** is the highest incident energy.

*Default:* None, **Ebeam** must be given if **production y**.

**Eback**

The lower end of the energy range at the back end of the target in MeV. This energy degradation is directly related to the effective thickness of the target. This keyword is only active if **production y**.

*Examples:*

**Eback 130.**

**Eback 12.**

*Range:*  $E_{\min} \leq \mathbf{Eback} < \mathbf{Ebeam}$ , where  $E_{\min}$  is the lowest incident energy.

*Default:*  $\mathbf{Eback} = \mathbf{Ebeam} - 5$  MeV.

### Ibeam

Particle beam current in mA. This keyword is only active if **production y**.

*Examples:*

**Ibeam 0.1**

**Ibeam 5.**

*Range:*  $0 \leq \mathbf{Ibeam} \leq 10000$ .

*Default:*  $\mathbf{Ibeam} 1$ . mA.

### Area

Area of the target in  $\text{cm}^2$ . This keyword is only active if **production y**.

*Examples:*

**Area 1.**

*Range:*  $0 \leq \mathbf{Area} \leq 10000$ .

*Default:*  $\mathbf{Area} 10$ .  $\text{cm}^2$ .

### rho

Material density of the target in  $\text{g}/\text{cm}^3$ . This keyword is only active if **production y**.

*Examples:*

**rho 10.**

*Range:*  $0 \leq \mathbf{rho} \leq 100$ .

*Default:*  $\mathbf{rho} 1$ . is read from a hardwired material density table.

### radiounit

Unit for radioactivity, to be used in the output files for isotope production. This keyword is only active if **production y**.

*The following units are possible:*

**radiounit Bq:** Becquerel

**radiounit kBq:** kiloBecquerel

**radiounit MBq:** MegaBecquerel

**radiounit GBq:** GigaBecquerel

**radiounit Ci:** Curie

**radiounit mCi:** milliCurie

**radiounit kCi:** kiloCurie

*Range:* **radiounit** should be equal to one of the units above.

*Default:* **radiounit Mbq.**

### yieldunit

Unit for isotope yield, in weight or number of isotopes. This keyword is only active if **production y**.

*The following units are possible:*

**yieldunit mug:** microgram

**yieldunit mg:** milligram

**yieldunit g:** gram

**yieldunit kg:** kilogram

**yieldunit num:** number of isotopes

*Range:* **yieldunit** should be equal to one of the units above.

*Default:* **yieldunit num.**

### Tirrad

Irradiation time. A general input for the irradiation time has been enabled. On the input line we read integer values and time units, which can be y (years), d (days), h (hours), m (minutes) or s (seconds). These all need to be separated by blanks. This keyword is only active if **production y**.

*Examples:*

**Tirrad      2 d 5 h**

**Tirrad      32 h 30 m**

**Tirrad      1 d 6 h 24 m 12 s**

*Range:* **0** <= **Tirrad** <= **1e6** for every time unit.

*Default:* **Tirrad 1 d.**

**Tcool**

Target cooling time. A general input for the cooling time has been enabled. On the input line we read integer values and time units, which can be y (years), d (days), h (hours), m (minutes) or s (seconds). These all need to be separated by blanks. This keyword is only active if **production y**.

*Examples:*

**Tcool 2 d 5 h**

**Tcool 32 h 30 m**

**Tcool 1 d 6 m 24 m 12 s**

*Range:*  $0 \leq \text{Tcool} \leq 1e6$  for every time unit.

*Default:* **Tcool 1 d**.

**6.2.11 Output**

The output can be made as compact or as extensive as you like. This can be specified by setting the following keywords. We especially wish to draw your attention to the several keywords that start with "file", at the end of this section. They can be very helpful if you directly want to have specific results available in a single file. Note that if you perform calculations with several incident energies, the files produced with these "file" keywords are incremented *during* the calculation. In other words, you can already plot intermediate results before the entire calculation has finished.

**outmain**

Flag for the main output. The header of TALYS is printed, together with the input variables and the automatically adopted default values. Also the most important computed cross sections are printed.

*Examples:*

**outmain y**

**outmain n**

*Range:* **y** or **n**

*Default:* **outmain y**

**outbasic**

Flag for the output of *all* basic information needed for the nuclear reaction calculation, such as level/bin populations, numerical checks, optical model parameters, transmission coefficients, inverse reaction cross sections, gamma and fission information, discrete levels and level densities. If **outbasic** is set

to **y** or **n**, the keywords **outpopulation**, **outcheck**, **outlevels**, **outdensity**, **outomp**, **outdirect**, **outdiscrete**, **outinverse**, **outgamma** and **outfission** (see below for their explanation) will all be set to the same value automatically. Setting **outbasic y** is generally not recommended since it produces a rather large output file. Less extensive output files can be obtained by enabling some of the aforementioned keywords separately.

*Examples:*

**outbasic y**

**outbasic n**

*Range:* **y** or **n**

*Default:* **outbasic n**

### **outpopulation**

Flag for the output of the population, as a function of excitation energy, spin and parity, of each compound nucleus in the reaction chain before it decays.

*Examples:*

**outpopulation y**

**outpopulation n**

*Range:* **y** or **n**

*Default:* the same value as **outbasic**: **outpopulation n**

### **fisfeed**

Flag for the output of the fission contribution per excitation energy bin. This allows to couple TALYS with e.g. fission yield software, by using the feeding per bin as input for normalization. The associated files have the name *fisZZZAAA.nex* where *ZZZ* is the charge number and *AAA* is the mass number in (i3.3) format.

*Examples:*

**fisfeed y**

**fisfeed n**

*Range:* **y** or **n**

*Default:* **fisfeed n**

**outcheck**

Flag for the output of various numerical checks. This is to check interpolation schemes for the transformation from the emission grid to the excitation energy grid and vice versa, and to test the WFC method by means of flux conservation in the binary compound nucleus calculation. Also, the emission spectra integrated over energy are compared with the partial cross sections, and summed exclusive channel cross sections are checked against total particle production cross sections and residual production cross sections.

*Examples:*

**outcheck y**

**outcheck n**

*Range:* **y** or **n**

*Default:* the same value as **outbasic**: **outcheck n**

**outlevels**

Flag for the output of discrete level information for each nucleus. All level energies, spins parities, branching ratios and lifetimes will be printed.

*Examples:*

**outlevels y**

**outlevels n**

*Range:* **y** or **n**

*Default:* the same value as **outbasic**: **outlevels n**

**outdensity**

Flag for the output of level density parameters and level densities for each residual nucleus.

*Examples:*

**outdensity y**

**outdensity n**

*Range:* **y** or **n**

*Default:* the same value as **outbasic**: **outdensity n**

**outomp**

Flag for the output of optical model parameters for each particle and energy.

*Examples:*

**outomp y**

**outomp n**

*Range:* **y** or **n**

*Default:* the same value as **outbasic**: **outomp n**

**outdirect**

Flag for the output of the results from the direct reaction calculation of ECIS (DWBA, giant resonances and coupled-channels).

*Examples:*

**outdirect y**

**outdirect n**

*Range:* **y** or **n**

*Default:* the same value as **outbasic**: **outdirect n**

**outinverse**

Flag for the output of particle transmission coefficients and inverse reaction cross sections.

*Examples:*

**outinverse y**

**outinverse n**

*Range:* **y** or **n**

*Default:* the same value as **outbasic**: **outinverse n**

**outtransenergy**

Flag for the output of transmission coefficients sorted per energy (**y**) or per angular momentum (**n**). **outtransenergy** is only active if **outinverse y**.

*Examples:*

**outtransenergy y**

**outtransenergy n**

*Range:* y or n

*Default:* outtransenergy y

**outecis**

Flag for keeping the various ECIS output files produced during a TALYS run. This is mainly for diagnostic purposes.

*Examples:*

**outecis y**

**outecis n**

*Range:* y or n

*Default:* outecis n

**outgamma**

Flag for the output of gamma-ray parameters, strength functions, transmission coefficients and reaction cross sections.

*Examples:*

**outgamma y**

**outgamma n**

*Range:* y or n

*Default:* the same value as **outbasic**: **outgamma n**

**outpreequilibrium**

Flag for the output of pre-equilibrium parameters and cross sections. **outpreequilibrium** is only active if **preequilibrium y**.

*Examples:*

**outpreequilibrium y**

**outpreequilibrium n**

*Range:* y or n

*Default:* outpreequilibrium n

**outfission**

Flag for the output of fission parameters, transmission coefficients and partial cross sections. **outfission** is only active if **fission y**.

*Examples:*

**outfission y**

**outfission n**

*Range:* y or n

*Default:* the same value as **outbasic**: **outfission n**

**outdiscrete**

Flag for the output of cross sections to each individual discrete state. This is given for both the direct and the compound component.

*Examples:*

**outdiscrete y**

**outdiscrete n**

*Range:* y or n

*Default:* the same value as **outbasic**: **outdiscrete n**

**adddiscrete**

Flag for the addition of energy-broadened non-elastic cross sections for discrete states to the continuum spectra. **adddiscrete** is only active if **outspectra y**.

*Examples:*

**adddiscrete y**

**adddiscrete n**

*Range:* y or n

*Default:* **adddiscrete y**

**addelastic**

Flag for the addition of energy-broadened elastic cross sections to the continuum spectra. This case is treated separately from **adddiscrete**, since sometimes the elastic contribution is already subtracted from the experimental spectrum. **addelastic** is only active if **outspectra y**.

*Examples:*

**addelastic y**

**addelastic n**

*Range:* y or n

*Default:* the same value as **addiscrete**: **addelastic y**

### **outspectra**

Flag for the output of angle-integrated emission spectra.

*Examples:*

**outspectra y**

**outspectra n**

*Range:* y or n

*Default:* **outspectra y** if only one incident energy is given in the input file, and **outspectra n** for more than one incident energy.

### **outbinspectra**

Flag for the output of emission spectra per compound nucleus bin. **outbinspectra** is only active if **outspectra y** and **population y**.

*Examples:*

**outbinspectra y**

**outbinspectra n**

*Range:* y or n

*Default:* **outbinspectra n**.

### **elwidth**

Width of elastic peak in MeV. For comparison with experimental angle-integrated and double-differential spectra, it may be helpful to include the energy-broadened cross sections for discrete states in the high-energy tail of the spectra. **elwidth** is the width of the Gaussian spreading that takes care of this. **elwidth** is only active if **outspectra y** or if **ddxmode 1, 2** or **3**.

*Examples:*

**elwidth 0.2**

*Range:*  $1.e - 6 \leq \text{elwidth} \leq 100$

*Default:* **elwidth 0.5**

**outangle**

Flag for the output of angular distributions for scattering to discrete states.

*Examples:*

**outangle y**

**outangle n**

*Range:* y or n

*Default:* **outangle n**

**outlegendre**

Flag for the output of Legendre coefficients for the angular distributions for scattering to discrete states.

**outlegendre** is only active if **outangle y**.

*Examples:*

**outlegendre y**

**outlegendre n**

*Range:* y or n

*Default:* **outlegendre n**

**ddxmode**

Option for the output of double-differential cross sections. There are 4 possibilities.

*Examples:*

**ddxmode 0:** No output.

**ddxmode 1:** Output per emission energy as a function of angle (angular distributions).

**ddxmode 2:** Output per emission angle as a function of energy (spectra).

**ddxmode 3:** Output per emission energy and per emission angle.

*Range:*  $0 \leq \text{ddxmode} \leq 3$

*Default:* **ddxmode 0**. If there is a **fileddxe** keyword, see p. 262, in the input file, **ddxmode 1** will be set automatically. If there is a **fileddxa** keyword, see p. 263, in the input file, **ddxmode 2** will be set automatically. If both **fileddxe** and **fileddxa** are present, **ddxmode 3** will be set automatically.

**outdwba**

Flag for the output of DWBA cross sections for the multi-step direct model.

*Examples:*

**outdwba y**

**outdwba n**

*Range:* y or n

*Default:* **outdwba n**

**outgamdis**

Flag for the output of discrete gamma-ray intensities. All possible discrete gamma transitions for all nuclei are followed. In the output they are given in tables per nuclide and for each decay from state to state.

*Examples:*

**outgamdis y**

**outgamdis n**

*Range:* y or n

*Default:* **outgamdis n**

**outexcitation**

Flag for the output of excitation functions, i.e. cross sections as a function of incident energy, such as residual production cross sections, inelastic cross sections, etc.

*Examples:*

**outexcitation y**

**outexcitation n**

*Range:* y or n

*Default:* **outexcitation n** if only one incident energy is given in the input file, and **outexcitation y** for more than one incident energy.

**endf**

Flag for the creation of various output files needed for the assembling of an ENDF-6 formatted file. Apart from the creation of various files that will be discussed for the following keywords, a file *endf.tot*

is created which contains the reaction, elastic and total cross sections (calculated by ECIS) on a fine energy grid. Also a file *decay.X* will be created, with X the ejectile symbol in (a1) format, that contains the discrete gamma decay probabilities for the binary residual nuclides. This will be used for gamma-ray production from discrete binary levels. In addition to all the output detailed below, the continuum gamma-ray spectra per residual nucleus and incident energy will be stored in files *gamZZZA-AAEYYY.YYY.tot*, where where *ZZZ* is the charge number and *AAA* is the mass number in (i3.3) format, and *YYY.YYY* is the incident energy in (f7.3) format. Setting **endf y** will automatically enable many of the “file” keywords given below. All these specific files will be written to output if **endfdetail y**, see the next keyword.

*Examples:*

**endf y**

**endf n**

*Range:* y or n

*Default:* **endf n**

### integral

Keyword to calculate the effective cross section for integral activation measurements, by folding the excitation functions by an experimental flux. In *talys/structure/flux*, we have stored more than 40 spectra, coming from the EASY package [432, 529], which have been used in past activation benchmarks. Obviously, this keyword does not produce a reliable answer for low energies, since TALYS does not cover the resonance range. On the input line, we read **integral**, the cross section filename and the name of the experimental spectrum. The latter should be equal to the extension of the *spectrum*. files in *talys/structure/flux*.

*Examples:*

**integral xs010000.L01 tud\_cucrzt**

**integral xs200000.tot cf252\_flux**

*Range:* Both the cross section file and the flux file should exist.

*Default:* **integral** is not used.

### endfdetail

Flag for detailed ENDF-6 information. Certain ENDF-6 data files, usually those for incident charged particles, only require lumped cross sections, spectra etc. and not all the exclusive channels. The **endfdetail** keyword enables to choose between this. For incident neutrons and photons, it is generally assumed that detailed ENDF-6 info, such as exclusive channels for all separate MT numbers, is required.

*Examples:*

**endfdetail y**

**endfdetail n**

*Range:* **y** or **n**

*Default:* **endfdetail y** for incident neutrons and photons, **endfdetail n** for incident charged particles.

### **ompenergyfile**

File with incident energies to calculate the total, elastic and reaction cross section on a sufficiently precise energy grid for ENDF-6 file purposes. On the input line, we read **ompenergyfile**, filename.

*Examples:*

**ompenergyfile energies.omp**

*Range:* **ompenergyfile** can be equal to any filename, provided it starts with a character. The incident energies should be in the range  $10^{-11}$  MeV to  $< 250$  MeV, whereby the **ompenergyfile** contains at least 1 and a maximum of **numen6** incident energies, where **numen6** is an array dimension specified in *talys.cmb*. Currently **numen6=10000**.

*Default:* **ompenergyfile** is not given in the input file,

### **filedensity**

Flag to write the level density and associated parameters on a separate file *ldZZZAAA.tot*, where *ZZZ* is the charge number and *AAA* is the mass number in (i3.3) format. **filedensity** is only active if **outdensity y**.

*Examples:*

**filedensity y**

**filedensity n**

*Range:* **y** or **n**

*Default:* **filedensity n**

### **fileelastic**

Flag to write the elastic angular distribution on a separate file *XXYYY.YYYang.L00*, where *XX* is the particle symbol in (2a1) format (e.g. *nn* for elastic scattering), and *YYY.YYY* the incident energy in (f7.3) format. The file contains the angle, and 3 columns containing the total, shape elastic, and compound elastic angular distribution, respectively. If in addition **outlegendre y**, the elastic scattering Legendre coefficients will be written on a file *XXYYY.YYYleg.L00*. This file contains the *L*-value, and 4 columns containing the total, direct, compound and normalized Legendre coefficient. **fileelastic** is only active if

**outangle y.***Examples:*

**fileelastic y**, giving files *nm014.000ang.L00*, and (if **outlegendre y**) *nm014.000leg.L00*, for an incident energy of 14 MeV.

**fileelastic n**

*Range:* **y** or **n**

*Default:* **fileelastic n**

**fileangle**

Designator for the output of the non-elastic angular distribution of one specific level on a separate file *PXYYY.YYYang.LMM*, where P and X are the particle symbols in (a1) format for the projectile and ejectile, respectively, YYY.YYY is the incident energy in (f7.3) format, and MM is the level number in (i2.2) format. The file contains the angle and 3 columns with the total inelastic, direct inelastic and compound inelastic angular distribution to the specified level. On the input line we read the level number. The **fileangle** keyword can appear more than once in an input file, one for each level that one is interested in. It will automatically produce files for all ejectiles. If in addition **outlegendre y**, the non-elastic scattering Legendre coefficients will be written on a file *PXYYY.YYYleg.LMM*. This file contains the *L*-value, and 4 columns containing the total, direct, compound and normalized Legendre coefficient. **fileangle** is only active if **outdiscrete y** and **outangle y**.

*Examples:*

**fileangle 2**, giving files *np014.000ang.L02* and (**outlegendre y**) *np014.000leg.L02*, for the (*n, p*) reaction to the second discrete level and an incident energy of 14 MeV, and similarly for the other ejectiles.

*Range:* **0** < **fileangle** < **numlev**. Currently, **numlev=30**

*Default:* **fileangle** not active.

**filechannels**

Flag to write the exclusive channel cross sections as a function of incident energy on separate files. The files will be called *xsNPDTHA.tot*, where N is the neutron number of the exclusive channel, P the proton number, etc., in (a1) format. For example *xs210000.tot* contains the excitation function for  $\sigma(n, 2np)$ , if the incident particle was a neutron. The files contain the incident energy and 3 columns with the exclusive cross section, the associated gamma-ray production cross section, and the fraction of this cross section relative to the total residual production cross section. If in addition isomers can be produced, files called *xsNPDTHA.LMM* will be created with MM the isomeric level number in (i2.2) format. If **filechannels y**, the exclusive binary continuum cross sections, such as continuum inelastic scattering, will also be written to files *PX.con*, where P and X are the particle symbols in (a1) format for

the projectile and ejectile, respectively. If *outspectra y*, the exclusive channel spectra will be written on files *spNPDTHAEYYY.YYY.tot* where YYY.YYY is the incident energy in (f7.3) format. The files contain the incident energy and 6 columns, with the spectra per outgoing particle type. **filechannels** is only active if **channels y**.

*Examples:*

**filechannels y**

**filechannels n**

*Range:* **y** or **n**

*Default:* **filechannels n**

### filespectrum

Designator for the output of the composite particle spectrum for a specific particle type on a separate file. On the input line we read the particle symbols. This will result in files *XspecYYY.YYY.tot*, where X is the outgoing particle symbol in (a1) format, and YYY.YYY the incident energy in (f7.3) format. The file contains the emission energy and 5 columns with the total, direct, pre-equilibrium, multiple pre-equilibrium and compound spectrum, respectively. **filespectrum** is only active if **outspectra y**.

*Examples:*

**filespectrum n p a**, giving files *nspec014.000.tot*, *pspec014.000.tot* and *aspec014.000.tot*, for an incident energy of 14 MeV.

*Range:* **n p d t h a**

*Default:* **filespectrum** not active.

### fileddxe

Designator for the output of double-differential cross sections per emission energy for a specific particle type. On the input line we read the particle type and the emission energy. This will result in files *XddxYYY.Y.mev*, where X is the particle symbol in (a1) format and YYY.Y the emission energy in (f5.1) format. The file contains the emission angle and 5 columns with the total, direct, pre-equilibrium, multiple pre-equilibrium and compound spectrum, respectively. The **fileddxe** keyword can appear more than once in an input file, one for each outgoing energy that one is interested in. If there is at least one **fileddxe** keyword in the input **ddxmode**, see p. 257, will automatically be enabled.

*Examples:*

**fileddxe n 60**. (giving a file *nddx060.0.mev*).

*Range:* **n p d t h a** for the particles and **0**. -  $E_{inc}$  for outgoing energies.

*Default:* **fileddxe** not active.

**fileddxa**

Designator for the output of double-differential cross sections per emission angle for a specific particle type. On the input line we read the particle type and the emission angle. This will result in files *XddxYYY.Y.deg*, where X is the particle symbol in (a1) format and YYY.Y the emission angle in (f5.1) format. The file contains the emission energy and 5 columns with the total, direct, pre-equilibrium, multiple pre-equilibrium and compound spectrum, respectively. The **fileddxa** keyword can appear more than once in an input file, one for each outgoing angle that one is interested in. If there is at least one **fileddxa** keyword in the input **ddxmode**, see p. 257, will automatically be enabled.

*Examples:*

**fileddxa n 30.** (giving a file *nddx030.0.deg*).

*Range:* **n p d t h a** for the particles and **0. - 180.** for outgoing angles.

*Default:* **fileddxa** not active.

**filegamdis**

Flag to write the discrete gamma-ray intensities as a function of incident energy to separate files. This will result in files *gamZZZAAAALYYLMM.tot*, where ZZZ is the charge number and AAA is the mass number in (i3.3) format, YY is the number of the initial discrete state and MM the number of the final discrete state. **filegamdis** is only active if **outgamdis y**.

*Examples:*

**filegamdis y**

**filegamdis n**

*Range:* **y** or **n**

*Default:* **filegamdis n**

**filetotal**

Flag to write all the total cross sections as a function of incident energy on a separate file *total.tot*. The file contains the incident energy, and 9 columns containing the non-elastic, total elastic, total, compound elastic, shape elastic, reaction, compound non-elastic, direct and pre-equilibrium cross section. In addition, the total particle production cross sections will be written on files *Xprod.tot*, with X the particle symbol in (a1) format. Finally, separate x-y tables will be made for the total cross section, on *totalxs.tot*, the total elastic cross section, on *elastic.tot*, and the total nonelastic cross section, on *nonelastic.tot*. **filetotal** is only active if **outexcitation y** or **endf y**.

*Examples:*

**filetotal y**

**filetotal n***Range: y or n**Default: filetotal n***fileresidual**

Flag to write all the residual production cross sections as a function of incident energy on separate files. The files for the total (i.e. the sum over ground state + isomers) residual production cross sections have the name *rpZZZAAA.tot* where *ZZZ* is the charge number and *AAA* is the mass number in (i3.3) format. If a residual nuclide contains one or more isomeric states, there are additional files *rpZZZAAA.LMM*, where *MM* is the number of the isomer (ground state=0) in (i2.2) format. The files contain the incident energy and the residual production cross section. **fileresidual** is only active if **outexcitation y** or **endf y**.  
*Examples:*

**fileresidual y****fileresidual n***Range: y or n**Default: fileresidual n***components**

Flag to write the direct, pre-equilibrium and compound components of the cross sections in the various output files.

*Examples:***components y****components n***Range: y or n**Default: components n***filerecoil**

Flag to write the recoil spectra of the residual nuclides as a function of incident energy on separate files. The files for the recoil spectra have the name *recZZZAAA.specYYY.YYY.tot* where *ZZZ* is the charge number and *AAA* is the mass number in (i3.3) format and *YYY.YYY* the incident energy in (f7.3) format. If in addition **flagchannels y**, there are additional files *spNPDTHAEYYY.YYY.rec*, where *N* is the neutron number of the exclusive channel, *P* the proton number, etc. The files contain the incident energy and the recoil.

*Examples:*

**filerecoil y**

**filerecoil n**

*Range:* y or n

*Default:* **filerecoil n**

### **filefission**

Flag to write all the fission cross sections as a function of incident energy on a separate file *fission.tot*. The file contains the incident energy and the total fission cross section. If in addition *filechannels y*, the exclusive fission cross sections will be written to files *fisNPDTHA.tot*, where N is the neutron number of the exclusive channel, P the proton number, etc., in (a1) format. For example, *fis200000.tot* contains the excitation function for  $\sigma(n, 2nf)$ , also known as the third chance fission cross section. **filefission** is only active if **fission y**.

*Examples:*

**filefission y**

**filefission n**

*Range:* y or n

*Default:* **filefission n**

### **filediscrete**

Designator for the output of the excitation function of one specific non-elastic level on a separate file *PX.LMM*, where P and X are the particle symbols in (a1) format for the projectile and ejectile, respectively, and MM is the level number in (i2.2) format. The file contains the incident energy and 3 columns with the total inelastic, direct inelastic and compound inelastic cross section to the specified level. On the input line we read the level number. The **filediscrete** keyword can appear more than once in an input file, one for each level that one is interested in. It automatically produces a file for each ejectile. **filediscrete** is only active if **outdiscrete y**.

*Examples:*

**filediscrete 2**, giving files *nn.L02*, *np.L02*, etc. for the excitation functions of (inelastic and other) neutron scattering to the second discrete level.

*Range:* **0 < filediscrete < numlev**. Currently, **numlev=30**

*Default:* **filediscrete** not active.

### 6.2.12 Energy-dependent parameter adjustment

TALYS contains hundreds of parameters and most of them are energy-independent. They are ingredients of phenomenological models which have been constructed with, indeed, energy-independent parameters. The OMP parameter  $r_V$ , or the height of the fission barrier, **fisbar** are examples. There are two reasons to deviate from this. First, since these models are a phenomenological representation of reality, there is no strict law that these parameters should be energy-independent. Suppose for example that one tries to use a simple Hill-Wheeler expression to approximate fission paths coming from microscopic analyses, which are supposedly built on a better physical basis. Heights and widths of the fission barriers which are dependent on (in this case, excitation) energy will probably emerge. Then, one may want to use those in calculations.

A second reason is that if physically adequate models fail to fit experimental data, such energy-dependent adjustment can be invoked as a last resort. As long as the deviation from the original model is not too large, unpleasant surprises in the various reaction channels are avoided.

To accommodate this, no less than 65 TALYS keywords (parameters) now have the possibility to be extended with such an energy-dependence.

On the input line, we read the usual keyword and its energy-independent value. If a local variation is required, one adds (1) 4 extra parameters, or (2) a filename, to the input line. With either method a multiplication factor deviating from 1 can be given, as a function of energy. The 4 extra parameters, Ea, Eb, Em and D, drive the following multiplication function

$$\begin{aligned}
 f(E) &= 1 + D' \frac{(E - E_a)^N}{(E - E_a)^N + (C - E_a)^N}, \text{ if } E < E_m \\
 (6.4) \quad &= 1 + D' \frac{(E_b - E)^N}{(E_b - E)^N + (C - E_b)^N}, \text{ if } E \geq E_m
 \end{aligned}$$

where  $N$  is currently fixed to 4, and

$$(6.5) \quad D' = (D - 1) \left(1 + \frac{1}{2}\right)^N$$

and

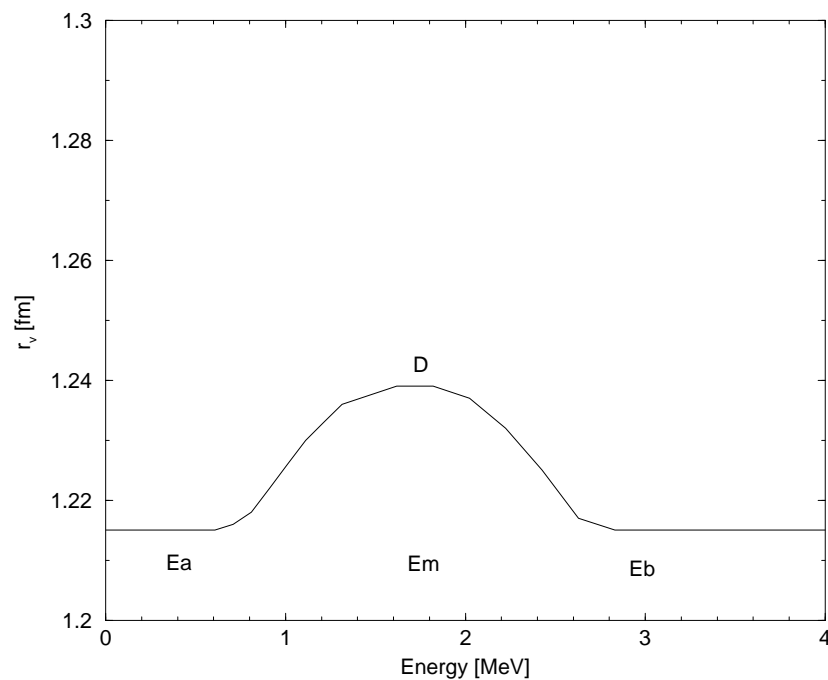
$$\begin{aligned}
 C &= E_a + \frac{1}{2}(E_m - E_a), \text{ if } E < E_m \\
 (6.6) \quad C &= E_m + \frac{1}{2}(E_b - E_m), \text{ if } E \geq E_m
 \end{aligned}$$

An input line would then look as follows:

```
keyword value(s) Ea Eb Em D
```

This means the following: the parameter has a constant value for all energies *outside* the begin energy Ea and end energy Eb. The multiplication function changes smoothly from Ea until Em, and at Em the deviation from the constant value has reached its maximum value D. Between Em and Eb the function changes in the opposite direction until the constant value is reached again at Eb. To ensure some smoothness, Eq. (6.4) was borrowed from the KD03 OMP expression for  $W_V(E)$ . An example for the real volume radius of the optical model is

## Local parameter adjustment

Figure 6.2: Local adjustment of the  $r_v$  parameter for  $^{93}\text{Nb}$ .

```
rvadjust n 1. 0.4 3. 1.7 1.02
```

Suppose we use this input line for neutrons on  $^{93}\text{Nb}$ . The default value for  $r_v$  is 1.215 fm. We do not change this globally, hence the parameter value 1. Next, we change  $r_v$  between 0.4 and 3 MeV with the top (D is positive in this case) at 1.7 MeV. The result is presented in figure rv. One may use several segments, i.e. several input lines, with such local deviations in the same input file, as long as the energy ranges do not overlap (TALYS tests this).

The other option is to use a table with multiplication factors, e.g.

```
rvadjust n myfile.adj
```

where *myfile.adj* looks e.g. as follows

```
0.0 1.
0.4 1.
1.7 1.1
3.0 1.
200 1.
```

which will simply produces a triangle with top at 1.7 MeV. For such simple cases, the use of Eq. (6.4) may be better.

The latter option may be interesting if one manages to fit, in some nuclear structure study, a phenomenological prescription available in TALYS to a more complex microscopic description of a nuclear process. For example, maybe a JLM OMP can be simulated by a Woods-Saxon OMP with energy dependent parameters, or a microscopic fission model by a Hill-Wheeler model with energy dependent fission parameters. The resulting fit can then be used as input file to TALYS.

The energy-dependent adjustment is currently possible for the following keywords.

Optical model: **avadjust, avdadjust, avsoadjust, awadjust, awdadjust, awsoadjust, d1adjust, d2adjust, d3adjust, lv1adjust, lvadjust, lvsoadjust, lw1adjust, lwadjust, lwsoadjust, rcadjust, rvadjust, rvdadjust, rvsoadjust, rwadjust, rwdadjust, rwsoadjust, tladjust, v1adjust, v2adjust, v3adjust, v4adjust, vso1adjust, vso2adjust, w1adjust, w2adjust, w3adjust, w4adjust, wso1adjust, wso2adjust, adpthcor, aradialcor**

Level density: **ctable, krotconstant, ptable, rspincut, s2adjust**

Gamma-ray strength function: **sgr, sgradjust, spr, spradjust, egr, egradjust, epr, epradjust, etable, ftable, ggr, ggradjust, gnorm, gpr, gpradjust**

Pre-equilibrium: **cbreak, cknock, cstrip, m2constant**

Fission: **fisbar, fisbaradjust, fishw, fishwadjust**

In a previous version of TALYS, this local adjustment was only applicable for the optical model parameters, with a different multiplication function, see e.g. **rvadjustF** on page 193. We now suggest the formalism described above for all parameters.

### 6.2.13 Input parameter table

From all the keywords given above you can see that certain default values depend on mass, energy or other parameters. In table 6.1 we summarize all these dependencies and give the full table of keywords including their relation with each other.

Table 6.1: The keywords of TALYS.

Keyword	Range	Default	Page
a	1. - 100.	table or systematics	227
aadjust	0.5 - 2.	1.	229
abundance	filename	no default	173
adddiscrete	y,n	y	255
addelastic	y,n	y	255
adepthcor	0.5 - 1.5	1.	200
alimit	1. - 100.	systematics	227
alphald	0.01 - 0.2	systematics	227
alphaomp	1 - 8	1	199
angles	1-numang	90	168
anglescont	1-numangcont (36)	36	169
anglesrec	1-numangrec (9)	9	171
aradialcor	0.5 - 1.5	1.	200
area	0. - 10000.	1.	248
astro	y,n	n	172
astroE	0.00001-1.	0.	172
astroex	y,n	n	173
astrogs	y,n	n	172
astroT	0.0001-10.	0.	173
asys	y,n	n	226
autorot	y,n	n	182
avadjust	0.5 - 2.	1.	186
avadjustF	-100 - 100	no default	193
avdadjust	0.5 - 2.	1.	188
avdadjustF	-100 - 100	no default	195
avsoadjust	0.5 - 2.	1.	191
avsoadjustF	-100 - 100	no default	196
awadjust	0.5 - 2.	1.	187
awadjustF	-100 - 100	no default	194
awdadjust	0.5 - 2.	1.	189
awdadjustF	-100 - 100	no default	195
awsoadjust	0.5 - 2.	1.	192
awsoadjustF	-100 - 100	no default	197
axtype	1-5	1 and 2,3 for $N > 144$	240
best	y,n	n	175
bestbranch	y,n	y	176
bestend	y,n	n	176
bestpath	pathname	no default	176
beta2	0. - 1.5	0.-1. (barrier dep.)	235
betafiscor	0.1 - 10.	1.	244
betald	0. - 0.5	systematics	227
bins	0, 2 - numbins (100)	40	160

Continuation of **Table 6.1.**

Keyword	Range	Default	Page
branch	0 - numlev	no default	164
breakupmodel	1 - 2	1	223
Cbreak	0. - 10.	1.	222
cfermi	0. - 1000.	10.	234
cfermibf	0. - 1000.	10.	234
cglobal	-10. - 10.	1.	236
channelenergy	y,n	n	171
channels	y,n	n	169
Cknock	0. - 10.	1.	222
class2	y,n	n	243
class2file	filename	no default	244
class2width	0.01 - 10.	0.2	244
colenhance	y,n [Z,A]	n	225
colldamp	y,n	n	225
components	y,n	n	264
compound	y,n	y	203
core	-1,1	-1	202
coulomb	y,n	y	184
cpang	y,n	n	185
Cstrip	0. - 10.	1.	222
ctable	-10. - 10.	1.	236
ctmglobal	y,n	n	225
D0	1.e-6 - 10000.	table	211
d1adjust	0.2 - 5.	1.	189
d2adjust	0.2 - 5.	1.	189
d3adjust	0.2 - 5.	1.	190
ddxmode	0 - 3	0	257
deformfile	filename	no default	202
deltaW	-20. - 20.	calculated	230
deuteronomp	1 - 5	1	199
disctable	1 - 3	1	163
dispersion	y,n	n	180
E0	-10. - 10.	calculated	231
E0adjust	0.1 - 10.	1.	232
E1file	filename	no default	212
Eback	0. - Ebeam	Ebeam - 5.	247
Ebeam	0. - Ein	no default	247
eciscalc	y,n	y	183
eciscompound	y,n	n	204
ecisdwba	y,n	y	223
ecissave	y,n	n	183

Continuation of **Table 6.1.**

Keyword	Range	Default	Page
egr	1. - 100.	table or systematics	209
egradjust	0.1 - 10.	1.	210
ejectiles	g n p d t h a	g n p d t h a	158
Ejoin	0. - 1000.	200.	192
electronconv	y,n	n	209
element	3 - 124 or Li - C4	no default	154
Elow	1.e-6 - 1.	$D_0$	166
elwidth	1.e-6 - 100.	0.5	256
Emsdmin	>0.	Eninc/5.	224
endf	y,n	n	258
endfdetail	y,n	y for n,g; n otherwise	259
endfecis	y,n	y	184
energy	1.e-11 - 250.	no default	155
epr	1. - 100.	no default	214
egradjust	0.1 - 10.	1.	215
equidistant	y,n	n	161
Estop	1.e-5 - 1000.	1000.	168
Esurf	0. - 38.	systematics	219
etable	-10. - 10.	0.	212
Exmatch	0.1 - 20.	calculated	231
Exmatchadjust	0.1 - 10.	1.	232
expmass	y,n	y	165
ffevaporation	y,n	n	247
ffspin	y,n	n	246
fileangle	0 - numlev	no default	261
filechannels	y,n	n	261
fileddxa	n,...,a 0. - 180.	no default	263
fileddxe	n,...,a 0. - energy	no default	262
filedensity	y,n	n	260
filediscrete	0 - numlev	no default	265
fileelastic	y,n	n	260
filefission	y,n	n	265
filegamdis	y,n	n	263
filerecoil	y,n	n	264
fileresidual	y,n	n	264
filespectrum	g n p d t h a	no default	262
filetotal	y,n	n	263
fisbar	0. - 100.	table or systematics	241
fisbaradjust	0.1 - 10.	1.	242
fisfeed	y,n	n	251
fishw	0.01 - 10.	table or systematics	241

Continuation of **Table 6.1.**

Keyword	Range	Default	Page
fishwadjust	0.1 - 10.	1.	242
fismodel	1 - 5	1	240
fismodelalt	3 - 4	4	240
fiso	0.01 - 100.	1.5, 2 or 5 (nuc-dep)	213
fission	y,n, $A \geq 56$	y for mass > 209, n for mass $\leq$ 209	239
ftable	0.1 - 10.	1.	212
fullhf	y,n	n	204
fymodel	1 - 3	1	245
g	0.1-100.	systematics	237
gamgam	0. - 10.	table or systematics	211
gamgamadjust	0.1 - 10.	1.	211
gammald	0.01 - 1.	systematics	228
gammashell1	0. - 1.	systematics	228
gammashell2	0. - 0.2	0.	228
gammax	1 - 6	2	207
gefran	1000 - 1000000	50000	246
ggr	1. - 100.	table or systematics	210
ggradjust	0.1 - 10.	1.	210
giantresonance	y,n	y for n,p; n otherwise	202
gn	0.1 - 100.	systematics	238
gnadjust	0.5 - 2.	1.	239
gnorm	0. - 100. or -1.	calculated	207
gp	0.1 - 100.	systematics	238
gpadjust	0.5 - 2.	1.	238
gpr	1. - 100.	no default	215
gpradjust	0.1 - 10.	1.	216
group	y,n	n	206
gshell	y,n	n	239
hbstate			243
hbtransfile	filename	no default	243
Ibeam	0. - 10000.	1.	248
incadjust	y,n	y	182
inccalc	y,n	y	184
integral	filenames	no default	259
isomer	0. - 1.e38	1.	166
jlmmode	0 - 3	1	180
jlmomp	y,n	n	180
Kph	1. - 100.	15.	237
Krotconstant	0.01 - 100.	1.	235
kvibmodel	1 - 2	2	229

Continuation of **Table 6.1.**

Keyword	Range	Default	Page
labddx	y,n	n	170
ldmodel	1 - 6 [Z,A]	1	224
ldmodelracap	1 - 3	1	213
levelfile	filename	no default	163
Liso	0 - numlev	no default	164
localomp	y,n	y	179
Ltarget	0 - numlev	0	159
lurr	1 - numl	2	205
lv1adjust	0.5 - 1.5	1.	198
lvadjust	0.5 - 1.5	1.	197
lvsoadjust	0.5 - 1.5	1.	198
lw1adjust	0.5 - 1.5	1.	198
lwadjust	0.5 - 1.5	1.	198
lwsoadjust	0.5 - 1.5	1.	199
M1file	filename	no default	212
M2constant	0. - 100.	1.	220
M2limit	0. - 100.	1.	220
M2shift	0. - 100.	1.	220
mass	0, 5 - 339	no default	155
massdir	filename	no default	166
massdis	y,n	n	246
massexcess	-500. - 500.	mass table	165
massmodel	1 - 3	3	164
massnucleus	A-0.5 - A+0.5	mass table	165
maxband	0 - 100	0	201
maxchannel	0 - 8	4	169
maxenrec	0 - numenrec (25)	10	171
maxlevelsbin	0 - numlev	10 (g,n,p,a) and 5 (d,t,h)	162
maxlevelsres	0 - numlev	10	162
maxlevelstar	0 - numlev	20	162
maxN	0 - numN-2	22	160
maxrot	0 - 10	2	201
maxZ	0 - numZ-2	10	159
micro	y,n	n	113
mpreeqmode	1 - 2	1	218
msdbins	2 - numenmsd/2-1 (8)	6	224
multipreeq	y,n or 0.001 - 250.	20.	217
Nlevels	0 - numlev	equal to maxlevelsres	163
Nlow	0 - 200	2	230
Ntop	0 - 200	table or equal to Nlevels	230
nonthermlev	0 - numlev	not used	173
nulldev	filename	no default	177
ompenergyfile	filename	no default	260

Continuation of **Table 6.1.**

Keyword	Range	Default	Page
omponly	y,n	n	181
onestep	y,n	n	223
optmod	filename	no default	178
optmodall	y,n	n	182
optmodfileN	filename	no default	179
optmodfileP	filename	no default	179
outangle	y,n	y for one energy, n for many	257
outbasic	y,n	n	250
outbinspectra	y,n	n	256
outcheck	y,n	equal to outbasic	252
outdensity	y,n	equal to outbasic	252
outdirect	y,n	equal to outbasic	253
outdiscrete	y,n	equal to outbasic	255
outdwba	y,n	n	258
outecis	y,n	n	254
outexcitation	y,n	n for one energy, y for many	258
outfission	y,n	equal to outbasic	255
outfy	y,n	n	246
outgamdis	y,n	n	258
outgamma	y,n	equal to outbasic	254
outinverse	y,n	equal to outbasic	253
outlegendre	y,n	n	257
outlevels	y,n	equal to outbasic	252
outmain	y,n	y	250
outomp	y,n	equal to outbasic	253
outpopulation	y,n	equal to outbasic	251
outpreequilibrium	y,n	n	254
outspectra	y,n	y for one energy, n for many	256
outtransenergy	y,n	y	253
pair	0. - 10.	systematics	230
pairconstant	0. - 30.	12.	229
pairmodel	1 - 2	1	220
parity	y,n	n	226
partable	y,n	n	175
pglobal	-10. - 10.	0.	237
phmodel	1 - 2	1	237
popeps	0. - 1000.	1.e-3	167
popMeV	y,n	n	168
preeqcomplex	y,n	y	219
preeqmode	1 - 4	2	217
preeqspin	y,n or 1-3	n	218

Continuation of **Table 6.1.**

Keyword	Range	Default	Page
preeqsurface	y,n	y	219
preequilibrium	y,n or 0.001 - 250.	Ex(NL)	216
production	y,n	n	247
projectile	n,p,d,t,h,a,g,0	no default	154
Pshift	-10. - 10.	systematics	233
Pshiftadjust	-10. - 10.	systematics	233
Pshiftconstant	-5. - 5.	0. or 1.09	233
ptable	-10. - 10.	0.	236
racap	y,n	n	213
radialfile	filename	no default	197
radialmodel	1 - 2	2	181
radiounit	(k,M,G)Bq, (m,k)Ci	Gbq	248
rcadjust	0.5 - 2.	1.	192
Rclass2mom	0.1 - 10.	1.	243
reaction	y,n	y	170
recoil	y,n	n	170
recoilaverage	y,n	n	171
relativistic	y,n	y	169
rescuefile	filename	no default	177
reslib	library name, default	default	206
Rfiseps	0. - 1.	1.e-3	245
Rgamma	0. - 100.	2.	222
rho	0. - 100.	from table	248
Rnunu	0. - 100.	1.	221
Rnupi	0. - 100.	1.	221
rotational	n p d t h a	n p	200
Rpinu	0. - 100.	1.	221
Rpipi	0. - 100.	1.	221
Rspincut	0. - 10.	1.	235
Rtransmom	0.1 - 10.	1.	242
rvadjust	0.5 - 2.	1.	186
rvadjustF	-100 - 100	no default	193
rvdadjust	0.5 - 2.	1.	188
rvdadjustF	-100 - 100	no default	195
rvsoadjust	0.5 - 2.	1.	191
rvsoadjustF	-100 - 100	no default	196
rwadjust	0.5 - 2.	1.	187
rwadjustF	-100 - 100	no default	194
rwdadjust	0.5 - 2.	1.	189
rwdadjustF	-100 - 100	no default	195

Continuation of **Table 6.1.**

Keyword	Range	Default	Page
rwsadjust	0.5 - 2.	1.	191
rwsadjustF	-100 - 100	no default	196
S0	0. - 10.	table	211
s2adjust	0.01 - 10.	1.	235
segment	1 - 4	1	161
sfexp	0. - 10.	table or 0.347	214
sfth	0. - 10.	table or 0.5	214
sgr	0. - 10000.	table or systematics	209
sgradjust	0.1 - 10.	1.	210
shellmodel	1 - 2	1	229
skipCN	[Z,A]	no default	207
soswitch	0.1 - 10.	3.	185
spherical	y,n	n	201
spincutmodel	1 - 2	1	226
spr	0. - 10000.	table or systematics	215
spradjust	0.1 - 10.	1.	215
statepot	y,n	n	182
strength	1 - 8	1 for n, 2 for others	208
strengthM1	1 - 2	2	208
strucpath	filename	no default	178
sysreaction	n p d t h a	d t h a	181
T	0.001 - 10.	calculated	231
Tadjust	0.1 - 10.	1.	232
Tcool	0. - 1.e6	1 d	250
Tirrad	0. - 1.e6	1 d	249
Tladjust	0.001 - 1000.	1.	197
transeps	0. - 1.	1.e-8	167
transpower	2 - 20	5	167
Tres	0. - 1.e12	293.16	207
twocomponent	y,n	n	219
Ufermi	0. - 1000.	30.	234
Ufermibf	0. - 1000.	45.	234
upbendc	0. - 1.e-5	0.	216
upbende	0. - 10.	0.	216
urr	y,n	n	205
urnjoy	y,n	y	205
v1adjust	0.2 - 5.	1.	185
v2adjust	0.2 - 5.	1.	185
v3adjust	0.2 - 5.	1.	186
v4adjust	0.2 - 5.	1.	186
vfiscor	0.1 - 10.	1.	245
Vinf	-200. - 0.	-30.	192
vsoladjust	0.2 - 5.	1.	190

Continuation of **Table 6.1.**

Keyword	Range	Default	Page
vso2adjust	0.2 - 5.	1.	190
w1adjust	0.2 - 5.	1.	187
w2adjust	0.2 - 5.	1.	187
w3adjust	0.2 - 5.	1.	188
w4adjust	0.2 - 5.	1.	188
wso1adjust	0.2 - 5.	1.	190
wso2adjust	0.2 - 5.	1.	191
widthfluc	y,n or 0.001 - 20.	S(n)	203
widthmode	0 - 3	1	204
xalphatherm	$10^{-20} - 10^{10}$	table or systematics	174
xscaptherm	$10^{-20} - 10^{10}$	table or systematics	174
xseps	0. - 1000.	1.e-7	167
xsptherm	$10^{-20} - 10^{10}$	table or systematics	175
yieldunit	num, mug, mg, g or kg	num	249



## Verification and validation, sample cases and output

TALYS has been tested both formally (“computational robustness”) and by comparison of calculational results with experimental data. This will be described in the present Chapter. Also a description of the output will be given.

### 7.1 Robustness test with DRIP

One way to test a nuclear model code is to let it calculate results for a huge number of nuclides, and the whole range of projectiles and energies. We have written a little code DRIP, not included in the release, that launches TALYS for complete calculations for all nuclides, from dripline to dripline. Besides checking whether the code crashes, visual inspection of many curves simultaneously, e.g.  $(n,2n)$  excitation functions for 50 different targets, may reveal non-smooth behaviour. Various problems, not only in the TALYS source code itself, but also in the nuclear structure database, were revealed with this approach in the initial development stages.

### 7.2 Robustness test with MONKEY

Chapter 6 contains a description of the more than 340 keywords that can be used in a problem for TALYS. Some of them are flags which can only be set to **y** or **n**. Other keywords can be set to a few or several integer values and there are also keywords whose values may cover a quasi-continuous range between the minimum and maximum possible value that we allow for them. Strictly speaking, the total number of possible input files for TALYS is huge (though theoretically finite, because of the finite precision of a computer), and obviously only a small subset of them corresponds to physically meaningful cases. Indeed, as with many computer codes it is not too difficult to bring a TALYS calculation to a formally successful end, i.e. without crashing, with an input file that represents a completely unphysical case.

Obviously, there is no way to prevent this - the user is supposed to have full responsibility for what she or he is doing - and we can never anticipate what input files are made by other users. Nevertheless, to test the robustness of our code, we wrote a little program called MONKEY which remotely simulates TALYS in the hands of an evil user: It creates an input file for TALYS, using *all* the keywords, with *random* values, and starts a run with it. Each keyword in this input file has a value that remains within the allowed (and very broad) range as specified in Chapter 6. If TALYS is compiled with all checking options (i.e. array out-of-bounds checks, divisions by zero, other over/underflow errors, etc.) enabled and runs successfully for thousands of such random input files without crashing, we can at least say we have tested *computational* robustness to some extent, and that we *may* have probed every corner of the code. We realize that this is not a full-proof method to test TALYS formally on the Fortran level (if there exists such a test!), but MONKEY has helped us to discover a few bugs during development which otherwise would have come to the surface sooner or later. We think it is better that *we* find them first. The ideal result of this procedure would be that TALYS never crashes or stops without giving an appropriate error message. We emphasize that this test alone does obviously not guarantee any physical quality of the results. For that, much more important are the input files that *are* physically meaningful. These are discussed in the next Section.

### 7.3 Validation with sample cases

With this manual, we hope to convince you that a large variety of nuclear reaction calculations can be handled with TALYS. To strengthen this statement, we will discuss many different sample cases. In each case, the TALYS input file, the relevant output and, if available, a graphical comparison with experimental data will be presented. The description of the first sample case is the longest, since the output of TALYS will be discussed in complete detail. Obviously, that output description is also applicable to the other sample cases. The entire collection of sample cases serves as (a) verification of TALYS: the sample output files should coincide, apart from numerical differences of insignificant order, with the output files obtained on your computer, and (b) validation of TALYS: the results should be comparable to experimental data for a widely varying set of nuclear reactions. Table 7.1 tells you what to expect in terms of computer time, and this shows that it thus may take a while (about two hours on a PC) before all sample cases have finished. Running the *verify* script will be worth the wait, since a successful execution of all sample cases will put you on safer ground for your own calculations. In general, we will explain the keywords again as they appear in the input files below. If not, consult Table 6.1, which will tell you where to find the explanation of a keyword.

Finally, from an extensive number of references [133]-[748], you may deduce whether TALYS is the appropriate code to perform the calculation you need.

Sample case	Time	Sample case	Time
1a	0 m 1.27 sec	1b	0 m 1.35 sec
1c	0 m 5.34 sec	1d	0 m 1.39 sec
1e	0 m 1.33 sec	1f	0 m 2.03 sec
1g	0 m 1.24 sec	1h	0 m 2.10 sec
1i	0 m 1.90 sec	2	0 m 34.93 sec
3a	0 m 0.42 sec	3b	0 m 0.41 sec
3c	0 m 0.41 sec	3d	1 m 10.53 sec
4a	0 m 14.19 sec	4b	0 m 9.69 sec
5	27 m 10.36 sec	6a	0 m 8.60 sec
6b	0 m 8.72 sec	7	0 m 10.61 sec
8	2 m 8.51 sec	9	0 m 2.73 sec
10a	0 m 9.04 sec	10b	0 m 27.21 sec
11	0 m 58.63 sec	12	0 m 2.92 sec
13	0 m 33.35 sec	14	17 m 57.55 sec
15	0 m 4.99 sec	16a	0 m 10.82 sec
16b	0 m 10.76 sec	16c	0 m 10.72 sec
16d	0 m 12.24 sec	17a	0 m 21.58 sec
17b	0 m 21.93 sec	17c	0 m 20.66 sec
18a	0 m 4.38 sec	18b	1 m 44.35 sec
19	0 m 1.52 sec	20	0 m 8.76 sec
21	0 m 32.11 sec	22	6 m 37.12 sec
23	29 m 51.22 sec	24	0 m 13.54 sec
25	0 m 10.00 sec	26a	4 m 21.47 sec
26b	4 m 43.42 sec	26c	6 m 39.52 sec
26d	5 m 12.07 sec	27a	0 m 12.81 sec
27b	1 m 15.14 sec	27c	0 m 59.76 sec

Table 7.1: Computation time for the sample cases, run on a Intel XEON X5472 3.0 GHz processor, and TALYS compiled with the Lahey/Fujitsu f95 compiler under Linux Red Hat Enterprise 6.

### 7.3.1 Sample 1: All results for 14 MeV n + <sup>93</sup>Nb

We have included 9 different versions of this sample case, in order to give an impression of the various types of information that can be retrieved from TALYS. Most, but not all, output options will be described, while the remainder will appear in the other sample cases. We have chopped the sample output after column 80 to let it fit within this manual. We suggest to consult the output files in the *samples/* directory for the full results.

#### Case 1a: The simplest input file

The first sample problem concerns the simplest possible TALYS calculation. Consider the following input file that produces the results for a 14 MeV neutron on <sup>93</sup>Nb:

```
#
# General
#
projectile n
element nb
mass 93
energy 14.
```

where the purpose of the lines starting with a “#” is purely cosmetic. This input file called *input* can simply be run as follows:

**talys < input > output**

An output file of TALYS consists of several blocks. Whether these blocks are printed or not depends on the status of the various keywords that were discussed in Chapter 6. By default, the so-called main output is always given (through the default **outmain y**), and we discuss this output in the present sample case. For a single incident energy, a default calculation gives the most important cross sections only. “Most important” is obviously subjective, and probably every user has an own opinion on what should always appear by default in the output. We will demonstrate in the other sample problems how to extract all information from TALYS. The output file starts with a display of the version of TALYS you are using, the name of the authors, and the Copyright statement. Also the physics dimensions used in the output are given:

TALYS-1.9 (Version: December 23, 2017)

Copyright (C) 2015 A.J. Koning, S. Hilaire and S. Goriely  
NRG CEA ULB

Dimensions - Cross sections: mb, Energies: MeV, Angles: degrees

The next output block begins with:

```
##### USER INPUT #####
```

Here, the first section of the output is a print of the keywords/input parameters. This is done in two steps: First, in the block

```
USER INPUT FILE
```

```
#
# General
#
projectile n
element nb
mass 93
energy 14.
```

an exact copy of the input file as given by the user is returned. Next, in the block

```
USER INPUT FILE + DEFAULTS
```

Keyword	Value	Variable	Explanation
#			
# Four main keywords			
#			
projectile	n	ptype0	type of incident particle
element	Nb	Starget	symbol of target nucleus
mass	93	mass	mass number of target nucleus
energy	14.000	eninc	incident energy in MeV
#			
# Basic physical and numerical parameters			
#			
ejectiles	g n p d t h a	outtype	outgoing particles
.....			

a table with all keywords is given, not only the ones that you have specified in the input file, but also all the defaults that are set automatically. The corresponding Fortran variables are also printed, together with a short explanation of their meaning. This table can be helpful as a guide to change further input parameters for a next run. You may also copy and paste the block directly into your next input file.

In the next output block

```
##### BASIC REACTION PARAMETERS #####
```

```
Projectile          : neutron      Mass in a.m.u.      : 1.008665
```

Target : 93Nb Mass in a.m.u. : 92.906378

Included channels:

gamma  
neutron  
proton  
deuteron  
triton  
helium-3  
alpha

1 incident energy (LAB):

14.000

Q-values for binary reactions:

Q(n,g): 7.22755  
Q(n,n): 0.00000  
Q(n,p): 0.69112  
Q(n,d): -3.81879  
Q(n,t): -6.19635  
Q(n,h): -7.72313  
Q(n,a): 4.92559

we print the main parameters that characterize the nuclear reaction: the projectile, target and their masses and the outgoing particles that are included as competitive channels. The incident energy or range of incident energies in the LAB system is given together with the binary reaction Q-values.

The block with final results starts with

```
##### RESULTS FOR E= 14.00000 #####
```

Energy dependent input flags

```
Width fluctuations (flagwidth) : n
Preequilibrium (flagpreeq) : y
Multiple preequilibrium (flagmulpre) : n
Number of continuum excitation energy bins: 40
```

with no further information for the present sample case since no further output was requested. When all nuclear model calculations are done, the most important cross sections are summarized in the main part of the output, in which we have printed the center-of-mass energy, the main (total) cross sections, the inclusive binary cross sections  $\sigma_{n,k}^{inc,bin}$ , see Eq. (3.19), the total particle production cross sections  $\sigma_{n,xn}$  of Eq. (3.20) and the multiplicities  $Y_n$  of Eq. (3.22), and the residual production cross sections. The latter are given first per produced nuclide and isomer. Next, nuclides with the same mass are summed to give mass yield curves. Also, the sum over all the residual cross sections is compared with the non-elastic cross section. Obviously, these two values should be approximately equal.

##### REACTION SUMMARY FOR E= 14.000 #####

Center-of-mass energy: 13.849

1. Total (binary) cross sections

Total = 3.98195E+03  
 Shape elastic = 2.21132E+03  
 Reaction = 1.77063E+03  
 Compound elastic= 6.00478E-04  
 Non-elastic = 1.77063E+03  
 Direct = 3.13938E+01  
 Pre-equilibrium = 4.15372E+02  
 Giant resonance = 6.25327E+01  
 Compound non-el = 1.26133E+03  
 Total elastic = 2.21132E+03

2. Binary non-elastic cross sections (non-exclusive)

gamma = 4.18076E+00  
 neutron = 1.69541E+03  
 proton = 3.82455E+01  
 deuteron= 4.95187E+00  
 triton = 1.81580E-01  
 helium-3= 7.05611E-10  
 alpha = 2.76590E+01

3. Total particle production cross sections

gamma = 2.20703E+03 Multiplicity= 1.24647E+00  
 neutron = 3.08077E+03 Multiplicity= 1.73993E+00  
 proton = 4.06703E+01 Multiplicity= 2.29694E-02  
 deuteron= 4.95187E+00 Multiplicity= 2.79667E-03  
 triton = 1.81580E-01 Multiplicity= 1.02551E-04  
 helium-3= 7.05612E-10 Multiplicity= 3.98509E-13  
 alpha = 2.83527E+01 Multiplicity= 1.60128E-02

4. Residual production cross sections

a. Per isotope

Z	A	nuclide	total cross section	level	isomeric cross section	isomeric ratio	lifetime
41	94	( 94Nb)	1.18322E+00	0	5.99984E-01	0.50708	
				1	5.83234E-01	0.49292	3.76000E+02 sec.
41	93	( 93Nb)	3.23646E+02	0	2.77623E+02	0.85780	

			1	4.60226E+01	0.14220	5.09000E+08 sec.
40	93 ( 93Zr)	2.98798E+01	0	2.98798E+01	1.00000	
41	92 ( 92Nb)	1.37164E+03	0	8.51757E+02	0.62098	
			1	5.19887E+02	0.37902	8.77000E+05 sec.
40	92 ( 92Zr)	1.57424E+01	0	1.57424E+01	1.00000	
40	91 ( 91Zr)	1.81576E-01	0	1.81576E-01	1.00000	
39	90 ( 90Y )	2.53059E+01	0	1.28873E+01	0.50926	
			2	1.24186E+01	0.49074	1.15000E+04 sec.
39	89 ( 89Y )	3.04682E+00	0	1.23419E+00	0.40508	
			1	1.81263E+00	0.59492	1.57000E+01 sec.

b. Per mass

A cross section

```

94 1.18322E+00
93 3.53525E+02
92 1.38739E+03
91 1.81576E-01
90 2.53059E+01
89 3.04682E+00

```

```

Total residual production cross section: 1770.62915
Non-elastic cross section                : 1770.62939

```

At the end of the output, the total calculation time is printed, followed by a message that the calculation has been successfully completed:

```

Execution time:  0 hours  0 minutes  3.88 seconds

```

The TALYS team congratulates you with this successful calculation.

### Case 1b: Discrete state cross sections and spectra

As a first extension to the simple input/output file given above, we will request the output of cross sections per individual discrete level. Also, the cumulated angle-integrated and double-differential particle spectra are requested. This is obtained with the following input file:

```

#
# General
#
projectile n
element nb
mass 93
energy 14.
#

```

```
# Output
#
outdiscrete y
outspectra y
ddxmode 2
filespectrum n p a
fileddxa n 30.
fileddxa n 60.
fileddxa a 30.
fileddxa a 60.
```

In addition to the information printed for case 1a, the cross sections per discrete state for each binary channel are given, starting with the  $(n, \gamma)$  channel,

#### 5. Binary reactions to discrete levels and continuum

(n,g) cross sections:

Inclusive:

Level	Energy	E-out	J/P	Direct	Compound	Total	Origin
0	0.00000	21.07609	6.0+	0.00000	0.00000	0.00000	Preeq
1	0.04090	21.03519	3.0+	0.00000	0.00000	0.00000	Preeq
.....							

after which the inelastic cross section to every individual discrete state of the target nucleus is printed, including the separation in direct and compound, see Eq. (3.16). These are summed, per contribution, to the total discrete inelastic cross section, see Eq. (3.15). To these cross sections, the continuum inelastic cross sections of Eq. (3.17) are added to give the total inelastic cross section (3.14). Finally, the  $(n, \gamma n)$  cross section is also printed. This output block looks as follows

Inelastic cross sections:

Inclusive:

Level	Energy	E-out	J/P	Direct	Compound	Total	Origin
1	0.03077	13.81777	0.5-	0.00670	0.00013	0.00683	Direct
2	0.68709	13.16145	1.5-	0.01311	0.00025	0.01336	Direct
3	0.74386	13.10468	3.5+	4.28791	0.00048	4.28839	Direct
4	0.80849	13.04005	2.5+	0.08705	0.00037	0.08741	Direct
5	0.81025	13.03829	2.5-	3.20756	0.00036	3.20792	Direct
6	0.94982	12.89872	6.5+	7.43461	0.00065	7.43526	Direct
7	0.97000	12.87854	1.5-	0.02590	0.00024	0.02614	Direct
8	0.97891	12.86963	5.5+	6.36403	0.00062	6.36465	Direct
9	1.08257	12.76597	4.5+	5.27768	0.00056	5.27823	Direct

10	1.12676	12.72178	2.5+	0.31992	0.00036	0.32028	Direct
11	1.28440	12.56414	0.5+	0.01591	0.00012	0.01603	Direct
12	1.29000	12.55854	1.5-	0.24336	0.00024	0.24360	Direct
13	1.29715	12.55139	4.5+	0.26629	0.00055	0.26684	Direct
14	1.31515	12.53339	2.5-	0.02135	0.00035	0.02170	Direct
15	1.33000	12.51854	1.5+	0.03001	0.00024	0.03025	Direct
16	1.33516	12.51338	8.5+	0.96835	0.00060	0.96895	Direct
17	1.36400	12.48454	3.5-	0.42107	0.00044	0.42152	Direct
18	1.36970	12.47884	1.5+	0.03173	0.00024	0.03197	Direct
19	1.39510	12.45344	2.5+	0.08954	0.00035	0.08990	Direct
20	1.45420	12.39434	0.5+	0.10706	0.00012	0.10718	Direct
				-----	-----	-----	
Discrete Inelastic:				29.21914	0.00727	29.22641	
Continuum Inelastic:				428.71729	1231.55090	1660.26819	
				-----	-----	-----	
Total Inelastic:				457.93640	1231.55823	1689.49597	
(n,gn) cross section:				1.05107			

This is repeated for the  $(n, p)$  and other channels,

(n,p) cross sections:

Inclusive:

Level	Energy	E-out	J/P	Direct	Compound	Total	Origin
0	0.00000	14.53966	2.5+	0.33165	0.00026	0.33191	Preeq
1	0.26688	14.27278	1.5+	1.10724	0.00017	1.10741	Preeq
2	0.94714	13.59252	0.5+	0.85027	0.00008	0.85035	Preeq
3	1.01800	13.52166	0.5+	0.24244	0.00008	0.24252	Preeq
.....							

The last column in these tables specifies the origin of the direct contribution to the discrete state. "Direct" means that this is obtained with coupled-channels, DWBA or, as in this case, weak coupling, whereas "Preeq" means that the pre-equilibrium cross section is collapsed onto the discrete states, as an approximate method for more exact direct reaction approaches for charge-exchange and pick-up reactions. We note here that the feature of calculating, and printing, the inelastic cross sections for a specific state is of particular interest in the case of excitations, i.e. to obtain this particular cross section for a whole range of incident energies. This will be handled in another sample case.

Since **outspectra y** was specified in the input file, the composite particle spectra for the continuum are also printed. Besides the total spectrum, the division into direct (i.e. smoothed collective effects and giant resonance contributions), pre-equilibrium, multiple pre-equilibrium and compound is given. First we give the photon spectrum,

## 7. Composite particle spectra

Spectra for outgoing gamma

Energy	Total	Direct	Pre-equil.	Mult. preeq	Compound
0.001	1.10530E+01	0.00000E+00	2.22494E-13	0.00000E+00	1.10530E+01
0.002	1.11348E+01	0.00000E+00	2.17671E-12	0.00000E+00	1.11348E+01
0.005	1.13792E+01	0.00000E+00	2.99265E-11	0.00000E+00	1.13792E+01
0.010	1.17873E+01	0.00000E+00	2.25661E-10	0.00000E+00	1.17873E+01
0.020	1.26069E+01	0.00000E+00	1.71084E-09	0.00000E+00	1.26069E+01
0.050	1.54725E+01	0.00000E+00	2.42110E-08	0.00000E+00	1.54725E+01
0.100	3.27488E+01	0.00000E+00	1.71082E-07	0.00000E+00	3.27488E+01
.....					

followed by the neutron spectrum

Spectra for outgoing neutron

Energy	Total	Direct	Pre-equil.	Mult. preeq	Compound
0.001	1.77195E+01	7.72138E-03	9.45985E-02	0.00000E+00	1.76172E+01
0.002	3.53846E+01	7.73366E-03	1.42810E-01	0.00000E+00	3.52340E+01
0.005	8.83650E+01	7.77059E-03	2.69012E-01	0.00000E+00	8.80882E+01
0.010	1.45726E+02	7.83249E-03	4.82712E-01	0.00000E+00	1.45236E+02
0.020	2.71007E+02	7.95765E-03	9.71034E-01	0.00000E+00	2.70028E+02
0.050	5.46087E+02	8.34413E-03	2.85497E+00	0.00000E+00	5.43223E+02
0.100	8.71934E+02	9.02631E-03	6.72888E+00	0.00000E+00	8.65196E+02
.....					

and the spectra for the other outgoing particles. Depending on the value of **ddxmode**, the double-differential cross sections are printed as angular distributions or as spectra per fixed angle. For the present sample case, **ddxmode 2**, which gives

9. Double-differential cross sections per outgoing angle

DDX for outgoing neutron at 0.000 degrees

E-out	Total	Direct	Pre-equil.	Mult. preeq	Compound
0.001	1.41397E+00	1.50567E-03	1.05321E-02	0.00000E+00	1.40193E+00
0.002	2.82124E+00	1.50806E-03	1.59003E-02	0.00000E+00	2.80383E+00
0.005	7.04130E+00	1.51527E-03	2.99548E-02	0.00000E+00	7.00983E+00
0.010	1.16128E+01	1.52734E-03	5.37603E-02	0.00000E+00	1.15575E+01
0.020	2.15979E+01	1.55174E-03	1.08185E-01	0.00000E+00	2.14882E+01
0.050	4.35484E+01	1.62711E-03	3.18426E-01	0.00000E+00	4.32283E+01
0.100	6.96037E+01	1.76013E-03	7.51868E-01	0.00000E+00	6.88501E+01
.....					

followed by the other angles and other particles. A final important feature of the present input file is that some requested information has been written to separate output files, i.e. besides the standard output file, TALYS also produces the ready-to-plot files

```
aspec014.000.tot
nspec014.000.tot
pspec014.000.tot
```

containing the angle-integrated neutron, proton and alpha spectra, and

```
addx030.0.deg
addx060.0.deg
nndx030.0.deg
nndx060.0.deg
```

containing the double-differential neutron and alpha spectra at 30 and 60 degrees.

### Case 1c: Exclusive channels and spectra

As another extension of the simple input file we can print the exclusive cross sections at one incident energy and the associated exclusive spectra. This is accomplished with the input file

```
#
# General
#
projectile n
element nb
mass 93
energy 14.
#
# Output
#
channels y
outspectra y
```

Contrary to the previous sample case, in this case no double-differential cross sections or results per separate file are printed (since it only concerns one incident energy). The exclusive cross sections are given in one table, per channel and per ground or isomeric state. It is checked whether the exclusive cross sections add up to the non-elastic cross section. Note that this sum rule, Eq. (3.25), is only expected to hold if we include enough exclusive channels in the calculation. If **maxchannel 4**, this equality should always hold for incident energies up to 20 MeV. This output block looks as follows:

```
6. Exclusive cross sections
6a. Total exclusive cross sections
```

Emitted particles						cross section	reaction	level	isomeric	i
n	p	d	t	h	a			cross section		
0	0	0	0	0	0	1.18344E+00	(n,g)			
								0	5.75062E-01	
								1	6.08379E-01	
1	0	0	0	0	0	3.26664E+02	(n,n')			
								0	2.74409E+02	
								1	5.22550E+01	
0	1	0	0	0	0	2.96168E+01	(n,p)			
0	0	1	0	0	0	1.04112E+01	(n,d)			
0	0	0	1	0	0	6.70822E-01	(n,t)			
0	0	0	0	0	1	2.73777E+01	(n,a)			
								0	1.35359E+01	
								2	1.38418E+01	
2	0	0	0	0	0	1.35982E+03	(n,2n)			
								0	8.46000E+02	
								1	5.13817E+02	
1	1	0	0	0	0	1.06861E+01	(n,np)			
1	0	0	0	0	1	3.14862E+00	(n,na)			
								0	1.27412E+00	
								1	1.87450E+00	
0	1	0	0	0	1	1.49401E-05	(n,pa)			
Sum over exclusive channel cross sections:						1769.57593				
(n,gn) + (n,gp) +... (n,ga) cross sections:						1.05321				
Total						:	1770.62915			
Non-elastic cross section						:	1770.62939			

Note that the  $(n, np)$  and  $(n, d)$  cross sections add up to the residual production cross section for  $^{92}\text{Zr}$ , as given in the first sample case.

Since **outspectra y**, for each exclusive channel the spectrum per outgoing particle is given. This output block begins with:

#### 6b. Exclusive spectra

Emitted particles						cross section	reaction	gamma cross section
n	p	d	t	h	a			
1	0	0	0	0	0	3.26664E+02	(n,n')	1.00870E+03

#### Outgoing spectra

Energy	gamma	neutron	proton	deuteron	triton	helium-3
0.001	4.06619E+00	2.14250E-03	0.00000E+00	0.00000E+00	0.00000E+00	0.00000E+00
0.002	4.08311E+00	4.22497E-03	0.00000E+00	0.00000E+00	0.00000E+00	0.00000E+00
0.005	4.13354E+00	1.04500E-02	0.00000E+00	0.00000E+00	0.00000E+00	0.00000E+00
0.010	4.21777E+00	2.08288E-02	0.00000E+00	0.00000E+00	0.00000E+00	0.00000E+00

```

0.020 4.38694E+00 4.16553E-02 0.00000E+00 0.00000E+00 0.00000E+00 0.00000E+00
0.050 4.92328E+00 1.04608E-01 0.00000E+00 0.00000E+00 0.00000E+00 0.00000E+00
0.100 6.46225E+00 2.10358E-01 0.00000E+00 0.00000E+00 0.00000E+00 0.00000E+00
.....
      Emitted particles      cross section reaction      gamma cross section
      n   p   d   t   h   a
      1   1   0   0   0   0      1.06861E+01  (n,np)              1.97965E+01

Outgoing spectra

Energy  gamma      neutron      proton      deuteron      triton      helium-3

0.001 6.35050E-02 1.87485E-01 0.00000E+00 0.00000E+00 0.00000E+00 0.00000E+00
0.002 6.94942E-02 3.74836E-01 0.00000E+00 0.00000E+00 0.00000E+00 0.00000E+00
0.005 8.74445E-02 9.36836E-01 0.00000E+00 0.00000E+00 0.00000E+00 0.00000E+00
0.010 1.17368E-01 1.88679E+00 0.00000E+00 0.00000E+00 0.00000E+00 0.00000E+00
0.020 1.77238E-01 3.89497E+00 0.00000E+00 0.00000E+00 0.00000E+00 0.00000E+00
0.050 3.57037E-01 6.03595E+00 0.00000E+00 0.00000E+00 0.00000E+00 0.00000E+00
0.100 6.57333E-01 8.96107E+00 0.00000E+00 0.00000E+00 0.00000E+00 0.00000E+00
0.200 1.58990E+00 1.04045E+01 0.00000E+00 0.00000E+00 0.00000E+00 0.00000E+00
0.300 1.88712E+00 9.88185E+00 0.00000E+00 0.00000E+00 0.00000E+00 0.00000E+00
0.400 2.01034E+00 9.03657E+00 0.00000E+00 0.00000E+00 0.00000E+00 0.00000E+00
0.500 1.41701E+00 8.28305E+00 0.00000E+00 0.00000E+00 0.00000E+00 0.00000E+00
0.600 5.68786E+00 7.59201E+00 0.00000E+00 0.00000E+00 0.00000E+00 0.00000E+00
0.700 8.64822E+00 6.60600E+00 0.00000E+00 0.00000E+00 0.00000E+00 0.00000E+00
0.800 4.28359E+00 5.86945E+00 0.00000E+00 0.00000E+00 0.00000E+00 0.00000E+00
0.900 2.37448E+00 5.09628E+00 0.00000E+00 0.00000E+00 0.00000E+00 0.00000E+00
1.000 2.20641E+00 4.19745E+00 1.23263E-07 0.00000E+00 0.00000E+00 0.00000E+00
.....

```

Note, as explained in Section 3.3.2, that the (n,np) channel is characterized by both a neutron and a proton spectrum.

### Case 1d: Nuclear structure

It is possible to have all the nuclear structure information in the output file. The simplest way is to set **outbasic y**, which means that about everything that can be printed, will be printed. This may be a bit overdone if one is only interested in e.g. discrete levels or level densities. If the keywords **outlevels** and/or **outdensity** are set to **y**, discrete level and level density information will always be given for the target nucleus and the primary compound nucleus. With **outgamma y**, photon strength function information is also given. If we would set, in addition, **outpopulation y**, this info will also be given for all the other residual nuclides that are reached in the reaction chain. The input file for this sample case is

```

#
# General
#

```

```

projectile n
element nb
mass 93
energy 14.
#
# Output
#
outlevels y
outdensity y
outgamma y

```

In addition to the output of case 1a, the separation energies for the six light particles are printed.

```

NUCLEAR STRUCTURE INFORMATION FOR Z= 41 N= 52 ( 93Nb)
Separation energies:
Particle      S
neutron       8.83126
proton        6.04337
deuteron     12.45360
triton       13.39081
helium-3     15.65202
alpha        1.93144

```

In the next output block, the discrete level scheme is printed for the first **maxlevelstar** levels. The discrete level info contains level number, energy, spin, parity, branching ratios and lifetimes of possible isomers. It is also indicated whether the spin (J) or parity (P) of a level is experimentally known or whether a value was assigned to it (see Section 5.4). The “string” of the original ENSDF database is also given, so that the user can learn about possible alternative choices for spin and parity. This output block begins with:

```
Discrete levels of Z= 41 N= 52 ( 93Nb)
```

Number	Energy	Spin	Parity	Branching	Ratio (%)	Lifetime(sec)	Assignment
0	0.0000	4.5	+				
1	0.0308	0.5	-			5.090E+08	
				---->	0	100.0000	
2	0.6871	1.5	-				
				---->	1	100.0000	
3	0.7439	3.5	+				
				---->	0	100.0000	
4	0.8085	2.5	+				
				---->	3	2.1751	
				---->	0	97.8249	
.....							

Since **outdensity y**, we print all the level density parameters that are involved, as discussed in Section 4.7: the level density parameter at the neutron separation energy  $a(S_n)$ , the experimental and theoretical

average resonance spacing  $D_0$ , the asymptotic level density parameter  $\tilde{a}$ , the shell damping parameter  $\gamma$ , the pairing energy  $\Delta$ , the shell correction energy  $\delta W$ , the matching energy  $E_x$ , the last discrete level, the levels for the matching problem, the temperature  $T$ , the back-shift energy  $E_0$ , the discrete state spin cut-off parameter  $\sigma$  and the spin cut-off parameter at the neutron separation energy. Next, we print a table with the level density parameter  $a$ , the spin cut-off parameter and the level density itself, all as a function of the excitation energy. This output block begins with:

Level density parameters for Z= 41 N= 52 ( 93Nb)

Model: Gilbert-Cameron

Collective enhancement: no

a(Sn) : 12.33543

Experimental D0 : 0.00 eV +- 0.00000

Theoretical D0 : 77.69 eV

Asymptotic a : 12.24515

Damping gamma : 0.09559

Pairing energy : 1.24434

Shell correction: 0.10845

Last disc. level: 20

Nlow : 5

Ntop : 15

Matching Ex : 7.63849

Temperature : 0.86816

E0 : -1.36134

Adj. pair shift : 0.00000

Discrete sigma : 2.78158

Sigma (Sn) : 4.57840

Level density per parity for ground state

(Total level density summed over parity)

Ex	a	sigma	total	JP= 0.5	JP= 1.5	JP= 2.5	JP= 3.5	JP= 4.5
----	---	-------	-------	---------	---------	---------	---------	---------

0.25	12.372	2.782	3.685E+00	4.465E-01	7.356E-01	7.987E-01	6.774E-01	4.734E-0
------	--------	-------	-----------	-----------	-----------	-----------	-----------	----------

0.50	12.372	2.782	4.915E+00	5.955E-01	9.810E-01	1.065E+00	9.035E-01	6.313E-0
------	--------	-------	-----------	-----------	-----------	-----------	-----------	----------

0.75	12.372	2.782	6.555E+00	7.942E-01	1.308E+00	1.421E+00	1.205E+00	8.420E-0
------	--------	-------	-----------	-----------	-----------	-----------	-----------	----------

1.00	12.372	2.782	8.742E+00	1.059E+00	1.745E+00	1.895E+00	1.607E+00	1.123E+0
------	--------	-------	-----------	-----------	-----------	-----------	-----------	----------

.....

Finally, a comparison of the total level density with the cumulative number of discrete levels is given,

Discrete levels versus total level density

Energy Level	N_cumulative
--------------	--------------

0.9498	6	7.125
--------	---	-------

0.9700	7	7.462
--------	---	-------

0.9789	8	7.614
--------	---	-------

1.0826	9	9.491
1.1268	10	10.363
1.2844	11	13.856
1.2900	12	13.992
1.2972	13	14.167

.....

Note also that, since **outdensity y** by default implies **filedensity y**, the files *ld041093.tot* and *ld041094.tot* have been created. They contain all level density parameters and a comparison between cumulated discrete levels and the integrated level density.

With **outgamma y** the gamma-ray information is printed. First, all relevant parameters are given: the total radiative width  $\Gamma_\Gamma$ , the s-wave resonance spacing  $D_0$ , the s-wave strength function  $S_0$  and the normalization factor for the gamma-ray strength function. Second, we print the giant resonance information. For each multipolarity, we print the strength of the giant resonance  $\sigma_0$ , its energy and its width. Next, the gamma-ray strength function and transmission coefficients for this multipolarity and as a function of energy are printed. This output block begins with:

```
##### GAMMA STRENGTH FUNCTIONS, TRANSMISSION COEFFICIENTS AND CROSS SECTIO
```

```
Gamma-ray information for Z= 41 N= 53 ( 94Nb)
```

```
S-wave strength function parameters:
```

```
Exp. total radiative width= 0.14500 eV +/- 0.01000 Theor. total radiative wid
Exp. D0                      = 80.00 eV +/- 10.00 Theor. D0
Exp. S-wave strength func.= 0.45000E-4 +/- 0.07000 Theor. S-wave strength fun
Normalization factor        = 0.70061
```

```
Gamma-ray strength function model for E1: Kopecky-Uhl
```

```
Normalized gamma-ray strength functions and transmission coefficients for l= 1
```

```
Giant resonance parameters :
```

```
sigma0(M1) = 2.515          sigma0(E1) = 192.148
  E(M1) = 9.017            E(E1) = 16.523
gamma(M1) = 4.000          gamma(E1) = 5.515
  k(M1) = 8.67373E-08      k(E1) = 8.67373E-08
```

E	f(M1)	f(E1)	T(M1)	T(E1)
0.001	0.00000E+00	1.36200E-08	0.00000E+00	8.55769E-17
0.002	7.39798E-13	1.36205E-08	3.71863E-20	6.84642E-16
0.005	1.84950E-12	1.36221E-08	1.45259E-18	1.06988E-14
0.010	3.69900E-12	1.36248E-08	2.32415E-17	8.56071E-14
0.020	7.39805E-12	1.36301E-08	3.71867E-16	6.85126E-13
0.050	1.84960E-11	1.36461E-08	1.45267E-14	1.07176E-11

```

0.100  3.69981E-11  1.36725E-08  2.32466E-13  8.59069E-11
.....

```

which is repeated for each  $l$ -value. Finally, the photoabsorption cross section is printed:

Photoabsorption cross sections

```

      E      reaction
0.001  2.2413E-04
0.002  5.5010E-04
0.005  1.2228E-03
0.010  2.3445E-03
0.020  4.5901E-03
0.050  1.1345E-02
0.100  2.2662E-02
0.200  4.5515E-02
0.300  6.8659E-02
0.400  9.2090E-02
0.500  1.1581E-01
.....

```

### Case 1e: Detailed pre-equilibrium information

The single- and double-differential spectra have already been covered in sample 1b. In addition to this, the contribution of the pre-equilibrium mechanism to the spectra and cross sections can be printed in more detail with the **outpreequilibrium** keyword. With the input file

```

#
# General
#
projectile n
element nb
mass 93
energy 14.
#
# Output
#
outpreequilibrium  y
outspectra        y
ddxmode           2

```

we obtain, in addition to the aforementioned output blocks, a detailed outline of the pre-equilibrium model used, in this case the default: the two-component exciton model. First, the parameters for the exciton model are printed, followed by the matrix elements as a function of the exciton number:

##### PRE-EQUILIBRIUM #####

+++++++ TWO-COMPONENT EXCITON MODEL ++++++

1. Matrix element for E= 21.076

Constant for matrix element : 1.000  
 p-p ratio for matrix element: 1.000  
 n-n ratio for matrix element: 1.500  
 p-n ratio for matrix element: 1.000  
 n-p ratio for matrix element: 1.000

p(p)	h(p)	p(n)	h(n)	M2pipi	M2nunu	M2pinu	M2nupi
0	0	1	0	2.63420E-05	3.95131E-05	2.63420E-05	2.63420E-05
0	0	2	1	1.08884E-04	1.63327E-04	1.08884E-04	1.08884E-04
1	1	1	0	1.08884E-04	1.63327E-04	1.08884E-04	1.08884E-04
0	0	3	2	1.76643E-04	2.64964E-04	1.76643E-04	1.76643E-04
1	1	2	1	1.76643E-04	2.64964E-04	1.76643E-04	1.76643E-04

.....

Next, the emission rates are printed: first as function of particle type and particle-hole number, and in the last column summed over particles:

2. Emission rates or escape widths

A. Emission rates ( /sec)

p(p)	h(p)	p(n)	h(n)	gamma	neutron	proton	deuteron	triton
0	0	1	0	2.16570E+18	0.00000E+00	0.00000E+00	0.00000E+00	0.00000E+0
0	0	2	1	5.29285E+17	1.63578E+21	0.00000E+00	0.00000E+00	0.00000E+0
1	1	1	0	5.58040E+17	8.15540E+20	2.32728E+20	2.79804E+19	0.00000E+0
0	0	3	2	1.26381E+17	4.52770E+20	0.00000E+00	0.00000E+00	0.00000E+0
1	1	2	1	1.08464E+17	3.04371E+20	1.11136E+19	3.36637E+18	9.21406E+1

.....

Also, the alternative representation in terms of the escape widths, see Eqs. (4.137) and (4.138), is given,

B. Escape widths (MeV)

p(p)	h(p)	p(n)	h(n)	gamma	neutron	proton	deuteron	triton
0	0	1	0	1.42549E-03	0.00000E+00	0.00000E+00	0.00000E+00	0.00000E+0
0	0	2	1	3.48382E-04	1.07669E+00	0.00000E+00	0.00000E+00	0.00000E+0
1	1	1	0	3.67309E-04	5.36798E-01	1.53184E-01	1.84170E-02	0.00000E+0
0	0	3	2	8.31858E-05	2.98019E-01	0.00000E+00	0.00000E+00	0.00000E+0



```

3.000  0.000  2.733  3.533  2.241E+01  3.745E+01  1.078E+02  1.354E+02  2.627E+01
4.000  0.000  2.733  3.533  2.988E+01  4.994E+01  1.965E+02  2.486E+02  5.453E+01
5.000  0.000  2.733  3.533  3.736E+01  6.242E+01  3.116E+02  3.959E+02  9.301E+01
6.000  0.000  2.733  3.533  4.483E+01  7.491E+01  4.530E+02  5.774E+02  1.417E+02

```

.....  
Particle-hole spin distributions

n	J= 0	J= 1	J= 2	J= 3	J= 4	J= 5	
1	1.7785E-02	4.3554E-02	4.8369E-02	3.6832E-02	2.1025E-02	9.3136E-03	3.
2	6.3683E-03	1.7261E-02	2.3483E-02	2.4247E-02	2.0773E-02	1.5284E-02	9.
3	3.4812E-03	9.7603E-03	1.4208E-02	1.6237E-02	1.5926E-02	1.3878E-02	1.
4	2.2659E-03	6.4613E-03	9.7295E-03	1.1698E-02	1.2277E-02	1.1642E-02	1.
5	1.6234E-03	4.6764E-03	7.1862E-03	8.9070E-03	9.7354E-03	9.7128E-03	8.

We print a table with the pre-equilibrium cross sections per stage and outgoing energy, for each outgoing particle. At the end of each table, we give the total pre-equilibrium cross sections per particle. Finally the total pre-equilibrium cross section summed over outgoing particles is printed,

+++++++ TOTAL PRE-EQUILIBRIUM CROSS SECTIONS ++++++

Pre-equilibrium cross sections for gamma

E	Total	p=1	p=2	p=3	p=4	p=5	p
0.001	2.2249E-13	9.1810E-14	5.0384E-14	3.8551E-14	4.1750E-14	0.0000E+00	0.000
0.002	2.1767E-12	8.9578E-13	4.9358E-13	3.7794E-13	4.0941E-13	0.0000E+00	0.000
0.005	2.9926E-11	1.2218E-11	6.8126E-12	5.2280E-12	5.6681E-12	0.0000E+00	0.000
0.010	2.2566E-10	9.0941E-11	5.1690E-11	3.9811E-11	4.3221E-11	0.0000E+00	0.000
0.020	1.7108E-09	6.7253E-10	3.9631E-10	3.0739E-10	3.3461E-10	0.0000E+00	0.000
0.050	2.4211E-08	8.9017E-09	5.7581E-09	4.5550E-09	4.9961E-09	0.0000E+00	0.000
0.100	1.7108E-07	5.7425E-08	4.1833E-08	3.4050E-08	3.7774E-08	0.0000E+00	0.000

19.000	1.3505E-01	1.3040E-01	4.3802E-03	2.6369E-04	4.8448E-06	0.0000E+00	0.000
19.500	1.2227E-01	1.1875E-01	3.4007E-03	1.2338E-04	6.6196E-07	0.0000E+00	0.000
20.000	1.1171E-01	1.0895E-01	2.7321E-03	3.1776E-05	0.0000E+00	0.0000E+00	0.000
21.000	0.0000E+00	0.0000E+00	0.0000E+00	0.0000E+00	0.0000E+00	0.0000E+00	0.000
22.000	0.0000E+00	0.0000E+00	0.0000E+00	0.0000E+00	0.0000E+00	0.0000E+00	0.000

1.2864E+00 1.1291E+00 1.2096E-01 2.6279E-02 1.0140E-02 0.0000E+00 0.000

Integrated: 1.28644

Pre-equilibrium cross sections for neutron

E	Total	p=1	p=2	p=3	p=4	p=5	p
---	-------	-----	-----	-----	-----	-----	---

```

0.001 9.4598E-02 0.0000E+00 2.6248E-02 2.5416E-02 2.0231E-02 1.4060E-02 8.642
0.002 1.4281E-01 0.0000E+00 3.9637E-02 3.8373E-02 3.0539E-02 2.1220E-02 1.304
0.005 2.6901E-01 0.0000E+00 7.4728E-02 7.2301E-02 5.7513E-02 3.9941E-02 2.453
0.010 4.8271E-01 0.0000E+00 1.3428E-01 1.2979E-01 1.0316E-01 7.1572E-02 4.391
0.020 9.7103E-01 0.0000E+00 2.7090E-01 2.6131E-01 2.0733E-01 1.4358E-01 8.790
.....
17.500 2.5293E-01 0.0000E+00 0.0000E+00 0.0000E+00 0.0000E+00 0.0000E+00 0.000
18.000 0.0000E+00 0.0000E+00 0.0000E+00 0.0000E+00 0.0000E+00 0.0000E+00 0.000
18.500 0.0000E+00 0.0000E+00 0.0000E+00 0.0000E+00 0.0000E+00 0.0000E+00 0.000
19.000 0.0000E+00 0.0000E+00 0.0000E+00 0.0000E+00 0.0000E+00 0.0000E+00 0.000

2.6727E+01 0.0000E+00 0.0000E+00 0.0000E+00 1.0326E-02 1.1088E-02 4.974

```

Integrated: 26.72690

Total pre-equilibrium cross section: 415.82114

### Case 1f: Discrete direct cross sections and angular distributions

More specific information on the characteristics of direct reactions can be obtained with the following input file,

```

#
# General
#
projectile n
element nb
mass 93
energy 14.
#
# Output
#
outdiscrete      Y
outangle         Y
outlegendre     Y
outdirect       Y
outspectra      Y

```

Now we obtain, through **outdirect y**, the direct cross sections from inelastic collective scattering and giant resonances. The output block begins with

```

+++++++ DIRECT CROSS SECTIONS ++++++
Direct inelastic cross sections
Level Energy E-out J/P Cross section Def. par.
1 0.03077 13.81777 0.5- 0.00670 B 0.00239

```

2	0.68709	13.16145	1.5-	0.01311	B	0.00338
3	0.74386	13.10468	3.5+	4.28791	B	0.04699
4	0.80849	13.04005	2.5+	0.08705	B	0.00873
5	0.81025	13.03829	2.5-	3.20756	B	0.04070
6	0.94982	12.89872	6.5+	7.43461	B	0.06216
.....						
92	12.99300	0.85554	0.5+	0.01342	B	0.01008
93	13.09000	0.75854	3.5-	0.00194	B	0.00797
94	13.54200	0.30654	2.5-	0.00680	B	0.00730
95	13.58100	0.26754	1.5+	0.00089	B	0.00437

Discrete direct inelastic cross section: 29.21914 Level 1- 20  
 Collective cross section in continuum : 45.69146

which for the case of <sup>93</sup>Nb gives the results of the weak-coupling model. For every level, the angular distribution is given, since **outangle y** was specified:

Direct inelastic angular distributions

Angle	Ex= 0.031 JP= 0.5-	Ex= 0.687 JP= 1.5-	Ex= 0.744 JP= 3.5+	Ex= 0.808 JP= 2.5+	Ex= 0.810 JP= 2.5-	Ex= 0.950 JP= 6.5+	E
0.0	1.06392E-03	2.02551E-03	1.31400E+00	1.33822E-02	9.82438E-01	2.27460E+00	1
2.0	1.06611E-03	2.03034E-03	1.30995E+00	1.34149E-02	9.79407E-01	2.26757E+00	1
4.0	1.07266E-03	2.04477E-03	1.29828E+00	1.35125E-02	9.70673E-01	2.24731E+00	1
6.0	1.08348E-03	2.06854E-03	1.28032E+00	1.36731E-02	9.57224E-01	2.21608E+00	1
8.0	1.09840E-03	2.10115E-03	1.25797E+00	1.38933E-02	9.40465E-01	2.17707E+00	1
10.0	1.11708E-03	2.14179E-03	1.23324E+00	1.41675E-02	9.21900E-01	2.13374E+00	1

The table with total giant resonance results is given next,

+++++++ GIANT RESONANCES ++++++

	Cross section	Exc. energy	Emis. energy	Width	Deform. par.
GMR :	0.00000	16.37500	-2.52646	3.00000	0.02456
GQR :	0.00000	14.34671	-0.49817	4.14092	0.14081
LEOR :	24.05840	6.84228	7.00626	5.00000	0.15788
HEOR :	0.00000	25.38264	-11.53410	7.36250	0.13210
Total:	24.05840				

followed, since **outspectra y**, by the associated spectra,

Giant resonance spectra

Energy	Total	GMR	GQR	LEOR	HEOR	Collective
0.001	7.7214E-03	0.0000E+00	0.0000E+00	7.7214E-03	0.0000E+00	0.0000E+00
0.002	7.7337E-03	0.0000E+00	0.0000E+00	7.7337E-03	0.0000E+00	0.0000E+00
0.005	7.7706E-03	0.0000E+00	0.0000E+00	7.7706E-03	0.0000E+00	0.0000E+00
0.010	7.8325E-03	0.0000E+00	0.0000E+00	7.8325E-03	0.0000E+00	0.0000E+00
0.020	7.9577E-03	0.0000E+00	0.0000E+00	7.9577E-03	0.0000E+00	0.0000E+00
0.050	8.3441E-03	0.0000E+00	0.0000E+00	8.3441E-03	0.0000E+00	0.0000E+00
.....						

The total, i.e. direct + compound cross section per discrete level of each residual nucleus was already described for sample 1b. In addition, we have now requested the angular distributions and the associated Legendre coefficients. First, the angular distribution for elastic scattering, separated by direct and compound contribution, is given. Since **outlegendre y** it is given first in terms of Legendre coefficients. This output block begins with:

#### 8. Discrete state angular distributions

##### 8a1. Legendre coefficients for elastic scattering

L	Total	Direct	Compound	Normalized
0	1.75971E+02	1.75971E+02	4.71035E-05	7.95776E-02
1	1.55728E+02	1.55728E+02	0.00000E+00	7.04232E-02
2	1.39720E+02	1.39720E+02	1.86062E-06	6.31840E-02
3	1.21488E+02	1.21488E+02	0.00000E+00	5.49390E-02
4	1.02659E+02	1.02659E+02	3.25580E-07	4.64241E-02
.....				

where the final column means division of the Legendre coefficients by the cross section. This is followed by the associated angular distribution. This output block begins with:

##### 8a2. Elastic scattering angular distribution

Angle	Total	Direct	Compound
0.0	6.69554E+03	6.69554E+03	6.12260E-05
2.0	6.62134E+03	6.62134E+03	6.11570E-05
4.0	6.40317E+03	6.40317E+03	6.09526E-05
6.0	6.05390E+03	6.05390E+03	6.06204E-05
8.0	5.59369E+03	5.59369E+03	6.01725E-05
10.0	5.04824E+03	5.04824E+03	5.96247E-05
12.0	4.44657E+03	4.44657E+03	5.89949E-05
.....			

Next, the Legendre coefficients for inelastic scattering to each discrete level, separated by the direct and compound contribution, is given. This output block begins with:

8b1. Legendre coefficients for inelastic scattering

```

Level 1

```

L	Total	Direct	Compound	Normalized
0	5.43660E-04	5.33254E-04	1.04057E-05	7.95775E-02
1	1.86109E-04	1.86109E-04	0.00000E+00	2.72415E-02
2	6.20916E-05	6.21244E-05	-3.27812E-08	9.08857E-03
3	1.66523E-05	1.66523E-05	0.00000E+00	2.43746E-03
4	-1.37214E-05	-1.35853E-05	-1.36110E-07	-2.00846E-03
5	-1.90397E-05	-1.90397E-05	0.00000E+00	-2.78691E-03
6	-1.61471E-05	-1.61584E-05	1.12224E-08	-2.36352E-03

.....

which is also followed by the associated angular distributions. This output block begins with:

8b2. Inelastic angular distributions

```

Level 1

```

Angle	Total	Direct	Compound
0.0	1.07320E-03	1.06392E-03	9.28143E-06
2.0	1.07540E-03	1.06611E-03	9.28519E-06
4.0	1.08196E-03	1.07266E-03	9.29647E-06
6.0	1.09280E-03	1.08348E-03	9.31533E-06
8.0	1.10774E-03	1.09840E-03	9.34185E-06
10.0	1.12646E-03	1.11708E-03	9.37618E-06
12.0	1.14844E-03	1.13902E-03	9.41848E-06

.....

Finally, the same is given for the  $(n, p)$  and the other channels.

### Case 1g: Discrete gamma-ray production cross sections

The gamma-ray intensity for each mother and daughter discrete level appearing in the reaction can be obtained with the following input file,

```

#
# General
#
projectile n
element nb
mass 93
energy 14.

```

```
#
# Output
#
outgamdis          y
```

For all discrete gamma-ray transitions, the intensity is printed. For each nucleus, the initial level and the final level is given, the associated gamma energy and the cross section. This output block begins with:

#### 10. Gamma-ray intensities

Nuclide: 94Nb

Initial level			Final level			Gamma Energy	Cross section	
no.	J/Pi	Ex	no.	J/Pi	Ex			
2	4.0+	0.0587	---->	1	3.0+	0.0409	0.01780	2.11853E-01
3	6.0+	0.0787	---->	0	6.0+	0.0000	0.07867	2.12745E-01
4	5.0+	0.1134	---->	0	6.0+	0.0000	0.11340	8.56884E-02
4	5.0+	0.1134	---->	2	4.0+	0.0587	0.05470	3.36955E-02
5	2.0-	0.1403	---->	1	3.0+	0.0409	0.09941	2.43882E-01
6	2.0-	0.3016	---->	5	2.0-	0.1403	0.16126	5.42965E-02
7	4.0+	0.3118	---->	2	4.0+	0.0587	0.25311	5.48060E-02

.....

When we discuss multiple incident energy runs in the other sample cases, we will see how the excitation functions for gamma production cross sections per level are accumulated and how they can be written to separate files for easy processing.

#### Case 1h: The full output file

In this sample case we print basically everything that can be printed in the main output file for a single-energy reaction on a non-fissile nucleus. The input file is

```
#
# General
#
projectile n
element nb
mass 93
energy 14.
#
# Output
#
outbasic          y
outpreequilibrium y
```

```

outspectra      Y
outangle        Y
outlegendre     Y
ddxmode        2
outgamdis       Y
partable        Y

```

resulting in an output file that contains all nuclear structure information, all partial results, and moreover all intermediate results of the calculation, as well as results of intermediate checking. Note that basically all flags in the "Output" block on top of the output file are set to **y**, the only exceptions being irrelevant for this sample case. In addition to the output that is already described, various other output blocks are present. First, since **outbasic y** automatically means **outomp y**, a block with optical model parameters is printed. The optical model parameters for all included particles are given as a function of incident energy. This output block begins with:

```
##### OPTICAL MODEL PARAMETERS #####
```

```
neutron on 93Nb
```

Energy	V	rv	av	W	rw	aw	Vd	rvd	avd	Wd	rwd	awd
0.001	51.02	1.215	0.663	0.14	1.215	0.663	0.00	1.274	0.534	3.32	1.274	0.53
0.002	51.02	1.215	0.663	0.14	1.215	0.663	0.00	1.274	0.534	3.32	1.274	0.53
0.005	51.02	1.215	0.663	0.14	1.215	0.663	0.00	1.274	0.534	3.32	1.274	0.53
0.010	51.02	1.215	0.663	0.14	1.215	0.663	0.00	1.274	0.534	3.33	1.274	0.53
0.020	51.02	1.215	0.663	0.14	1.215	0.663	0.00	1.274	0.534	3.33	1.274	0.53

In the next part, we print general quantities that are used throughout the nuclear reaction calculations, such as transmission coefficients and inverse reaction cross sections. The transmission coefficients as a function of energy are given for all particles included in the calculation. Depending upon whether **outtransenergy y** or **outtransenergy n**, the transmission coefficient tables will be grouped per energy or per angular momentum, respectively. The latter option may be helpful to study the behavior of a particular transmission coefficient as a function of energy. The default is **outtransenergy n**, leading to the following output block,

```
##### TRANSMISSION COEFFICIENTS AND INVERSE REACTION CROSS SECTIONS #####
```

```
Transmission coefficients for incident neutron at 0.00101 MeV
```

L	T(L-1/2,L)	T(L+1/2,L)	Tav(L)
0	0.00000E+00	8.82145E-03	8.82145E-03
1	1.45449E-04	2.56136E-04	2.19240E-04

```
Transmission coefficients for incident neutron at 0.00202 MeV
```

L	T(L-1/2,L)	T(L+1/2,L)	Tav(L)
0	0.00000E+00	1.24534E-02	1.24534E-02
1	4.11628E-04	7.24866E-04	6.20454E-04
2	2.55785E-08	1.88791E-08	2.15588E-08

Transmission coefficients for incident neutron at 0.00505 MeV

L	T(L-1/2,L)	T(L+1/2,L)	Tav(L)
0	0.00000E+00	1.96205E-02	1.96205E-02
1	1.62890E-03	2.86779E-03	2.45483E-03
2	2.52135E-07	1.86214E-07	2.12582E-07

.....

which is repeated for each included particle type. Next, the (inverse) reaction cross sections is given for all particles on a LAB energy grid. For neutrons also the total elastic and total cross section on this energy grid is printed for completeness. This output block begins with:

Total cross sections for neutron

E	total	reaction	elastic	OMP reaction
0.00101	1.1594E+04	6.2369E+03	5.3566E+03	6.2369E+03
0.00202	1.0052E+04	4.7092E+03	5.3430E+03	4.7092E+03
0.00505	8.8645E+03	3.5518E+03	5.3127E+03	3.5518E+03
0.01011	8.4660E+03	3.1918E+03	5.2741E+03	3.1918E+03
0.02022	8.4357E+03	3.2208E+03	5.2148E+03	3.2208E+03
0.05054	8.9304E+03	3.8249E+03	5.1055E+03	3.8249E+03
0.10109	9.6344E+03	4.5808E+03	5.0536E+03	4.5808E+03
0.20217	1.0198E+04	5.0370E+03	5.1609E+03	5.0370E+03
0.30326	1.0068E+04	4.7878E+03	5.2799E+03	4.7878E+03
0.40434	9.6390E+03	4.3377E+03	5.3013E+03	4.3377E+03
0.50543	9.1158E+03	3.8893E+03	5.2264E+03	3.8893E+03
0.60651	8.5881E+03	3.5056E+03	5.0825E+03	3.5056E+03
0.70760	8.0915E+03	3.1968E+03	4.8946E+03	3.1968E+03

.....

The final column "OMP reaction" gives the reaction cross section as obtained from the optical model. This is not necessary the same as the adopted reaction cross section of the middle column, since sometimes (especially for complex particles) this is overruled by systematics, see the **sysreaction** keyword, page 181. For the incident energy, we separately print the OMP parameters, the transmission coefficients and the shape elastic angular distribution,

+++++++ OPTICAL MODEL PARAMETERS FOR INCIDENT CHANNEL ++++++

neutron on 93Nb

Energy	V	rv	av	W	rw	aw	Vd	rvd	avd	Wd	rwd	awd
14.000	46.11	1.215	0.663	0.98	1.215	0.663	0.00	1.274	0.534	6.84	1.274	0.53

Optical model results

Total cross section : 3.9819E+03 mb

Reaction cross section: 1.7706E+03 mb

Elastic cross section : 2.2113E+03 mb

Transmission coefficients for incident neutron at 14.000 MeV

L	T(L-1/2,L)	T(L+1/2,L)	Tav(L)
0	0.00000E+00	7.46404E-01	7.46404E-01
1	8.02491E-01	7.78050E-01	7.86197E-01
2	7.77410E-01	8.08483E-01	7.96054E-01
3	7.75550E-01	6.94249E-01	7.29092E-01
4	9.15115E-01	9.53393E-01	9.36381E-01
5	6.01374E-01	6.19435E-01	6.11226E-01
6	7.00430E-01	4.72026E-01	5.77443E-01
7	1.15102E-01	1.90743E-01	1.55444E-01
8	1.59959E-02	1.88919E-02	1.75291E-02
9	2.36267E-03	2.49532E-03	2.43249E-03
10	3.55525E-04	3.61442E-04	3.58625E-04
11	5.38245E-05	5.39431E-05	5.38864E-05
12	8.20113E-06	8.17260E-06	8.18630E-06
13	1.26174E-06	1.25428E-06	1.25788E-06

Shape elastic scattering angular distribution

Angle	Cross section
0.0	6.69554E+03
2.0	6.62134E+03
4.0	6.40317E+03
6.0	6.05390E+03
8.0	5.59369E+03
10.0	5.04824E+03
12.0	4.44657E+03
14.0	3.81867E+03
16.0	3.19323E+03
18.0	2.59561E+03
20.0	2.04638E+03

.....

At some point during a run, TALYS has performed the direct reaction calculation and the pre-equilibrium calculation. A table is printed which shows the part of the reaction population that is left for the formation of a compound nucleus. Since the pre-equilibrium cross sections are calculated on an emission energy grid, there is always a small numerical error when transferring these results to the excitation energy grid. The pre-equilibrium spectra are therefore normalized. The output block looks as follows

```
##### POPULATION CHECK #####

Particle Pre-equilibrium Population

gamma          1.28644      1.27794
neutron        428.71729    410.91696
proton         25.24361     25.20203
deuteron       3.50197      3.49032
triton         0.09480      0.09451
helium-3       0.00000      0.00000
alpha          26.72690     26.64193

+++++++ Normalization of reaction cross section ++++++

Reaction cross section          : 1770.63000 (A)
Sum over T(j,l)                 : 1770.62537 (B)
Compound nucleus formation c.s. : 1243.46240 (C)
Ratio C/B                       :    0.70227
```

After the compound nucleus calculation, the results from the binary reaction are printed. First, the binary cross sections for the included outgoing particles are printed, followed by, if **outspectra y**, the binary emission spectra. If also **outcheck y**, the integral over the emission spectra is checked against the cross sections. The printed normalization factor has been applied to the emission spectra. This output block begins with:

```
##### BINARY CHANNELS #####

+++++++ BINARY CROSS SECTIONS ++++++

gamma   channel to Z= 41 N= 53 ( 94Nb): 2.23665E+00
neutron channel to Z= 41 N= 52 ( 93Nb): 1.68950E+03
proton  channel to Z= 40 N= 53 ( 93Zr): 3.79183E+01
deuteron channel to Z= 40 N= 52 ( 92Zr): 1.04112E+01
triton  channel to Z= 40 N= 51 ( 91Zr): 6.70826E-01
helium-3 channel to Z= 39 N= 52 ( 91Y ): 2.35820E-08
alpha   channel to Z= 39 N= 51 ( 90Y ): 2.98966E+01

Binary emission spectra

Energy  gamma      neutron      proton      deuteron      triton      helium-3
```

0.001	1.14462E-06	1.89788E+00	0.00000E+00	0.00000E+00	0.00000E+00	0.00000E+00	0.00000E+00
0.002	2.28923E-06	3.74165E+00	0.00000E+00	0.00000E+00	0.00000E+00	0.00000E+00	0.00000E+00
0.005	5.72311E-06	9.25456E+00	0.00000E+00	0.00000E+00	0.00000E+00	0.00000E+00	0.00000E+00
0.010	1.14464E-05	1.84461E+01	0.00000E+00	0.00000E+00	0.00000E+00	0.00000E+00	0.00000E+00
0.020	2.28940E-05	3.68901E+01	0.00000E+00	0.00000E+00	0.00000E+00	0.00000E+00	0.00000E+00
0.050	5.72550E-05	9.26411E+01	0.00000E+00	0.00000E+00	0.00000E+00	0.00000E+00	0.00000E+00
0.100	1.14633E-04	1.86293E+02	0.00000E+00	0.00000E+00	0.00000E+00	0.00000E+00	0.00000E+00
0.200	2.30055E-04	3.28686E+02	2.64905E-30	1.35926E-43	0.00000E+00	0.00000E+00	0.00000E+00
0.300	7.48114E-04	4.14446E+02	3.56019E-23	9.99027E-34	9.03852E-41	0.00000E+00	0.00000E+00
0.400	1.81798E-03	4.97986E+02	5.12047E-19	1.48517E-27	3.14528E-33	0.00000E+00	0.00000E+00
0.500	2.88939E-03	5.48371E+02	3.42302E-16	1.47275E-23	2.43692E-28	0.00000E+00	0.00000E+00
0.600	3.96241E-03	5.39365E+02	4.07677E-14	1.28871E-20	9.22918E-25	0.00000E+00	0.00000E+00
0.700	5.03710E-03	5.29973E+02	1.64259E-12	2.45195E-18	5.46266E-22	0.00000E+00	0.00000E+00

.....  
 ++++++++ CHECK OF INTEGRATED BINARY EMISSION SPECTRA ++++++++

	Continuum cross section	Integrated spectrum	Compound normalizatio
gamma	2.19555E+00	2.19555E+00	1.00011E+00
neutron	1.66025E+03	1.64343E+03	1.01805E+00
proton	3.43220E+01	3.43220E+01	1.00226E+00
deuteron	3.51689E+00	3.51689E+00	1.02829E+00
triton	9.54471E-02	9.54471E-02	1.01145E+00
helium-3	2.86109E-10	2.86109E-10	0.00000E+00
alpha	2.86177E+01	2.86176E+01	9.99189E-01

Since **outpopulation y**, the population that remains in the first set of residual nuclides after binary emission is printed,

+++++++ POPULATION AFTER BINARY EMISSION ++++++++

Population of Z= 41 N= 53 ( 94Nb) after binary gamma emission: 2.23665E+00  
 Maximum excitation energy: 21.076 Discrete levels: 10 Continuum bins: 40 Conti

bin	Ex	Popul.	J= 0.0-	J= 0.0+	J= 1.0-	J= 1.0+	J= 2.0-	J= 2.0
0	0.000	3.206E-07	0.000E+00	0.000E+00	0.000E+00	0.000E+00	0.000E+00	0.000E+
1	0.041	1.889E-07	0.000E+00	0.000E+00	0.000E+00	0.000E+00	0.000E+00	0.000E+
2	0.059	2.525E-07	0.000E+00	0.000E+00	0.000E+00	0.000E+00	0.000E+00	0.000E+
3	0.079	1.528E-03	0.000E+00	0.000E+00	0.000E+00	0.000E+00	0.000E+00	0.000E+
4	0.113	3.443E-03	0.000E+00	0.000E+00	0.000E+00	0.000E+00	0.000E+00	0.000E+
5	0.140	1.051E-02	0.000E+00	0.000E+00	0.000E+00	0.000E+00	1.051E-02	0.000E+
6	0.302	9.579E-03	0.000E+00	0.000E+00	0.000E+00	0.000E+00	9.579E-03	0.000E+
7	0.312	1.818E-03	0.000E+00	0.000E+00	0.000E+00	0.000E+00	0.000E+00	0.000E+
8	0.334	4.717E-03	0.000E+00	0.000E+00	0.000E+00	0.000E+00	0.000E+00	0.000E+
9	0.396	6.486E-03	0.000E+00	0.000E+00	0.000E+00	0.000E+00	0.000E+00	0.000E+
10	0.450	3.014E-03	0.000E+00	0.000E+00	0.000E+00	0.000E+00	0.000E+00	0.000E+
11	0.708	3.665E-02	2.036E-04	1.520E-04	1.592E-03	1.152E-03	3.293E-03	2.540E-

```

12  1.224 5.702E-02 2.592E-04 1.935E-04 2.065E-03 1.494E-03 4.428E-03 3.415E-
.....

```

where in this case bins 0-10 concern discrete levels and bins 11-50 concern continuum bins.

After this output of the binary emission, we print for each nuclide in the decay chain the population as a function of excitation energy, spin and parity *before* it decays. This loop starts with the initial compound nucleus and the nuclides formed by binary emission. When all excitation energy bins of the nucleus have been depleted, the final production cross section (per ground state/isomer) is printed. The feeding from this nuclide to all its daughter nuclides is also given. If in addition **outspectra y**, the emission spectra for all outgoing particles from this nucleus are printed. At high incident energies, when generally **multipreeq y**, the result from multiple pre-equilibrium emission is printed (not included in this output). If **outcheck y**, it is checked whether the integral over the emission spectra from this nucleus is equal to the corresponding feeding cross section. This output block begins with:

```
##### MULTIPLE EMISSION #####
```

```
Population of Z= 41 N= 53 ( 94Nb) before decay: 3.58813E+00
```

```
Maximum excitation energy: 21.076 Discrete levels: 10 Continuum bins: 40 Conti
```

bin	Ex	Popul.	J= 0.0	J= 1.0	J= 2.0	J= 3.0	J= 4.0	J= 5.0
0	0.000	1.050E-06	0.000E+00	0.000E+00	0.000E+00	0.000E+00	0.000E+00	0.000E+
1	0.041	6.181E-07	0.000E+00	0.000E+00	0.000E+00	6.181E-07	0.000E+00	0.000E+
2	0.059	8.266E-07	0.000E+00	0.000E+00	0.000E+00	0.000E+00	8.266E-07	0.000E+
3	0.079	1.525E-03	0.000E+00	0.000E+00	0.000E+00	0.000E+00	0.000E+00	0.000E+
4	0.113	3.436E-03	0.000E+00	0.000E+00	0.000E+00	0.000E+00	0.000E+00	3.436E-
5	0.140	1.049E-02	0.000E+00	0.000E+00	1.049E-02	0.000E+00	0.000E+00	0.000E+
6	0.302	9.558E-03	0.000E+00	0.000E+00	9.558E-03	0.000E+00	0.000E+00	0.000E+
7	0.312	1.814E-03	0.000E+00	0.000E+00	0.000E+00	0.000E+00	1.814E-03	0.000E+
8	0.334	4.706E-03	0.000E+00	0.000E+00	0.000E+00	4.706E-03	0.000E+00	0.000E+
9	0.396	6.472E-03	0.000E+00	0.000E+00	0.000E+00	6.472E-03	0.000E+00	0.000E+
10	0.450	3.008E-03	0.000E+00	0.000E+00	0.000E+00	3.008E-03	0.000E+00	0.000E+
11	0.708	3.657E-02	1.517E-04	1.150E-03	2.536E-03	3.531E-03	3.593E-03	2.702E-
12	1.224	5.693E-02	1.939E-04	1.497E-03	3.419E-03	5.023E-03	5.489E-03	4.513E-
13	1.739	6.580E-02	1.843E-04	1.443E-03	3.395E-03	5.210E-03	6.036E-03	5.335E-
14	2.255	7.347E-02	1.744E-04	1.381E-03	3.323E-03	5.274E-03	6.390E-03	5.973E-

```
.....
Emitted flux per excitation energy bin of Z= 41 N= 53 ( 94Nb):
```

bin	Ex	gamma	neutron	proton	deuteron	triton	heli
0	0.000	0.00000E+00	0.00000E+00	0.00000E+00	0.00000E+00	0.00000E+00	0.00000
1	0.041	0.00000E+00	0.00000E+00	0.00000E+00	0.00000E+00	0.00000E+00	0.00000
2	0.059	2.11853E-01	0.00000E+00	0.00000E+00	0.00000E+00	0.00000E+00	0.00000
3	0.079	2.12745E-01	0.00000E+00	0.00000E+00	0.00000E+00	0.00000E+00	0.00000
4	0.113	1.19384E-01	0.00000E+00	0.00000E+00	0.00000E+00	0.00000E+00	0.00000

```

5   0.140 2.43882E-01 0.00000E+00 0.00000E+00 0.00000E+00 0.00000E+00 0.00000
6   0.302 5.42965E-02 0.00000E+00 0.00000E+00 0.00000E+00 0.00000E+00 0.00000

```

.....  
Emission cross sections to residual nuclei from Z= 41 N= 53 ( 94Nb):

```

gamma    channel to Z= 41 N= 53 ( 94Nb): 2.66180E+00
neutron  channel to Z= 41 N= 52 ( 93Nb): 1.05107E+00
proton   channel to Z= 40 N= 53 ( 93Zr): 1.67352E-03
deuteron channel to Z= 40 N= 52 ( 92Zr): 1.07608E-06
triton   channel to Z= 40 N= 51 ( 91Zr): 2.06095E-08
helium-3 channel to Z= 39 N= 52 ( 91Y ): 1.07027E-16
alpha    channel to Z= 39 N= 51 ( 90Y ): 4.69800E-04

```

Emission spectra from Z= 41 N= 53 ( 94Nb):

Energy	gamma	neutron	proton	deuteron	triton	helium-3
0.001	1.14218E-02	5.11503E-03	0.00000E+00	0.00000E+00	0.00000E+00	0.00000E+00
0.002	1.19276E-02	1.10501E-02	0.00000E+00	0.00000E+00	0.00000E+00	0.00000E+00
0.005	1.34434E-02	3.25383E-02	0.00000E+00	0.00000E+00	0.00000E+00	0.00000E+00
0.010	1.59698E-02	7.24291E-02	0.00000E+00	0.00000E+00	0.00000E+00	0.00000E+00
0.020	2.10227E-02	1.27402E-01	0.00000E+00	0.00000E+00	0.00000E+00	0.00000E+00
0.050	4.45166E-02	2.33433E-01	0.00000E+00	0.00000E+00	0.00000E+00	0.00000E+00

.....  
+++++++ CHECK OF INTEGRATED EMISSION SPECTRA ++++++

	Cross section	Integrated spectrum	Average emission energy
gamma	2.66180E+00	2.66180E+00	1.776
neutron	1.05107E+00	1.05107E+00	1.174
proton	1.67352E-03	1.67334E-03	5.377
deuteron	1.07608E-06	7.97929E-07	5.635
triton	2.06095E-08	0.00000E+00	0.000
helium-3	1.07027E-16	0.00000E+00	0.000
alpha	4.69800E-04	4.69563E-04	10.831

Final production cross section of Z= 41 N= 53 ( 94Nb):

```

Total      : 1.18344E+00
Ground state: 5.75062E-01
Level 1    : 6.08379E-01

```

Note that once a new nucleus is encountered in the reaction chain, all nuclear structure information for that nucleus is printed as well.

**Case 1i: No output at all**

It is even possible to have an empty output file. With the following input file,

```
#  
# General  
#  
projectile n  
element nb  
mass 93  
energy 14.  
#  
# Output  
#  
outmain n
```

it is specified that even the main output should be suppressed. The sample output file should be empty. This can be helpful when TALYS is invoked as a subroutine from other programs and the output from TALYS is not required (if the communication is done e.g. through shared arrays or subroutine variables). We have not yet used this option ourselves.

### 7.3.2 Sample 2: Excitation functions: $^{208}\text{Pb}$ (n,n'), (n,2n), (n,p) etc.

Often we are not interested in only one incident energy, but in excitation functions of the cross sections. If more than one incident energy is given in the file specified by the **energy** keyword, it is helpful to have the results, for each type of cross section, in a table as a function of incident energy. TALYS will first calculate all quantities that remain equal for all incident energy calculations, such as the transmission coefficients. Next, it will calculate the results for each incident energy. When the calculation for the last incident energy has been completed, the cross sections are collected and printed as excitation functions in the output if **outexcitation y** (which is the default if there is more than one incident energy). Moreover, we can provide the results in separate files: one file per reaction channel. Consider the following input file

```
#
# General
#
projectile n
element pb
mass 208
energy energies
#
# Parameters
#
gnorm 0.35
Rgamma 2.2
gn 81 208 9.4
gp 81 208 6.2
egr      82 209 12.0      E1 1
optmodfileN 82 pb.omp
#
# Output
#
channels y
filechannels y
filetotal y
fileresidual y
outdiscrete y
```

which provides all partial cross sections for neutrons incident on  $^{208}\text{Pb}$  for 46 incident energies, from 1 to 30 MeV, as given in the file *energies* that is present in this sample case directory. In the main output file, first the results per incident energy are given. At the end of the output file, there is an output block that begins with:

```
##### EXCITATION FUNCTIONS #####
```

The first table contains the most important total cross sections as a function of incident energy. This output block begins with:

## 1. Total (binary) cross sections

Energy	Non-elastic	Elastic	Total	Comp. el.	Shape el.	Reaction
1.000E+00	5.4614E-01	4.8367E+03	4.8372E+03	1.7271E+03	3.1096E+03	1.7276E+03
1.200E+00	6.0181E-01	4.7812E+03	4.7818E+03	1.8195E+03	2.9618E+03	1.8201E+03
1.400E+00	6.7627E-01	4.9406E+03	4.9413E+03	1.9485E+03	2.9921E+03	1.9492E+03
1.600E+00	7.6416E-01	5.2462E+03	5.2469E+03	2.1039E+03	3.1423E+03	2.1046E+03
1.800E+00	8.6914E-01	5.6345E+03	5.6353E+03	2.2653E+03	3.3692E+03	2.2662E+03
2.000E+00	1.0015E+00	6.0464E+03	6.0474E+03	2.4110E+03	3.6354E+03	2.4120E+03
.....						

Next, the binary cross sections are printed. This output block begins with:

## 2. Binary non-elastic cross sections (non-exclusive)

Energy	gamma	neutron	proton	deuteron	triton	helium-3
1.000E+00	1.9672E-01	0.0000E+00	0.0000E+00	0.0000E+00	0.0000E+00	0.0000E+00
1.200E+00	2.4416E-01	0.0000E+00	0.0000E+00	0.0000E+00	0.0000E+00	0.0000E+00
1.400E+00	3.0773E-01	0.0000E+00	0.0000E+00	0.0000E+00	0.0000E+00	0.0000E+00
1.600E+00	3.8879E-01	0.0000E+00	0.0000E+00	0.0000E+00	0.0000E+00	0.0000E+00
1.800E+00	4.9418E-01	0.0000E+00	0.0000E+00	0.0000E+00	0.0000E+00	0.0000E+00
2.000E+00	6.3274E-01	0.0000E+00	0.0000E+00	0.0000E+00	0.0000E+00	0.0000E+00
.....						

Next, the total particle production cross sections are printed. Parts of this output block look as follows:

## 3. Total particle production cross sections

gamma production

Energy Cross section Multiplicity

1.000E+00	2.47648E-01	1.43346E-04
1.200E+00	3.14552E-01	1.72825E-04
1.400E+00	4.06594E-01	2.08595E-04
1.600E+00	5.23101E-01	2.48546E-04
1.800E+00	6.76670E-01	2.98596E-04
2.000E+00	8.80247E-01	3.64945E-04
2.200E+00	1.14449E+00	4.52788E-04
2.400E+00	1.48925E+00	5.70753E-04
.....		

neutron production

Energy Cross section Multiplicity

```

1.000E+00 4.26190E-03 2.46692E-06
1.200E+00 9.15765E-03 5.03151E-06
1.400E+00 1.71089E-02 8.77738E-06
1.600E+00 3.18516E-02 1.51339E-05
1.800E+00 5.42068E-02 2.39200E-05
2.000E+00 8.89349E-02 3.68719E-05
2.200E+00 1.41778E-01 5.60908E-05
2.400E+00 2.20738E-01 8.45971E-05
2.600E+00 3.30648E-01 1.24267E-04
2.800E+00 3.16809E+02 1.17802E-01
.....

```

Next in the output are the residual production cross sections. The output block begins with:

#### 4. Residual production cross sections

Production of Z= 82 A=209 (209Pb) - Total

```

Q-value      =    3.937307
E-threshold=    0.000000

```

Energy Cross section

```

1.000E+00 1.92452E-01
1.200E+00 2.35002E-01
1.400E+00 2.90625E-01
1.600E+00 3.56940E-01
1.800E+00 4.39971E-01
2.000E+00 5.43801E-01
2.200E+00 6.70818E-01
2.400E+00 8.26660E-01
2.600E+00 1.02344E+00
.....

```

and the remaining isotopes follow in decreasing order of mass and isotope.

The final part of the output, for this input file at least, concerns the exclusive reaction cross sections. This output block begins with:

#### 6. Exclusive cross sections

```

      Emitted particles      reaction
      n  p  d  t  h  a
      0  0  0  0  0  0      (n,g)

```

```

Q-value      =    3.937307
E-threshold=    0.000000

```

Energy    Cross section    Gamma c.s.    c.s./res.prod.cs

```

1.000E+00 1.92452E-01 3.48872E-01 1.00000E+00
1.200E+00 2.35002E-01 4.35691E-01 1.00000E+00
1.400E+00 2.90625E-01 5.54769E-01 1.00000E+00
1.600E+00 3.56940E-01 6.97846E-01 1.00000E+00
1.800E+00 4.39971E-01 8.82793E-01 1.00000E+00
2.000E+00 5.43801E-01 1.12074E+00 1.00000E+00

```

.....

```

      Emitted particles        reaction
      n   p   d   t   h   a
      1   1   0   0   0   0        (n,np)

```

Q-value        =    -8.003758

E-threshold=    8.042576

Energy    Cross section    Gamma c.s.    c.s./res.prod.cs

```

1.000E+00 0.00000E+00 0.00000E+00 0.00000E+00
1.200E+00 0.00000E+00 0.00000E+00 0.00000E+00
1.400E+00 0.00000E+00 0.00000E+00 0.00000E+00
1.600E+00 0.00000E+00 0.00000E+00 0.00000E+00
1.800E+00 0.00000E+00 0.00000E+00 0.00000E+00
2.000E+00 0.00000E+00 0.00000E+00 0.00000E+00
2.200E+00 0.00000E+00 0.00000E+00 0.00000E+00

```

.....

```

2.000E+01 3.12374E+00 2.18877E+00 5.08526E-01
2.200E+01 8.55243E+00 8.69348E+00 6.06418E-01
2.400E+01 1.70454E+01 2.30865E+01 6.79074E-01
2.600E+01 2.70534E+01 4.51648E+01 7.31295E-01
2.800E+01 3.62134E+01 6.92506E+01 7.66934E-01
3.000E+01 4.31314E+01 9.02171E+01 7.89711E-01

```

For plotting data, or processing into ENDF-6 data files, it is more practical to have the data in individual output files. Note that, since **filechannels y**, several files with names as e.g. *xs200000.tot* have been created in your working directory. These files contain the entire excitation function per reaction channel. Besides these exclusive cross sections, residual production cross section files are produced (**fileresidual y**). Note that for this reaction, *rp082207.tot* and *xs200000.tot* obviously have equal contents.

We illustrate this sample case with various comparisons with measurements. Since **filetotal y**, a file *total.tot* is created with, among others, the total cross section. The resulting curves are shown in Figs. 7.1 and 7.2.

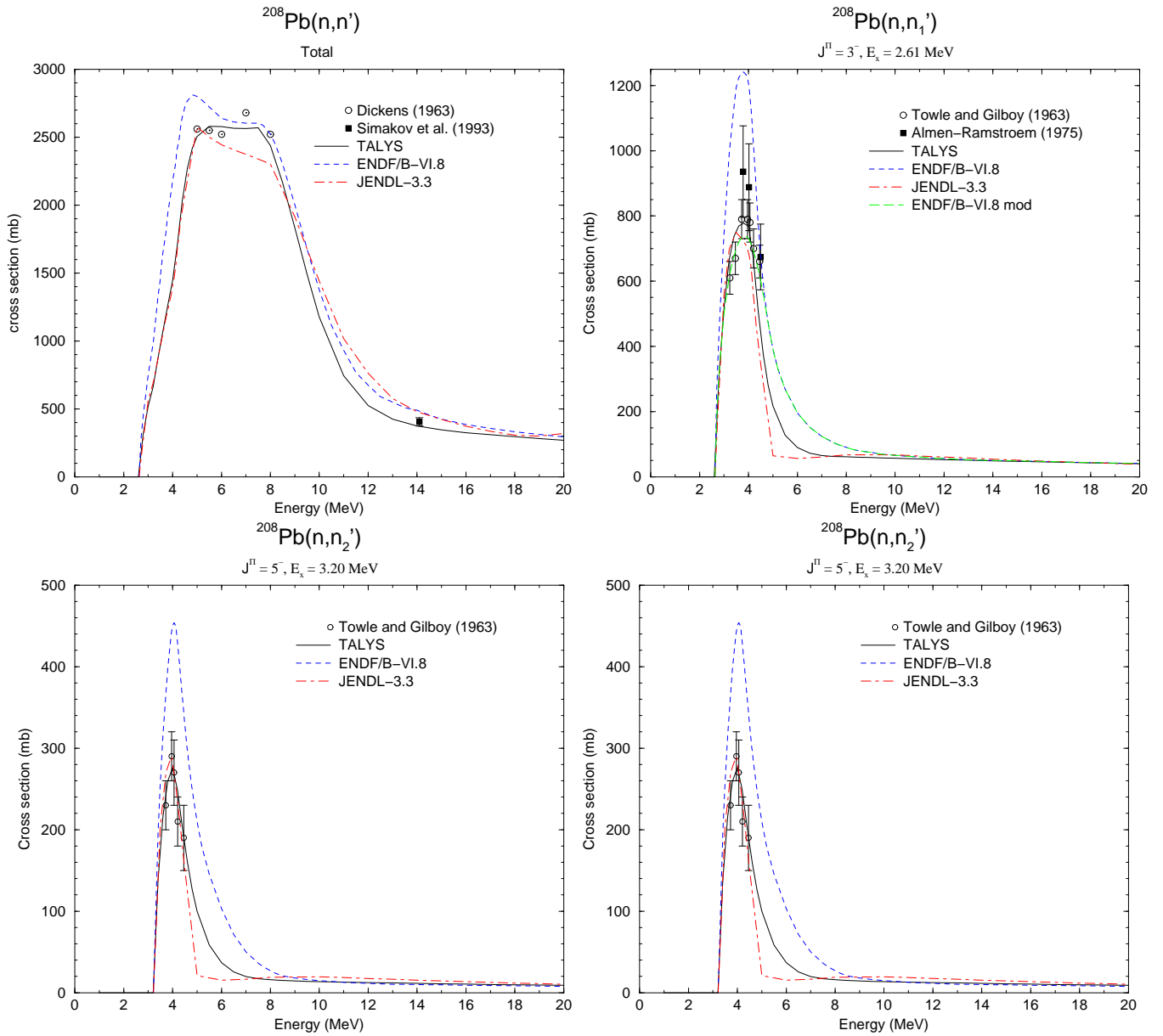
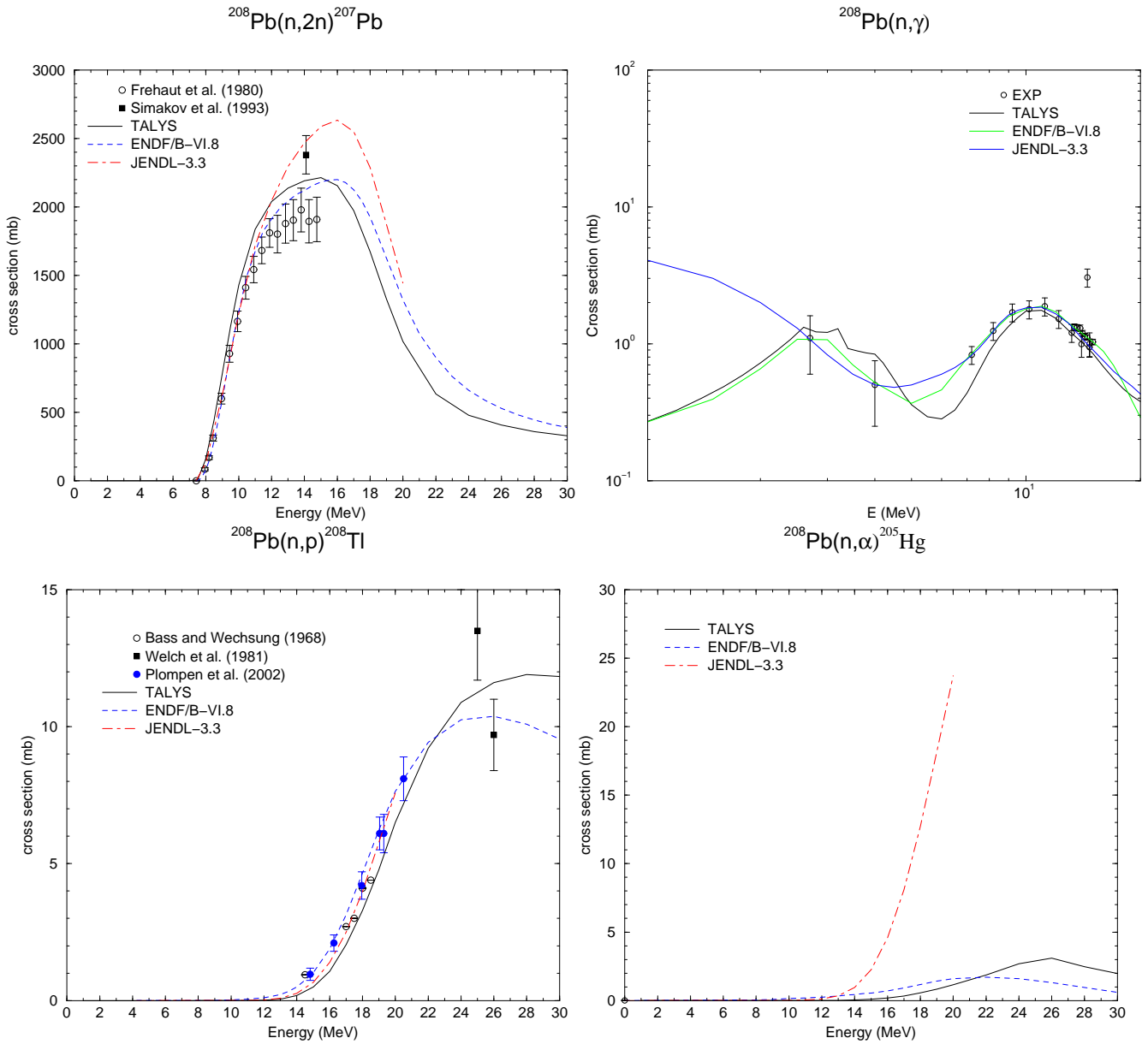


Figure 7.1: Partial cross sections for neutrons incident on  $^{208}\text{Pb}$ .

Figure 7.2: Partial cross sections for neutrons incident on  $^{208}\text{Pb}$ .

### 7.3.3 Sample 3: Comparison of compound nucleus WFC models: 10 keV n + <sup>93</sup>Nb

In this sample case, we demonstrate the difference between the various models for the width fluctuation correction in compound nucleus reactions, as discussed extensively in Ref. [183]. As sample case, we take 10 keV neutrons incident on <sup>93</sup>Nb and we ask for various compound nucleus models to calculate cross sections and angular distributions (**outangle y**), and to put the result for the elastic scattering angular distribution on a separate file, called *nn000.010ang.L00*. Since the GOE calculation (**widthmode 3**) is rather time-consuming, we reduce the number of bins to 20 for all cases. We wish to check whether the flux is conserved in the compound nucleus model for the various WFC models, so we set **outcheck y**. This means that for each set of quantum numbers, unitarity is checked by means of Eq. (4.189).

#### Case 3a: Hauser-Feshbach model

The following input file is used

```
#
# General
#
projectile n
element nb
mass 93
energy 0.01
#
# Parameters
#
bins 20
widthmode 0
#
# Output
#
outcheck y
outangle y
fileelastic y
```

This only new output block, i.e. not discussed before, is

```
+++++++ CHECK OF FLUX CONSERVATION OF TRANSMISSION COEFFICIENTS ++++++
Hauser-Feshbach model

Parity-- J= 3.0 j= 1.5 l= 1 T(j,l)= 7.98822E-03 Sum over outgoing channels
Parity-- J= 4.0 j= 0.5 l= 1 T(j,l)= 4.54100E-03 Sum over outgoing channels
Parity-- J= 4.0 j= 1.5 l= 1 T(j,l)= 7.98822E-03 Sum over outgoing channels
Parity-- J= 5.0 j= 0.5 l= 1 T(j,l)= 4.54100E-03 Sum over outgoing channels
Parity-- J= 5.0 j= 1.5 l= 1 T(j,l)= 7.98822E-03 Sum over outgoing channels
Parity-- J= 6.0 j= 1.5 l= 1 T(j,l)= 7.98822E-03 Sum over outgoing channels
.....
```

Model	$\sigma^{comp-el}$
Hauser-Feshbach	2410.89 mb
Moldauer	2617.22 mb
HRTW	2752.25 mb
GOE	2617.12 mb

Table 7.2: Compound elastic cross section for 4 different compound nucleus models for 10 keV neutrons incident on  $^{93}\text{Nb}$ .

in which the aforementioned unitarity is checked.

### Case 3b: Moldauer model

As for case a, but now with **widthmode 1** in the input file.

### Case 3c: HRTW model

As for case a, but now with **widthmode 2** in the input file.

### Case 3d: GOE model

As for case a, but now with **widthmode 3** in the input file.

Table 7.2 lists the obtained compound nucleus elastic cross section for the 4 cases.

Fig. 7.3 displays the elastic angular distribution for the 4 models. Results like these made us conclude in Ref. [183] that Moldauer's model, which is closest to the exact GOE result, is the one to use in practical applications, especially when considering the calculation times as printed in Table 7.1. Obviously, this sample case can be extended to one with various incident energies, so that the differences between excitation functions can be studied, see also Ref. [183].

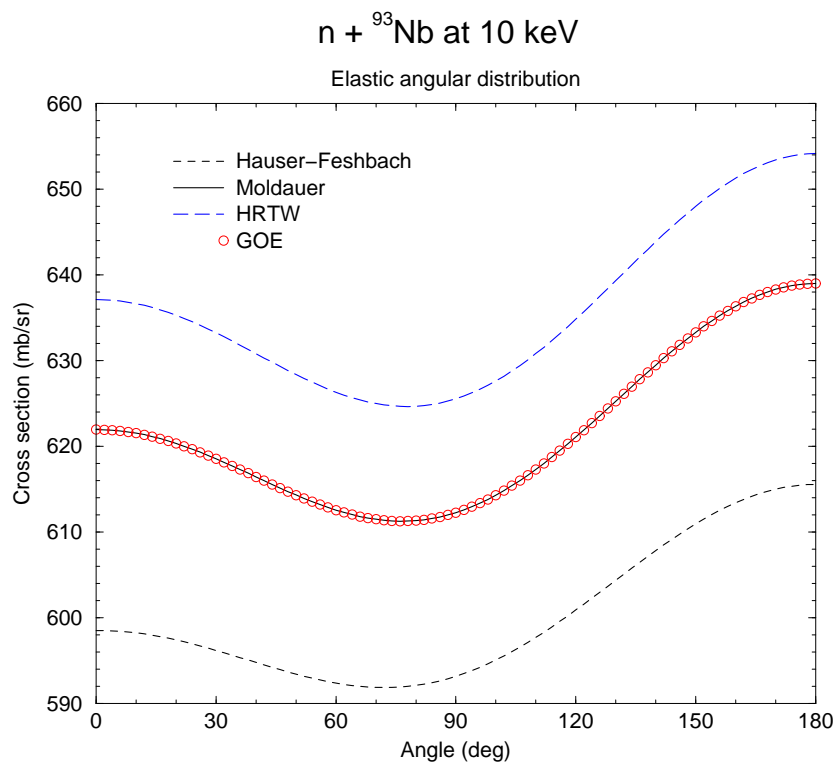


Figure 7.3: Total elastic angular distribution for 4 different compound nucleus models for 10 keV neutrons incident on  ${}^{93}\text{Nb}$ .

### 7.3.4 Sample 4: Recoils: 20 MeV n + <sup>28</sup>Si

In this sample case, we calculate the recoils of the residual nuclides produced by 20 MeV neutrons incident on <sup>28</sup>Si reaction. Two methods are compared.

#### Case 4a: “Exact” approach

In the exact approach, each excitation energy bin of the population of each residual nucleus is described by a full distribution of kinetic recoil energies. The following input file is used

```
#
# General
#
projectile n
element si
mass 28
energy 20.
#
# Parameters
#
m2constant 0.70
sysreaction p d t h a
spherical y
#
# Output
#
recoil y
filerecoil y
```

For increasing incident energies, this calculation becomes quickly time-expensive. The recoil calculation yields separate files with the recoil spectrum per residual nucleus, starting with *rec*, followed by the Z, A and incident energy, e.g. *rec012024spec020.000.tot*. Also following additional output block is printed:

#### 8. Recoil spectra

Recoil Spectrum for 29Si

Energy	Cross section
--------	---------------

0.018	0.00000E+00
0.053	0.00000E+00
0.088	0.00000E+00

.....

0.676	3.21368E+00
0.720	3.22112E+00
0.763	3.21215E+00

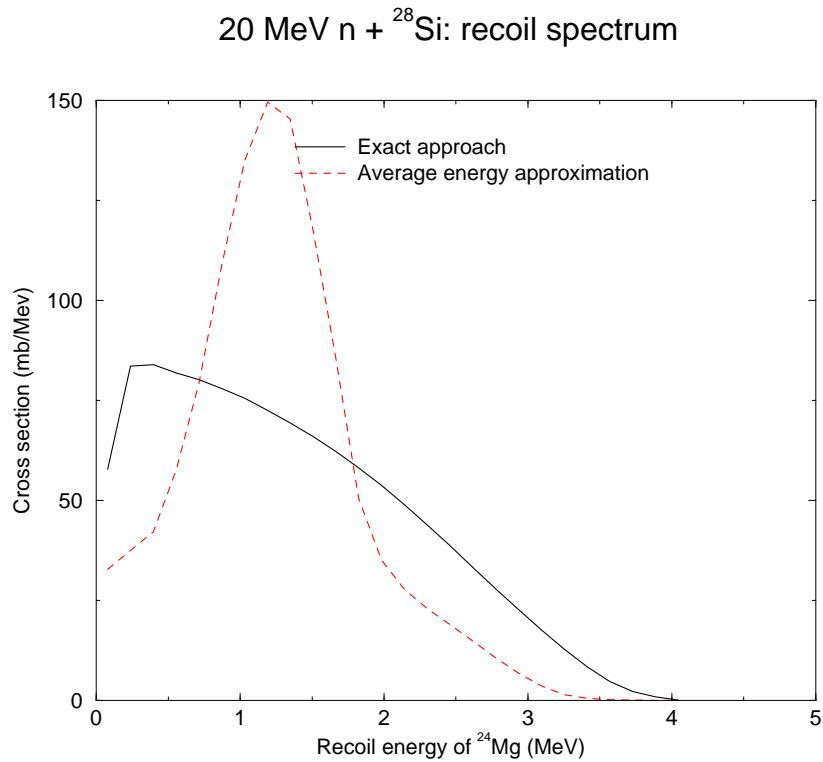


Figure 7.4: Recoil energy distribution of  $^{24}\text{Mg}$  for 20 MeV n +  $^{28}\text{Si}$  according to the exact and approximative approach.

```
0.807 3.10619E+00
0.851 2.60156E+00
0.894 2.30919E-01
```

```
Integrated recoil spectrum      : 1.04358E+00
Residual production cross section: 9.71110E-01
```

#### Case 4b: Approximative approach

As an approximation, each excitation energy bin of the population of each residual nucleus is described by a an average kinetic recoil energy. For this, we add one line to the input file above,

```
recoilaverage y
```

The results, together with those of case (a), are compared in Fig. 7.4.

### 7.3.5 Sample 5: Fission cross sections: $n + {}^{232}\text{Th}$

It is well known that a systematic approach for fission is difficult to achieve. It is possible to obtain very satisfactory fits to fission data with TALYS, but at the expense of using many adjustable input parameters. We are performing extensive model calculations to bring somewhat more structure in the collection of fitting parameters. In the meantime, we include here a sample case for the description of the fission cross section of  ${}^{232}\text{Th}$ . We use the following input file,

```
#
# General
#
projectile n
element      Th
mass         232
energy       energies
#
# Models and output
#
outfission y
partable y
bins 40
channels y
filechannels y
best y
```

Note that, although no adjustable parameters are visible above, this is certainly no “default” calculation. Instead, this sample case illustrates the use of so-called “best files”. By using the **best y** keyword, the file *talys/structure/best/Th232/n-Th232.best* is automatically invoked. The contents of that file are

```
colldamp y
asys y
class2 y
maxrot 5
gnorm 9.
t          90 233  0.41756  1
e0         90 233 -0.90113  1
exmatch   90 233  5.89461  1
t          90 233  0.56780  2
e0         90 233 -2.52108  2
exmatch   90 233  6.63983  2
fisbar     90 233  6.41136  1
fishw     90 233  0.61550  1
class2width 90 233  0.2      1
fisbar     90 233  5.23377  2
t          90 232  0.46845
e0         90 232 -0.39156
Exmatch    90 232  5.55627  0
a          90 232 31.90038
t          90 232  0.41262  1
```

e0	90	232	-1.66339	1
exmatch	90	232	6.74958	1
t	90	232	0.44833	2
e0	90	232	-0.51471	2
exmatch	90	232	6.45816	2
class2width	90	232	0.10013	1
fisbar	90	232	6.31815	2
a	90	231	26.62965	
t	90	231	0.45494	
e0	90	231	-0.91497	
exmatch	90	231	4.92684	0
t	90	231	0.47007	1
e0	90	231	-2.16775	1
exmatch	90	231	5.98780	1
t	90	231	0.68793	2
e0	90	231	-2.79424	2
exmatch	90	231	6.74959	2
a	90	230	26.21683	
t	90	230	0.47155	
e0	90	230	-0.33802	
exmatch	90	230	5.52092	0
t	90	230	0.45039	1
e0	90	230	-1.14073	1
exmatch	90	230	6.80289	1
t	90	230	0.41118	2
e0	90	230	-1.25432	2
exmatch	90	230	6.52706	2

The above parameters are the usual ones to be adjusted to get good agreement with experimental data: level density and fission parameters for the ground state or on top of the barriers. The resulting file *fission.tot* is plotted together with experimental data in Fig. 7.5.

Due to the presence of **outfission y** in the input file, all nuclear structure related to the fission process is given in the output for the target and the compound nucleus

Fission information for Z= 90 N=142 (232Th)

Number of fission barriers : 2  
 Number of sets of class2 states : 1

Parameters for fission barrier 1

Type of axiality : 1  
 Height of fission barrier 1 : 5.800  
 Width of fission barrier 1 : 0.900  
 Rtransmom : 0.600  
 Moment of inertia : 87.657  
 Number of head band transition states: 8  
 Start of continuum energy : 0.800

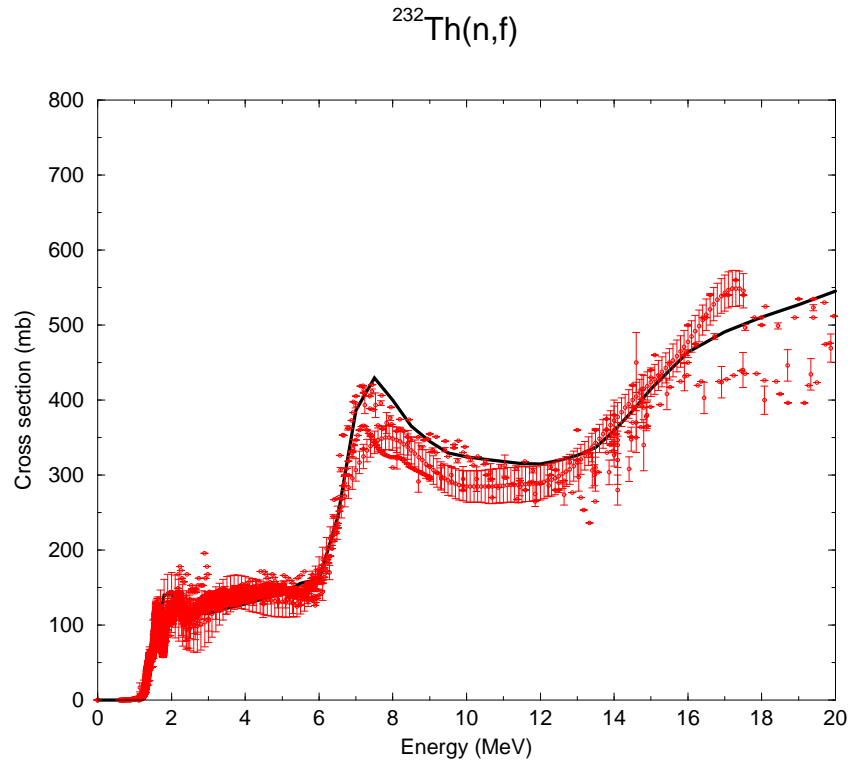


Figure 7.5: Neutron induced fission cross section of  $^{232}\text{Th}$  compared with experimental data.

Head band transition states

no.	E	spin	parity
1	0.000	0.0	+
2	0.500	2.0	+
3	0.400	0.0	-
4	0.400	1.0	-
5	0.500	2.0	+
6	0.400	2.0	-
7	0.800	0.0	+
8	0.800	0.0	+

Rotational bands

no.	E	spin	parity
1	0.000	0.0	+
2	0.034	2.0	+
3	0.114	4.0	+
4	0.240	6.0	+
5	0.400	1.0	-

6	0.400	2.0	-
7	0.411	8.0	+
8	0.411	1.0	-
9	0.423	2.0	-
10	0.434	3.0	-

.....

Parameters for fission barrier 2

Type of axiality	:	2
Height of fission barrier 2	:	6.318
Width of fission barrier 2	:	0.600
Rtransmom	:	1.000
Moment of inertia	:	154.212
Number of head band transition states:	:	4
Start of continuum energy	:	0.500

Head band transition states

no.	E	spin	parity
1	0.000	0.0	+
2	0.500	2.0	+
3	0.200	0.0	-
4	0.500	1.0	-

.....

Moreover, the corresponding fission transmission coefficients are printed for all excitation energies encountered in the calculation

Fission transmission coefficients for Z= 90 N=143 (233Th) and an excitation energy of

J	T(J,-)	T(J,+)
0.5	4.02053E-08	6.51894E-08
1.5	0.00000E+00	0.00000E+00

.....

The fission information for all residual nuclides can be obtained in the output file as well by adding *outpopulation y* to the input file.

### 7.3.6 Sample 6: Continuum spectra at 63 MeV for Bi(n,xp)...Bi(n,x $\alpha$ )

In this sample case, we calculate angle-integrated and double-differential particle spectra for 63 MeV neutrons on  $^{209}\text{Bi}$ , see Ref. [422].

#### Case 6a: Default calculation

The following input file is used

```
#
# General
#
projectile n
element bi
mass 209
energy 63.
#
# Output
#
ddxmode 2
filespectrum n p d t h a
fileddxa p 20.
fileddxa p 70.
fileddxa p 110.
fileddxa d 20.
fileddxa d 70.
fileddxa d 110.
fileddxa t 20.
fileddxa t 70.
fileddxa t 110.
fileddxa h 20.
fileddxa h 70.
fileddxa h 110.
fileddxa a 20.
fileddxa a 70.
fileddxa a 110.
```

Note that we request that angle-integrated spectra for all particles are written on separate files through *filespectrum n p d t h a*. At 20, 70 and 110 degrees, we also ask for the double-differential spectrum for protons up to alpha-particles. The resulting files *pspec063.000.tot*, *pddx020.0.deg*, etc. are presented, together with experimental data, in Figs. 7.6 and 7.7.

#### Case 6b: Adjusted matrix element

The default results of case (a) for the proton spectra are a bit high. Therefore, as a second version of this sample case, we adjust a pre-equilibrium parameter and add the following to the input above:

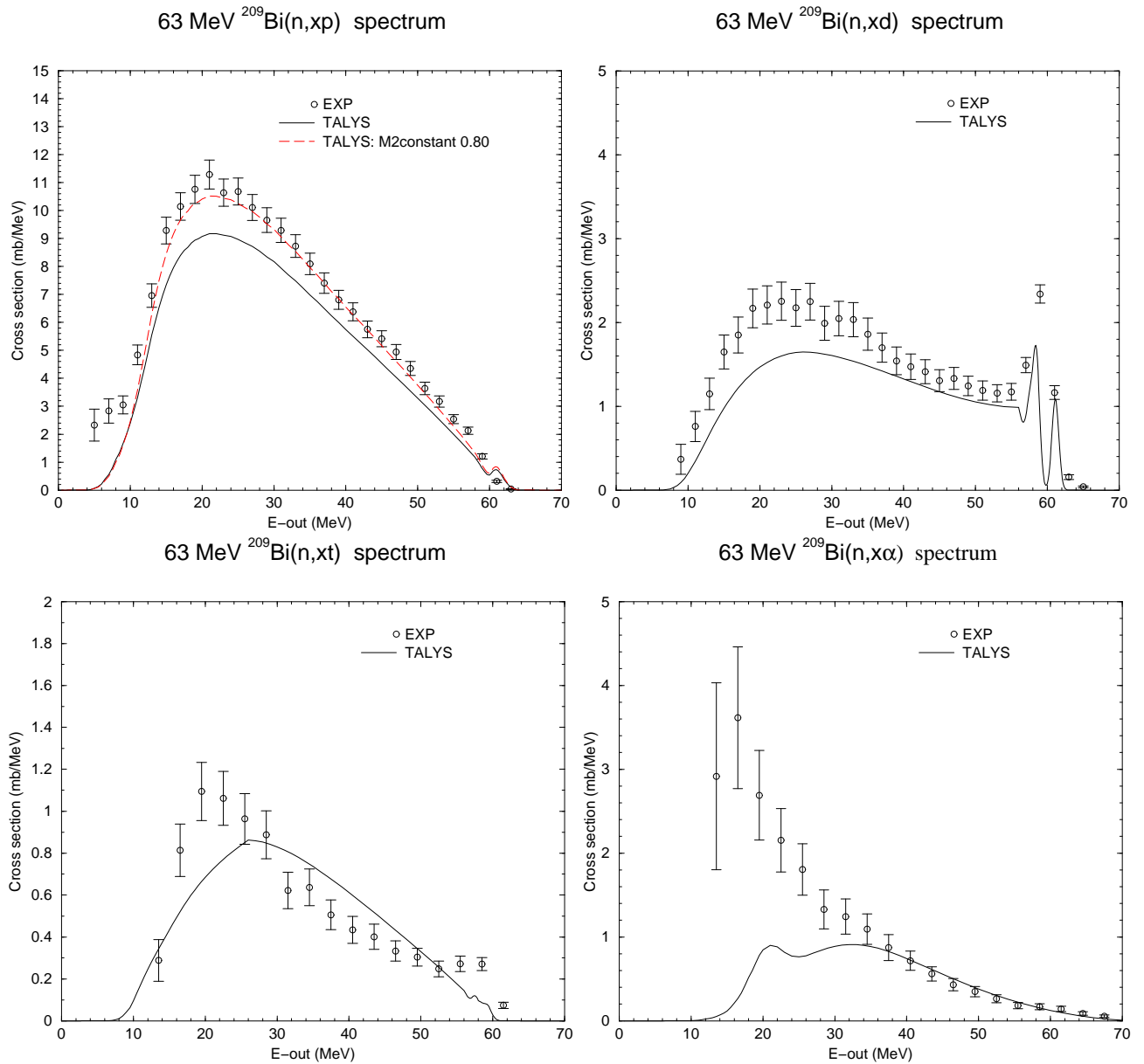


Figure 7.6: Angle-integrated proton, deuteron, triton and alpha emission spectra for 63 MeV neutrons on  $^{209}\text{Bi}$ . The experimental data are from [422].

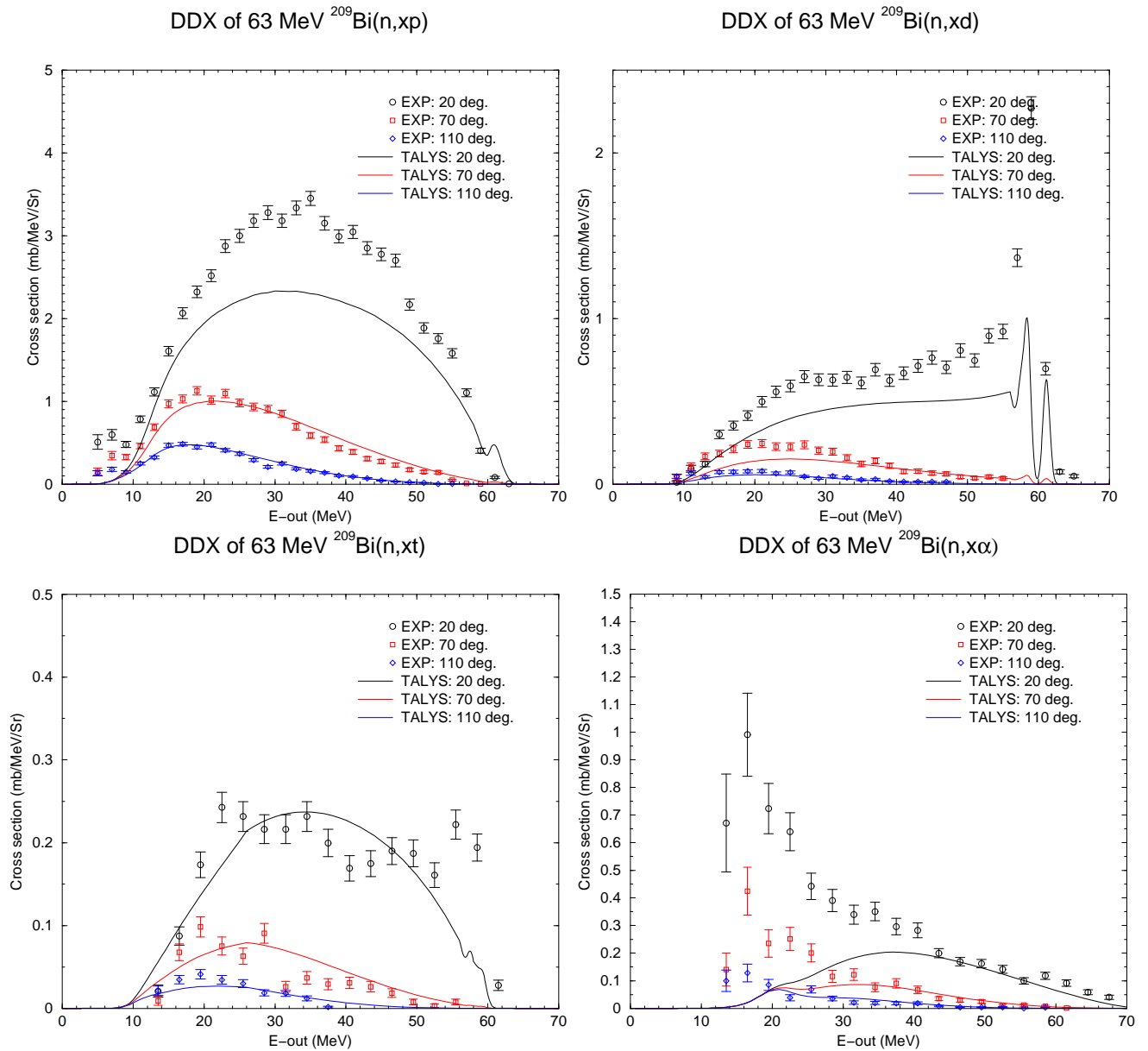


Figure 7.7: Double-differential proton, deuteron, triton and alpha emission spectra for 63 MeV neutrons on  $^{209}\text{Bi}$ . The experimental data are from [422].

```
#  
# Parameters  
#  
M2constant 0.80
```

By decreasing **M2constant** by 20% (which is a common and acceptable deviation from the average), we favor the pre-equilibrium emission rate over the rate rate, leading to a harder spectrum. The result is shown in Fig. 7.6 for the proton spectrum.

### 7.3.7 Sample 7: Pre-equilibrium angular dist. and multiple pre-equilibrium emission

At high incident energies, multiple pre-equilibrium reactions play a significant role. In this sample case, we show the results for this mechanism in the output file. Also, as an alternative to the previous sample case, we present another way of producing double-differential cross sections, namely as a function of angle at a fixed outgoing energy. With the following input file, the reaction of 120 MeV protons incident on  $^{90}\text{Zr}$  is simulated:

```
#
# General
#
projectile p
element zr
mass 90
energy 120.
#
# Output
#
outpopulation y
ddxmode 1
filespectrum n p
fileddxe p 20.
fileddxe p 40.
fileddxe p 60.
fileddxe p 80.
fileddxe p 100.
```

The results are presented in Figs. 7.8 and 7.9. For this sample case, since **outpopulation y**, after each print of the population for each residual nucleus (as already described in the first sample case), a block with multiple pre-equilibrium decay information is printed. This output block begins with

Multiple preequilibrium emission from Z= 41 N= 49 (  $^{90}\text{Nb}$ ):

bin	Ex	Mpe ratio	neutron		proton		Feeding terms from			
			emission	emission	emission	emission	1 1 0 0	0 0 1 1	1 0 0 1	0 1 1 0
11	2.208	0.00000	0.000E+00	0.000E+00	0.000E+00	0.000E+00	5.287E-01	0.000E+00		
12	4.980	0.00000	0.000E+00	0.000E+00	0.000E+00	0.000E+00	1.249E+00	0.000E+00		
13	7.752	0.00000	0.000E+00	0.000E+00	0.000E+00	0.000E+00	1.961E+00	0.000E+00		
14	10.524	0.00001	0.000E+00	4.343E-05	0.000E+00	0.000E+00	2.645E+00	0.000E+00		
15	13.296	0.00555	3.214E-04	1.999E-02	0.000E+00	0.000E+00	3.300E+00	0.000E+00		
16	16.067	0.04999	5.901E-03	2.049E-01	0.000E+00	0.000E+00	3.928E+00	0.000E+00		
17	18.839	0.10870	2.305E-02	5.024E-01	0.000E+00	0.000E+00	4.527E+00	0.000E+00		
18	21.611	0.17335	5.014E-02	8.952E-01	0.000E+00	0.000E+00	5.098E+00	0.000E+00		
.....										

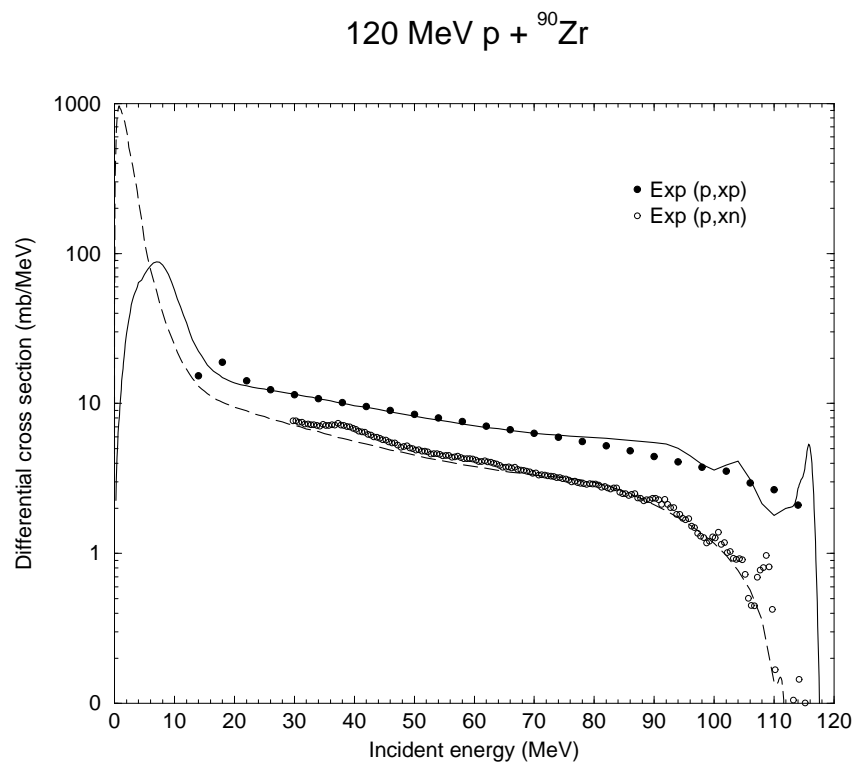


Figure 7.8: Angle-integrated (p,xn) and (p,xp) spectra for 120 MeV protons on  $^{90}\text{Zr}$ . Experimental data are taken from [127, 128]

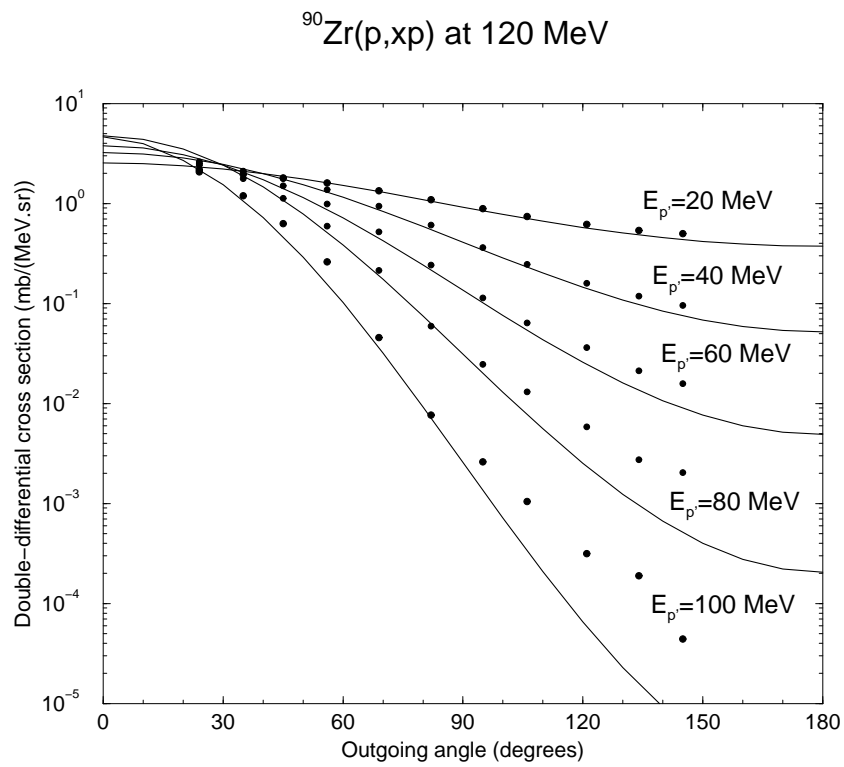


Figure 7.9: Double-differential (p,xp) spectra for 120 MeV protons on  $^{90}\text{Zr}$ . Experimental data are taken from [127]

For each continuum bin, with excitation energy  $E_x$ , we print the fraction of the population that is emitted as multiple pre-equilibrium. Also the total neutron and proton emission per residual nucleus is printed, as well as the feeding terms from previous particle-hole configurations. With this input file, files *nspec120.000.tot* and *pspec120.000.tot* are created through the *filespectrum n p* keyword. The results are displayed in Fig. 7.8. Also, the combination of **ddxmode 1** and the various **fileddxe** keywords generate the *pddx100.0.mev*, etc. files that are compared with experimental data in Fig. 7.9.

### 7.3.8 Sample 8: Residual production cross sections: $p + {}^{nat}\text{Fe}$ up to 100 MeV

In this sample case, we calculate the residual production cross sections for protons on  ${}^{nat}\text{Fe}$  for incident energies up to 100 MeV. A calculation for a natural target is launched, meaning that successive TALYS calculations for each isotope are performed, after which the results are weighted with the natural abundance. We restrict ourselves to a calculation with all nuclear model parameters set to their default values. The following input file is used:

```
#
# General
#
projectile p
element fe
mass 0
energy energies
#
# Output
#
fileresidual      y
```

The file *energies* contains 34 incident energies between 1 and 100 MeV. Obviously, this sample case can be extended to more incident energies, e.g. up to 200 MeV, by simply adding numbers to the *energies* file. In that case, we recommend to include more energy bins in the calculation, (e.g. **bins 80**) to avoid numerical fluctuations, although this will inevitably take more computer time. Note that we have enabled the **fileresidual** keyword, so that a separate cross sections file for each final product is produced. The results from the files *rp027056.tot*, *rp027055.tot*, *rp025054.tot* and *rp025052.tot* are presented, together with experimental data, in Fig. 7.10.

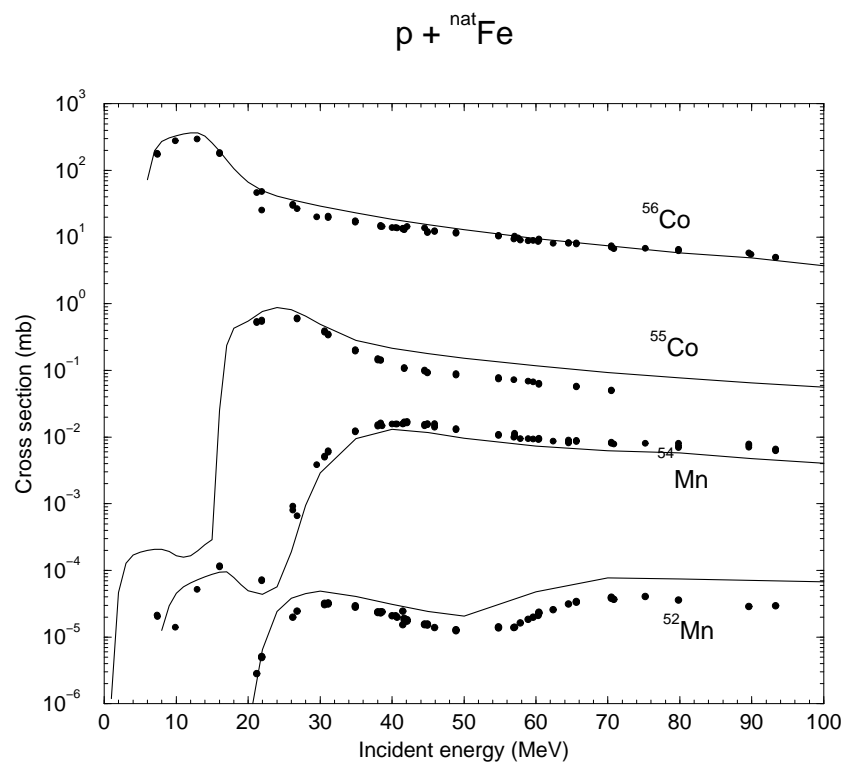


Figure 7.10: Residual production cross sections for protons incident on  ${}^{\text{nat}}\text{Fe}$ . Experimental data are obtained from [129].

### 7.3.9 Sample 9: Spherical optical model and DWBA: $n + {}^{208}\text{Pb}$

Three types of optical model calculations are included in the set of sample cases. In this first one, we treat  ${}^{208}\text{Pb}$  as a spherical nucleus and request calculations for the elastic angular distributions and inelastic angular distributions at a few incident energies. This is accomplished with the input file

```
#
# General
#
projectile n
element pb
mass 208
energy energies
#
# Avoid unnecessary calculations and output
#
ejectiles n
preequilibrium n
compound n
maxZ 0
maxN 0
bins 5
fileresidual n
filetotal n
#
# Output
#
outangle y
fileelastic y
fileangle 1
fileangle 2
```

where the file *energies* consists of the energies 11., 13.7, 20., 22., and 25.7 MeV (for which experimental data exists). The keyword *fileelastic y* has created the files *nn011.000ang.L00*, etc. which contain the elastic scattering angular distribution and are compared with experimental data in Fig. 7.11. With **fileangle 1** and **fileangle 2** we have created the files *nn010.000ang.L01*, etc. with the inelastic scattering angular distribution to the first and second discrete state. These are also plotted in Figs. 7.11. Note that the keywords in the middle block (**ejectiles n** up to **filetotal n**) have been added to avoid a full calculation of all the cross sections. For the present sample case we assume that only elastic scattering and DWBA angular distributions are of interest, so we economize on output options, number of bins, ejectiles and nuclides that can be reached. Obviously, for reliable results for all observables this middle block would have to be deleted. See also sample case (1f) for obtaining more specific information from the output.

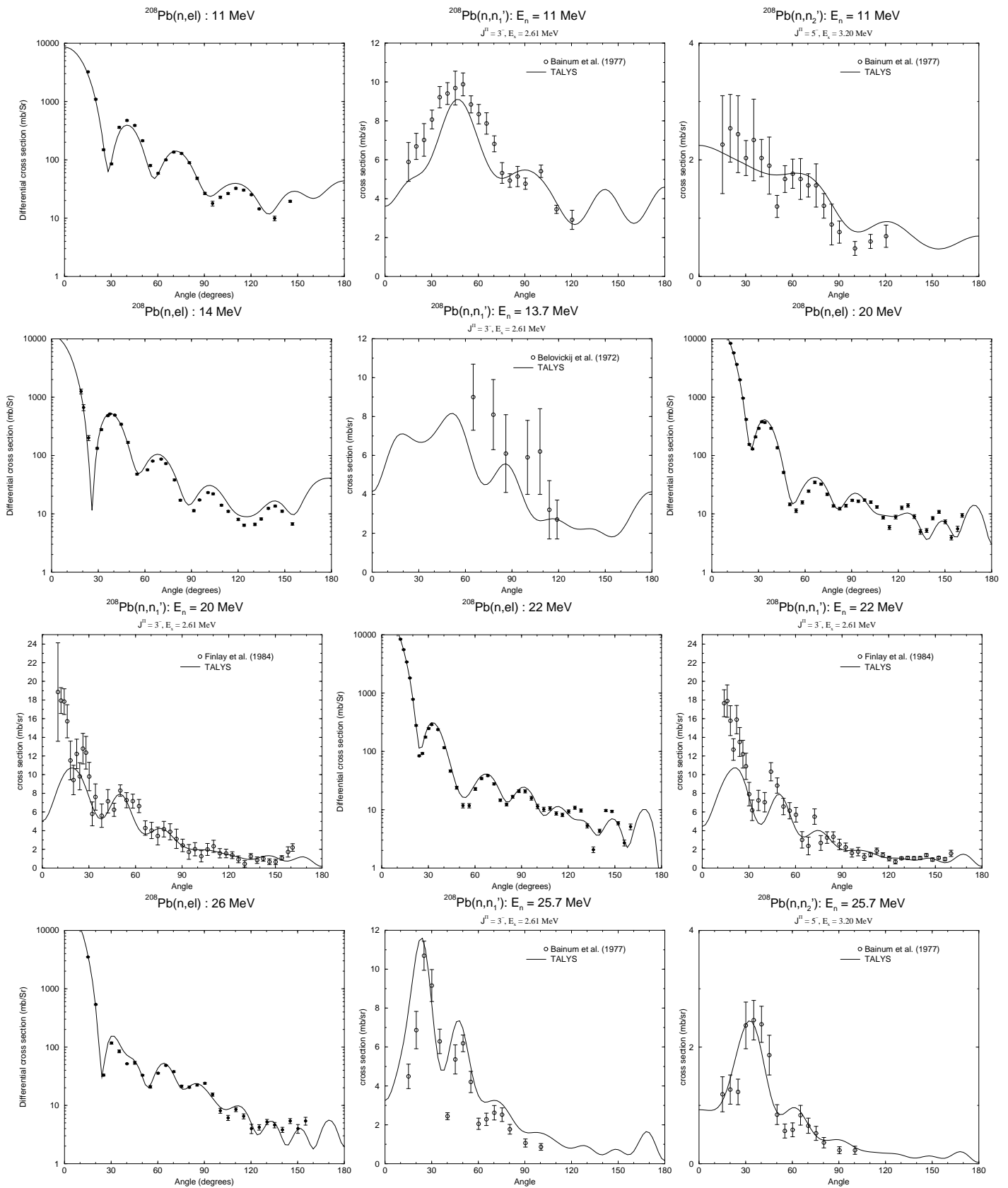


Figure 7.11: Elastic and inelastic scattering angular distributions between 11 and 26 MeV for  $^{208}\text{Pb}$ .

### 7.3.10 Sample 10: Coupled-channels rotational model: $n + {}^{28}\text{Si}$

In this sample case, we consider spherical OMP and rotational coupled-channels calculations for the deformed nucleus  ${}^{28}\text{Si}$ .

#### Case 10a: Spherical optical model

In the first case, we treat  ${}^{28}\text{Si}$  as a spherical nucleus and include the first ( $2^+$ ), second ( $4^+$ ) and sixth ( $3^-$ ) level as weakly coupled levels, i.e. the cross sections are calculated with DWBA. The input file is

```
#
# General
#
projectile n
element si
mass 28
energy energies
#
# Parameters
#
spherical y
#
# Output
#
channels y
filechannels y
```

For the default calculation, TALYS will look in the *deformation/exp* database to see whether a coupling scheme is given. Since this is the case for  ${}^{28}\text{Si}$ , we have to put **spherical y** to enforce a spherical calculation.

#### Case 10b: Symmetric rotational model

In the second case, we include the first and second level of the ground state rotational band and the  $3^-$  state in the coupling scheme. This is accomplished with the input file

```
#
# General
#
projectile n
element si
mass 28
energy energies
#
# Output
#
```

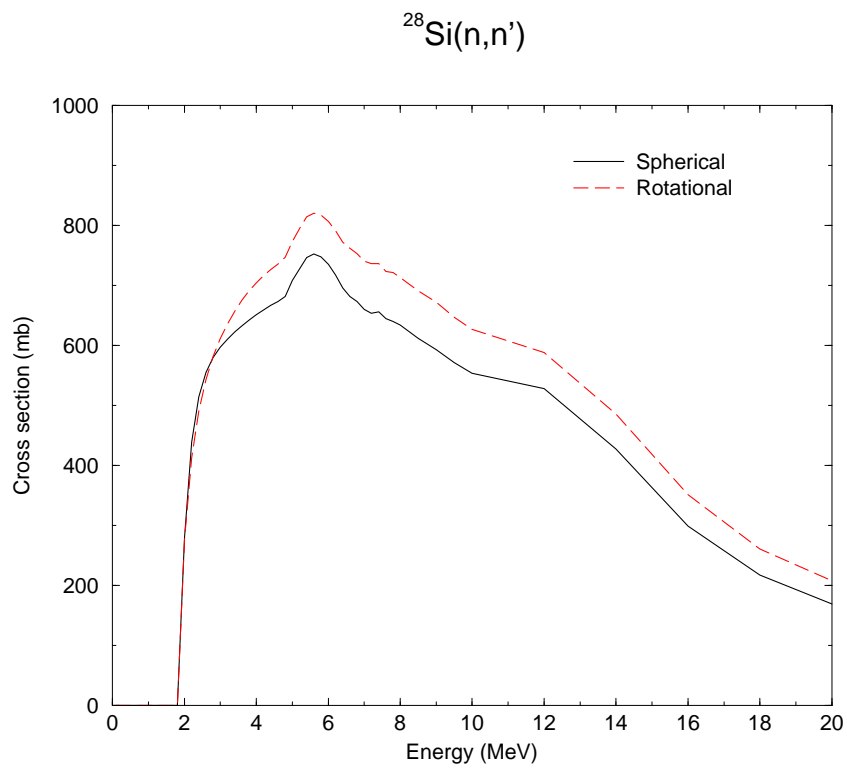
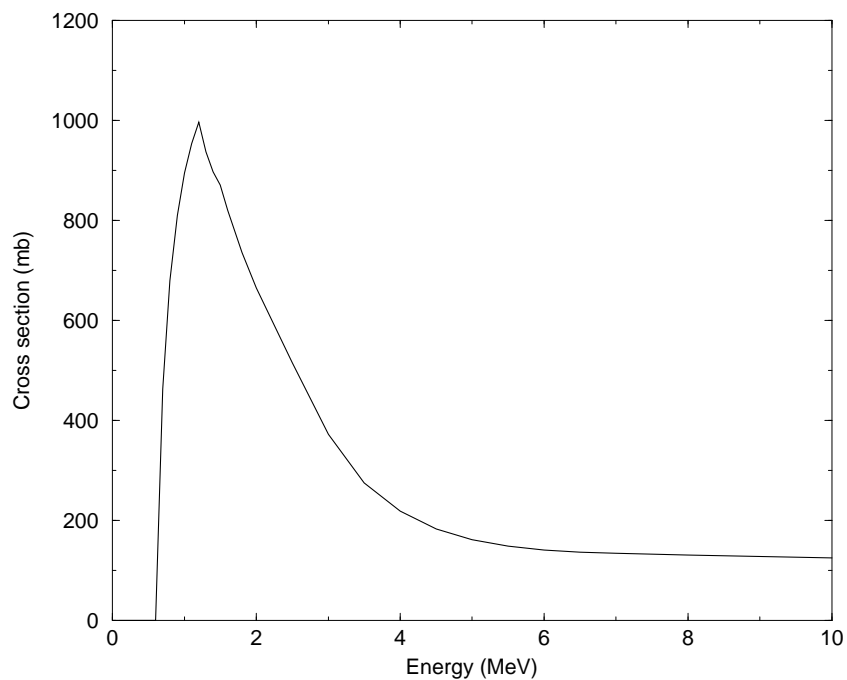


Figure 7.12: Total inelastic neutron scattering off  $^{28}\text{Si}$  for a spherical and a deformed OMP.

```
channels y
filechannels y
```

In Fig. 7.12, the calculated total inelastic scattering for cases a and b are plotted.

$^{74}\text{Ge}(n,n')$ : first discrete stateFigure 7.13: Inelastic scattering to the first discrete state of  $^{74}\text{Ge}$ .**7.3.11 Sample 11: Coupled-channels vibrational model:  $n + ^{74}\text{Ge}$** 

In this sample case we consider a neutron-induced reaction on the vibrational nucleus  $^{74}\text{Ge}$  which consists of a one-phonon state ( $2^+$ ) followed by a ( $0^+, 2^+, 4^+$ ) triplet of two-phonon states, and a  $3^-$  phonon state. The coupling scheme as stored in *structure/deformation/Ge.def* is automatically adopted. The following input file is used:

```
#
# General
#
projectile n
element ge
mass 74
energy energies
#
# Output
#
outexcitation n
outdiscrete y
filediscrete 1
```

In Fig. 7.13, the calculated inelastic scattering to the first discrete state is plotted.

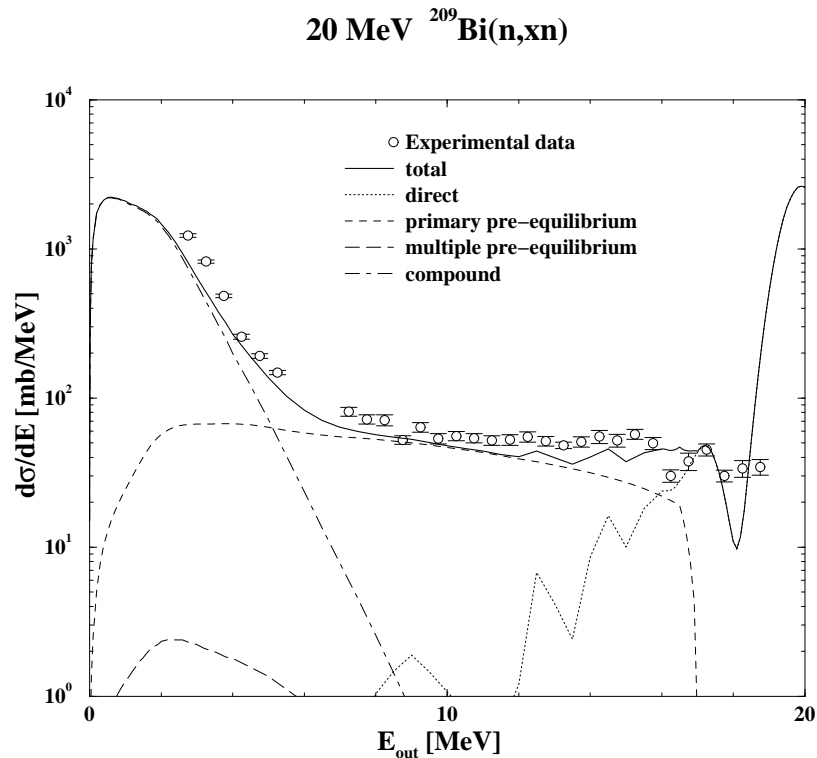


Figure 7.14:  $^{209}\text{Bi}(n,xn)$  spectrum at 20 MeV. Experimental data are obtained from [131].

### 7.3.12 Sample 12: Inelastic spectra at 20 MeV: Direct + Preeq + GR + Compound

For pre-equilibrium studies, it may be worthwhile to distinguish between the various components of the emission spectrum. This was already mentioned in sample case (1c). As an extra sample case, we compare the calculated  $^{209}\text{Bi}(n,xn)$  spectrum at 20 MeV with experimental data. This is accomplished with the following input file,

```
#
# General
#
projectile n
element bi
mass 209
energy 20.
#
# Parameters
#
ddxmode 2
filespectrum n
```

The various components of the spectrum, and the total, as present in the file *nspec020.000.tot*, are plotted in Fig. 7.14.

### 7.3.13 Sample 13: Gamma-ray intensities: $^{208}\text{Pb}(n, n\gamma)$ and $^{208}\text{Pb}(n, 2n\gamma)$

This feature could simply have been included in the sample case on excitation functions for  $^{208}\text{Pb}$ , but in order not to overburden the description of that sample case we include it here. With the input file

```
#
# General
#
projectile n
element pb
mass 208
energy energies
#
# Parameters
#
isomer 1.e-4
maxZ 0
gnorm 0.35
Rgamma 2.2
egr      82 209 12.0      E1 1
optmodfileN 82 pb.omp
#
# Output
#
channels y
filechannels y
fileresidual y
outgamdis y
```

all discrete gamma lines are printed and stored in separate files. To avoid the production of too many data files, we have put **maxZ 0** so that only the gamma-ray production files for Pb-chain are created. Also, we include a special OMP with the file *pb.omp* and we set **isomer 1.e-4** to allow for gamma decay of some rather short-lived levels. Experimental data exists for the  $^{208}\text{Pb}(n, n'\gamma)$  cross section for level 1 to level 0 and the  $^{208}\text{Pb}(n, 2n'\gamma)$  cross section for level 2 to level 0 and for level 1 to level 0. These data have been plotted together with the results of the calculated files *gam082208L01L00.tot*, *gam082207L02L00.tot* and *gam082207L01L00.tot*, in Fig. 7.15.

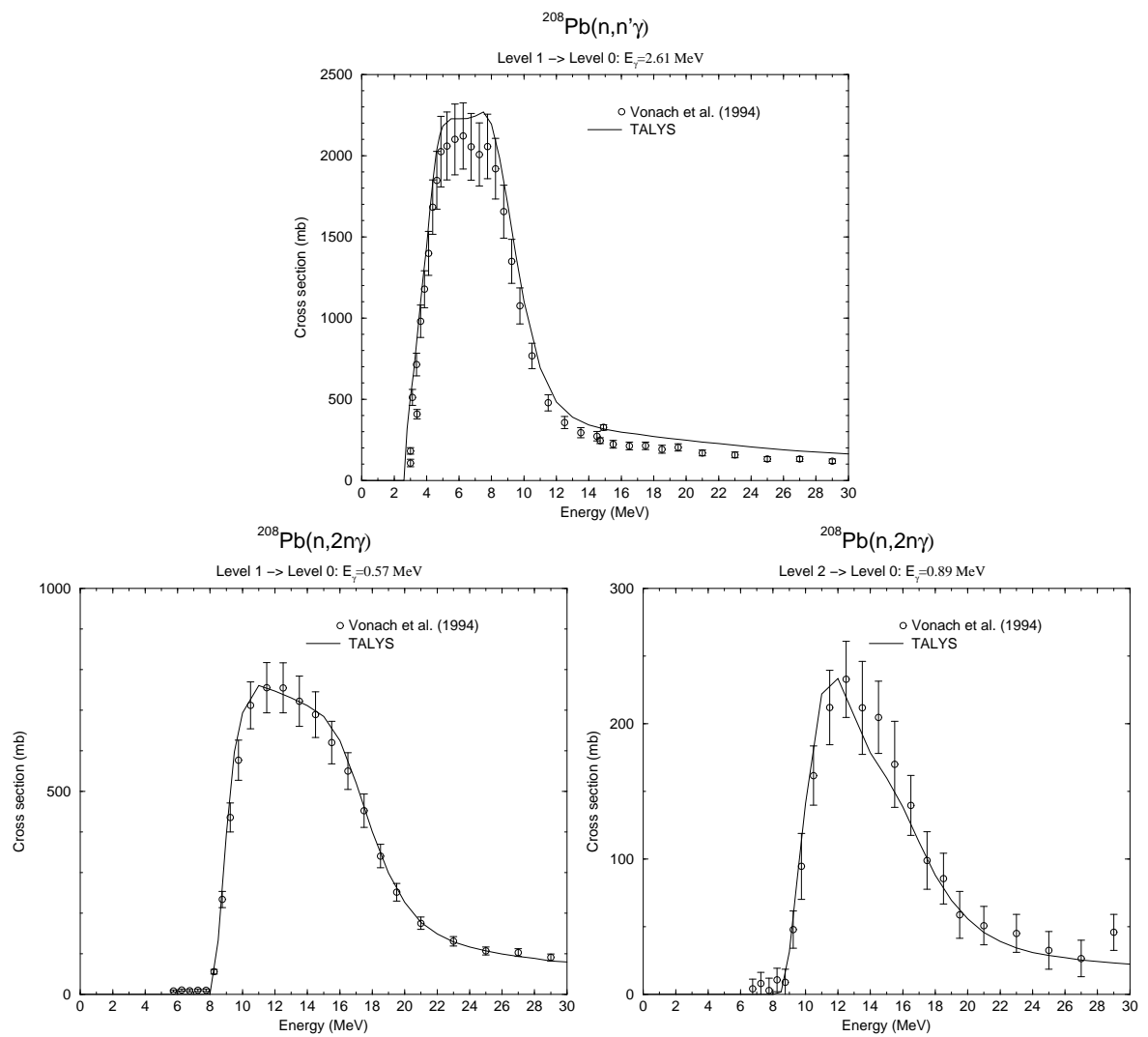


Figure 7.15: Gamma-ray production lines for a few transitions in  $^{208}\text{Pb}(n,n')$  and  $^{208}\text{Pb}(n,2n)$  reactions. The experimental data are from [132].

### 7.3.14 Sample 14: Fission yields for $^{238}\text{U}$

In this sample case we compute fission fragment/product mass/isotope yields. The fission fragment mass yield curve is determined for neutrons on  $^{238}\text{U}$  at incident energies of 1.6 and 5.5 MeV (these incident energies are given in the file *energies*). The following input file is used:

```
projectile n
element     U
mass       238
energy     energies
partable y
bins      40
channels y
filechannels y
autorot y
best y
ecissave y
massdis y
ffevaporation y
```

The long list of adjustable parameters, not visible here but automatically taken from *talys/structure/best/U238/n-U238.best* through the **best y** keyword, is mainly needed to give a decent (though not yet perfect) description of the total fission cross section. For completeness, we show the results for  $^{238}\text{U}$  we obtained for incident energies of 1, 1.6, 3.5, 5.5, 7.5 and 10 MeV. The TALYS results for the pre-neutron emission mass yields can be found in *yield001.600.fis* and *yield005.500.fis* and are given in the upper plot of Fig. 7.16. The two other plots show a comparison of the normalized yields with experimental data [122].

Since we have added the keyword *ffevaporation y* to the input, we have also calculated the fission product isotope yields. Fig. 7.17 contains the result for the production of the fission products  $^{115}\text{Cd}$  and  $^{140}\text{Ba}$ . The left plot shows the cumulative yield (obtained after adding the calculated independent yields of all beta-decay precursors). The normalized cumulative yields are compared to experimental data [123, 124] in the other two plots.

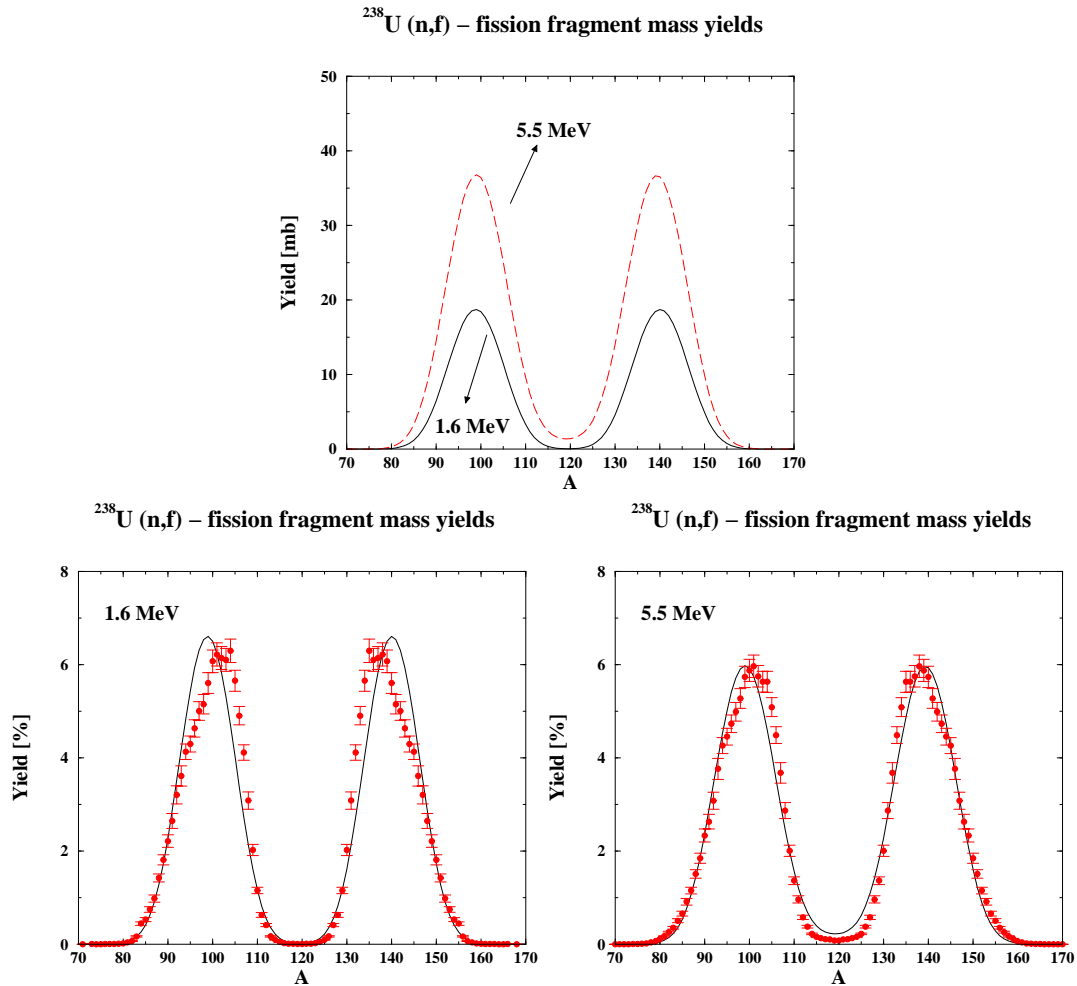


Figure 7.16: Fission fragment mass yield curves as function of the mass number  $A$ , produced by 1.6 MeV and 5.5 MeV neutrons on  $^{238}\text{U}$ . The upper curve shows the results as they are produced by TALYS and the other two plots contain the comparison with experimental data in terms of normalized yields [122].

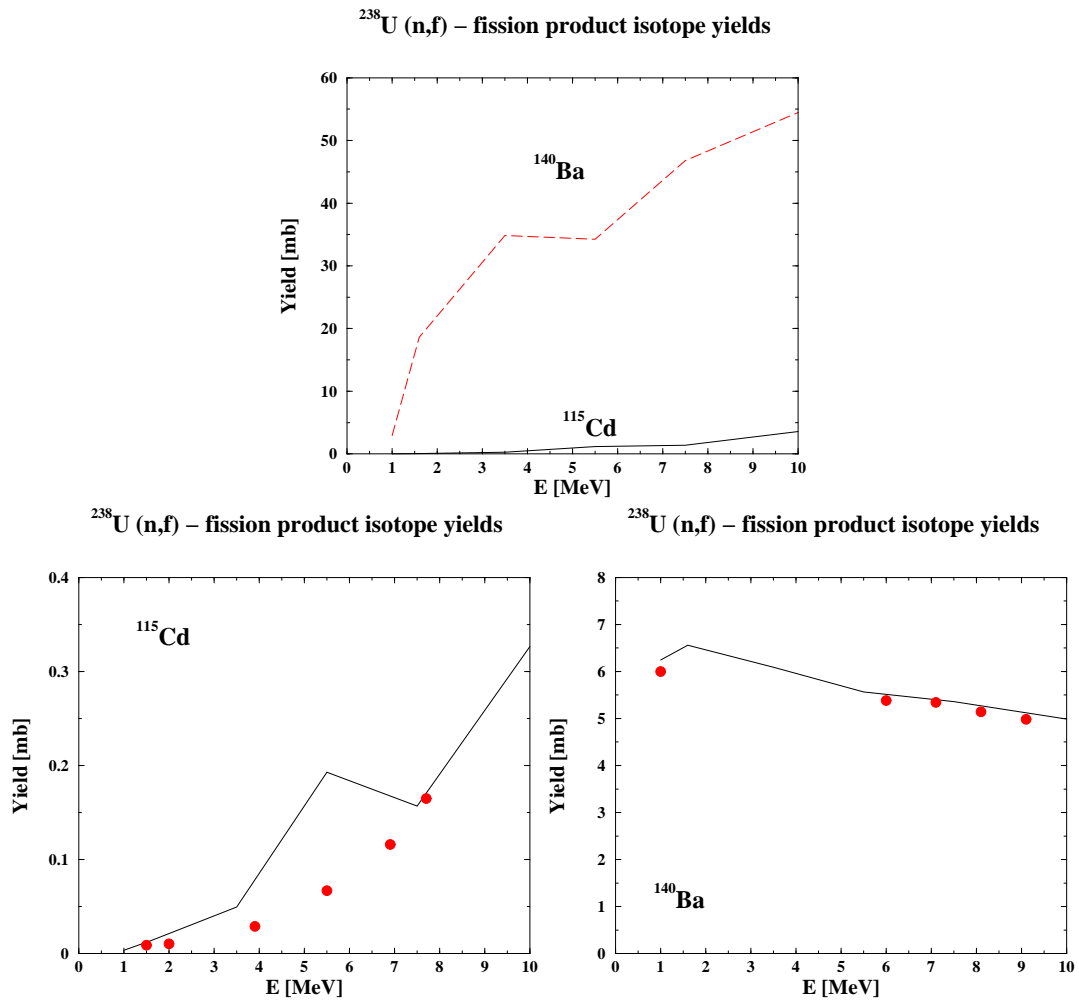


Figure 7.17: Fission product isotope yields produced by neutrons on  $^{238}\text{U}$  as function of the mass number A. The upper plot shows the results for  $^{115}\text{Cd}$  and  $^{140}\text{Ba}$  as they are produced by TALYS and the other two plots contain the comparison with experimental data in terms of normalized yields [123, 124].

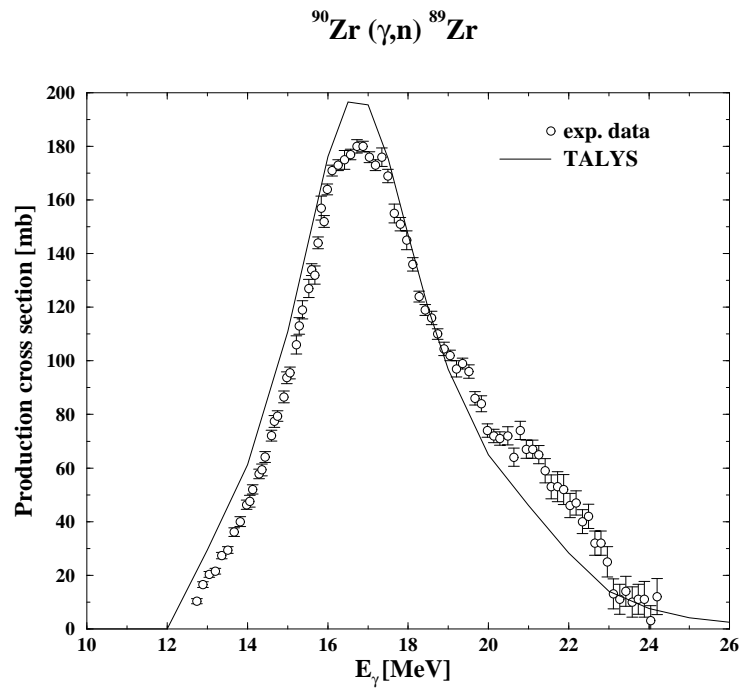


Figure 7.18: Photonuclear reaction on  $^{90}\text{Zr}$ . Experimental data are obtained from [130].

### 7.3.15 Sample 15: Photonuclear reactions: $g + ^{90}\text{Zr}$

This sample case illustrates the capabilities of TALYS to treat photonuclear reactions. We calculate the  $(\gamma,n)$  reaction on  $^{90}\text{Zr}$  as a function of incident energy, with default model parameters, and compare the result to experimental data. The following input file is used

```
#
# General
#
projectile g
element zr
mass 90
energy energies
```

Fig. 7.18 displays the resulting production cross section of  $^{89}\text{Zr}$ , as obtained in file *rp040089.tot*.

### 7.3.16 Sample 16: Different optical models : $n + {}^{120}\text{Sn}$

To demonstrate the variety of optical models that we have added recently to TALYS, we include a sample case in which 4 OMP's for neutrons on  ${}^{120}\text{Sn}$  are compared. The results are given in Fig. 7.19 for the total cross section and in Fig.7.20 for the total inelastic cross section.

#### Case 16a: Koning-Delaroche local potential

The input file is

```
#
# General
#
projectile n
element    sn
mass      120
energy    energies
```

This is the default calculation: TALYS will find a local OMP in the structure database and will use it.

#### Case 16b: Koning-Delaroche global potential

The input file is

```
#
# General
#
projectile n
element    sn
mass      120
energy    energies
#
# Parameters
#
localomp n
```

#### Case 16c: Koning-Delaroche local dispersive potential

The input file is

```
#
# General
#
projectile n
element    sn
```

```
mass      120
energy    energies
#
# Parameters
#
dispersion y
```

**Case 16d: Bauge-Delaroche JLM potential**

The input file is

```
#
# General
#
projectile n
element    sn
mass      120
energy    energies
#
# Parameters
#
jlmomp y
```

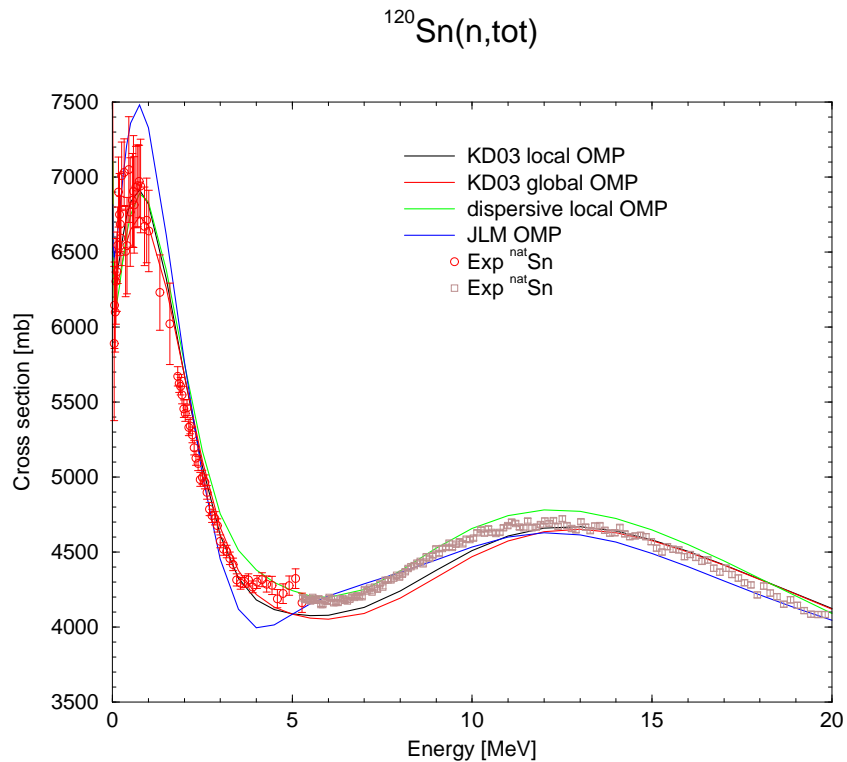


Figure 7.19: Total cross section for neutrons incident on  $^{120}\text{Sn}$  for different optical model potentials.

### 7.3.17 Sample 17: Different level density models : $n + ^{99}\text{Tc}$

To demonstrate the variety of level density models that we have added recently to TALYS, we include a sample case in which 3 different models are compared. The results are given in Fig. 7.21 for the cumulative number of discrete levels and in Fig.7.22 for the  $(n,p)$  cross section.

#### Case 17a: Constant Temperature Model

The input file is

```
#
# General
#
projectile n
element tc
mass 99
energy energies
#
# Parameters
#
outdensity y
filedensity y
```

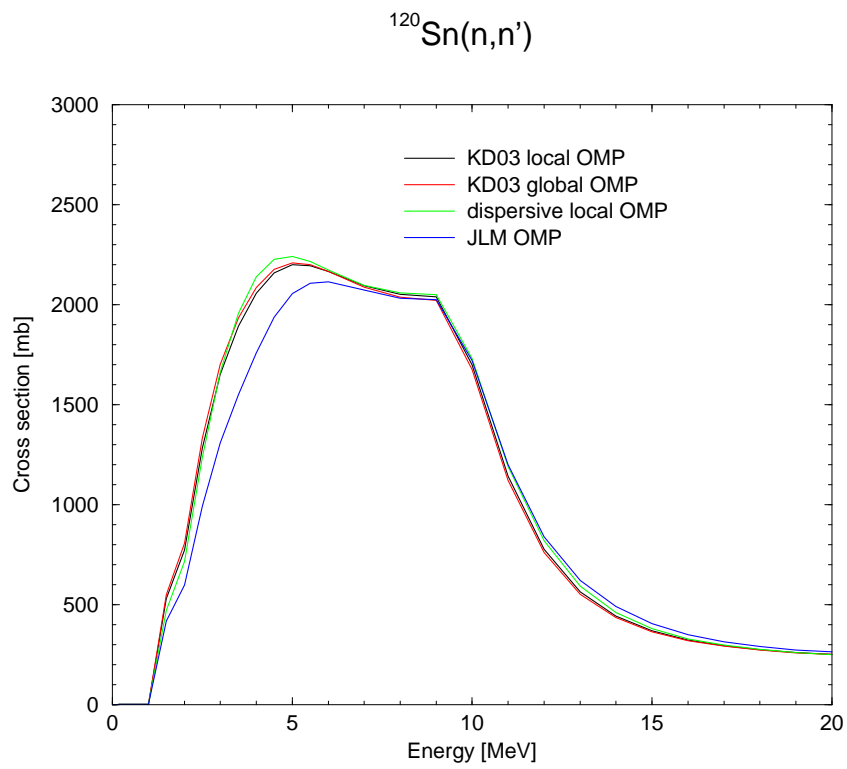


Figure 7.20: Total inelastic cross section for neutrons incident on  $^{120}\text{Sn}$  for different optical model potentials.

```
ldmodel 1
```

This is the default calculation: TALYS use the local CTM level density for its calculations

### Case 17b: Back-shifted Fermi gas Model

The input file is

```
#  
# General  
#  
projectile n  
element tc  
mass 99  
energy energies  
#  
# Parameters  
#  
outdensity y  
filedensity y  
ldmodel 2
```

### Case 17c: Hartree-Fock Model

The input file is

```
#  
# General  
#  
projectile n  
element tc  
mass 99  
energy energies  
#  
# Parameters  
#  
outdensity y  
filedensity y  
ldmodel 5
```

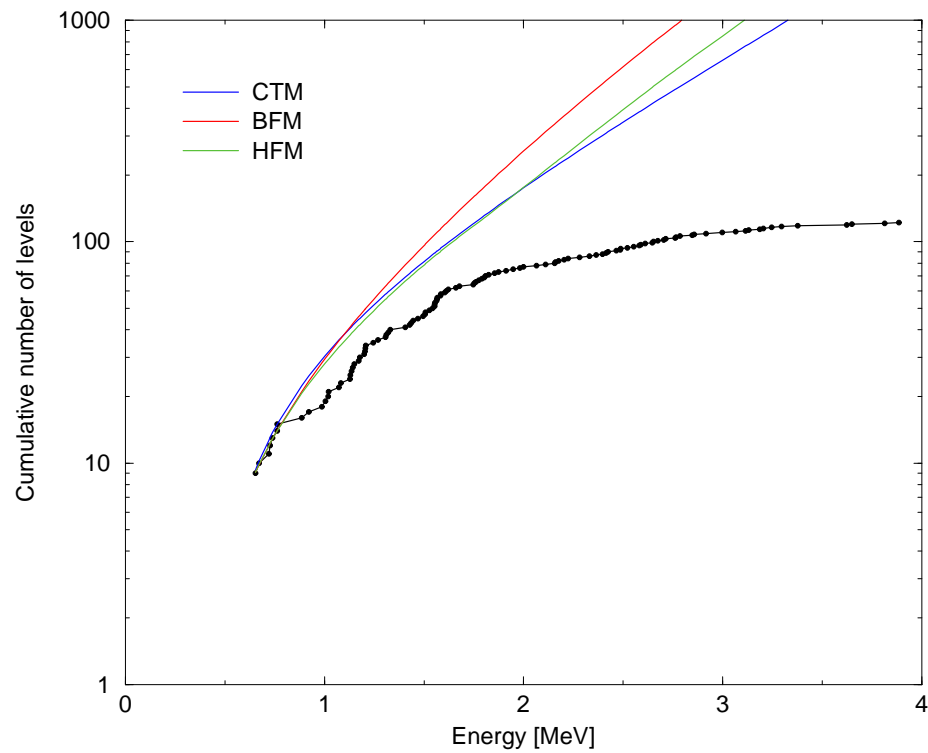


Figure 7.21: Cumulative number of discrete levels of  $^{99}\text{Tc}$  for different level density models.

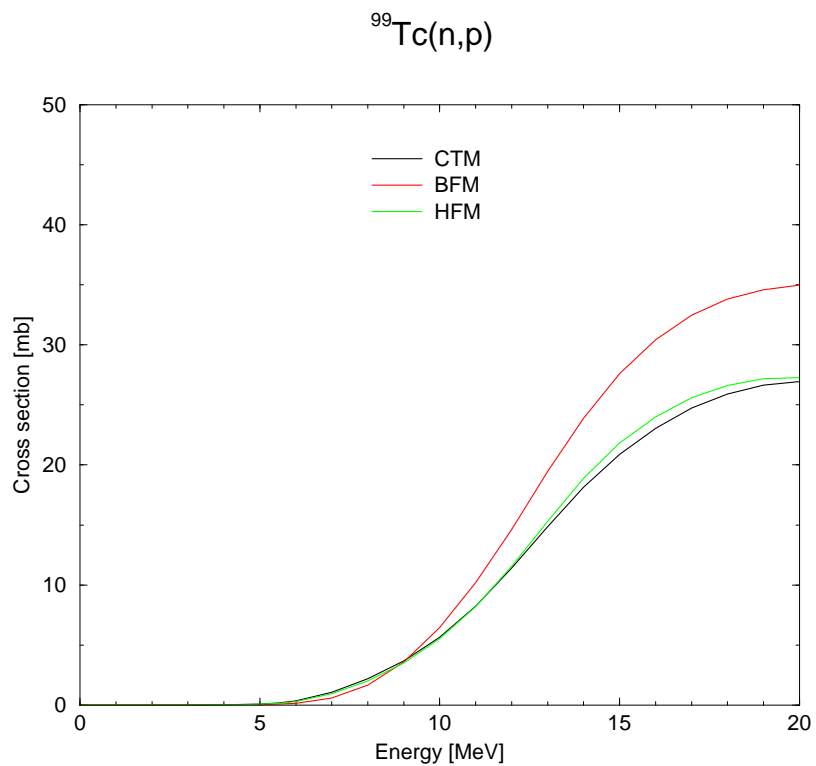


Figure 7.22:  $^{99}\text{Tc}(n,p)$  cross section for different level density models.

### 7.3.18 Sample 18: Astrophysical reaction rates : $n + {}^{187}\text{Os}$

Since TALYS-1.2, astrophysical reaction rates can be calculated, see section 4.12. As sample case, we took the work done in Ref.[728] where the  ${}^{187}\text{Os}(n,\gamma)$  was studied for the derivation of the age of the galaxy withing the Re-Os cosmochronology.

#### Case 18a: ${}^{187}\text{Os}(n,\gamma)$ cross section

First, the calculated  ${}^{187}\text{Os}(n,\gamma)$  was compared with experimental data, using the following input file

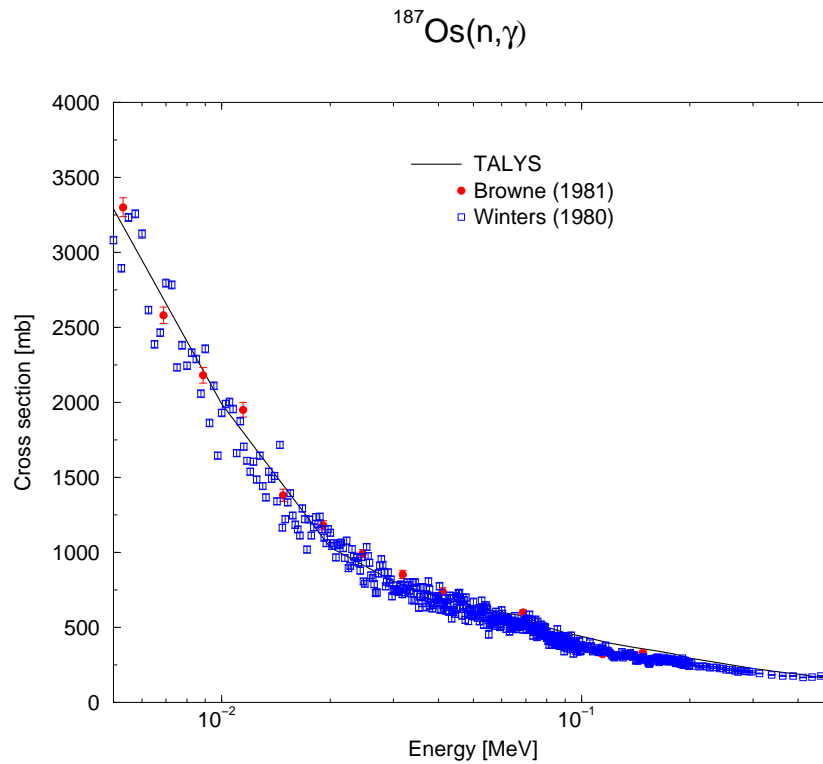
```
#
# General
#
projectile n
element    os
mass      187
energy    energies
#
# Parameters
#
ldmodel   5
asys n
strength  2
gnorm 0.27
```

where obviously **gnorm** was used as adjustment parameter. The results are given in Fig.7.23.

#### Case 18b: ${}^{187}\text{Os}(n,\gamma)$ astrophysical reaction rate

Next, the astrophysical reaction rates for neutrons on  ${}^{187}\text{Os}$  are computed with the following input file

```
#
# General
#
projectile n
element    os
mass      187
energy    energies
#
# Parameters
#
ldmodel   5
asys n
strength  2
gnorm 0.27
astro y
astrops n
```

Figure 7.23:  $^{187}\text{Os}(n,\gamma)$  cross section.

which produces various output files in which the reaction rates as function of temperature are given. The  $(n,\gamma)$  rate as given in the output file is

## 8. Thermonuclear reaction rates

Reaction rate for  $Z=76$   $A=188$  ( $^{188}\text{Os}$ )

T	G(T)	Rate
0.0001	1.00000E+00	5.46242E+08
0.0005	1.00000E+00	4.96512E+08
0.0010	1.00000E+00	4.45882E+08
0.0050	1.00000E+00	3.52813E+08
0.0100	1.00002E+00	3.01755E+08
0.0500	1.20827E+00	2.03467E+08
0.1000	1.64630E+00	1.87256E+08
0.1500	1.95860E+00	1.82416E+08
0.2000	2.21894E+00	1.80436E+08
0.2500	2.48838E+00	1.79690E+08
0.3000	2.79031E+00	1.79474E+08
0.4000	3.49874E+00	1.79716E+08
0.5000	4.31540E+00	1.80165E+08
0.6000	5.20597E+00	1.80375E+08
0.7000	6.15215E+00	1.80187E+08
0.8000	7.14759E+00	1.79580E+08
0.9000	8.19300E+00	1.78579E+08

```
1.0000 9.29313E+00 1.77221E+08  
.....
```

The same numbers can be found in the separate file *astrorate.g*. In *astrorate.tot* the rates for all reactions can be found.

**7.3.19 Sample 19: Unresolved resonance range parameters: n + <sup>136</sup>Ba**

Since the release of TALYS-1.4, parameters for the unresolved resonance range (URR) can be produced. The following input file is used

```
#
# General
#
projectile n
element ba
mass 136
energy energies
urr y
```

where the line **urr y** results in a set of URR output files which are described page 205. The top of the general output file *urr.dat* looks as follows:

```
#
# Resonance parameters for Z= 56 A= 136 (136Ba) Target spin= 0.0
# Thermal capture cross section= 6.70000E+02 mb Sn= 6.90561E+00 MeV
#
# Einc[MeV]= 1.00000E-03
# Rprime[fm]= 4.39731E+00
# l J D(l)[eV] D(l,J)[eV] S(l) S(l,J) Gx(l,J)[eV] Gn(l,J)[e
0 0.5 1.20855E+03 1.20855E+03 1.80190E+00 1.80190E+00 0.00000E+00 2.17768E-
1 0.5 4.17392E+02 1.20855E+03 9.29906E-01 1.16255E+00 0.00000E+00 1.40500E-
1 1.5 4.17392E+02 6.37595E+02 9.29906E-01 8.52357E-01 0.00000E+00 5.43458E-
#
# Einc[MeV]= 2.00000E-03
# Rprime[fm]= 4.38034E+00
# l J D(l)[eV] D(l,J)[eV] S(l) S(l,J) Gx(l,J)[eV] Gn(l,J)[e
0 0.5 1.20703E+03 1.20703E+03 1.78817E+00 1.78817E+00 0.00000E+00 2.15838E-
```

### 7.3.20 Sample 20: Maxwellian averaged cross section at 30 keV: $n + {}^{138}\text{Ba}$

In this sample case, the Maxwellian averaged cross section (MACS) at 30 keV is calculated. The following input file is used

```
#
# General
#
projectile n
element ba
mass 138
energy 1.
astroE 0.03
```

where the line **astroE 0.03** determines the energy in MeV for which the average is calculated. Note that the line **energy 1.** is irrelevant, but must nevertheless be given. The file *astrorate.g* looks as follows:

```
# Reaction rate for 138Ba(n,g) at <E>= 0.03000 MeV (Excited States Contribution : n)
#   T      Rate      MACS
  0.3481 5.49792E+05 3.79831E+00
```

in which the temperature, reaction rate and MACS is given. For this case, the deviation from a normal 30 keV calculation (which can be obtained by removing the **astroE** line and using **energy 0.03**) is small, since the latter is 3.75 mb.

**7.3.21 Sample 21: Medical isotope production with  $p + {}^{100}\text{Mo}$** 

In this sample case, the activity of all the produced isotopes from the reaction  $p + {}^{100}\text{Mo}$  are given, for a 150  $\mu\text{A}$  proton accelerator, as a function of time. The following input file is used

```
#
# General
#
projectile p
element Mo
mass 100
energy 8. 30. 0.5
#
# Spherical OMP
#
spherical y
#
# Medical isotope production
#
production y
Ibeam 0.15
Ebeam 24.
Eback 10.
```

Note the use of the **energy** keyword, available since TALYS-1.6: Cross sections are calculated for incident energies between 8 and 30 MeV with 0.5 MeV energy steps. The keyword **production y** means that activities of all radioactive products as a function of bombarding and/or decay time will be produced in tables. The incident energy of the particle beam is 24 MeV, and the required thickness of the target (which is given in the output) is such that at the back of the target the energy is 10 MeV. Other keywords relevant for isotope production, such as **Tcool**, see page 250, **Tirrad**, see page 249, **rho**, see page 248, **area**, see page 248, **radiounit**, see page 248, **yieldunit**, see page 249, have their default values in this sample case.

We like to point out an efficient option for medical isotope calculations. Suppose one is interested in varying several accelerator options, such as e.g. **Ebeam**. Once the first calculation, like the sample case above, has been done, one may rerun that case and add the extra line **reaction n** to the input file. Then, TALYS will *not* redo the nuclear reaction calculations, but use the various *rpZZZAAA.tot*, etc. cross section output files which are already available in the work directory. Obviously, **Ebeam** and **Eback** must always fall inside the energy grid for which the cross sections are calculated, in this case between 8 and 30 MeV.

The tail of the standard output files contains some general parameters:

Summary of isotope production

```
Maximal irradiation time : 0 years 1 days 0 hours 0 minutes 0 seconds
Cooling time             : 0 years 1 days 0 hours 0 minutes 0 seconds
Energy range             : 24.000 --> 10.000 MeV
```

```

Beam current           : 0.150 mA
Target material density : 10.220 g/cm^3
Target area           : 1.000 cm^2
Effective target thickness : 0.085 cm
Effective target volume : 0.085 cm^3
Effective target mass   : 0.865 g
Number of target atoms  : 5.20730E+21
Number of incident particles: 9.36226E+14 s^-1
Produced heat in target : 2.100 kW

```

More interesting are probably the files with the produced activity (in Bq or Ci) per isotope. These yields are in files *YZZZAAA.tot* where *ZZZ* is the charge number and *AAA* is the mass number in (i3.3) format. For produced isomers, and ground states, there are additional files *pZZZAAA.LMM*, where *MM* is the number of the isomer (ground state=0) in (i2.2) format. For the above sample case, *Y043099.L02*, i.e. the production of  $^{99m}\text{Tc}$  looks as follows:

```

# Reaction: p + 100Mo Production of 99Tc Isomer= 1
# Half life           : 0 years 0 days 6 hours 0 minutes 36 seconds
# Maximum production at: 0 years 3 days 18 hours 0 minutes 32 seconds
# Initial production rate: 1.08493E-10 [s^-1] Decay rate: 3.20368E-05 [s^-1]
# # time points =100
# Time [h] Activity [GBq] #isotopes [ ] Yield [GBq/mAh] Isotopic frac.
 0.5 3.16572E+01 9.88152E+14 4.22096E+02 0.11878
 1.0 6.15404E+01 1.92093E+15 3.98443E+02 0.11551
 1.5 8.97491E+01 2.80144E+15 3.76115E+02 0.11233
 2.0 1.16377E+02 3.63261E+15 3.55039E+02 0.10925
 2.5 1.41513E+02 4.41720E+15 3.35144E+02 0.10628
 3.0 1.65240E+02 5.15783E+15 3.16363E+02 0.10342
 3.5 1.87638E+02 5.85695E+15 2.98635E+02 0.10067
 4.0 2.08780E+02 6.51689E+15 2.81900E+02 0.09801
 4.5 2.28738E+02 7.13986E+15 2.66103E+02 0.09545
 5.0 2.47577E+02 7.72791E+15 2.51191E+02 0.09298
 5.5 2.65361E+02 8.28301E+15 2.37115E+02 0.09060
 6.0 2.82148E+02 8.80701E+15 2.23828E+02 0.08831
 6.5 2.97994E+02 9.30164E+15 2.11285E+02 0.08609
 7.0 3.12953E+02 9.76855E+15 1.99445E+02 0.08396
 7.5 3.27073E+02 1.02093E+16 1.88268E+02 0.08190
 8.0 3.40402E+02 1.06253E+16 1.77718E+02 0.07991

```

where the final column denotes the fraction of the produced isotope relative to all isotopes of that element. Fig. 7.24 shows the  $^{99m}\text{Tc}$  production as a function of time. Note that the curve is not a straight line due to the decay of  $^{99m}\text{Tc}$  to the ground state.

### 7.3.22 Sample 22: Calculations up to 500 MeV for $p + ^{209}\text{Bi}$

Since TALYS-1.8, the maximum allowed incident energy has formally been extended to 1 GeV. The term 'formally' means that the code seems to produce reasonable results, without crashing, while we are well

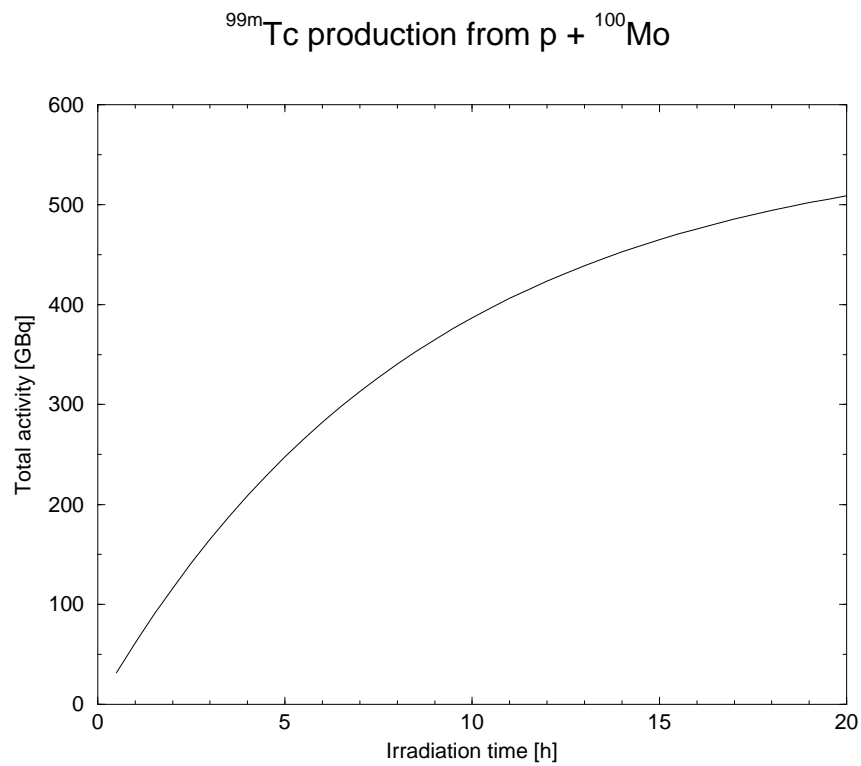


Figure 7.24: Total activity of  $^{99m}\text{Tc}$  produced by a 24 MeV proton accelerator of  $150\ \mu\text{A}$  and a  $^{100}\text{Mo}$  target with an energy of 10 MeV at the back of the target.

aware that the physics beyond about 200 MeV is different from that at lower energies. The question is at which energy the “low-energy” models will start to fail. To investigate this, the extension to 1 GeV has been made. In this sample case we perform calculations for  $p + {}^{209}\text{Bi}$  at 5 different energies,

```
#
# General
#
projectile p
element bi
mass 209
energy 100. 500. 100.
bins 60
```

Here we use the option to give equidistant incident energies from 100 to 500 MeV with steps of 100 MeV. All results can be found in the usual files, e.g. the residual production cross sections of  ${}^{204}\text{Pb}$  are in *rp082204.tot*, which look as follows

```
# p + 209Bi: Production of 204Pb - Total
# Q-value      =-4.42737E+00 mass= 203.973043
# E-threshold= 4.44871E+00
# # energies = 5
#   E           xs
1.000E+02 2.81964E+01
2.000E+02 3.70364E+01
3.000E+02 4.09552E+01
4.000E+02 3.84491E+01
5.000E+02 3.62129E+01
```

Obviously, the user may extend this case up to 1 GeV and with a finer incident energy grid.

### 7.3.23 Sample 23: Neutron multiplicities and fission yields for $n + {}^{242}\text{Pu}$

TALYS contains a partial implementation of the GEF code by Karl-Heinz Schmidt and Beatriz Jurado. Part of GEF has been translated by Vasily Simutkin and Michail Onegin into a Fortran subroutine. In this sample case, the prompt neutron multiplicity as a function of mass,  $\bar{\nu}(A)$ , number of neutrons,  $P(\nu)$ , and the total average,  $\bar{\nu}$ , are calculated, as well as the pre- and post-neutron fission yields as a function of  $N$  and  $A$ . The following input file is used

```
#
# General
#
projectile n
element Pu
mass 242
energy n0-20.grid
#
# Parameters and models
```

```

#
maxrot 2
fymodel 2
best y
#
# Output
#
channels y
filechannels y
ecissave y
inccalc y
eciscalc y
massdis y
# In a second run, you may set
# eciscalc n
# inccalc n
# for time-efficient variations of this input file

```

Note the comment given at the end of the input file. Note also that a hardwired energy grid is used through *n0-20.grid*. The prompt average neutron multiplicity  $\bar{\nu}$  is given in the output file *nubar.tot*. Fig. 7.25 shows a comparison with experimental data and some of the world nuclear data libraries. Fig. 7.26 presents the distribution of  $\bar{\nu}(A)$  as a function of fission product mass, for an incident energy of 1 MeV. This is given in output file *nuA001.000.fis*. Fig. 7.27 presents the distribution of  $\nu$  as a function of number of neutrons, for an incident energy of 1 MeV. This is given in output file *Pnu001.000.fis*.

#### 7.3.24 Sample 24: Local parameter adjustment for $n + {}^{93}\text{Nb}$

```

#
# General
#
projectile n
element nb
mass 93
energy 0.2 5. 0.2
outomp y
#
# Local parameter adjustment
#
rvadjust 1.02 1. 3. 2. 1.10
avadjust 1.02 1. 3. 2. 0.95

##### OPTICAL MODEL PARAMETERS #####

      neutron  on  93Nb

```

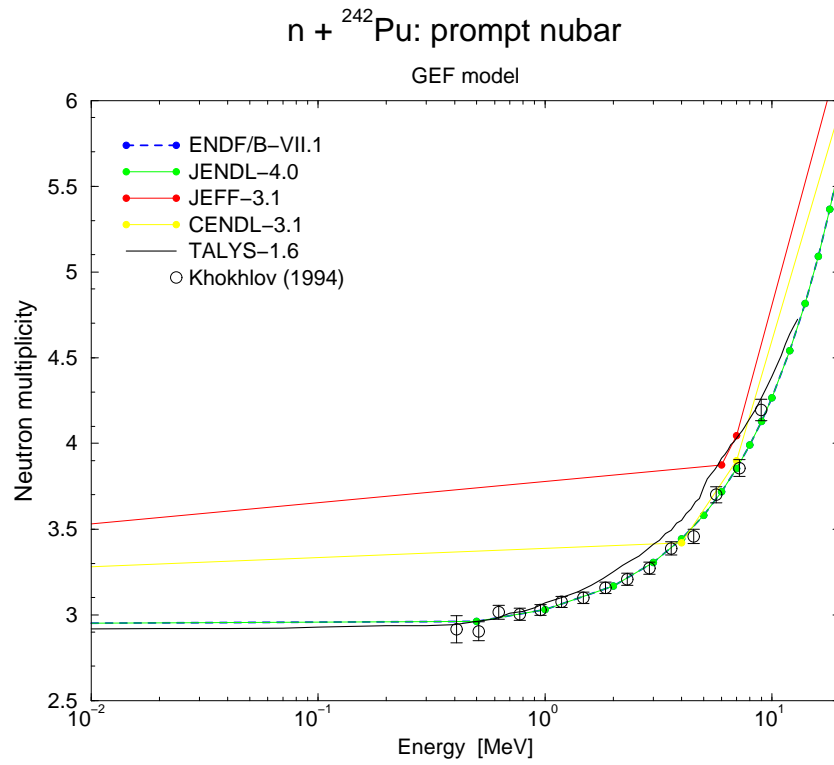


Figure 7.25: Average prompt neutron multiplicity  $\bar{\nu}$  for  $n + {}^{242}\text{Pu}$ , with the GEF model, compared with experimental data and nuclear data libraries.

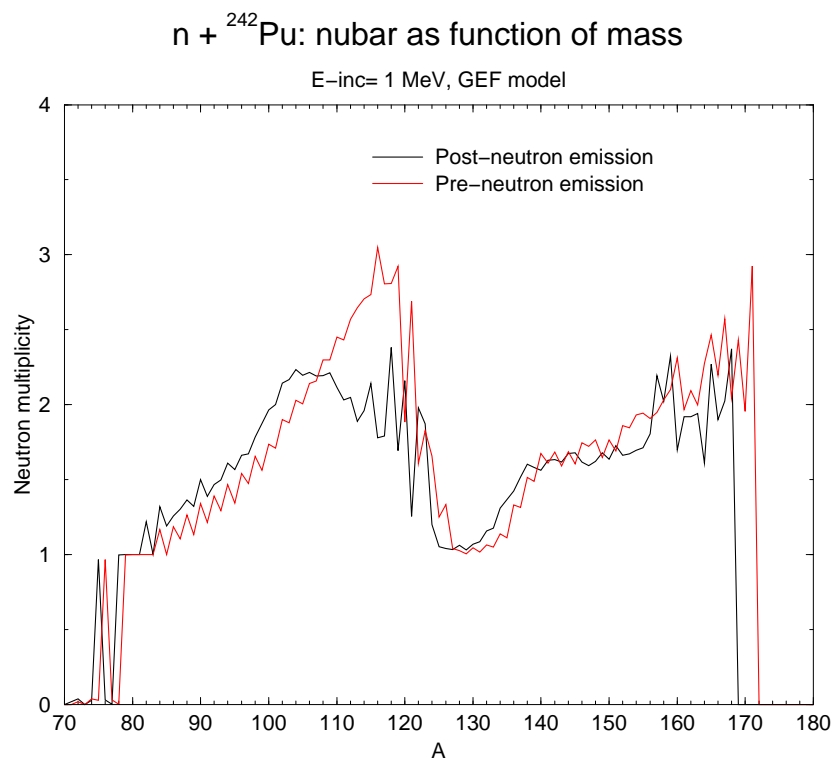


Figure 7.26: Average prompt neutron multiplicity  $\bar{\nu}(A)$ , as a function of fission product mass, for  $n + {}^{242}\text{Pu}$ , with the GEF model.

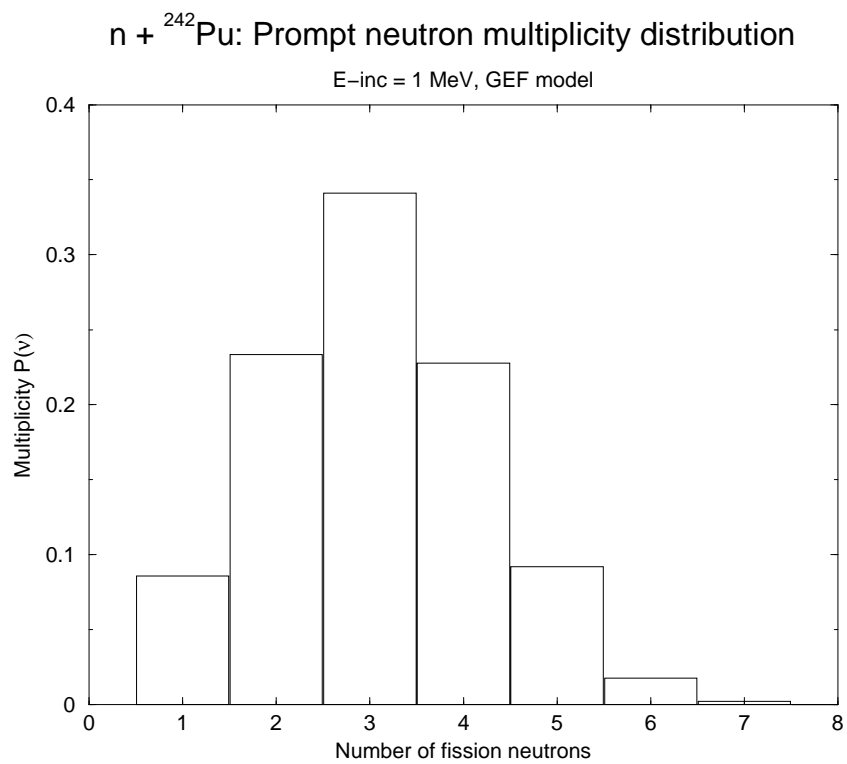


Figure 7.27: Prompt neutron multiplicity distribution  $P(\nu)$ , as a function of the number of neutrons, for  $n + {}^{242}\text{Pu}$ , with the GEF model.

Energy	V	rv	av	W	rw	aw	Vd	rvd	avd	Wd	rwd
0.001	51.02	1.239	0.676	0.14	1.239	0.676	0.00	1.274	0.534	3.32	1.274
0.002	51.02	1.239	0.676	0.14	1.239	0.676	0.00	1.274	0.534	3.32	1.274
.....											
0.910	50.69	1.239	0.676	0.17	1.239	0.676	0.00	1.274	0.534	3.80	1.274
1.011	50.66	1.239	0.676	0.18	1.239	0.676	0.00	1.274	0.534	3.85	1.274
1.112	50.62	1.240	0.676	0.18	1.239	0.676	0.00	1.274	0.534	3.90	1.274
1.213	50.58	1.244	0.675	0.18	1.239	0.676	0.00	1.274	0.534	3.95	1.274
1.314	50.55	1.257	0.671	0.19	1.239	0.676	0.00	1.274	0.534	4.00	1.274
1.415	50.51	1.282	0.665	0.19	1.239	0.676	0.00	1.274	0.534	4.05	1.274
1.516	50.47	1.309	0.657	0.20	1.239	0.676	0.00	1.274	0.534	4.10	1.274
1.617	50.44	1.331	0.651	0.20	1.239	0.676	0.00	1.274	0.534	4.15	1.274
1.718	50.40	1.346	0.647	0.20	1.239	0.676	0.00	1.274	0.534	4.20	1.274
1.820	50.37	1.355	0.645	0.21	1.239	0.676	0.00	1.274	0.534	4.24	1.274
1.921	50.33	1.360	0.643	0.21	1.239	0.676	0.00	1.274	0.534	4.29	1.274
2.022	50.29	1.363	0.643	0.22	1.239	0.676	0.00	1.274	0.534	4.34	1.274
2.224	50.22	1.352	0.646	0.22	1.239	0.676	0.00	1.274	0.534	4.43	1.274
2.426	50.15	1.323	0.653	0.23	1.239	0.676	0.00	1.274	0.534	4.52	1.274
2.628	50.08	1.270	0.668	0.24	1.239	0.676	0.00	1.274	0.534	4.61	1.274
2.830	50.00	1.241	0.676	0.25	1.239	0.676	0.00	1.274	0.534	4.70	1.274
3.033	49.93	1.239	0.676	0.26	1.239	0.676	0.00	1.274	0.534	4.78	1.274
3.235	49.86	1.239	0.676	0.27	1.239	0.676	0.00	1.274	0.534	4.86	1.274
3.437	49.79	1.239	0.676	0.28	1.239	0.676	0.00	1.274	0.534	4.95	1.274
.....											

Note that outside 1 and 3 MeV both rv and av have their constant values while in between these energies the parameters vary according to the prescription given in Section 6.2.12.

### 7.3.25 Sample 25: Direct neutron capture for $n + {}^{89}\text{Y}$

For this sample case we use the input file

```
#
# General
#
projectile n
element y
mass 89
energy n0-5.grid
#
# Parameters
#
gnorm 0.35
racap y
```

The contribution of the direct capture process can be found in the last column of *total.tot*.

### 7.3.26 Sample 26: Different alpha-particle optical model potentials: $\alpha + {}^{165}\text{Ho}$

To demonstrate the variety of (spherical) optical model potentials for alpha-particles available in TALYS, we include a sample case in which 4 OMPs for alpha-particles on  ${}^{165}\text{Ho}$  are compared. The results are given in Fig. 7.28 for the  $(\alpha,n)$  reaction cross sections within the incident-energy range of most recent measured data [24] below the Coulomb barrier.

#### Case 26a: Watanabe folding approach with Koning-Delaroche nucleon potentials

The input file is

```
#
# General
#
projectile a
element Ho
mass 165
energy energies
#
# Model
#
alphaomp 1
#
# Output
#
outomp y
```

where the file energies consists of energies between 7 and 15.5 MeV with 0.5 MeV energy steps, corresponding to the energy range of the measured data. This is the default calculation. Fig. 7.28 displays the resulting  $(\alpha,n)$  reaction cross sections for the target nucleus  ${}^{165}\text{Ho}$ , as obtained in the file rp069168.tot.

#### Case 26b: McFadden-Satchler [21] potential

The input file, using the alphaomp keyword value of 2, is

```
#
# General
#
projectile a
element Ho
mass 165
energy energies
#
# Model
#
```

```
alphaomp 2
#
# Output
#
outomp y
```

**Case 26c: Demetriou, Grama and Goriely [22] double folding dispersive potential**

The input file, using the alphaomp keyword value of 5, is

```
#
# General
#
projectile a
element Ho
mass 165
energy energies
#
# Model
#
alphaomp 5
#
# Output
#
outomp y
```

**Case 26d: Avrigeanu et al. [25] potential**

The input file, using the alphaomp keyword additional value of 6, is

```
#
# General
#
projectile a
element Ho
mass 165
energy energies
#
# Model
#
alphaomp 6
#
# Output
#
outomp y
```

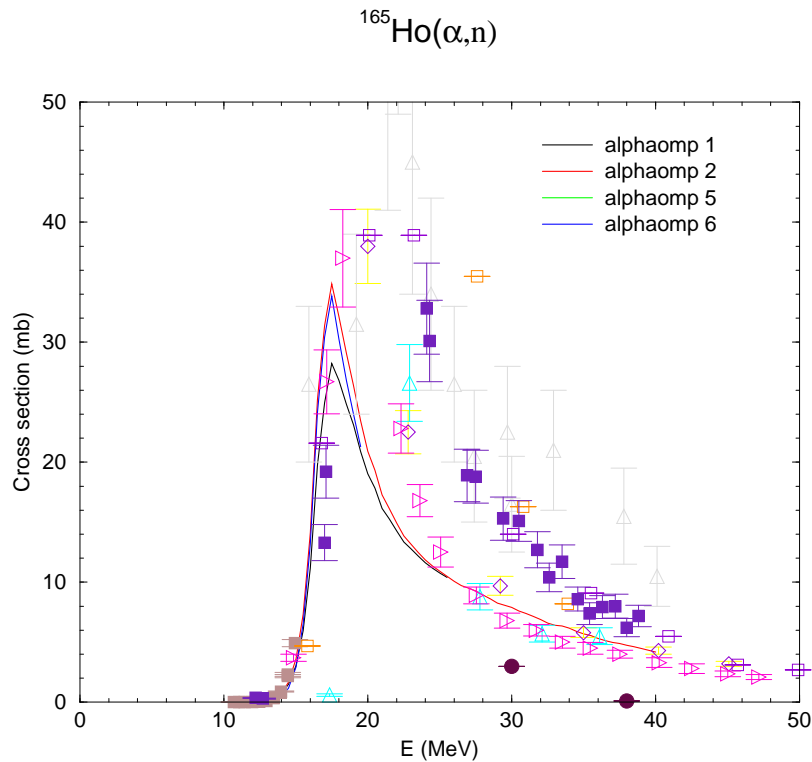


Figure 7.28:  $^{165}\text{Ho}(\alpha,n)^{168}\text{Tm}$  reaction cross sections.

where the file energies consists in addition of energies up to 33 MeV corresponding to all energy ranges which are considered in Table II of Ref. [25].

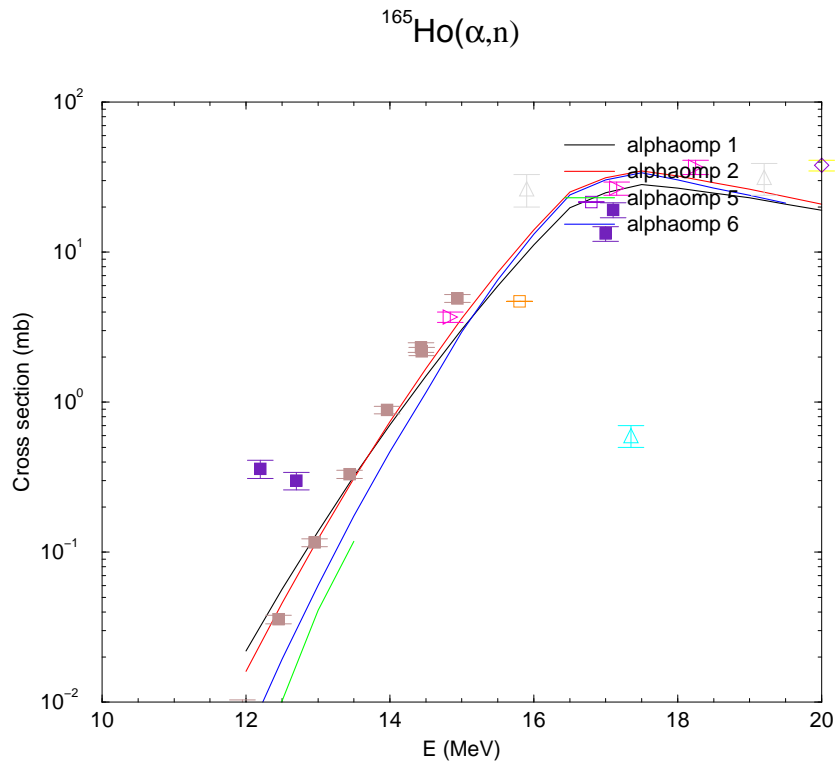
### 7.3.27 Sample 27: Low energy resonance data for $n + ^{107}\text{Ag}$

TALYS can read in resonance parameters, from various possible sources, and call the RECENT code of Red Cullen's PREPRO package, in TALYS included as a subroutine. Low energy pointwise resonance cross sections will then be added to channels like total, elastic, fission and capture.

#### Case 27a: Resonance input file: Standard

The input file is

```
#
# General
#
projectile n
element Y
mass 89
energy n0-2.grid
#
```

Figure 7.29:  $^{165}\text{Ho}(\alpha, n)^{168}\text{Tm}$  reaction cross sections near threshold.

```
# Model
#
resonance y
#
# Output
#
channels y
filechannels y
```

where *n0-2.grid* is the built-in TALYS energy grid for neutrons between 0 and 2 MeV.

#### Case 27b: Resonance input file: Temperature broadening

The input file is

```
#
# General
#
projectile n
element Y
mass 89
energy n0-2.grid
```

```
#  
# Model  
#  
resonance y  
Tres 1200.  
#  
# Output  
#  
channels y  
filechannels y
```

### Case 27c: Resonance input file: Group structure

The input file is

```
#  
# General  
#  
projectile n  
element Y  
mass 89  
energy n0-2.grid  
#  
# Model  
#  
resonance y  
group y  
#  
# Output  
#  
channels y  
filechannels y
```

The results are depicted in Fig. 7.30. Note the discontinuity between the end of the resonance range and the statistical model energy range of TALYS. Obviously, this needs to be studied case by case.

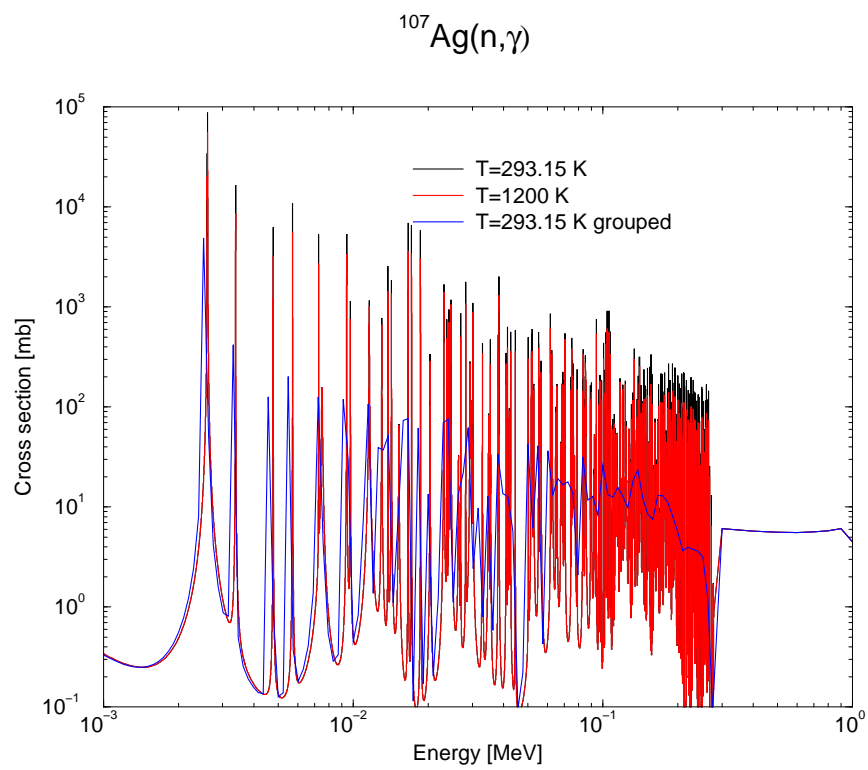


Figure 7.30:  $^{107}\text{Ag}(n,\gamma)$  cross section, at 293.15 K, 1200 K, and grouped.



# Computational structure of TALYS

## 8.1 General structure of the source code

The source of TALYS-1.9 is mostly written in Fortran77, and so far we see that it can be successfully compiled with any f77 or f90/f95/f03/f08 compiler. We have aimed at a setup that is as modular as Fortran77 allows it to be, using programming procedures that are consistent throughout the whole code. In total, there are 316 Fortran subroutines, which are connected through one file, *talys.cmb*, in which all global variables are declared and stored in common blocks. This adds up to a total of more than 90000 lines, of which about 45% are comments. These numbers do not include the *ecis06t* subroutine (23761 lines), see below. On a global level, the source of TALYS consists of 3 main parts: Input, initialisation and reaction calculation. This structure can easily be recognized in the main program, *talys*, which consists merely of calls to the following 5 subroutines:

```
TALYS
|--machine
|--constants
|--talysinput
|--talysinitial
|--talysreaction
|--natural
```

### 8.1.1 machine

In this subroutine, the database is set for the directories with nuclear structure information and possible other operating system dependent settings. Only this subroutine should contain the machine-dependent statements.

### 8.1.2 constants

In this subroutine the fundamental constants are defined. First, in the block data module **constants0** the nuclear symbols and the fundamental properties of particles are defined. Also, the magic numbers, character strings for the two possible parity values and a few fundamental constants are initialized. From these constants, other constants that appear in various reaction formulae are directly defined in subroutine *constants*. Examples are  $2\pi/\hbar$ ,  $\hbar c$ ,  $1/\pi^2\hbar^2c^2$ ,  $1/\pi^2\hbar^3c^2$  and  $amu/\pi^2\hbar^3c^2$ . In the initialisation, they are directly defined in units of MeV and mb. Also, a few other constants are set.

### 8.1.3 talysinput

Subroutine for the user input of keywords and their defaults.

### 8.1.4 talysinitial

Subroutine for the initialisation of nuclear structure and other basic parameters.

### 8.1.5 talysreaction

Subroutine with reaction models.

### 8.1.6 natural

For calculations of reactions on natural elements a fifth subroutine may be called, namely a subroutine to handle natural elements as target. In this subroutine, another loop over *talysinput*, *talysinitial* and *talysreaction* is performed, for each isotope of the element.

### 8.1.7 ecis06t

Another integral part of TALYS that should explicitly be mentioned is Raynal's multi-disciplinary reaction code ECIS-06, which we have included as a subroutine. It is called several times by TALYS for the calculation of basic reaction cross sections, angular distributions and transmission coefficients, for either spherical or deformed nuclei. To enable the communication between ECIS-06 and the rest of TALYS, a few extra lines were added to the original ECIS code. In the source *ecis06t.f* our modifications, not more than 30 lines, can be recognized by the extension *ak000000* in columns 73-80.

We will now describe the main tasks of the three main subroutines mentioned above. We will start with the calling sequence of the subroutines, followed by an explanation of each subroutine. A subroutine will only be explained the first time it appears in the calling tree. Moreover, if a subtree of subroutines has already been described before in the text, we put a ">" behind the name of the subroutine, indicating it can be found in the text above.

## 8.2 Input: talysinput

The subroutine *talysinput* deals with the user input of keywords and their defaults and consists of calls to the following subroutines:

```
talysinput
|--readinput
|--input1
  |--getkeywords
  |--abundance
|--input2
  |--getkeywords
|--input3
  |--getkeywords
|--input4
  |--getkeywords
|--input5
  |--getkeywords
|--input6
  |--getkeywords
|--checkkeyword
  |--getkeywords
|--checkvalue
```

### 8.2.1 readinput

This subroutine reads in all the lines from the user input file as character strings and transfers them to lower case, for uniformity. The actual reading of the keywords from these lines is done in the next six subroutines.

### 8.2.2 input1

In *input1*, the four main keywords **projectile**, **element**, **mass** and **energy** are read and it is determined whether there is only one incident energy (directly given as a number in the input file) or a range of incident energies (given in an external file), after which the energy or range of energies are read in. The maximal incident energy is determined, the incident particle is identified, and the numerical  $Z$ ,  $N$  and  $A$  values for the target are set. A few other keywords can be read in here as well. If a reaction start with an excited nucleus, the population is read in this subroutine. The same holds for the reading of the collection of “best” input parameters. The keywords are read from the input line using the following subroutine,

#### **getkeywords**

With *getkeywords*, all separate words are read from each input line. From each input line we retrieve the keyword, the number of values, and the values themselves. These are all stored in strings to enable an

easy setting of variables in the input subroutines.

For natural targets, *input1* also calls the following subroutine,

### **abundance**

In *abundance*, the isotopic abundances are read from the database or from a user input file, if present.

### **8.2.3 input2, input3, input4, input5, input6**

In the other 5 subroutines, all other keywords that can be present in the input file are identified. Most of them are first set to their default values at the beginning of the subroutine, after which these values can be overwritten by means of a read statement. In all input subroutines, checks are built in for the most flagrant input errors. For example, if a character string is read from the input file where a numerical value is expected, TALYS warns the user and gracefully stops. Subroutine *input2* deals with general physical parameters, *input3* deals with choices for nuclear models, *input4* deals with choices for the output, *input5* deals with nuclear model parameters, and *input6* deals with output to be written to specific files. The order of these subroutines, and the information in them, is important since sometimes defaults are set according to previously set flags.

### **8.2.4 checkkeyword**

In this subroutine, we check whether all keywords given by the user are valid. If for example the wrongly typed keyword **proprojectile** appears in the input, TALYS stops after giving an error message.

### **8.2.5 checkvalue**

This subroutine performs a more intelligent check on erroneous input values. Values of parameters which are out of the ranges that were specified in Chapter 6, and are thus beyond physically reasonable values, are detected here. In such cases the program also gives an error message and stops. Sufficiently wide ranges are set, i.e. the input values have to be really ridiculous before TALYS stops.

## **8.3 Initialisation: talysinitial**

In subroutine *talysinitial*, nuclear structure and other basic parameters are initialised. It consists of calls to the following subroutines:

```
talysinitial
|--particles
|--nuclides
|--grid
```

```
|--mainout
|--timer
```

### 8.3.1 particles

In *particles*, it is determined, on the basis of the **ejectiles** keyword (page 158), which particles are included and which are skipped as competing particles in the calculation. The default is to include all particles from photons to alpha's as competing channels. If specific outgoing particles in the input are given, only those will be included as competing channels. This sets the two logical variables **parinclude** and **parskip**, which are each others' opposite and are used throughout TALYS.

### 8.3.2 nuclides

In *nuclides* the properties of the involved nuclides are set. The following subroutines are called:

```
nuclides
|--strucinitial
|--masses
|--separation
|--structure
|--weakcoupling
|--radwidththeory
|--sumrules
|--kalbachsep
|--egridastro
```

First, in *nuclides* we assign the Z, N, and A of all possible residual nuclei. In TALYS we make use of both absolute and relative designators to describe the nuclides. This is illustrated in Fig. 8.1.

ZZ, NN, AA, Zinit, Ninit, Ainit, Ztarget, Ntarget, Atarget, represent true values of the charge, neutron and mass number. The extension 'init' indicates the initial compound nucleus and 'target' corresponds to the target properties. Zix, Nix, Zcomp and Ncomp are indices relative to the initial compound nucleus. The initial compound nucleus (created by projectile + target) has the indices (0,0). The first index represents the number of protons and the second index the number of neutrons away from the initial compound nucleus. Example: For the reaction  $p + {}^{208}\text{Pb}$ , the set (0,0) represents  ${}^{209}\text{Bi}$  and the set (1,2) represents  ${}^{206}\text{Pb}$ . In the calculation Zix and Nix are used in loops over daughter nuclides and Zcomp and Ncomp are used in loops over decaying mother nuclides. In addition, TALYS makes use of the arrays Zindex and Nindex, which are the first two indices of many other arrays. At any point in the reaction calculation, given the indices of the mother nucleus Zcomp, Ncomp and the particle type, these relative nuclide designators will be directly known through the arrays we initialize in this subroutine.

As an example for the  ${}^{56}\text{Fe}(n,p){}^{56}\text{Mn}$  reaction: Ztarget=26, Ntarget=30, Zcomp=0 (primary compound nucleus), Ncomp=0 (primary compound nucleus), Zindex=1, Nindex=0, Zinit=26, Ninit=31, ZZ=25, NN=31. Next, many structure and model parameters are set. This is done by calling the subroutines mentioned above. Nuclear structure properties for the target, Q-values and the Coulomb barriers are

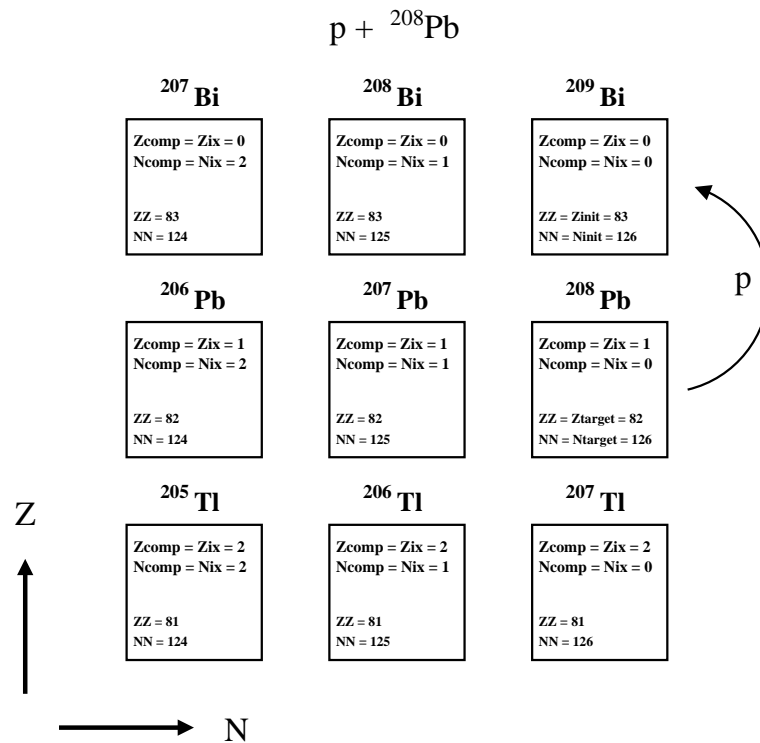


Figure 8.1: Illustration of the various nuclide designators used throughout TALYS.

also set in *nuclides*. Finally, some set-off energies for pre-equilibrium and width fluctuation corrections are set here. The subroutines called are:

### strucinitial

This subroutine merely serves to initialize a lot of arrays. Also, the energy grid for tabulated level densities are set.

### masses

In *masses* the nuclear masses are read from the mass table. The following subroutines are called:

```
masses
|--duflo
```

We read both the experimental masses, of Audi-Wapstra, and the theoretical masses from the mass table. The experimental nuclear mass is adopted, when available. We also read the experimental and theoretical mass excess, to enable a more precise calculation of separation energies. If a residual nucleus is not in the experimental/theoretical mass table, we use the analytical formula of Duflo-Zuker. Finally, the so-called reduced and specific masses are calculated for every nucleus.

*duflo*

Subroutine with the analytical mass formula of Dufflo-Zuker.

**separation**

In *separation*, the separation energies for all light particles on all involved nuclides are set. For consistency, separation energies are always calculated using two nuclear masses of the same type, i.e. both experimental or both theoretical. Hence if nucleus A is in the experimental part of the table but nucleus B is not, for both nuclides the theoretical masses are used.

**structure**

This is a very important subroutine. In *structure*, for each nuclide that can be reached in the reaction chain the nuclear structure properties are read in from the nuclear structure and model database. If the nuclear parameters are not available in tabular form they are determined using models or systematics. TALYS is written such that a call to *structure* only occurs when a new nuclide is encountered in the reaction chain. First, it is called for the binary reaction. Later on, in *multiple*, the call to *structure* is repeated for nuclides that can be reached in multiple emission. The full calling tree is as follows:

```

structure
|--levels
|--gammadecay
|--deformpar
|--resonancepar
|--gammapar
|--omppar
|--radialtable
|--fissionpar
|--densitypar
|--densitytable
|--densitymatch
|--phdensitytable
|--thermalxs
|--partable

```

*levels*

In *levels*, the discrete level information is read. First, for any nuclide, we assign a 0+ ground state to even-even and odd-odd nuclei and a 1/2+ ground state to odd nuclei. Of course, if there is information in the discrete level file, this will be overwritten by the full discrete level info. The amount of information that is read in is different for the first several levels and higher lying levels. For the discrete levels that explicitly appear in the multiple Hauser-Feshbach decay (typically the first 20 levels), we need all information, i.e. the energy, spin, parity, lifetime and branching ratio's. We also read extra levels which

are used only for the level density matching problem or for direct reactions (deformation parameters) in the continuum. The branching ratios and lifetimes are not read for these higher levels. In *levels*, it is also determined whether the target nucleus is in an excited state, in which case the level properties are read in.

#### *gammadecay*

For ENDF-6 data files, specific information on gamma-ray branching ratios, namely the cumulated flux originating from a starting level, needs to be handled. This is performed in *gammadecay*.

#### *deformpar*

In *deformpar*, the deformation parameters or deformation lengths are read, together with the associated coupling scheme for the case of coupled-channels calculations. In the case of vibrational nuclides, simple systematical formulae are used for the first few excited states if no experimental information is available. Spherical (S), vibrational (V) or rotational (R) coupled-channels calculations are automated. Finally, the deformation parameter for rotational enhancement of fission barrier level densities is read in from the nuclear structure database.

#### *resonancepar*

The experimental values from the resonance parameter file,  $D_0$ ,  $\Gamma_\gamma$ , and  $S_0$  are read here. A simple systematics for  $\Gamma_\gamma$  derived by Kopecky (2002), is provided in the block data module **gamdata** for nuclides not present in the table.

#### *gammapar*

In *gammapar*, the default giant dipole resonance parameters for gamma-ray strength functions are read from the database. Also the default values for M1, E1, E2 etc., are set using systematics if no value is present in the database [163]. Also, Goriely's microscopic gamma ray strength functions can be read in this subroutine.

#### *omppar*

The optical model parameters for nucleons are read from the database. If there are no specific parameters for a nuclide, they are determined by a global optical model for neutrons and protons. Also possible user-supplied input files with optical model parameters are read here.

*radialtable*

The radial matter densities for protons and neutrons are read from the database, to perform semi-microscopic OMP calculations. Also possible user-supplied input files with radial matter densities are read here.

*fissionpar*

In *fissionpar*, the fission barrier parameters are read, using the following subroutines:

```
fissionpar
|--barsierk
  |--plegendre
|--rldm
|--wkb
|--rotband
|--rotclass2
```

Several databases with fission barrier parameters can be read. There are also calls to two subroutines, *barsierk* and *rldm*, which provide systematical predictions for fission barrier parameters from Sierk's model and the rotating liquid drop model, respectively. As usual, it is also possible to overrule these parameters with choices from the user input. If *fismodel 1*, also the head band states and possible class II states are read in this subroutine. If *fismodel 5*, the WKB approximation as implemented in *wkb.f* is used. Finally, rotational bands are built on transition and class II states. Note that next to the chosen fission model (**fismodel**), there is always an alternative fission model (**fismodelalt**) which comes into play if fission parameters for the first choice model are not available.

*barsierk*

Using the rotating finite range model, the  $l$ -dependent fission barrier heights are estimated with A.J. Sierk's method. This subroutine returns the fission barrier height in MeV. It is based on calculations using yukawa-plus-exponential double folded nuclear energy, exact Coulomb diffuseness corrections, and diffuse-matter moments of inertia [103]. The implementation is analogous to the subroutine "asierk" written by A.J. Sierk (LANL, 1984). This subroutine makes use of the block data module *fisdata*.

*plegendre*

This function calculates the Legendre polynomial.

*rldm*

Using the rotating liquid drop model [104], the fission barrier heights are estimated. This subroutine returns the fission barrier height in MeV and is based on the subroutine FISROT incorporated in ALICE-

91 [3]. This subroutine makes use of the block data module *fisdata*.

### *wkb*

This subroutines computes fission transmission coefficients according to the WKB approximation. The subroutine itself calls various other subroutines and functions.

### *rotband*

Here, the rotational bands are built from the head band transition states, for fission calculations.

### *rotclass2*

Here, the rotational bands are built from the class II states. For this, the maximum energy of class II states is first determined.

### *densitypar*

In *densitypar*, parameters for the level density are set, or read from the database. The following subroutines are called:

```
densitypar
|--mliquid1
|--mliquid2
```

The  $N_L$  and  $N_U$  of the discrete level region where the level density should match are read or set. Next the spin cut-off parameter for the discrete energy region is determined. All parameters of the Ignatyuk formula are determined, either from systematics or from mutual relations, for the level density model under consideration. Pairing energies and, for the generalized superfluid model, critical functions that do not depend on energy, are set. There are many input possibilities for the energy-dependent level density parameter of the Ignatyuk formula. The required parameters are *alev*, *alimit*, *gammald* and *deltaW*. The Ignatyuk formula implies that these parameters can not *all* be given at the same time in the input file, or in a table. All possibilities are handled in this subroutine. Also, the single-particle state density parameters are set.

### *mliquid1*

Function to calculate the Myers-Swiatecki liquid drop mass for spherical nuclei.

### *mliquid2*

Function to calculate the Goriely liquid drop mass for spherical nuclei.

*densitytable*

This subroutine reads in microscopic tabulated level densities.

*phdensitytable*

This subroutine reads in microscopic tabulated particle-hole level densities.

*densitymatch*

The following subroutines are called:

```
densitymatch
|--ignatyuk
|--colenhance
|--fermi
|--matching
|--poll
|--dtheory
```

In *densitymatch*, the matching levels for the temperature and Fermi gas level densities are determined, and the level density matching problem is solved for both ground-state level densities and level densities on fission barriers. The matching problem is solved by calling *matching*.

*ignatyuk*

The level density parameter as function of excitation energy is calculated here.

*colenhance*

In *colenhance*, the collective (vibrational and rotational) enhancement for fission level densities is calculated. Here, a distinction is made between (a) **colenhance n**: collective effects for the ground state are included implicitly in the intrinsic level density, and collective effects on the barrier are determined relative to the ground state, and (b) **colenhance y**: both ground state and barrier collective effects are included explicitly. The calling tree is:

```
colenhance
|--ignatyuk
```

*fermi*

In *fermi*, the Fermi gas level density is calculated. The calling tree is:

```
fermi
|--spincut
```

### *spincut*

In *spincut*, the spin cut-off parameter is calculated. Above the matching energy, this is done by an energy-dependent systematical formula. Below the matching energy, the value for the spin cut-off parameter is interpolated from the value at the continuum energy and the value from the discrete energy region. For the generalized superfluid model, the spin cut-off parameter is related to its value at the critical energy.

### *matching*

In *matching*, the matching problem of Eq. (4.271) is solved. First, we determine the possible region of the roots of the equation, then we determine the number of solutions and finally we choose the solution for our problem. The calling tree is:

```
matching
|--ignatyuk
|--zbrak
|--rtbis
|--match
  |--poll
```

### *zbrak*

This subroutine finds the region in which the matching equation has a root (“bracketing” a function).

### *rtbis*

This function finds the roots of a function.

### *match*

This function represents Eq. (4.271).

### *poll*

Subroutine for interpolation of first order.

*dtheory*

Subroutine to calculate the theoretical average resonance spacing from the level density. The following subroutines are called:

```
dtheory
|--levels
|--density
```

*density*

This is the function for the level density. It is calculated as a function of the excitation energy, spin, parity, fission barrier and model identifier. On the basis of **ldmodel**, the level density model is chosen. The following subroutines are called:

```
density
|--ignatyuk
|--densitytot
|--spindis
|--locate
```

*densitytot*

This is the function for the total level density. It is calculated as a function of the excitation energy, fission barrier and model identifier. On the basis of **ldmodel**, the level density model is chosen. The following subroutines are called:

```
densitytot
|--ignatyuk
|--colenhance >
|--gilcam
  |--fermi >
|--bsfgmodel
  |--fermi >
  |--spincut >
|--superfluid
  |--fermi >
  |--spincut >
|--locate
```

*spindis*

In *spindis*, the Wigner spin distribution is calculated. The calling tree is:

```
spindis
|--spincut >
```

*locate*

Subroutine to find a value in an ordered table.

*gilcam*

In *gilcam*, the Gilbert-Cameron level density formula is calculated with the constant temperature and the Fermi gas expression.

*bsfgmodel*

In *bsfgmodel*, the Back-shifted Fermi gas formula is calculated with the Grossjean-Feldmeier approximation at low energy.

*superfluid*

In *superfluid*, the generalized superfluid model level density is calculated.

### 8.3.3 thermalxs

In *thermalxs*, experimental cross sections at thermal energies are read in.

*partable*

Subroutine to write model parameters per nucleus to a separate output file.

### weakcoupling

Subroutine *weakcoupling* is only called for odd target nuclides. The even-even core is determined and its deformation parameters, if any, are retrieved. These are then re-distributed over the levels of the odd-nucleus, so that later on DWBA calculations with the even core can be made. The selection of the odd-nucleus levels is automatic, and certainly not full proof. The following subroutines are called:

```
weakcoupling
|--deformpar >
|--levels >
```

**radwidththeory**

Subroutine for the calculation of the theoretical total radiative width, using gamma-ray strength functions and level densities. The following subroutines are called:

```
radwidththeory
|--levels >
|--density >
```

**sumrules**

Using sum rules for giant resonances, the collective strength in the continuum is determined. The deformation parameters of the collective low lying states are subtracted from the sum, so that the final GR deformation parameters can be determined.

**kalbachsep**

In *kalbachsep*, the separation energies for the Kalbach systematics are computed. We use the Myers-Swiatecki parameters as used by Kalbach [71].

**egridastro**

Subroutine to calculate the default incident energy grid for astrophysical rates. For astrophysical calculations, no use is made of an incident energy as supplied by the user, but instead is hardwired.

**8.3.4 grid**

In subroutine *grid*, the outgoing energy grid to be used for spectra and the transmission coefficients and inverse reaction cross section calculation is fixed. This non-equidistant grid ensures that the calculation for outgoing energies of a few MeV (around the evaporation peak) is sufficiently precise, whereas at higher energies a somewhat coarser energy grid can be used. For the same reason, this energy grid is used for the calculation of transmission coefficients. The begin and end of the energy grid for charged particles is set. The energy grid for which TALYS uses extrapolation (basically from thermal energies up to the first energy where we believe in a nuclear model code) is set. Also a few parameters for the angular grid, the transmission coefficient numerical limit, and temperatures for astrophysical calculations are set here. The following subroutines are called:

```
grid
|--energies
  |--locate
|--locate
```

**energies**

This subroutine is called for each new incident energy. The center-of-mass energy and the wave number are calculated (relativistic and non-relativistic), the upper energy limit for the energy grid is set, as well as the outgoing energies that belong to discrete level scattering. Finally, several incident energy-dependent flags are disabled and enabled.

**8.3.5 mainout**

Subroutine *mainout* takes care of the first part of the output. The output of general information such as date, authors etc., is printed first. Next, the basic reaction parameters are printed. The following subroutines are called:

```
mainout
|--inputout
  |--yesno
|--levelsout
|--densityout
  |--aldmatch
  |--spincut >
  |--ignatyuk
  |--colenhance >
  |--densitytot >
  |--density >
|--fissionparout
```

**inputout**

In this subroutine, the (default) values of all input keywords are written. This will appear at the top of the output file.

*yesno*

Function to assign the strings 'y' and 'n' to the logical values .true. and .false..

**levelsout**

In *levelsout*, all discrete level information for the nucleus under consideration is printed.

**densityout**

In *densityout*, all level density parameters are written, together with a table of the level density itself. For fissile nuclides, also the level densities on top of the fission barriers are printed. Cumulative level

densities are calculated and written to files.

#### *aldmatch*

For fission, the effective level density parameter, which we only show for reference purposes, is obtained in three steps: (1) create the total level density in Fermi gas region, (2) apply a rotational enhancement to the total level density (3) determine the effective level density parameter by equating the rotational enhanced level density by a new effective total level density. The calling tree is:

```
aldmatch
|--ignatyuk
|--fermi >
|--spindis >
|--colenhance >
|--spincut >
```

#### **fissionparout**

In this subroutine, we write the main fission parameters, such as barrier heights and widths, and the head band transition states, rotational band transition states and class II states.

#### **8.3.6 timer**

Subroutine for the output of the execution time and a congratulation for the successful calculation.

## **8.4 Nuclear models: talysreaction**

The main part of TALYS, *talysreaction*, contains the implementation of all the nuclear reaction models. First it calls *basicxs*, for the calculation of transmission coefficients, inverse reaction cross sections, etc. which are to be calculated only once (i.e. regardless of the number of incident energies). Next, for either one or several incident energies, subroutines for the nuclear reaction models are called according to the flags set by default or by input. During these nuclear model calculations, information such as cross sections, spectra, angular distributions, and nuclide populations, is collected and stored. At the end, all results are collected and transferred to the requested output. Finally, a message that the calculation was successful should be printed. The following subroutines are called:

```
talysreaction
|--basicxs
|--preeqinit
|--excitoninit
|--compoundinit
|--astroinit
```

```
|--energies >  
|--reacinitial  
|--incident  
|--exgrid  
|--recoilinit  
|--direct  
|--preeq  
|--population  
|--compnorm  
|--comptarget  
|--binary  
|--angdis  
|--multiple  
|--channels  
|--totalxs  
|--spectra  
|--massdis  
|--residual  
|--totalrecoil  
|--normalization  
|--thermal  
|--output  
|--finalout  
|--astro  
|--endf  
|--timer
```

### 8.4.1 basicxs

The transmission coefficients and inverse reaction cross sections for the outgoing energy grid need to be calculated only once for all particles and gamma's, for energies up to the maximal incident energy. The following subroutines are called:

```
basicxs  
|--basicinitial  
|--inverse  
|--gamma
```

#### **basicinitial**

In *basicinitial*, all arrays that appear in this part of the program are initialized.

**inverse**

Subroutine *inverse* organises the calculation of total, reaction and elastic cross sections and transmission coefficients for all outgoing particles and the whole emission energy grid (the inverse channels). The following subroutines are called:

```
inverse
|--inverseecis
|--inverseread
|--inversenorm
|--inverseout
```

*inverseecis*

In this subroutine the loop over energy and particles is performed for the basic ECIS calculations. For each particle and energy, the optical model parameters are determined by calling *optical*. The subroutine *ecisinput* is called for the creation of the ECIS input files. At the end of this subroutine, *ecis06t* is called to perform the actual ECIS calculation. The following subroutines are called:

```
inverseecis
|--ecisinput
  |--optical
  |--mom
|--optical
|--ecis06t >
```

*ecisinput*

This subroutine creates a standard ECIS input file for spherical or coupled-channels calculations.

*optical*

This is the main subroutine for the determination of optical model parameters. The following subroutines are called:

```
optical
|--opticaln
  |--soukhovitskii
|--opticalp
  |--soukhovitskii
|--opticald
  |--opticaln
  |--opticalp
|--opticalt
```

```

|--opticaln
|--opticalp
|--opticalh
|--opticaln
|--opticalp
|--opticala
|--opticaln
|--opticalp

```

### *opticaln, opticalp*

Subroutines for the neutron and proton optical model parameters. If an optical model file is given with the **optmod** keyword, see page 178, we interpolate between the tabulated values. In most cases, the general energy-dependent form of the optical potential is applied, using parameters per nucleus or from the global optical model, both from subroutine *omppar*.

### *soukhovitskii*

Subroutine for the global optical model for actinides by Soukhovitskii et al. [44].

### *opticald, opticalt, opticalh, opticala*

Subroutines for deuteron, triton, helion and alpha optical potentials. In the current version of TALYS, we use the Watanabe method [15] to make a composite particle potential out of the proton and neutron potential.

### *mom*

Subroutine for the semi-microscopic JLM optical model. This is basically Eric Bauge's MOM code turned into a TALYS subroutine. Inside this subroutine, there are many calls to other local subroutines. It also uses the file *mom.cmb*, which contains all common blocks and declarations for *mom.f*.

### *inverseread*

In this subroutine the results from ECIS are read. For every particle and energy we first read the reaction (and for neutrons the total and elastic) cross sections. Next, the transmission coefficients are read into the array *Tjl*, which has four indices: particle type, energy, spin and l-value. For spin-1/2 particles, we use the array indices -1 and 1 for the two spin values. For spin-1 particles, we use -1, 0 and 1 and for spin-0 particles we use 0 only. For rotational nuclei, we transform the rotational transmission coefficients into their spherical equivalents for the compound nucleus calculation. Also, transmission coefficients averaged over spin are put into separate arrays. For each particle and energy, the maximal l-value is determined to constrain loops over angular momentum later on in the code.

*inversenorm*

In *inversenorm*, a semi-empirical formula for the reaction cross section can be invoked to overrule the results from the optical model. This is sometimes appropriate for complex particles. The normalization is only performed if the option for semi-empirical reaction cross sections is enabled. The semi-empirical results have a too sharp cut-off at low energies. Therefore, for the lowest energies the optical model results are normalized with the ratio at the threshold. The following subroutines are called:

```
inversenorm
|--tripathi
    |--radius
```

*tripathi*

Function for semi-empirical formula for the reaction cross section by Tripathi et al.. The original coding (which is hard to understand) does not coincide with the formulae given in Ref. [39] though the results seem to agree with the plotted results.

*radius*

Function for the radius, needed for the Tripathi systematics.

*inverseout*

This subroutine takes care of the output of reaction cross sections and transmission coefficients. Depending on the **outtransenergy** keyword, see page 253, the transmission coefficients are grouped per energy or per angular momentum.

**gamma**

This subroutine deals with calculations for gamma cross sections, strength functions and transmission coefficients. The following subroutines are called:

```
gamma
|--gammanorm
|--gammaout
```

*gammanorm*

In this subroutine, we normalize the gamma-ray strength functions by imposing the condition that the transmission coefficients integrated from zero up to neutron separation energy are equal to the ratio of the experimental mean gamma width and mean level spacing for s-wave neutrons. The gamma transmission

coefficients are generated through calls to the strength function *fstrength*. The gamma-ray cross sections are also normalized. The following subroutines are called:

```
gammanorm
|--density >
|--fstrength
|--gammamaxs
|--fstrength
```

### *fstrength*

In *fstrength*, the gamma-ray strength functions according to Kopecky-Uhl or Brink-Axel are calculated, or are interpolated from Goriely's HFB or HFBCS tables.

### *gammamaxs*

In *gammamaxs*, the photo-absorption cross sections are calculated. They consist of a GDR part and a quasi-deuteron part.

### *gammaout*

In *gammaout*, the gamma-ray strength functions, transmission coefficients and cross sections are written to output. The following subroutines are called:

```
gammaout
|--fstrength
```

## 8.4.2 preeqinit

General quantities needed for pre-equilibrium calculations are set, such as factorials, spin distribution functions and Pauli correction factors. The following subroutines are called:

```
preeqinit
|--bonetti
|--mom >
|--optical >
```

### **bonetti**

In this subroutine, the average imaginary volume potential for the internal transition rates is calculated.

### 8.4.3 excitoninit

Quantities needed for exciton model calculations are set, such as preformation factors, factors for the emission rates and charge conserving Q-factors.

### 8.4.4 compoundinit

Quantities needed for compound nucleus model calculations are set, such as factors for width fluctuation and angular distribution calculations. The following subroutines are called:

```
compoundinit
|--gaulag
|--gauleg
```

### 8.4.5 astroinit

Quantities needed for astrophysical reaction calculations are initialized.

#### **gaulag**

This subroutine is for Gauss-Laguerre integration.

#### **gauleg**

This subroutine is for Gauss-Legendre integration.

### 8.4.6 reacinitial

In *reacinitial*, all arrays that appear in the nuclear reaction model part of the program are initialized.

### 8.4.7 incident

Subroutine *incident* handles the calculation of total, reaction, elastic cross section, transmission coefficients and elastic angular distribution for the incident energy. Also, some main parameters for the current incident energy are set. The following subroutines are called:

```
incident
|--yesno
|--incidentecis
  |--optical    >
  |--mom       >
```

```

|--ecisinput >
|--incidentread
|--incidentnorm
|--tripathi >
|--incidentgamma
|--fstrength
|--gammamaxs >
|--radwidththeory >
|--gammanorm >
|--spr
|--incidentout

```

### **incidentecis**

In this subroutine the basic ECIS calculation for the incident particle and energy is performed for either a spherical or a deformed nucleus. The optical model parameters are determined by calling *optical*. The subroutine *ecisinput* is called for the creation of the ECIS input files. At the end of this subroutine, *ecis06t* is called to perform the actual ECIS calculation.

### **incidentread**

In this subroutine the results from ECIS are read for the incident particle and energy. We first read the reaction (and for neutrons the total and elastic) cross section. Next, the transmission coefficients are read into the array *Tjline*, which has four indices: particle type, energy, spin and *l*-value. For spin-1/2 particles, we use the indices -1 and 1 for the two spin values. For spin-1 particles, we use -1, 0 and 1 and for spin-0 particles we use 0 only. For rotational nuclei, we transform the rotational transmission coefficients into their spherical equivalents for the compound nucleus calculation. Also, transmission coefficients averaged over spin are put into separate arrays. The maximal *l*-value is determined to constrain loops over angular momentum later on in the code. The direct reaction Legendre coefficients and angular distribution are also read in. For coupled-channels calculations, we also read the discrete inelastic angular distributions and cross sections.

### **incidentnorm**

In *incidentnorm*, the transmission coefficients can be normalized with values obtained from semi-empirical systematics for the reaction cross section, if required.

### **incidentgamma**

Here, the transmission coefficients for the incident gamma channel, in the case of photo-nuclear reactions, are generated.

**spr**

In *spr*, the S, P and R resonance parameters for low incident neutron energies are calculated and, if requested, written to file.

**incidentout**

In this subroutine the basic cross sections, transmission coefficients and possible resonance parameters for the incident channel are written to output.

**8.4.8 exgrid**

In *exgrid*, the possible routes to all reachable residual nuclei are followed, to determine the maximum possible excitation energy for each nucleus, given the incident energy. From this, the excitation energy grid for each residual nucleus is determined. The first NL values of the excitation energy grid  $E_x$  correspond to the discrete level excitation energies of the residual nucleus. The NL+1th value corresponds to the first continuum energy bin. The continuum part of the nuclides are then divided into energy bins. The Q-values for the residual nuclides are also determined. Finally, the calculation of level densities in TALYS can be done outside many loops of various quantum numbers performed in other subroutines. Therefore, in *exgrid* we store the level density as function of residual nucleus, excitation energy, spin and parity. The following subroutines are called:

```
exgrid
|--density >
|--spincut >
```

**8.4.9 recoilinit**

In this subroutine the basic recoil information is initialized. Various arrays are initialized and the maximum recoil energies for all residual nuclides are determined. Recoil energy and angular bins are determined.

**8.4.10 direct**

Subroutine *direct* takes care of the calculation of direct cross sections to discrete states that have not already been covered as coupled-channels for the incident channel, such as DWBA and giant resonance cross sections. The following subroutines are called:

```
direct
|--directecis
  |--ecisinput >
|--directread
```

```
|--giant
|--directout
```

### **directecis**

In this subroutine the basic DWBA calculation for a spherical nucleus is performed. The subroutine *ecisinput* is called for the creation of the ECIS input files. At the end of this subroutine, *ecis06t* is called to perform the actual ECIS calculation.

### **directread**

In this subroutine the results from ECIS are read for the DWBA calculation. We first read the direct cross section for the collective discrete states. The direct reaction Legendre coefficients and angular distribution are also read in. The procedure is repeated for the giant resonance states.

### **giant**

In *giant*, the DWBA cross sections for the continuum are smeared into spectra. The same is done for other collective states that are in the continuum.

### **directout**

In this subroutine the direct cross sections for discrete states and giant resonances are written to output.

## **8.4.11 preeq**

Subroutine *preeq* is the general module for pre-equilibrium reactions. Particle-hole numbers for the reaction under consideration are initialized. Depending on the chosen pre-equilibrium model, the following subroutines may be called:

```
preeq
|--surface
|--exciton
|--excitonout
|--exciton2
|--exciton2out
|--msd
|--msdplusmsc
|--preeqcomplex
|--preeqcorrect
|--preeqttotal
|--preeqang
|--preeqout
```

**surface**

This function evaluates the effective well depth for pre-equilibrium surface effects.

**exciton**

This is the main subroutine for the one-component exciton model. For each exciton number, we subsequently calculate the emission rates and the lifetime of the exciton state according to the never-come-back approximation. There is also a possibility to create J-dependent pre-equilibrium cross sections using the spin distribution. As an alternative (which is the default), the Hauser-Feshbach spin distribution is adopted. The following subroutines are called:

```
exciton
|--emissionrate
  |--ignatyuk
  |--preeqpair
  |--phdens
    |--finitewell
|--lifetime
  |--lambdaplus
    |--matrix
    |--ignatyuk
    |--preeqpair
    |--finitewell
    |--phdens      >
```

*emissionrate*

This subroutine delivers the particle and photon emission rates (4.121), (4.125), (4.142) for the one-component exciton model.

*preeqpair*

In this subroutine, the pre-equilibrium pairing correction according to either Fu, see Eq. 4.91, or to the compound nucleus value is calculated.

*phdens*

The function *phdens* computes the one-component particle-hole state density (4.123).

*finitewell*

The function *finitewell* computes the finite well function (4.96).

*lifetime*

In this subroutine, the lifetime of the exciton state (4.126) is calculated, according to the never-come-back approximation.

*lambdaplus*

The function *lambdaplus* delivers the transition rates (4.129) in either analytical or numerical form, for the one-component exciton model based on matrix elements or on the optical model.

*matrix*

This function computes the matrix element (4.132) for the one-component model, and (4.112) for the two-component model.

**excitonout**

In *excitonout* all information of the one-component exciton model, such as matrix elements, emission rates and lifetimes, is written.

**exciton2**

This is the main subroutine for the two-component exciton model. For each exciton number, we subsequently calculate the emission rates and exchange terms (both in subroutine *exchange2*) and the lifetime of the exciton state. There is also a possibility to create J-dependent pre-equilibrium cross sections using the spin distribution. As an alternative (which is the default), the Hauser-Feshbach spin distribution is adopted. The following subroutines are called:

```
exciton2
|--exchange2
  |--emissionrate2
    |--ignatyuk
    |--preeqpair
    |--phdens2
      |--finitewell
  |--lambdapiplus
    |--matrix
    |--ignatyuk
    |--preeqpair
    |--finitewell
    |--phdens2    >
  |--lambdanuplus
    |--matrix
```

```

|--ignatyuk
|--preeqpair
|--finitewell
|--phdens2    >
|--lambdapinu
|--matrix
|--ignatyuk
|--preeqpair
|--finitewell
|--phdens2    >
|--lambdanupi
|--matrix
|--ignatyuk
|--preeqpair
|--finitewell
|--phdens2    >
|--lifetime2

```

#### *exchange2*

In *exchange2*, the probabilities (4.101) for the strength of the exciton state are calculated.

#### *phdens2*

The function *phdens2* computes the two-component particle-hole state density (4.90).

#### *emissionrate2*

This subroutine delivers the particle and photon emission rates for the two-component exciton model.

#### *lambdapiplus, lambdanuplus*

The function *lambdapiplus* delivers the proton transition rates (4.103) in either analytical or numerical form, for the two-component exciton model based on matrix elements or the optical model. Similarly for *lambdanuplus*.

#### *lambdapinu, lambdanupi*

The function *lambdapinu* delivers the proton-neutron transition rates (4.103) in either analytical or numerical form, for the two-component exciton model based on matrix elements or the optical model. Similarly for *lambdanupi*.

*lifetime2*

In this subroutine, the lifetime of the exciton state through the quantity of Eq. (4.100) is calculated.

**exciton2out**

In *exciton2out* all information of the two-component exciton model, such as matrix elements, emission rates and lifetimes, is written.

**msd**

This subroutine calculates pre-equilibrium cross sections according to the macroscopic multi-step direct (MSD) model. The MSD model is implemented for neutrons and protons only. The following subroutines are called:

```

msd
|--msdinit
  |--interangle
|--dwbaecis
  |--ecisdwbamac
    |--optical >
  |--dwbaread
  |--dwbaout
  |--dwbaint
  |--onecontinuumA
    |--ignatyuk
    |--omega
      |--phdens >
  |--onestepA
    |--ignatyuk
    |--omega >
    |--locate
    |--pol2
|--msdcalc
  |--onestepB
    |--cmsd
  |--onecontinuumB
  |--cmsd
  |--multistepA
  |--multistepB
  |--locate
  |--pol2
|--msdtotal
|--msdout

```

*msdinit*

This subroutine initializes various arrays for the multi-step direct calculation, such as the MSD energy grid and the intermediate angles through a call to *interangle*.

*interangle*

Subroutine *interangle* produces the intermediate angles for MSD model, by the addition theorem. For multi-step reactions, this is necessary to transform the ingoing angle of the second step and link it with the outgoing angle of the first step.

*dwbaecis*

This subroutine takes care of all the ECIS calculations that need to be performed for the various steps of the multi-step reaction. Subsequently, DWBA calculations are performed for the first exchange one-step reaction, the inelastic one-step reaction and the second exchange one-step reaction. For this, various subroutines are called.

*dwbaecis*

Subroutine *ecisdwbamac* creates the ECIS input file for a macroscopic DWBA calculation. Potentials for the incident, transition and outgoing channel are calculated.

*dwbaread*

In this subroutine the results from ECIS are read. For every energy and spin we read the total DWBA cross section and the angle-differential DWBA cross section.

*dwbaread*

This subroutine takes care of the output of the DWBA cross sections.

*dwbaint*

In *dwbaint*, the DWBA cross sections are interpolated on the appropriate energy grid.

*onecontinuumA*

In *onecontinuumA*, the continuum one-step cross sections to be used in multi-step calculations are calculated by multiplying the DWBA cross sections by particle-hole state densities.

*omega*

This is a function of the particle-hole state density per angular momentum.

*onestepA*

In *onestepA*, the unnormalized one-step direct cross sections for the outgoing energy grid are calculated (these will be normalized in subroutine *onestepB*).

*pol2*

Subroutine for interpolation of second order.

*msdcalc*

This is the general subroutine for the final MSD calculations.

*onestepB*

In *onestepB*, the one-step direct cross sections are calculated using a final normalization.

*onecontinuumB*

In *onecontinuumB*, the final one-step direct cross sections for use in the multi-step calculations are computed using the final normalization.

*multistepA*

In *multistepA*, the multi-step direct cross sections (second and higher steps) are calculated using a final normalization.

*multistepB*

In *multistepB*, the multi-step direct cross sections are interpolated on the final outgoing energy grid.

*msdtotal*

In *msdtotal*, the total multi-step direct cross sections are calculated.

*msdout*

In *msdout*, the multi-step direct cross sections are written to output.

**msdplusmsc**

In this subroutine, the MSD cross sections are put in the general pre-equilibrium cross sections.

**preeqcomplex**

Subroutine *preeqcomplex* handles pre-equilibrium complex particle emission. The implemented complex particle emission model is described in Section 4.4.4. Note that several purely empirical fixes to the model were needed to prevent divergence of certain cross section estimates. The subroutine consists of two main parts: One for stripping/pickup and one for alpha knock-out reactions. The following subroutines are called:

```
preeqcomplex
|--phdens2    >
```

**preeqcorrect**

This subroutine handles the correction of pre-equilibrium cross sections for direct discrete cross sections. If the cross sections for discrete states have *not* been calculated by a direct reaction model, we collapse the continuum pre-equilibrium cross sections in the high-energy region on the associated discrete states. After this, the pre-equilibrium cross sections in the discrete energy region are set to zero. The following subroutines are called:

```
preeqcorrect
|--locate
```

**preeqtotal**

In *preeqtotal*, the total pre-equilibrium cross sections are calculated. The pre-equilibrium spectra and spectra per exciton number are summed to total pre-equilibrium cross sections. Special care is taken for the continuum bin with the highest outgoing energy, i.e. the one that overlaps with the energy corresponding to the last discrete state. In line with unitarity, the summed direct + pre-equilibrium cross section may not exceed the reaction cross section. In these cases, we normalize the results. Also, the discrete pre-equilibrium contribution is added to the discrete state cross sections.

**preeqang**

In *preeqang*, the pre-equilibrium angular distribution is calculated. Also here, there is a correction of the pre-equilibrium cross sections for direct discrete angular distributions. If the angular distributions for discrete states have *not* been calculated by a direct reaction model, we collapse the continuum pre-equilibrium angular distributions in the high energy region on the associated discrete states. For the exciton model, the pre-equilibrium angular distributions are generated with the Kalbach systematics. The following subroutines are called:

```
preeqang
|--kalbach
```

*kalbach*

This is the function for the Kalbach systematics [71].

**preeqout**

In *preeqout*, the output of pre-equilibrium cross sections is handled. The following subroutines are called:

```
preeqout
|--ignatyuk
|--phdens      >
|--phdens2     >
```

**8.4.12 population**

In *population*, the pre-equilibrium spectra are processed into population bins. The pre-equilibrium cross sections have been calculated on the emission energy grid. They are interpolated on the excitation energy grids of the level populations (both for the total and the spin/parity-dependent cases) to enable further decay of the residual nuclides. also, the pre-equilibrium population cross section are normalized. Due to interpolation, the part of the continuum population that comes from pre-equilibrium is not exactly equal to the total pre-equilibrium cross section. The normalization is done over the whole excitation energy range. The following subroutines are called:

```
population
|--locate
|--poll
```

### 8.4.13 compnorm

There is a small difference between the reaction cross section as calculated by ECIS and the sum over transmission coefficients. We therefore normalize the level population accordingly in this subroutine. The compound nucleus formation cross section *xsflux* and the associated normalization factors are created.

### 8.4.14 comptarget

In *comptarget*, the compound reaction for the initial compound nucleus is calculated. First, the level densities and transmission coefficients are prepared before the nested loops over all quantum numbers are performed. Next the following nested loops are performed:

- compound nucleus parity
- total angular momentum  $J$  of compound nucleus
- $j$  of incident channel
- $l$  of incident channel
- outgoing particles and gammas
- outgoing excitation energies
- residual parity
- residual spin
- $j$  of outgoing channel
- $l$  of outgoing channel

There are two possible types of calculation for the initial compound nucleus. If either width fluctuation corrections or compound nucleus angular distributions are wanted, we need to sum explicitly over all possible quantum numbers before we calculate the width fluctuation or angular factor. If not, the sum over  $j$  and  $l$  of the transmission coefficients can be lumped into one factor, which decreases the calculation time. In the latter case, the partial decay widths *enumhf* are calculated in subroutine *compprepare*.

In order to get do-loops running over integer values, certain quantum numbers are multiplied by 2, which can be seen from a 2 present in the corresponding variable names. For each loop, the begin and end point is determined from the triangular rule.

For every  $J$  and  $P$  (parity), first the denominator (total width) *denomhf* for the Hauser-Feshbach formula is constructed in subroutine *compprepare*. Also width fluctuation variables that only depend on  $J$  and  $P$  and not on the other angular momentum quantum numbers are calculated in subroutine *widthprepare*. For the width fluctuation calculation, all transmission coefficients need to be placed in

one sequential array. Therefore, a counter `tnum` needs to be followed to keep track of the proper index for the transmission coefficients.

Inside the nested loops listed above, compound nucleus calculations for photons, particles and fission are performed. In the middle of all loops, we determine the index for the width fluctuation calculation and call the subroutine that calculates the correction factor. Also, compound angular distributions, i.e. the Legendre coefficients, for discrete states are calculated.

The following subroutines are called:

```
comptarget
|--densprepare
|--tfission
|--comppprepare
|--widthprepare
|--widthfluc
|--clebsch
|--racah
|--tfissionout
|--raynalcomp
```

### **densprepare**

In *densprepare*, we prepare the energy grid, level density and transmission coefficient information for the compound nucleus and its residual nuclides. For various types of decay (continuum to discrete, continuum to continuum, etc.) we determine the energetically allowed transitions. These are then taken into account for the determination of integrated level densities. To get the transmission coefficients on the excitation energy grid from those on the emission energy grid, we use interpolation of the second order. Finally, the fission level densities are calculated.

The following subroutines are called:

```
densprepare
|--fstrength
|--locate
|--pol2
|--density >
```

### **tfission**

In this subroutine, the fission transmission coefficients are calculated. The fission transmission coefficients decrease very rapidly with excitation energy. Therefore, we calculate them at the end points and at the middle of each excitation energy bin. With this information, we can do logarithmic integration. Calls to subroutine *tbarrier* are done for 1, 2 and 3 barriers. Also transmission coefficients corrected for the presence of class II states are calculated.

The following subroutines are called:

```

tfission
|--tlbarrier
  |--thill

```

**tlbarrier**

Subroutine *tlbarrier* handles the fission transmission coefficient for one barrier. Both discrete states and the continuum are taken into account.

**thill**

Function for the Hill-Wheeler formula.

**compprepare**

In *compprepare*, information for the initial compound nucleus is prepared. The transmission coefficients are put in arrays for possible width fluctuation calculations. Also the total width *denomhf* appearing in the denominator of the compound nucleus formula is created. Note that the complete subroutine is performed inside the loop over compound nucleus spin  $J$  and parity  $P$  in subroutine *comptarget*.

**widthprepare**

In this subroutine, the preparation of width fluctuation calculations is done. All width fluctuation variables that only depend on  $J$  and  $P$  and not on the other angular momentum quantum numbers are calculated. The following subroutines are called:

```

widthprepare
|--molprepare
|--hrtwprepare
|--goeprepare
  |--prodm
  |--prodp

```

**molprepare**

This subroutine takes care of the preparation of the Moldauer width fluctuation correction (information only dependent on  $J$  and  $P$ ).

**hrtwprepare**

This subroutine takes care of the preparation of the HRTW width fluctuation correction (information only dependent on  $J$  and  $P$ ).

**goeprepare**

This subroutine takes care of the preparation of the GOE triple integral width fluctuation correction (information only dependent on  $J$  and  $P$ ).

**prodm, prodp**

Functions to calculate a product for the GOE calculation.

**widthfluc**

General subroutine for width fluctuation corrections. The following subroutines are called:

```
widthfluc
|--moldauer
|--hrtw
|--goe
  |--func1
```

**moldauer**

Subroutine for the Moldauer width fluctuation correction.

**hrtw**

Subroutine for the HRTW width fluctuation correction.

**goe**

Subroutine for the GOE width fluctuation correction.

**clebsch**

Function for the calculation of Clebsch-Gordan coefficients.

**racah**

Function for the calculation of Racah coefficients.

**tfissionout**

Subroutine *tfissionout* takes care of the output of fission transmission coefficients.

**raynalcomp**

Using subroutine *raynalcomp*, a compound nucleus run by ECIS can be performed, in addition to the calculation by TALYS. The results as calculated by ECIS will however not be used for TALYS but are just for comparison. The following subroutines are called:

```
raynalcomp
|--eciscompound
  |--optical    >
```

**eciscompound**

In *eciscompound*, an ECIS input file for a compound nucleus calculation is prepared.

**8.4.15 binary**

In *binary*, the binary reaction cross section are accumulated. The direct and pre-equilibrium cross sections are processed into population arrays. Binary feeding channels, necessary for exclusive cross sections, are determined. Also the population after binary emission is printed. The following subroutines are called:

```
binary
|--ignatyuk
|--spindis    >
|--binariespectra
  |--binemission
    |--locate
    |--poll
|--binaryrecoil
```

**binariespectra**

Subroutine to interpolate decay, from one bin to another, on the emission spectrum. The binary and compound emission spectra are constructed.

**binemission**

In *binemission*, the decay from the primary compound nucleus to residual nuclei is converted from the excitation energy grid to emission energies. Due to interpolation errors, there is always a small difference

between the binary continuum cross section and the integral of the spectrum over the continuum. The spectrum is accordingly normalized. The interpolation is performed for both inclusive and exclusive channels.

### **binaryrecoil**

Subroutine *binaryrecoil* calculates the recoil and ejectile spectra in the LAB frame from the ejectile spectra calculated in the CM frame. The following subroutines are called:

```
binaryrecoil
|--cm2lab
|--labsurface
  |--belongs
  |--binsurface
    |--intri
      |--sideline
    |--intersection
      |--belongs
    |--invest
      |--belongs
```

### **cm2lab**

Subroutine *cm2lab* performs the classical kinematical transformation from the center of mass frame to the LAB frame. For massive ejectiles the CM emission energy is converted into a CM emission velocity and is then vectorially coupled with the CM velocity to deduce the LAB velocity. No coupling is performed for photons. The same subroutine is used to calculate the recoil velocities.

### **labsurface**

Subroutine *labsurface* is used to calculate the way the area of a triangle defined by three points is distributed in a given bidimensional grid.

### **belongs**

This function tests if a real number is inside or outside a given bin.

### **binsurface**

This subroutine returns the area of a given bidimensional bin covered by a triangle.

**intri**

This function tests if a point is inside or outside a triangle.

**sideline**

This function tells if a point is on one side or on the other side of a given line.

**intersection**

Subroutine *intersection* determines the intersection points of a straight line with a given bidimensional bin.

**invect**

This function tests if a point is within a segment or not.

**8.4.16 angdis**

In *angdis*, angular distributions for discrete states are calculated. This is done through Legendre polynomials for direct, compound and the total contribution per discrete state. The following subroutines are called:

```
angdis
|--plegendre
|--angdisrecoil
```

**angdisrecoil**

Subroutine *angdisrecoil* calculates the recoil and ejectile spectra in the LAB frame from the ejectile spectra calculated in the CM frame. The following subroutines are called:

```
angdisrecoil
|--cm2lab
|--labsurface >
```

**8.4.17 multiple**

This is the subroutine for multiple emission. We loop over all residual nuclei, starting with the initial compound nucleus ( $Z_{\text{comp}}=0$ ,  $N_{\text{comp}}=0$ ), and then according to decreasing  $Z$  and  $N$ . For each encountered residual nuclide in the chain, we determine its nuclear structure properties. In total, the following nested loops are performed for multiple Hauser-Feshbach decay:

- compound nuclides  $Z_{\text{comp}}, N_{\text{comp}}$
- mother excitation energy bins
- compound nucleus parity
- total angular momentum  $J$  of compound nucleus
- (in *compound*) outgoing particles and gammas
- (in *compound*) outgoing excitation energies
- (in *compound*) residual parity
- (in *compound*) residual spin
- (in *compound*)  $j$  of outgoing channel
- (in *compound*)  $l$  of outgoing channel

Before the *compound subroutine* is entered there is a call to the multiple pre-equilibrium subroutine *multipreeq(2)* to deplete the flux if enough fast-particle flux is present. The following subroutines are called:

```
multiple
|--excitation
|--structure >
|--exgrid >
|--basicxs >
|--levelsout
|--densityout >
|--fissionparout
|--cascade
|--densprepare >
|--multipreeq2
|--multipreeq
|--tfission >
|--compound
|--tfissionout
|--compemission
|--kalbach
```

### **excitation**

Subroutine for initial population of a nucleus. If there is no nuclear reaction specified, both the starting condition is a populated nucleus, in this subroutine the initial population is redistributed over the excitation energy bins.

**cascade**

Subroutine for the gamma-ray cascade. The discrete gamma line intensities are stored.

**multipreeq2**

Subroutine for the two-component multiple preequilibrium model. A loops over all possible particle-hole excitations of the mother bin is performed. From each configuration, a new exciton model calculation is launched (**mpreeqmode 1**) or a simple transmission coefficient method is used (**mpreeqmode 2**). The particle-hole configurations of all residual nuclides are populated with the emitted pre-equilibrium flux. The depletion factor to be used for multiple compound emission is determined. The following subroutines are called:

```
multipreeq2
|--ignatyuk
|--phdens2      >
|--exchange2
|--lifetime2
|--locate
```

**multipreeq**

Subroutine for the one-component multiple preequilibrium model. A loops over all possible particle-hole excitations of the mother bin is performed. From each configuration, a new exciton model calculation is launched (**mpreeqmode 1**) or a simple transmission coefficient method is used (**mpreeqmode 2**). The particle-hole configurations of all residual nuclides are populated with the emitted pre-equilibrium flux. The depletion factor to be used for multiple compound emission is determined. The following subroutines are called:

```
multipreeq
|--ignatyuk
|--phdens      >
|--emissionrate >
|--lifetime >
|--locate
```

**compound**

Subroutine with the Hauser-Feshbach model for multiple emission. the nested loops are the same as those described for *comptarget*, with the exception of  $j$  and  $l$  of the incident channel, since we start from an excitation energy bin with a  $J, P$  value. In order to get do-loops running over integer values, certain quantum numbers are multiplied by 2, which can be seen from a 2 present in the corresponding variable names. For each loop, the begin and end point is determined from the triangular rule.

For every  $J$  and  $P$  (parity), first the denominator (total width) `denomhf` for the Hauser-Feshbach formula is constructed. Inside the nested loops, compound nucleus calculations for photons, particles and fission are performed.

### **compemission**

In *compemission*, the compound nucleus emission spectra are determined from the multiple Hauser-Feshbach decay scheme. The decay from compound to residual nuclei is converted from the excitation energy grid to emission energies. The spectrum is obtained by spreading the decay over the mother bin and, in the case of continuum-continuum transitions, the residual bin. For each mother excitation energy bin, we determine the highest possible excitation energy bin for the residual nuclei. As reference, we take the top of the mother bin. The maximal residual excitation energy is obtained by subtracting the separation energy from this. Various types of decay are possible:

- Decay from continuum to continuum. For most residual continuum bins, no special care needs to be taken and the emission energy that characterizes the transition is simply the average between the highest energetic transition that is possible and the lowest.
- Decay from continuum to discrete. The lowest possible mother excitation bin can not entirely decay to the discrete state. For the residual discrete state, it is checked whether the mother excitation bin is such a boundary case. This is done by adding the particle separation energy to the excitation energy of the residual discrete state.

When the decay type has been identified, the decay from the population is distributed over the emission energy bins. All possible end point problems are taken into account. The following subroutines are called:

```
compemission
|--locate
|--comprecoil
```

### **comprecoil**

If **recoil y**, the recoil and/or light particle spectra in the LAB frame are calculated in *comprecoil*. The following subroutines are called:

```
comprecoil
|--kalbach
|--cm2lab
|--labsurface >
```

### 8.4.18 channels

In *channels*, the exclusive reaction cross sections and spectra as outlined in Section 3.2.2 are calculated. A loop over all residual nuclides is performed and it is determined whether the residual nucleus under consideration can be reached by a certain particle combination. The associated gamma-ray production and isomeric exclusive cross sections are also computed. Finally, numerical checks with the total cross sections are performed. The following subroutines are called:

```
channels
|--specemission
  |--locate
```

### specemission

In *specemission*, the exclusive emission spectra are computed. The procedure is analogous to that of *compemission*.

### 8.4.19 totalxs

In this subroutine, a few total cross sections are cumulated, such as the continuum exclusive cross section, the total particle production cross section and the total fission cross section.

### 8.4.20 spectra

In *spectra*, smoothed discrete cross sections are added to the emission spectra. A more precise energy grid at the high-energy tail is created to account for the structure of discrete states. This is done for both angle-integrated and double-differential spectra. The following subroutines are called:

```
spectra
|--locate
```

### 8.4.21 massdis

In *massdis* the fission fragment and product yields are calculated. A loop over all fissioning systems is performed. Some of the excitation energy bins are lumped into larger energy bins to save computation time. The fission yields per fissioning system are weighted with the fission cross section and added to form the total yield. The following subroutines are called:

```
massdis
|--brosafy
  |--spline
  |--ignatyuk
```

```

|--trans
  |--funcfismode
    |--ignatyuk
    |--splint
    |--density    >
  |--trapzd
    |--funcfismode
|--splint
|--neck
  |--bdef
    |--fcoul
    |--fsurf
  |--ignatyuk
  |--fmin
  |--rpoint
    |--vr2
  |--vr1
  |--vr2
  |--vr3
  |--rtbis
  |--evap
    |--bdef
  |--sform
  |--rhodi
  |--fidi
    |--vr1
    |--vr2
    |--vr3

```

### **brosafy**

In this subroutine the fission fragment and product mass yields are determined per fissioning system. The relative contribution of each fission mode is calculated. Subsequently, the fission yields per fission mode are calculated and summed with the fission mode weight.

### **spline**

This subroutine performs a spline fit to the fission mode barrier parameters and the deformation parameters used in the subroutine *neck*.

### **trans**

This subroutine calculates the fission transmission coefficient per fission mode to determine the relative contribution of each fission mode.

**funcfismode**

This function corresponds to the expression of the fission transmission coefficient.

**splint**

This subroutine uses the spline fit obtained in the subroutine *spline* to interpolate.

**neck**

In this subroutine the actual fission fragment and product mass yield per fission mode is computed based on the Random-neck Rupture model.

**bdef**

This subroutine computes the binding energy of a deformed nucleus with an eccentricity by the droplet model without shell corrections.

**fcoul**

This function contains the form factor for the Coulomb self energy.

**fsurf**

This function contains the form factor for the surface energy.

**fmin**

This subroutine searches the minimal value of a function.

**rpoint**

This subroutine is used to calculate the rupture point  $z_{riss}$  for a given nucleon number hidden in the left-hand side of the dinuclear complex.

**vr1**

This function gives the volume of the projectile-like section.

**vr2**

This function gives the volume of the neck.

**vr3**

This function gives the volume of the target-like section.

**evap**

This function is used to determine the number of evaporated neutrons for a given fission fragment.

**sform**

This function determines the form factor for the coulomb interaction energy between two spheroids.

**rhodi**

This function computes the shape of the dinuclear system.

**fdi**

This function determines the exact shape of the dinuclear complex.

**8.4.22 residual**

In *residual*, the residual production cross sections, both total and isomeric, are stored in arrays.

**8.4.23 totalrecoil**

In this subroutine, the total recoil results are assembled.

**8.4.24 normalization**

In this subroutine, cross sections can be normalized to experimental or evaluated data.

**8.4.25 thermal**

In *thermal*, the cross sections down to thermal energies are estimated. For non-threshold channels, the cross sections are extrapolated down to 1.e-5 eV. Capture values at thermal energies are used. For

energies up to 1 eV, the  $1/\sqrt{E}$  law is used. Between 1 eV and the first energy at which TALYS performs the statistical model calculation, we use logarithmic interpolation. The following subroutines are called:

```
thermal  
|--poll
```

### 8.4.26 output

Subroutine *output* handles the output of all cross sections, spectra, angular distributions, etc. per incident energy. The following subroutines are called:

```
output  
|--totalout  
|--binaryout  
|--productionout  
|--residualout  
|--fissionout  
|--discreteout  
|--channelsout  
|--spectraout  
|--recoilout  
|--angleout  
|--ddxout  
  |--locate  
|--gamdisout
```

#### **totalout**

Subroutine for the output of total cross sections, such as total, non-elastic, pre-equilibrium, direct, etc.

#### **binaryout**

Subroutine for the output of the binary cross sections.

#### **productionout**

Subroutine for the output of particle production cross sections and total fission cross section.

#### **residualout**

Subroutine for the output of residual production cross sections.

**fissionout**

Subroutine for the output of fission cross sections per fissioning nuclide.

**discreteout**

Subroutine for the output of cross sections for discrete states for inelastic and other non-elastic channels.

**channelsout**

Subroutine for the output of exclusive channel cross sections and spectra, including ground state and isomer production and fission.

**spectraout**

Subroutine for the output of angle-integrated particle spectra.

**recoilout**

Subroutine for the output of recoil information.

**angleout**

Subroutine for the output of angular distributions for elastic scattering, inelastic scattering to discrete states and non-elastic scattering to other discrete states.

**ddxout**

Subroutine for the output of double-differential cross sections.

**gamdisout**

Subroutine for the output of discrete gamma-ray production.

**8.4.27 finalout**

In *finalout*, all results are printed as a function of incident energy, i.e. all excitation functions. This information appears in the main output file and/or in separate output files per reaction channel. Also, general nuclear model parameters are written to the parameter file.

**8.4.28 astro**

Subroutine for astrophysical reaction rates. The following subroutines are called:

```
|--stellarrate  
  |--partfunc  
|--astroout
```

**stellarrate**

Subroutine for the calculation of the reaction rate for a Maxwell-Boltzmann distribution.

**partfunc**

Partition function for astrophysical calculations.

**astroout**

Subroutine for the output of astrophysical reaction rates.

**8.4.29 endf**

Subroutine for the output of cross sections and information for the production of an ENDF-6 file. The following subroutines are called:

```
endf  
|--endfinfo  
|--endfenergies  
|--endfecis  
  |--optical >  
  |--ecisinput >  
|--endfread  
  |--tripathi >
```

**endfinfo**

Subroutine for writing the general information (i.e. the main reaction parameters) needed to create an ENDF-6 file.

**endfenergies**

Subroutine to create the energy grid for cross sections for an ENDF-6 file. This grid ensures that the total, elastic and reaction cross section are calculated on a sufficiently precise energy grid. Thresholds for all partial cross sections are also added to this grid.

**endfecis**

In this subroutine the loop over the energy grid created in *endfenergies* is done to perform basic ECIS calculations. The optical model parameters are determined by calling *optical*. The subroutine *ecisinput* is called for the creation of the ECIS input files. At the end of this subroutine, *ecis06t* is called to perform the actual ECIS calculation.

**endfread**

In this subroutine the results from ECIS are read. For every incident energy we read the reaction (and for neutrons the total and elastic) cross sections. These are then written to a separate file for ENDF-6 formatting.

## 8.5 Programming techniques

In general, we aim to apply a fixed set of programming rules consistently throughout the whole code. Here are some of the rules we apply to enforce readability and robustness:

- We use descriptive variable names as much as possible.
- Every variable in a subroutine, apart from dummy variables appearing in e.g. a do loop, is explained once in the comment section. In addition, we aim to give as much explanation as possible for the used algorithms.
- We use **implicit none** as the first line of *talys.cmb* and all stand-alone subroutines and functions. This means that every variable must be declared, which is a powerful recipe against typing errors.
- We program directly “from the physics”, as much as possible, i.e. we use array indices which correspond one-to-one to the indices of the physical formulae from articles and books.
- Cosmetical features:
  - Different tasks within a subroutine are clearly separated. A block, which contains one sub-task, is separated by asterisks, e.g.

```
c
c ***** Constants *****
c
```

The last asterisk is always in column 72. In the first block, the labels are numbered 10, 20, 30, etc. In the second block, the labels are numbered 110, 120, 130, etc.

- We indent two blanks in do loops and if statements.
- In the file *talys.cmb*, we systematically store variables of type logical, character, integer, real and double precision in separate common blocks. The order of appearance of variables in *talys.cmb* follows that of the subroutines.
- Every subroutine has the same heading structure: We give the author, date and task of the subroutine. Next, the file *talys.cmb* is included, followed by the inclusion of declarations for possible local variables.
- We use nuclear model parameterisations that are as general as possible within the programmed nuclear reaction mechanisms, to enable easy implementation of future refinements. For example, level densities will never be hardwired “on the spot”, but will be called by a function *density*. An improvement, or alternative choice, of a level density model will then have a consistent impact throughout the whole code.
- If there are exceptions to the procedures outlined above, it is probably since a few subroutines have been adopted from other sources, such as the collection of old style subroutines for the fission yields model.

As a general rule, although we aim to program as clever as possible, we always prefer readability over speed and memory economy. Some nuclear physicists are more expensive than computers, or at least should be.

## 8.6 Changing the array dimensions

As explained in the previous sections, almost all arrays are defined in the common block file *talys.cmb*. At the top of *talys.cmb*, the parameters are set for the dimensions of the various arrays. Their names all start with **num**. Most of these parameters should be left untouched, because they determine basic quantities of a nuclear model calculation. Some of them can however be changed. They can be reduced, for the case that the working memory of your computer is too small, or be increased, in cases where you want to perform more extensive or precise calculations than we thought were necessary. However, in normal cases you only need to change the keyword values in the input file and not the parameters in *talys.cmb*. In the standard version of TALYS, the latter already have reasonable values. Nevertheless, the following parameters can be changed and will have a significant effect:

- **memorypar**: general multiplication factor for dimensions of several arrays. Use a small value for a small computer. Normally, changing this parameter does not require any further changes of the parameters that follow below.
- **numbins**: the maximum number of continuum excitation energy bins in the decay chains. Obviously, this could be increased to allow for more precision.

- **numZchan**, **numNchan** and **numchantot**: the depth to which exclusive reaction channels are followed can be set by these parameters. However, as mentioned in Section 3.2.2, exclusive channels that go beyond 4 outgoing particles are rarely of interest (only for certain activation codes that work at high energies). Also, since the exclusive reaction calculation involves some large arrays, one may easily run into memory problems by choosing too large values. If one works on e.g. a 64 Mb machine it may be helpful, or even necessary, to choose smaller values if one is not interested in exclusive calculations at all. Table 8.1 displays the values that are theoretically possible. In this table, we use

$$(8.1) \quad \text{numchantot} = \sum_{m=0}^{\text{numchannel}} \binom{m+5}{m}$$

which is the total number of channels for 6 different outgoing particles (neutrons up to alpha particles) if we go **numchannels** particles deep. In practice, less are needed since many channels never open up and this is what we have assumed by setting the value for **numchantot** in *talys.cmb*.

- **numZ** and **numN**: The maximum number of proton and neutron units, respectively, away from the initial compound nucleus that can be reached after multiple emission. If you want to try your luck with TALYS at very high incident energies, these parameters may need to be increased.
- **numlev**: The maximum number of included discrete levels.
- **numang**: The maximum number of outgoing angles for discrete states.
- **numangcont**: The maximum number of outgoing angles for the continuum.

Obviously, after increasing these values you still need to set the associated keywords in the input file to use the increased limits, although some of them, e.g. **maxZ**, are always by default set to their maximum value. You could increase a parameter and simultaneously reduce another one that is of no relevance to the particular problem under study, to remain within the available memory of your computer. Of course, you should always completely re-compile TALYS after changing anything in *talys.cmb*.

Table 8.1: Theoretical number of exclusive channels for outgoing particles of 6 different types

numchannel	number of channels	numchantot
0	1	1
1	6	7
2	21	28
3	56	84
4	126	210
5	252	462
6	462	924
7	792	1716
8	1287	3003
9	2002	5005
10	3003	8008



## Outlook and conclusions

This manual describes TALYS-1.9, a nuclear reaction code developed at NRG Petten and CEA Bruyères-le-Châtel. After several years of development, and application in various areas, by many users [133]-[748], we decided that after the previous (TALYS-0.64, TALYS-0.72) beta releases, the first official Version 1.0 of the code could be released at the end of 2007. After the release of TALYS-1.2 in december 2009, TALYS-1.4 in december 2011, TALYS-1.6 in december 2013, TALYS-1.8 in december 2015, TALYS-1.9 is the next update.

We note that various extensions are possible for the physics included in TALYS, and some will be mentioned below. Obviously, we can not guarantee that these will be included in a future release (if any). This depends on the required effort, future careers of the authors, your willingness to share your extensions with us, our willingness to implement them, and in the case of significant extensions, financial input from research programs that require nuclear data.

In general, the nuclear structure database can still be extended with more tables based on microscopic nuclear structure calculations. Through a trivial change in the TALYS code, the impact of these ingredients on reaction calculations can immediately be tested.

The default local and global spherical and deformed optical models that are used in TALYS are quite powerful. However, it would be good to extend the optical model database with more cases. A connection with the RIPL OMP database is then the most obvious. Another extension is needed for light nuclides ( $A < 24$ ). Also, TALYS is already being used with microscopic OMPs, but only with the spherical JLM method. An extension to deformed JLM has been made available by Eric Bauge, but is not yet implemented. A few direct reaction items, such as the prediction of the Isobaric Analogue State, are also yet to be completed.

One type of observable still missing is the fission neutron spectrum. For this, both phenomenological and more physical approaches (in the latter, one would perform a loop over all excited fission fragments) are possible. Also, models for simulating the number of prompt and delayed neutrons could be included. In general, the fission parameter database for TALYS still needs to be settled, although significant progress has been made recently. This will probably be added in the next version of the code,

when the entire GEF module will become available. A general analysis of all actinides simultaneously should result in a stable, ready-to-use fission database. It is clear that the theoretical fission models themselves are also not yet mature, even though microscopic fission paths are now included.

Concerning continuum reactions, there exists a microscopic multi-step direct code, MINGUS, for quantum-mechanical pre-equilibrium calculations (MSD/MSD) [81], which still needs to be merged with TALYS.

Coupling with high-energy intranuclear cascade (INC) codes is possible, now that TALYS is able to take a pre-defined population distribution as the starting point. The INC code would take care of energies above e.g. 200 MeV, while TALYS takes over below that cut-off energy. The well-validated pre-equilibrium and Hauser-Feshbach approach at lower energies may then lead to more precise simulated data (including isomer production), even for reactions in the GeV

As for computational possibilities, the current day computer power enables to use nuclear model codes in ways that were previously thought impossible. Activities that have already proven to be possible are the generation of nuclear-model based covariances with Monte Carlo methods, automatic multi-parameter fitting of all partial cross sections to the existing experimental data, and dripline-to-dripline generation of all cross sections over the entire energy and projectile range, see e.g. the TENDL link on our website. The applications range from basic science (e.g. astrophysics) to the production of nuclear data libraries for existing and future nuclear technologies.

We are considering a complete upgrade of TALYS to Fortran90/95. For the moment, however, we have restricted ourselves to adding as much modules to TALYS as possible, using Fortran77, without letting that project interfere with the use of other programming languages. Once we feel TALYS has reached a certain level, in terms of included physics and options, that calls for a global upgrade to a more modern language, we will certainly do so and we will apply such an update to the whole code *at once*. At the moment, all authors of TALYS master at least Fortran77, which is a strong argument in favor of the present approach. However, TALYS-1.9 is the last version for which we insist on full Fortran77 compatibility. A huge extra effort would be needed to make our methods fully quality assured, even though we know that we are already deviating, in a positive sense, from those currently practised in computational nuclear science.

There are two important satellite codes for TALYS, written at NRG, that have appeared in the literature: TASMAN [491], for determining nuclear model based covariances and automatic optimization to experimental data, and TEFAL [463], for translating the results of TALYS into ENDF-6 data libraries. However, this is proprietary software, and it is not yet foreseen that this software becomes generally available. The current plan is to include both in a new Fortran90/95/03/08 version of TALYS, which would be called TALYS-2.0.

The development of TALYS has always followed the “first completeness, then quality” principle. This merely means that, in our quest for completeness, we tried to divide our effort equally among all nuclear reaction types. We think that, with the exception of a few issues the code is indeed *complete* in terms of predicted quantities. We now hope that TALYS also qualifies for “completeness and quality”. Nevertheless, it is certain that future theoretical enhancements as suggested above are needed to bring our computed results even closer to measurements.

# Bibliography

First, the references for this manual are listed .

Next, all publications in which TALYS has been used are listed, from new to old, for the following categories:

General publications and code releases  
Development of nuclear reaction mechanisms  
Analysis of measurements below 20 MeV  
Analysis of measurements above 20 MeV  
Evaluated nuclear data libraries  
Uncertainties, covariances and Monte Carlo  
Global testing and cross section tables  
Fusion  
High energy codes and applications  
Medical applications  
Astrophysics  
Other applications

## References used for this manual

- [1] S. Goriely and J.-P. Delaroche, “The isovector imaginary neutron potential: A key ingredient for the r-process nucleosynthesis”, *Phys. Lett. B* 653 (2007) 178183.
- [2] P.G. Young, E.D. Arthur, and M.B. Chadwick, in *Workshop on Computation and Analysis of Nuclear Data Relevant to Nuclear Energy and Safety*, edited by M.K. Mehta and J.J. Schmidt, Feb. 10 - March 13 1992, Trieste, Italy, (1993), p. 622.
- [3] M. Blann, in *Workshop on Computation and Analysis of Nuclear Data Relevant to Nuclear Energy and Safety*, edited by M.K. Mehta and J.J. Schmidt, Feb. 10 - March 13 1992, Trieste, Italy, (1993), p. 622.

- [4] M. Uhl and B. Strohmaier, *Computer code for particle induced activation cross sections and related quantities*, IRK report No. 76/01, Vienna (1976).
- [5] M. Herman, in *Workshop on Nuclear Reaction Data and Nuclear Reactors: Physics, Design and Safety*, edited by N. Paver, M. Herman and A. Gandini, March 13 - April 14 2000, Trieste Italy, (2001), p. 137.
- [6] J. Raynal, *Notes on ECIS94*, CEA Saclay Report No. CEA-N-2772, (1994).
- [7] A.M. Baldin, *Kinematics of Nuclear Reactions*, Oxford University Press, (1961).
- [8] M.J. Lopez Jimenez, B. Morillon and P. Romain, *Ann. Nucl. Energy* 32, 195 (2005).
- [9] B. Morillon, H. Duarte and P. Romain, "New BRC Neutron Evaluations of Actinides with the TALYS code : Modelization and First Validation Tests" in: A. Chatillon, H. Faust, G. Fioni, D. Goutte, H. Goutte [Eds], *Proceedings of the 4th International Workshop on Nuclear Fission and Fission-Product Spectroscopy*, Cadarache, France, May 13-16, AIP Conference Proceedings, p.79 (2009).
- [10] M.B. Chadwick, P.G. Young, S. Chiba, S.C. Frankle, G.M. Hale, G. Hughes, A.J. Koning, R.C. Little, R.E. Macfarlane, R.E. Prael, and L.S. Waters, *Nucl. Sci. Eng.* **131** (1999), 293.
- [11] M.B. Chadwick, P.G. Young, R.E. Macfarlane, and A.J. Koning, "High Energy Nuclear Data Libraries for Accelerator-Driven Technologies: Calculational Method for Heavy Recoils", *Second International Conference on Accelerator-Driven Transmutation Technologies and Applications*, Kalmar, Sweden, June 3-7 1996, 483.
- [12] A.J. Koning, "Extension of TALYS to 1 GeV", *Proceedings of ND-2013*, New York (2014).
- [13] S. Typel, O. Riedl, H.H. Wolter, *NUC. PHYS.* **A709**, 299 (2002).
- [14] S. Chiba *et al.*, in *SPEC. MEET. ON THE NUCLEON NUCLEUS OPTICAL MODEL UP TO 200 MEV*, BRUYERES-LE-CHATEL (1996).
- [15] S. Watanabe, *Nucl. Phys.* **8**, 484 (1958).
- [16] D.G. Madland, in *Proceedings of a Specialists' Meeting on preequilibrium nuclear reactions*, Semmering, Austria, February 10-12 (1988), p. 103.
- [17] W.W. Daehnick, J.D. Childs, Z. Vrcelj, *Phys. Rev C* 21, 2253 (1980).
- [18] J. Bojowald et al, *Phys. Rev. C* 38, 1153 (1988).
- [19] Y. Han, Y. Shi and Q. Shen, *Phys. Rev. C* 74, 044615 (2006).
- [20] Haixia An and Chonghai Cai, *Phys. Rev. C* 73, 054605 (2006).
- [21] L. McFadden, G.R. Satchler, *Nucl. Phys.* 84 (1966) 177.
- [22] P. Demetriou, C. Grama and S. Goriely, *Nucl. Phys.* A707, 253 (2002).

- [23] D.E. Cullen, PREPRO 2015 - 2015 ENDF-6 Pre-processing codes, Technical report IAEA-NDS-39 (Rev.14), IAEA (2010).
- [24] J. Glorius et al., Phys. Rev.C 89, 065808 (2014).
- [25] V. Avrigeanu et al. Phys. Rev. C 90, 044612 (2014).
- [26] Nolte et al., Phys. Rev. C 36, 1312 (1987).
- [27] V. Avrigeanu et al. Phys. Rev. C 49, 2136 (1994).
- [28] E. Bauge, J.P. Delaroche, M. Girod, Phys. Rev. C **63**, 024607 (2001).
- [29] F. Maréchal, T. Suomijärvi, Y.Blumenfeld, A. Azhari, E. Bauge, D. Bazin, J.A. Brown, P.D. Cottle, J.P. Delaroche, M. Fauerbach, M. Girod, T. Glassmacher, S.E. Hirzebruch, J.K. Jewel, J.H. Kelley, K.W. Kemper, P.F. Mantica, D.J. Morissey, L.A. Riley, J.A. Scarpaci, H. Sheit, M. Steiner, Phys. Rev C **60**, 034615 (1999).
- [30] H. Sheit, F. Maréchal, T. Glassmacher, E. Bauge, Y.Blumenfeld, J.P. Delaroche, M. Girod, R.W. Ibbotson, K.W. Kemper, J. Libert, B. Pritychenko, T. Suomijärvi, Phys. Rev. C **63** 014604 (2000).
- [31] E. Khan, T. Suomijärvi, Y.Blumenfeld, Nguyen Van Giai, N. Alamanos, F. Auger, E. Bauge, D. Beaumel, J.P. Delaroche, P. Delbourgo-Salvador, A. Drouart, S. Fortier, N. Frascaria, A. Gilibert, M. Girod, C. Jouanne, K.W. Kemper, A. Lagoyannis, V. Lapoux, A. Lépine-Szily, I. Lhenry, J. Libert, F. Maréchal, J.M. Maison, A. Mussumara, S. Ottini-Hustache, P. Piattelli, S. Pita, E.C. Pollaco, P. Roussel-Chomaz, D. Santonocito, J.E. Sauvestre, J.A. Scarpacci, T. Zerguerras, Nucl. Phys A **694**, 103 (2001).
- [32] E. Bauge, J.P. Delaroche, M. Girod, G. Haouat, J. Lachkar, Y. Patin, J. Sigaud, J. Chardine, Phys. Rev. C **61**, 034306 (2000).
- [33] J.P. Jeukenne, A. Lejeune, and C. Mahaux, Phys. Rep. **25C**, 83 (1976).
- [34] J.P. Jeukenne, A. Lejeune, and C. Mahaux, Phys. Rev. C **10**, 1391 (1974).
- [35] J.P. Jeukenne, A. Lejeune, and C. Mahaux, Phys. Rev. C **15**, 10 (1977).
- [36] J.P. Jeukenne, A. Lejeune, and C. Mahaux, Phys. Rev. C **16**, 80 (1977).
- [37] E.Bauge, J.P. Delaroche, M. Girod, Phys. Rev. C **58** 1118 (1998).
- [38] R.R. Scheerbaum, Nucl. Phys. **A257**, 77 (1976).
- [39] R.K. Tripathi, F.A. Cucinotta and J.W. Wilson, NASA technical paper 3621, January 1997.
- [40] T. Tamura, Rev. Mod. Phys. **37**, 679 (1965).
- [41] J.P. Delaroche, in Proceedings of the International Symposium on *Nuclear Data Evaluation Methodology*, ed. C.L. Dunford, October 12-16 1992, Brookhaven, USA, p. 347.
- [42] N. Olsson, E. Ramström, and B. Trostell, Nucl. Phys. **A513**, 205 (1990).

- [43] B.V. Carlsson, in *Workshop on Nuclear Reaction Data and Nuclear Reactors: Physics, Design and Safety*, edited by N. Paver, M. Herman and A. Gandini, March 13 - April 14 2000, Trieste Italy, (2001), p. 61.
- [44] E. Sh Soukhovitskii, S. Chiba, J.-Y. Lee, O. Iwamoto and T. Fukahori, *J. Phys. G: Nucl. Part. Phys.* **30**, 905 (2004).
- [45] P.P. Guss, R.C. Byrd, C.R. Howell, R.S. Pedroni, G. Tungate, R.L. Walter, and J.P. Delaroche, *Phys. Rev. C* **39**, 405 (1989).
- [46] G.R. Satchler, *Direct Nuclear Reactions*, Oxford University Press, New York, 1983.
- [47] P.E. Hodgson, *Nuclear Reactions and Nuclear Structure*, Clarendon Press, Oxford, 1971.
- [48] A. van der Woude, in *Electric and Magnetic Giant Resonances in Nuclei*, edited by J. Speth (World Scientific, Singapore, 1991), p. 99-232.
- [49] C. Kalbach, *Phys. Rev. C* **62**, 44608 (2000).
- [50] D.M. Brink, *Nucl. Phys.* **4**, 215 (1957); P. Axel, *Phys. Rev.* **126**, 671 (1962).
- [51] J. Kopecky and M. Uhl, *Phys. Rev. C* **41**, 1941 (1990).
- [52] J. Kopecky, M. Uhl and R.E. Chrien, *Phys. Rev. C* **47**, 312 (1993).
- [53] D.G. Gardner, in *Neutron Radiative Capture*, OECD/NEA Series on Neutron Physics and Nuclear Data in Science and Technology, eds. A. Michaudon et al., p. 62 (1984).
- [54] J. Kopecky, private communication.
- [55] M.B. Chadwick, P. Oblozinsky, P.E. Hodgson, and G. Reffo, *Phys. Rev. C* **44**, 814 (1991); *Handbook on photonuclear data for applications: Cross sections and spectra*, IAEA-TECDOC-1178 (2000).
- [56] H. Gruppelaar, P. Nagel, and P.E. Hodgson, *Riv. Nuovo Cimento* **9**, No. 7, 1 (1986).
- [57] E. Gadioli and P.E. Hodgson, *Pre-equilibrium nuclear reactions*, Oxford Univ. Press (1992).
- [58] C. Kalbach, *Phys. Rev. C* **33**, 818 (1986).
- [59] C.K. Cline and M. Blann, *Nucl. Phys.* **A172**, 225 (1971).
- [60] J. Dobeš and E. Běták, *Zeit. Phys.* **A310**, 329 (1983).
- [61] E. Běták and J. Dobeš, *Zeit. Phys.* **A279**, 319 (1976).
- [62] C.Y. Fu, *Nucl. Sci. Eng.* **86**, 344 (1984).
- [63] C. Kalbach, *Phys. Rev. C* **32**, 1157 (1985).
- [64] C. Kalbach-Cline, *Nucl. Phys.* **A210**, 590 (1973).

- [65] F. C. Williams, Nucl. Phys. **A166**, 231 (1971).
- [66] J.M. Akkermans and H. Gruppelaar, Phys. Lett. **157B**, 95 (1985).
- [67] H. Gruppelaar, *IAEA Advisory Group Meeting on Basic and Applied Problems on Nuclear Level Densities* (Brookhaven National Laboratory report, 1983), p. 143.
- [68] C. Kalbach, Phys. Rev. C **71**, 034606 (2005).
- [69] C. Kalbach, private communication (2007).
- [70] A.J. Koning and J.M. Akkermans, Ann. Phys. **208**, 216 (1991).
- [71] C. Kalbach, Phys. Rev. C **37**, 2350 (1988).
- [72] W.D. Myers and W.J. Swiatecki, Nucl. Phys. **81**, 1 (1966).
- [73] H.M. Hofmann, J. Richert, J.W. Tepel and H.A. Weidenmüller, Ann. Phys. (N.Y.) **90**, 403 (1975).
- [74] J.W. Tepel, H.M. Hofmann and H.A. Weidenmüller, Phys. Lett. **49B**, 1 (1974).
- [75] H.M. Hofmann, T. Mertelmeier, M. Herman and J.W. Tepel, Zeit. Phys. **A297**, 153 (1980).
- [76] P.A. Moldauer, Phys. Rev. C **14**, 764 (1976).
- [77] P.A. Moldauer, Nucl. Phys. **A344**, 185 (1980).
- [78] J.J.M. Verbaarschot, H.A. Weidenmüller and M.R. Zirnbauer, Phys. Rep. **129**, 367 (1985).
- [79] H. Gruppelaar and G. Reffo, Nucl. Sci. Eng. **62**, 756 (1977).
- [80] M.B. Chadwick, P.G. Young, D.C. George and Y. Watanabe, Phys. Rev. C **50**, 996 (1994).
- [81] A.J. Koning and M.B. Chadwick, Phys. Rev. C **56**, 970 (1997).
- [82] T. Ericson, Adv. Phys. **9**, 425 (1960).
- [83] A. Gilbert and A.G.W. Cameron, Can. J. Phys. **43**, 1446 (1965).
- [84] W. Dilg, W. Schantl, H. Vonach, and M. Uhl, Nucl. Phys. **A217**, 269 (1973).
- [85] H. Baba, Nucl. Phys. **A159**, 625 (1970).
- [86] A.V. Ignatyuk, G.N. Smirenkin and A.S. Tishin, Sov. J. Nucl. Phys. **21**, no. 3, 255 (1975).
- [87] G. Audi and A.H. Wapstra, Nucl. Phys. **A729**, 129 (2003).
- [88] A. Mengoni and Y. Nakajima, J. Nucl. Sci. Techn. **31**, 151 (1994).
- [89] S. Goriely, Nucl. Phys. **A605**, 28 (1996).
- [90] S. Hilaire, PhD thesis, unpublished (1997).

- [91] S.F. Mughabghab and C. Dunford, Phys. Rev. Lett. **81**, 4083 (1998).
- [92] A.S. Iljinov, M.V. Mebel, N. Bianchi, E. De Sanctis, C. Guaraldo, V. Lucherini, V. Muccifora, E. Polli, A.R. Reolon, and P. Rossi, Nucl. Phys. **A543**, 517 (1992).
- [93] M.K. Grossjean and H. Feldmeier, Nucl. Phys. **A444**, 113 (1985).
- [94] O.T. Grudzevich, A.V. Ignatyuk, V.I. Plyaskin, A.V. Zelenetsky, in Proc. Nuclear Data for Science and Technology (Mito, JAERI), p 187 (1988)
- [95] A.R. Junghans, M. de Jong, H.-G. Clerc, A.V. Ignatyuk, G.A. Kudyaev, and K.-H. Schmidt, Nucl. Phys. **A629**, 635 (1998).
- [96] G. Hansen and A.S. Jensen, Nucl. Phys. **A406**, 236 (1983).
- [97] P. Demetriou and S. Goriely, Nucl. Phys. **A695**, 95 (2001).
- [98] S. Goriely, F. Tondeur, J.M. Pearson, Atom. Data Nucl. Data Tables **77**, 311 (2001).
- [99] S.F. Mughabghab, Atlas of Neutron Resonances, 5<sup>th</sup> edition, Elsevier Publisher, 2006.
- [100] E.V. Gaï, A.V. Ignatyuk, N.S. Rabotnov, G.N. Smirenkin, 1969. *Physics and Chemistry of Fission*, I.A.E.A., Vienna, p.337.
- [101] A.V. Ignatyuk, K.K. Istekov, and G.N. Smirenkin, Sov. J. Nucl. Phys. **29**, no. 4, 450 (1979).
- [102] A.V. Ignatyuk, J.L. Weil, S. Raman, and S. Kahane, Phys. Rev. **C47**, 1504 (1993).
- [103] A. J. Sierk, Phys. Rev. C **33**, 2039 (1986).
- [104] S. Cohen, F. Plasil, and W. J. Swiatecki, *Ann. of Phys.* **82**, 557 (1974).
- [105] M. Sin, R. Capote and A. Ventura, Phys. Rev. C **74**, 014608 (2006).
- [106] A. Mamdouh, J.M. Pearson, M. Rayet and F. Tondeur, Nucl. Phys. **A679**, 337 (2001).
- [107] A. D'Arrigo *et al.*, Journ. Phys. G **20**, 365 (1994).
- [108] U. Brosa, S. Großmann and Müller, Phys. Rep. **197**, 167 (1990).
- [109] M.C. Duijvestijn, A.J. Koning, and F.-J. Hamsch, Phys. Rev. C **64**, 014607 (2001).
- [110] W.D. Myers and W.S. Swiatecki, Ark. Fysik **36**, 593 (1967).
- [111] B.D. Wilkins, E.P. Steinberg, and R. R. Chasman, Phys. Rev. C **14**, 1832 (1976).
- [112] J. Kopecky, M.G. Delfini, H.A.J. van der Kamp and D. Nierop: Revisions and extensions of neutron capture cross-sections in the European Activation File EAF-3, ECN-C-92-051, July 1992.
- [113] S. Lemaire, P. Talou, T. Kawano, M.B. Chadwick, and D.G. Madland, Phys. Rev. C **72**, 024601 (2005).

- [114] J.A. Holmes, S.E. Woosley, W.A. Fowler, B.A. Zimmerman, *At. Data Nucl. Data Tables* **18**, 306 (1976).
- [115] K.-H. Schmidt and B. Jurado, *Phys. Rev. C* **82** (2011) 014607.
- [116] H. Bateman, *Proc. Cambridge Phil. Soc.* **15**, 423 (1910).
- [117] W. Rubinson, *J. Chem. Phys.* **17**, 542 (1949).
- [118] W. R. Leo, "Techniques for Nuclear and Particle Physics Experiments", Springer Verlag, Berlin, 1994.
- [119] S. Goriely and J.M. Pearson, *Phys. Rev. Lett.* **102**, 152503 (2009).
- [120] P. Möller, J.R. Nix, W.D. Myers and W.J. Swiatecki, *Atomic Data Nucl. Data Tab.* **59**, 185 (1995).
- [121] J. Duflo and A. Zuker, unpublished.
- [122] F. Vivès, F. -J. Hamsch, H. Bax, and S. Oberstedt, *Nucl. Phys.* **A662**, 63 (2000).
- [123] S. Nagg, K.F. Flynn, J.E. Gindler, J.W. Meadows, and L.E. Glendening, *Phys. Rev. C* **17**, 163 (1978).
- [124] T.C. Chapman, G.A. Anzelon, G.C. Spitale, and D.R. Nethaway *Phys. Rev. C* **17**, 1089 (1978).
- [125] T.C. Chapman, G.A. Anzelon, G.C. Spitale, and D.R. Nethaway *Phys. Rev. C* **17**, 1089 (1978).
- [126] S. Goriely, *Phys. Lett. B* **436**, 10 (1998).
- [127] A.A. Cowley, A. van Kent, J.J. Lawrie, S.V. Förtsch, D.M. Whittal, J.V. Pilcher, F.D. Smit, W.A. Richter, R. Lindsay, I.J. van Heerden, R. Bonetti, and P.E. Hodgson, *Phys. Rev. C* **43**, 678 (1991).
- [128] W. Scobel, M. Trabandt, M. Blann, B. A. Pohl, B. A. Remington, R. C. Byrd, C. C. Foster, R. Bonetti, C. Chiesa, and S. M. Grimes, *Phys. Rev. C* **41**, 2010 (1990).
- [129] R. Michel, R. Bodemann, H. Busemann, R. Daunke, M. Gloris, H.-J. Lange, B. Klug, A. Krins, I. Leya, M. Luepke, S. Neumann, H. Reinhardt, M. Schnatz-Buettgen, U. Herpers, TH. Schiekkel, F. Sudbrock, B. Holmqvist, H. Conde, P. Malmborg, M. Suter, B. Dittrich-Hannen, P.-W. Kubik, H.-A. Sinal, D. Filges, *Nucl. Inst. Meth.* **B129**, 153 (1997).
- [130] B.L. Berman, J.T. Caldwell, R.R. Harvey, M.A. Kelly, R.L. Bramblett, S.C. Fultz, *Phys. Rev.* **162**, 1098 (1967).
- [131] A. Marcinkowski, J. Rapaport, R. Finlay, X. Aslanoglou, and D. Kielan, *Nucl. Phys.* **A530**, 75 (1991).
- [132] H. Vonach, A. Pavlik, M.B. Chadwick, R.C. Haight, R.O. Nelson, S.A. Wender, and P.G. Young, *Phys. Rev. C* **50**, 1952 (1994).

## All references to TALYS

### General publications and code releases

- [133] A.J. Koning, S. Hilaire and M.C. Duijvestijn, “TALYS-1.0”, *Proceedings of the International Conference on Nuclear Data for Science and Technology - ND2007*, May 22 - 27, 2007, Nice, France, editors O.Bersillon, F.Gunsing, E.Bauge, R.Jacqmin, and S.Leray, EDP Sciences, p. 211-214 (2008).
- [134] S. Hilaire, S. Goriely, A.J. Koning, and E. Bauge, “Towards universal predictions with the Talys code”, *Proceedings of 2nd International Conference on Frontiers in Nuclear Structure, Astrophysics and Reactions Aghios Nikolaos, Crete, Greece, September 10-14, (2007)*.
- [135] A.J. Koning, S. Hilaire and M.C. Duijvestijn, “Predicting nuclear reactions with TALYS”, *Proceedings of the Workshop on Neutron Measurements, Evaluations and Applications - 2*, October 20-23, 2004 Bucharest, Romania (2006), ed. A. Plompen, [http://www.irmm.jrc.be/html/publications/technical\\_reports/index.htm](http://www.irmm.jrc.be/html/publications/technical_reports/index.htm)
- [136] A.J. Koning, “Current status and future of nuclear model-based data evaluation”, in *Perspectives on Nuclear Data for the Next Decade*, CEA-DIF Bruyères-le-Châtel, France, September 26-28 2005, p. 1-7, NEA report (2006).
- [137] A.J. Koning, S. Hilaire and M.C. Duijvestijn, “TALYS: Comprehensive nuclear reaction modeling”, *Proceedings of the International Conference on Nuclear Data for Science and Technology - ND2004*, AIP vol. 769, eds. R.C. Haight, M.B. Chadwick, T. Kawano, and P. Talou, Sep. 26 - Oct. 1, 2004, Santa Fe, USA, p. 1154 (2005).

### Development of nuclear reaction mechanisms

- [138] S. Hilaire, M. Girod, S. Goriely and A.J. Koning, “Temperature dependent combinatorial level densities with the DIM Gogny force”, to be published (2013).
- [139] Yi Xu and Stephane Goriely, “Systematic study of direct neutron capture”, *Phys. Rev. C* 86, 045801 (2012).
- [140] E. Bauge et al, “Coherent investigation of nuclear data at CEA DAM: Theoretical models, experiments and evaluated data”, *Eur. Phys. Journ. A* 48, 113 (2012).
- [141] K. Gul, “A theoretical study of the excitation functions for the  $^{197}\text{Au}(d,2n)$ ,  $^{197}\text{Au}(d,4n)$  reactions and isomeric cross section ratios up to 40 MeV deuteron energy”, *Nucl. Instr. Meth. B* 280, 131 (2012).
- [142] G. Boutoux et al., “Study of the surrogate-reaction method applied to neutron-induced capture cross sections”, *Phys. Lett. B* 712, 319 (2012).

- [143] Y.S. Perkasa, A. Waris R. Kurniadi, Z. Suud, "Implementation of new fission barrier model in TALYS code", *Appl. Mech. and Mat.* 110-116, 2475 (2012).
- [144] Y.S. Perkasa, A. Waris, R. Kurniadi and Z. Su'ud, "Calculation of fission yield using fission barrier from optimal shapes of liquid drop model", 3rd Int Conf. on advances in Nucl. Sci. and Eng. 2011: ICANSE 2011, AIP Conf. Proc. 1448, 297 (2012).
- [145] S. Goriely, S. Hilaire, A.J. Koning and R. Capote, "Towards improved evaluation of neutron-induced cross section on actinides", *Phys. Rev. C* 83, 034601 (2011).
- [146] G. Boutoux et al., "Neutron-induced Capture Cross Sections via the Surrogate Reaction Method", Proceedings of the International Conference on Nuclear Data for Science and Technology, April 26-30, 2010, Jeju, Korea, *Journ. Kor. Phys. Soc.* 59, no. 23, 1924 (2011).
- [147] J.J. Jeremiah, B.M.A. Jyrwa, "Poschl Teller model for the total cross sections of neutron scattering from  $^{232}\text{Th}$ ", *Indian Journal of Pure and Applied Physics* 50 (2012).
- [148] A. Avdeenkov, S. Goriely, S. Kamerdzhiev, and S. Krewald, "Self-consistent calculations of the strength function and radiative neutron capture cross section for stable and unstable tin isotopes", *Phys. Rev. C* 83, 064316 (2011). "Impact of the Phonon Coupling on the Dipole Strength and Radiative Neutron Capture", Proceedings of the International Conference on Nuclear Data for Science and Technology, April 26-30, 2010, Jeju, Korea, *Journ. Kor. Phys. Soc.* 59, no. 23, 967 (2011).
- [149] S. Hilaire, M. Girod, S. Goriely and A.J. Koning, "Temperature dependent combinatorial level densities with the DIM Gogny force", submitted to *Phys Rev C* (2012).
- [150] S. Goriely, S. Hilaire, A.J. Koning and M. Girod, "Nuclear ingredients for cross section calculation of exotic nuclei", Conference on Nuclear Physics in Astrophysics V, Eilat, April 3-8 (2011).
- [151] K. Gul, "A theoretical study of excitation functions of isomers and isomeric cross section ratios in alpha induced reactions on  $^{107,109}\text{Ag}$ ", *Nucl. Instr. Meth.* B269, 764 (2011).
- [152] J.J. Jeremiah, D. Surchiang and B.M. Jyrwa, "Excitation functions and isotopic effects in (n,p) reactions for stable iron isotopes from reaction threshold to 20 MeV", *Ann. Nuc. En.* 43, 208 (2012).
- [153] S. Goriely, S. Hilaire, A.J. Koning, and R. Capote, "Towards improved evaluation of neutron-induced fission cross section", Proceedings of the International Conference on Nuclear Data for Science and Technology, April 26-30, 2010, Jeju, Korea, *Journ. Kor. Phys. Soc.* 59, no. 23, 979 (2011).
- [154] S. Hilaire, A.J. Koning and S. Goriely, "Microscopic cross sections: an utopia?", Proceedings of the EFNUDAT Workshop on Measurements and Models of Nuclear Reactions, May 25-27, 2010, Paris, France, *Europ. Phys. Journ* 8, 02004 (2010).
- [155] S. Hilaire, A.J. Koning and S. Goriely, "Towards many body theory based nuclear data evaluations", Proceedings of the International Conference on Nuclear Data for Science and Technology, April 26-30, 2010, Jeju, Korea, *Journ. Kor. Phys. Soc.* 59, no. 23, 767 (2011).

- [156] S. Hilaire, S. Goriely, M. Girod, A.J. Koning, R. Capote and M. Sin, "Combinatorial level densities for practical applications", CNR\*09 - Second International Workshop on Compound Nuclear Reactions and Related Topics, eds. L. Bonneau, N. Dubray, F. Gunsing, B. Jurado, 05 - 08 October 2009, Bordeaux, France, *European Physical Journal*, vol. 2, 04005 (2010).
- [157] M. Sabri and M. Haddad, "Calculation of fission product yields for some nuclei with TALYS code", CNR\*09 - Second International Workshop on Compound Nuclear Reactions and Related Topics, eds. L. Bonneau, N. Dubray, F. Gunsing, B. Jurado, 05 - 08 October 2009, Bordeaux, France, *European Physical Journal*, vol. 2, 14003 (2010).
- [158] A. C. Larsen and S. Goriely, "Impact of a low-energy enhancement in the g-ray strength function on the neutron-capture cross section" *Phys. Rev. C* 82, 014318 (2010).
- [159] A.C. Larsen, U. Agvaanluvsan, L.A. Bernstein, A. Brger, R. Chankova, S. Goriely, M. Guttormsen, T. Lonnroth, G.E. Mitchell, H.T. Nyhus, S. Siem, N.U.H. Syed, H.K. Toft and A. Voinov, "Soft structure of gamma-ray strength functions studied with the Oslo method", CNR\*09 - Second International Workshop on Compound Nuclear Reactions and Related Topics, eds. L. Bonneau, N. Dubray, F. Gunsing, B. Jurado, 05 - 08 October 2009, Bordeaux, France, *European Physical Journal*, vol. 2, 03001 (2010).
- [160] T. Kawano, P. Talou, M.B. Chadwick, T. Watanabe, "Monte Carlo simulation for particle and gamma-ray emissions in statistical Hauser-Feshbach model", *Journ. Nucl. Sc. Techn.* 47(5) 462 (2010).
- [161] T. Watanabe, T. Kawano, M.B. Chadwick, R.O. Nelson, S. Hilaire, E. Bauge, P. Dossantos-Usarralde, "Calculation of prompt fission product average cross sections for neutron-induced fission of  $^{235}\text{U}$  and  $^{239}\text{Pu}$ ", *Journ. Nucl. Sci. Techn.*, 47(5), 470 (2010).
- [162] M. Aiche, G. Boutoux, B. Jurado, G. Barreau, L. Matthieu, D. Dassie, B. Haas, V. Meot, O. Roig, L. Gaudefroy, J. Taieb, N. Pillet, T. Faul, O. Serot, E. Bauge and F. Gunsing, "Neutron-induced capture cross sections of short-lived actinides with the surrogate reaction method", *EPJ Web of conferences* 2, 06002 (2010).
- [163] R. Capote, M. Herman, P. Oblozinsky, P.G. Young, S. Goriely, T. Belgia, A.V. Ignatyuk, A.J. Koning, S. Hilaire, V. Plujko, M. Avrigeanu, O. Bersillon, M.B. Chadwick, T. Fukahori, S. Kailas, J. Kopecky, V.M. Maslov, G. Reffo, M. Sin, E. Soukhovitskii, P. Talou, H. Yinlu, and G. Zhigang, "RIPL - Reference Input Parameter Library for calculation of nuclear reactions and nuclear data evaluation", *Nucl. Data Sheets* 110, 3107 (2009).
- [164] S. Goriely, S. Hilaire, A.J. Koning, M. Sin and R. Capote, "Towards prediction of fission cross section on the basis of microscopic nuclear inputs", *Phys. Rev. C* 79, 024612 (2009).
- [165] S. P. Weppner, R. B. Penney, G. W. Diffendale, and G. Vittorini, "Isospin dependent global nucleon-nucleus optical model at intermediate energies", *Phys. Rev. C* 80, 034608 (2009).
- [166] S. Perez-Martin, S. Hilaire, and E. Bauge, "A methodology to compute fission prompt neutron multiplicity by statistical decay of fragments", *Proceedings of the 4th International Workshop on*

- nuclear fission and fission-product spectroscopy, Oct 15 (2009), AIP Conf. Proc. 1175, issue 1, 103 (2009).
- [167] S Goriely and S Hilaire, and N. Chamel, “Nuclear inputs for nucleosynthesis applications”, The Thirteenth International Symposium on Capture Gamma-Ray Spectroscopy and Related Topics, Aug. 25-29 2008, Cologne, Germany, (eds. A. Blazhev, J. Jolie, N. Warr, A. Zilges, AIP Conference proceedings Vol. 1090, New York) (2009).
- [168] A.J. Koning, S. Hilaire and S. Goriely, “Global and local level density models”, Nucl Phys. A810, 13-76 (2008).
- [169] S. Goriely, S. Hilaire and A.J. Koning, “Improved microscopic nuclear level densities within the HFB plus combinatorial method”, Phys. Rev. C 78, 064307 (2008).
- [170] S. Hilaire, S. Goriely and A.J. Koning, “Drip line to drip line microscopic nuclear level densities”, Kernz-08 - International Conference on Interfacing Structure and Reactions at the Centre of the Atom, Dec. 1-5 2008, Queenstown, New Zealand, to be published (2009).
- [171] S. Hilaire, S. Goriely, A.J. Koning, M. Sin and R. Capote, “Towards prediction of fission cross section on the basis of microscopic nuclear inputs”, Kernz-08 - International Conference on Interfacing Structure and Reactions at the Centre of the Atom, Dec. 1-5 2008, Queenstown, New Zealand, to be published (2009).
- [172] S. Hilaire, E. Bauge, A.J. Koning, and S. Goriely, “Towards microscopic predictions of cross sections with TALYS”, Kernz-08 - International Conference on Interfacing Structure and Reactions at the Centre of the Atom, Dec. 1-5 2008, Queenstown, New Zealand, to be published (2009).
- [173] S. Goriely, S. Hilaire, A.J. Koning, M. Sin and R. Capote, “Towards predictions of neutron-induced fission cross section”, The Thirteenth International Symposium on Capture Gamma-Ray Spectroscopy and Related Topics, Aug. 25-29 2008, Cologne, Germany, (eds. A. Blazhev, J. Jolie, N. Warr, A. Zilges, AIP Conference proceedings Vol. 1090, New York) (2009).
- [174] M. Sin, R. Capote, S. Goriely, S. Hilaire and A.J. Koning, “Neutron-induced fission cross section on actinides using microscopic fission energy surfaces”, Proceedings of the International Conference on Nuclear Data for Science and Technology, April 22-27, 2007, Nice, France, editors O.Bersillon, F.Gunsing, E.Bauge, R.Jacqmin, and S.Leray, EDP Sciences, 2008, p. 313-316. (2008).
- [175] S. Hilaire, S. Goriely and A.J. Koning, “Global microscopic nuclear level densities within the HFB plus combinatorial method for practical applications”, Proceedings of the International Conference on Nuclear Data for Science and Technology, April 22-27, 2007, Nice, France, editors O.Bersillon, F.Gunsing, E.Bauge, R.Jacqmin, and S.Leray, EDP Sciences, 2008, p. 199-202. (2008).
- [176] E. Betal, A. Likar and T. Vidmar, “Radiative nucleon capture—a dual approach” Proceedings of the International Conference on Nuclear Data for Science and Technology, April 22-27, 2007, Nice, France, editors O.Bersillon, F.Gunsing, E.Bauge, R.Jacqmin, and S.Leray, EDP Sciences, (2008).

- [177] M. Avrigeanu, R.A. Forrest, A.J. Koning, F.L. Roman, V. Avrigeanu, "On the role of activation and particle-emission data for reaction model validation", Proceedings of the International Conference on Nuclear Data for Science and Technology, April 22-27, 2007, Nice, France, editors O.Bersillon, F.Gunsing, E.Bauge, R.Jacqmin, and S.Leray, EDP Sciences, 2008, p. 223-226. (2008).
- [178] S. Perez-Martin, S. Hilaire, and E. Bauge, "Fission prompt neutron and gamma multiplicity by statistical decay of fragments", Seminar on fission: Corsenk Priory Belgium, 18-21 Sep 2007, p. 147 (2007).
- [179] M.C. Duijvestijn and A.J. Koning, "Exciton model calculations up to 200 MeV: the optical model points the way", *Proceedings of the International Conference on Nuclear Data for Science and Technology - ND2004*, AIP vol. 769, eds. R.C. Haight, M.B. Chadwick, T. Kawano, and P. Talou, Sep. 26 - Oct. 1, 2004, Santa Fe, USA, p. 1150 (2005).
- [180] M.C. Duijvestijn and A.J. Koning, "Fission yield predictions with TALYS", *Proceedings of the International Conference on Nuclear Data for Science and Technology - ND2004*, AIP vol. 769, eds. R.C. Haight, M.B. Chadwick, T. Kawano, and P. Talou, Sep. 26 - Oct. 1, 2004, Santa Fe, USA, p. 1225 (2005).
- [181] A.J. Koning and M.C. Duijvestijn, "A global pre-equilibrium analysis from 7 to 200 MeV based on the optical model potential", *Nucl. Phys.* **A744**, 15 (2004).
- [182] A.J. Koning and J.P. Delaroche, "Local and global nucleon optical models from 1 keV to 200 MeV", *Nucl. Phys.* **A713**, 231 (2003).
- [183] S. Hilaire, Ch. Lagrange, and A.J. Koning, "Comparisons between various width fluctuation correction factors for compound nucleus reactions", *Ann. Phys.* **306**, 209 (2003).

#### Analysis of measurements below 20 MeV

- [184] H. C. Pandey, B. Pandey, H.M. Agrawal, "Pre-equilibrium effects on (n,p) reactions of Gd and Dy isotopes from threshold to 20 MeV", *Ann. Nucl. En.* 64, 8 (2014).
- [185] D. Suchiang, J. J. Jeremiah, B.M. Jyrwa, L. Khongiang, "Excitation functions of the 90,91,92,94,96Zr(n,p) reactions from reaction threshold to 20 MeV", *Ann. Nuc. En.*, 65, March 2014, 97 (2014).
- [186] M. Kerveno, J.C. Thiry, A. Bacquias, C. Borcea, P. Dessagne, J.C. Drohe, S. Goriely, S. Hilaire, E. Jericha, H. Karam, A. Negret, A. Pavlik, A.J.M. Plompen, P. Romain, C. Rouki, G. Rudolf, and M. Stanoiu, "Measurement of  $^{235}\text{U}(n,n'g)$  and  $^{235}\text{U}(n,2n)$  reaction cross sections", *Phys. Rev.* C87, 024609 (2013).
- [187] J.J. Jeremiah, D. Suchiang, B.M. Jyrwa, "Excitation functions of (n,2n) reactions for stable lead isotopes from reaction threshold to 20 MeV", *Ann. Nuc. En.* 56, 44 (2013).
- [188] Y. Zhang, L. Zhao, X. Kong, R. Liu and J. Li, "Cross-sections for (n,2n) and (n,p) reactions on neodymium isotopes and  $^{160}\text{Gd}(n,a)^{157}\text{Sm}$  at neutron energy between 13.5 and 14.7 MeV", *Ann. Nuc. En.* 53, 99 (2013).

- [189] h. Aytekin and B. Ridvan, "Pre-equilibrium and equilibrium calculations of (n, p) reactions on  $^{32}\text{S}$ ,  $^{64}\text{Zn}$ ,  $^{67}\text{Zn}$ ,  $^{89}\text{Y}$ ,  $^{90}\text{Zr}$  and  $^{153}\text{Eu}$  targets used for production of  $^{32}\text{P}$ ,  $^{64}\text{Cu}$ ,  $^{67}\text{Cu}$ ,  $^{89}\text{Sr}$ ,  $^{90}\text{Y}$  and  $^{153}\text{Sm}$  therapeutic radionuclides", *Ann. Nuc. En.* 53, 439 (2013)
- [190] C. Bhatia, S. W. Finch, M. E. Gooden, and W. Tornow, " $^{40}\text{Ar}(n,p)^{40}\text{Cl}$  reaction cross section between 9 and 15 MeV", *Phys. Rev. C* 86, 041602 (2012).
- [191] J.J. Jeremiah, D. Suchiang, B.M. Jyrwa, "Excitation functions of (n,2n) reactions for stable iron isotopes from reaction threshold to 20 MeV", *Ann. Nuc. En.* 43, 208 (2012).
- [192] C. Plaisir, F. Hannachi, F. Gobet, M. Tarisien, M. M. Aleonard, V. Meot, G. Gosselin, P. Morel, B. Morillon, "Measurement of the  $^{85}\text{Rb}(g,n)^{84m}\text{Rb}$  cross-section in the energy range 10-19 MeV with bremsstrahlung photons", *Eur. Phys. Journ.* A48, 68 (2012).
- [193] M. Serris et al, "Experimental and theoretical study of the (n,2n) reaction on Hf-174,176 isotopes", *Phys. Rev. C* 86, 034602 (2012).
- [194] I. Vishnevskii, V. Zheltonozhskii, A. Savrasov, "Investigating  $\text{Np}^{237}$  and  $\text{Am}^{241}$  photofission", *Bull. Rus. Acad. Sci.* 76, 8, 901 (2012).
- [195] P.K. Saran, M. Nandy, P.K. Sarkar, S.L. Goyal, "Production of long-lived  $^{26}\text{Al}$  and  $^{24}\text{Na}$  from neutron interaction in Al target", *Indian Journ. Pure and Applied Physics* 50 (7), 509 (2012).
- [196] A. Plompen, P. Archier, A. Bacquias, C. Borcea, D. Deleanu, C. De Saint-Jean, P. Dessagne, E. Gasser, S. Hilaire, M. Kerveno, A. Koning, L. Leal, A. Negret, G. Noguere, P. Romain, C. Rouki, G. Rudolf, J.C. Thiry, C. Vaglio-Gaudard, "Neutron inelastic scattering, recent experiments and their interpretation", *Proceedings of the 13th International Conference on nuclear reaction mechanisms, Varenna (Italy), June 11 - 15, (2012).*
- [197] A. Bacquias, C. Borcea, Ph. Dessagne, E. Gasser, S. Goriely, S. Hilaire, M. Kerveno, J.C. Drohe, A.J. Koning, N. Nankov, A.L. Negret, A. Plompen, P. Romain, C. Rouki, G. Rudolf, M. Stanoiu, J.C. Thiry, "Study of (n,xng) reactions on  $^{235,238}\text{U}$ ", *Proceedings of the 13th International Conference on nuclear reaction mechanisms, Varenna (Italy), June 11 - 15, (2012).*
- [198] S.P. Simakov, V.G. Pronyaev, R. Capote, R.O. Nelson "  $^{48}\text{Ti}(n,ng)$  gamma production reaction as a candidate for a reference cross section", *Proceedings of the 13th International Conference on nuclear reaction mechanisms, Varenna (Italy), June 11 - 15, (2012).*
- [199] B.S. Ishkhanov, S. Yu. Troschiev and V.A. Chetvertkova, "Yields of photonuclear reactions on Sn isotopes at an energy of 19.1 MeV", *Bull. Russ. Ac. Sci.: Physics* 76, 481 (2012).
- [200] M. Beard, S. Frauendorf, B. Kaempfer, R. Schwengner and M. Wiescher, "Photonuclear and radiative-capture reaction rates for nuclear astrophysics and transmutation:  $^{92-100}\text{Mo}$ ,  $^{88}\text{Sr}$ ,  $^{90}\text{Zr}$  and  $^{139}\text{La}$ ", *Phys. Rev. C* 85, 065808 (2012).
- [201] C. Oprea, A. Oprea and A. Mihul, "Cross section evaluation in the photodisintegration of  $^{152}\text{Sm}$  isotope", *Physics Procedia* 31, 178 (2012).

- [202] R. Crasta et al., “Measurement of  $^{232}\text{Th}(n,g)$  and  $^{232}\text{Th}(n,2n)$  reaction cross-sections at neutron energies of 8.04 and 11.90 MeV”, *Ann. Nuc. En.* 47, 160 (2012).
- [203] I.A. Reyhancan, “Measurements and model calculations of isomeric cross sections for (n,alpha) reaction on Ce140 isotope around 14 MeV neutrons”, *Ann. Nuc. En.* 47, 81 (2012).
- [204] P.M. Prajapati et al., “Measurement of the neutron capture cross sections of  $^{232}\text{Th}$  at 5.9 MeV and 15.5 MeV”, *Eur. Phys. Journ A48*, 35 (2012).
- [205] B. S. Shivashankar, H. Naik, S. V. Suryanarayana, P. M. Prajapati, V. K. Mulik, K. C. Jagadeesan, S. V. Thakare, A. Goswami, S. Ganesan, “Measurement of reaction cross-sections for  $^{64}\text{Ni}(n,g)^{65}\text{Ni}$  at  $E_n = 0.025$  eV and  $^{58}\text{Ni}(n,p)^{58}\text{Co}$  at  $E_n = 3.7$  MeV ” *Journal of Radioanalytical and Nuclear Chemistry*, (2012).
- [206] B. Lalremruata, N. Otuka, G. J. Tambave, V. K. Mulik, B. J. Patil, S. D. Dhole, A. Saxena, S. Ganesan, and V. N. Bhoraskar, “Systematic study of (n,p) reaction cross sections from the reaction threshold to 20 MeV”, *Phys. Rev. C* 85, 024624 (2012).
- [207] N. Dzysiuk, A. Kadenko, I. Kadenko G. Primenko, “Measurement and systematic study of (n,x) cross sections for Dy, Er and Yb isotopes at 14.7 MeV neutron energy”, *Phys. Rev. C* 86, 034609 (2012).
- [208] M. Avrigeanu, V. Avrigeanu and A.J. Koning, “Investigation of deuteron breakup and deuteron-induced fission on actinide nuclei at low incident energies”, *Phys. Rev. C* 85, 034603 (2012).
- [209] H. Naik, et al., “Mass distribution in the 50-, 60-, and 70-MeV bremsstrahlung-induced fission of  $\text{Th}^{232}$ ”, *Phys. Rev. C* 85, 024623 (2012).
- [210] H. Naik, A. Goswami, G. N. Kim, M. W. Lee, K. S. Kim, S. V. Suryanarayana, E. A. Kim, S. G. Shin, and M.-H. Cho, “Mass-yield distributions of fission products from photofission of  $^{232}\text{Th}$  induced by 45- and 80-MeV bremsstrahlung”, *Phys. Rev. C* 86, 054607 (2012).
- [211] M. Avrigeanu, V. Avrigeanu and F.L. Roman, “Deuteron-induced reaction mechanisms at low energies”, *Proceedings of CNR\*11 : Third International Workshop on Compound Nuclear Reactions and Related Topics*, Prague, 2011, *EPJ Web of Conferences* 21, 07003 (2012).
- [212] M. Avrigeanu, V. Avrigeanu and F.L. Roman, “On neutron-induced reaction mechanisms at medium energies”, *Proceedings of CNR\*11 : Third International Workshop on Compound Nuclear Reactions and Related Topics*, Prague, 2011, *EPJ Web of Conferences* 21, 07004 (2012).
- [213] V.M. Mazur, Z.M. Bigan, D.M. Symochko, and T.V. Poltorzhytska, “Cross-sections of isomeric state excitation of the  $^{119}\text{Te}$  and  $^{121}\text{Te}$  nuclei in (g,n) reactions in an energy range of 9-20 MeV”, *Phys. Part and Nuclei Letters* 9, 248 (2012).
- [214] M. Avrigeanu, V. Avrigeanu and F.L. Roman, “On neutron-induced reaction mechanisms at medium energies”, *Proceedings of CNR\*11 : Third International Workshop on Compound Nuclear Reactions and Related Topics*, Prague, 2011, *EPJ Web of Conferences* 21, 07004 (2012).

- [215] M. Avrigeanu, V. Avrigeanu, M. Diakaki and R. Vlastou, "Isomeric cross sections of fast-neutron-induced reactions on  $^{197}\text{Au}$ ", *Phys. Rev. C* 85, 044618 (2012).
- [216] C. Gustavsson, J. Blomgren, C. Hellesen, A. Oehrn, S. Pomp and the SCANDAL collaboration, "Inelastic neutron scattering from carbon, iron, yttrium and lead", *Proceedings of CNR\*11 : Third International Workshop on Compound Nuclear Reactions and Related Topics, Prague, 2011, EPJ Web of Conferences* 21, 03004 (2012).
- [217] J.R. Tompkins, C.W. Arnold, H.J. Karwowski, G.C. Rich, L.G. Sobotka and C.R. Howell, "Measurement of the  $^{48}\text{Ca}(g,n)$  reaction", *Phys. Rev. C* 84, 044331 (2011)
- [218] N.K. Skobelev, V. Kroha, A.A. Kulko, Yu.E. Penionzhkevich, R. Kalpakchieva, "Excitation functions of the isotopes  $^{44}\text{Sc}$ ,  $^{46}\text{Sc}$  and  $^{47}\text{Sc}$  in the reactions  $^{45}\text{Sc} + d$  and  $^{45}\text{Sc} + ^6\text{He}$ ", *Proceedings of NPAE, Kyiv 2010* (2011).
- [219] H. K. Toft, A. C. Larsen, A. Brger, M. Guttormsen, A. Grgen, H. T. Nyhus, T. Renstrm, S. Siem, G. M. Tveten, and A. Voinov, "Evolution of the pygmy dipole resonance in Sn isotopes", *Phys. Rev. C* 83, 044320 (2011).
- [220] V.K. Mulik, B.S. Shivashankar, P.M. Prajapati, S.V. Suryanarayana, H. Naik, K.C.Jagadeesan, S.V.Thakare, S.C. Sharma, P.V. Bhagwat, A.Goswami, S.Ganesan, S.D. Dhole and V.N. Bhora, "Measurements of  $^{56}\text{Fe}(n,p)^{56}\text{Mn}$  reaction cross-section at neutron energy of 15.5 MeV", *Proceedings of the DAE Symp. on Nucl. Phys.* 56 (2011).
- [221] S.V. Surayanarayana, H. Naik, V. K. Mulik, P. M. Prajapati, B. S. Sivashankar, K. C .Jagadeesan, S.V.Thakare, D. Raj, S.C. Sharma, P.V. Bhagwat, S. D. Dhole, S. Ganesan and V.N. Bhoras, "Measurement of the neutron capture cross-section of  $^{238}\text{U}$  using the neutron activation technique", *Proceedings of the DAE Symp. on Nucl. Phys.* 56 (2011).
- [222] B. Pandey, H.M. Agrawal, "Excitation Functions of neutron induced reactions on Ytterbium isotopes", *Proceedings of the DAE Symp. on Nucl. Phys.* 56 (2011).
- [223] P.K. Saran, M. Nandy, P.K. Sarkar, S.L. Goyal, "Excitation functions for the production of radioisotopes  $^{62}\text{Cu}$  and  $^{63}\text{Ni}$  from  $^{63}\text{Cu}$ " *Proceedings of the DAE Symp. on Nucl. Phys.* 56 (2011).
- [224] P. Mohr, "Total reaction cross sections from  $^{141}\text{Pr}(a,a)^{141}\text{Pr}$  elastic scattering and  $a$ -induced reaction cross sections at low energies", *Phys. Rev. C* 84, 055803 (2011).
- [225] V.A. Zheltonozhsky and A.N. Savrasov, "Investigating the excitation of 8- isomers in the odd-odd nuclei of  $^{116-120}\text{Sb}$  in the  $(p,n)$  reaction", *Bull. Russ. Ac. Sci.: Physics* 75(9), 1274 (2011).
- [226] V. Semkova, R. Jaime Tornin, N. Janeva, N. Koyumdjieva, A. Moens, A.J. Plompen and K. Volev, "Neutron-induced Activation Cross Sections on Hafnium Isotopes from the Threshold to 20 MeV", *Proceedings of the International Conference on Nuclear Data for Science and Technology, April 26-30, 2010, Jeju, Korea, Journ. Kor. Phys. Soc.* 59, no. 23, 1737 (2011).
- [227] A. Negret, C. Borcea and A.J. Plompen, "Cross Sections for Neutron Inelastic Scattering on  $^{28}\text{Si}$ ", *Proceedings of the International Conference on Nuclear Data for Science and Technology, April 26-30, 2010, Jeju, Korea, Journ. Kor. Phys. Soc.* 59, no. 23, 1765 (2011).

- [228] M. Hagiwara, T. Sanami, Y. Iwamoto, N. Matsuda, Y. Sakamoto, Y. Nakane, H. Nakashima, K. Masumoto and Y. Uwamino, "Spectrum Measurement of Neutrons and Gamma-rays from Thick H<sub>2</sub> 18O Target Bombarded with 18 MeV Protons" Proceedings of the International Conference on Nuclear Data for Science and Technology, April 26-30, 2010, Jeju, Korea, Journ. Kor. Phys. Soc. 59, no. 23, 2035 (2011).
- [229] N.-C. Shu, Y.-J. Chen, T.-J. Liu, Z.-J. Sun, X.-Z. Wu, T.-S. Fan, J. Qian and R.-R. Xu, "Semi-empirical Study on the Yield Energy-dependence of the <sup>235</sup>U+n Fission", Proceedings of the International Conference on Nuclear Data for Science and Technology, April 26-30, 2010, Jeju, Korea, Journ. Kor. Phys. Soc. 59, no. 23, 1353 (2011).
- [230] Y. Gledenov, G. Zhang, P. Koehler, M. Sedysheva, J. Zhang, H. Wu, J. Liu, J. Cheng, G. Khuukhenkhuu and P. Szalanski, "Investigation of (n,) Reaction for Rare-earth Elements in the MeV Neutron Energy Region", Proceedings of the International Conference on Nuclear Data for Science and Technology, April 26-30, 2010, Jeju, Korea, Journ. Kor. Phys. Soc. 59, no. 23, 1693 (2011).
- [231] H. Benhabiles Mezhoud, J. Kiener, J. P. Thibaud, V. Tatischeff, I. Deloncle, A. Coc, J. Duprat, C. Hamadache, A. Lefebvre Schuhl, J. C. Dalouzy, F. de Grancey, F. de Oliveira, F. Dayras, N. de Sereville, M. G. Pellegriti, L. Lamia and S. Ouichaoui "Measurements of nuclear gamma-ray line emission in interactions of protons and alpha particles with N, O, Ne, and Si", Phys. Rev. C83, 024603 (2011).
- [232] R. Crasta, H. Naik, S.V. Suryanarayana, Ganesh Sanjeev, P.M. Prajapati, M. Kumar, T.N. Nathaniel, V.T. Nimje, K.C. Mittal, "Measurement of photoneutron cross section of <sup>93</sup>Nb at end point brehmsstrahlung energy of 10 MeV", Proceedings of the DEA symposium on Nuclear physics 56, 1022 (2011).
- [233] R. Crasta, H. Naik, S.V. Suryanarayana, P.M. Prajapati, K.C. Jagadisan, S.V. Thakare, S. Ganesh, V.T. Nimje, K.C. Mittal, A. Goswami, "Photo-neutron cross section of <sup>100</sup>Mo", Journ. Radioan. nucl. chem. 290(2), 367 (2011).
- [234] H. Naik, V.T. Nimje, D. Raj, S.V. Suryanarayana, A. Goswami, Sarbjit Singh, S.N. Acharya, K.C. Mittal, S. Ganesan, P. Chandrachoodan, V.K. Manchanda, V. Venugopal, S. Banarjee, "Mass distribution in the Bremsstrahlung-induced fission of <sup>232</sup>Th, <sup>238</sup>U and <sup>240</sup>Pu", Nucl. Phys. A853, 1 (2011).
- [235] A. Tsinganis, M. Diakaki, M. Kokkoris, A. Lagoyannis, E. Mara, C.T. Papadopoulos and R. Vlastou, "Isomeric cross section of the <sup>197</sup>Au(n,2n) reaction", Phys. Rev. C83, 024609 (2011).
- [236] N. N. Kalmykov, O. P. Shustova, A. V. Uryson, "Spectra and Mass Composition of Ultrahigh-Energy Cosmic Rays from Point Sources", Journ. Cosm. Astr. Part. Phys. 2012, 035 (2012).
- [237] O.P. Shustova, N.N. Kalmykov and A.V. Uryson, "Influence of background radiation on the composition of ultrahigh energy cosmic rays in propagating from their source to an earth based facility", Bull. Russ. Ac. Sci: physics 75 (3), 313 (2011).

- [238] R. Raut, A.S. Crowell, B. Fallin, C.R. Howell, C. Huibregtse, J.H. Kelley, T. Kawano, E. Kwan, G. Rusev, A.P. Tonchev, W. Tornow, D.J. Vieira and J.B. Wilhelmy, "Cross section measurements of neutron-induced reactions on GaAs using monoenergetic beams from 7.5 to 15 MeV", *Phys. Rev. C* 83,044621 (2011).
- [239] H. Naik, P.M. Prajapati, S.V. Suryanarayana, et al, "Measurement of the neutron capture cross section of  $^{232}\text{Th}$  using the neutron activation technique", *Europ. Phys. Journ A* 47, no 4, 51 (2011).
- [240] B.S. Ishkhanov, V.N. Orlin and S. Yu. Troschiev, "Photodisintegration of tantalum", *Phys. Atomic Nuclei* 75, 253 (2012).
- [241] B.S. Ishkhanov and S. Yu. Troschiev, "Simulation of photodisintegration of heavy nuclei", *Moscow Univ. Phys. Bull.* 66 (3), 219 (2011).
- [242] B.S. Ishkhanov, V.N. Orlin and S. Yu. Troschiev, "Photonuclear reactions on mercury isotopes in the region of the giant-dipole-resonance energy", *Phys. At. Nuclei* 74, 706 (2011).
- [243] S. R. Elliott, V. E. Guiseppe, B. H. LaRoque, R. A. Johnson, and S. G. Mashnik, "Fast-neutron activation of long-lived isotopes in enriched Ge", *Phys. Rev. C* 82, 054610 (2010).
- [244] J.C. Thiry, C. Borcea, P. Dessagne, J.C. Drohe, E. Jericha, H. Karam, M. Kerveno, A.J. Koning, A. Negret, A. Pavlik, A. Plompen, P. Romain, C. Rouki, G. Rudolf, and M. Stanoiu, "Measurement of (n,xng) reactions of interest for the new nuclear reactors", *Proceedings of the International Conference on Nuclear Data for Science and Technology*, April 26-30, 2010, Jeju, Korea, *Journ. Kor. Phys. Soc.* 59, no. 23, 1880 (2011).
- [245] Maelle Kerveno, Catalin Borcea, Philippe Dessagne, Jean Claude Drohe, Erwin Jericha, Habib Karam, Arjan J. Koning, Alexandru Negret, Andreas Pavlik, Arjan J. M. Plompen, Chariklia Rouki, Gerard Rudolf, Mihai Stanoiu, Jean Claude Thiry, "Measurement of (n,xn) reactions of interest for the new nuclear reactors", *Proceedings of the NEMEA-6 Workshop on Neutron Measurements, Evaluations and Applications: Exploring the frontiers of nuclear data and measurements, their uncertainties and covariances*, October 25-28, 2010 Krakow, Poland (2011), p. 93 (2010), also *NEA Nuclear Science NEA/NSC/DOC(2011)* 4.
- [246] J. C. Thiry, C. Borcea, P. Dessagne, J.C. Drohe, E. Jericha, H. Karam, M. Kerveno, A.J. Koning, A. Negret, A. Pavlik, A.J.M. Plompen, C. Rouki, G. Rudolf, M. Stanoiu, "Measurement of (n,xng) reactions at high precision", *Proceedings of the NEMEA-6 Workshop on Neutron Measurements, Evaluations and Applications: Exploring the frontiers of nuclear data and measurements, their uncertainties and covariances*, October 25-28, 2010 Krakow, Poland, p. 121 (2010), also *NEA Nuclear Science NEA/NSC/DOC(2011)* 4.
- [247] N. Dzysiuk, I. Kadenko, A.J. Koning, "Cross sections for (d-t) neutron interaction with germanium isotopes", *Nuc. Phys.* A858, 1 (2011).
- [248] N. Dzysiuk, I. Kadenko, A.J. Koning, R. Yermolenko, "Cross sections for fast neutron interaction with Lu, Tb and Ta isotopes", *Phys. Rev. C* 81, 014610 (2010).

- [249] V.M. Bondar, O.M. Gorbachenko, I.M. Kadenko, B.Y. Leshchenko, Y.M. Onishchuk, V. Plujko, "Spectra of gamma rays in (n,xn) reactions on ferrum and bismuth nuclei" Nucl. Phys. At. En. 11(3), 246 (2010).
- [250] C. Sage, V. Semkova, O. Bouland, P. Dessagne, A. Fernandez, F. Gunsing, C. Naestren, G. Nogure, H. Ottmar, A. J. M. Plompen, P. Romain, G. Rudolf, J. Somers, and F. Wastin, "High resolution measurements of the  $^{241}\text{Am}(n,2n)$  reaction cross section", Phys. Rev. C81, 064604 (2010).
- [251] V.M. Mazur, Z.M. Bigan, D.M. Symochko, "Population of metastable states in Rb isotopes in the photoneutron reactions", Journ. Phys. G 37, 035101 (2010).
- [252] G. Noguere, "Neutron average cross sections of  $^{237}\text{Np}$ ", Phys. Rev. C81, 044607 (2010).
- [253] V.S. Bokhinuk, Z.M. Bigan, O.M. Parlag, I.V. Sokoluk, D.M., Symochko, T.J. Marynets, "Excitation of  $^{117}\text{In}$  1/2-isomeric state in (g,p) reactions", Journal of Physical Studies, 14(1) (2010).
- [254] J. Luo, C. Li, Z. Liu, X. Wang, R. Liu, L.Jiang, "Measurement of neutron-induced activation cross sections of lanthanum at 14.8 MeV", Journ. Radioan. Nucl. Chem. 283(2), 421 (2010).
- [255] Y.M. Gledenov, G. Zhang, G. Khuukhenkhoo, M.V. Sedysheva, P.J. Szalanski, P.E., Koehler, et al, "Cross-section measurement and analysis for the  $^{149}\text{Sm}(n,a)^{146}\text{Nd}$  reaction at 6.0 MeV", Phys. Rev. C82, 014601 (2010).
- [256] V.A. Zheltonozhskii and A.N. Savrasov, "Investigation of the near-threshold (g,n) reaction on the  $^{116}\text{Cd}$  and  $^{121}\text{Sb}$  nuclei", Bull. Russ Ac. Sciences: physics 74, 829 (2010).
- [257] G. Zhang, H. Wu, J. Zhang, J. Liu, J. Chen, Y.M. Gledenov, M.V. Sedysheva, G. Khuukhenkhoo and P.J. Szalansky, "Cross-section measurement for the  $^{67}\text{Zn}(n,a)^{64}\text{Ni}$  reaction at 6.0 MeV", European Physical Journal A, 43(1), 1 (2010).
- [258] M. Erhard, A. R. Junghans, C. Nair, R. Schwengner, R. Beyer, J. Klug, K. Kosev, A. Wagner, and E. Grosse, "Experimental study of the electric dipole strength in the even Mo nuclei and its deformation dependence", Phys. Rev. C81, 034319 (2010).
- [259] C. Koumeir, F. Haddad, V. Metivier, N. Servagent and N. Michel, "A new facility for high energy PIXE at the ARRONAX facility", Proceedings of the European Conference on X-ray spectrometry, June 20-25 2010, Figueira da Foz, Coimbra, (2010).
- [260] I.M. Vyshnevskiy, O.I. Davidoskaya, V.O. Zheltonozhsky, A.M. Savrasov, P.M. Trifonov, V.M. Mazur, D.M. Symochko, "Investigation of isomeric yields ratio in (g,n)-reaction in nucleus of  $^{121}\text{Sb}$ ", Nuclear = Physics and Atomic Energy 10(4), 352-356 (2009).
- [261] A. Makinaga, R. Schwengner, G. Rusev, F. Donau, S. Frauendorf, D. Bemmerer, R. Beyer, P. Crespo, M. Erhard, A. R. Junghans, J. Klug, K. Kosev, C. Nair, K. D. Schilling, and A. Wagner, "Dipole strength in  $^{139}\text{La}$  below the neutron-separation energy", Phys. Rev. C 82, 024314 (2010).
- [262] V. Semkova, E. Bauge, A.J.M. Plompen, D.L. Smith, "Neutron activation cross sections for zirconium isotopes", Nucl. Phys. A832, 149 (2010).

- [263] N.R. Dzysiuk, I.M. Kadenko, V.K. Maidanyuk, G.I. Primenko, R.V. Yermolenko, "The cross sections for (n,x) nuclear reactions on terbium and lutetium isotopes", *Nuclear Physics and Atomic Energy*, 9(2), 34-38 (2008).
- [264] A. Hutcheson, C. Angell, J.A. Becker, A.S. Crowell, D. Dashdorj, B. Fallin, N. Fotiadis, C.R. Howell, H.J. Karwowski, T. Kawano, J.H. Kelley, E. Kwan, R.A. Macri, R.O. Nelson, R.S. Pedroni, A.P. Tonchev, W. Tornow, "Cross sections for  $^{238}\text{U}(n,n'\gamma)$  and  $^{238}\text{U}(n,2n\gamma)$  reactions at incident neutron energies between 5 and 14 MeV, *Phys. Rev. C* 80, 014603 (2009).
- [265] Zheng Na, Zhong Chunlai, Ma Liyong, Li Xiangqing, Chen Jinxiang, Fan Tieshuan, "The dependence of cumulative  $^{238}\text{U}(n,f)$  fission yield on incident-neutron energy", *Nucl. Sci and Techn.* 20(5) (2009).
- [266] O.A. Bezshyyko, A.N. Dovbnya, L.O. Golinka-Bezshyyko, I.M. Kadenko, I.S. Kulakov, V.A. Kushnir, V.V. Mitrochenko, S.N. Olejnik, G.E. Tuller, A.N. Vodin, "Isomer ratios of photonuclear reaction products of silver and indium isotopes for Bremsstrahlung energies above 35 MeV", *Problems of atomic science and technology N5, series: nuclear physics investigations* 52, 23 (2009).
- [267] F.M.D. Attar, S.D. Dhole, S. Kailas and V.N. Bhoraskar, "Cross sections for the formation of isomeric pair  $^{75}\text{Ge}^{m,g}$  through (n,2n), (n,p) and (n, $\alpha$ ) reactions measured over 13.73 to 14.77 MeV and calculated from near threshold to 20 MeV neutron energies", *Nucl. Phys.* A828, 253 (2009).
- [268] Yu. M. Gledenov, M.V. Sedysheva, V.A. Stolupin, G. Zhang, J. Zhang, J. Liu, J. Chen, G. Khuukhenkhuu, P.E. Koehler, P.J. Szalanski, "Cross sections of the  $^{143}\text{Nd}(n,\alpha)^{140}\text{Ce}$  and  $^{147}\text{Sm}(n,\alpha)^{144}\text{Nd}$  reactions in the MeV neutron region", *Phys. Rev. C* 80, 044602 (2009).
- [269] P. Reimer, A.J. Koning, A.J.M. Plompen, S.M. Qaim, and S. Sudar, "Neutron induced reaction cross sections for the radioactive target nucleus  $^{99}\text{Tc}$ ", *Nuc. Phys.* A815, 1-17 (2009).
- [270] B. Lalremruata, S.D. Dhole, S. Ganesan, V.N. Bhoraskar, "Double differential cross-sections of (n, $\alpha$ ) reactions in aluminium and nickel at 14.77 MeV neutrons", *Nucl. Phys.* A821, 23 (2009).
- [271] B. Lalremruata, S. Ganesan, V.N. Bhoraskar, S.D. Dhole, "Excitation functions and isotopic effects in (n, p) reactions for stable nickel isotopes from", *Ann. Nuc. En.* 36, 458 (2009).
- [272] B. Lalremruata, S. D. Dhole, S. Ganesan, and V. N. Bhoraskar, "Excitation function of the  $^{93}\text{Nb}(n,2n)^{92}\text{Nb}$  reaction from threshold to 24 MeV ", *Phys. Rev. C* 80, 014608 (2009).
- [273] O.A. Bezshyyko, A.N. Vonin, L.O. Golinka-Bezshyyko, A.N. Dovbnya, I.M. Kadenko, O.A. Kovalenko, A. Kushnir, A.I. Levon, V.V. Mitrochenko, S.N. Olejnik, G.E. Tuller, "Isomer ratios of photonuclear reaction products for indium isotopes in the energy region above 33 MeV", *Nucl. Phys. and At. Energy* 10(2), 32 (2009).
- [274] I.N. Vishnevsky, V.A. Zheltonozhsky, A.N. Savrasov, N.V. Strilchuk, "Isomeric yield ratio in nuclei  $^{190}\text{Ir}$  and  $^{150,152}\text{Eu}$ ", *Phys. Rev. C* 79, 014615 (2009).
- [275] A.V. Avdeenkov, S. Goriely and S.P. Kamerdzhiev, "Impact of the phonon coupling of the radiative neutron capture", *Phys. At. Nucl.* 73, no 7, 1119 (2010).

- [276] G. Rusev, R. Schwengner, R. Beyer, M. Erhard, E. Grosse, A. R. Junghans, K. Kosev, C. Nair, K. D. Schilling, A. Wagner, F. Dnau, and S. Frauendorf, "Enhanced electric dipole strength below particle-threshold as a consequence of nuclear deformation", *Phys. Rev. C* **79**, 061302 (2009).
- [277] V. Semkova, P. Reimer, T. Altzitzoglou, A.J. Koning, A.J.M. Plompen, S.M. Qaim, C. Quétel, D.L. Smith, S. Sudar, "Neutron activation cross sections on lead isotopes", *Phys. Rev. C* **80**, 024610 (2009).
- [278] R. Kurniadi, Y.S. Perkasa, K. Basar, A. Waris, "Fission cross section calculation using TALYS based on two different level density models", 2nd International conference on advances in nuclear science and engineering 2009-ICANSE, *AIP Conf Proc.* **1244**, 300 (2010).
- [279] Y.S. Perkasa, R. Kurniadi, K. Basar, A. Waris, "Fission cross section and fission yield calculation of Am-241(n,f), Th-232(n,f) and U-235(N,F) using TALYS", *Proceedings of the 2nd Int Conf. on advances in nuclear science and engineering - ICANSE 2009* (2010).
- [280] Y.S. Perkasa, R. Kurniadi, A. Waris, "Application of TALYS code for calculation of fission cross section and fission yield of several heavy nuclides", *Indonesian Journ. Phys.* **20**(3) (2009).
- [281] F.M.D. Attar, R. Mandal, S.D. Dhole, A. Saxena, Ashokkumar, S. Ganesan, S. Kailas, V.N. Bhorkar, "Cross-sections for formation of  $^{89}\text{Zr}$  through  $^{90}\text{Zr}(n,2n)^{89}\text{Zr}$  reaction over neutron energy range 13.73 MeV to 14.77 MeV", *Nucl. Phys.* **A802**, 1 (2008).
- [282] V.E. Guiseppe, M. Devlin, S.R. Elliott, N. Fotiades, A. Hime, D.-M. Mei, R.O. Nelson, and D.V. Perepelitsa, "Neutron inelastic scattering and reactions in natural Pb as a background in neutrinoless double-beta decay experiments", *Phys. Rev. C* **79**, 054604 (2008).
- [283] J. Hasper, S. Muller, D. Savran, L. Schnorrenberger, K. Sonnabend, A. Zilges, "Investigation of photoneutron reactions close to and above the neutron emission threshold in the rare earth region", *Phys. Rev. C* **77**, 015803 (2008).
- [284] M. Avrigeanu, H. Leeb, W. von Oertzen, F.L. Roman, and V. Avrigeanu, "Low energy deuteron elastic scattering on light and medium nuclei", *International Conference on Nuclear Data for Science and Technology*, April 22-27, 2007, Nice, France, editors O.Bersillon, F.Gunsing, E.Bauge, R.Jacqmin, and S.Leray, *EDP Sciences*, (2008).
- [285] L.C. Mihailescu, C. Borcea, P. Baumann, Ph. Dessagne, E. Jericha, H. Karam, M. Kerveno, A.J. Koning, N. Leveque, A. Pavlik, A.J.M. Plompen, C. Quétel, G. Rudolf, I. Tresl, "Measurement of  $(n, xn\gamma)$  cross sections for  $^{208}\text{Pb}$  from threshold up to 20 MeV", *Nucl. Phys.* **A811**, 1 (2008).
- [286] V.A. Zheltonozhsky, V.M. Mazur, Z.M. Bigan, D.M. Symochko, "Investigation of isomeric ratios in  $(g, n)$  reactions of rubidium isotopes in giant dipole resonance energy region", *Nuclear Physics and Atomic Energy*, **9**(2), 13-17 (2008).
- [287] L.C. Mihailescu, C. Borcea, A.J. Koning, A. Pavlik, A.J.M. Plompen, "High resolution measurement of neutron inelastic scattering and  $(n, 2n)$  cross sections for  $^{209}\text{Bi}$ ", *Nucl. Phys.* **A799**, no. 1, p. 1-29 (2008).

- [288] V. Semkova, A. Moens, A. Plompen, R.J. Tornin, "Measurement of neutron-induced reaction cross sections on Ni, Zr, Ta and W isotopes with activation technique", 1st Workshop on Accelerator Radiation induced activation", Oct. 13 2008, PSI Switzerland, [aria.web.psi.ch](http://aria.web.psi.ch) (2008).
- [289] N.-C. Shu, T.-J. Liu, H.-W. Yu and Y.-J. Chen, "Systematics study of the Zp model for the U235 + n fission" Proceedings of the International Conference on Nuclear Data for Science and Technology, April 22-27, 2007, Nice, France, editors O.Bersillon, F.Gunsing, E.Bauge, R.Jacqmin, and S.Leray, EDP Sciences, 2008, p. 347 (2008).
- [290] V. Semkova, R.J. Tornin, A.J. Koning, A. Moens, A. Plompen, "New cross section measurements for neutron-induced reactions on Cr, Ni, Cu, Ta and W isotopes obtained with the activation technique", Proceedings of the International Conference on Nuclear Data for Science and Technology, April 22-27, 2007, Nice, France, editors O.Bersillon, F.Gunsing, E.Bauge, R.Jacqmin, and S.Leray, EDP Sciences, p. 559-562 (2008).
- [291] L.C. Mihailescu, P. Baumann, C. Borcea, P. Dessagne, E. Jericha, M. Kerveno, S. Lukic, A.J. Koning, A. Pavlik, A.J.M. Plompen, G. Rudolf, "High resolution neutron (n,xn) cross section measurements for 206,207,208Pb and 209Bi from threshold up to 20 MeV", Proceedings of the International Conference on Nuclear Data for Science and Technology, April 22-27, 2007, Nice, France, editors O.Bersillon, F.Gunsing, E.Bauge, R.Jacqmin, and S.Leray, EDP Sciences, p. 567-570 (2008).
- [292] V. Semkova and A.J. Plompen, "Neutron-induced dosimetry reaction cross-section measurements from the threshold up to 20 MeV", Rad. prot. Dos. 126, 126 (2007).
- [293] L.C. Mihailescu, C. Borcea, A.J.M. Plompen, and A.J. Koning, "High resolution measurement of neutron inelastic scattering and (n,2n) cross-sections for 52Cr" Nucl. Phys A786, p. 1-23 (2007).
- [294] R. Schwengner, G. Rusev, N. Benouaret, R. Beyer, M. Erhard, E. Grosse, A. R. Junghans, J. Klug, K. Kosev, L. Kostov, C. Nair, N. Nankov, K. D. Schilling, and A. Wagner, "Dipole response of 88Sr up to the neutron-separation energy", Phys. Rev. C 76, 034321 (2007).
- [295] O.A. Bezshyyko, L.O. Golinka-Bezshyyko, I.M. Kadenko, A.O. Lymanets, "Analysis of characteristics of the photonuclear reactions with charged particles in output channel using EMPIRE II and TALYS", Problems of At. Science and techn. Nuclear physics investigations 48, p. 18 (2007).
- [296] V. Avrigeanu, S.V. Chuvaev, R. Eichin, A.A. Filatenkov, R.A. Forrest, H. Freiesleben, M. Herman, A.J. Koning and K. Seidel, "Pre-equilibrium reactions on the stable tungsten isotopes at low energy", Nucl. Phys. A765, p. 1 (2006).
- [297] M. Erhard, C. Nair, R. Beyer, E. Grosse, A.R. Junghans, J. Klug, K. Kosev, N. Nankov, G. Rusev, K.D. Schilling, R. Schwengner, and A. Wagner, "Electromagnetic, excitations in nuclei: from photon scattering to photodisintegration", Internation symposium on Nuclear Astrophysics - Nuclei in the Cosmos IX, Cern (2006).
- [298] X. Ledoux, I. Lantuejoul, N. Arnal, J.M. Laborie, J.P. Lochard, P. Pras, C. Varignon, "An improved experimental set-up for (n,xn) reaction studies", Proceedings of the International Workshop on Fast neutron detectors, Univ. Cape Town, South-Africa, April 3-6, 2006, Proceedings of Science (2006).

- [299] M. Erhard, A.R. Junghans, R. Beyer, E. Grosse, J. Klug, K. Kosev, C. Nair, N. Nankov, G. Ru-sev, K.D. Schilling, R. Schwengner, A. Wagner, “Photodissociation of p-process nuclei studied by Bremsstrahlung induced activation”, *Eur. Phys. J. A* 27 135-140 (2006).
- [300] P. Baumann, C. Borcea, E. Jericha, S. Jokic, M. Kerveno, S. Lukic, L. C. Mihailescu, A. Pavlik, A.J.M. Plompen, and G. Rudolf “ $^{207}\text{Pb}(n,2\gamma)^{206}\text{Pb}$  Cross-Section Measurements by In-Beam Gamma-Ray Spectroscopy”, *Proceedings of Capture gamma-ray spectroscopy and related topics: 12th International Symposium*, AIP Conf. Proc. 819, p. 561 (2006).
- [301] V. Avrigeanu, R. Eichin, R.A. Forrest, H. Freiesleben, M. Herman, A.J. Koning, and K. Seidel, “Sensitivity Of Activation Cross Sections Of Tungsten To Nuclear Reaction Mechanisms”, *Proceedings of the International Conference on Nuclear Data for Science and Technology - ND2004*, AIP vol. 769, eds. R.C. Haight, M.B. Chadwick, T. Kawano, and P. Talou, Sep. 26 - Oct. 1, 2004, Santa Fe, USA, p. 1501 (2005).
- [302] V. Semkova, A.J.M. Plompen, D.L. Smith, “Measurement of  $^{58}\text{Ni}(n,t)^{59}\text{Fe}$  and  $^{63}\text{Cu}(n,\alpha)^{60}\text{Co}$  reaction cross sections from 14 to 20 MeV”, *Proceedings of the International Conference on Nuclear Data for Science and Technology - ND2004*, AIP vol. 769, eds. R.C. Haight, M.B. Chadwick, T. Kawano, and P. Talou, Sep. 26 - Oct. 1, 2004, Santa Fe, USA, p. 1501 (2005).
- [303] V. Semkova, A.J.M. Plompen, D.L. Smith, “Light charged-particle production activation cross sections of Zr isotopes from 14 to 20 MeV”, *Proceedings of the International Conference on Nuclear Data for Science and Technology - ND2004*, AIP vol. 769, eds. R.C. Haight, M.B. Chadwick, T. Kawano, and P. Talou, Sep. 26 - Oct. 1, 2004, Santa Fe, USA, p. 1501 (2005).
- [304] A. Plompen, “Cross section measurements in the fast neutron energy range”, *Proceedings of the International Workshop on “Nuclear data Needs for Generation IV Nuclear energy systems*, Antwerpen, April 5-7, 2005, ed. P. Rullhusen, World Scientific p. 208 (2006).
- [305] A. Plompen, “Gamma production cross sections for inelastic scattering and (n,2n) reactions”, in *Perspectives on Nuclear Data for the Next Decade*, CEA-DIF Bruyères-le-Châtel, France, September 26-28 2005 (2006).
- [306] K.Y. Hara, H. Harada, F. Kitatani, S. Goko, S. Hohara, T. Kaihori, A. Makinaga, H. Utsunomiya, H. Toyokawa, K. Yamada and Y. Watanabe, “Photonuclear reaction cross section of  $^{152}\text{Sm}$ ”, *Proceedings of NEMEA-3 Workshop on Neutron Measurements, Evaluations and Applications*, 25-28 October 2006. Borovets, Bulgaria, EUR 22794 EN (2006).
- [307] S. Goko, H. Utsunomiya, A. Makinaga, T. Kaihori, S. Hohara, H. Akimune, T. Yamagata, S. Goriely, A.J. Koning, S. Hilaire, H. Toyokawa, Y.-W. Lui, “Photodisintegration of  $^{181}\text{Ta}$  leading to the isomeric state  $^{180\text{m}}\text{Ta}$ ”, *Proceedings of the International Symposium on Nuclear Astrophysics - Nuclei in the Cosmos - IX*. 25-30 June 2006, CERN., p.253.1 (2006).
- [308] V. Semkova, V. Avrigeanu, A.J. Koning, A.J.M. Plompen, D.L. Smith, and S. Sudar, “A systematic investigation of reaction cross sections and isomer ratios up to 20 MeV on Ni-isotopes and  $^{59}\text{Co}$ ”

by measurements with the activation technique and new model studies of the underlying reaction mechanisms”, Nucl. Phys. **A730**, 255 (2004).

- [309] P. Reimer, V. Avrigeanu, S.V. Chuvaev, A.A. Filatenkov, T. Glodariu, A.J. Koning, A.J.M. Plompen, S.M. Qaim, D.L. Smith, and H. Weigmann, “Reaction mechanisms of fast neutrons on stable Mo isotopes below 21 MeV”, Phys. Rev. C71, 044617 (2003).
- [310] V. Semkova, V. Avrigeanu, A.J.M. Plompen, P. Reimer, D.L. Smith, S. Sudar, A. Koning, R. Forrest, “Neutron activation cross sections for safety of nuclear reactors”, European Commission JRC report, EUR Report 20820 EN, ISBN 92-894-6095-4 (2003).

#### **Analysis of measurements above 20 MeV**

- [311] F. Ditroi, F. Tarkanyi, S. Takacs, A. Hermanne, H. Yamazaki, A. Mohammadi and A.V. Ignatyuk, “Investigation of activation cross-section data of proton induced reactions on natural rhenium”, to be published (2013).
- [312] F. Ditroi, F. Tarkanyi, S. Takacs, A. Hermanne, H. Yamazaki, A. Mohammadi, “Activation cross-sections of longer lived products of proton induced nuclear reactions on manganese up to 70 MeV”, to be published (2013).
- [313] F. Ditroi, F. Tarkanyi, S. Takacs, A. Hermanne, H. Yamazaki, A. Mohammadi, “Activation cross-sections of longer lived products of proton induced nuclear reactions on cobalt up to 70 MeV”, to be published (2013).
- [314] F. Tarkanyi, F. Ditroi, S. Takacs, A. Hermanne, H. Yamazaki, M. Baba, A. Mohammadi, A.V. Ignatyuk, “Activation cross-sections of longer lived products of deuteron induced nuclear reactions on ytterbium up to 40 MeV”, to be published (2013).
- [315] F. Tarkanyi, A. Hermanne, S. Takacs, A.V. Ignatyuk, “Investigation of production routes for  $^{161}\text{Ho}$  Auger-electron emitting radiolanthanide, a candidate for therapy”, to be published (2013).
- [316] F. Tarkanyi, F. Ditroi, A. Hermanne, S. Takacs, R. Adam-Rebeles, N. Walravens, O. Cichelli and A.V. Ignatyuk, “Investigation of activation cross-sections of proton induced nuclear reactions on nat-Tl up to 42 MeV: Review, new data and evaluation”, Appl. Rad. Isot. 74, 109 (2013).
- [317] S.A. Kandil and M. Al-Abyad, “Cross section measurements and theoretical calculations of proton induced nuclear reactions on natural tellurium”, Radiochimica Acta 101, 67 (2013).
- [318] A. Kulko, N. K. Skobelev, V. Kroha, Yu. E. Penionzhkevich, J. Mrazek, V. Burjan, Z. Hons, E. Simeckova, S. Piskor and A. Kugler, et al., “Excitation functions for deuterium-induced reactions on  $^{194}\text{Pt}$  near the coulomb barrier”, Physics of Particles and Nuclei Letters Volume 9, Numbers 6-7 (2012), 502-507 (2012).
- [319] I. Rovni, M. Szieberth, and S. Feher, “Secondary charged particle activation method for measuring the tritium production rate in the breeding blankets of a fusion reactor”, Nucl. Instr. Meth A690, 85 (2012).

- [320] A. Kaplan, "Investigation of Neutron-Production Cross Sections of the Structural Fusion Material  $^{181}\text{Ta}$  for  $(a, xn)$  Reactions up to 150 MeV Energy", *Journ. Fus. En.* (2012).
- [321] A. Aydin, I. H. Sarpun, A. Kaplan and E. Tel, "Calculations of Double Differential Deuteron Emission Cross Sections at 62 MeV Proton Induced Reactions", *Journ. Fus. En.* (2012).
- [322] R. Adam Rebeles, P. Van den Winkel, A. Hermanne, F. Tarkanyi, S. Takacs, "Experimental excitation functions of deuteron induced reactions of natural thallium up to 50 MeV", *Nucl. Instr. Meth. B288*, 94 (2012).
- [323] A.A. Cowley, "Pre-equilibrium emission of alpha-particles with energies down to the region of those from compound nucleus decay", *Proceedings of CNR\*11 : Third International Workshop on Compound Nuclear Reactions and Related Topics, Prague, 2011, EPJ Web of Conferences 21, 9002* (2012).
- [324] S. Pomp et al., "A Medley with over ten years of (mostly) light-ion production measurements at the Svedberg Laboratory" *Proceedings of the EFNUDAT Workshop on Measurements and Models of Nuclear Reactions*, May 25-27, 2010, Paris, France, *Europ. Phys. Journ 8*, 07013 (2012).
- [325] Y.S. Perkasa, A. Waris, R. Kurniadi and Z. Su'ud, "Prediction of nat-Pb and  $^{209}\text{Bi}$  neutron induced fission cross section using TALYS for energy up to 200 MeV", 3rd international conference on advances in nuclear science and engineering 2011, Bali Indonesia (2011).
- [326] M.A. Norsworthy, "Active interrogation source based on deuteron reactions", *Nuclear Science Symposium and medical imaging conference*, 1362 (2011).
- [327] Megan E. Bennett, Dmitriy A. Mayorov, Kyle D. Chapkin, Marisa C. Alfonso, Tyler A. Werke, Charles M. Folden III, "Measurement of the natLu(p,x) $^{175}\text{Hf}$  excitation function", *Nucl. Instr. Meth. B276*, 62 (2012).
- [328] O. Svoboda, J. Vrzalova, A. Krasa, A. Kugler, M. Majerle, V. Wagner, "Three years of cross section measurements of  $(n, xn)$  threshold reactions at TSL Uppsala and NPI Rez", *Proceedings of the EFNUDAT Workshop on Measurements and Models of Nuclear Reactions*, May 25-27, 2010, Paris, France, *Europ. Phys. Journ 8*, 07003 (2012).
- [329] S. MacMullin, M. Boswell, M. Devlin, S. R. Elliott, N. Fotiades, V. E. Guiseppe, R. Henning, T. Kawano, B. H. LaRoque, R. O. Nelson, J. M. O'Donnell, "Neutron-induced gamma-ray production cross sections for the first excited-state transitions in Ne-20 and Ne-22", to be published (2012).
- [330] S. MacMullin, M. Boswell, M. Devlin, S. R. Elliott, N. Fotiades, V. E. Guiseppe, R. Henning, B. LaRoque, R. O. Nelson, J. M. O'Donnell, "Partial gamma-ray cross sections for  $(n, xn\gamma)$  reactions in natural argon from 1-30 MeV", *Phys. Rev. C85*, 064614 (2012).
- [331] J. Vrzalova, O. Svoboda, A. Kugler, M. Suchopar and V. Wagner, "Cross-section measurements of neutron threshold reactions in various materials", *Physics Procedia* 126 (2012).
- [332] J. Vrzalova, O. Svoboda, A. Kugler, M. Suchopar and V. Wagner, "Measurements of cross-sections of  $(n, xn)$  threshold reactions in various materials", *Proceedings of CNR\*11 : Third International*

- Workshop on Compound Nuclear Reactions and Related Topics, Prague, 2011, EPJ Web of Conferences 21, 10007 (2012).
- [333] M. Al-Abyad, F. Tarkanyi, F. Ditroi and S. Takacs, "Excitation function of  $^3\text{He}$  induced nuclear reactions on nat-Pt up to 26 MeV", *Appl. Rad. Isot.* 72, 73 (2013).
- [334] M. Al-Abyad, A.S. Abdel-Hamid, F. Tarkanyi, F. Ditroi, S. Takacs, U. Seddik and I.I. Bashter", "Cross-section measurements and nuclear model calculation for proton induced nuclear reaction on zirconium", *Appl. Rad. Isot.* 7, 257 (2012).
- [335] F. Ditroi, F. Tarkanyi, S. Takacs, A. Hermanne, A.V. Ignatyuk, M. Baba "Activation cross sections of deuteron induced reactions on natural palladium", *Nucl. Instr. Meth.* B270, 61 (2012).
- [336] E. Simeckova et al., " $^{65}\text{Cu}(d,p)$  excitation function at deuteron energies up to 20 MeV", *Proceedings of the EFNUDAT Workshop on Measurements and Models of Nuclear Reactions*, May 25-27, 2010, Paris, France, *Europ. Phys. Journ* 8, 07002 (2012).
- [337] F. Ditroi, F. Trknyi, S. Takacs, R. Dczi, A. Hermanne, A.V. Ignatyuk, "Study of excitation function of deuteron induced reactions on natKr up to 20 MeV", *Appl. Rad. Iso.*, Vol. 70 (4), 574 (2012).
- [338] F. Ditroi, A. Hermanne, F. Tarkanyi, S. Takacs, A.V. Ignatyuk, "Investigation of the  $\alpha$ -particle induced nuclear reactions on natural molybdenum", *Nucl. Instr. Meth.* B285, 125 (2012).
- [339] R. Bevilacqua, S. Pomp, et al, "Study of pre-equilibrium emission of light complex particles from Fe and Bi induced by intermediate energy neutrons", *Journ. Phys. Conf. Ser.* 312, 082013 (2011).
- [340] I.C. Sagrado Garcia et al, "Neutron production in neutron-induced reactions at 96 MeV on  $^{56}\text{Fe}$  and  $^{208}\text{Pb}$ ", *Phys. Rev.* C84, 044619 (2011).
- [341] M. Bielewicz, S. Kilim, E. Strugalska-Gola, M. Szuta and A. Wojciechowski, "Yttrium as a New Threshold Detector for Fast Neutron Energy Spectrum ( $\geq 10$  MeV) Measurement", *Proceedings of the International Conference on Nuclear Data for Science and Technology*, April 26-30, 2010, Jeju, Korea, *Journ. Kor. Phys. Soc.* 59, no. 23, 2014 (2011).
- [342] M.S. Uddin, S. Sudr and S.M. Qaim, "Formation of the isomeric pair  $^{194}\text{Ir}_{m,g}$  in interactions of alpha particles with  $^{192}\text{Os}$ ", *Phys. Rev.* C84, 024605 (2011).
- [343] I. Leya and R. Michel, "Cross sections for neutron-induced reactions up to 1.6 GeV for target elements relevant for cosmochemical, geochemical and technological applications", *Nucl. Instr. Meth.* B269, 2487 (2011).
- [344] M. Hayashi et al, "Measurement of light-ion production at the new Uppsala facility", *Proceedings of the International Conference on Nuclear Data for Science and Technology*, April 22-27, 2007, Nice, France, editors O.Bersillon, F.Gunsing, E.Bauge, R.Jacqmin, and S.Leray, EDP Sciences (2008).
- [345] I.C. Sagrado Garcia et al, " $(n,xn)$  measurements at 96 MeV", *Proceedings of the International Conference on Nuclear Data for Science and Technology*, April 22-27, 2007, Nice, France, editors O.Bersillon, F.Gunsing, E.Bauge, R.Jacqmin, and S.Leray, EDP Sciences (2008).

- [346] A.A. Alharbi, J. Alzahrani and A. Azzam, "Activation cross section measurements of some proton induced reactions on Ni, Co and Mo for proton activation analysis (PAA) purposes", *Radiochim Acta* 99 (12), 763 (2011).
- [347] M. Al-Abyad, I. Spahn, B. Scholten, S. Spellerberg, M.N. Comsan, S.M. Qaim and H.H. Coenen, "Cross Section Measurements of Proton Induced Reactions on  $^{55}\text{Mn}$  and Comparison of Experimental Results with Different Nuclear Model Calculations", *Proceedings of the International Conference on Nuclear Data for Science and Technology*, April 26-30, 2010, Jeju, Korea, *Journ. Kor. Phys. Soc.* 59, no. 23, 1888 (2011).
- [348] I.V. Ryzhov et al., "Measurement of Fragment Mass Yields in Neutron-induced Fission of  $^{232}\text{Th}$  and  $^{238}\text{U}$  at 33, 45 and 60 MeV", *Proceedings of the International Conference on Nuclear Data for Science and Technology*, April 26-30, 2010, Jeju, Korea, *Journ. Kor. Phys. Soc.* 59, no. 23, 1864 (2011).
- [349] M.U. Khandaker, K. Kim, M.W. Lee, K.S. Kim and G.N. Kim, "Excitation Functions for the  $^{27}\text{Al}(p,x)^{22,24}\text{Na}$  Nuclear Reactions up to 40 MeV", *Proceedings of the International Conference on Nuclear Data for Science and Technology*, April 26-30, 2010, Jeju, Korea, *Journ. Kor. Phys. Soc.* 59, no. 23, 1821 (2011).
- [350] S. Kunieda, S. Hirayama, T. Fukahori and Y. Watanabe, "Applicability of Pre-equilibrium Coalescence Model to Evaluation of Alpha-particle Production Cross Sections", *Proceedings of the International Conference on Nuclear Data for Science and Technology*, April 26-30, 2010, Jeju, Korea, *Journ. Kor. Phys. Soc.* 59, no. 23, 911 (2011).
- [351] M. Avrigeanu and V. Avrigeanu, "Analysis of Deuteron Breakup and Induced Activation on Medium Nuclei", *Proceedings of the International Conference on Nuclear Data for Science and Technology*, April 26-30, 2010, Jeju, Korea, *Journ. Kor. Phys. Soc.* 59, no. 23, 903 (2011).
- [352] U. Tippawan et al., "Light-ion Production in 175 MeV Neutron-induced Reactions on Oxygen", *Proceedings of the International Conference on Nuclear Data for Science and Technology*, April 26-30, 2010, Jeju, Korea, *Journ. Kor. Phys. Soc.* 59, no. 23, 1979 (2011).
- [353] Md. Shakilur Rahman, Manwoo Lee, Kyung-Sook Kim, Guinyun Kim, Eunae Kim, Moo-Hyun Cho, Valery Shvetshov, Pham Duc Khue, Nguyen Van Do, "Measurement of isomeric-yield ratios of  $^{109\text{m}}\text{gPd}$  and  $^{115\text{m}}\text{gCd}$  with 50-, 60-, and 70-MeV bremsstrahlung", *Nucl. Instr. Meth. B* 276, 44 (2012).
- [354] M.S. Rahman, K.S. Kim, M.W. Lee, G.N. Kim, V.D. Nguyen, P.D. Khue, M.H. Cho and W. Namkung, "Measurements of Isomeric Yield Ratios of  $^{44\text{m}}\text{gSc}$  and  $^{85\text{m}}\text{gY}$  with Intermediate Energy Bremsstrahlung", *Proceedings of the International Conference on Nuclear Data for Science and Technology*, April 26-30, 2010, Jeju, Korea, *Journ. Kor. Phys. Soc.* 59, no. 23, 1749 (2011).
- [355] R. Bevilacqua, "New neutron data measurements at 175 MeV for Accelerator Driven Systems", *Proceedings of International Congress on Advances in Nuclear Power Plants (ICAPP 2011)*, 2828 (2011).

- [356] R. Bevilacqua et al., "Light-Ion Production in the Interaction of 175 MeV Neutrons with Iron and Bismuth", Proceedings of the International Conference on Nuclear Data for Science and Technology, April 26-30, 2010, Jeju, Korea, Journ. Kor. Phys. Soc. 59, no. 23, 1701 (2011).
- [357] T. Kajimoto, N. Shigyo, K. Ishibashi, D. Moriguchi, Y. Nakamura, H. Arakawa, S. Kunieda, T. Watanabe and R.C. Haight, "Measurements of Neutron-induced Neutron-production Double-differential Cross Sections from 50 to 150 MeV", Proceedings of the International Conference on Nuclear Data for Science and Technology, April 26-30, 2010, Jeju, Korea, Journ. Kor. Phys. Soc. 59, no. 23, 1721 (2011).
- [358] V. Avrigeanu and M. Avrigeanu, "Key Issues for Consistent Description of Neutron-induced Reactions on Cr Isotopes", Proceedings of the International Conference on Nuclear Data for Science and Technology, April 26-30, 2010, Jeju, Korea, Journ. Kor. Phys. Soc. 59, no. 23, 891 (2011).
- [359] O. Svoboda, J. Vrzalov, A. Krsa, A. Kugler, M. Majerle and V. Wagner, "Cross-Section Measurements of (n,xn) Threshold Reactions in Au, Bi, I, In and Ta", Proceedings of the International Conference on Nuclear Data for Science and Technology, April 26-30, 2010, Jeju, Korea, Journ. Kor. Phys. Soc. 59, no. 23, 1709 (2011).
- [360] E. Simeckova, P. Bem, M. Honusek, M. Stefanik, U. Fischer, S.P. Simakov, R.A. Forrest, A.J. Koning, J.-C. Sublet, M. Avrigeanu, F.L. Roman, and V. Avrigeanu, "Low and medium energy deuteron-induced reactions on  $^{63,65}\text{Cu}$  nuclei", Phys. Rev. C84, 014605 (2011).
- [361] E. Simeckova, P. Bem, M. Honusek, L. Zavorka, U. Fischer, S.P. Simakov, R.A. Forrest, M. Avrigeanu, V. Avrigeanu and F.L. Roman, "On Low and Medium Energy Deuteron-induced Reactions on  $^{63,65}\text{Cu}$ ", Proceedings of the International Conference on Nuclear Data for Science and Technology, April 26-30, 2010, Jeju, Korea, Journ. Kor. Phys. Soc. 59, no. 23, 1928 (2011).
- [362] A.V. Voinov, S.M. Grimes, C.R. Brune, A. Burger, A. Gorgen, M. Guttormsen, A.C. Larsen, T.N. Massey, S. Siem, C. Kalbach, "Equilibrium and pre-equilibrium processes in the  $^{55}\text{Mn}(^6\text{Li},\text{xp})$  and  $^{57}\text{Fe}(^{\text{a}},\text{xp})$  reactions", Phys. Rev. C83, 054605 (2011).
- [363] A. Pichard, J. Mrazek, M. Assie, M. Hass, G. Lhersonneau, F. de Oliveira de Santos, M.-G. Saint-Laurent and E. Simeckova, "A new cross section measurement of reactions induced by  $^3\text{He}$ -particles on a carbon target", Europ. Phys. Journ. A - Hadrons and Nuclei 47(6), 72 (2011).
- [364] F. Tarkanyi, F. Ditroi, S. Takacs, A. Hermanne, M. Baba, A.V. Ignatyuk, "Investigation of activation cross sections of deuteron induced reactions on vanadium up to 40 MeV", Nucl. Instr. Meth. B269, 1792 (2011).
- [365] F. Tarkanyi, F. Ditroi, A. Hermanne, S. Takacs, B. Kiraly, M. Baba, A.V. Ignatyuk, "Experimental study of the excitation functions of deuteron induced reactions on natSn up to 40 MeV", Nucl. Instr. Meth. B269(4), 405 (2011).
- [366] F. Tarkanyi, F. Ditroi, A. Hermanne, S. Takacs, B. Kiraly, H. Yamazaki and A.V. Ignatyuk, "Activation cross sections of deuteron induced reactions on gold up to 40 MeV", Nucl. Instr. Meth. B269, 1389 (2011).

- [367] H. Naik, P. M. Prajapati, S. V. Suryanarayana, P. N. Pathak, D. R. Prabhu, V. Chavan, D. Raj, P. C. Kalsi, A. Goswami and S. Ganesan, et al, “ $^{233}\text{Pa}(2\text{nth},\text{f})$  cross-section determination using a fission track technique” *Europ. Phys. Journ. A* 47, (8), 100 (2011).
- [368] H. Naik, S. Singh, A. Goswami, V. K. Manchanda, G. Kim, K.S. Kim, M.W. Lee, M.S. Rahman, D. Raj, S. Ganesan, S. Suryanarayana, M.H. Cho and W. Namkung, “Measurement of photo-neutron cross-sections in  $^{208}\text{Pb}$  and  $^{209}\text{Bi}$  with 50-70 MeV Bremsstrahlung”, *Nucl. Instr. Meth. B* 269, 1417 (2011).
- [369] K.S. Kim et al, “Measurement of isomeric yield ratios for  $^{93}\text{Nb}(\text{g},4\text{n})^{89\text{m,g}}\text{Nb}$  and  $\text{nat-Mo}(\text{g},\text{xn}1\text{p})^{95\text{m,g}}\text{Nb}$  reactions with 50, 60 and 70 MeV Bremsstrahlung, *Journ. Radioanal. and Nucl. Chem.* 287, vol 3, 869 (2011).
- [370] A.A. Kulko et al, “Excitation functions for  $^{44}\text{Sc}$ ,  $^{46}\text{Sc}$  and  $^{47}\text{Sc}$  radionuclides produced in the interaction of  $^{45}\text{Sc}$  with deuterons and  $^6\text{He}$ ”, *Bull. Russ. Ac. Sci.* 75, 4, 538 (2011).
- [371] M.U. Khandaker, K. Kim, M. Lee, K.S. Kim, G. Kim, N. Otuka, “Investigations of  $^{89}\text{Y}(\text{p},\text{x})^{86,88,89}\text{gZr}$ ,  $^{86\text{m}+\text{g},87\text{g},87\text{m},88\text{g}}\text{Y}$ ,  $^{85}\text{gSr}$ , and  $^{84}\text{gRb}$  nuclear processes up to 42 MeV”, *Nucl. Instr. Meth. B* 271, 72 (2011).
- [372] M.U. Khandaker, K. Kim, M. Lee, K.S. Kim, G. Kim, “Excitation functions of (p,x) reactions on natural nickel up to 40MeV”, *Nucl. Inst. Methods B* 269, 1140 (2011).
- [373] A. Oehrns, C. Gustavsson, M. Blann, V. Blideanu, J. Blomgren, S. Chiba, H. Duarte, F. Haddad, C. Kalbach, J. Klug, A. Koning, C. Le Brun, C. Lebrun, F.R. Lecolley, X. Ledoux, N. Marie-Noury, P. Mermoud, L. Nilsson, M. Osterlund, S. Pomp, A. Prokofiev, U. Tippawan, and Y. Watanabe, “Measurements of inelastic neutron scattering at 96 MeV from carbon, iron, yttrium and lead”, *Proceedings of the International Conference on Nuclear Data for Science and Technology*, April 26-30, 2010, Jeju, Korea, *Journ. Kor. Phys. Soc.* 59, no. 23, 1817 (2011).
- [374] O. Svoboda, J. Vrzalova, A. Krasa, A. Kugler, M. Majerle, V. Wagner, “Cross-section measurements of (n,xn) threshold reactions in Au, Bi, I, In and Ta”, *Proceedings of the International Conference on Nuclear Data for Science and Technology*, April 26-30, 2010, Jeju, Korea, to be published (2011)
- [375] U. Tippawan, S. Pomp, J. Blomgren, S. Dangtip, C. Gustavsson, J. Klug, P. Nadel-Turonski, M. Osterlund, L. Nilsson, N. Olsson, O. Jonsson, A.V. Prokofiev, V. Corcalciuc, A.J. Koning, and Y. Watanabe, “Double-Differential Cross Sections and Kerma Coefficients for Light-Charged Particles Produced by 96 MeV Neutrons on Carbon”, *Radiation Measurements* 45, 1134-1138 (2010).
- [376] F. Ditroi, F. Tarkanyi, S. Takacs, A. Hermanne, M. Baba, and A.V. Ignatyuk, “Investigation deuteron-induced reactions on cobalt”, *Nucl. Instr. Meth. B* 268, 2571 (2010).
- [377] P. Demetriou, Th. Keutgen, R. Prieels, and Y. El Masri, “Fission properties of actinide nuclei from proton-induced fission at 26.5 and 62.9 MeV incident proton energies”, *Phys. Rev. C* 82, 054606 (2010).

- [378] R. Bevilacqua, S. Pomp, V.D. Simutkin, U. Tippawan, P. Andersson, J. Blomgren et al, "Neutron induced light-ion production from iron and bismuth at 175 MeV", *Rad. Meas.*, 45, 1145 (2010).
- [379] F. Simonelli, K. Abbas, P. Chau Huu-Tai, U. Holzwarth, I. Cydzik, "Measurement of excitation functions for production of cerium radioisotopes by deuteron induced reactions on natural cerium for nanobioscience applications", *Rad. chim. Acta*, 98(4), 187 (2010).
- [380] M. Al-Abyad, I. Spahn, S.M. Qaim, "Experimental studies and nuclear model calculations on proton induced reactions on manganese up to 45MeV with reference to production of  $^{55}\text{Fe}$ ,  $^{54}\text{Mn}$  and  $^{51}\text{Cr}$ ", *Appl. Rad. Isot.* 68(12), 2393 (2010).
- [381] M. Avrigeanu and V. Avrigeanu, "Deuteron breakup effects on activation cross sections at low and medium energies", *Journ. Phys. Conference series* 205 012014 (2010).
- [382] M.U. Khandaker, K. Kim, G. Kim, N. Otuka, "Cyclotron Production of the  $^{105}\text{Ag}$ ,  $^{106m}\text{Ag}$ ,  $^{100}\text{Pd}$ ,  $^{100m}\text{Pd}$ ,  $^{101m}\text{Pd}$ ,  $^{105}\text{Rh}$  Radionuclides by natPd (p, x) Nuclear Processes, *Nucl. Instr. Meth. B*268 (14) 2303 (2010).
- [383] U. Tippawan, S. Pomp, J. Blomgren, S. Dangtip, C. Gustavsson, J. Klug, L. Nilsson, M. Osterlund, N. Olsson, A.V. Prokofiev, P.-U. Renberg, P. Nadel-Turonski, V. Corcalciuc, Y. Watanabe and A.J. Koning, "Light-ion production in the interaction of 96 MeV neutrons with carbon", *Phys. Rev. C*79, 064611 (2009).
- [384] H. Naik, S. Singh, A. V. R. Reddy, V. K. Manchanda, S. Ganesan, D. Raj, Md. Shakilur Rahman, K. S. Kim, M. W. Lee and G. Kim, et al, "Measurement of photo-fission yields and photo-neutron cross-sections in  $^{209}\text{Bi}$  with 50 and 65 MeV Bremsstrahlung", *Eur. Phys. J. A*41, 323 (2009).
- [385] F. Ditroi, A. Hermanne, E. Corniani, S. Takacs, F. Tarkanyi, J. Csikai, Yu. N. Shubin, "Investigation of proton induced reactions on niobium at low and medium energies", *Nucl. Instr. Meth. B*267, 3364 (2009).
- [386] A. Hermanne, L. Daraban, F. Tarkanyi, S. Takacs, F. Ditroi, A. Ignatyuk, R. Adam Rebeles, M. Baba, "Excitation functions for some W, Ta and Hf radionuclides obtained by deuteron irradiation of  $^{181}\text{Ta}$  up to 40 MeV", *Nucl. Instr. Meth. B*267, 3293 (2009).
- [387] M.U. Khandaker, K. Kim, M.W. Lee, K.S. Kim, G.N. Kim and, "Investigations of the nat-Ti (p,x)  $^{43}\text{Ti}$ ,  $^{44m}\text{Ti}$ ,  $^{44g}\text{Ti}$ ,  $^{46}\text{Ti}$ ,  $^{47}\text{Ti}$ ,  $^{48}\text{Sc}$ ,  $^{48}\text{V}$  nuclear processes up to 40MeV", *Appl. Rad. Isot.* 67, 1348 (2009).
- [388] M.U. Khandaker, K. Kim, M.W. Lee, K.S. Kim, G.N. Kim and, "Experimental determination of proton-induced cross-sections on natural zirconium", *Appl. Rad. Isot.* 67, 1341 (2009).
- [389] M.U. Khandaker, K. Kim, K.S. Kim, M. Lee, Y.S. Lee, G. Kim, and, "Excitation functions of the proton-induced nuclear reactions on nat-Sn up to 40MeV", *Nucl. Instr. Methods B*267, 23 (2009).
- [390] M.S. Rahman, K.-S. Kim, M. Lee, G.N. Kim, Y. Oh, H.-S. Lee, M.-H. Cho, I.S. Ko, W. Namkung, N. van Do, P.D. Khue, K.T. Thanh and T.-I. Ro, "Measurement of isomeric yield ratios for  $^{90}\text{Zr}(g,n)^{89m,g}\text{Zr}$ , natZr(g,xn1p) $^{86m,g}\text{Y}$ , and  $^{89}\text{Y}(g,xn)^{87m,g,86m,g}\text{Y}$  reactions with 50-, 60-, and 70-MeV Bremsstrahlung", *Nucl. Instr. Meth. B*267(21-22), 3511 (2009).

- [391] I. Leya, J.C. David, S. Leray, R. Wieler and R. Michel, "Production of noble gas isotopes by proton-induced reactions on bismuth", Nucl. Instr. Meth. B266, 1030 (2008).
- [392] M.U. Khandaker, K. Kim, M.W. Lee, K.S. Kim, G.N. Kim and, "Production cross-sections for the residual radionuclides from the nat-Cd (p, x) nuclear processes", Nucl. Inst. Meth. B266, 4877 (2008).
- [393] M.U. Khandaker, K. Kim, K.S. Kim, M. Lee, G. Kim, Y.S. Cho and, "Production cross-sections of residual radionuclides from proton-induced reactions on nat-Ag up to 40 MeV", Nucl. Inst. Meth. B266, 5101 (2008).
- [394] M.U. Khandaker, M.S. Uddin, K. Kim, M.W. Lee, K.S. Kim, Y.S. Lee, G.N. Kim, Y.S. Cho, Y.O. Lee, "Excitation functions of proton induced nuclear reactions on natW up to 40 MeV", Nucl. Instr. Meth. B266, 1021 (2008).
- [395] G. Kim, M.U. Khandaker, K. Kim, M. Lee, K.S. Kim, Y.S. Lee, S. Uddin, "Measurement of excitation functions for proton induced nuclear reactions on natW", Nuclear Science Symposium 2008, Honolulu (2008).
- [396] K. Ammon, I. Leya, B. Lavielle, E. Gilabert, J.-C. David, U. Herpers, R. Michel, "Cross sections for the production of helium, neon and argon isotopes by proton-induced reactions on iron and nickel", Nucl. Instr. Meth. B266, 2 (2008).
- [397] S. Isaev, R. Prieels, Th. Keutgen, J. van Mol, P. Demetriou, "Proton-induced fission on actinide nuclei at energies 27 and 63 MeV", Nucl. Phys. A809, 1 (2008).
- [398] S. Pomp, V. Blideanu, J. Blomgren, P. Eudes and A. Guertin, "Neutron-induced light-ion production from Fe, Pb and U at 96 MeV", Rad. Prot. Dosim. 126, 123 (2007).
- [399] M. Avrigeanu, S.V. Chuvaev, A.A. Filatenkov, R.A. Forrest, M. Herman, A.J. Koning, A.J.M. Plompen, F.L. Roman, V. Avrigeanu, "Fast neutron induced preequilibrium reactions on 55Mn and 63,65Cu at energies up to 40 MeV", Nucl. Phys. A806, p. 15-39 (2008).
- [400] M.S. Uddin, M. Baba, M. Hagiwara, F. Tarkanyi, F. Ditroi, "Experimental determination of deuteron-induced activation cross sections of yttrium", Radioch. Acta. 95, no. 4, 187 (2007).
- [401] U. Tippawan, S. Pomp, J. Blomgren, S. Dangtip, C. Johansson, J. Klug, P. Mermod, L. Nilsson, A. Ohrn, M. Osterlund, N. Olsson, A.V. Prokofiev, P. Nadel-Turonski, V. Corcalciuc, A.J. Koning, and Y. Watanabe, "Light charged particle production in 96 MeV neutron-induced reactions on carbon and oxygen", Radiation Protection Dosimetry, vol 126 no. 1-4, p. 35-39, 2007; doi: 10.1093/rpd/ncm008, Proceedings of the Tenth Symposium on Neutron Dosimetry, Uppsala, June 12-16 2006. (2007).
- [402] M Avrigeanu and FL Roman, "On the need of microscopic models for evaluation of deuteron activation data", Proceedings of NEMEA-3 Workshop on Neutron Measurements, Evaluations and Applications, 25-28 October 2006. Borovets, Bulgaria, EUR 22794 EN (2006).

- [403] P. Mermod, J. Blomgren, C. Johansson, A. Ohrn, M. Osterlund, S. Pomp, B. Bergenwall, J. Klug, L. Nilsson, N. Olsson, U. Tippawan, P. Nadel-Turonski, O. Jonsson, A. Prokofiev, P.-U. Renberg, Y. Maeda, H. Sakai, A. Tamii, K. Amos, R. Crespo, and A. Moro, “95 MeV neutron scattering on hydrogen, deuterium, carbon, and oxygen”, *Phys. Rev. C* **74**, 054002 (2006).
- [404] U. Tippawan, S. Pomp, A. Atac, B. Bergenwall, J. Blomgren, S. Dangtip, A. Hildebrand, C. Johansson, J. Klug, P. Mermod, L. Nilsson, M. Osterlund, N. Olsson, A.V. Prokofiev, P. Nadel-Turonski, V. Corcalciuc, and A.J. Koning, “Light-ion production in the interaction of 96 MeV neutrons with oxygen”, *Phys. Rev. C* **73**, 034611 (2006).
- [405] Y. El Masri, Ch. Dufauquez, V. Roberfroid, J. Cabrera, Th. Keutgen, J. Van Mol, P. Demetriou, D. Bertrand and R. Charity, “Microscopic studies of light charged particle and neutron production in natSi using proton and alpha beams of energies between 20 and 65 MeV”, *Journ. Phys. Conf. series* **41**, 248 (2006).
- [406] Ch. Dufauquez, Y. El Masri, V. Roberfroid, J. Cabrera, Th. Keutgen, J. Van Mol, P. Demetriou, R. Charity, “Light charged particle and neutron production in proton- and particle-induced reactions on natSi at energies between 20 and 65 MeV”, *Nucl. Phys. A* **773**, 24 (2006).
- [407] M.S. Uddin, M. Baba, M. Hagiwara, F. Tarkanyi and F. Ditroi, “Experimental studies of the deuteron-induced activation cross-sections on nat-Ag”, *Appl. Rad. Isot.* **64**, no. 9, 1013 (2006).
- [408] P. Demetriou, Ch. Dufauquez, E. El Masri, and A.J. Koning, “Light charged-particle production from proton and alpha-induced reactions on <sup>nat</sup>Si at energies from 20 to 65 MeV: A theoretical analysis”, *Phys Rev C* **72**, 034607 (2005).
- [409] Udomrat Tippawan, Stephan Pomp, Ayse Atac, Bel Bergenwall, Jan Blomgren, Somsak Dangtip, Angelica Hildebrand, Cecilia Johansson, Joakim Klug, Philippe Mermod, Leif Nilsson, Michael Osterlund, Klas Elmgren, Nils Olsson, Olle Jonsson, Alexander Prokofiev, P.-U. Renberg, Pawel Nadel-Turonski, Valentin Corcalciuc, Yukinobu Watanabe, Arjan Koning, “Light-ion production in the interaction of 96 MeV neutrons with silicon” *Proceedings of the International Conference on Nuclear Data for Science and Technology - ND2004*, AIP vol. 769, eds. R.C. Haight, M.B. Chadwick, T. Kawano, and P. Talou, Sep. 26 - Oct. 1, 2004, Santa Fe, USA, p. 1592 (2005).
- [410] R. Michel, M. Gloris, J. Protoschill, M.A.M. Uosif, M. Weug, U. Herpers, J. Kuhnenn, P.-W. Kubik, D. Schumann, H.-A. Synal, R. Weinreich, I. Leya, J.C. David, S. Leray, M. Duijvestijn, A. Koning, A. Kelic, K.H. Schmidt, and J. Cugnon, “From The HINDAS Project: Excitation Functions For Residual Nuclide Production By Proton-Induced Reactions”, *Proceedings of the International Conference on Nuclear Data for Science and Technology - ND2004*, AIP vol. 769, eds. R.C. Haight, M.B. Chadwick, T. Kawano, and P. Talou, Sep. 26 - Oct. 1, 2004, Santa Fe, USA, p. 1551 (2005).
- [411] R. Michel, W. Glasser, U. Herpers, H. Schuhmacher, H.J. Brede, V. Dangendorf, R. Nolte, P. Malmberg, A.V. Prokofiev, A.N. Smirnov, I. Rishkov, D. Kollar, J.P. Meulders, M. Duijvestijn, and A. Koning, “Residual Nuclide Production From Iron, Lead, And Uranium By Neutron-Induced Reactions Up To 180 MeV”, *Proceedings of the International Conference on Nuclear Data for Science and Technology - ND2004*, AIP vol. 769, eds. R.C. Haight, M.B. Chadwick, T. Kawano, and P. Talou, Sep. 26 - Oct. 1, 2004, Santa Fe, USA, p. 861 (2005).

- [412] M.A.M. Uosif, R. Michel, U. Herpers, P.-W. Kubik, M. Duijvestijn, and A. Koning, "Residual Nuclide Production By Proton-Induced Reactions On Uranium For Energies Between 20 MeV And 70 MeV", *Proceedings of the International Conference on Nuclear Data for Science and Technology - ND2004*, AIP vol. 769, eds. R.C. Haight, M.B. Chadwick, T. Kawano, and P. Talou, Sep. 26 - Oct. 1, 2004, Santa Fe, USA, p. 1547 (2005).
- [413] Vilen P. Eismont, Nikolay P. Filatov, Andrey N. Smirnov, Gennady A. Tutin, Jan Blomgren, Henri Conde, Nils Olsson, Marieke C. Duijvestijn, and Arjan J. Koning, "On Nuclear Structure Effects in the Nucleon-Induced Fission Cross Sections of Nuclei Near 208Pb at Intermediate Energies", *Proceedings of the International Conference on Nuclear Data for Science and Technology - ND2004*, AIP vol. 769, eds. R.C. Haight, M.B. Chadwick, T. Kawano, and P. Talou, Sep. 26 - Oct. 1, 2004, Santa Fe, USA, p. 629 (2005).
- [414] Vilen P. Eismont, Nikolay P. Filatov, Sergey N. Kirillov, Andrey N. Smirnov, Jan Blomgren, Henri Conde, Nils Olsson, Marieke C. Duijvestijn, and Arjan J. Koning, "Angular Anisotropy of Intermediate Energy Nucleon-Induced Fission of Pb Isotopes and Bi", *Proceedings of the International Conference on Nuclear Data for Science and Technology - ND2004*, AIP vol. 769, eds. R.C. Haight, M.B. Chadwick, T. Kawano, and P. Talou, Sep. 26 - Oct. 1, 2004, Santa Fe, USA, p. 633 (2005).
- [415] Andrey N. Smirnov, Vilen P. Eismont, Nikolay P. Filatov, Sergey N. Kirillov, Jan Blomgren, Henri Conde, Nils Olsson, Marieke C. Duijvestijn, and Arjan J. Koning, "Correlation of Intermediate Energy Proton- and Neutron-Induced Fission Cross Section in the Lead-Bismuth Region", *Proceedings of the International Conference on Nuclear Data for Science and Technology - ND2004*, AIP vol. 769, eds. R.C. Haight, M.B. Chadwick, T. Kawano, and P. Talou, Sep. 26 - Oct. 1, 2004, Santa Fe, USA, p. 637 (2005).
- [416] Oleg I. Batenkov, Vilen P. Eismont, Mikhail I. Majorov, Andrey N. Smirnov, Kjell Aleklett, Walter Loveland, Jan Blomgren, Henri Conde, Marieke C. Duijvestijn, and Arjan J. Koning, "Comparison of Experimental and Calculated Mass Distributions of Fission Fragments in Proton-Induced Fission of  $^{232}\text{Th}$ ,  $^{235}\text{U}$ ,  $^{238}\text{U}$  and  $^{237}\text{Np}$  in the Intermediate Energy Region", *Proceedings of the International Conference on Nuclear Data for Science and Technology - ND2004*, AIP vol. 769, eds. R.C. Haight, M.B. Chadwick, T. Kawano, and P. Talou, Sep. 26 - Oct. 1, 2004, Santa Fe, USA, p. 625 (2005).
- [417] C. Dufauquez, Y. El Masri, V. Roberfroid, J. Cabrera, Th. Keutgen, J. van Mol, V. Demetriou, and A.J. Koning, "Light charged and neutral particles emission in proton and alpha induced reactions on  $^{nat}\text{Si}$  between 20 and 65 MeV", *Proceedings of the International Conference on Nuclear Data for Science and Technology - ND2004*, AIP vol. 769, eds. R.C. Haight, M.B. Chadwick, T. Kawano, and P. Talou, Sep. 26 - Oct. 1, 2004, Santa Fe, USA, p. 941 (2005).
- [418] U. Tippawan, S. Pomp, A. Atac, B. Bergenwall, J. Blomgren, S. Dangtip, A. Hildebrand, C. Johansson, J. Klug, P. Mermod, L. Nilsson, M. Osterlund, N. Olsson, K. Elmgren, O. Jonsson, A.V. Prokofiev, P.-U. Renberg, P. Nadel-Turonski, V. Corcalciuc, Y. Watanabe, and A.J. Koning, "Light-ion production in the interaction of 96 MeV neutrons with silicon", *Phys. Rev. C* **69**, 064609 (2004).

- [419] I. Slypen, N. Nica, A.J. Koning, E. Raeymackers, S. Benck, J.P. Meulders, and V. Corcalciuc, "Light charged particle emission induced by fast neutrons with energies between 25 and 65 MeV on Iron", *Journ. Phys.* **G30**, 45 (2004).
- [420] M. Kerveno, P. Baumann, A. Nachab, G. Rudolf, A. Pavlik, E. Jericha, S. Jokic, S. Lukic, L. Mihailescu, A. Plompen, R. Nolte, M. Reginatto, J.P. Meulders, J. Jeknic, S. Hilaire, A.J. Koning, and the n-TOF collaboration, "Measurements of (n,xn) cross sections for hybrid systems", Proceedings of the 8th Information Exchange Meeting on Actinide and Fission Product Partitioning and Transmutation, Las Vegas, USA Nov 9-11 2004 (2005).
- [421] A. Guertin, N. Marie, S. Auduc, V. Blideanu, Th. Delbar, P. Eudes, Y. Foucher, F. Haddad, T. Kirchner, Ch. Le Brun, C. Lebrun, F. R. Lecolley, J. F. Lecolley, X. Ledoux, F. Lefebvres, T. Lefort, M. Louvel, A. Ninane, Y. Patin, Ph. Pras, G. Riviere and C. Varignon, "Neutron and light-charged-particle productions in proton-induced reactions on 208Pb at 62.9 MeV", *Eur. Phys. J. A23*, 49-60 (2005).
- [422] E. Raeymackers, S. Benck, N. Nica, I. Slypen, J.P. Meulders, V. Corcalciuc and A.J. Koning, "Light charged particle emission in fast neutron (25-65 MeV) induced reactions on  $^{209}\text{Bi}$  nuclei", *Nucl. Phys.* **A726**, 175 (2003).
- [423] E. Raeymackers, S. Benck, I. Slypen, J.P. Meulders, N. Nica, V. Corcalciuc and A. Koning, "Light charged particle production in the interaction of fast neutrons (25-65 MeV) with Uranium nuclei", *Phys. Rev. C* **68**, 24604 (2003)
- [424] M. Pandurovic, S. Lukic, P. Baumann, S. Hilaire, J. Jeknic, E. Jericha, S. Jokic, M. Kerveno, C. Mihailescu, A. Pavlik, A. Plompen, and G. Rudolf, "Measurement of (n, xn'gamma) Reaction Cross-Sections on Natural Lead Using in-Beam Gamma-Ray Spectroscopy", *Nucl. Techn. Rad. Prot.* **18**, no. 1, 22 (2003).
- [425] A.J. Koning, "HINDAS: Experiments, models and data libraries below 200 MeV", Proceedings of the International Workshop on Nuclear Data for the Transmutation of Nuclear Waste, eds. A. Kelic and K.-H. Schmidt, GSI Darmstadt, Sep 1-5 2003. <http://www-wnt.gsi.de/tramu/> (2004).
- [426] R. Michel, W. Glasser, M. Gloris, S. Neumann, J. Protoschill, M.A.M. Uosif, M. Weug, U. Herpers, J. Kuhnenn, F. Sudbrock, P. Malmborg, P.-W. Kubik, J.C. David, S. Leray, M. Duijvestijn, A.J. Koning, A. Kelic, K.H. Schmidt, H. Schuhmacher, H.J. Brede, V. Dangendorf, R. Nolte, A.N. Smirnov, I. Rishkov, A.V. Prokofiev, D. Kollar, J.P. Meulders, "Production of residual nuclides by neutron- and proton-induced reactions", Proceedings of the International Workshop on Nuclear Data for the Transmutation of Nuclear Waste, eds. A. Kelic and K.-H. Schmidt, GSI Darmstadt, Sep 1-5 2003. <http://www-wnt.gsi.de/tramu/>, ISBN 3-00-012276-1s. (2004).
- [427] A.J. Koning, H. Beijers, J. Benlliure, O. Bersillon, J. Blomgren, J. Cugnon, M. Duijvestijn, P. Eudes, D. Filges, F. Haddad, S. Hilaire, C. Lebrun, F.-R. Lecolley, S. Leray, J.-P. Meulders, R. Michel, R. Neef, R. Nolte, N. Olsson, R. Ostendorf, E. Ramstroem, K.-H. Schmidt, H. Schuhmacher, I. Slypen, H.-A. Synal, R. Weinreich, "HINDAS: A European nuclear data program for

accelerator-driven systems”, Proceedings of the International Conference on Nuclear Data for Science and Technology, Oct. 7-12, 2001, Tsukuba, Ibaraki, Japan, ed. K. Shibata, Journ. Sci. Techn., Suppl. 2 p. 1161 (2002).

- [428] J.P. Meulders, E. Raeymackers, I. Slypen, S. Benck, N. Nica, V. Corcalciuc and A.J. Koning, “Neutron-induced Light-charged particle production ( $E_n=25-65$  MeV) on elements of ADS-interest, AccApp’03, Accelerator Applications in a Nuclear Renaissance, San Diego, USA, June 1-5 2003 (2003).
- [429] M. Kerveno, F. Haddad, Ph. Eudes, T. Kirchner, C. Lebrun, I. Slypen, J.P. Meulders, C. Le Brun, F.R. Lecolley, J.F. Lecolley, F. Lefèbvres, S. Hilaire and A.J. Koning, ”Hydrogen isotope double-differential production cross sections induced by 62.7 MeV neutrons on a lead target”, Phys. Rev. C **66**, 014601 (2002).

#### Evaluated nuclear data libraries

- [430] D. Rochman, A.J. Koning, J. Kopecky, J.-C. Sublet, P. Ribon and M. Moxon, “From average parameters to statistical resolved resonances”, Ann. Nuc. En. 51, 60 (2013).
- [431] A.J. Koning and D. Rochman, “Modern nuclear data evaluation with the TALYS code system”, Nucl. Data Sheets 113 (12), 2841 (2012).
- [432] J.-C. Sublet, J. Eastwood, G. Morgan, A. Koning and D. Rochman, “EASY-II(12): modern modelling of n, d, p, g, a activation and transmutation processes”, Proceedings of the 12th International Conference on Radiation Shielding, Sep 2-7 2012, Nara, Japan, Progress in Nuclear Science and Technology (2013).
- [433] D. Rochman and A.J. Koning, “TENDL-2011: TALYS-based Evaluated Nuclear Data Library”, PHYSOR2012 Advances in Reactor Physics, Knoxville Tennessee, USA, April 15-20 (2012).
- [434] D. Rochman and A.J. Koning, “Evaluating and adjusting  $^{239}\text{Pu}$ ,  $^{56}\text{Fe}$ ,  $^{28}\text{Si}$  and  $^{95}\text{Mo}$  nuclear data with a Monte Carlo technique”, PHYSOR2012 Advances in Reactor Physics, Knoxville Tennessee, USA, April 15-20 (2012).
- [435] D. Rochman and A.J. Koning, “Evaluation and adjustment of the neutron-induced reactions of  $^{63,65}\text{Cu}$ ”, Nucl. Sci. Eng. 170 (3), 265 (2012).
- [436] P.M. Prajapati, “Measurement of neutron-induced reaction cross sections in zirconium isotopes at thermal, 2.45 MeV and 9.85 MeV energies”, Nucl. Sci. Eng. 171 (1), 78 (2012).
- [437] Y. Tur et al, “Analysis of integral experiment on erbia-loaded thermal spectrum cores using Kyoto University Critical Assembly by MCNP code with various cross section libraries”, Journ. Sci. Techn. 49, 10, 1028 (2012).
- [438] M. Kostal et al., “The effect of biological shielding on fast neutron and photon transport in the VVER-1000 mock-up model placed in the LR-0 reactor”, Appl. Rad. Isot. 75, 37 (2013).

- [439] M. Kostal et al., "Neutron and photon transport in Fe with the employment of TENDL2009, CENDL3.1, JENDL4 and JENDL4 evolution from JENDL3.3 in case of Fe", *NUcl. Eng. Des.* 249, 275 (2012).
- [440] M.B. Chadwick, M. Herman, P. Oblo?insk, M.E. Dunn, Y. Danon, A.C. Kahler, D.L. Smith, B. Pritychenko, G. Arbanas, R. Arcilla, R. Brewer, D.A. Brown, R. Capote, A.D. Carlson, Y.S. Cho, H. Derrien, K. Guber, G.M. Hale, S. Hoblit, S. Holloway, et al., "ENDF/B-VII.1 Nuclear Data for Science and Technology: Cross Sections, Covariances, Fission Product Yields and Decay Data", *Nucl. Data Sheets* 112 (12), 2887 (2011).
- [441] L.W. Packer, J.-C. Sublet, J. Kopecky and R.A. Forrest, "Recent Progress in Neutron-, Proton- and Deuteron-induced Reaction Nuclear Data for EAF-2010 and the European Activation System", *Proceedings of the International Conference on Nuclear Data for Science and Technology*, April 26-30, 2010, Jeju, Korea, *Journ. Kor. Phys. Soc.* 59, no. 23, 1100 (2011).
- [442] G. Noguere, P. Archier, B. Habert, C.D. Jean, D. Bernard and J. Tommasi, "Fission Product Cross Section Evaluations using Integral Experiments", *Proceedings of the International Conference on Nuclear Data for Science and Technology*, April 26-30, 2010, Jeju, Korea, *Journ. Kor. Phys. Soc.* 59, no. 23, 1343 (2011).
- [443] U. Fischer, P. Batistoni, E. Dupont, R.A. Forrest, H. Henriksson, J. Izquierdo and J.-C. Sublet, "The European Effort on the Evaluation and Validation of Nuclear Data for Fusion Technology Applications", *Proceedings of the International Conference on Nuclear Data for Science and Technology*, April 26-30, 2010, Jeju, Korea, *Journ. Kor. Phys. Soc.* 59, no. 23, 1369 (2011).
- [444] P. Pereslavtsev, A. Konobeyev, L. Leal and U. Fischer, "Evaluation of 50Cr, 52Cr, 53Cr, 54Cr Neutron Cross Section Data for Energies up to 200 MeV", *Proceedings of the International Conference on Nuclear Data for Science and Technology*, April 26-30, 2010, Jeju, Korea, *Journ. Kor. Phys. Soc.* 59, no. 23, 931 (2011).
- [445] H.I. Kim, M. Mun, D.H. Kim and Y.-O. Lee, "Nuclear Data Evaluations for Silicon Isotopes Induced by Proton, Deuteron and Alpha", *Proceedings of the International Conference on Nuclear Data for Science and Technology*, April 26-30, 2010, Jeju, Korea, *Journ. Kor. Phys. Soc.* 59, no. 23, 1023 (2011).
- [446] D. Brown et al., "Overview of the 2009 Release of the Evaluated Nuclear Data Library (ENDL2009)", *Proceedings of the International Conference on Nuclear Data for Science and Technology*, April 26-30, 2010, Jeju, Korea, *Journ. Kor. Phys. Soc.* 59, no. 23, 1084 (2011).
- [447] D. Rochman and A.J. Koning, "How to randomly evaluate nuclear data: a new method applied to Pu-239", *Nucl. Sci. Eng.* 169(1), 68 (2011).
- [448] D. Rochman, A.J. Koning, D.F. da Cruz, P. Archier, J. Tommasi, "On the evaluation of 23Na neutron-induced reactions and validations", *Nucl. Instr. Meth.* A612, 374 (2010).
- [449] A.J. Koning and D. Rochman, "Modern nuclear data evaluation: Straight from nuclear physics to applications", *Proceedings of the International Conference on Nuclear Data for Science and Technology*, April 26-30, 2010, Jeju, Korea, *Journ. Kor. Phys. Soc.* 59, no. 23, 773 (2011).

- [450] D.A. Brown, B. Beck, M.-A. Descalle, R. Hoffman, E. Ormand, P. Navratil, N. Summers, I. Thompson, R. Vogt, W. Younes, R. Barnowski, "Overview of the release of the 2009 evaluated nuclear data library (ENDL2009)" LLNL report LLNL-PROC-430652 (2010).
- [451] Y-S. Cho, Y.-O. Lee, G. Kim, "A new approach for cross section evaluations in the high energy region", Nucl. Instr. Meth B267, 1882 (2009).
- [452] D. Brown, M.-A. Descalle, R. Hoffman, K. Kelley, P. Navratil, J. Pruet, N. Summers, I. Thompson, "Release of the 2008 evaluated nuclear data library (ENDL2008)" LLNL report UCRL-TR-413190 (2009).
- [453] H.I. Kim and Y.O. Lee, "Nuclear data evaluation for proton-induced reaction on Aluminum with TALYS", Journ. Korean Phys. Soc. 52(3), 837 (2008).
- [454] D. Rochman and A.J. Koning, "Pb and Bi neutron data libraries with full covariance evaluation and improved integral tests", Nucl. Instr. Meth. A589, p. 85-108 (2008).
- [455] E. Dupont, I. Raskinyte, A.J. Koning and D. Ridikas, "Photonuclear data evaluations of actinides up to 130 MeV", Proceedings of the International Conference on Nuclear Data for Science and Technology, April 22-27, 2007, Nice, France, editors O.Bersillon, F.Gunsing, E.Bauge, R.Jacqmin, and S.Leray, EDP Sciences, p. 685-688 (2008).
- [456] A.J. Koning and M.C. Duijvestijn, "New nuclear data evaluations for Ca and Sc isotopes" Journ. Nucl. Sci. Techn. 44, no.6, p. 823-837 (2007).
- [457] A.J. Koning, M.C. Duijvestijn, S.C. van der Marck, R. Klein Meulekamp, and A. Hogenbirk, "New nuclear data libraries for Pb and Bi and their impact on ADS design", Nucl. Sci. Eng. 156, p. 357-390 (2007).
- [458] D. Brown, N. Summers, I. Thompson, W. Younes, "Proposed  $^{237}\text{U}$  evaluation for the next ENDL release", LLNL report UCRL-TR-237309 (2007).
- [459] P. Romain, B. Morillon, and A.J. Koning, "Neutron actinides evaluations with the TALYS code", *Proceedings of the Workshop on Neutron Measurements, Evaluations and Applications - 2*, October 25-28, 2006 Borovets, Bulgaria 2006, EUR 22794 EN, p. 113-116 (2007).
- [460] M.C. Duijvestijn and A.J. Koning, "New intermediate-energy nuclear data libraries for Fe", Ann. Nuc. En. 33, 1196 (2006).
- [461] A.J. Koning and M.C. Duijvestijn, "New nuclear data evaluations for Ge isotopes" Nucl. Instr. Meth. B248, 197 (2006).
- [462] G. Noguere, O. Bouland, A. Courcelle, E. Dupont, O. Serot, J.C. Sublet, "Nuclear data evaluation for Generation-IV", Proceedings of the International Workshop on "Nuclear data Needs for Generation IV Nuclear energy systems, Antwerpen, April 5-7, 2005, ed. P. Rullhusen, World Scientific, p. 253 (2006).

- [463] A.J. Koning, M.C. Duijvestijn, S.C. van der Marck, R. Klein Meulekamp, and A. Hogenbirk, "New nuclear data evaluations for Ca, Sc, Fe, Ge, Pb, and Bi isotopes" *Proceedings of the International Conference on Nuclear Data for Science and Technology - ND2004*, AIP vol. 769, eds. R.C. Haight, M.B. Chadwick, T. Kawano, and P. Talou, Sep. 26 - Oct. 1, 2004, Santa Fe, USA, p. 422 (2005).
- [464] E. Dupont, E. Bauge, S. Hilaire, A. Koning, and J.-C. Sublet, "Neutron Data Evaluation and Validation of Rhodium-103", *Proceedings of the International Conference on Nuclear Data for Science and Technology - ND2004*, AIP vol. 769, eds. R.C. Haight, M.B. Chadwick, T. Kawano, and P. Talou, Sep. 26 - Oct. 1, 2004, Santa Fe, USA, p. 95 (2005).

### Uncertainties, covariances and Monte Carlo

- [465] H. Sjostrand, E. Alhassan, J. Duan, C. Gustavsson, S. Pomp, D. Rochman, A. Koning, M. Osterlund, "Total Monte Carlo evaluation of the European lead-cooled train reactor", proceedings of the Wonder workshop (2012).
- [466] D.F. da Cruz, D. Rochman, and A.J. Koning, "Uncertainty analysis on reactivity and discharged inventory due to U235,238, Pu239,240,241 and fission products nuclear data uncertainties - application to a pressurized water reactor fuel assembly", to be published (2012).
- [467] D.F. da Cruz, D. Rochman and A.J. Koning, "Uncertainty analysis on reactivity and discharged inventory for a pressurized water reactor fuel assembly due to 235,238U nuclear data uncertainties", Proceedings of ICAPP'12, Chicago USA, June 24-28, 2012.
- [468] D. Rochman, A.J. Koning and D. da Cruz, "Propagation of 235,236,238U and 239Pu nuclear data uncertainties for a typical PWR fuel element", to be published (2012).
- [469] P. Dossantos-Uzarralde, H.-P. Jacquet, G. Dejonghe, I. Kodeli, "Methodology investigations on uncertainties propagation in nuclear data evaluation", Nucl. Eng. Design 246, 49 (2011).
- [470] D. Neudecker, S. Gundacker, T. Srdinko, V. Wildpaner and H. Leeb, "Comparison of Covariance Matrices Obtained by Different Methods", Proceedings of the International Conference on Nuclear Data for Science and Technology, April 26-30, 2010, Jeju, Korea, Journ. Kor. Phys. Soc. 59, no. 23, 1272 (2011).
- [471] D. Neudecker, S. Gundacker, H. Leeb, T. Srdinko, and V. Wildpaner, "Prior of structural materials", Proceedings of 2nd workshop on neutron cross section covariances, Wien 2011, EPJ Web of Conferences 27, 00003 (2012).
- [472] V. Wildpaner, D. Neudecker, T. Srdinko, and H. Leeb, "Status of GENEUS", Proceedings of 2nd workshop on neutron cross section covariances, Wien 2011, EPJ Web of Conferences 27, 00003 (2012).
- [473] H. Leeb, S. Gundacker, D. Neudecker, T. Srdinko and V. Wildpaner, "The GENEUS Project - Development of an Evaluation Tool", Proceedings of the International Conference on Nuclear Data for Science and Technology, April 26-30, 2010, Jeju, Korea, Journ. Kor. Phys. Soc. 59, no. 23, 959 (2011).

- [474] H. Leeb, S. Gundacker, D. Neudecker, T. Srdinko and V. Wildpaner, "Bayesian Based Uncertainties of Neutron-induced Reaction Cross Sections of Mn-55", Proceedings of the International Conference on Nuclear Data for Science and Technology, April 26-30, 2010, Jeju, Korea, Journ. Kor. Phys. Soc. 59, no. 23, 1230 (2011).
- [475] A.Y. Konobeyev, U. Fischer and P.E. Pereslavytsev, "Computational Approach for Evaluation of Nuclear Data Including Covariance Information", Proceedings of the International Conference on Nuclear Data for Science and Technology, April 26-30, 2010, Jeju, Korea, Journ. Kor. Phys. Soc. 59, no. 23, 923 (2011).
- [476] E. Bauge and P. Dossantos-Uzarralde, "Evaluation of the Covariance Matrix of  $^{239}\text{Pu}$  Neutronic Cross Sections in the Continuum Using the Backward-forward Monte-Carlo Method", Proceedings of the International Conference on Nuclear Data for Science and Technology, April 26-30, 2010, Jeju, Korea, Journ. Kor. Phys. Soc. 59, no. 23, 1218 (2011).
- [477] T. Sugawara, M. Sarotto, A. Stankovskiy, G. Van den Eynde, "Nuclear data sensitivity/uncertainty analysis for XT-ADS", Ann. Nucl. En. 38(5) 1098 (2011).
- [478] D. Rochman, A.J. Koning, S.C. van der Marck, A. Hogenbirk and C.M. Sciolla, "Nuclear data uncertainty propagation: perturbation vs. Monte Carlo", Ann. Nuc. En. 38(5), 942 (2011).
- [479] D. Rochman, A.J. Koning, D.F. da Cruz, "Uncertainties for the Kalimer Sodium Fast Reactor: void coefficient, keff, Beff, burn-up and radiotoxicity", Jap. Journ. Sci. Techn. 48 (8) 1193 (2011).
- [480] D. Rochman, A.J. Koning, S.C. van der Marck, A. Hogenbirk, and D. van Veen, "Propagation of nuclear data uncertainty: Exact or with covariances", Proceedings of the EFNUDAT Workshop on Measurements and Models of Nuclear Reactions, May 25-27, 2010, Paris, France, Europ. Phys. Journ 8, 04003 (2010).
- [481] D. Rochman, A.J. Koning, S.C. van der Marck, A. Hogenbirk, and D. van Veen, "Nuclear data uncertainty propagation: Total Monte Carlo vs. covariances", Proceedings of the International Conference on Nuclear Data for Science and Technology, April 26-30, 2010, Jeju, Korea, Journ. Kor. Phys. Soc. 59, no. 23, 1236 (2011).
- [482] D. Rochman, A.J. Koning, D.F. da Cruz, "Nuclear data uncertainty propagation for a Sodium Fast Reactor", Proceedings of the International Conference on Nuclear Data for Science and Technology, April 26-30, 2010, Jeju, Korea, Journ. Kor. Phys. Soc. 59, no. 23, 1195 (2011).
- [483] G. Noguere, P. Blaise, O. Litaize, D. Bernard, J.-M. Ruggieri, "Group-average covariance matrices for the hafnium isotopes of interest for light water reactor applications", Ann. Nucl. En. 36, 1059 (2009).
- [484] D. Rochman, A.J. Koning and S.C. van der Marck, "Uncertainties for criticality-safety benchmarks and keff distributions", Ann. Nuc. En. 36, 810 (2009).
- [485] A.J. Koning and D. Rochman, "Towards sustainable nuclear energy: Putting nuclear physics to work", Ann. Nuc. En. 35, p. 2024-2030 (2008).

- [486] A.J. Koning, “New working methods for nuclear data evaluation: how to make a nuclear data library?”, Proceedings of the International Conference on Nuclear Data for Science and Technology, April 22-27, 2007, Nice, France, editors O.Bersillon, F.Gunsing, E.Bauge, R.Jacqmin, and S.Leray, EDP Sciences, p. 679-684 (2008).
- [487] E. Bauge, S. Hilaire and P. Dossantos-Uzarralde, “Evaluation of the covariance matrix of neutronic cross sections with the Backward-Forward Monte Carlo method”, Proceedings of the International Conference on Nuclear Data for Science and Technology, April 22-27, 2007, Nice, France, editors O.Bersillon, F.Gunsing, E.Bauge, R.Jacqmin, and S.Leray, EDP Sciences, (2008).
- [488] M. Salvatores et al, “Uncertainty and target accuracy assessment for innovative systems using recent covariance data evaluations”, WPEC Subgroup-26, NEA report, OECD ISBN 978-92-64-99053-1, www.nea.fr (2008).
- [489] H. Leeb, D. Neudecker, Th. Srdinko, “Consistent procedure for nuclear data evaluation based on modeling”, Nucl. Data Sheets 109, 2762 (2008).
- [490] M.B. Chadwick, T. Kawano, P. Talou, E. Bauge and S. Hilaire, “Yttrium ENDF/B-VII Data from Theory and LANSCE/GEANIE Measurements and Covariances Estimated using, Nucl. Data Sheets 108, 2742 (2007).
- [491] A.J. Koning, “Generating covariance data with nuclear models”, Proceedings of the International Workshop on “Nuclear data Needs for Generation IV Nuclear energy systems, Antwerpen, April 5-7, 2005, ed. P. Rullhusen, World Scientific, p. 153 (2006).

#### **Global testing and cross section tables**

- [492] E. Dupont, A.J. Koning and N. Otsuka, “Exploratory data analysis of the EXFOR database”, Proceedings of the International Conference on Nuclear Data for Science and Technology, April 26-30, 2010, Jeju, Korea, Journ. Kor. Phys. Soc. 59, no. 23, 1333 (2011).
- [493] A. Yu. Konobeyev, U. Fischer, A.J. Koning, H. Leeb, S. Leray and Y. Yariv, “What can we expect from the use of nuclear models implemented in MCNPX at projectile energies below 150 MeV? Detailed comparison with experimental data”, Proceedings of the International Conference on Nuclear Data for Science and Technology, April 26-30, 2010, Jeju, Korea, Journ. Kor. Phys. Soc. 59, no. 23, 927 (2011).
- [494] A. Yu. Konobeyev, U. Fischer, A.J. Koning, P.E. Pereslavitsev, and M. Blann, “Implementation of the geometry dependent hybrid model in TALYS”, Proceedings of the International Conference on Nuclear Data for Science and Technology, April 26-30, 2010, Jeju, Korea, Journ. Kor. Phys. Soc. 59, no. 23, 935 (2011).
- [495] Y.A. Korovin, A.A. Natalenko, A.Y. Stankovskiy, S.G. Mashnik, A.Y. Konobeyev, “High energy activation data library (HEAD-2009)”, Nucl. Instr. Meth. A624(1), 20 (2010).
- [496] A. Konobeyev, C.H.M. Broeders, U. Fischer, L. Mercatali, I. Schmuck and S.P. Simakov, “The proton activation data file PADF-2007”, Proceedings of the International Conference on Nuclear

- Data for Science and Technology, April 22-27, 2007, Nice, France, editors O.Bersillon, F.Gunsing, E.Bauge, R.Jacqmin, and S.Leray, EDP Sciences, p. 709 (2008).
- [497] L. Mercatali, A.Y. Konobeyev, and C.H.M. Broeders, "On the uncertainty in the nuclear model calculation of neutron and proton induced reaction cross sections", International Conference on Nuclear Data for Science and Technology, April 22-27, 2007, Nice, France, editors O.Bersillon, F.Gunsing, E.Bauge, R.Jacqmin, and S.Leray, EDP Sciences, (2008).
- [498] C.H.M. Broeders, U. Fischer, A.Y. Konobeyev, L. Mercatali, "Proton Activation Data File to Study Activation and Transmutation of Materials Irradiated with ", Journ. Nucl. Sc. Techn. 44, 933 (2007).
- [499] Yury A. Korovin, Alexander Yu. Konobeyev, Gennady B. Pilnov, Alexey Yu. Stankovskiy, "Neutron- and proton-induced evaluated transport library up to 150 MeV", Nucl. Instr. Meth. 562, 721 (2006).
- [500] C.H.M. Broeders, A.Yu. Konobeyev, L. Mercatali, "Investigation of nuclear model predictions for proton-induced reaction cross sections up to 150 MeV", Kerntechnik 72, no 5/6, 274 (2007).
- [501] C.H.M. Broeders, A.Yu. Konobeyev, L. Mercatali, "Global comparison of TALYS and ALICE code calculations and evaluated data from ENDF/B, JENDL, FENDL and JEFF files with measured neutron induced reaction cross-sections at energies above 0.1 MeV" Journ. Nucl. Radiochem. Sciences, 7(1), S.N1-N4 (2006).

### Fusion

- [502] W. Guanbo et al., "Thermal-to-fusion neutron convertor and Monte Carlo coupled simulation of deuteron/triton transport and secondary products generation", submitted to Nucl. Instr. Meth. B (2012).
- [503] T.S. Reshid, "Calculation of excitation function of some structural fusion material for (n,p) reactions up to 25 MeV", Journ. Fusion Energy 10.1007 (2012).
- [504] A. Kaplan, "Investigation of neutron-production cross sections of the structural fusion material  $^{181}\text{Ta}$  for (a,xn) reactions up to 150 MeV Energy" Journ. Fusion Energy (2012).
- [505] Daniel Lopez, Javier Sanz, Francisco Ogando, "Radioactive waste assessment for the IFMIF/EVEDA facility ", Fus. Eng. Design, to be published (2012).
- [506] B. Jansky, Z. Turzik, E. Novak, M. Svadlenkova, M. Barta, L.A. Trykov and A.I. Blokhin, "Neutron and Gamma Spectra Measurement and Calculations Using Different Data Libraries on Nickel Benchmark Assembly", Proceedings of the International Conference on Nuclear Data for Science and Technology, April 26-30, 2010, Jeju, Korea, Journ. Kor. Phys. Soc. 59, no. 23, 1154 (2011).
- [507] U. Fischer, A. Klix, J. Li, P. Pereslavstev, S.P. Simakov, R. Forrest, F. Wasastjerna, "State-of-the-art of Computational Tools and Data for IFMIF Neutronics and Activation Analyses", Journ. Nucl. Mat. 417, 1311 (2011).

- [508] V. Blideanu, M. Garca, P. Joyer, D. Lopez, A. Mayoral, F. Ogando, F. Ortiz, J. Sanz, P. Sauvan, "Deuteron Cross Section Evaluation for Safety and Radioprotection Calculations of Ifmif/Eveda Accelerator Prototype", *Journ. Nucl. Mat.* 417, 1271 (2011).
- [509] A. Mayoral, J. Sanz, P. Sauvan, D. Lopez, M. Garcia and F. Ogando, "Relevance of d-D interactions on neutron and tritium production in IFMIF-EVEDA accelerator prototype", *Journ. Nucl. Mat.* 417, 1288 (2011).
- [510] M. Hagiwara, T. Itoga, M. Baba, S. Uddin, M. Sugimoto, "Experimental Studies on Deuteron-induced Activation Reactions in IFMIF Accelerator Structural Elements", *Journ. Nucl. Mat.* 417, 1267 (2011).
- [511] D. Rochman, A.J. Koning and S.C. van der Marck, "Exact nuclear data uncertainty propagation for fusion design", *Fusion Engineering and Design* 85, 669-682 (2010).
- [512] D. Rochman, A.J. Koning, S.C. van der Marck, "Exact nuclear data uncertainty propagation for fusion design", *Proceedings of the International Conference on Nuclear Data for Science and Technology*, April 26-30, 2010, Jeju, Korea, *Journ. Kor. Phys. Soc.* 59, no. 23, 1386 (2011).
- [513] P. Sauvan, A. Mayoral, J. Sanz, A.J. Koning, F. Ogando, M. Garcia, D. Lopez, A. Ibarra, "Computational tools and nuclear data for radioprotection studies in low energy light ions accelerators", *Proceedings of the International Conference on Nuclear Data for Science and Technology*, April 26-30, 2010, Jeju, Korea, *Journ. Kor. Phys. Soc.* 59, no. 23, 1195 (2011).
- [514] P. Sauvan, J. Sanz, F. Ogando, "New capabilities for Monte Carlo simulation of deuteron transport and secondary products generation", *Nucl. Instr. Meth.* A614, 323 (2010).
- [515] P. Bem, E. Simeckova, M. Honusek, U. Fischer, S. P. Simakov, R. A. Forrest, M. Avrigeanu, A. C. Obreja, F. L. Roman, and V. Avrigeanu, "Low and medium energy deuteron-induced reactions on  $^{27}\text{Al}$ ", *Phys. Rev.* C79, 044610 (2009).
- [516] J.C. Sublet, R.A. Forrest, J. Kopecky, "The EAF-2007 neutron, deuteron, and proton activation libraries", *Nuclear Technology*, 168(2), 279-283 (2009).
- [517] J. Sanz, M. Garcia, F. Ogando, A. Mayoral, P. Sauvan, B. Branas, "First IFMIF/EVEDA radioprotection studies for the preliminary design of the accelerator beam dump", *Proceedings of the ANS topical meeting on the technology of fusion energy no. 18*, San Francisco, 28-09-2008, *Fus. Sci. Techn.* vol 56, 273 (2009).
- [518] R.A. Forrest, J. Kopecky and A.J. Koning, "Detailed analysis of (n,p) and (n,a) cross sections in the EAF-2007 and TALYS-generated libraries", *Fusion Engineering and Design* 83, p. 634-643 (2008).
- [519] K. Ochiai, M. Nakao, N. Kubota, S. Sato, M. Yamaguchi, N. Ishioka, T. Nishitani, and C. Konno, "Deuteron induced activation cross section measurement for IFMIF", *Proceedings of the International Conference on Nuclear Data for Science and Technology*, April 22-27, 2007, Nice, France, editors O.Bersillon, F.Gunsing, E.Bauge, R.Jacqmin, and S.Leray, *EDP Sciences* (2008).

- [520] R.A. Forrest, J. Kopecky and A.J. Koning, "Revisions and improvements of neutron capture cross sections for EAF-2009 and validation of TALYS calculations", UKAEA report UKAEA FUS 546 (2008).
- [521] R.A. Forrest and J. Kopecky, "EASY-2007: a new generation of activation modelling including neutron-, proton- and deuteron-induced reactions", Proceedings of the International Conference on Nuclear Data for Science and Technology, April 22-27, 2007, Nice, France, editors O.Bersillon, F.Gunsing, E.Bauge, R.Jacqmin, and S.Leray, EDP Sciences (2008).
- [522] R.A. Forrest and J. Kopecky, "Statistical analysis of cross sections - A new tool for data validation", *Fus. Eng. Des.* 82, 73 (2007).
- [523] R.A. Forrest, "Deuteron-induced activation data in EAF for IFMIF calculations", *Fus. Eng. Design* 82, 2478 (2007).
- [524] R.A. Forrest and M.J. Loughlin, "Neutron and deuteron activation calculations for IFMIF", *Journ. Nucl. Mat.* 367-370, 1568 (2007).
- [525] R.A. Forrest, J. Kopecky and J.-Ch. Sublet, "The European Activation File: EAF-2007 neutron-induced cross section library", EASY documentation series UKAEA report FUS 535 (2007).
- [526] R.A. Forrest, "The European Activation File: EAF-2007 deuteron- and proton-induced cross section libraries", EASY documentation series UKAEA report FUS 536 (2007).
- [527] T. Itoga, M. Hagiwara, T. Oishi, S. Kamada, M. Baba, "Measurement of 40 MeV Deuteron Induced Reaction on Fe and Ta for Neutron Emission Spectrum and Activation Cross Section", *JAEA Symposium on Nuclear Data*, 124 (2006).
- [528] R.A. Forrest, "Data requirements for neutron activation: Part 1: Cross sections" *Fus. Eng. Des.* 81, issue 18, 2143 (2006).
- [529] R.A. Forrest and J. Kopecky, "EASY-2005: Validation and new tools for data checking", *Fus. Eng. Des.* 82, 2471 (2007).
- [530] R.A. Forrest, "Extending the energy range of materials activation modeling" *Journ. Nucl. Mat.* 329, 1633 (2004).
- [531] R.A. Forrest, J. Kopecky and J.-Ch. Sublet, "The European Activation File: EAF-2005 cross section library", Euratom UKAEA Fusion, EASY documentation series, UKAEA report FUS 515 (2005).
- [532] R.A. Forrest, J. Kopecky and J.-Ch. Sublet, "The European Activation File: EAF-2003 cross section library", Euratom UKAEA Fusion, EASY documentation series, UKAEA report FUS 486 (2002).

### **High energy codes and applications**

- [533] C.J. Diez, O. Cabellos, D. Rochman, A.J. Koning, J.S. Martinez, "Monte Carlo uncertainty propagation approaches in ADS burn-up calculations", *Ann. Nuc. En.* 54, 27 (2013).

- [534] M. Nandy and C. Lahiri, "Radioactivity generation in Pb target by protons - A comparative study from MeV to GeV", *Indian, Journ. of Pure and Appl. Phys.* 50, 761 (2012).
- [535] V. Wagner, O. Svoboda, J. Vrzalova, M. Suchopar, B. Geier, A. Kugler and M. Honusek, "Measurement of Neutrons in Different Pb/U Setups Irradiated by Relativistic Protons and Deuterons by means of Activation Samples", *Journ. Phys.* 366, 012047 (2012).
- [536] M. Ghergherehchi et al., "Dosimetry and microdosimetry of 10-220 MeV proton beams with CR-39 and their verifications by calculation of reaction cross sections using ALICE, TALYS and GEANT4 codes", *Radiation measurements* 47, 410 (2012).
- [537] K.S. Babu, Y.O. Lee, S. Mukherjee, "Analysis of charged particle induced reactions for beam monitor applications" *Nucl. Instr. Meth.* B283, 46 (2012).
- [538] E. Mendoza, "A new physics model for the charged particle transport with GEANT4", *Nuclear Science Symposium and medical imaging conference*, 2242 (2011).
- [539] C. Bhatia and V. Kumar, "Status, evaluation and role of (n,xn) reaction cross sections in ADS materials" *Proceedings of the International Conference on Mathematics and Computational Methods M and C 2011, Rio de Janeiro, May 8-12 (2011)*.
- [540] N. Shigyo et al., "Measurement of Deuteron Induced Thick Target Neutron Yields at 9 MeV", *Proceedings of the International Conference on Nuclear Data for Science and Technology, April 26-30, 2010, Jeju, Korea, Journ. Kor. Phys. Soc.* 59, no. 23, 1725 (2011).
- [541] A. Yu. Konobeyev, U. Fischer, L. Zanini, "Analysis of nuclide production in the MEGAPIE target", *Nucl. Instr. Meth.* A605, 224 (2009).
- [542] C. Bhatia and V. Kumar, "Impact of spallation neutrons on criticality" *Proceedings of the International Symposium on Nuclear Physics (2009)*.
- [543] A.Y. Stankovskiy and A.Y. Konobeyev, "CASCADEX - A combination of intranuclear cascade model from CASCADE/INPE with the HauserFeshbach evaporation/fission calculations from TALYS", *Nucl. Inst. Meth.* A594, 420 (2008).
- [544] Young-Sik Cho, Cheol-Woo Lee, Young-Ouk Lee, "Evaluation of proton cross-sections for radiation sources in the proton accelerator", *Nucl. Instr. Meth.* A579, 468 (2007).
- [545] E.J. Buis, H. Beijers, S. Brandenburg, A.J.J. Bos, "Measurement and simulation of proton induced activation of LaBr<sub>3</sub>: Ce", *Nucl. Inst. Meth.* A578, 239 (2007).
- [546] E.J. Buis, F. Quarati, S. Brandenburg, A.J.J. Bos and, "Proton induced activation of LaBr<sub>3</sub>: Ce and LaCl<sub>3</sub>: Ce", *Nucl. Inst. Meth.* A580, 902 (2007).

### Medical applications

- [547] T. Kakavand, M. Aref, S. Rajabifar and R. Razavi, "Cyclotron production of <sup>94m</sup>Tc via <sup>94</sup>Mo (p, n) <sup>94m</sup>Tc reaction", *Indian Journ. Pure and Appl. Phys.* 51 (2013).

- [548] M.K. Bakht, M. Sadeghi, S.J. Ahmadi, S.S. Sadjadi, C. Tenreiro, "Preparation of radioactive praseodymium oxide as a multifunctional agent in nuclear medicine: expanding the horizons of cancer therapy using nanosized neodymium oxide", *Nucl. Med. Comm.* 34, 5 (2013).
- [549] A. Hermanne, R. Adam-Rebeles, F. Tarkanyi, S. Takacs, M.P. Takacs, A.V. Ignatyuk, M.S. Uddin, "Excitation functions of deuteron induced reactions on nat-Os up to 50 MeV: Experiments and comparison with theoretical codes", *Nucl. Instr. Meth.* B297, 75 (2013).
- [550] A. Hermanne, S. Takacs, R. Adam-Rebeles, F. Tarkanyi, M.P. Takacs, "New measurements and evaluation of database for deuteron induced reactions on Ni up to 50 MeV", *Nucl. Instr. Meth.* B299, 8 (2013).
- [551] S. Takacs, M.P. Takacs, A. Hermanne, F. Trknyi, R. Adam Rebeles, "Cross sections of proton-induced reactions on natSb", *Nucl. Instr. Meth.* B297, 44 (2013).
- [552] Z. Riazi, H. Afarideh and R. Sadighi-Bonabi, "Influence of ridge filter material on the beam efficiency and secondary neutron production in a proton therapy system", *Zeit. Med. Physik*, 22, 231 (2012).
- [553] L. M. Oranj, T. Kakavand, M. Sadeghi and M.A. Rovias, "Monte Carlo FLUKA code simulation for study of  $^{68}\text{Ga}$  production by direct proton-induced reaction" *Nucl. Instr. Meth.* A677, 22 (2012).
- [554] E. Seravalli et al., "Monte Carlo calculations of positron emitter yields in proton radiotherapy", *Phys. Med. Biol.* 57, 1659 (2012).
- [555] Abdulrahman Alfuraih, Khalid Alzimami, Andy K. Ma and Ali Alghamdi, "Optimization of  $^{89}\text{Zr}$  production using Monte Carlo simulations", *Journal of Radioanalytical and Nuclear Chemistry* 2012, DOI: 10.1007/s10967-012-2074-6 (2012).
- [556] S.M. Qaim, S. Sudar, B. Scholten, A.J. Koning and H.H. Coenen, "Evaluation of excitation functions of  $^{100}\text{Mo}(p,d+pn)^{99}\text{Mo}$  and  $^{100}\text{Mo}(p,2n)^{99m}\text{Tc}$  reactions : Estimation of long-lived Tc-impurity and its implication on the specific activity of cyclotron-produced  $^{99m}\text{Tc}$ ", to be published in *Appl. Rad. Isot.* (2012).
- [557] B. Braunn, A. Boudard, J.C. David, S. Leray and A.J. Koning, "A new nuclear database for proton therapy application", submitted to *Phys. Med. Biol.* (2012).
- [558] J.M. Verburg, H.A. Shih and J. Seco, "Simulation of prompt gamma-ray emission during proton radiotherapy", *Physics in Medicine and Biology* 57 (17), 5459 (2012).
- [559] M.U. Khandaker, K. Kim and G. Kim, "Production parameters of the therapeutic  $^{105}\text{Rh}$  radionuclide using medium energy cyclotron", *Pramana Journal of physics* 79, 2, 243 (2012).
- [560] N. Zandi, M. Sadeghi, H. Afarideh, M. Yarmohamadi, "Radiochemical studies relevant to cyclotron production of the therapeutic radionuclide  $^{167}\text{Tm}$ ", *Radiochim. Acta*, to be published (2012).
- [561] N. Zandi, M. Sadeghi, H. Afarideh, "Evaluation of the cyclotron production of  $^{165}\text{Er}$  by different reactions", *Journ. Radioan. nucl. chem.* (2012).

- [562] Mahdi Sadeghi, Nadia Zandi and Hossein Afarideh, "Targetry and specification of  $^{167}\text{Tm}$  production parameters by different reactions", *Journ. Radioan. Nuclear Chem.* 291, 3, 731-738 (2012).
- [563] A. Alfuraih, K. Alzimami, A.K. Ma, A. Alghamdi, "Optimization of  $^{89}\text{Zr}$  production using Monte Carlo simulations", *Journ. Radioan. Nucl. Chem.* (2012).
- [564] M. Taghilo, T. Kakavand, S. Rajabifar and P. Sarabadani, "Cyclotron production of  $^{89}\text{Zr}$ : A potent radionuclide for positron emission tomography", *Int. Journ. Phys. Sci.* 7, 1321 (2012).
- [565] Mahdi Sadeghi, Mahdi Bakhtiari, M.K. Bakht, M. Anjomrouz and L. Mokhtari, "Overview of mercury radionuclides and nuclear model calculations of  $^{195}\text{Hg}(m,g)$  and  $^{197}\text{Hg}(m,g)$  to evaluate experimental cross section data", *Phys. Rev. C* 85, 034605 (2012).
- [566] Mahdi Sadeghi, Nadia Zandi, Mahdi Bakhtiari, "Nuclear model calculation for cyclotron production of  $^{61}\text{Cu}$  as a PET imaging", *Journ. Radioan. Nucl. Chem.* 292, 777 (2012).
- [567] Mayeen Uddin Khandaker, H. Haba, J. Kanaya, N. Otuka, "Excitation functions of (d,x) nuclear reactions on natural titanium up to 24 MeV", *Nucl. Instr. Meth. B* 296, 14 (2012).
- [568] Mayeen Uddin Khandaker, Kwangsoo Kim, Guinyun Kim, "Production cross sections of short-lived silver radionuclides from  $\text{natPd}(p,xn)$  nuclear processes", *Nucl. Instr. Meth. B* 274, 148 (2012).
- [569] Mayeen Uddin Khandaker, Kwangsoo Kim, Man-Woo Lee, Kyung-Sook Kim, Guinyun Kim, Naohiko Otuka, "Investigations of  $^{89}\text{Y}(p,x)^{86,88,89}\text{Zr}$ ,  $^{86m+g,87g,87m,88g}\text{Y}$ ,  $^{85}\text{gSr}$ , and  $^{84}\text{gRb}$  nuclear processes up to 42 MeV", *Nucl. Instr. Meth. B* 271, 72 (2012).
- [570] Mahdi Sadeghi, Milad Enferadi, Mahdi Bakhtiari, "Accelerator production of the positron emitter zirconium-89", *Ann. Nuc. En.* 41, 97 (2012).
- [571] A. Mihailescu, N. Verga, M.A. Popovici, L. Strasses, D. Filipescu, G. Cata-Danil, "Residual radioactivity induced by protons and  $^{12}\text{C}$  ions in biomedical materials", *Rom. Rep. Phys.* 63 (2), 729 (2011).
- [572] S. Takcs, M.P. Takcs, A. Hermanne, F. Trknyi, R. Adam Rebeles, "Cross sections of deuteron-induced reactions on  $\text{natSb}$  up to 50 MeV", *Nucl. Instr. Meth. B* 278, 93 (2012).
- [573] A. Hermanne, F. Trknyi, S. Takcs, R. Adam-Rebeles, A. Ignatyuk, "Activation cross sections for deuteron induced reactions on  $\text{Si}$  up to 50 MeV", *Nucl. Instr. Meth. B* 285, 43 (2012).
- [574] A. Hermanne, S. Takacs, F. Tarkanyi, R. Adam-Rebeles, A. Ignatyuk, "Excitation function for  $^7\text{Be}$  production in carbon by deuteron irradiations up to 50 MeV", *Appl. Rad. Iso.* 70 (6), 911 (2012).
- [575] F. Tarkanyi, F. Ditroi, A. Hermanne, S. Takacs, A.V. Ignatyuk, "Investigation of activation cross-sections of proton induced nuclear reactions on  $\text{natMo}$  up to 40 MeV: New data and evaluation" *Nucl. Instr. Meth. B* 280, (1), 45 (2012).
- [576] F. Tarkanyi, F. Ditroi, S. Takacs, A. Hermanne, and A.V. Ignatyuk, "Excitation functions of deuteron induced reactions on  $\text{nat-Xe}$ : new data up to 20 MeV", submitted to *Appl. Rad. Iso.* (2012).

- [577] F. Tarkanyi, A. Hermanne, S. Takacs, F. Ditroi, I. Spahn and A.V. Ignatyuk, "Activation cross-sections of proton induced reactions on thulium in the 20-45 MeV energy range", *Appl. Rad. Isot.* 70, 309 (2012)
- [578] F. Trknyi, F. Ditri, S. Takcs, B. Kirly, A. Hermanne, M. Sonck, M. Baba, A.V. Ignatyuk, "Investigation of activation cross-sections of deuteron induced nuclear reactions on natural Mo up to 50 MeV", *Nucl. Instr. Meth. B274*, 1 (2012).
- [579] M. Maiti, "New measurement of cross sections of evaporation residues from the natPr + 12C reaction: A comparative study on the production of 149Tb", *Phys. Rev. C84* (4) 044615 (2011).
- [580] M. Sadeghi and M. Enferadi, "Production and radiochemical separation of no-carrier added 88Y by liquid-liquid extraction", *Radiochemistry* 53(5), 539 (2011).
- [581] Z. Alipoor, Z. Gholamzadeh, M. Sadeghi, M. Aref, "Data evaluation acquired TALYS-1.0 code to produce 111In from various accelerator-based reactions", *Int. J. Modern Pys. E20* (5) 1307 (2011).
- [582] M.N. Aslam, S. Sudar, M. Hussain, A.A. Malik and S.M. Qaim, "Evaluation of excitation functions of proton, 3He and alpha-particle induced reactions for production of the medically interesting positron-emitter bromine-76", *Appl. Rad. Isot.* 69, 1490 (2011).
- [583] M. Hussain, S. Sudar, M.N. Aslam, R. Ahmad, H.A. Shah, A.A. Malik and S.M. Qaim, "Evaluations of Charged Particle Data for Production of the Therapeutic Radionuclides 103Pd, 186Re and 67Cu, Proceedings of the International Conference on Nuclear Data for Science and Technology, April 26-30, 2010, Jeju, Korea, *Journ. Kor. Phys. Soc.* 59, no. 23, 1987 (2011).
- [584] F. Ditri, S. Takcs, F. Trknyi, M. Baba and R.W. Smith, "Investigation of Proton and Deuteron Induced Reactions on Cobalt", *Proceedings of the International Conference on Nuclear Data for Science and Technology, April 26-30, 2010, Jeju, Korea, Journ. Kor. Phys. Soc.* 59, no. 23, 1697 (2011).
- [585] F. Ditroi, F. Tarkanyi, S. Takacs, A. Hermanne, H. Yamazaki, M. Baba, A. Mohammadi and A. V. Ignatyuk, "Study of activation cross sections of deuteron induced reactions on rhodium up to 40 MeV", *Nucl. Instr. Meth. B269* (18), 1963 (2011).
- [586] F. Ditroi, F. Tarkanyi, S. Takacs, A. Hermanne, H. Yamazaki, M. Baba, A. Mohammadi and A. V. Ignatyuk, "Activation cross sections of deuteron induced nuclear reactions on manganese up to 40 MeV", *Nucl. Instr. Meth. B269* (17) 1878 (2011).
- [587] M. Enferadi, M. Sadeghi and H. Nadi, "72As, a powerful positron emitter for immunoimaging and receptor mapping: Study of the cyclotron production", *Radiochemistry* 53 (4), 407 (2011).
- [588] P. Saidi, M. Sadeghi, M. Enferadi and G. Aslani, "Investigation of palladium-103 production and IR07-103Pd brachytherapy seed preparation", *Ann. Nuc. En.* 38, 2168 (2011).
- [589] D. Wittwer, R. Dressler, R. Eichler, H.W. Gaeggeler, D. Piguet, A. Serov, A. Tuerler and A. Voegelé, "The thermal release of scandium from titanium metal - a simple way to produce pure 44Sc for PET application", *Radiochim. Acta* 99 (3), 193 (2011).

- [590] S. Takacs, F. Tarkanyi, A. Hermanne, R. Adam Rebeles, "Activation cross sections of deuteron induced nuclear reactions on natural hafnium", *Nucl. Instr. Meth. B269* (23), 2824 (2011).
- [591] M.S. Uddin, A. Hermanne, S. Sudr, M.N. Aslam, B. Scholten, H.H. Coenen, S.M. Qaim, "Excitation functions of alpha-particle induced reactions on enriched  $^{123}\text{Sb}$  and  $\text{natSb}$  for production of  $^{124}\text{I}$ ", *Appl. Rad. Isot.* 69(4), 699 (2011).
- [592] F. Tarkanyi, A. Hermanne, S. Takacs, M. Sonck, Z. Szuacutecs, B. Kiraly, et al, "Investigation of alternative production routes of  $^{99\text{m}}\text{Tc}$ : Deuteron induced reactions on  $^{100}\text{Mo}$ ", *Appl. Rad. Isot.*, 69(1), 18-25 (2011).
- [593] M.N. Aslam, S. Sudar, M. Hussain, A.A. Malik, S.M. Qaim, "Evaluation of excitation functions of  $^3\text{He}$ - and  $\alpha$ -particle induced reactions on antimony isotopes with special relevance to the production of iodine-124", *Appl. Rad. Isot.*, 69(1), 94-104 (2011).
- [594] F. Tarkanyi, A. Hermanne, B. Kiraly, S. Takacs, F. Ditroi, M. Baba, et al., "Investigation of activation cross sections of deuteron induced reactions on indium up to 40 MeV for production of a  $^{113}\text{Sn}/^{113\text{m}}\text{In}$  generator", *Appl. Rad. Isot.* 69(1), 26-36 (2011).
- [595] A. Hermanne, R. Adam Rebeles, F. Tarkanyi, S. Takacs, M. Takacs, J. Csikai and A.V. Ignatyuk, "Cross sections of deuteron induced reactions on  $^{45}\text{Sc}$  up to 50 MeV: Experiments and comparison with theoretical codes", *Nucl. Instr. Meth. B270*, 106 (2012).
- [596] A. Hermanne, R. Adam Rebeles, F. Tarkanyi, S. Takacs, M. Takacs and A.V. Ignatyuk, "Cross sections of deuteron induced reactions on  $\text{nat-Cr}$  up to 50 MeV: Experiments and comparison with theoretical codes", *Nucl. Instr. Meth. B269* (21) 2563 (2011).
- [597] A. Hermanne, F. Tarkanyi, S. Takacs, R. Adam Rebeles, S. Spellerberg and R. Schweikert, "Limitation of the long lived  $^{121}\text{Te}$  contaminant in production of  $^{123}\text{I}$  through the  $^{124}\text{Xe}$  (p, x) route", *Appl. Rad. Isot.* 69(2), 358 (2011).
- [598] T. Kakavand and M. Sadeghi, "Determination of  $^{89}\text{Zr}$  production parameters via different reactions using ALICE and TALYS codes", *Kerntechnik* 76, 362 (2011).
- [599] A. Hermanne, R. Adam Rebeles, F. Tarkanyi, S. Takacs, B. Kiraly, A.V. Ignatyuk, "Cross sections for production of longer lived  $^{170}, ^{168}, ^{167}\text{Tm}$  in 16 MeV proton irradiation of  $\text{natEr}$ ", *Nucl. Instr. Meth. B269*(7), 695 (2011).
- [600] M. Sadeghi and M. Enferadi, "Nuclear model calculations on the production of  $^{119}\text{Sb}$  via various nuclear reactions", *Ann. Nucl. En.* 38(4), 825 (2011).
- [601] M.K. Bakht, M. Sadeghi and C. Tenreiro, "A novel technique for simultaneous diagnosis and radioprotection by radioactive cerium oxide nanoparticles: study of cyclotron production of  $^{137\text{m}}\text{Ce}$ ", *Journ. Radioan. Nucl. Chem.* 292, 53-59 (2012).
- [602] M. Sadeghi, M.K. Bakht and L. Mokhtari, "Practicality of the cyclotron production of radiolanthanide  $^{142}\text{Pr}$ : a potential for therapeutic applications and biodistribution studies", *Journ. Radioanal. Nucl. Chem.* 288, no 3 937 (2011).

- [603] M. Sadeghi, M. Enferadi, M. Aboudzadeh and P. Sarabadani, "Production of  $^{122}\text{Sb}$  for the study of environmental pollution" *Journ. Radioanal. Nucl. Chem.* 287, no 2 585 (2011).
- [604] M. Enferadi, M. Sadeghin and H. Nadi, " $^{45}\text{Ti}$ , a candidate for positron emission tomography: Study of the cyclotron production", *Radiochemistry* 53 (4), 411 (2011).
- [605] TAGHILO M. ; KAKAVAND T. ; SADEGHI M "Determination of  $^{89}\text{Zr}$  production parameters via different reactions using ALICE and TALYS codes", *Kerntechnik* 76, 362 (2011).
- [606] M. Enferadi, M. Sadeghi, " $^{122}\text{Sb}$  - a potential radiotracer: Evaluation of cyclotron production via novel routes", *Nucl. Techn. Rad. Prot.* 26, issue 1, 58 (2011).
- [607] M. Enferadi, M. Sadeghi, "Nuclear data for the cyclotron production of  $^{117}\text{Sb}$  and  $^{90}\text{Nb}$ ", *Chinese Physics C* 35(3), 248 (2011).
- [608] H.E. Hassan and S.M. Qaim, "A critical survey of experimental cross section data, comparison with nuclear model calculations and estimation of production yields of  $^{77}\text{Br}$  and  $^{77}\text{Kr}$  in no-carrier-added form via various nuclear processes", *Nucl. Instr. Meth.* B269, 1121 (2011).
- [609] M. Sadeghi, Z. Alipoor, A. Majdabadi, "Nuclear model calculation on charged particle induced reaction on Rb and Kr targets and targetry for  $^{82}\text{Sr}$  production", *Journ. Radioanal. Nucl. Chem.* 288, no 3 745 (2011).
- [610] M.S. Uddin, B. Scholten, A. Hermanne, S. Sudar, H. Coenen, and S.M. Qaim, "Radiochemical determination of cross sections of  $\alpha$ -particle induced reactions on  $^{192}\text{Os}$  for the production of the therapeutic radionuclide  $^{193\text{m}}\text{Pt}$ ", *Appl. Rad. Isot.* 68(10), 2001 (2010).
- [611] S.M. Qaim, K. kettern, Y.N. Shubin, S. Sudar, "Excitation functions of nuclear reactions leading to the soft-radiation emitting radionuclides  $^{45}\text{Ca}$ ,  $^{49}\text{V}$  and  $^{204}\text{Tl}$  in beam collimator materials used in proton therapy", *Rad. chim. Acta* 98, 447 (2010).
- [612] M.N. Aslam, S. Sudar, M. Hussain, A.A. Malik, H.A. Shah, and S.M. Qaim, "Evaluation of excitation functions of proton and deuteron induced reactions on enriched tellurium isotopes with special relevance to the production of iodine-124", *Appl. Rad. Isot.* 68, 1760 (2010).
- [613] M. Sadeghi, A. Ghanbarzadeh, M. Enferadi, "Nuclear data for cyclotron production of  $^{114\text{m}}\text{In}/^{114}\text{In}$  and  $^{140}\text{Nd}/^{140}\text{Pr}$  used in gamma camera monitoring, RIT, ERT and PET", *Kern-technik* 75(6), 363 (2010).
- [614] P.S. Bidokhti, M. Sadeghi, B. Fateh, M. Matloobi, G. Aslani, "Nuclear data measurement of  $^{186}\text{Re}$  production via various reactions", *Nucl. Eng. Techn.* 42(5), 600 (2010).
- [615] M. Sadeghi, M. Enferadi, H. Nadi, "Study of the cyclotron production of  $^{172}\text{Lu}$ : An excellent radiotracer", *Journ. Radioanal. Nucl. Chem.* 286(1), 259 (2010).
- [616] M. Sadeghi, M. Enferadi, H. Nadi, C. Tenreiro, "A novel method for the cyclotron production no-carrier-added  $^{93\text{m}}\text{Mo}$  for nuclear medicine", *Journ. Radioanal. Nucl. Chem.*, 286(1), 141 (2010).

- [617] M. Hussain, S. Sudar, M.N. Aslam, A.A. Malik, R. Ahmad, S.M. Qaim, "Evaluation of charged particle induced reaction cross section data for production of the important therapeutic radionuclide  $^{186}\text{Re}$ ", *Rad. chim. Acta*, 98(7), 385 (2010).
- [618] S. Takacs, F. Tarkanyi and A. Hermanne, "Activation cross sections of deuteron induced nuclear reactions on hafnium", *Nucl. Instr. Meth. B268* (22), 3443 (2010).
- [619] F. Tarkanyi, A. Hermanne, S. Takacs, F. Ditroi, B. Kiraly, H. Yamazaki, M. Baba, A. Mohammadi, A.V. Ignatyuk, "New measurements and evaluation of excitation functions for (p,xn), (p,pxn) and (p,2pxn) reactions on  $^{133}\text{Cs}$  up to 70 MeV proton energy", *Appl. Rad. Isot.* 68, 47 (2010).
- [620] S. Mahdi et al, "Data evaluation of Yb-169-producing reactions by charged particles", *Nucl. Sci. Techn.* 21, 110 (2010).
- [621] A. Hermanne, R. Adam Rebeles, F. Tarkanyi, S. Takacs, I. Spahn, and A.V. Ignatyuk, "High yield production of the medical radioisotope  $^{167}\text{Tm}$  by the  $^{167}\text{Er}(d,2n)$  reaction", *Appl. Rad. Isot.* 69, 475 (2010).
- [622] F. Tarkanyi, A. Hermanne, S. Takacs, B. Kiraly, I. Spahn, A.V. Ignatyuk, "Experimental study of the excitation functions of proton induced nuclear reactions on  $^{167}\text{Er}$  for production of medically relevant  $^{167}\text{Tm}$ " *Appl. Rad. Isot.* 68, 250 (2010).
- [623] F. Tarkanyi, F. Ditroi, B. Kiraly, S. Takacs, H. Yamazaki, M. Baba, A. Mohammadi and A.V. Ignatyuk, "Study of activation cross sections of proton induced reactions on barium: Production of  $^{131}\text{Ba}$ – $^{131}\text{Cs}$ " *Appl. Rad. Isot.* 68(10) 1869 (2010).
- [624] M. Sadeghi, T. Kakavand, and Z. Alipoor, " $^{85}\text{Sr}$  Production via Proton Induced on Various Targets Using Talys 1.0 Code", *Mod. Phys. Lett. A* 25, 1541 (2010).
- [625] M. Sadeghi, S. Seyyedi, Z. Gholamzadeh, "Comparison of nuclear data of  $^{64}\text{Cu}$  production using an accelerator by TALYS-1.0 code", *Nucl. Techn. Rad. Prot.* 62 (2010).
- [626] T. Kakavand and M. Taghilo, "Calculations of excitation functions to produce  $^{88}\text{Y}$  via various nuclear reactions by ALICE/91 and TALYS-1.0 codes", 18th International conference on nuclear engineering vol 3, May 17-21 2010 Xian, p. 285 (2010).
- [627] S.M. Qaim, K. Hilgers, S. Sudar, H.H. Coenen, "Excitation function of the  $^{192}\text{Os}(3\text{He},4n)$ -reaction for production of  $^{191}\text{Pt}$ ", *Appl. Rad. Isot.* 67, 1074 (2009).
- [628] M. Aslam, S. Sudar, M. Hussain, A. A. Malik, H. A. Shah and Syed M. Qaim, "Charged particle induced reaction cross section data for production of the emerging medically important positron emitter  $^{64}\text{Cu}$ : A comprehensive evaluation", *Radio. Chim. Acta* 97, 667 (2009).
- [629] M. Hussain, S. Sudar, M.N. Aslam, H.A. Shah, R. Ahmad, A.A. Malik, S.M. Qaim, "A comprehensive evaluation of charged-particle data for production of the therapeutic radionuclide  $^{103}\text{Pd}$ ", *Appl. Rad. Iso.* 67, 1842 (2009).

- [630] F. Tarkanyi, A. Hermanne, S. Takacs, F. Ditroi, H. Yamazaki, M. Baba, A. Mohammadi, and A.V. Ignatyuk, "Activation cross sections of proton induced nuclear reactions on ytterbium up to 70 MeV", *Nucl. Instr. Meth. B* 267, 2789 (2009).
- [631] F. Tarkanyi, A. Hermanne, S. Takacs, R.A. Rebeles, P. van den Winkel, B. Kiraly, F. Ditroi, A.V. Ignatyuk, "Cross section measurements of the  $^{131}\text{Xe}(p,n)$  reaction for production of the therapeutic nuclides  $^{131}\text{Cs}$ ", *Appl. Rad. Iso.* 67, 1751 (2009).
- [632] M. Sadeghi, T. Kakavand, L. Mokhtari and Z. Gholamzadeh, "Determination of  $^{68}\text{Ga}$  production parameters by different reactions using ALICE and TALYS codes, *Pramana Journ. of Phys.* 72, no.2, 335 (2009).
- [633] M. Sadeghi, M. Aboudzadeh, A. Zali and M. Mirzaii, "Radiochemical studies relevant to  $^{86}\text{Y}$  production via  $^{86}\text{Sr}(p, n)^{86}\text{Y}$  for PET imaging", *App. Rad. Isot.* 67, no. 1, 7 (2009).
- [634] M. Maiti and S. Lahiri, "Theoretical approach to explore the production routes of astatine radionuclides", *Phys. Rev. C* 79, 0247611 (2009).
- [635] E. Betak, E. Rurarz, S. Mikolajewski, and J. Wojtkowska, "A new method of pure  $^{111}\text{In}$  production by proton-induced nuclear reactions with enriched  $^{112}\text{Sn}$ ", *Nukleonika* 52, 17 (2007).
- [636] A.J. Koning and M.C. Duijvestijn, "Nuclear theory for high-energy nuclear reactions of biomedical relevance", *Radiation Protection Dosimetry* 2007; doi: 10.1093/rpd/ncm008, *Proceedings of the Tenth Symposium on Neutron Dosimetry*, Uppsala, June 12-16 2006 (2007)

### Astrophysics

- [637] R. Trappitsch and I. Leya, "Cosmogenic production rates and recoil loss effects in micrometeorites and interplanetary dust particles", *Meteoritics and planetary science*, to be published (2013).
- [638] A. Palumbo, W.P. Tan, J. Gorres, M. Wiescher, N. Ozkan, R. T. Guray, and C. Yalcin, "Measurement of  $^{120}\text{Te}(a,n)$  cross sections relevant to the astrophysical p process", *Phys. Rev. C* 85, 028801 (2012).
- [639] D. Robertson, J. Gres, P. Collon, M. Wiescher and H.-W. Becker, "New measurement of the astrophysically important  $^{40}\text{Ca}(a,g)^{44}\text{Ti}$  reaction", *Phys. Rev. C* 85, 045810 (2012).
- [640] Ruo-Yu Liu and Xiang-Yu Wang, "Energy spectrum and chemical composition of ultra-high energy cosmic rays from semi-relativistic hypernovae", *Astroph. Journ* 746, 40 (2012).
- [641] C. Lahiri and G. Gangopadhyay, "Low-energy proton reactions of astrophysical interest in the  $A=90-100$  region", *Phys. Rev. C* 86, 047601 (2012).
- [642] S. Mukerji et al., "Measurement of  $^{232}\text{Th}(n,g)$  and  $^{232}\text{Th}(n,2n)$  cross-sections at neutron energies of 13.5, 15.5 and 17.28 MeV using neutron activation techniques", *Physics and astronomy* 79, 249 (2012).
- [643] I. Daoutidis and S. Goriely, "Large-scale continuum random-phase approximation predictions of dipole strength for astrophysical applications", *Phys. Rev. C* 86, 034328 (2012).

- [644] T. Kondo, H. Utsunomiya, S. Goriely, I. Daoutidis, C. Iwamoto, H. Akimune, A. Okamoto, T. Yamagata, M. Kamata, O. Itoh, H. Toyokawa, Y.-W. Lui, H. Harada, F. Kitakani, S. Hilaire, and A.J. Koning, “Total and partial photoneutron cross sections for Pb isotopes”, submitted to Phys. Rev. C (2012).
- [645] L.I. Miroshnichecenko and W.Q. Gan, “Particle acceleration and gamma rays in solar flares: Recent observations and new modeling”, *Advances in Space Research* 50, 6, 736 (2012).
- [646] W. Chen and W.Q. Gan, “The effect of Compton scattering of gamma-ray spectra of the 2005 january 20 flare”, *Research in Astron. Astrop.* 12, 10, 1439 (2012).
- [647] W. Chen and W.Q. Gan, “The Calculation of Solar Gamma-Rays by TALYS”, *Chinese Astronomy and Astrophysics* 36, 49 (2012).
- [648] E. Kafexhiu, F. Aharonian, G.S. Vila, “Nuclear reactions in hot astrophysical plasmas with  $T > 10^{10}$  K” *Intern. Journ. Mod. Phys. D21*, 1250009 (2012).
- [649] L. Csige, M. Csatlos, T. Faestermann, J. Gulyas, D. Habs, R. Hertenberg, M. Hunyadi, A. Krasznahorkay, H.J. Maier, P.G. Thirolf, H.F. Wirth, “Transmission resonance spectroscopy in the third minimum of 232Pa”, *Phys. Rev. C85*, 054306 (2012).
- [650] S. Goriely, A. Bauswein, and H.T. Janka, “R-process nucleosynthesis during the decompression of neutron star crust material”, *Journ. Phys. Conf. Series* 337, 012039 (2012).
- [651] L. Csige, M. Csatlos, T. Faestermann, J. Gulyas, D. Habs, R. Hertenberg, M. Hunyadi, A. Krasznahorkay, H.J. Maier, P.G. Thirolf, H.F. Wirth, “High resolution spectroscopy in the third minimum of 232Pa”, *Acta Polonica* 42 (2012).
- [652] O. Lebeda, V. Lozza, P. Schrock, J. Stursa, K. Zuber, “Excitation functions of proton-induced reactions on natural Nd in the 10-30 MeV energy range, and production of radionuclides relevant for double-beta decay”, *Phys. Rev. C85*, 014602 (2012).
- [653] R. Raut, W. Tornow, A.P. Tonchev, G. Rusev, J.H. Kelley, A.C. Crowell, M.W. Ahmed, S.C. Stave, C. Iliadis, M. Lugaro, J. Buntain, R. Schwengner, A. Banu, “Photodisintegration studies at HIgS: Addressing the few and the many”, to be published (2012).
- [654] Gy. Gyurky, P. Mohr, Zs. Fulop, Z. Halasz, G. G. Kiss, T. Szucs, and E. Somorjai “Relation between total cross sections from elastic scattering and a-induced reactions: The example of 64Zn”, *Phys. Rev. C86*, 041601 (2012).
- [655] Gy. Gyurky, J. Farkas, Z. Halasz, Zs. Fulop, E. Somorjai, P. Mohr, A. Wallner, “Experimental study of a-induced reactions on 64Zn for the astrophysical g-process”, *Journ. Phys. Conf. Ser.* 337, 012009 (2012).
- [656] R. Raut, A Banu, C Iliadis, J H Kelley, G Rusev, R Schwengner, A P Tonchev and W Tornow, “Cross-Section Measurements of the 86Kr(g, n) Reaction to Probe the s-Process Branching at 85Kr”, *J. Phys.: Conf. Ser.* 337 012048 (2012).

- [657] A. Coc, S. Goriely, Y. XU, M. Saimpert, E. Vangioni, “Standard big-bang nucleosynthesis up to CNO with an improved extended nuclear network”, *Astrophys Journ. Suppl.* 744, 158 (2012).
- [658] A. Coc, “Variation of fundamental constants and the triple-alpha reaction in Population III stars and BBN”, *J. Phys.: Conf. Ser.* 337 012037 (2012).
- [659] A. Coc, S. Goriely, M. Saimpert, E. Vangioni, and Yi Xu “Nuclear uncertainties in CNO production by Big Bang nucleosynthesis” *AIP Conf. Proc.* 1484, pp. 354-359; doi:<http://dx.doi.org/10.1063/1.4763419>, ORIGIN OF MATTER AND EVOLUTION OF GALAXIES 2011, November 2011, Wako, Japan (2012)
- [660] Li Zhihong et al., “Study of the primordial Lithium abundance”, *Sci. Chin.* G54, s67 (2011).
- [661] A. Arcones and G. Martnez-Pinedo, “Dynamical r-process studies within the neutrino-driven wind scenario and its sensitivity to the nuclear physics input”, *Phys. Rev. C* 83, 045809 (2011).
- [662] A. C. Larsen, S. Goriely, et al, “Gamma-ray strength functions and their relation to astrophysics”, *AIP Conf Proc* 1377, 239 (2011), *Frontiers in nuclear structure, astrophysics and reactions: FINUSTAR 3*.
- [663] G.F. Herzog, M.W. Caffee, T. Faestermann, R. Hertenberg, G. Korschinek, I. Leya, R. Reedy, J.M. Sisterson, “Cross sections from 5 to 35 MeV for the reactions  $\text{natMg}(3\text{He},x)26\text{Al}$ ,  $27\text{Al}(3\text{He},x)26\text{Al}$ ,  $\text{natCa}(3\text{He},x)41\text{Ca}$  and  $\text{natCa}(3\text{He},x)36\text{Cl}$ : implications for early irradiation in the solar system”, *Meteoritics and planetary science* 46(10), 1427 (2011).
- [664] F. Kitatani, H. Harada, S. Goko, H. Utsunomiya, H. Akimune, H. Toyokawa, K. Yamada, “Measurement of  $76\text{Se}$  and  $78\text{Se}(g,n)$  cross sections”, *Journ. Nucl. Sci. Techn.* 48(7) 1017 (2011).
- [665] G. Gyurky, J. Farkas, Z. Halasz, Z. Fulop, E. Somorjai, T. Szucs, P. Mohr and A. Wallner, “Experimental study of alpha-induced reactions on  $64\text{Zn}$  for the astrophysical g-process”, submitted to *Journ Phys.* (2011).
- [666] W. Chen and W.Q. Gan, “The calculation of solar gamma rays by TALYS”, *Chinese Astron. Astrop.* 36, 49 (2012).
- [667] A. Sauerwein, H.W. Becker, H. Dombrowski, M. Elvers, J. Endres, U. Giesen, J. Hasper, A. Hennig, L. Nettelton, T. Rauscher, D. Rogalla, K.O. Zell and A. Zilges, “Determination of  $141\text{Pr}(a,n)144\text{Pm}$  cross section at energies of relevance for the astrophysical p process using the gg coincidence method”, *Phys. Rev. C* 84, 045808 (2011).
- [668] S. Goriely, N. Chamel, H.T. Janka and J.M. Pearson, “The decompression of the outer neutron star crust and r-process nucleosynthesis”, *Astron. Astrop.* 531, A78 (2011).
- [669] S. Goriely, N. Chamel and J.M. Pearson, “HFB Mass Models for Nucleosynthesis Applications”, *Proceedings of the International Conference on Nuclear Data for Science and Technology*, April 26-30, 2010, Jeju, Korea, *Journ. Kor. Phys. Soc.* 59, no. 23, 2100 (2011).

- [670] F. Kaeppler, A. Mengoni, M. Mosconi, K. Fujii, M. Heil, C. Domingo-Pardo and the nTOF Collaboration, “Neutron Studies for Dating the Universe”, Proceedings of the International Conference on Nuclear Data for Science and Technology, April 26-30, 2010, Jeju, Korea, Journ. Kor. Phys. Soc. 59, no. 23, 2094 (2011).
- [671] H. Utsunomiya, S. Goriely, H. Akimune, H. Harada, F. Kitatani, S. Goko, H. Toyokawa, K. Yamada and Y.-W. Lui, “The gSF Method - Determination of Radiative Neutron Capture Cross Sections for Unstable Nuclei”, Proceedings of the International Conference on Nuclear Data for Science and Technology, April 26-30, 2010, Jeju, Korea, Journ. Kor. Phys. Soc. 59, no. 23, 1713 (2011).
- [672] H. Utsunomiya, S. Goriely, M. Kamata, H. Akimune, T. Kondo, O. Itoh, C. Iwamoto, T. Yamagata, H. Toyokawa, Y.-W. Lui, H. Harada, F. Kitatani, S. Goko, S. Hilaire, and A.J. Koning, “Photoneutron cross sections for 118-124Sn and the gamma-ray strength function method”, Phys. Rev. C84, 055805 (2011).
- [673] M. Ahlers and J. Salvado, “Cosmogenic gamma-rays and the composites of cosmic rays”, submitted to High energy astroph. phenomena (2011).
- [674] S. Goriely, A. Bauswein, and H.T. Janka, “R-process nucleosynthesis in dynamically ejected matter of neutron star mergers”, Astrop. Journ. Lett. 738 L32 (2011).
- [675] J. Glorius, M. Knörzer, S. Müller, N. Pietralla, A. Sauerwein, K. Sonnabend, C. Wälzlein and M. Wiescher, “p-process nucleosynthesis: Activation experiments”, Progr. Part. Nucl Phys. 66(2), 379 (2011).
- [676] B. Oginni, C. Iliadis, A. Champagne, “Theoretical evaluation of the reaction rates for  $^{26}\text{Al}(n,p)^{26}\text{Mg}$  and  $^{26}\text{Al}(n,a)^{23}\text{Na}$ ”, Phys. Rev. C83, 025802 (2011).
- [677] H. Utsunomiya, S. Goriely, H. Akimune, H. Harada, F. Kitatani, S. Goko, H. Toyokawa, K. Yamada, T. Kondo, O. Itoh, M. Kamata, T. Yamagata, Y.-W. Lui, I. Daoutidis, D.P. Arteaga, S. Hilaire, and A.J. Koning, “Gamma-ray strength function method and its application to  $^{107}\text{Pd}$ ”, Phys. Rev. C82, 064610 (2010).
- [678] H. Utsunomiya, H. Akimune, H. Harada, F. Kitatani, S. Goko, H. Toyokawa, S. Goriely, Y.-W. Lui, S. Hilaire, A. Koning, K. Yamada, T. Yamagata, T. Kondo, C. Iwamoto and A. Okamoto, “Study of neutron capture cross sections for  $^{93}\text{Zr}$  and  $^{107}\text{Pd}$  with the gamma-ray strength function method”, 2011 Annual Meeting of Atomic Energy Society of Japan, Fukui (Japan), (2011).
- [679] H. Utsunomiya, S. Goriely, H. Akimune, T. Yamagata, H. Toyokawa, H. Harada, F. Kitatani, Y.-W. Lui, I. Daoutidis, D.P. Arteaga, S. Hilaire, and A.J. Koning, “Gamma-ray strength function method and applications”, 2011 Oslo Workshop.
- [680] I. Leya, “Cosmogenic effects on  $^7\text{Li}/^6\text{Li}$ ,  $^{10}\text{B}/^{11}\text{B}$ , and  $^{182}\text{W}/^{184}\text{W}$  in CAIs from carbonaceous chondrites”, Geoch. Cosmoch. Acta 75(6), 1507 (2011).

- [681] R.J. Murphy, B. Kozlovsky, and G.H. Share, “Nuclear cross sections for gamma-ray deexcitation line production by secondary neutrons in the earth’s atmosphere”, *Journ. Geophys. Res.* 116, A03308 (2011).
- [682] E. Kafexhiu, G.S. Vila, F. Aharonian, “Excitation and destruction of nuclei in hot astrophysical plasmas around black holes”, 11th symposium on nuclei in the cosmos, NIC XI, July 19-23, 2010, Heidelberg, Germany, *Proceedings of Science* (2010).
- [683] S. Cebrian, H. Gomez, G. Luzon, J. Morales, A. Tomas, J.A. Villar, “Cosmogenic activation in germanium and copper for rare event searches”, *Astroparticle Physics* 33, 316 (2010).
- [684] G.H. Share, R.J. Murphy, A.J. Tylka, B. Kozlovsky, J.M. Ryan, C. Gwon, “Physics of Solar Neutron Production: Questionable Detection of Neutrons from the 2007 December 31 Flare”, *Journ. Geophys. Res.* 116, A03102 (2011).
- [685] H. Utsunomiya, S. Goriely, H. Akimune, H. Harada, F. Kitatani, S. Goko, H. Toyokawa, K. Yamada, T. Kondo, O. Itoh, M. Kamata, T. Yamagata, Y.-W. Lui, S. Hilaire, and A.J. Koning, “Photoneutron cross sections for  $^{96}\text{Zr}$ : a systematic study of photoneutron and radiative neutron capture cross section for zirconium isotopes”, *Phys. Rev. C* 81, 035801 (2010).
- [686] Z.-B. Yin, D.-M. Mei, S.R. Elliott, “Studies on cosmogenic production as a background for rare physics processes”, *Nucl. Phys. A* 834, 823c (2010).
- [687] S. Hilaire, S. Goriely, A.J. Koning, M. Girod, “Nuclear ingredients for cross section calculation of exotic nuclei”, 3rd international conference on “Frontiers In Nuclear Structure, Astrophysics and Reactions” (FINUSTAR 3), August 23-27 2010, Rhodos (2011).
- [688] H. Utsunomiya, S. Goriely, H. Akimune, T. Yamagata, T. Kondo, C. Iwamoto, A. Okamoto, H. Harada, F. Kitatani, S. Goko, H. Toyokawa, K. Yamada, Y.-W. Lui, S. Hilaire, and A.J. Koning, “The gamma-ray Strength Function Method”, 3rd international conference on “Frontiers In Nuclear Structure, Astrophysics and Reactions” (FINUSTAR 3), August 23-27 2010, Rhodos (2011).
- [689] H. Utsunomiya, S. Goriely, H. Akimune, T. Yamagata, T. Kondo, C. Iwamoto, M. Kamata, O. Itoh, H. Harada, F. Kitatani, S. Goko, H. Toyokawa, K. Yamada, Y.-W. Lui, S. Hilaire, and A.J. Koning, “Application of the SF Method to Palladium”, 3rd international conference on “Frontiers In Nuclear Structure, Astrophysics and Reactions” (FINUSTAR 3), August 23-27 2010, Rhodos (2011).
- [690] J. Hasper, M. B. Bussing, M. Elvers, J. Endres and A. Zilges, “In-beam experiments on (p,g) and (a,g) reactions for the astrophysical p process”, *J. Phys. Conf. Ser.* 202 01 2005 (2010).
- [691] A. Matic, A. M. van den Berg, M. N. Harakeh, H. J. Woertche, G. P. A. Berg, M. Couder, J. Goerres, P. LeBlanc, S. O’Brien, M. Wiescher, K. Fujita, K. Hatanaka, Y. Sakemi, Y. Shimizu, Y. Tameshige, A. Tamii, M. Yosoi, T. Adachi, Y. Fujita, Y. Shimbara, H. Fujita, T. Wakasa, B. A. Brown and H. Schatz “High-precision (p,t) reaction to determine  $^{25}\text{Al}(p,g)^{26}\text{Si}$  reaction rates”, *Phys. Rev. C* 82, 025807 (2010).

- [692] M. Mosconi, M. Heil, F. Kaeppler, R. Plag, and A. Mengoni, “Neutron physics of the Re/Os clock. II. The (n,n) cross section of  $^{187}\text{Os}$  at 30 keV neutron energy”, *Phys. Rev. C* 82, 015803 (2010).
- [693] K. Fujii et al. (The nTOF Collaboration) “Neutron physics of the Re/Os clock. III. Resonance analyses and stellar (n,g) cross sections of  $^{186,187,188}\text{Os}$ ”, *Phys. Rev. C* 82, 015804 (2010).
- [694] D.-M. Mei, C. Zhang, K. Thomas, F. Gray, “Early results on radioactive background characterization for Sanford Laboratory and DUSEL experiments”, *Astroparticle Physics* 34, 33 (2010).
- [695] G. Gangopadhyay, “Low-energy (p,g) reactions in Ni and Cu nuclei using a microscopic optical model”, *Phys. Rev. C* 82, 027603 (2010)
- [696] M. Wiescher and T. Rauscher, “Nuclear reactions”, *Lect. Notes Phys.* 812, 461 (2011).
- [697] I.V. Panov and I.Y. Korneev, T Rauscher, G. Martinez-Pinedo, A. Kelic-Heil, N.T. Zinner, F.-K. Thieleman, “Neutron-induced astrophysical reaction rates for translead nuclei”, *Astronomy and Astrophysics* 513 id.A61 (2010).
- [698] M. Ahlers and A.M. Taylor, “Analytic Solutions of Ultra-High Energy Cosmic Ray Nuclei Revisited”, *Phys. Rev. D* 82, 123005 (2010).
- [699] C. Nair, A.R. Junghans, M. Erhard, D. Bemmerer, R. Beyer, E. Grosse, K. Kosev, M. Marta, G. Rusev, K.D. Schilling, R. Schwengner, and A. Wagner, “Dipole strength in  $^{144}\text{Sm}$  studied via (g,n), (g,p) and (g,a) reactions”, *Phys. Rev. C* 81, 055806 (2010).
- [700] D.-M. Mei, Z.-B. Yin, J. Spaans, M. Koppang, A. Hime, C. Keller, and V. M. Gehman, “Prediction of underground argon content for dark matter experiments”, *Phys. Rev. C* 81, 055802 (2010).
- [701] K. Ammon, J. Masarik and I. Leya, “New model calculations for the production rates of cosmogenic nuclides in iron meteorites”, *Meteorics and Planetary Science* 44(4), 485 (2010).
- [702] H. Utsunomiya, S. Goriely, M. Kamata, T. Kondo, O. Itoh, H. Akimune, T. Yamagata, H. Toyokawa, Y.-W. Lui, S. Hilaire, and A.J. Koning, “Gamma-ray strength function for  $^{116,117}\text{Sn}$  with pygmy dipole resonance balanced in the photoneutron and neutron capture channels”, *Phys. Rev. C* 80, 055806 (2009).
- [703] I. Leya, M. Schonbachler, U. Krahenbuhl, and A.N. Halliday, “New Titanium isotopes data for Allende and Efremovka CAIs”, *Astroph. Journ.* 702(2), 1118 (2009).
- [704] A. Makinaga, H. Utsunomiya, S. Goriely, T. Kaihori, S. Goko, H. Akimune, T. Yamagata, H. Toyokawa, T. Matsumoto, H. Harano, H. Harada, F. Kitatani, Y.K. Hara, S. Hohara, Y.-W. Lui, “Photodisintegration  $^{80}\text{Se}$ : Implications for the s-process branching at  $^{79}\text{Se}$ ”, *Phys. Rev. C* 79, 025801 (2009).
- [705] R.T. Guray, N. Ozkan, C. Yalcin, A. Palumbo, R. deBoer, J. Gorres, P.J. Leblanc, S. O’Brien, E. Strandberg, W.P. Tan, M. Wiescher, Zs. Fulop, E. Somorjai, H.Y. Lee, J.P. Greene, “Measurements of proton-induced reaction cross sections on  $^{120}\text{Te}$  for the astrophysical p process”, *Phys. Rev. C* 80, 035804 (2009).

- [706] I. Dillmann, C. Domingo-Pardo, M. Heil, F. Kppeler, A. Wallner, O. Forstner, R. Golser, W. Kutschera, A. Priller, P. Steier, A. Mengoni, R. Gallino, M. Paul, and C. Vockenhuber, “Determination of the stellar (n,g) cross section of  $^{40}\text{Ca}$  with accelerator mass spectrometry”, *Phys. Rev. C* 79, 065805 (2009).
- [707] D.L. Cook, E. Berger, T. Faestermann, G.F. Herzog, K. Knie, G. Korschinek, M. Poutivtsev, G. Rugel, and F. Serefidin, “ $^{60}\text{Fe}$ ,  $^{10}\text{Be}$  and  $^{26}\text{Al}$  in lunar cores 12025/8 and 60006/7: Search for a nearby supernovae”, 40th Lunar and Planetary Science Conference (2009).
- [708] R.J. Murphy, B. Kozlovsky, J. Kiener and G.H. Share, “Nuclear gamma-ray de-excitation lines and continuum from accelerated-particle interactions in solar flare”, *Astroph. Journ. Suppl Series* 183, 142 (2009).
- [709] I. Leya, J. Masarik, “Cosmogenic nuclides in stony meteorites revisited”, *Meteoritics and planetary science* 44(7), 1061 (2009).
- [710] M. Mei, Z.B. Yin and S.R. Elliott, “Cosmogenic Production as a Background in Searching for Rare Physics Processes”, *Astroparticle Phys.* 31, 417 (2009).
- [711] M.-C. Liu and K.D. McKeegan, “On an irradiation origin for magnesium isotope anomalies in meteoritic hibonite”, *Astroph. Journ.* 697, L145 (2009).
- [712] K.H. Kampert, J.K. Kulbartz, N. Nierstenhoefer, M. Risse, and G. SIgl, “Propagation of ultra-high energy nuclei with CRPopa”, proceedings of the 31st ICRC, Lodz (2009).
- [713] C. Fitoussi, J. Duprat, V. Tatischeff, J. Kiener, F. Naulin, G. Raisbeck, M. Assuncao, C. Bourgeois, M. Chabot, A. Coc, C. Engrand, M. Gounelle, F. Hammache, A. Lefebvre, M.-G. Porquet, J.-A. Scarpaci, N. De Sereville, J.-P. Thibaud, and F. Yiou, “Measurement of the  $^{24}\text{Mg}(^3\text{He},p)^{26}\text{Al}$  cross section: Implication for  $^{26}\text{Al}$  production in the early solar system”, *Phys. Rev. C* 78, 044613 (2008).
- [714] S.I. Fujimoto, R. Matsuba and K. Arai, “Lithium production on a low mass secondary in a black hole soft X-ray transient”, *Astro. Journ. Lett.* 673, L51 (2008).
- [715] K. Sonnabend, S. Muller, N. Pietralla, D. Savran, and S. Krewald, “Self-consistent calculations of the strength function and radiative neutron capture cross section for stable and unstable tin isotopes”, *Phys. Rev. C* 83, 064316 (2011). L. Schnorrenberger, J. Hasper, A. Zilges, “Experiments on photon-induced reactions for p-processes nucleosynthesis”, 10th symposium on Nuclei in the cosmos, july 2008, Mackinac Island, USA (2008).
- [716] S. Goriely, S. Hilaire and A.J. Koning, “Improved predictions of nuclear reaction rates with the TALYS reaction code for astrophysical applications”, *Astronomy and Astrophysics Journal* 487, 767-774 (2008).
- [717] H. Utsunomiya, S. Goriely, T. Kondo, T. Kaihori, A. Makinaga, S. Goko, H. Akimune, T. Yamagata, H. Toyokawa, T. Matsumoto, H. Harano, S. Hohara, Y.-W. Lui, S. Hilaire, S. Peru, and A.J. Koning, “M1 strength for zirconium nuclei in the photoneutron channel”, *Phys. Rev. Lett.* 100, 162502 (2008).

- [718] C. Nair, A.R. Junghans, M. Erhard, D. Bemmerer and R. Beyer, "Photodisintegration studies on p-nuclei: the case of Mo and Sm isotopes", *Journ. Phys. G35*, 014036 (2008).
- [719] A. Spyrou, A. Lagoyannis, P. Demetriou, S. Harissopulos, "Cross section measurements of (p, $\gamma$ ) reactions on Pd isotopes relevant to the p process", *Phys. Rev. C77*, 065801 (2008).
- [720] D.M. Mei, C. Zhang, A. Hime, M. Ito and, "Evaluation of (alpha, n) Induced Neutrons as a Background for Dark Matter Experiments", *Nucl. Instrum. Meth. A606*, 651 (2008).
- [721] J. Duprat and V. Tatischeff, "On non-thermal nucleosynthesis of Short-Lived Radionuclei in the early solar system", *New Astronomy Reviews* 52, 463 (2008).
- [722] S. Goriely, S. Hilaire and A.J. Koning, "Improved predictions of reaction rates for astrophysics applications with the TALYS reaction code", *Kernz-08 - International Conference on Interfacing Structure and Reactions at the Centre of the Atom*, Dec. 1-5 2008, Queenstown, New Zealand, to be published (2009).
- [723] S. Goriely, S. Hilaire and A.J. Koning, "Improved reaction rates for astrophysics applications with the TALYS reaction code", *The Thirteenth International Symposium on Capture Gamma-Ray Spectroscopy and Related Topics*, Aug. 25-29 2008, Cologne, Germany, to be published (2009).
- [724] H. Utsunomiya, S. Goriely, T. Kondo, M. Kamata, O. Itoh, H. Toyokawa, T. Matsumoto, S. Hilaire and A.J. Koning, "Low-lying strength in Sn photoneutron reactions", *The Thirteenth International Symposium on Capture Gamma-Ray Spectroscopy and Related Topics*, Aug. 25-29 2008, Cologne, Germany, to be published (2009).
- [725] H. Utsunomiya, H. Akimune, T. Yamagata, T. Kondo, M. Kamata, O. Itoh, H. Toyokawa, K. Yamada, T. Matsumoto, H. Harada, F. Kitatani, S. Goko, S. Goriely, S. Hilaire, A.J. Koning, "Photon Probe in Nuclear Astrophysics", *6th Japan-Italy symposium on Heavy Ion Physics (11-15th Nov. 2008)*, Tokai, Japan (2009).
- [726] J. Kiener, A. Belhout, V. Tatischeff, and H. Benhabiles-Mezhoud, "Nuclear reaction studies for solar flares", *Proceedings of the DAE Symposium on Nuclear Physics*, Vol. 53, Roorkee, India, 22-26 December, 2008 editors R. K. Choudhury, Alok Saxena, B. J. Roy, Indian Institute of Technology, Roorkee, Uttarakhand, (2008).
- [727] J. Duprat and V. Tatischeff, "Energetic Constraints on In Situ Production of Short-Lived Radionuclei in the Early Solar System", *Astro. Journ. Letters* 671, L69 (2007).
- [728] M. Segawa, T. Masaki, Y. Nagai, Y. Temma, T. Shima, K. Mishima, M. Igashira, S. Goriely, A. Koning, and S. Hilaire, "Neutron capture cross sections of  $^{186}\text{Os}$ ,  $^{187}\text{Os}$ , and  $^{189}\text{Os}$  for the Re-Os chronology", *Phys. Rev. C* 76, 022802 (2007)
- [729] S. Goriely, S. Hilaire and A.J. Koning, "Improved predictions of nuclear reaction rates for astrophysics applications with the TALYS reaction code", *Proceedings of the International Conference on Nuclear Data for Science and Technology*, April 22-27, 2007, Nice, France, editors O. Bersillon, F. Gunsing, E. Bauge, R. Jacqmin, and S. Leray, EDP Sciences, p. 1329-1332 (2008).

- [730] A. Belhout, J. Kiener, A. Coc, J. Duprat, C. Engrand, C. Fitoussi, M. Gounelle, A. Lefebvre-Schuhl, N. de Srville, V. Tatischeff, J.-P. Thibaud, M. Chabot, F. Hammache, and H. Benhabiles-Mezhoud, “ $\gamma$ -ray production by proton and  $\alpha$ -particle induced reactions on  $^{12}\text{C}$ ,  $^{16}\text{O}$ ,  $^{24}\text{Mg}$ , and  $^{56}\text{Fe}$ ”, *Phys. Rev. C* 76, 034607 (2007).
- [731] S. Goriely, “Nucleosynthesis by accelerated particles to account for the surface composition of HD 101065”, *Astronomy and Astrophysics* 466, 619 (2007).
- [732] E. Khan, “Astrophysical roles for giant resonances in exotic nuclei”, *Nucl. Phys. A* 788, 121 (2007).
- [733] C. Vockenhuber, I. Dillmann, M. Heil, F. Kaeppler, N. Winckler, W. Kutschera, A. Wallner, M. Bichler, S. Dababneh, S. Bisterzo, and R. Gallino, “Stellar  $(n,\gamma)$  cross sections of  $^{174}\text{Hf}$  and radioactive  $^{182}\text{Hf}$ ”, *Phys. Rev. C* 75, 015804 (2007).
- [734] H. Utsunomiya, S. Goriely, A.J. Koning, S. Hilaire, S. Goko, A. Makinaga, T. Kaihori, T. Kondo, T. Yamagata, H. Akimune, H. Toyokawa, T. Matsumoto, H. Harano and Y.-W. Lui, “Enhanced photoneutron cross sections for zirconium isotopes near threshold: evidence for extra M1 strength?”, *Proceedings of 2nd International Conference on Frontiers in Nuclear Structure, Astrophysics and Reactions Aghios Nikolaos, Crete, Greece, September 10-14, 2007* (2008).
- [735] S. Goko, H. Utsunomiya, S. Goriely, A. Makinaga, T. Kaihori, S. Hohara, H. Akimune, T. Yamagata, Y.-W. Lui, H. Toyokawa, A.J. Koning, and S. Hilaire, “Partial photoneutron cross sections for the isomeric state  $^{180\text{m}}\text{Ta}$ ”, *Phys. Rev. Lett.* 96, 192501 (2006).
- [736] V. Tatischeff, B. Kozlovsky, J. Kiener, R. J. Murphy, “Delayed X and GammaRay Line Emission from Solar Flare Radioactivity”, *Astro. Journ. Supp. Series*, 165:606-617 (2006).
- [737] E. Khan, S. Goriely, D. Allard, E. Parizot, T. Suomijarvi, A.J. Koning, S. Hilaire, and M.C. Duijvestijn, “Impact of the giant dipole resonance on the photodisintegration of ultrahigh energy cosmic rays”, *Astroparticle physics Volume 23, Issue 2*, 191 (2005).

#### Other applications

- [738] R. Luis, J. G. Marques, T. Stora, P. Vaz and L. Zanini, “Optimization studies of the CERN-ISOLDE neutron converter and fission target system”. *European Physical Journal A - Hadrons and Nuclei* Volume 48, Number 6 (2012), 90, DOI: 10.1140/epja/i2012-12090-9 (2012).
- [739] A. Stankovskyi and G. van den Eynde, “Advanced method for calculations of burn-up, activation of structural materials, and spallation products accumulation in accelerator-driven systems”, *Science and technology of nuclear installations 2012*, 545103 (2012).
- [740] A. Milocco et al, “Monte Carlo simulation of the experimental pulse height spectra produced in diamond detectors by quasi-mono-energetic neutrons”, *Nucl. Instr. Meth. A* to be published (2013).
- [741] T Y Hirsh, D Berkovits, M Hass, P Jardin, A Pichard, M L Rappaport, Y Shachar and I Silverman, “Towards an intense radioactive  $^8\text{Li}$  beam at SARAF Phase I”, *Nuclear Physics in Astrophysics V, Eilat 2011, Journal of Physics Conference Series* 337 012010 (2012).

- [742] E. Aprile et al. (XENON100 Collaboration), “Study of the electromagnetic background in the XENON100 experiment”, *Phys. Rev. D* 83, 082001 (2011).
- [743] M.M. Guenther, K. Sonnabend, E. Brambrink, K. Vogt, V. Bagnoud, K. Harres and M. Roth, “A novel nuclear pyrometry for the characterization of high-energy Bremsstrahlung and electrons produced in relativistic laser-plasma interactions’ *Physics of plasmas* 18, 083102 (2011).
- [744] P.J. Griffin and C.D. Peters, “Use of Model-based Covariance Estimates in Dosimetry Applications”, *Proceedings of the International Conference on Nuclear Data for Science and Technology*, April 26-30, 2010, Jeju, Korea, *Journ. Kor. Phys. Soc.* 59, no. 23, 1248 (2011).
- [745] E.P. Hartouni, “An assessment of nuclear isomers as an energy storage medium”, LLNL report LLNL-PROC-409454 (2009).
- [746] J. Blomgren and A.J. Koning, “Neutron physics research for the development of accelerator-driven systems”, in *Nuclear reactors: Research, technology and safety*, ed. Nova science, ISBN 978-1-60692-508-9 (2009).
- [747] J. Blomgren, S. Pomp, J.-C. Bourselier, M. Oesterlund, A. Prokofiev, A.J. Koning, “Mono-energy neutron testing of single event effects”, *Proceedings of the International Conference on Nuclear Data for Science and Technology*, April 22-27, 2007, Nice, France, editors O.Bersillon, F.Gunsing, E.Bauge, R.Jacqmin, and S.Leray, EDP Sciences, p. 1287-1290 (2008).
- [748] S.C. van der Marck, A.J. Koning, D. Rochman, “Photoproduction data for heating calculations”, in *International Conference on the physics of reactors*, Physor 2008 (2008).
- [749] T. Zagar, J. Galy, J. Magill and M. Kellett, “Laser-generated nanosecond pulsed neutron sources: scaling from VULCAN to table-top”, *New journ phys.* 7, 253 (2005).



## Log file of changes since the release of TALYS-1.0

Development of TALYS since release of TALYS-1.0

- December 21, 2007

\*\*\*\*\* Release of TALYS-1.0 \*\*\*\*\*

- January 11, 2008

Repaired little bug for angular distributions in isomeric reactions in  
angleout.f, discovered by Neil Summers, LLNL

- January 17 2008

Added protection for average radiative width in resonancepar.f  
gamgam is never larger than 10.  
Only required for extreme cases.

- January 22 2008

Suggestion from Stephane Goriely:  
Added HFB deformations, consistent with the HFB masses  
Added keyword deformmodel to choose between Moeller deformations  
(deformmodel 1) and HFB deformations (deformmodel 2)

- March 4 2008

Suggestion by Emmeric Dupont: small format change for writing D0 in partable.f

- March 4 2008

Advice of Stephane Goriely:

Removed unphysical behavior of pre-equilibrium gamma emission for extremely neutron rich nuclides. Changed emissionrate.f, emissionrate2.f and preeqttotal.f

- March 4 2008

Added very small preequilibrium contribution to inelastic cross section, in preeqcorrect.f, to prevent discontinuous inelastic cross sections.

- March 11 2008

Emmeric Dupont spotted a small omission in partable.f for the second GDR Lorentzian. Solved.

- March 13 2008

Removed an error for Kopecky-Uhl gamma-ray strength functions. They are now computed at every incident energy since the model is incident energy dependent.

- March 29 2008

Introduced keywords aadjust, gnadjust, gpadjust, gamgamadjust (all default 1.) to make relative changes to level density and other parameters. This avoid looking up the default values of a, etc. and changing them.

- April 8 2008

Stephane Hilaire found an important initialization problem for the case 'projectile 0'; the maximum l-value was zero instead of gamma. This is repaired in densprepare.f

- April 18 2008

Changed a few 0 energies in the file hbstates.eo by energy 0.01 as given in Maslov's report. This was pointed out by Emmeric Dupont.

- May 5 2008

Error with 'segment' variable in spectra.f. Found by Ian Thompson.

- May 19 2008

Added extra if statement for calculation of radiative widths in nuclides.f. Test case 9 crashed for Vittorio Zecca.

- May 24, 2008

Corrected gamma-ray branching ratios with electron conversion, following advice of Olivier Bersillon and Arjan Plompen.

Default is now 'electronconv y'.

Also the branching ratios in the levels database have changed.

- June 20 2008

Pascal Romain found a problem with indexing optical model files, for cases where more than 1 external potential per particle is given. Therefore, the array index for omplines has been enlarged to 3 dimensions.

- June 30 2008

Small normalization problem solved for pre-equilibrium. The pre-equilibrium cross section could be slightly negative, and this is repaired in preeq.f, preeqtot.f and binary.f. Found by Stephane Hilaire.

-July 29 2008

Solved a bug found by Arnd Junghans. Small change in basicinitial.f where lmax is set to gamma for gamma's. This caused problems for calculations with ompall y.

- August 1 2008

Added the possibility to use microscopic particle-hole configurations, as generated from Stephane Hilaire's HFB software. A directory structure/density/ph has been added in the nuclear structure database, which contains 2-component particle-hole state densities for many configurations per nuclide. A new keyword has been introduced, phmodel, where phmodel 1 is used for the (default) analytical densities and phmodel 2 is used for the

tabulated densities. Various subroutines were generalized to accommodate the choice between these different types of *ph*-densities. A subroutine *phdensitytable.f* was added to read in the values from the structure database. Inside *phdens.f* and *phdens2.f* there is now a choice for the model.

- August 4 2008

Added a keyword *endfecis*, similar to *inccalc* and *eciscalc*, such that calculations for a more precise ENDF-6 energy grid can be kept from a previous run.

- August 14 2008

Added a keyword *omonly*, so that Talys runs can be done in which ONLY an optical model calculation is done, i.e. Talys simply acts as a driver for ECIS.

- August 20 2008

Stephane Goriely sent a table with ground state and spins predicted by HFB calculations. This has now been added to the nuclear structure database. If the ground state spin and/or parity is not known experimentally, we now take it from the HFB table instead of a simple 0+ (even) or 0.5+ (odd) assignment.

- August 20 2008

A keyword *jlmmode* has been added to enable different normalizations for the imaginary potential, as explained in

``The isovector imaginary neutron potential:

A key ingredient for the *r*-process nucleosynthesis'',

S. Goriely, , J.-P. Delaroche, *Physics Letters B* 653 (2007) 178183

Obviously, this keyword only works if '*jlmomp y*'.

- August 20 2008

On advice of Stephane Goriely, the possibility to include Pygmy resonance parameters for gamma-ray strength functions was included. Three new keywords '*epr*', '*gpr*' and '*tpr*' were defined.

- September 6 2008

Repaired small error with *nbins* in *input2.f*

- September 11 2008

Added correction factor for gamma-ray strength function to take into account isospin -forbidden transitions, and the associated fiso keyword. Also included strength function model 5 for Goriely's hybrid strength model. Added a keyword micro to do a completely microscopic calculation, i.e. without any phenomenological models or adjustment

- September 21 2008

Added a keyword 'best' to adopt a set of adjusted best parameters for a particular reaction. Such parameter sets can be stored in the structure/best directory.

- October 17 2008

Added the flexibility to use user-defined thermal capture, (n,p), and (n,alpha) cross sections. Also created a new subroutine thermalxs.f to handle these values there.

- November 1 2008

Changed the default for multiple preequilibrium reactions, i.e. mpreeqmode 2 is now the default. This means that the transmission coefficient method of Chadwick is used instead of multiple exciton model. This may increase the speed of TALYS at higher energies by several factors.

- November 17 2008

Corrected small database reading bug for strength=5 in gammapar.f. Discovered by Stephane Goriely.

Stephane Goriely discovers a Lab/CM bug in his stellarrate subroutine which may be non-negligible for light nuclides. Corrected version adopted.

- December 1 2008

Solved a problem encountered by Arjan Plompen for JLM based exciton model transitions in bonetti.f (fluctuating behaviour at low outgoing energies). For negative energies, the JLM results are normalized to the phenomenological imaginary potential. This only applies if 'preeqmode 3' and 'jlmomp y'.

- December 2 2008

External optical model input files can now also be made adjustable through the `rvadjust`, etc. keywords. Changed `opticaln.f`, ... `opticala.f` for this.

- December 16 2008

Implemented several corrections and options by Pascal Romain for fission calculations:

- Increased maximum possible number of rotational levels to 20 in `checkvalue.f`
- Possibility to read in head band and `class2` states for 3 barriers in `fissionpar.f`
- Increased maximum number of incident energies to 500 in `talys.cmb`
- Increased maximum number of rotational states to 700 in `talys.cmb`
- Updated the subroutine `tfission.f` with improved equations for the treatment of class-II states.
- Re-introduced the keyword `colldamp`. If '`colldamp y`' fission calculations according to the method of Pascal Romain of CEA Bruyeres-le-Chatel are performed. This means different options for the spin cutoff parameter and the collective enhancement. Also different defaults for some level density parameters are used.

- January 13 2009

TALYS can now produce a table with average resonance parameters, for the description of the Unresolved Resonance Range (URR). A keyword '`urr`' has been added. If '`urr y`', a file called `urr.dat` will be produced, which for each incident energy contains the relevant neutron and gamma strength functions  $S$ , mean level spacings  $D(J,1)$  and decay widths  $G_n(J,1)$  and  $G_g(J,1)$ . To enable this, the subroutines `radwidththeory.f` and `spr.f` are now called for every incident neutron energy.

- February 9 2009

Amir A Bahadori found a problem for emission spectra in a natural element calculation. The emission energy grids for the various isotopes were out of sync. I revised the subroutine `natural.f` to solve this.

- February 20 2009

Added the possibility to normalize certain reaction channels in TALYS directly to experimental or evaluated data. A new subroutine normalization.f was written and the keyword 'rescuefile' was added. With a "rescue file" normalization factors can be given on an incident energy grid, after which the cross sections are normalized. The difference is then corrected for in the elastic cross section. Use with care.

- March 20 2009

Change default of including class 2 states. The default is now class2 y.

- March 20 2009

Corrected little error in densityout.f. The name of the nucleus was written incorrectly to the ld\* files

- April 1 2009

Change the default for deformed OMP calculations: If the incident particle is a neutron or a proton, only for that particle (as projectile and ejectile) a deformed OMP is adopted. The default for the other particle is set to false. As usual this can all be overwritten with the 'rotational' keyword.

- April 6 2009

Ian Thompson found unphysical oscillatory behavior for Al26(n,n') excitation functions. The cause of this lies in a too large pre-equilibrium alpha contribution. Therefore, I changed some C/A terms in preeqcomplex.f into C/(max(A,40)).

- April 9 2009

Added isotopic specification for natural targets, for recoil output files on advice of Reto Trappitsch. Changed recoilout.f and natural.f.

- April 14 2009

For very short-lived target nuclei the definition of 'isomer' is overwritten with the lifetime of the target level. This means that if e.g. the lifetime of the target nucleus is 1 ms,

then all other levels with a lifetime longer than 1 ms will be treated as "isomer". This overwrites the isomer default or value given in the input. Change made in levels.f.

- April 16 2009

Changed maximum value of eninflow in grid.f to prevent array overflow. Only relevant for very exotic nuclei.

- April 23 2009

Updated preeqcomplex.f after discussions with Connie Kalbach on complex particle pre-equilibrium emission. Changed lab energy into CM energy at a few formula's

- April 23 2009

Made a correction in recoilinit.f. For reactions with very large Q-values, e.g.  $\text{Li-7(d,n)}$  the recoil energy grid was not well defined. Problem encountered by Markus Lauscher.

- April 29 2009

Added the latest mass and deformation tables from Stephane Goriely, as published in Phys Rev Lett 102, 152503 (2009).

- April 29 2009

Included default normalization factors for microscopic fission calculations as published in Goriely et al Phys Rev C79, 024612 (2009).

- April 29 2009

Introduced logarithmic interpolation for tabulated level densities, instead of linear. Changed densitot.f and phdens.f, phdens2.f.

- May 5 2009

Updated preeqcomplex.f after discussions with Connie Kalbach: included pairing correction

- May 5 2009

Generalized nuclear mass, deformation and discrete level tables. Nuclear masses are now read from different subdirectories instead of from one file. This will allow easier addition of alternative mass models in the future.

Also the number of theoretical deformation parameter databases is extended. For both masses and deformation parameters, HFB calculations based on the Gogny D1M force are now also an option.

For discrete levels, HFB based ground state spins and parities are added to the discrete level database for nuclides for which no experimental information exists.

The nuclear structure database, masses.f deformation.f and levels.f were changed for this.

- May 10 2009

Further changes to the masses, deformation, and ground state property tables. I removed the 'deformmodel' keyword again (introduced after the release of TALYS-1.0, so no problems with angry users). It is obvious that theoretical deformation parameters should be taken from the same model as that of the masses. The structure/deformation directory is also cleaned. It now only consists of the subdirectory exp/ where the coupling schemes for coupled channels (and possibly deformation parameters) are given. The theoretical deformation parameters are now found in the mass tables. However, they can be overruled by other values in the deformation/exp files. In most cases however, only the coupling scheme and vibrational deformation parameters (from Raman and Kibedi) remain.

For all (or at least most) stable nuclides above Z=30 and actinides a coupling scheme is provided in deformation/exp. This will soon be finalized for all nuclides, enabling default coupled-channel calculations.

I also changed the numbering of the massmodels.

0: Duflo-Zuker (analytical formula for the masses, no deformation and ground state spins, instead, take these from 'massmodel 2')

1: Moller

2: HFB-17 (Skyrme force): this is the default when exp data is not available

3: HFBD1M (Gogny force)

- May 11 2009

The keywords "addelastic" and "adddiscrete", to fold in direct peaks in secondary spectra, for easy comparison with experiment, have been made energy dependent, similar to that of e.g. the "preequilibrium" keyword. Possibilities are now e.g.

addelastic y  
addelastic n  
addelastic 25.

and similarly for adddiscrete.

- May 18 2009

After one year, I ran the monkey code again, and included all new keywords for testing. This means running Talys with random input files with about 300 keywords, and the requirement that it does not crash, run out of array boundaries etc. A few minor problems were solved in several subroutines.

- May 19 2009

Introduced new keyword strengthM1, to vary between M1 strength functions. The default is strengthM1 = 2 (RIPL-2 prescription) while a value of 1 corresponds to the older prescription of RIPL-1.

- May 22 2009

Adopted the Duflo-Zuker formula from 1996 (from the RIPL-2 website) and replaced the older version. This is only used for masses outside the masstables.

- May 22 2009

Adopted the suggestion of David Perticone to use the longest-lived nuclide as default for natural element calculations for elements without stable isotopes. In other words 'element Tc' in combination with 'mass 0' will no longer give an error message but instead A=98 will be adopted.

- May 22 2009

Added the isotope number to double-differential spectra in the case of natural targets. David Perticone discovered that this was missing.

- June 9 2009

Added the possibility to give 'nbins 0' in the input. In this case, TALYS tries to adopt a clever number of bins, depending on the incident

energy, rather than a constant number of bins (the default).

- June 9 2009

Since all theoretical deformations are now in the mass directory, there is only one set of data left in the structure/deformation/, the subdirectory exp/ is therefore removed, and the structure/deformation/ directory now merely contains the coupling schemes. Added many coupling schemes in this directory

- June 9 2009

Removed an input inconsistency for D0. Both in the input and from the structure database they are now read in keV.

- August 5 2009

Improved some of the ECIS flags for low incident energies for deformed nuclides, according to suggestions of Pascal Romain. Also introduced the keyword 'soswitch' to set the energy where deformed spin-orbit calculations and sequential iterations begin.

Introduced the keyword 'coulomb' to (de-)activate Coulomb excitation calculations by ECIS

Reprogrammed the energy dependence of fstrength.f (again!), after discussion with Pascal Romain and Roberto Capote.

- August 24 2009

Solved a problem with angular distributions for reactions on isomeric states. Incorrect levels were read in (in other words, elastic and inelastic angular distributions were mixed.)

- October 28 2009

Included new thermal cross section database of Mughabghab in structure database. This will change the low energy extension down to thermal energies.

- December 1 2009

Added new keywords rvadjustF, avadjustF, to enable energy-dependent

geometry parameters for the optical model. This is useful for local optimization of the optical model. We can now slightly deviate from constant values, in a smooth manner, and for a restricted energy range given by the user.

- December 11 2009

Added a keyword bestpath to allow a different directory to store input files with best TALYS input parameters

- December 17 2009

Smoothened microscopical particle-hole states read from table.

# Appendix **B**

## Log file of changes since the release of TALYS-1.2

Development of TALYS since release of TALYS-1.2

- December 23, 2009

\*\*\*\*\* Release of TALYS-1.2 \*\*\*\*\*

- January 6, 2010

Changed some of the defaults for 'micro y' (fully microscopic option). Among others, the phmodel is kept to 1. Also 'strength 4' if 'micro y'.

- January 8, 2010

Tiny correction by Stephane Goriely  
in levels.f, line 153

```
    if (massmodel.ne.2) then  
has been changed into  
    if (massmodel.le.1) then
```

since in the case of D1M (massmodel=3), a spin and parity is also assigned.

- January 21, 2010

Solved a problem with Elow (eninclow in the source code) found by Dimitri Rochman: If the highest incident energy is smaller than Elow, Elow is set to zero (otherwise there would be no output of cross sections).

- February 1, 2010

Corrected an indexing problem for exclusive channels in channels.f  
For exotic nuclei sometimes the exclusive channel does not open up  
at the right moment, so the idnum index is incorrect. This caused  
a wrong extrapolation at thermal energies for Th-150(n,n')

Added a small output extension for the branching ratios of  
residual products

- February 24 2010

Added a correction for the indexing of exclusive channels  
(see also Feb 1). In the case of using 'rescue' files the capture  
channel may appear to be closed while the (n,gf) channel, which is  
not normalized, remains open. Variables chanopen, in channels.f,  
and chanexist, in strucinitial.f, are now reinitialized to true  
for the capture channel.

Nikolaj Filatov found a few small bugs, or potential problems, in the Brosa  
subroutines. for fission yield calculations. These have now been corrected

- March 2 2010

Solved a precision problem in molprepare.f for width fluctuation  
calculations Very small numbers were multiplied with very large numbers,  
leading to NaN's in some cases.

The thermal (n,a) cross section in the thermal database was a factor a  
million too high. This is corrected.

- March 7 2010

Erich Ormand found a Bug in Fu's pairing correction, important if  
pairmodel 1 (the default is pairmodel 2). The formula contains a factor  
(U/delta)\*\*0.68 and not (U/delta\*0.68) as coded. Formula corrected.

- March 11 2010

Solved an old problem, first mentioned by Arjan Plompen and now also by  
Alexander Konobeyev: Different compilers produce different answers for  
the gamma spectrum at low energies. This was visible in sample case 6.

Solved this by a small correction in `specemission.f` and `compemission.f`.

After advice of Yan Shengquan, I added a print of the compound nucleus formation cross section per spin and parity value. This will only be done if `flagcheck y`.

- March 12 2010

On the advice of Stephane Hilaire, `S(Zcomp,Ncomp,1)` was changed into `S(Zcomp,Ncomp,k0)` in the Kopecky-Uhl generalized Lorentzian part of `fstrength.f`

- March 26 2010

Separated subroutine `preeqcomplex` into subroutines `stripping`, `knockout` and `breakup`.

- March 28 2010

Implemented Kalbach's new model for break-up reactions, documented in a FENDL-3 report (March 2010). For this, the `Cbreak` keyword was introduced, similar to `Cknock` and `Cstrip`. The new model is in subroutine `breakup`.

- March 30 2010

After a problem discovered by Mihai Horoi, and on the advice of Stephane Goriely, the limits to take transmission coefficients and cross sections (`popeps`, etc.) into account are lowered for astrophysical calculations.

- April 9 2010

Repaired a problem found by Tak Pui Lou. If 'compound n', as in sample case 9, no subroutine or function calculating gamma ray strength functions should be called. This was ensured by changing an if statement near the end of `incident.f`

- April 14 2010

Erich Ormand found a bug for the exciton model emission rates for the use of `pairmodel=1` (Fu's pairing correction). The exciton number of the residual system should be taken in `preeqpair`, when appropriate.

Changed emissionrate.f and emissionrate2.f for this.

- May 20 2010

Added the recoil flag to the endf.inf file, for ENDF evaluations

- June 25 2010

Ronald Murphy discovered an error for angular distributions to discrete states for reactions other than inelastic scattering. This problem occurs for low incident energies of complex particles such as alpha's. Subroutine angdis.f was corrected for this.

- June 28 2010

Ronald Murphy discovered another error for continuum angular distributions. An if statement was removed from spectra.f

- September 2 2010

Generalized input of characters: filenames and other strings can now also be given in uppercase

- December 7 2010

An input file of Mahdi Bakhtiari and Mahdi Sadeghi led me to a problem on interpolation of (input) tabulated OMP parameters with the optmod keyword. Solved in subroutine omppar.f.

Also, they spotted an error in the manual on the outexcitation keyword that I corrected, and it TALYS now stops if a microscopic level density model (ldmodel 4,5) is used in combination with colenhance y (which only works for phenomenological models).

- December 27 2010

On the advice of Stephane Goriely, I wiped a problem with the JLM OMP under the carpet: for very neutron-rich nuclides the JLM potential by Bauge and Delaroche may produce negative reaction cross sections. Instead of stopping the TALYS calculation directly, we now set the reaction cross section to zero. Changed incidentread.f and directread.f for this.

- December 29 2010

Adopted Stephane Goriely's double folding alpha potential.  
A new subroutine foldalpha.f was added, and now alphaomp runs from 1 to 5. The default for the alpha OMP remains unchanged.

- January 3 2011

Extended the flexibility for using level densities. It is now possible, in one and the same calculation, to use different level density models for different nuclides. If the input file contains e.g.

```
ldmodel 5
```

```
ldmodel 24 52 1
```

```
ldmodel 24 53 2
```

then ldmodel 5 will be used for all nuclides, with the exception of Cr-52 and Cr-53 for which ldmodel 1 and 2, respectively, will be used. The level density model thus becomes an adjustable parameter of integer type.

- January 5 2011

Changed the meaning of the keyword adddiscrete. For (n,p)...(n,alpha) reactions discrete state cross sections are now always added to the energy spectrum of the cumulative (n,xp)...(n,xa) spectra.

- January 10 2011

Changed a small cross section limit in preeqcorrect.f to allow calculation of very small alpha-induced cross sections of astrophysical interest

- February 3 2011

Solved an error in the extrapolation of partial (n,p) cross sections to thermal values.

- February 22 2011

Solved a consistency error in the GSM in densitypar.f, found by Heedong Choi. After determination of the critical level density parameters, the global l.d. alimit should not be redefined.

- April 13 2011

Changed the lower input boundary for the Pygmy resonance width to 0.1 MeV, due to a problem found by Samantha Hammond.

- May 10 2011

Added 4 global deuteron OMP's, since the default model coming from standard Watanabe folding does not perform well. A keyword 'deuteronomp' has been made to make a choice between the models:

```
deuteronomp 1 --> Watanabe potential
deuteronomp 2 --> Daehnick potential
deuteronomp 3 --> Bojowald potential
deuteronomp 4 --> Han potential
deuteronomp 5 --> Haixia An potential
```

- May 11 2011

Added flexibility in the OMP adjustment factors. If necessary, all geometrical parameters can now be independently varied (e.g. we no longer necessarily have  $rw=rv$ , etc.)

- May 11 2011

Adopted new egridastro.f subroutine from Stephane Goriely for a finer energy grid in astrophysical calculations

- June 27 2011

On the advice of Kevin Kelley, I allowed the combination 'ecissave y' and 'eciscalc n'. TALYS now checks whether transmission coefficients are available from a previous run. If not, it will create them.

- June 30 2011

Corrected the treatment of the URR: there was an error in the rules for possible angular momentum combinations in urr.f, discovered by Paul Koehler. I also included the calculation of the average gamma width for the URR in the correct place, as suggested by Gilles Noguere. All URR related actions in TALYS can now be found by searching for the variable flagurr.

- July 1 2011

Included the possibility to calculate the effective cross section for integral activation measurements, by folding the excitation functions by an experimental flux. In talys/structure/flux, we have stored more than 40 spectra, coming from the EASY package, which have been used in past activation benchmarks. Such benchmark activities should eventually be performed using (processed) nuclear data libraries, especially for reactions containing a low energy resonance range, but it is helpful to get an idea of the performance directly with TALYS as well. A new keyword 'integral' has been introduced for this.

- September 19 2011

Adopted Gilles Noguere's subroutines for the calculation of unresolved resonance parameters. The urr keyword now acts like the widthfluc keyword: it can be y, n or a value between 0 and 20 MeV for the on-set of the URR calculations. For more flexibility, also the keyword lurr (maximal l-value for URR calculations) and urrnjoy (to normalize capture and fission widths according to the NJOY URR method). The URR subroutines are urr.f, urROUT.f, csunr2.f, unfac.f, gnrl.f and strengthfunc.f

- September 19 2011

In addition to making ldmodel nuclide-dependent, the same was done for the colenhance keyword, i.e. for every nuclide in the chain the collective enhancement for the level density can be turned on and off.

- November 17 2011

Added the possibility to print the direct, pre-equilibrium and compound components of each cross section in the output files. This can be enabled with a new keyword: components

- December 22 2011

Added the possibility to calculate Maxwellian averaged cross sections (MACS). This was already implicitly available for the calculation of astrophysical reaction rates, but now with the keywords 'astroE' and 'astroT' the MACS can be calculated at a user-specified energy, e.g. 30 keV, or temperature.



## Log file of changes since the release of TALYS-1.4

Development of TALYS since release of TALYS-1.4

- December 28, 2011

\*\*\*\*\* Release of TALYS-1.4 \*\*\*\*\*

- December 30, 2011

Introduced non-equidistant binning for the excitation energy grid. The excitation energies can now be given on a logarithmic grid, and this has also become the default. It allows to use less excitation energy bins while not losing precision. The old situation, of TALYS-1.4 and before, can be invoked with the new 'equidistant' keyword, but from now on the default will be 'equidistant n'. Especially for cross sections above 100 MeV the improvement is significant: smoothness and more reliable absolute values. TALYS can now technically be used up to 600 MeV, though I did not validate that with experimental data yet.

- January 2, 2012

Added the extra MT numbers 152-200, introduced in the ENDF-6 format in 2010, in the normalization subroutine.

- January 9, 2012

Multiplied the normalization factor for stripping reactions for helions with a factor of 5 to better fit (n,h) data.

- January 16, 2012

Added the statement "Positive parity" to the level density output file in case of parity-dependent level densities, on the advice of Goran Arbanas.

- January 17, 2012

Solved a problem reported by Patric Granholm. At energies far below the Coulomb Barrier, some excitation functions showed discontinuities. This was due to a too strict choice of pre-equilibrium spin distributions in subroutine binary.f. A popepsA constant is now added.

- January 17, 2012

Turned a few TALYS-errors into warnings (TALYS no longer stops) in integral.f. Also changed the naming of the associated data into talys/structure/integral in which experimental data and fluxes can be found.

- January 21, 2012

Patric Granholm's problem of jan 17 motivated me to extend the 'preeqspin' keyword. There are now 3 possibilities:  
preeqspin 1 (equivalent to the old 'preeqspin n'): the pre-eq spin distribution is made equal to the relative spin-dependent population after compound nucleus emission  
preeqspin 2: the spin distribution from total level densities is adopted  
preeqspin 3 (equivalent to the old 'preeqspin y'): the pre-eq spin distribution is based on particle-hole state densities  
The input is backward compatible, i.e.  
preeqspin y is transformed into preeqspin 3  
preeqspin n is transformed into preeqspin 1  
Total number of possibilities: preeqspin can be equal to y,n,1,2,3

- February 1, 2012

Added more adjustment flexibility. With the tljadjust keyword the transmission coefficients for the outgoing channel can be changed in a

certain energy range.

- February 3, 2012

Added more adjustment flexibility. With the 'branch' keyword the branching ratio for any discrete level in the database can easily be overwritten in the user input. This may be necessary to adjust isomeric cross sections.

- February 13, 2012

Corrected a bug found by Yuki Watanabe: for charged-particle elastic and inelastic scattering the compound components are not written to output. Corrected angdis.f for this.

- February 13, 2012

Fixed a problem with the calculation of D0 for the case of incident photons, (used for level density studies) found by Stephane Goriely. I changed dtheory.f for this.

- February 14, 2012

Removed a bug in rldm.f, introduced just before the release of TALYS-1.4: A min() function was introduced to prevent an array running out of bounds. However, this gives huge fission cross sections for neutrons on subactinides (or any other case where the RLDM is needed), as discovered by Stephane Goriely.

- February 16, 2012

On the advice of Stephane Goriely, I made a change in fissionpar.f: if no fission barriers are found in the tables with phenomenological values, first the tables of Mamdouh (fismodel 2) are scanned for values, before an analytical model is used.

- February 20, 2012

After a question by Yuki Watanabe, I decided to introduce the 'cpang' keyword, to enable the calculation of discrete level compound nucleus angular distributions for incident charged particles

- February 25, 2012

Changed the order of reading lines from files of the best/ directory such that the "best" parameters are now also used for natural targets.

- March 6, 2012

Added radiative capture model for direct and semi-direct capture cross section. For this the 'racap' keyword was made. By default, 'racap n'.

- March 11, 2012

Added new microscopic level densities, this time generated from temperature-dependent HFB calculations and the Gogny D1M nucleon force. This option is now 'ldmodel 6'

- March 27, 2012

Automatically increased the number of included discrete levels for a highly excited isomer.

- March 27, 2012

To increase fitting flexibility I added the keywords egradjust, ggradjust, sgradjust, epradjust, gpradjust, spradjust, E0adjust, Exmatchadjust, Tadjust, fisbaradjust and fishwadjust, all with a default value of 1.

- March 27, 2012

About 70 keywords can now have energy-dependent values. After the keyword and its value are given in the input, an energy range can be specified over which the corresponding model parameter is altered.

- March 29, 2012

Incident energies can now be given in any order, not necessarily in ascending order. They will be sorted first. Also double energy points will be removed. TALYS will thus no longer stop when this is provided.

- April 11 2012

Solved an output bug found by Mahdi Baktiari. At energies far below the Coulomb barrier the direct elastic angular distribution for charged

particles is not copied into the total column.

- April 21 2012

Changed nexout into nexout2 in do loop around line 70 in specemission.f  
That error has been there for several years.

- April 26 2012

Generalized a few energy grids, so that TALYS can be used up to 600 MeV.

- May 7 2012

Vivian Demetriou found a problem in the alpha folding potential  
which I corrected.

- August 12 2012

Added keyword 'production' for (medical) isotope production.  
Added decay data subroutine.

- August 15 2012

Extended nucleon OMP to 1 GeV. For this the keywords Vinf, Ejoin,  
w3adjust and w4adjust give some extra flexibility. TALYS can now  
technically be used up to 1 GeV.

- August 28 2012

Added all other routines for medical isotope production. With  
the 'production' keyword, excitation functions are automatically  
transferred into isotope production rates in MBq. Various  
extra keywords are included for flexibility.

- September 11 2012

Corrected an error for particle multiplicities found by Pedro Arce.  
The yields should be defined relative to the nonelastic cross section  
and not to the reaction cross section. This makes a difference at  
low energies and will change charged-particle nuclear data libraries,  
which use this information.

- September 15 2012

Added possibility to locally adjust the OMP parameters for outgoing channels only, with the keyword 'incadjust'. If 'incadjust n' then OMP adjustments are not performed for the incident channel. This gives more fitting flexibility. Physical argument is that the magnitude of the approximation to regard inverse channels as occurring from the ground state, is unknown. (temperature dependent OMP). The default is however still 'incadjust y'.

- September 15 2012

Arnd Junghans discovered a reading error in the RIPL file for S0. Some of the values do not have a decimal point, resulting in a factor of 100 difference for some nuclides. Fortunately S0 is not used, apart from reference, but the error is now corrected anyway. At his advice, I also removed the printing of the neutron strength function at the wrong place (it was in the middle of the gamma data).

- October 6 2012

Introduced a keyword Liso to enforce the isomeric number of the target (by default it is determined from the discrete level database).

- October 15 2012

Added a keyword fisfeed to output the fission per excitation energy bin. This allows to couple TALYS with a fission yields code, like GEF. To enable this, a few outlets in multiple.f had to be made.

- December 10 2012

Changed a statement in the output about level densities. The 'total' column is given per parity. (issue discovered by Paul Koehler).

- December 21 2012

Revised the direct radiative capture model together with Stephane Goriely. Three new keywords were introduced: ldmodelracap, sfexp and sfth.

- December 21 2012

The resulting intermediate code version is called TALYS-1.50

- March 19 2013

Complemented RIPL discrete level database with levels calculated from microscopic densities. A new keyword 'disctable' was introduced to include or exclude such additions. The default is now 'disctable 1', i.e. RIPL discrete levels file + levels added up to level number 100 if missing from RIPL.

- April 27 2013

Changed 'ecis06' into 'ecis' for filenames etc., to make the filenames independent of the version of ECIS.

- May 18 2013

Increased boundaries for keyword massexcross from 0.500 to 0.600 a.m.u.

- May 20 2013

Put an if statement around loop 150 in comptarget.f to solve an NaN problem found by Satoshi Chiba for astrophysical calculations.

- May 21 2013

Enforced that the non-elastic cross section is non-negative by putting a max around xsnonel in binary.f

- May 21 2013

Changed an .lt. into an .le. in tripathi.f which solves a strange ifort compilation problem.

- May 27 2013

Problem found by Mahdi Bakhtiari for elastic scattering angular distributions for natural targets. For charged particles these were not summed to the natural value. Corrected natural.f

- June 4 2013

Wrote more parameters to parameters.dat file

- June 24 2013

Corrected two problems found by Peter Mohr: if `cpang y` then the charged-particle compound elastic angular distribution should be anisotropic (though symmetric). Corrected `angdis.f` for this. Also, for incident charged particles, direct discrete contributions are not taken into account if a coupling scheme is given. The default for the 'spherical' keyword is changed for this.

- June 30 2013

Added call for GEF subroutine, created by Vasily Simutkin and Michail Onegin, to `massdis.f` to use the Schmidt-Jurado model for fission observables. Introduced the `fymodel` keyword to choose FY model `fymodel 1= Brosa`, `fymodel 2 = GEF`. `fymodel 1` is now also the default.

- August 18 2013

As requested by Paul Koehler, added the average alpha and proton widths in the output of the URR subroutines.

- August 22 2013

Disabled the renormalization of the URR by the NJOY method, as a default at least, to avoid unstable results for the competitive width.

- September 24 2013

Added `radiounit` and `yieldunit` keywords to specify units for medical isotope production

- October 11 2013

Repaired an error in optical model adjustment, discovered by Vlad and Marilena Avrigeanu, the Coulomb radius was not adjusted with `rcadjust`.

- December 1 2013

Added new version of GEF subroutine, created by Vasily Simutkin and Michail Onegin, called `geftalys.f`. Fission yields,  $P(\nu)$ , `nubar`, and `nu` as function of  $Z$  and  $A$  are added to the output. Introduced two extra keywords: `outfy`, to give detailed output of the GEF calculation,

and gefran, for the number of random events to be fed to GEF.



## Log file of changes since the release of TALYS-1.6

Development of TALYS since release of TALYS-1.6

- December 23, 2013

\*\*\*\*\* Release of TALYS-1.6 \*\*\*\*\*

- January 10, 2014

Stephane Goriely found an error in densitytable.f where for ldmodel=6 no parity-dependence was included. This is corrected.

- January 23, 2014

Introduced extra adjustment to pairing shift with keyword Pshiftadjust. This works for the Backshifted Fermi Gas model and avoids looking up the actual value for Pshift for adjustment.

- January 26, 2014

Extended the range of gamgamadjust. Lower limit is now 0.01.

- February 10, 2014

Fixed a problem for FY calculation spotted after calculating a test case for Charlotte Duchemin.

An extra check is done in `massdis.f` to speed up the FY calculations considerably. Charlotte also noted that not all FP files are present. A correction in `massdisout.f` was made. In addition, total FP cross sections per A (cumulative cross section) are now given.

- February 13, 2014

Re-introduced the possibility to fit average radiative width for masses below 100. This is now performed if the `gamgamadjust` keyword is explicitly given in the input file.

- February 21, 2014

Added low energy resonance cross sections to the output. For this, the keyword 'resonance' was introduced. If resonance y, TALYS will read in resonance parameters, from various possible sources, and call the RECENT code of Red Cullen's PREPRO package, which is included as a subroutine. Low energy pointwise resonance cross sections will be added to channels like total, elastic, fission and capture. Choices for various libraries can be made with the `reslib` keyword, which can be equal to default, `endfb7.1`, `jeff3.1`, `jendl4.0`

- March 10, 2014

Extended the resonance option with the `SIGMA1` code, for resonance broadening, and `GROUPIE`, for groupwise cross sections, of the PREPRO package. Introduced the new keywords 'Tres' and 'group' for this. Giving e.g. `Tres 100`.  
`group y`  
will produce groupwise cross sections at 100 Kelvin Doppler broadening.

- April 1, 2014

Sort of solved an indexing problem for exclusive channels, found after a crash (indeed!) of TALYS with an input case of Arjen van Vliet. When `maxchannel` is high, e.g. 8, so many channels are open that an indexing problem occurs. The ultimate correction has not been found but a small change in `channels.f`, when we jump out of the loop if the index reaches `numchantot-10`, seems to do the trick.

- April 1, 2014

Solved a problem discovered by Ismail Sarpun. The GSM model was insensitive

to variations of the level density parameter  $a$  in the input. This is because the GSM model contains a critical level density parameter  $a_{crit}$  that is solved by iteration. Now ' $a$ ' from the input is set equal to  $a_{limit}$ .

- May 29, 2014

Solved a problem for medical isotope production found by Will Webster. TALYS was not protected against using a very fine incident energy. This has now been solved and up to 2000 incident energies can be used. Also some indices for the radioactive decay chain were wrongly assigned, which is solved now.

- June 21, 2014

Added the absorption cross section to the output. This was missing so far. The absorption cross section is the sum of all partial cross sections that do not have the initial particle (usually a neutron) in the exit channel. While it is not needed for any application, EXFOR contains some data sets that can be compared with this.

- July 7, 2014

Added a keyword `bestend` to insert a structure/best file at the end of the input file instead of at the beginning. This gives more flexibility for overruling parameter values.

- July 14, 2014

Replaced HFB masses by HFB24.

- July 14, 2014

Replaced microscopic  $\rho$ -densities by latest version from Stephane Hilaire.

- July 14, 2014

Added strength 6,7,8 models for gamma-ray strength functions. Added a new keyword `Elfile` to read in user-defined gamma-ray strength functions.

- July 29, 2014

Added keyword `Estop` to stop calculation if incident energy gets above `Estop` (while not changing the file with incident energies which may go beyond `Estop`)

- August 6, 2014

Changed acceptable range for aadjust, gnadjust and gpadjust into 0.1 - 10. Also extended a few other ranges to accommodate random variations for TASMAN.

- August 8, 2014

Continue calculation if number of built rotational or class2 states exceeds numrot (currently 700). Instead of an error message we simply stop building more states.

- August 18, 2014

Solved a problem for medical isotope production found by Ismail Sarpun. The wrong lifetime is read from the decay data file for the ground state if a nuclide has more than 1 isomer. Solved this in decaydata.f.

- August 27, 2014

Extended the range of elements up to  $Z=124$ , with nuclear symbols Rg(111), Cn(112), Fl(114) and Lv(116), B3(113), B5(115), B7-9(117-119), C0-4(120-124)

- August 28, 2014

Unified the output in separate files a bit more. Everything is now in lp,e12.5 format. This makes processing by TEFAL and TASMAN easier.

- September 8, 2014

Added the stand-alone Fortran version of the GEF code as a subroutine to enable, in principle, the evaporation of fission fragments by TALYS. For this, TALYS "loops over itself", i.e. it is restarted internally for every excited fission fragment. The option for this is fymodel 3.

- October 8, 2014

Added extra security in compound.f to prevent division by zero in the case of fission. A rare NaN by TALYS was found for 160 MeV helions on Bi-203.

- October 22, 2014

Re-indexed the excitation energies in case of an incident population grid.

This was corrected before but not written down. Olivier Delaune pointed me to that error of TALYS-1.6. Created a new keyword `popMeV`. If `popMeV y`, the population grid is given as a spectrum per MeV (like before). If `popMeV n` (the default), the table represents pure histograms.

- November 25, 2014

Added alpha global OMP by Avrigeanu et al and Nolte et al. The range for `alphaomp` has now been extended to 8.

- December 21, 2014

Added keyword `bestbranch` to enable the adoption of adjusted branching ratios from the `structure/levels/branch/` directory, for better description of isomeric cross sections and gamma-ray cross sections.

- April 13 2015

Corrected an error in the manual, the default GSF is Kopecky-Uhl for incident neutrons only, otherwise it is Brink-Axel. Found by David Walz.

- May 1 2015

Started implementing breakup model by Marilena Avrigeanu. There is now a keyword `breakupmode` which can have the values 1 (Kalbach) or 2 (Avrigeanu). The implementation is not yet complete.

- May 7 2015

On the advice of Stefan Buller, I added a keyword `outbinspectra`, which prints the emission spectra per compound nucleus bin. Obviously, the default is `outbinspectra n`, since it generates a lot of output.

- September 6 2015

Solved a problem for astrophysical reaction rates, found by Stylianos Nikas. The non-equidistant binning of excitation energies was not properly coded in `partfunc.f` leading to wrong astrophysical reaction rates, especially for high temperatures.

- September 24 2015

Defined `deltaEx(0)` to be half the energy of the first discrete level.

It used to be zero.

- October 3 2015

Added keyword `ffspin` to enable a choice between spin dependent excitation functions for excited fission fragments as emerging from GEF, or assignment of spin distributions by TALYS

Added keyword `skipCN` to skip the decay of a compound nucleus altogether.

- October 10 2015

Generalized GSM for fission according to suggestions of Michael Onegin. Various level density parameters for the GSM now have an extra fission barrier index.

# Appendix E

## Log file of changes since the release of TALYS-1.6

Development of TALYS since release of TALYS-1.8

- December 28, 2015

\*\*\*\*\* Release of TALYS-1.8 \*\*\*\*\*

- January 21, 2016

Dimitri Rochman managed to crash TALYS, a rare feat indeed!  
For ldmodel 6, it was possible to have an undefined value for D0,  
leading to possible incident energies of 0 MeV, which crashes ECIS.  
Therefore a minimum value for eninclo, 1.e-11 MeV, was set in grid.f

- February 12, 2016

Solved an error found by Vlad Avrigeanu. Contrary to what is stated in the man  
alphaomp was NOT yet the default in TALYS-1.8. To use the best alpha OMP, you  
have to explicitly put alphaomp 6.  
This is solved now in input4.f

- June 1, 2016

Implemented the possibility to read external files for M1 strength functions,  
and also the possibility to scale them with the etable and ftable keywords.  
Changes were suggested by Stephane Goriely. etable and ftable are now extended

e.g. etable 40 93 1.2 M1

A new keyword mlfile was introduced.

- June 2, 2016

Replace RECENT, SIGMA1 and GROUPIE subroutines of PREPRO-2013 to PREPRO-2015.

- July 9, 2016

Revised Kalbach parametrization for break up reactions, according to the latest

- July 16, 2016

Added keyword massdir to add your own masstables to the talys/structure/mass/

- September 7, 2016

Corrected an error in the deformed OMP for actinides of Soukhovitskii et al, as reported by Fabio Zeisler. The Fermi energy in the OMP definition was taken from the Soukhovitskii OMP while the Soukhovitskii OMP uses specific Fermi energies per nucleus.

- September 19, 2016

Corrected an error found by Bernard Erasmus: medical isotope production. Results were different for a second run in which the TALYS results were already precalculated. Solved this by initializing the discrete levels for non-binary (this was omitted when 'reaction n').

- November 2, 2016

Stephane Goriely added 2 new keywords upbendc and upbende to adjust gamma-ray

- November 8, 2016

Stephane Goriely added 2 new keywords astroex and nonthermlev to account for cross sections. To accommodate this I introduced variables MaxZastro and MaxNastro to keep the cross sections under control.

- November 16, 2016

Solved a problem for low lying 0+ states. ECIS seems to produce inelastic cross sections for the reaction cross section. In case of a weakcoupling model, if the first discrete level is 0+, we replace it by 2+.





## Derivation of the isotope production equations

For the target nuclide we have

$$(F.1) \quad \frac{dN_T(t)}{dt} = -R_T N_T(t).$$

This is easily integrated to give

$$(F.2) \quad N_T(t) = N_T(0) e^{-R_T t}.$$

For every parent nuclide we have

$$(F.3) \quad \frac{dN_p(t)}{dt} = R_{T \rightarrow p} N_T(t) - \lambda_p N_p(t).$$

Multiplying both sides with  $e^{\lambda_p t}$  gives

$$(F.4) \quad e^{\lambda_p t} \frac{dN_p(t)}{dt} = e^{\lambda_p t} [R_{T \rightarrow p} N_T(t) - \lambda_p N_p(t)],$$

or,

$$(F.5) \quad e^{\lambda_p t} \frac{dN_p(t)}{dt} + e^{\lambda_p t} \lambda_p N_p(t) = e^{\lambda_p t} R_{T \rightarrow p} N_T(t),$$

or,

$$(F.6) \quad \frac{d[e^{\lambda_p t} N_p(t)]}{dt} = e^{\lambda_p t} R_{T \rightarrow p} N_T(t).$$

Integrating this, after insertion of Eq. (F.2), gives

$$(F.7) \quad \begin{aligned} e^{\lambda_p t} N_p(t) &= N_T(0) R_{T \rightarrow p} \int dt e^{(\lambda_p - R_T)t} \\ &= \frac{N_T(0) R_{T \rightarrow p}}{\lambda_p - R_T} e^{(\lambda_p - R_T)t} + C, \end{aligned}$$

or,

$$(F.8) \quad N_p(t) = \frac{N_T(0)R_{T \rightarrow p}}{\lambda_p - R_T} e^{-R_T t} + C e^{-\lambda_p t}.$$

Inserting the initial condition  $N_p(t = 0) = 0$  gives

$$(F.9) \quad 0 = \frac{N_T(0)R_{T \rightarrow p}}{\lambda_p - R_T} + C,$$

giving the solution for the parent nuclide,

$$(F.10) \quad N_p(t) = \frac{N_T(0)R_{T \rightarrow p}}{\lambda_p - R_T} [e^{-R_T t} - e^{-\lambda_p t}].$$

For every isotope  $i$ , directly produced by a nuclear reaction on the target isotope or from decay of the parent nuclide, we have

$$(F.11) \quad \frac{dN_i(t)}{dt} = \lambda_{p \rightarrow i} N_p(t) + R_{T \rightarrow i} N_T(t) - \lambda_i N_i(t).$$

Multiplying both sides with  $e^{\lambda_i t}$  gives analogous to Eqs. (F.4)-(F.6),

$$(F.12) \quad \frac{d[e^{\lambda_i t} N_i(t)]}{dt} = e^{\lambda_i t} [\lambda_{p \rightarrow i} N_p(t) + R_{T \rightarrow i} N_T(t)],$$

or, after insertion of the solutions for  $N_T$ , Eq. (F.2), and  $N_p$ , Eq. (F.10),

$$(F.13) \quad \frac{d[e^{\lambda_i t} N_i(t)]}{dt} = e^{\lambda_i t} \left[ \lambda_{p \rightarrow i} \frac{N_T(0)R_{T \rightarrow p}}{\lambda_p - R_T} (e^{-R_T t} - e^{-\lambda_p t}) + N_T(0)R_{T \rightarrow i} e^{-R_T t} \right]$$

Integrating this gives

$$(F.14) \quad \begin{aligned} e^{\lambda_i t} N_i(t) &= \frac{N_T(0)\lambda_{p \rightarrow i}R_{T \rightarrow p}}{\lambda_p - R_T} \left[ \int dt e^{(\lambda_i - R_T)t} + \int dt e^{(\lambda_i - \lambda_p)t} \right] \\ &+ N_T(0)R_{T \rightarrow i} \int dt e^{(\lambda_i - R_T)t} + C, \end{aligned}$$

or,

$$(F.15) \quad \begin{aligned} N_i(t) &= \frac{N_T(0)\lambda_{p \rightarrow i}R_{T \rightarrow p}}{\lambda_p - R_T} \left[ \frac{e^{-R_T t}}{\lambda_i - R_T} + \frac{e^{-\lambda_p t}}{\lambda_i - \lambda_p} \right] \\ &+ \frac{N_T(0)R_{T \rightarrow i}}{\lambda_i - R_T} e^{-R_T t} + C e^{-\lambda_i t}. \end{aligned}$$

Inserting the initial condition  $N_i(t = 0) = 0$  gives

$$(F.16) \quad 0 = \frac{N_T(0)\lambda_{p \rightarrow i}R_{T \rightarrow p}}{\lambda_p - R_T} \left[ \frac{1}{\lambda_p - R_T} + \frac{1}{\lambda_i - \lambda_p} \right] + \frac{N_T(0)R_{T \rightarrow i}}{\lambda_i - R_T} + C,$$

so we finally obtain

$$(F.17) \quad N_i(t) = N_T(0) \frac{R_{T \rightarrow i}}{\lambda_i - R_T} [e^{-R_T t} - e^{-\lambda_i t}] + N_T(0) \frac{\lambda_{p \rightarrow i}R_{T \rightarrow p}}{\lambda_p - R_T} \left[ \frac{e^{-R_T t} - e^{-\lambda_i t}}{\lambda_i - R_T} - \frac{e^{-\lambda_p t} - e^{-\lambda_i t}}{\lambda_i - \lambda_p} \right].$$

The three solutions of interest are thus given by Eqs. (F.2), (F.10), and (F.17).

## TERMS AND CONDITIONS FOR COPYING, DISTRIBUTION AND MODIFICATION

1. This License applies to any program or other work which contains a notice placed by the copyright holder saying it may be distributed under the terms of this General Public License. The "Program", below, refers to any such program or work, and a "work based on the Program" means either the Program or any derivative work under copyright law: that is to say, a work containing the Program or a portion of it, either verbatim or with modifications and/or translated into another language. (Hereinafter, translation is included without limitation in the term "modification".) Each licensee is addressed as "you".

Activities other than copying, distribution and modification are not covered by this License; they are outside its scope. The act of running the Program is not restricted, and the output from the Program is covered only if its contents constitute a work based on the Program (independent of having been made by running the Program). Whether that is true depends on what the Program does.

2. You may copy and distribute verbatim copies of the Program's source code as you receive it, in any medium, provided that you conspicuously and appropriately publish on each copy an appropriate copyright notice and disclaimer of warranty; keep intact all the notices that refer to this License and to the absence of any warranty; and give any other recipients of the Program a copy of this License along with the Program.

You may charge a fee for the physical act of transferring a copy, and you may at your option offer warranty protection in exchange for a fee.

3. You may modify your copy or copies of the Program or any portion of it, thus forming a work based on the Program, and copy and distribute such modifications or work under the terms of Section 1 above, provided that you also meet all of these conditions:

- a) You must cause the modified files to carry prominent notices stating that you changed the files and the date of any change.
- b) You must cause any work that you distribute or publish, that in whole or in part contains or is derived from the Program or any part thereof, to be licensed as a whole at no charge to all third parties under the terms of this License.
- c) If the modified program normally reads commands interactively when run, you must cause it, when started running for such interactive use in the most ordinary way, to print or display an announcement including an appropriate copyright notice and a notice that there is no warranty (or else, saying that you provide a warranty) and that users may redistribute the program under these conditions, and telling the user how to view a copy of this License. (Exception: if the Program itself is interactive but does not normally print such an announcement, your work based on the Program is not required to print an announcement.)

These requirements apply to the modified work as a whole. If identifiable sections of that work are not derived from the Program, and can be reasonably considered independent and separate works in themselves, then this License, and its terms, do not apply to those sections when you distribute them as separate works. But when you distribute the same sections as part of a whole which is a work based on the Program, the distribution of the whole must be on the terms of this License, whose permissions for other licensees extend to the entire whole, and thus to each and every part regardless of who wrote it.

Thus, it is not the intent of this section to claim rights or contest your rights to work written entirely by you; rather, the intent is to exercise the right to control the distribution of derivative or collective works based on the Program.

In addition, mere aggregation of another work not based on the Program with the Program (or with a work based on the Program) on a volume of a storage or distribution medium does not bring the other work under the scope of this License.

4. You may copy and distribute the Program (or a work based on it, under Section 2) in object code or executable form under the terms of Sections 1 and 2 above provided that you also do one of the following:
  - a) Accompany it with the complete corresponding machine-readable source code, which must be distributed under the terms of Sections 1 and 2 above on a medium customarily used for software interchange; or,
  - b) Accompany it with a written offer, valid for at least three years, to give any third party, for a charge no more than your cost of physically performing source distribution, a complete machine-readable copy of the corresponding source code, to be distributed under the terms of Sections 1 and 2 above on a medium customarily used for software interchange; or,
  - c) Accompany it with the information you received as to the offer to distribute corresponding source code. (This alternative is allowed only for noncommercial distribution and only if you received the program in object code or executable form with such an offer, in accord with Subsection b above.)

The source code for a work means the preferred form of the work for making modifications to it. For an executable work, complete source code means all the source code for all modules it contains, plus any associated interface definition files, plus the scripts used to control compilation and installation of the executable. However, as a special exception, the source code distributed need not include anything that is normally distributed (in either source or binary form) with the major components (compiler, kernel, and so on) of the operating system on which the executable runs, unless that component itself accompanies the executable.

If distribution of executable or object code is made by offering access to copy from a designated place, then offering equivalent access to copy the source code from the same place counts as distribution of the source code, even though third parties are not compelled to copy the source along with the object code.

5. You may not copy, modify, sublicense, or distribute the Program except as expressly provided under this License. Any attempt otherwise to copy, modify, sublicense or distribute the Program is void, and will automatically terminate your rights under this License. However, parties who have received copies, or rights, from you under this License will not have their licenses terminated so long as such parties remain in full compliance.
6. You are not required to accept this License, since you have not signed it. However, nothing else grants you permission to modify or distribute the Program or its derivative works. These actions are prohibited by law if you do not accept this License. Therefore, by modifying or distributing the Program (or any work based on the Program), you indicate your acceptance of this License to do so, and all its terms and conditions for copying, distributing or modifying the Program or works based on it.
7. Each time you redistribute the Program (or any work based on the Program), the recipient automatically receives a license from the original licensor to copy, distribute or modify the Program subject to these terms and conditions. You may not impose any further restrictions on the recipients' exercise of the rights granted herein. You are not responsible for enforcing compliance by third parties to this License.
8. If, as a consequence of a court judgment or allegation of patent infringement or for any other reason (not limited to patent issues), conditions are imposed on you (whether by court order, agreement or otherwise) that contradict the conditions of this License, they do not excuse you from the conditions of this License. If you cannot distribute so as to satisfy simultaneously your obligations under this License and any other pertinent obligations, then as a consequence you may not distribute the Program at all. For example, if a patent license would not permit royalty-free redistribution of the Program by all those who receive copies directly or indirectly through you, then the only way you could satisfy both it and this License would be to refrain entirely from distribution of the Program.

If any portion of this section is held invalid or unenforceable under any particular circumstance, the balance of the section is intended to apply and the section as a whole is intended to apply in other circumstances.

It is not the purpose of this section to induce you to infringe any patents or other property right claims or to contest validity of any such claims; this section has the sole purpose of protecting the integrity of the free software distribution system, which is implemented by public license practices. Many people have made generous contributions to the wide range of software distributed through that system in reliance on consistent application of that system; it is up to the author/donor to decide if he or she is willing to distribute software through any other system and a licensee cannot impose that choice.

This section is intended to make thoroughly clear what is believed to be a consequence of the rest of this License.

9. If the distribution and/or use of the Program is restricted in certain countries either by patents or by copyrighted interfaces, the original copyright holder who places the Program under this License may add an explicit geographical distribution limitation excluding those countries, so that distribution is permitted only in or among countries not thus excluded. In such case, this License incorporates the limitation as if written in the body of this License.
10. The Free Software Foundation may publish revised and/or new versions of the General Public License from time to time. Such new versions will be similar in spirit to the present version, but may differ in detail to address new problems or concerns.

Each version is given a distinguishing version number. If the Program specifies a version number of this License which applies to it and "any later version", you have the option of following the terms and conditions either of that version or of any later version published by the Free Software Foundation. If the Program does not specify a version number of this License, you may choose any version ever published by the Free Software Foundation.

11. If you wish to incorporate parts of the Program into other free programs whose distribution conditions are different, write to the author to ask for permission. For software which is copyrighted by the Free Software Foundation, write to the Free Software Foundation; we sometimes make exceptions for this. Our decision will be guided by the two goals of preserving the free status of all derivatives of our free software and of promoting the sharing and reuse of software generally.

**\*NO WARRANTY\***

12. BECAUSE THE PROGRAM IS LICENSED FREE OF CHARGE, THERE IS NO WARRANTY FOR THE PROGRAM, TO THE EXTENT PERMITTED BY APPLICABLE LAW. EXCEPT WHEN OTHERWISE STATED IN WRITING THE COPYRIGHT HOLDERS AND/OR OTHER PARTIES PROVIDE THE PROGRAM "AS IS" WITHOUT WARRANTY OF ANY KIND, EITHER EXPRESSED OR IMPLIED, INCLUDING, BUT NOT LIMITED TO, THE IMPLIED WARRANTIES OF MERCHANTABILITY AND FITNESS FOR A PARTICULAR PURPOSE. THE ENTIRE RISK AS TO THE QUALITY AND PERFORMANCE OF THE PROGRAM IS WITH YOU. SHOULD THE PROGRAM PROVE DEFECTIVE, YOU ASSUME THE COST OF ALL NECESSARY SERVICING, REPAIR OR CORRECTION.
13. IN NO EVENT UNLESS REQUIRED BY APPLICABLE LAW OR AGREED TO IN WRITING WILL ANY COPYRIGHT HOLDER, OR ANY OTHER PARTY WHO MAY MODIFY

AND/OR REDISTRIBUTE THE PROGRAM AS PERMITTED ABOVE, BE LIABLE TO YOU FOR DAMAGES, INCLUDING ANY GENERAL, SPECIAL, INCIDENTAL OR CONSEQUENTIAL DAMAGES ARISING OUT OF THE USE OR INABILITY TO USE THE PROGRAM (INCLUDING BUT NOT LIMITED TO LOSS OF DATA OR DATA BEING RENDERED INACCURATE OR LOSSES SUSTAINED BY YOU OR THIRD PARTIES OR A FAILURE OF THE PROGRAM TO OPERATE WITH ANY OTHER PROGRAMS), EVEN IF SUCH HOLDER OR OTHER PARTY HAS BEEN ADVISED OF THE POSSIBILITY OF SUCH DAMAGES.